University of Oxford

Department of Chemistry



Group 4 Permethylpentalene Complexes as Polymerisation Catalysts

Maureen Georges

Linacre College

Trinity 2021

This thesis is submitted in partial fulfilment of the requirement for the degree of Doctor of Philosophy at the University of Oxford

Preface

The work described in this thesis was carried out in the Chemistry Research Laboratory at the University of Oxford between October 2017 and June 2021 under the supervision of Professor Dermot O'Hare. All the work was performed by the author unless otherwise stated, and no part has been previously submitted for any other degree.

Abstract

Group 4 Permethylpentalene Complexes as Polymerisation Catalysts

Maureen Georges **D.Phil Thesis**

Linacre College **Hilary Term 2021**

The primary aims of this thesis were to: (1) prepare new permethylpentalene complexes and to investigate their performance as homogeneous and heterogeneous α-olefins polymerisation catalysts, (2) investigate the polymerisation of polar monomers and (3) discover new (hydro)permethylpentalene catalysts for the Ring Opening Polymerisation (ROP) of lactide monomers.

The thesis begins by offering an introduction to the chemistry of pentalene and its metal derivatives including ligand synthesis, organometallic chemistry and catalytic performances. The application of Cp^*TiCl_3 ($Cp^* = \eta\text{-}C_5Me_5$) and $Pn^*(H)TiCl_3$ ($Pn^*H = \eta^5\text{-}C_8Me_6H$) as olefin polymerisation catalysts, in both solution phase and immobilised on an insoluble methylaluminoxane (sMAO) support is described. Very high activities are observed for the styrene polymerisation using the supported $Pn^*(H)TiCl_3$. The systems were able to produce atactic polystyrene as well as high density polyethylene (HDPE). The ethylene/styrene copolymerisation ability of the catalysts is then demonstrated. A negative comonomer effect is described as well a low styrene incorporation. A variety of polymerisation conditions were studied, including the effects of temperature, styrene volume and solvent. Polymerisation of *para*-functionalised styrenes was studied using Cp^*TiCl_3 and $Pn^*(H)TiCl_3$. *Para*-functionalised styrenes containing electron donating groups NR_2 (R = H, Me) and OMe lead to very high activities whereas the catalysts perform poorly in the presence of the electron-withdrawing substituent, Br. It was found that Cp^*TiCl_3 and $Pn^*(H)TiCl_3$ exhibited some of the highest activities for p*ara*-aminostyrene polymerisation reported in literature. Copolymerisations of 4-NR_2-styrene with ethylene were attempted but no reaction occurred after poisoning of the catalyst by the comonomer.

The (hydro)permethylpentalene titanium alkoxide and aryloxide complexes, $Pn^*(H)TiCl_2(OR)$ were tested as ethylene and styrene polymerisation catalysts in solution and slurry phases. $Pn^*(H)TiCl_2(O\text{-}Si(Me)_2{}^tBu)$ exhibited high styrene homopolymerisation activities in both phases. The three pre-catalysts tested produced high molecular weight polyethylene ($M_w > 10^6$ g/mol) but were unable to copolymerise other olefins. These complexes were also found to be initiators for the ROP of lactide. The kinetics of polymerisation, rates, effect of temperature, initiator concentration are discussed. The polymers were characterised by a range of physical methods to determine the tacticity, molecular weights and chain end groups.

Finally, eight amidinate permethylpentalene complexes ($Pn^*ZrCl_{1-x}[(NR')_2CR'']_x$) were prepared and investigated as slurry phase olefin polymerisation catalysts. Electronic and steric effects were studied by varying the amidinate substituents. Overall, low homopolymerisation activities were observed and these catalysts were unable to copolymerise ethylene with styrene and 4-NH_2-styrene.

The thesis concludes with experimental details and all characterisations performed as appendices.

Acknowledgements

Firstly, I would like to thank my supervisor Professor Dermot O'Hare for giving me the opportunity to study in and be part of his research group, and for his advice and help throughout my DPhil. Secondly, I am grateful to SCG Chemicals Co., Ltd (Thailand) for their financial support which has allowed me to undertake this project.

Thanks also goes to JC and Zoë for their constant guidance and support over the years. I highly appreciated your help as well as the patience you demonstrated to teach me. I'm also grateful to the people who have helped me with some techniques: Nick for solid-state and solution NMR, Zoë for single crystal X ray diffraction, Norner AS (Norway) for PE GPC, Clem for SEM, and Justin and Meng for powder XRD and TGA. I would also like to thank everyone who took on their personal time to proof read this thesis.

A huge thank you goes to the O'Hare group and more particularly S3 for bearing with me and making the past few years so enjoyable and entertaining. I must start with Gabi (10/10) for making the best use of my dolls (you'll get there !), Phil for being the only one enjoying my company when I clearly lacked of sleep, Rebecca, my first real fumehood neighbour, thanks for the laughs and jokes and not abandoning me, Peace for her constant help, kind words and encouragements, Justin and Bean for always be up for a chat to relax. Matt, thanks for letting me use your space and good luck with this adventure. I'd also like to thank Justin, the king of Photoshop for making me laugh every time I checked my phone, and Meng for sharing memes during the writing period. For sharing the pain and turning it into motivation, thanks to Jess and Archie.

Outside of the lab, I want to thank Lisa for her encouragements and nice times around a cup of tea. Thanks to Camille for keeping me going with amazing cakes, and helping me

discovering Oxford's surroundings. I'd also like to thank "my friend Dan" for teaching how to live like a proper adult. I also want to hugely thank Alex for always being by my side, for listening to me, supporting me and giving me the extra push I needed. Last but not least, I am grateful to my family for their continuous help, for answering the phone in the middle of the night and taking regular trips to Oxford. I would not be where I am today without you all and I am incredibly lucky to have such a caring family.

Nomenclature

Term	Definition
$\{^1H\}$	Proton decoupled
α	Ring tilt angle
a.u.	Arbitrary unit
b	Broad
BnOH	Benzyl alcohol, $C_6H_5CH_2OH$
CGC	Constrained geometry catalyst
COSY	2D correlation spectroscopy
Cp	Cyclopentadienyl, $C_5H_5^-$
Cp*	Pentamethylcyclopentadienyl, $C_5Me_5^-$
CPMAS	Cross-polarisation magic-angle spinning
d	Doublet
DPMAS	Direct polarisation magic angle spinning
Dipp	Di*iso*propylphenyl (2,6-^{i}Pr-C_6H_3)
DSC	Differential scanning calorimetry
Đ	Dispersities, M_w/M_n
δ	Chemical shift
GPC	Gel permeation chromatography
ΔH_m	Enthalpy of melting
η	Hapticity
HDPE	High-density polyethylene
HMBC	Heteronuclear multiple bond correlation
HSQC	Heteronuclear single-quantum correlation spectroscopy
Ind	Indenyl, $C_9H_7^-$
κ-bound	hapticity
k_{obs}	Observed rate constant
k_p	Propagation rate constant

LA	Lactide
LDPE	Low-density polyethylene
m	Multiplet
MALDI-TOF	Matrix-assisted laser desorption/ionisation time of flight
MAO	Methylaluminoxane
Mes	Mesityl (2,4,6-Me-C_6H_2)
MMAO	Modified methylaluminoxane
M_n	Number average molecular weight
MS	Mass spectrometry
M_w	Weight average molecular weight
MWD	Molecular weight distribution, M_w/M_n
μ	Bridging
NMR	Nuclear magnetic resonance
p	Pentet
PDLA	Poly-*D*-lactide
PE	Polyethylene
PLA	Polylactide
PLLA	Poly-*L*-lactide
P_m	Probability of forming a *meso* linkage
Pn	Pentalene, C_8H_6
Pn*	Permethylpentalene, $C_8Me_6^-$
Pn*(H)	(Hydro)permethylpentalene, C_8Me_6H
ppm	Parts per million
P_r	Probability of forming a *racemic* linkage
PS	Polystyrene
pyr	Pyridine (C_5H_5N)
q	Quartet
ROP	Ring-opening polymerisation
RT	Room temperature
s	Singlet

SEM	Scanning electron microscopy
sMAO	Solid polymethylaluminoxane
sPS	Syndiotactic polystyrene
ssNMR	Solid-state nuclear magnetic resonance
t	Triplet
T_g	Glass transition temperature
THF	Tetrahydrofuran, C_4H_8O
TiBA	Triisobutylaluminium, Al^iBu_3
T_m	Melting temperature
TMA	Trimethylaluminium, $AlMe_3$
TMEDA	*N,N,N',N'*-tetramethyl-ethane-1,2-diamine
Tol	Tolyl, (6-Me-C_6H_4)
XRD	X-ray diffraction
Xyl	Xylyl, (2,6-Me-C_6H_3)

Complex identification

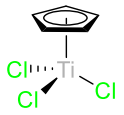

$CpTiCl_3$

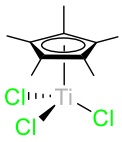

Cp^*TiCl_3 (1)

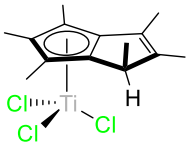

$Pn^*(H)TiCl_3$ (2)

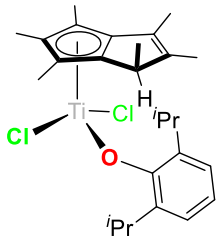

$Pn^*(H)TiCl_2(O\text{-}2,6\text{-}^i Pr\text{-}C_6H_3)$ (3)

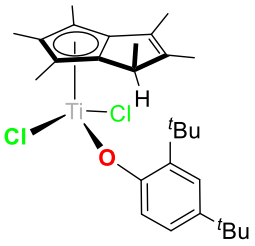

$Pn^*(H)TiCl_2(O\text{-}2,4\text{-}^t Bu\text{-}C_6H_3)$ (4)

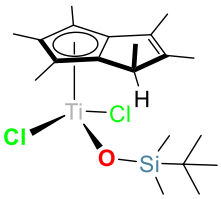

$Pn^*(H)TiCl_2(O\text{-}Si(Me)_2{}^t Bu)$ (5)

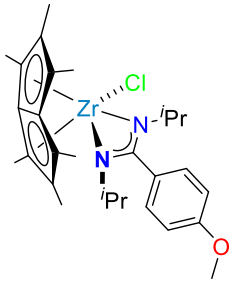

$Pn^*ZrCl[(N^iPr)_2C(4\text{-}OMe\text{-}C_6H_4)]$ (6)

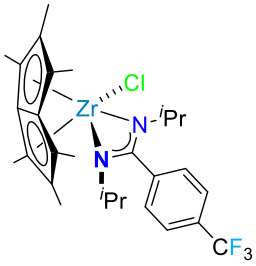

$Pn^*ZrCl[(N^iPr)_2C(4\text{-}CF_3\text{-}C_6H_4)]$ (7)

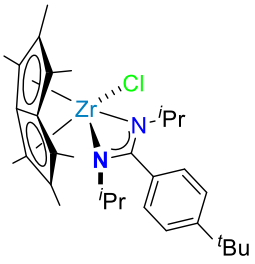

$Pn^*ZrCl[(N^iPr)_2C(4\text{-}^t Bu\text{-}C_6H_4)]$ (8)

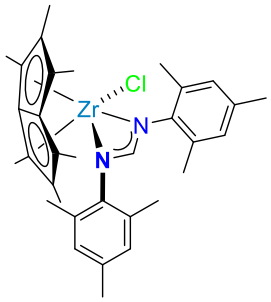

$Pn^*ZrCl[(NMes)_2CH]$ (9)

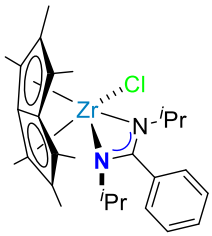

$Pn^*ZrCl[(N^iPr)_2C(C_6H_5)]$ (10)

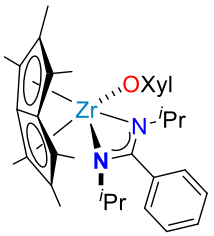

$Pn^*Zr(OXyl)[(N^iPr)_2C(C_6H_5)]$ (11)

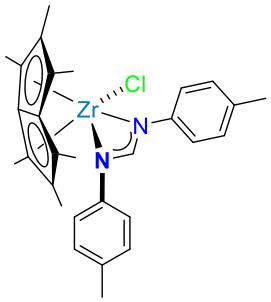

$Pn^*ZrCl[(N^pTol)_2CH]$ (12)

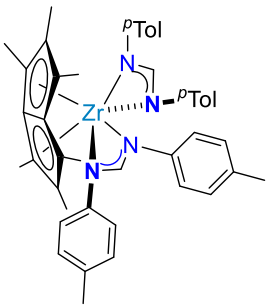

$Pn^*Zr[(N^pTol)_2CH]_2$ (13)

Complex numbering

Number	Name
1	Cp^*TiCl_3
2	$Pn^*(H)TiCl_3$
3	$Pn^*(H)TiCl_2(O\text{-}2,6\text{-}^{i}Pr\text{-}C_6H_3)$
4	$Pn^*(H)TiCl_2(O\text{-}2,4\text{-}^{t}Bu\text{-}C_6H_3)$
5	$Pn^*(H)TiCl_2(O\text{-}Si(Me)_2{}^{t}Bu)$
6	$Pn^*ZrCl[(N^{i}Pr)_2C(4\text{-}OMe\text{-}C_6H_4)]$
7	$Pn^*ZrCl[(N^{i}Pr)_2C(4\text{-}CF_3\text{-}C_6H_4)]$
8	$Pn^*ZrCl[(N^{i}Pr)_2C(4\text{-}^{t}Bu\text{-}C_6H_4)]$
9	$Pn^*ZrCl(NMes)_2CH]$
10	$Pn^*ZrCl[(N^{i}Pr)_2C(C_6H_5)]$
11	$Pn^*Zr(OXyl)[(N^{i}Pr)_2C(C_6H_5)]$
12	$Pn^*ZrCl(N^{p}Tol)_2CH]$
13	$Pn^*Zr(N^{p}Tol)_2CH]_2$

Table of Contents

Preface i

Abstract ii

Acknowledgements iii

Nomenclature v

Complex identification viii

Complex numbering ix

Table of Contents x

Chapter One Introduction 1

1.1 Overview 1

1.2 α-Olefin Polymerisation 3

1.2.1 Mechanism 4

1.2.2 Methylaluminoxane co-catalyst and scavenger 6

1.2.3 Tacticity control and stereospecificity 8

1.2.4 Copolymerisations of olefins 11

1.3 Ring-Opening Polymerisation of Lactide 14

1.3.1 Renewable polymers 14

1.3.2 Structure of Polylactide 14

1.3.3 Mechanism of ROP 16

1.3.4 Initiators for the ROP of lactide 18

1.3.5 PLA tacticity 20

1.4 Pentalene chemistry 22

1.4.1 Nomenclature 22

1.4.2 Synthesis of the pentalene molecule and permethylation 22

1.4.3 Coordination modes of pentalene 25

1.4.4 η^5 hydropentalene complexes Pn*(H) 28

1.4.5 Pentalene complexes in catalysis 29

1.5 Scope of the thesis 32

1.6 References 33

Chapter Two Cyclopentadienyl and Permethylpentalene trichloride complexes for Olefin Polymerisations 45

2.1 Introduction 45

2.2 Polymerisation of styrene 48

2.2.1 Preliminary study for the solution-phase polymerisation of styrene 48

2.2.2 Immobilisation of complexes on solid-MAO 51

2.2.3 Solution and slurry-phase polymerisation of styrene 52

2.2.4 Polymer characterisation 54

2.3 Ethylene homopolymerisation study 63

2.3.1 Temperature dependence 63

2.3.2 Polymer characterisation 65

2.4 Copolymerisation of ethylene with styrene 72

2.4.1 Solvent effect 72

2.4.2 Temperature effect 75

2.4.3 Effect of the styrene comonomer concentration 78

2.4.4 Polymer characterisation 80

2.5 Conclusion 84

2.6 References 86

Chapter Three Polymerisation of Polar Styrene Monomers 91

3.1 Introduction 91

3.2 Homopolymerisation of substituted styrene monomers 94

3.2.1. Influence of temperature 95

3.2.2. Polymer characterisation 98

3.3 Copolymerisation of ethylene with 4-NR_2-styrene (R = H, Me) 104

3.3.1. Preliminary studies 105

3.3.2. Influence of the amount of 4-NR_2-styrene (R= H and Me) 109

3.3.2.1. 4-NH_2-styrene 109

3.3.2.2. 4-NMe_2-styrene 112

3.4 Conclusion 113

3.5 References 115

Chapter Four (Hydro)permethylpentalene complexes as Olefin Polymerisation catalysts ····119

4.1 Introduction 119

4.2 Synthesis and characterisation of new Pn*(H)MCl_2(OR) (M = Ti and Zr) complexes 121

4.2.1 Complex synthesis 121

4.2.2 Complex characterisation 123

4.2.3 Alternative synthetic routes 126

4.3 Homopolymerisation of styrene 128

4.3.1 Solution phase styrene polymerisation 128

4.3.2 Slurry-phase styrene polymerisation 133

4.4 Homopolymerisation of ethylene 139

4.4.1 Solution phase ethylene polymerisations 139

4.4.2 Slurry-phase ethylene polymerisation 142

4.5 Copolymerisation of ethylene and styrene 148

4.6 Conclusion 152

4.7 References 153

Chapter Five Ring Opening Polymerisation of Lactide 157

5.1. Introduction 157

5.2. Ring-Opening Polymerisation of lactide 158

5.2.1 ROP of *L*-lactide 159

5.2.1.1 Effect of the alkoxide/aryloxide 159

5.2.1.2 Initiator concentration dependency 162

5.2.1.3 Temperature variation 165

5.2.1.4 Co-initiator dependency 168

5.2.1.5 Solvent variation 170

5.2.2 ROP of *D*-lactide 171

5.2.3 ROP of *meso*-lactide 173

5.2.4 ROP of *rac*-lactide 176

5.3. Conclusion 179

5.4. References 181

Chapter Six Permethylpentalene Zirconium Amidinate complexes for Olefin Polymerisation **184**

6.1. Introduction 184

6.2. Synthesis of formamidine/amidine ligands and complexes 187

6.3. Homopolymerisation of olefins 191

6.3.1 Slurry-phase homopolymerisation of styrene 193

6.3.2 Slurry-phase homopolymerisation of ethylene 201

6.4. Copolymerisations of ethylene with α-olefins 211

6.4.1 Ethylene/styrene copolymerisations 211

6.4.2 Ethylene/4-NH_2-styrene copolymerisations 220

6.5. Conclusion 222

6.6. References 224

Concluding Remaks and Perspectives **229**

Chapter Seven Experimental details **234**

7.1 General methods 234

7.1.1 Air- and moisture-sensitive techniques 234

7.1.2 Solvent preparation 234

7.1.3 Commercially supplied reagents 235

7.1.4 Synthesis of literature compounds 235

7.1.5 Solution NMR spectroscopy 235

7.1.6 Solid-state NMR spectroscopy 236

7.1.7 Differential scanning calorimetry 236

7.1.8 Scanning electron microscopy 237

7.1.9 Gel permeation chromatography 237

7.1.10 Mass spectrometry 238

7.1.11 Single crystal X-ray diffraction 238

7.1.12 Powder X-ray diffraction (PXRD) 239

7.1.13 Elemental analysis 239

7.1.14 Fourier transform infrared (FTIR) spectroscopy 239

7.1.15 General procedure for immobilising catalysts on solid support. 239

7.1.16 General procedure for solution phase polymerisation of styrene 240
7.1.17 General procedure for solution phase polymerisation of ethylene 240
7.1.18 General procedure for slurry-phase polymerisation of styrene 241
7.1.19 General procedure for slurry-phase polymerisation of ethylene 241
7.1.20 General procedure for slurry-phase copolymerisation.....241
7.1.21 General procedure for solution phase copolymerisation 242
7.2 Experimental details for Chapter 2 243
7.2.1 sMAO-Cp*$TiCl_3$ (1_{sMAO}) 243
7.2.2 sMAO-Pn*(H)$TiCl_3$ (2_{sMAO}) 243
7.2.3 Typical NMR spectroscopy data of polystyrene samples 243
7.2.4 Typical NMR spectroscopy data of polyethylene samples 244
7.3 Experimental details for Chapter 3 245
7.3.1 Typical NMR spectroscopy data of poly(4-methoxy-styrene) 245
7.3.2 Typical NMR spectroscopy data of poly(4-amino-styrene) 245
7.3.3 Typical NMR spectroscopy data for poly(4-bromo-styrene) 246
7.3.4 Typical NMR spectroscopy data for 4-dimethylaminostyrene dimer 246
7.4 Experimental details for Chapter 4 248
7.4.1 Pn*(H)$TiCl_2$(O-2,6-^{i}Pr-C_6H_3) (3) 248
7.4.2 Pn*(H)$TiCl_2$(O-2,4-^{t}Bu-C_6H_3) (4) 249
7.4.3 Pn*(H)$TiCl_2$(O-Si(Me)$_2$^{t}Bu) (5) 250
7.4.4 sMAO-Pn*(H)$TiCl_2$(O-2,6-^{i}Pr-C_6H_3) (3_{sMAO}).....250
7.4.5 sMAO-Pn*(H)$TiCl_2$(O-2,4-^{t}Bu-C_6H_3) (4_{sMAO}).....251
7.4.6 sMAO-Pn*(H)$TiCl_2$(O-Si(Me)$_2$^{t}Bu) (5_{sMAO}).....251
7.5 Experimental details for Chapter 5 252
7.5.1 Lactide polymerisation 252
7.6 Experimental details for chapter 6 253
7.6.1 Li[(N^{i}Pr)$_2$C(4-OMe-C_6H_4)].....253
7.6.2 Li[(N^{i}Pr)$_2$C(4-CF_3-C_6H_4)].....254
7.6.3 Li[(N^{i}Pr)$_2$C(4-^{t}Bu-C_6H_4)] 255
7.6.4 K{[N(2,4,6-Me-C_6H_2)]$_2$CH} 256
7.6.5 General procedure for the synthesis of Pn*ZrCl[(NR′)$_2$CR].....256
7.6.6 Pn*ZrCl[(N^{i}Pr)$_2$C(4-OMe-C_6H_4)] (6).....257
7.6.7 Pn*ZrCl[(N^{i}Pr)$_2$C(4-CF_3-C_6H_4)] (7).....257
7.6.8 Pn*ZrCl[(N^{i}Pr)$_2$C(4-^{t}Bu-C_6H_4)] (8).....258

7.6.9 Pn*ZrCl[[N(2,4,6-Me-C_6H_2)$_2$]CH] (9) 259
7.6.10 General procedure for the synthesis of Pn*TiCl[(NR')$_2$CR] 259
7.6.11 Pn*TiCl[[N(2,4,6-Me-C_6H_2)$_2$]CH] 259
7.6.12 Pn*TiCl[[N(2,6-^{i}Pr-C_6H_3)$_2$]CH] 260
7.6.13 sMAO-Pn*ZrCl[(N^{i}Pr)$_2$C(4-OMe-C_6H_4)] (6_{sMAO}) 260
7.6.14 sMAO-Pn*Zr[(N^{i}Pr)$_2$C(4-CF_3-C_6H_4)] (7_{sMAO}) 261
7.6.15 sMAO-Pn*ZrCl[(N^{i}Pr)$_2$C(4-^{t}Bu-C_6H_4)] (8_{sMAO}) 261
7.6.16 sMAO-Pn*ZrCl[(NMes)$_2$CH] (9_{sMAO}) 261
7.6.17 sMAO-Pn*Zr(OXyl)[(N^{i}Pr)$_2$C(C_6H_5)] (11_{sMAO}) 261
7.6.18 sMAO-Pn*ZrCl[(N^{p}Tol)$_2$CH] (12_{sMAO}) 262
7.6.19 sMAO-Pn*Zr[(N^{p}Tol)$_2$CH]$_2$ (13_{sMAO}) 262
7.7 References 263

APPENDIX A-1

Chapter 2 ..... A-2
Chapter 3 ..... A-29
Chapter 4 ..... A-38
Chapter 5 ..... A-60
Chapter 6 ..... A-69

Chapter One

Introduction

1.1 Overview

The production of polyolefins, around 180 million tonnes per year, represents more than half of the worldwide plastics production making them by far the most important industrial polymers.[1–4] Their chemical and physical properties such as flexibility, lightweight and recyclability makes them one of the most important synthetic polymers with use in various domains such as food packaging, car bumpers, toys, prosthetics.[5,6] However, polyolefins are non-biodegradable and their decomposition takes hundreds of years.[7–9] Biodegradable and biorenewable polymers (for example, polylactide) are of major interest in the context of environmentally friendly alternatives to polymers derived from fossil fuel sources, though the sustainability of the monomer feedstocks and the products of biodegradation must also be carefully considered.[10,11]

While polyolefins are also produced commercially by methods such as radical polymerisation, organometallic catalysts play a prominent role in their global production and they are a key focus in the synthesis of biodegradable polymers. For over 50 years, the pentalene molecule has sparked interest in organometallic chemistry. Once a challenging molecule to synthesise, strategies have been developed to overcome its

instability and make it applicable in a large range of domains such as small molecule activation and coordination chemistry. The use of pentalene as an organometallic ligand has been extensively reviewed in the literature.[12,13]

This chapter discusses some aspects of homogeneous and heterogeneous polymerisation of α-olefins by group 4 catalysts. It also serves as a brief introduction to ring-opening polymerisation (ROP) and synthesis of biodegradable polymers such as polylactic acid, including how polymer properties can be tuned. Finally, the use of pentalene and its derivatives in organometallic chemistry is discussed.

1.2 α-Olefin Polymerisation

In the 1950s, Ziegler and Natta discovered that the combination of titanium halides and organo-aluminium species promoted the polymerisation of olefins such as ethylene and propylene.[14–16] This breakthrough won them the Nobel Prize in 1963 and since then academic and industrial research has been oriented towards developing new olefin polymerisation catalysts for high performances.[1] The catalysts generally used in olefin polymerisation undergo a coordination-insertion mechanism where the monomer coordinates to the metal centre.[17–19] Coordination-insertion polymerisations present the huge advantage of allowing control of the nature of the polymer by tuning the catalyst. Indeed, it is possible to control the stereochemistry as well as the molecular weight of the polyolefins by varying the catalyst's architecture.[20–23]

Most of the industrially-used catalysts nowadays are inspired by Ziegler-Natta catalysts, *e.g.* $TiCl_4$ supported on $MgCl_2$ or other heterogeneous systems such as Phillips' chromium oxides[17,24,25]. However, recent research has been focused on single-site group 4 catalysts.[26–30] Metallocene systems such as Cp_2MCl_2 (M = Zr, Ti) can polymerise olefins such as ethylene and propylene in the presence of an aluminium alkyl (Figure 1.1, a)).[31,32] More recently, half-metallocene have attracted interest for the ability to tune the ancillary ligands and the properties of the polymers.[3334] Notably, piano-stool half-titanocenes were developed by Ishihara and Nomura for the stereospecific polymerisation of styrene as well as for the copolymerisation of ethylene with styrene (Figure 1.1, b) and c)).[33,35–37]

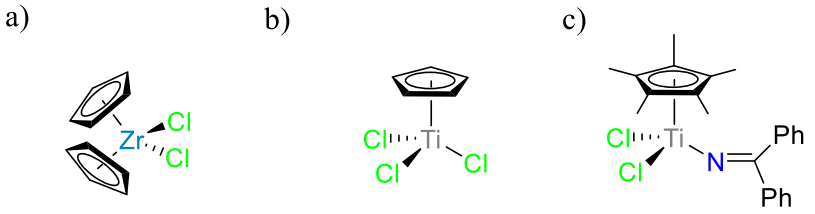

Figure 1.1. Examples of group 4 metallocene and half-metallocene catalysts for the polymerisation of olefins.

1.2.1 Mechanism

The mechanism for olefin polymerisation using transition metal catalysts has been thoroughly studied.[38–41] In the majority of cases, a Cossee-Arlman insertion-migration mechanism takes place where successive insertions of an olefin monomer in a metal-carbon bond produce a polyolefin, such as polyethylene (Scheme 1.1).[42–44] The first step of polymerisation is the formation of the active species. By substituting a ligand (*e.g.* chloride, alkyl or alkoxide) by an alkyl group, the aluminium alkyl (*e.g.* methylaluminoxane, MAO) activates the pre-catalyst. A cationic species $[L_2MMe]^+$ is then produced by abstraction. In the propagation step, an olefin monomer approaches the coordination sphere and coordinates to form a π complex. Then, the methylene carbon attacks one of the olefin carbons leading to a four-membered ring transition state. Finally, the electron-rich olefin migrates and inserts in the metal-carbon bond and an olefin monomer is added to the starting species. The migration opens a vacant site and the polymer chain then grows by the addition of monomer units. The polyolefin is obtained after termination. Several termination pathways exist including chain transfer to the aluminium co-catalyst, β-hydride elimination where a metal hydride species is formed, and transfer to another olefin monomer.[41,45,46] Other mechanisms have been proposed such as the Green-Rooney mechanism for example, which involves reaction of olefins with a carbene complex to give a metaalacyclobutane intermediate.[47]

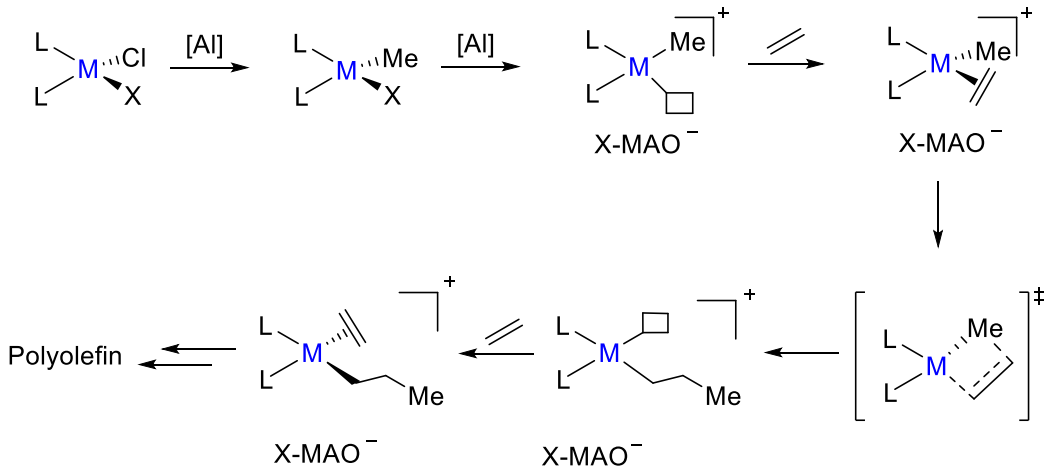

Scheme 1.1. Cossee-Arlman mechanism for the polymerisation of ethylene by a group 4 complex.

Styrene can be polymerised *via* many different techniques such as radical, anionic, cationic and thermal polymerisations.[48–51] Commercial polystyrene is mostly obtained *via* free radical polymerisation initiated by benzoyl peroxide.[52] More recently, styrene polymerisation by metal complexes has emerged as a solution to obtain good control over the morphology and molecular weight distribution of the polymers.[53–56] The process follows a typical insertion-coordination mechanism and allows for the formation of different stereoregularity.

Although the homopolymerisations of ethylene and styrene follow the same coordination-insertion mechanism, the active species from group 4 catalysts responsible for producing the polymer chain is different. While group 4 metals in the (+IV) oxidation state (M^{IV}) are catalysing ethylene homopolymerisation, (+III) species control the polymerisation of styrene.[54,57] It has been suggested that the (+III) state is favoured to (+IV) because of enhanced back-donation from the more electron-rich metal centre to the monomer.[54,58,59] In the case of styrene, the active M^{III} species is formed after reduction of the M^{IV} centre by aluminium alkyls. While Nomura *et al.* proposed that neutral Ti^{III} is responsible for styrene polymerisation,[60–62] other authors have postulated that cationic

Ti^{III} was the active species for the polymerisation of styrene.[54,63,64] The propagation and termination steps are the same as for ethylene polymerisation. Two modes of insertion can be observed depending on the carbon involved: 1,2-insertion and 2,1-insertion (Scheme 1.2).[57,65,66]

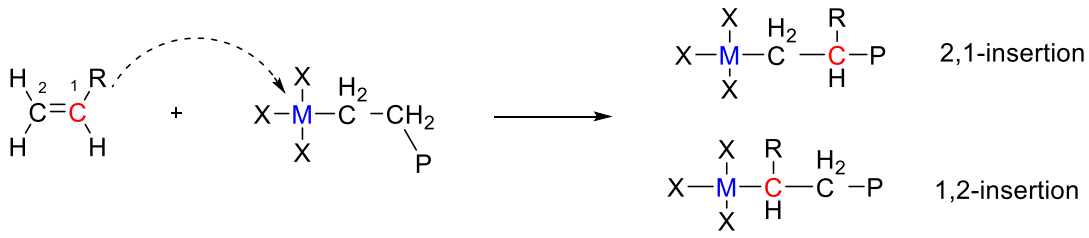

Scheme 1.2. Regiospecific polymerisation of 1-alkene.

1.2.2 Methylaluminoxane co-catalyst and scavenger

Single-site catalysts became the focus of olefin polymerisation after metallocenes such as $CpTiCl_2$ were combined with alkyl aluminium species to polymerise ethylene.[67,68] Although the catalysts allowed for the formation of polymers, they displayed low activity. Reichert, Breslow and Kaminsky first investigated the activation of the catalytic species by adding water in the systems and reported better activities due to the *in-situ* formation of methylaluminoxane (MAO) from the reaction of alkyl aluminium (*e.g.* $AlMe_3$) with water.[69–71] In the presence of MAO, the catalysts displayed higher stability and an increase in polymerisation activity, which made this activator the focus of polymerisation chemistry by metallocenes.

MAO is predominantly synthesised by the partial hydrolysis of trimethylaluminium (TMA) and contains a mixture of polymeric compounds $(Me_{\sim 1.5}AlO_{\sim 0.75})_n$ and significant amounts of TMA.[72–74] For this reason, the structure of MAO is complex and consists of cages, sheets and nanotubes with various sizes and motif repetitions (Figure 1.2).[75–77]

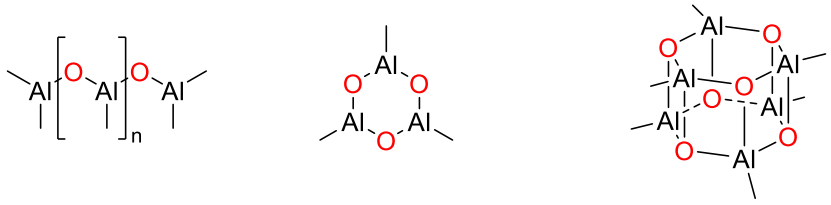

Figure 1.2. Possible structure of MAO.[75–77]

MAO is the most common activator used in homogeneous α-olefin polymerisations.[76,78–80] However, high quantities of MAO (200-5000 eq.) are required to reach high polymerisation activities due to the dual function of the co-catalyst: it generates and stabilises the active species and acts as a scavenger, removing traces of impurities in the system.[75] The large excess needed represents one of the major industrial challenges associated with the use of MAO.

Alternatively, a different form of MAO, insoluble polymethylaluminoxane (sMAO), can be employed as a dual cocatalyst. Its structure is as complex as its soluble analogue and still undefined.[81] When introduced in the system, it acts as an activator and scavenger as well as a support on which the catalyst can be immobilised. Reported polymerisations using sMAO show an increase in activity compared to free MAO and better control over the morphology of the resulting polymers compared to unsupported catalysts.[82,83]

The principal aim for immobilising catalysts onto solid supports such as sMAO is to keep the advantages of homogeneous polymerisation such as high activities while improving the polymer morphology and preventing fouling (*i.e.* accumulation of a polymer layer on the reaction vessel).[84,85] It is generally accepted that slurry-phase olefin polymerisation begins in the pores of the solid catalysts and a polymer coating forms around the catalyst particles.[2] The morphology of the support is replicated in the resulting polymer.

Alkyl aluminium species, especially trialkyl species, are often added to the reactor during slurry-phase polymerisations to act as scavengers that remove traces of water and oxygen.[86] Most common species include trimethylaluminium (TMA), triethylaluminium (TEA) and triisobutylaluminium (TiBA).[86,87] When these are employed, a low amount is added as their concentration influences the polymerisation activities. At a high concentration, the trialkylaluminium species can deactivate the catalyst as well as interact with the MAO, which is one of the main reasons for reduced activity and reactor fouling.[84,88,89]

1.2.3 Tacticity control and stereospecificity

Factors such as the catalysts ligands and their symmetry can influence the polymerisation activity and determine the stereochemistry of the polyolefin.[21] When prochiral olefins are employed for polymerisation, the main chain of the resultant polyolefin contain chiral carbons. The respective configurations of consecutive monomer units determine the stereoregularity of the polymer. The latter is crucial to define the physical properties of the materials.

Styrene is a substituted olefin and its polymerisation process can lead to stereoregularity.[56,59]. Depending on the insertion that takes place, two monomer units arrange themselves in the same fashion (*meso*) or an opposite manner (*rac*). On a larger scale, the succession of *meso*- and *rac*- blocks promotes the formation of polystyrene chains with three different macro-tacticities (Figure 1.3).[90] Atactic polystyrene, where the phenyl groups are randomly arranged on each side of the carbon backbone, is amorphous and widely used industrially for its transparency and stiffness.[91] In isotactic polystyrene, the phenyl substituents are on the same side of the backbone. It is a semi-crystalline polymer that can easily be synthesised using Ziegler-Natta catalysts.[42,92,93] Because of its

slow crystallisation rate, isotactic polystyrene is not produced commercially. Syndiotactic polystyrene contains phenyl groups that alternate on each side of the main chain. This semi-crystalline material has attracted much attention over the past 20 years, due to its unique properties such as fast crystallisation rate, high melting temperature, low density, low dielectric constant and high modulus.[55,56,94–96] Syndiotactic polystyrene has diverse applications such as plugs and sockets, as well as in automotive systems where it is used in power distribution centres.[94]

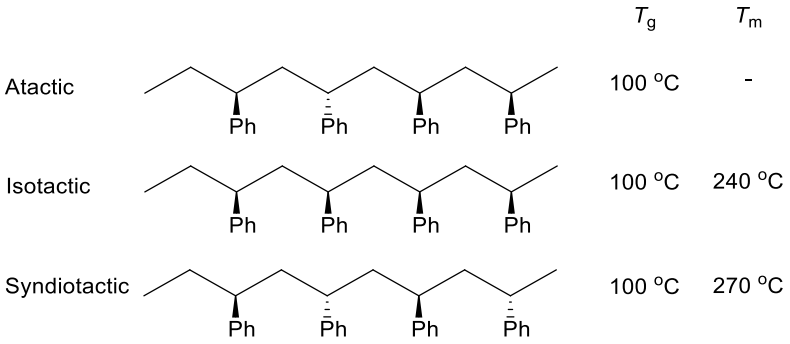

Figure 1.3. Different polystyrene tacticities.

Ishihara *et al.* reported the first synthesis of syndiotactic polystyrene by $CpTiCl_3$ in 1986.[36] Since then, many half-titanocenes systems have been developed to promote syndiotacticity.[97–101] Efficient syndiotactic polymer catalysts have been reported that display simple structure modifications from the work by Ishihara. Specifically, Nomura and co-workers have been pioneers in the development of catalysts such as $Cp^RTiCl_2(OAr)$ (Ar = 2,6-^{i}Pr$_2$-C_6H_3) and Cp^RTiCl_3 (Cp^R = Cp, Cp*, 1,3-Me-C_5H_3).[102–105] They indeed reported that, in the presence of MAO, $Cp^RTiCl_2(OAr)$ was an active catalyst for the polymerisation of syndiotactic polystyrene with activities increasing with the temperature.[105] The highest activity obtained was 16 000 $kgs_{PS}/mol_{Ti}/h$ at 85 °C.

Since Johnson *et al.* reported the first NMR spectroscopic study of polystyrene, extensive efforts have been made to use ^{1}H and $^{13}C\{^{1}H\}$ NMR spectroscopy to determine the stereoregularity of the polymers.[106–112] Many controversies however remain and the assignments are ambiguous. One key method to determine polystyrene tacticity is to compare the NMR spectra to known structures and proceed by analogy. Generally, when $^{13}C\{^{1}H\}$ NMR spectroscopy is used to study the arrangement of the monomer units, three carbons are important: the aromatic ipso carbon (144-146 ppm), the methylene carbon (42-47 ppm) and the methine carbon (40-41 ppm).

Lee and co-workers highlighted the differences in the $^{13}C\{^{1}H\}$ NMR spectra obtained for the three macro-tacticities in the regions of the methine and methylene carbons.[111] Isotactic and syndiotactic polystyrene only exhibits two singlets with the syndiotactic methylene carbon at a lower field than the isotactic analogue. The spectrum of the atactic polystyrene is more complex with multiplets in the methylene region resulting from a random arrangement of the carbons.[111]

With stereospecific polymers, it is possible to determine the degree of regularity by the probability to form a new *rac* or *meso* diad. This probability is expressed by P_r or P_m respectively and both are linked by the simple relation $P_r = 1–P_m$. If $P_r = P_m = 0.5$, the polystyrene is composed by randomly arranged units and thus is atactic. When $P_r = 1$, the polystyrene is isotactic and syndiotactic polymer is synthesised if $P_m = 1$. These probabilities P_r and P_m can be obtained by considering each tetrad and their intensities after deconvolution of NMR spectra.[111]

Table 1.1. Probability of each tetrad in polymer chains for a one-parameter Bernoullian statistical calculation.[107]

Tetrad	Probability
mmm	P_m^3
mmr	$2\ P_m^2(1-P_m)$
rmr	$P_m\ (1-P_m)^2$
mrm	$P_m^2(1-P_m)$
mrr	$2\ P_m(1-P_m)^2$
rrr	$(1-P_m)^3$

1.2.4 Copolymerisations of olefins

Different physical properties can be achieved by synthesising homopolymers with controlled molecular weight and stereospecificity as discussed above. Alternatively, introducing a second monomer in the system widens the types of polymers attainable. For example, incorporation of another olefin such as 1-hexene in polyethylene chains affects the crystallinity, the density and the melting point of the resulting copolymer.[113–115]

Ethylene/α-olefin copolymers started attracting attention around 1990. Before that, attempts to synthesise the copolymer by a Ziegler-Natta or radical mechanism failed or achieved very low comonomer incorporation due to their reactivity differences.[116–120] Stevens *et al.* developed a route *via* homogeneous insertion using group 4 constrained geometry catalysts and MAO.[121] The half-titanocenes complexes Cp^RTiX_3 (Cp^R= Cp, Cp*, X= halide, alkyl, alkoxide, aryloxide) have been tested for ethylene/styrene copolymerisations but they were not able to selectively generate the copolymer. Indeed, in most cases, a mixture of polyethylene, polystyrene and copolymer was observed.[122–126] The formation of a mixture of polymers was attributed to the coexistence of different active titanium species.[127] Evidence of the presence of several catalytic species was

studied by Ishihara *et al.* using half-titanocene systems.[128] More recently, Nomura and co-workers identified both Ti^{III} and Ti^{IV} cyclopentadienyl-based catalysts as responsible for producing the mixture of polymers.[60] Indeed they postulated that two active species were formed in the system during the copolymerisation with half-titanocenes Cp^*TiX_2Y and a co-catalyst: Ti^{IV} and Ti^{III}.[129,130] They hypothesised that the cationic Ti^{IV} active species intervenes in the copolymerisation and the neutral Ti^{III} species plays a role in the styrene homopolymerisation (Scheme 1.3).[60–62]

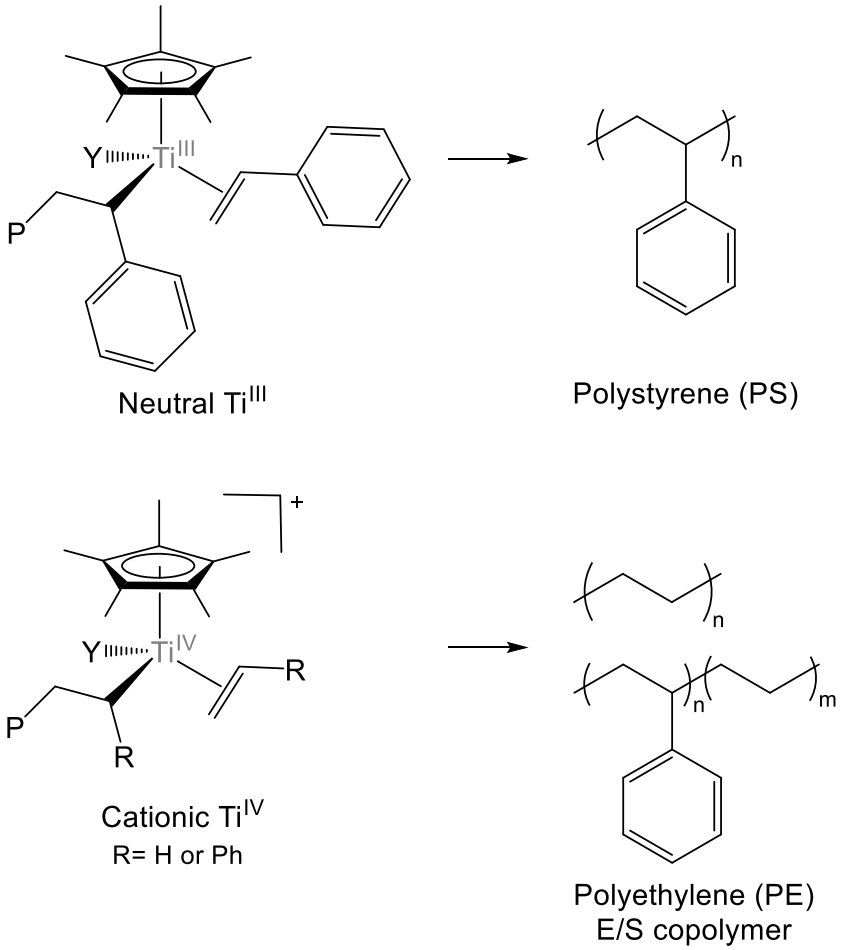

Scheme 1.3. Neutral Ti^{III} and cationic Ti^{IV+} active species for the polymerisation of olefins, adapted from Nomura et al.[60,61]

$CpTi(OPh)_3$ exhibited good activity with high styrene incorporation of 54.5% when used with MAO at 60 °C.[123] However, a polymer mixture was still obtained. The relative ratio

of each depends on the initial amount of $AlMe_3$ and MAO employed. Styrene content, activities and stereoregularity distribution highly depend on the nature of the anionic ligands and the polymerisation conditions.

Using modified titanium half-metallocene appears as one of the solutions to the mixture of polymers usually obtained. Nomura *et al.* investigated the copolymerisation capacity of aryloxide half-titanocenes $Cp^RTiCl_2(O\text{-}2,6\text{-}^iPr_2C_6H_3)$ (Cp^R= 1,2,3-$Me_3C_5H_2$, 1,3-$Me_2C_5H_3$, $^tBuC_5H_4$).[131,132] With these complexes, exclusive formation of the ethylene/styrene copolymer was reported without homopolymer by-products. The aryloxide ligands promoted relatively high molecular weights (M_w = 3.5–17.10^4 g/mol) and narrow molecular weight distribution between 1.6 and 2.1. An increase in the amount of styrene comonomer introduced in the system led to a slight decrease in the activity of $Cp^RTiCl_2(O\text{-}2,6\text{-}^iPr_2C_6H_3)$ (Cp^R= 1,2,3-Me_3CH_2) and a large increase in styrene incorporation (up to 73.6%). Similarly, the ketimide complex, $Cp^*TiCl_2(N{=}C^tBu_2)$ displayed living copolymerisation character in presence of MAO.[130] The living character of the polymerisation appeared independent of the amount of MAO, the pressure of ethylene, temperature and styrene content.

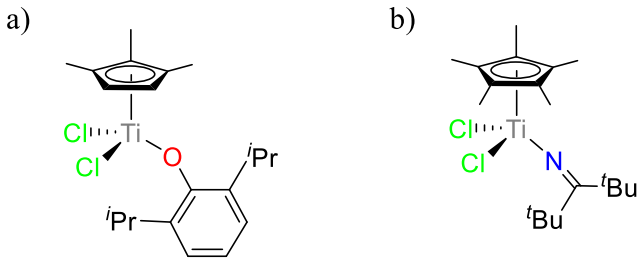

Figure 1.4. Examples of half-metallocene catalysts developed by Nomura *et al.* for olefin copolymerisation.

1.3 Ring-Opening Polymerisation of Lactide

1.3.1 Renewable polymers

The recent years have seen the rapid growth of renewable polymer production. While polyolefins are omnipresent in modern life, their slow degradation process presents a threat to the environment.[9,133,134] The development of biodegradable and biocompatible polymers as an alternative to polyolefins emerged as a necessity to reduce industrial waste. The global bioplastic market is growing exponentially whereby 2.1 million metric tons were generated in 2020 and the production is estimated to reach over 2.8 million metric tons in 2025.[135]

A more sustainable option can be attained by polyesters with readily available monomer sourcing which upon degradation generates small molecules such as CO_2 and H_2O.[136–138] Polylactides (PLAs) represent the majority of biodegradable polymers produced due to their physical and chemical properties such as low toxicity and mechanical strength.[139,140] Industrially, lactic acid and lactide (LA) are produced by a bacterial fermentation process using products like corn, beet, cane sugar as well as agricultural waste materials.[140–144] The versatile properties of PLAs make them valuable materials with diverse applications. It is useful for disposable tableware for example, and also has applications in surgery where PLA-based degradable stitches are used.[145,146]

1.3.2 Structure of Polylactide

Polylactides can be synthesised *via* two different pathways: polycondensation of lactic acid or ring-opening polymerisation (ROP) of lactide. The polycondensation has many disadvantages such as the removal of water generated during the polymerisation, the need for high temperatures and long reaction time. It mostly yields polymers of low molecular

weights.[140] To overcome the limitations, lactide is often preferred as a monomer. Lactide is produced by the oligomerisation of lactic acid followed by the depolymerisation of a low molecular weight pre-polymer producing the cyclic monomer.[137,147,148] The ROP of lactide enables the formation of high molecular weight polymers.

Lactic acid possesses two configurations (*S* and *R*), due to the single stereocentre, referred to as *L*- and *D*-lactic acid respectively. The dimeric lactide thus has two chiral centres with three possible isomers: *L*-lactide (*S, S*), *D*-lactide (*R, R*) and *meso*-lactide (*R,S*). *Rac*-lactide refers to a 1:1 mixture of *L*- and *D*-lactide (Scheme 1.4).[149,150] Consequently, the ROP of lactide results in different distributions of the stereocentres that determine the physical properties of the polymers.[11,151] There are four possible tacticities of PLA: isotactic, heterotactic, syndiotactic and atactic (Scheme 1.4). Two types of isotactic PLA exist; poly(*L*-lactide) (*SSSS*) and poly(*D*-lactide) (*RRRR*) are made of adjacent monomers with the same stereochemistry and are typically crystalline.[152] Heterotactic PLA, (*SSRR*), consists of adjacent monomers with the opposite stereochemistry. It can be produced from *rac*- and *meso*-lactide and is generally amorphous.[153–155] Syndiotactic PLA, where stereocentres are alternating (*SRSRSR*), is produced by the ROP of *meso*-lactide and is crystalline.[156,157] Atactic polymer formed by random sequences of sterocentres is synthesised from *rac*-LA and is amorphous.[157]

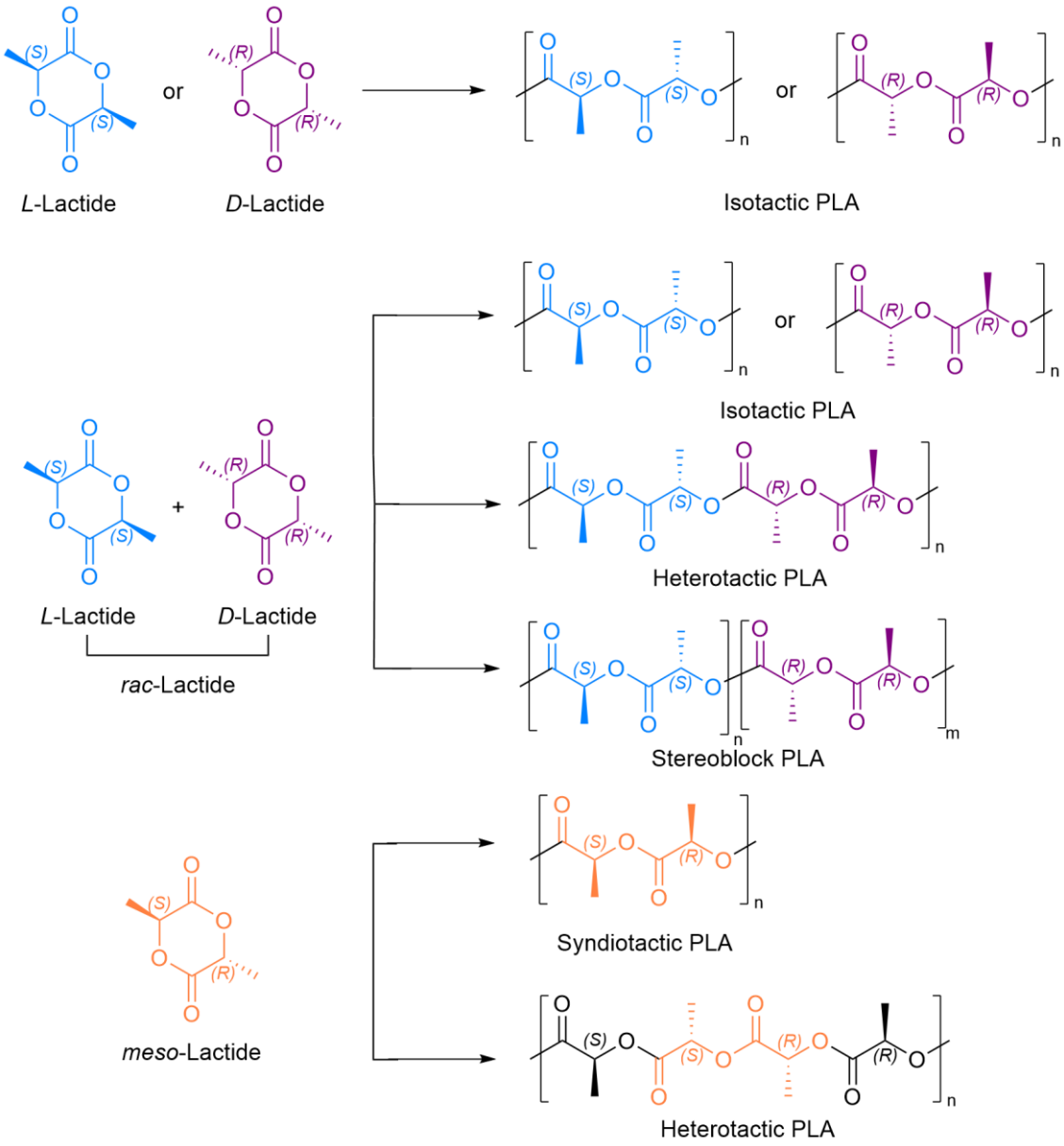

Scheme 1.4. Isomers of lactide and possible PLA tacticities.

1.3.3 Mechanism of ROP

The most efficient synthetic pathway to polylactide is the ring-opening polymerisation (ROP) of lactide monomer using metal catalysts.[148,158–163] The nature of the catalyst used for the ROP determines the type of polymerisation mechanism among cationic,[164,165] anionic,[166,167] organocatalytic,[168,169] coordination-insertion mechanisms,[170,171] or by Lewis pairs.[172] Anionic and cationic mechanisms have major limitations: side reactions

such as epimerisation, transesterification and chain termination result in a lack of molecular weight and dispersity.[151,164,173]

Alternatively, ROP of lactide monomers *via* coordination-insertion can produce polymers with high stereocontrol and high molecular weights with controlled dispersity (Scheme 1.5). Initially, a lactide monomer coordinates to the Lewis acidic metal centre through the carbonyl group. Insertion then takes place *via* nucleophilic addition of the alkoxide or aryloxide species to the carbonyl and a strained four-membered ring transition state is formed. The ring-opening of the lactide monomer breaks the acyl-oxygen bond and releases a free coordination site on the metal centre. Insertion of new lactide monomers enables the polymer to grow and termination occurs by hydrolysis of the active polymer chain.[151,170] Equations 1.1 defines the rate law for polymerisation *via* the coordination-insertion mechanism.

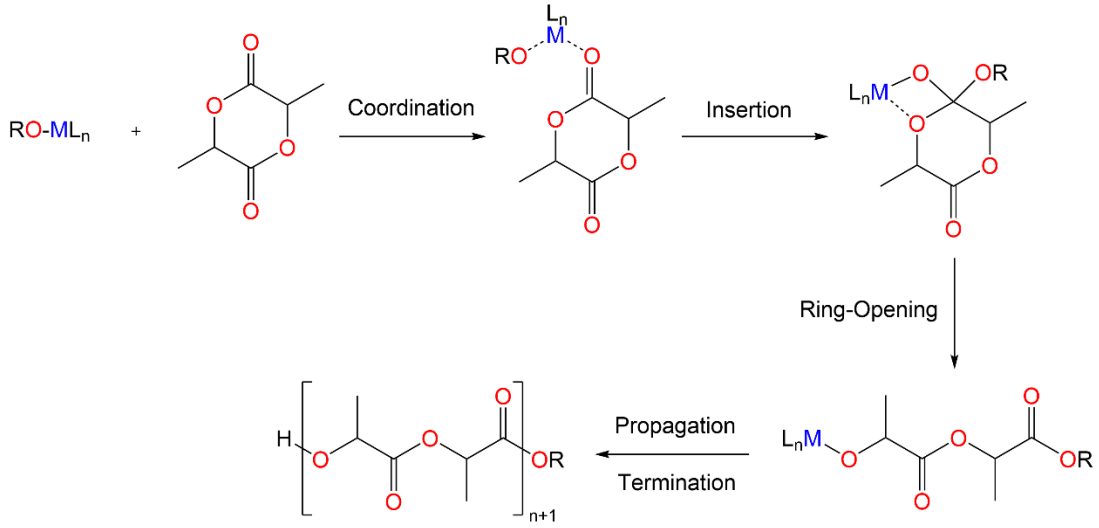

Scheme 1.5. Coordination insertion mechanism for the ROP of lactide.

$$\frac{d[\mathrm{LA}]}{d\mathrm{T}} = \mathrm{k_p}[\mathrm{LA}]^{\mathrm{a}}[\mathrm{cat}]_0^{\mathrm{b}} \qquad \text{with} \qquad \mathrm{k_{obs}} = \mathrm{k_p}[\mathrm{cat}]_0^{\mathrm{b}} \qquad \text{Equation 1.1}$$

1.3.4 Initiators for the ROP of lactide

The ROP of lactide is predominantly initiated by metal alkoxides.[162,174,175] The latter are often generated *in situ* by the addition of a protic co-initiator in the system. Tin bis(2-ethylhexanoate) or $Sn(Oct)_2$ is one of the main initiators employed industrially due to its wide availability and solubility in organic solvents (Figure 1.5).[176] The real initiators are tin(II) alkoxides that are formed in the presence of protic reagents such as alcohols.[151,177] The most common activator is benzyl alcohol.

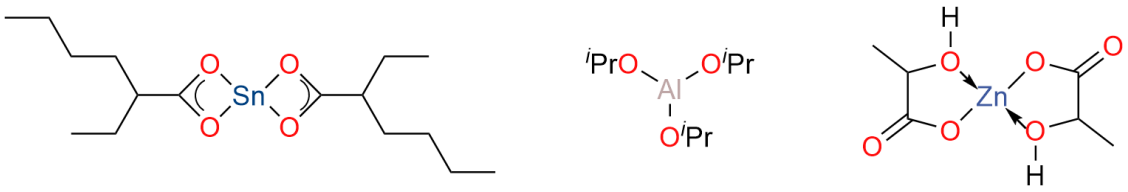

Figure 1.5. Examples of ROP initiators: $Sn(Oct)_2$, $Al(O^iPr)_3$ and $Zn(Lact)_2$.

Other examples of initiators used in industry include aluminium isopropoxides $Al(O^iPr)_3$ and zinc lactate $Zn(Lact)_2$ which is preferred for biomedical applications due to its non-toxicity compared to $Sn(Oct)_2$ (Figure 1.5).[175,178–180] These highly active catalysts, however, present the major disadvantage of multiple polymer chains growing from one metal, resulting in a poor control over molecular weights.[151] Designing single-site catalysts to promote the polymerisation of lactide with control over molecular weights, dispersity, rate of reaction and stereochemistry is therefore particularly interesting.[151,158]

A wide range of salen-type ligands has been studied with metals such as indium, yttrium, scandium and lanthanum.[181–185] Phosphasalen catalysts have been reported to be more active than their salen analogues due to the greater electron-donating ability of the ligand that reduces the Lewis acid character of the metal thus increasing the polymerisation rate.[186] For example, phosphasalen indium and yttrium initiators showed high activities

for the ROP of *rac*-lactide with high tacticity control, producing isotactic PLA with indium (P_m = 0.87) and heterotactic PLA with yttrium (P_r > 0.87).[183,187]

Group 4 complexes as ROP initiators have been less investigated. Lunn *et al.* reported group 4 amine tris(phenolate) alkoxides as highly active initiators for the ROP of *rac*-lactide in solvent-free conditions. Hafnium species reached 95% conversion after 30 minutes and produced heterotactic PLA with high molecular weights and narrow dispersity (M_n = 71×10^3 g/mol, Đ = 1.19).[188]

More recently, zirconium permethylindenyl initiators have been reported by O'Hare and co-workers (Figure 1.6, a). They observed a second-order dependence on monomer concentration in the presence of benzyl alcohol and a range of PLA tacticities depending on the stereoregularity of the monomer employed.[189,190] Group 4 permethylpentalene (Pn*) aryloxides and alkoxides are good initiators for the ROP of *L*- and *rac*-lactide.[191,192] (Hydro)permethylpentalene (Pn*(H)) initiators were ranked in the order Zr > Hf > Ti, however, no stereocontrol was observed and atactic PLA was produced despite the chiral centre on the Pn*(H) ligand (Figure 1.6, b).[192] Zirconium η^8-Pn* alkoxide and aryloxide catalysts generated isotactic PLA from the ROP of *L*-lactide and atactic enriched PLA from *rac*-lactide (Figure 1.6, c). Pn*Zr(O-2,6-^{i}Pr-C$_6$H$_3$) and Pn*Zr(O-2,6-Me-C$_6$H$_3$) displayed similar polymerisation rates for *L*-lactide (k_{obs} = 0.35 and 0.30 h^{-1} respectively) suggesting that steric bulk of the aryloxide does not affect the insertion of the lactide monomer.[191]

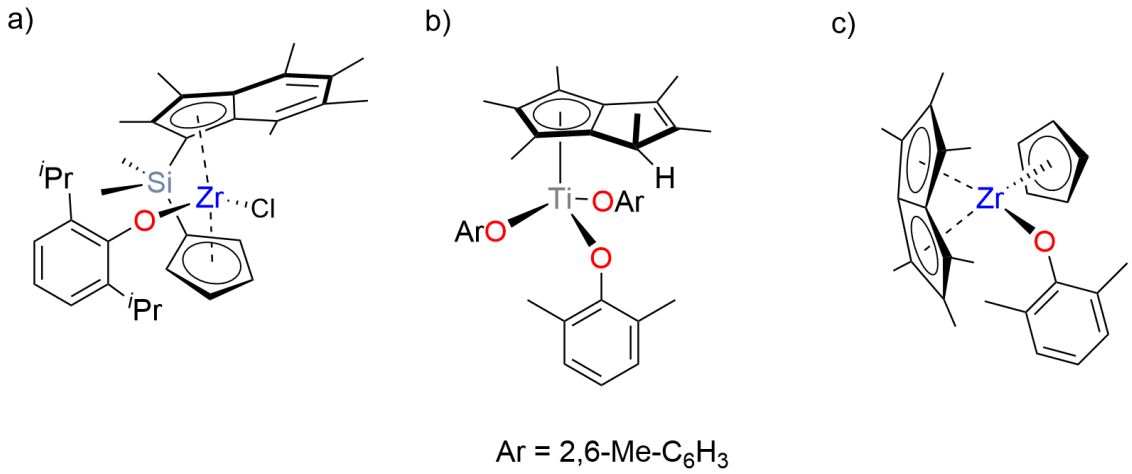

Figure 1.6. Example of initiators for the ROP of lactide monomer developed by O'Hare and co-workers.[190–192]

1.3.5 PLA tacticity

The polymer tacticity can be influenced by various factors such as the lactide monomer, as well as side reactions like epimerisation, transesterification or racemisation during the polymerisation.[149,193] NMR spectroscopy is commonly used to determine the tacticity of PLA at the tetrad level.[149,150,194–197] Using homonuclear decoupled $^{1}H\{^{1}H\}$ spectroscopy of the methine proton region, the resonances can be attributed to the various *meso* (*m*, *RR* and *SS*) and racemic (*r*, *RS* and *SR*) linkages (Figure 1.7).[198]

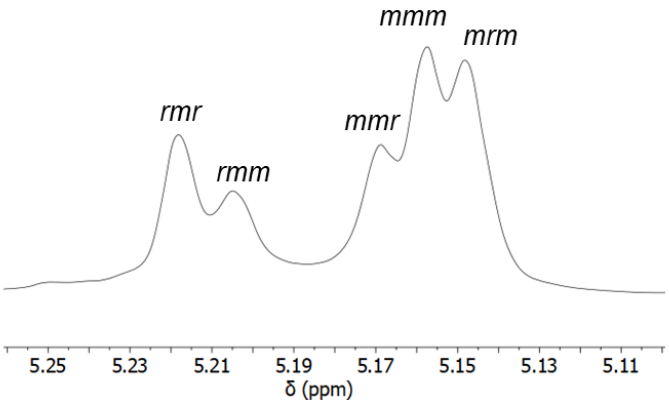

Figure 1.7. Example of a homonuclear decoupled $^{1}H\{^{1}H\}$ NMR spectrum of heterotactic enriched PLA (P_r = 0.52).

The probability of forming *rac* or *meso* bonds are defined at P_r and P_m. $P_r = 1$ represents heterotactic PLA, $P_m = 1$ corresponds to isotactic PLA and atactic polymer is produced when P_r or $P_m = 0.5$.[198] P_r and P_m can be calculated from the intensity of the resonances after deconvolution of the homonuclear decouples spectra assuming the values follow a Bernoullian statistics (Table 1.2).[189,199,200]

Table 1.2. Tetrad probabilities base on Bernouillian statistics.

Tetrad	**Probability**[a]
rmr	$\frac{P_r^2}{2}$
rmm	$\frac{P_r P_m}{2}$
mmr	$\frac{P_r P_m}{2}$
mmm	$P_m^2 + \frac{P_r P_m}{2}$
mrm	$\frac{P_r^2 + P_r P_m}{2}$

[a] $P_r + P_m = 1$.

1.4 Pentalene chemistry

1.4.1 Nomenclature

In the work presented in this thesis, the term "pentalene" refers to any pentalene derivative, neutral and charged. This includes dihydropentalene [C_8H_8], pentalene [C_8H_6] and the pentadienyl dianion [$C_8H_6]^{2-}$. The numbering system used for the carbon framework is shown in Figure 1.8. Carbon 4 and carbon 8 will be referred to as "bridgehead" carbons. The 8 carbons can be divided into wingtip carbons (2 and 6, WT) and non-wingtip carbons (1, 3, 5 and 7, NWT).

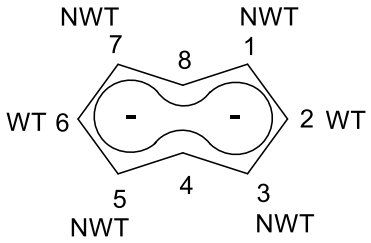

Figure 1.8. Pentalene numbering system and nomenclature. NWT = non-wingtip, WT = wingtip.

1.4.2 Synthesis of the pentalene molecule and permethylation

Pentalene, C_8H_6, is a neutral hydrocarbon molecule containing 8 π-electrons that can be considered as two Cp rings fused at the bridgehead carbons, or as a cycloocatetraene with a transannular bond across the eight-membered ring[201–203]

Neutral pentalene is unstable and has only been isolated in matrices at –196 °C. Above this temperature, it undergoes a cycloaddition reaction, leading to a dimer consisting of two fulvenes isolated from each other by a cyclobutane (Scheme 1.6).[203,204]

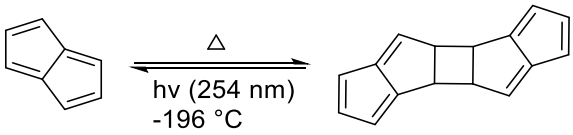

Scheme 1.6. The dimerisation of pentalene.

Due to the difficulties of synthesis of the Pn ligand, the chemistry of pentalene has not been widely investigated. The anion Pn^{2-}, however, is aromatic with 10π electrons and is consequently stable at room temperature, making it a synthetic target to reach pentalene chemistry. It is a stronger donor for acidic metal centres compared to neutral 10π molecules such as naphthalene. Additionally, the two rings allow for the charges to be distributed which enables hapticity shifts.[205] There are three major synthetic paths to obtain the Pn^{2-} dianion: pyrolytic routes, thermal cyclisations and rearrangements.

In 2007, O'Hare *et al.* reported a novel route for the synthesis of the lithium permethylpentalene anion Li_2Pn^* that does not involve dihydropentalene.[206–208] The starting material for this route is the Weiss-H_4 compound (Scheme 1.7). The reaction of Weiss-H_4 with methyl iodide and K_2CO_3 followed by hydrolysis and decarboxylation by HCl led to the diketone 2,4,6,8-tetramethylbicyclo[3.3.0]octane-3,7-dione (Scheme 1.7). Further oxidation with bromine allows for the formation of a dienone. Substitution followed by dehydration of the cyclic dienone allows for the preparation of a neutral isomer of permethylpentalene. The dilithium permethylpentalene anion can be isolated after further reduction and deprotonation of the intermediate.

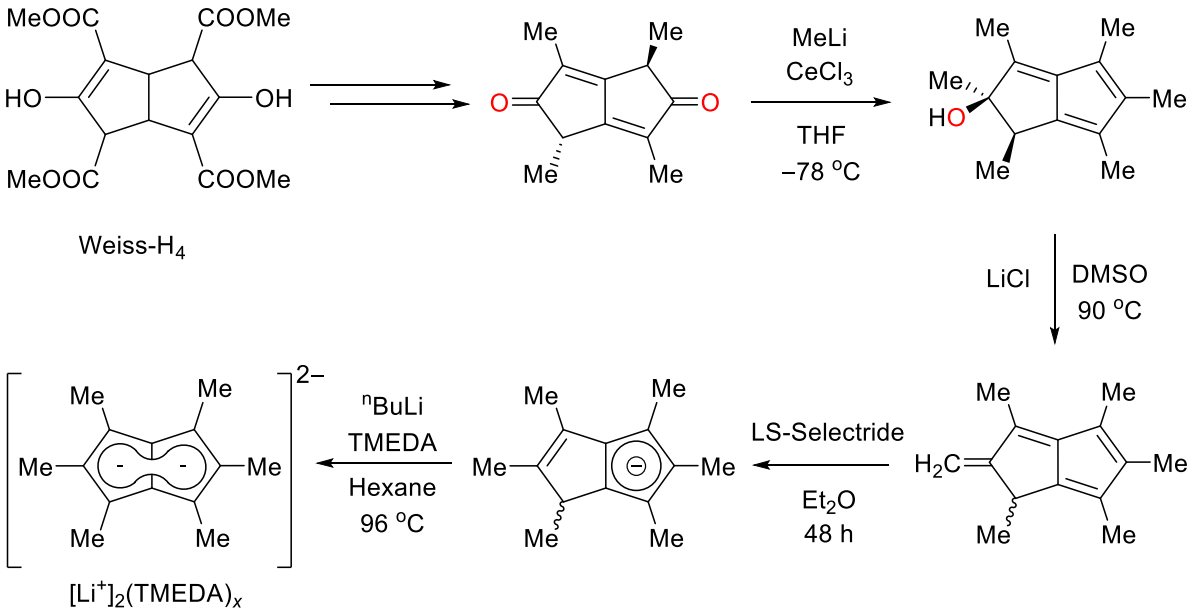

Scheme 1.7. Synthesis of Li_2Pn^* developed by O'Hare *et al.*[206]

The inductive-donor effect of the six methyl substituents stabilises the pentalene molecule which can be isolated at room temperature. Adding substituents has been proven to highly increase the stability, solubility and crystallinity of the pentalene complexes in a manner resembling the replacement of Cp by the pentamethylcyclopentadienyl Cp* ligands in organometallic chemistry.[209–211]. Few substituted pentalene compounds were studied and shown to be isolable at room temperature.[204,212,213]

1.4.3 Coordination modes of pentalene

The pentalene ligand possesses 10 π electrons available for coordination to a metal centre and thus shows a variety of bonding modes (Figure 1.9).[13]

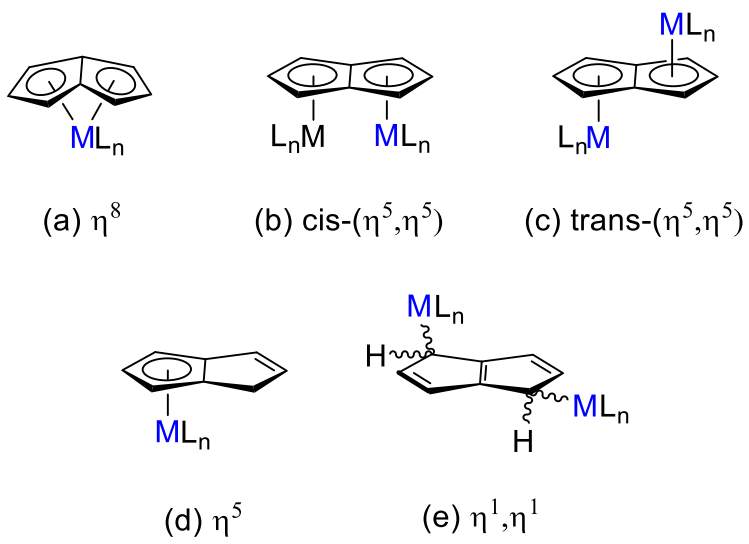

Figure 1.9. Coordination modes of pentalene.[13]

In the η^8 bonding mode, the pentalene ligand acts as an L_3X_2 donor with all eight carbons participating in the coordination. This g mode results in a folding of the ligand on its bridgehead. This umbrella-like distortion is accompanied by a disruption of the aromaticity but helps the steric stabilisation of the metal centre. The fold angle typically characterises the angle by which the pentalene ligand deviates from planarity (Figure 1.10).

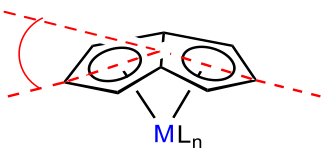

Figure 1.10. Illustration of the fold angle for η^8-Pn complexes.

The fold angle generally decreases with an increased size of metal centres.[214] Jonas *et al.* first studied (η^8-Pn)MCp complexes and reported an increase in the fold angle from Ti to V (37.0º to 43.0º) which corresponds to the decrease in metal radii (0.670 Å for Ti versus 0.640 Å for V).[215,216] O'Hare *et al.* reported that for the group 4 Pn* series Pn*MCpCl (M=Ti, Zr and Hf). The fold angle remains unaffected by a change in the metal centre (31º to 30.7º) and near-identical angles for Ti and Hf were observed despite the larger size of the hafnium centre..[217].

Additionally, metals can bind in an η^5 fashion to each ring of the pentalene in two different conformations, *cis* or *trans*. The (hydro)pentalene ligand acts then as a L_2X donor and can facilitate the interaction between the two metal centres. This coordination fashion is very similar to that of Cp metallocenes with each ring donating 5 electrons to the metals. This binding mode is usually encountered in bimetallic complexes, even though more complexes have been reported presenting the *trans* conformation.[218,219] Metathesis reaction of Li_2Pn_2 performed by Katz *et al.* promoted the formation of *cis* complexes Pn_2M_2 (M= Co, Ni) in low yields.[220,221] O'Hare and co-workers investigated the formation of bimetallic sandwich complexes with V, Cr, Mn, Co and Ni in which each metal centre binds to two permethylpentalene ligands in an η^5 mode (Figure 1.11).[222] Permethylation of the rings allowed for the entire series of double metallocenes to be characterised in the solid state by X-ray diffraction.

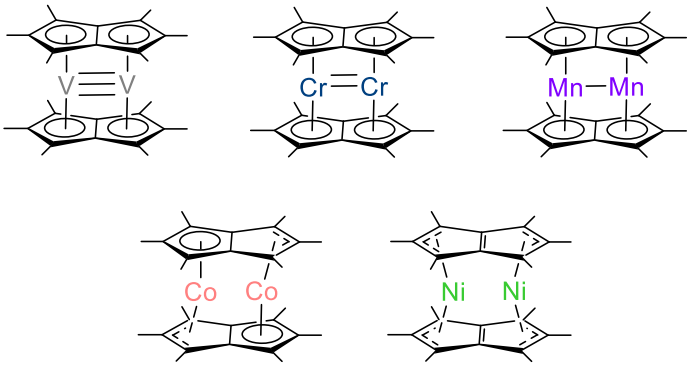

Figure 1.11. Examples of bimetallic permethylpentalene sandwiches.[222]

The simplest bonding mode, η^1, is commonly observed with p-block elements such as in Sn(IV) complexes (Figure 1.11). In 1987, Ustynyuk *et al.* described the synthesis of mono and bis(trimethylstannyl)dihydropentalenes *via* tin amides.[223] Monosubstituted isomers 1-η^1-(Me_3Sn)Pn(H) and 2-η^1-(Me_3Sn)Pn(H) were obtained from the reaction of $PnH_2$with $Me_3Sn(NEt_2)$ in heptane. Using two equivalents of the tin compound under the same conditions exclusively formed 1,4-(Me_3Sn)Pn in moderate yields (57%). η^1 tin species can also act as ligand transfer agent for synthesising hydropermethylpentalene complexes. For example, [1,5–Pn*($SnMe_3$)$_2$] is used in the synthesis of [Pn*TiCl(μ–Cl)]$_2$ (Figure 1.12).[224]

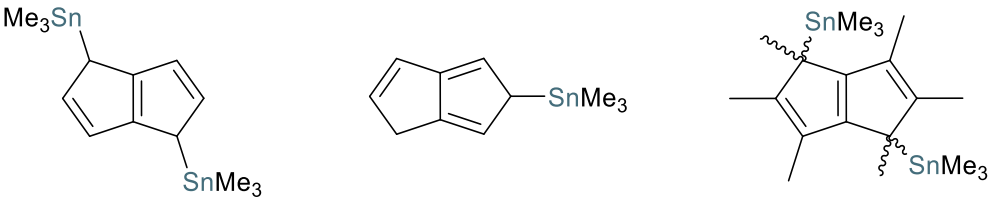

Figure 1.12. Examples of η^1-Pn and η^1-Pn* compounds.

1.4.4 η^5 hydropentalene complexes Pn*(H)

In the hydropentalenyl ligand, the Pn fragment contains one aromatic ring, the second ring presenting a localised double bond. The ligand thus behaves like a cyclopentadienyl ligand donating 5 electrons when coordinating to a metal centre. In 1962, Burns *et al.* reported the first (hydro)pentalene complex, $Mn(\eta^5\text{-}Pn(H))(CO)_3$ was synthesised by the reaction of acetylene with manganese carbonyl (Scheme 1.8).[225]

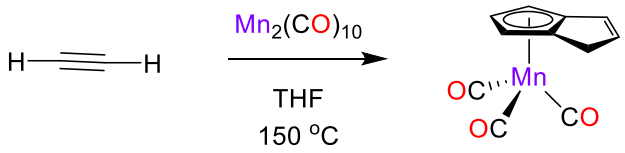

Scheme 1.8. Synthesis of $Mn(\eta^5\text{-}Pn(H))(CO)_3$.[225]

A synthetic route used to make hydropentalene complexes was reported by Katz *et al.* and consists of employing the lithium salt of the anion, LiPn(H). They synthesised a ferrocene-type compound, $Fe(\eta^5\text{-}Pn(H))_2$ in which the metal is bound in an η^5-manner to each pentalene ring (Figure 1.13).[226] These complexes are valuable for the synthesis of metallocene polymers. Indeed, the deprotonation of $Fe(\eta^5\text{-}Pn(H))_2$ by LiBu leads to $Li[Fe(\eta^5\text{-}Pn(H))(\eta^5\text{-}Pn)]$ and $Li_2[Fe(\eta^5\text{-}Pn)_2]$ which are precursors of metallocene polymers. [227,228]

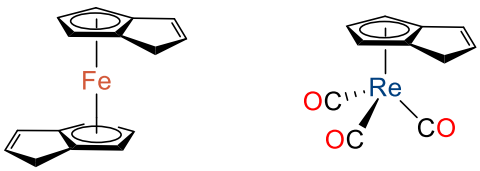

Figure 1.13. Examples of η^5-Pn complexes.[227–229]

Similarly to TlCp, TlPn(H) is a transmetalation agent for d block precursors.[230] Katz and Mrowca obtained the ferrocene analogues $Fe(\eta^5\text{-}Pn(H))_2$ by reacting $FeCl_2$ with TlPn(H)

in THF in moderate yield (47%).[231] η^5-(COD)Rh[Pn(H)] can be synthesised in the same manner by the reaction of the thallium transmetallation agent with $[Rh(COD)Cl]_2$.

In 2005, O'Hare *et al.* reported that the deprotonation of the dihydropentalene molecule by TlOEt generated TlPn(H).[229] Further reaction of TlPn(H) with $[Re(CO)_3(THF)Br]_2$ in the absence of light led to the formation of the η^5 coordinated complex Re(η^5-Pn(H))$(CO)_3$. The manganese complex Mn(η^5-Pn(H))$(CO)_3$ could also be obtained by the reaction of TlPn(H) with $[Mn(CO)_3(py)_2Br]$ in THF.

1.4.5 Pentalene complexes in catalysis

Following the discovery of synthetic routes for stable pentalene and substituted pentalene ligands, pentalene complexes have been investigated for their catalytic properties in the same manner as their cyclopentadienyl (Figure 1.14).[6,23,26,27,232]

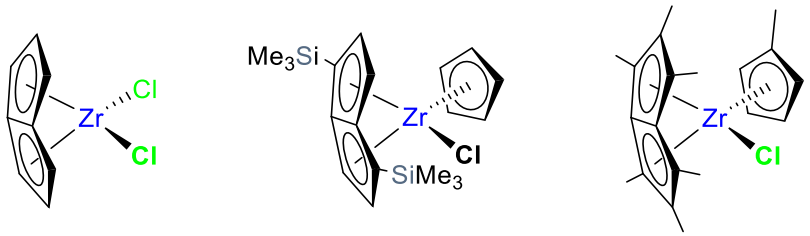

Figure 1.14. Examples of pentalene zirconocene used in catalysis.[233,234]

Jonas *et al.* first studied zirconium complexes $PnZrCl_2$, $PnZr(C_3H_5)_2$ and PnZr(Ind)Cl as ethylene polymerisation catalysts.[235] They reported good to high activities according to the Gibson scale with the indenyl-substituted complexes giving the highest activity of 712 $kg_{PE}/mol_{Zr}/h/bar$.[236] Similarly, the catalytic ability of silylated pentalene complexes was tested by Cloke and co-workers.[233] Pn(1,4-$SiMe_3)_2$ZrCpCl and Pn(1,4-$SiMe_3)_2$ZrCp*Cl, however, showed poor catalytic activity for polymerisation. Hlatky and

co-workers reported unsymmetrical zirconocenes bearing indenyl and pentalene ligands as catalysts in the copolymerisations of cyclic olefins with ethylene (Scheme 1.9).[32,237]

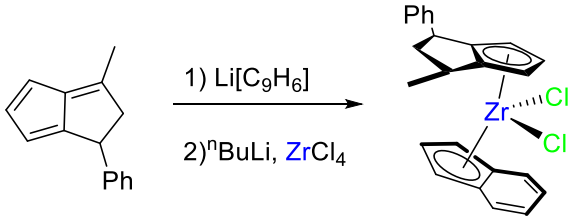

Scheme 1.9. Synthesis of unsymmetrical zirconocene based pentalene.[32,237]

O'Hare and co-workers synthesised dialkyl permethylpentalene complexes Pn*TiR_2 (R= Me, CH_2Ph, CH_2SiMe_3, $CH_2{}^tBu$) and showed their moderate catalytic activity in the polymerisation of ethylene in the presence of a borate co-catalyst.[238] More recently, they reported solution-phase ethylene polymerisation with a series of group 4 complexes Pn*$MCp_{2-x}Cl_x$ (M= Zr, Hf and Ti; x= 0, 1) and Pn*MCp^RX (R= Me, ^{t}Bu, ^{n}Bu, Me_3 and Ind; X= Cl, Me).[82,234] The zirconium complexes appeared highly active on the Gibson scale for ethylene polymerisation with methylaluminoxane (MAO) with the most active species being Pn*ZrIndCl (3585 $kg_{PE}/mol_{Zr}/h/bar$). Slurry-phase polymerisations of ethylene were also investigated in which Pn*MCp^RX complexes were immobilised on various solid supports such as sMAO, MAO-modified silica and MAO-modified layered double hydroxide. The sMAO polymerisations gave higher catalytic activities than their homogeneous analogues with Pn*$ZrCp^{Me}Me$ reaching 4486 $kg_{PE}/mol_{Zr}/h/bar$.

Few examples exist of pentalene complexes used outside of olefin polymerisation. Hydropermethylpentalene complexes Pn*(H)MX_3 and Pn*(H)MCl_2OR (M= Zr, Ti, Hf) were synthesised and fully characterised by Turner *et al.* (Figure 1.15).[192] The group 4 complexes were tested as catalysts for the ring-opening polymerisation of lactide and were shown to be effective. The initiation rate of the ring-opening polymerisation was

observed to increase following the order Zr > Hf > Ti (k_{obs} = 0.479, 0.391 and 0.113 h^{-1}). Surprisingly, the hydropermethylpentalene ligand showed no impact on the stereoselectivity as atactic polymers were obtained from the ROP of *rac*-lactide.

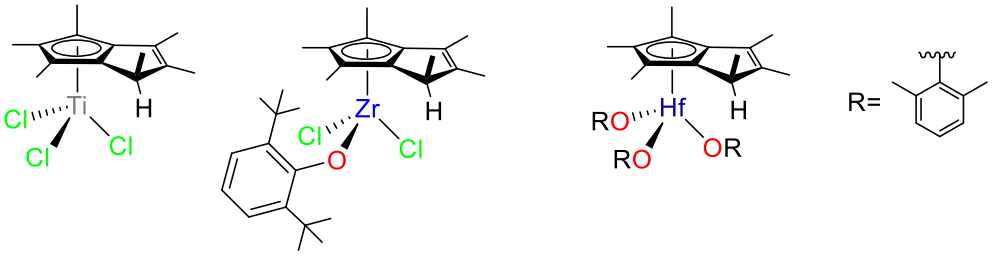

Figure 1.15. Examples of hydropermethylpentalene group 4 complexes for the ring-opening polymerisation of lactides.[192]

1.5 Scope of the thesis

This thesis aims at investigating new permethylpentalene complexes for their capacity of polymerising olefins such as styrene reaching high activity and good control over the properties of the polymers.

In the first section of this thesis, the (hydro)pentalene chloride complex is compared with cyclopentadienyl trichloride regarding the polymerisation of styrene and ethylene. The polymerisation activities were studied in solution-phase with MAO as an activator, and in slurry-phase with MAO-supported complexes. Chapter 3 then presents the ability of the (hydro)permethylpentalene and pentamethylcyclopentadienyl trichloride compounds to function as polar monomer polymerisation catalysts. Chapter 4 focuses on the synthesis and characterisation of ayloxides and alkoxides (hydro)permethylpentalene complexes. Their ability to polymerise styrene is investigated and the effects of the alkoxide/aryloxide substituents on the activity are discussed. Chapter 5 showcases the use of the aryloxide and alkoxide (hydro)permethylpentalene complexes as initiators for the ROP of lactide. The effect of the different substituents on the kinetics are explored under various polymerisation conditions. Finally, Chapter 6 discusses the preparation and characterisation of a series of permethylpentalene amidinate complexes and showcases the ability of the heterogeneous catalysts to polymerise olefins.

1.6 References

1 C. Chen, *Nat. Rev. Chem.*, 2018, **2**, 6–14.

2 J. R. Severn and J. C. Chadwick, *Tailor-made polymers : via immobilization of alpha-olefin polymerization catalysts*, Wiley-VCH, 2008.

3 D. W. Sauter, M. Taoufik, C. Boisson, D. W. Sauter, M. Taoufik and C. Boisson, *Polymers*, 2017, **9**, 185.

4 R. Geyer, J. R. Jambeck and K. L. Law, *Sci. Adv.*, 2017, **3**, e1700782.

5 C. Vasile, *Handbook of Polyolefins*, CRC Press, 2000, vol. 59.

6 J. Scheirs and W. Kaminsky, *Metallocene-based polyolefins : preparation, properties, and technology*, Wiley, 2000.

7 C. Romera-Castillo, M. Pinto, T. M. Langer, X. A. Álvarez-Salgado and G. J. Herndl, *Nat. Commun.*, 2018, **9**, 1–7.

8 S. Ghatge, Y. Yang, J. H. Ahn and H. G. Hur, *Appl. Biol. Chem.*, 2020, 63, 1–14.

9 S. Bonhomme, A. Cuer, A. M. Delort, J. Lemaire, M. Sancelme and G. Scott, *Polym. Degrad. Stab.*, 2003, **81**, 441–452.

10 R. A. Gross and B. Kalra, *Science*, 2002, **297**, 803–807.

11 R. E. Drumright, P. R. Gruber and D. E. Henton, *Adv. Mater.*, 2000, **12**, 1841–1846.

12 O. T. Summerscales and F. G. N. Cloke, *Coord. Chem. Rev.*, 2006, **250**, 1122–1140.

13 F. G. N. Cloke, J. C. Green, A. F. R. Kilpatrick and D. O'Hare, *Coord. Chem. Rev.*, 2017, **344**, 238–262.

14 P. Galli and G. Vecellio, *Prog. Polym. Sci.*, 2001, **26**, 1287–1336.

15 P. Cossee, *J. Catal.*, 1964, **3**, 80–88.

16 G. Natta, *Angew. Chem. Int. Ed.*, 1964, **76**, 553–566.

17 S. Ronca, *Polyethylene*, Elsevier Inc., 2017.

18 B. P. Carrow and K. Nozaki, *Macromolecules*, 2014, **47**, 2541–2555.

19 W.-F. Su, *Principles of Polymer Design and Synthesis*, Springer, Berlin, Heidelberg, 2013, vol. 82.

20 G. W. Coates, *Chem. Rev.*, 2000, **100**, 1223–1252.

21 L. Resconi, L. Cavallo, A. Fait and F. Piemontesi, *Chem. Rev.*, 2000, **100**, 1253–1346.

22 U. Zucchini and G. Cecchin, in *Industrial Developments*, Springer-Verlag, 2005, pp. 101–153.

23 H. G. Alt and A. Köppl, *Chem. Rev.*, 2000, **100**, 1205–1221.

24 M. P. McDaniel, in *Handbook of Transition Metal Polymerization Catalysts*, John Wiley & Sons, Inc., Hoboken, NJ, USA, 2018, pp. 401–571.

25 A. Klaue, M. Kruck, N. Friederichs, F. Bertola, H. Wu and M. Morbidelli, *Ind. Eng. Chem. Res.*, 2019, **58**, 886–896.

26 W. Kaminsky, A. Funck and H. Hähnsen, *Dalton Trans.*, 2009, 8803–8810.

27 W. Kaminsky and A. Laban, *Appl. Catal. A Gen.*, 2001, **222**, 47–61.

28 M. C. Baier, M. A. Zuideveld and S. Mecking, *Angew. Chem. Int. Ed.*, 2014, **53**, 9722–9744.

29 R. K. J. Bott, M. Hammond, P. N. Horton, S. J. Lancaster, M. Bochmann and P. Scott, *Dalton Trans.*, 2005, 3611–3613.

30 G. J. Clarkson, V. C. Gibson, P. K. Y. Goh, M. L. Hammond, P. D. Knight, P. Scott, T. M. Smit, A. J. P. White and D. J. Williams, *Dalton Trans.*, 2006, 5484–5491.

31 R. A. Collins, A. F. Russell and P. Mountford, *Appl. Petrochemical Res.*, 2015, **5**, 153–171.

32 G. G. Hlatky, *Coord. Chem. Rev.*, 1999, **181**, 243–296.

33 K. Osakada, Ed., *Organometallic Reactions and Polymerization*, Springer, 2014.

34 H. Tsurugi, K. Yamamoto, R. Rochat and K. Mashima, *Polym. J.*, 2015, 47, 2–17.

35 N. Ishihara, M. Kuramoto and M. Uoi, *Macromolecules*, 1988, **21**, 3356–3360.

36 N. Ishihara, T. Seimiya, M. Kuramoto and M. Uoi, *Macromolecules*, 1986, **19**, 2464–2465.

37 K. Nomura, J. Yamada, W. Wang and J. Liu, *J. Organomet. Chem.*, 2007, **692**, 4675–4682.

38 L. Guo, W. Liu and C. Chen, *Mater. Chem. Front.*, 2017, 1, 2487–2494.

39 A. R. Siedle, W. M. Lamanna, R. A. Newmark and J. N. Schroepfer, *J. Mol. Catal. A Chem.*, 1998, **128**, 257–271.

40 M. Lamberti, M. Mazzeo, D. Pappalardo and C. Pellecchia, *Coord. Chem. Rev.*,

2009, 253, 2082–2097.

41 A. K. Rappé, W. M. Skiff and C. J. Casewit, *Chem. Rev.*, 2000, **100**, 1435–1456.

42 P. Cossee, *J. Catal.*, 1964, **3**, 80–88.

43 G. Allegra, *Die Makromol. Chemie*, 1971, **145**, 235–246.

44 J. I. Martínez-Araya, R. Quijada and A. Toro-Labbé, *J. Phys. Chem. C*, 2012, **116**, 21318–21325.

45 K. Thorshaug, J. A. Støvneng, E. Rytter and M. Ystenes, *Macromolecules*, 1998, **31**, 7149–7165.

46 E. Quintanilla, F. Di Lena and P. Chen, *Chem. Commun.*, 2006, 4309–4311.

47 In *Encyclopedia of Inorganic and Bioinorganic Chemistry*, John Wiley & Sons, Ltd, Chichester, UK, 2005.

48 C. Stretch and G. Allen, *Polymer*, 1961, **2**, 151–160.

49 A. Husain and A. E. Hamielec, *J. Appl. Polym. Sci.*, 1978, **22**, 1207–1223.

50 L. H. Tung, A. T. Hu, S. V. McKinley and A. M. Paul, *J. Polym. Sci. Polym. Chem. Ed.*, 1981, **19**, 2027–2039.

51 S. V. Kostjuk and F. Ganachaud, *Macromolecules*, 2006, **39**, 3110–3113.

52 F. R. Mayo, *J. Am. Chem. Soc.*, 1953, **75**, 6133–6141.

53 R. Tanaka and T. Shiono, in *Encyclopedia of Polymeric Nanomaterials*, Springer, Berlin, Heidelberg, 2015, pp. 474–480.

54 J. Schellenberg, *Syndiotactic polystyrene : synthesis, characterization, processing, and applications*, Wiley, 2010.

55 J. Schellenberg, *Prog. Polym. Sci.*, 2009, **34**, 688–718.

56 J. Schellenberg and N. Tomotsu, *Prog. Polym. Sci.*, 2002, **27**, 1925–1982.

57 N. Tomotsu, N. Ishihara, T. H. Newman and M. T. Malanga, *J. Mol. Catal. A Chem.*, 1998, **128**, 167–190.

58 L. S. Baugh and D. N. Schulz, *Macromolecules*, 2020, 53, 3627–3631.

59 R. Pó and N. Cardi, *Prog. Polym. Sci.*, 1996, **21**, 47–88.

60 J. Yi, N. Nakatani and K. Nomura, *Dalton Trans.*, 2020, **49**, 8008–8028.

61 K. Nomura, I. Izawa, J. Yi, N. Nakatani, H. Aoki, H. Harakawa, T. Ina, T. Mitsudome, N. Tomotsu and S. Yamazoe, *Organometallics*, 2019, **38**, 4497–4507.

62 J. Yi, N. Nakatani, N. Tomotsu, K. Nomura and M. Hada, *Organometallics*, 2021, **40**, 643–653.

63 Q. H. Zhou, H. Q. Liang, Y. J. Long, Q. Wu, H. Y. Gao, G. D. Liang and F. M. Zhu, *J. Organomet. Chem.*, 2015, **798**, 347–353.

64 A. Grassi, A. Zambelli and F. Laschi, *Organometallics*, 1996, **15**, 480–482.

65 A. Zambelli, P. Longo, C. Pellecchia and A. Grassi, *Macromolecules*, 1987, **20**, 2035–2037.

66 C. Pellecchia, P. Longo, A. Grassi, P. Ammendola and A. Zambelli, *Die Makromol. Chemie, Rapid Commun.*, 1987, **8**, 277–279.

67 D. S. Breslow and N. R. Newburg, *J. Am. Chem. Soc.*, 1957, **79**, 5072–5073.

68 G. Natta, P. Pino, G. Mazzanti, U. Giannini, E. Mantica and M. Peraldo, *J. Polym. Sci.*, 1957, **26**, 120–123.

69 K. H. Reichert and K. R. Meyer, *Die Makromol. Chemie*, 1973, **169**, 163–176.

70 W. P. Long and D. S. Breslow, *Justus Liebigs Ann. Chem.*, 1975, 463–469.

71 W. Kaminsky and H. Sinn, *Justus Liebigs Ann. Chem.*, 1975, 424–437.

72 S. J. Obrey and A. R. Barron, *Dalton Trans.*, 2001, 2456–2458.

73 A. Andresen, H.-G. Cordes, J. Herwig, W. Kaminsky, A. Merck, R. Mottweiler, J. Pein, H. Sinn and H.-J. Vollmer, *Angew. Chem. Int. Ed.*, 1976, **15**, 630–632.

74 L. Resconi, S. Bossi and L. Abis, *Macromolecules*, 1990, **23**, 4489–4491.

75 H. S. Zijlstra and S. Harder, *Eur. J. Inorg. Chem.*, 2015, **2015**, 19–43.

76 E. Zurek and T. Ziegler, *Theoretical studies of the structure and function of MAO (methylaluminoxane)*, Pergamon, 2004, vol. 29.

77 M. Linnolahti and S. Collins, *ChemPhysChem*, 2017, **18**, 3369–3374.

78 W. Kaminsky and R. Steiger, *Polyhedron*, 1988, **7**, 2375–2381.

79 C. Janiak, U. Versteeg, K. C. H. Lange, R. Weimann and E. Hahn, *J. Organomet. Chem.*, 1995, **501**, 219–234.

80 W. Kaminsky, *J. Polym. Sci. Part A Polym. Chem.*, 2004, **42**, 3911–3921.

81 A. F. R. R. Kilpatrick, J.-C. C. Buffet, P. Nørby, N. H. Rees, N. P. Funnell, S. Sripothongnak, D. O'Hare and D. O'Hare, *Chem. Mater.*, 2016, **28**, 7444–7450.

82 D. A. X. Fraser, Z. R. Turner, J.-C. Buffet and D. O'Hare, *Organometallics*, 2016, **35**, 2664–2674.

83 T. A. Q. Arnold, Z. R. Turner, J.-C. Buffet and D. O'Hare, *J. Organomet. Chem.*, 2016, **822**, 85–90.

84 V. F. Tisse, F. Prades, R. Briquel, C. Boisson and T. F. L. McKenna, *Macromol. Chem. Phys.*, 2010, **211**, 91–102.

85 A. Entezami and P. Najafi Moghadam, *Polym. Int.*, 2005, **54**, 1326–1329.

86 M. A. Bashir, V. Monteil, C. Boisson and T. F. L. McKenna, *J. Appl. Polym. Sci.*, 2018, **135**, 45670.

87 N. Senso, S. Khaubunsongserm, B. Jongsomjit and P. Praserthdam, *Molecules*, 2010, **15**, 9323–9339.

88 H. Hammawa, T. M. Mannan, D. T. Lynch and S. E. Wanke, *J. Appl. Polym. Sci.*, 2004, **92**, 3549–3560.

89 D. E. Babushkin, V. N. Panchenko, M. N. Timofeeva, V. A. Zakharov and H. H. Brintzinger, *Macromol. Chem. Phys.*, 2008, **209**, 1210–1219.

90 C.-L. Huang, Y.-C. Chen, T.-J. Hsiao, J.-C. Tsai and C. Wang, *Macromolecules*, 2011, **44**, 6155–6161.

91 K. Nijenhuis, *Thermoreversible Networks*, Springer, Berlin, Heidelberg, 1997, vol. 130.

92 K. Soga, T. Uozumi, H. Yanagihara and T. Siono, *Die Makromol. Chemie, Rapid Commun.*, 1990, **11**, 229–234.

93 N. Nakata, T. Toda, Y. Saito, T. Watanabe, A. Ishii, N. Nakata, T. Toda, Y. Saito, T. Watanabe and A. Ishii, *Polymers*, 2016, **8**, 31.

94 J. Schellenberg and H.-J. Leder, *Adv. Polym. Technol.*, 2006, **25**, 141–151.

95 A. J. Pasztor, B. G. Landes and P. J. Karjala, *Thermochim. Acta*, 1991, **177**, 187–195.

96 M. Jaymand, *Polym. Chem.*, 2014, **5**, 2663–2690.

97 J. Liu, H. Ma, J. Huang and Y. Qian, *Eur. Polym. J.*, 2000, **36**, 2055–2058.

98 R. E. Campbell, T. H. Newman and M. T. Malanga, *Macromol. Symp.*, 1995, **97**, 151–160.

99 G. M. Miyake and E. Y.-X. Chen, *Polym. Chem.*, 2011, **2**, 2462.

100 A.-S. Rodrigues, E. Kirillov and J.-F. Carpentier, *Coord. Chem. Rev.*, 2008, **252**, 2115–2136.

101 G. Xu and D. Cheng, *Macromolecules*, 2000, **33**, 2825–2831.

102 K. Nomura, N. Naga, M. Miki and K. Yanagi, *Macromolecules*, 1998, **31**, 7588–7597.

103 K. Nomura, K. Oya, T. Komatsu and Y. Imanishi, *Macromolecules*, 2000, **33**, 3187–3189.

104 K. Nomura, N. Naga, M. Miki, K. Yanagi and A. Imai, *Organometallics*, 1998, **17**, 2152–2154.

105 J. B. Doo, A. Fudo, A. Tanaka, M. Fujiki and K. Nomura, *Macromolecules*, 2004, **37**, 5520–5530.

106 L. F. Johnson, F. Heatley and F. A. Bovey, *Macromolecules*, 1970, **3**, 175–177.

107 J. C. Randall, *J. Polym. Sci. Polym. Phys. Ed.*, 1975, **13**, 889–899.

108 H. Sato, Y. Tanaka and K. Hatada, *J. Polym. Sci. Polym. Phys. Ed.*, 1983, **21**, 1667–1674.

109 F. Feil and S. Harder, *Macromolecules*, 2003, **36**, 3446–3448.

110 T. Kawamura, N. Toshima and K. Matsuzaki, *Macromol. Rapid Commun.*, 1994, **15**, 479–486.

111 H. N. Cheng and G. H. Lee, *Int. J. Polym. Anal. Charact.*, 1996, **2**, 439–455.

112 J. Xu, J. Ouyang, Z. Fan, D. Chen, L. Feng and Y. Yang, *Polym. J.*, 1998, **30**, 720–722.

113 K. Nomura, K. Oya and Y. Imanishi, *J. Mol. Catal. A Chem.*, 2001, **174**, 127–140.

114 F. F. Karbach, T. Macko and R. Duchateau, *Macromolecules*, 2016, **49**, 1229–1241.

115 R. Quijada, J. Dupont, M. S. L. Miranda, R. B. Scipioni and G. B. Galland, *Macromol. Chem. Phys.*, 1995, **196**, 3991–4000.

116 N. Galdi, A. Buonerba and L. Oliva, *Polymers*, 2016, **8**, 405–417.

117 K. Soga, D. ho Lee and H. Yanagihara, *Polym. Bull.*, 1988, **20**, 237–241.

118 I. H. Anderson, G. M. Burnett and W. C. Geddes, *Eur. Polym. J.*, 1967, **3**, 181–186.

119 Y. V. Kissin, Y. Y. Goldfarb, B. A. Krentsel and H. Uyliem, *Eur. Polym. J.*, 1972, **8**, 487–499.

120 B. Baker and P. J. T. Tait, *Polymer*, 1967, **8**, 225–235.

121 J. C. Stevens, F. J. Timmers, D. R. Wilson, G. F. Schmidt, P. N. Nickias, R. K. Rosen, G. W. Knight, S-Y. Lai, EP0416815A2, 1990.

122 D.-H. Lee, K.-B. Yoon, H.-J. Kim, S.-S. Woo and S. K. Noh, *J. Appl. Polym. Sci.*, 1998, **67**, 2187–2198.

123 G. X. and and S. Lin, *Macromolecules*, 1997, **30**, 685–693.

124 C. Pellecchia, D. Pappalardo, M. D'Arc and A. Zambelli, *Macromolecules*, 1996, **29**, 1158–1162.

125 L. Oliva, S. Mazza and P. Longo, *Macromol. Chem. Phys.*, 1996, **197**, 3115–3122.

126 P. Longo, A. Grassi and L. Oliva, *Die Makromol. Chemie*, 1990, **191**, 2387–2396.

127 A. Muoz-Escalona, V. Cruz, N. Mena, S. Martínez and J. Martinez-Salazar, *Polymer*, 2002, **43**, 7017–7026.

128 K. Yokota, T. Kohsaka, K. Ito and N. Ishihara, *J. Polym. Sci. Part A Polym. Chem.*, 2005, **43**, 5041–5048.

129 H. Zhang, D.-J. Byun and K. Nomura, *Dalton Trans.*, 2007, 1802–1806.

130 Z. Hao, K. Nomura, H. Zhang and K. Nomura, *Macromolecules*, 2005, **39**, 5266–5274.

131 K. Nomura, T. Komatsu and I. Yukio, *Macromolecules*, 2000, **33**, 8122–8124.

132 N. Kotohiro, H. Okumura, T. Komatsu and N. Naga, *Macromolecules*, 2002, **35**, 5388–5395.

133 O. Agboola, R. Sadiku, T. Mokrani, I. Amer and O. Imoru, *Polyolefin Fibres*, 2017, 89–133.

134 J. Rychlý and L. Rychlá, in *Polyolefin Compounds and Materials*, Springer, 2016, pp. 285–314.

135 N.-I. European Bioplastics, World plastics production 1950-2019.

136 G. E. Luckachan and C. K. S. Pillai, *J. Polym. Environ.*, 2011, **19**, 637–676.

137 Y. Zhu, C. Romain and C. K. Williams, *Nature*, 2016, 540, 354–362.

138 C. Williams and M. Hillmyer, *Polym. Rev.*, 2008, **48**, 1–10.

139 V. Nagarajan, A. K. Mohanty and M. Misra, *ACS Sustain. Chem. Eng.*, 2016, 4, 2899–2916.

140 J. Ahmed and S. K. Varshney, *Int. J. Food Prop.*, 2011, **14**, 37–58.

141 R. P. John, A. G.S., K. M. Nampoothiri and A. Pandey, *Biotechnol. Adv.*, 2009, 27, 145–152.

142 R. P. John, D. Gangadharan and K. Madhavan Nampoothiri, *Bioresour. Technol.*,

2008, **99**, 8008–8015.

143 R. P. John, K. M. Nampoothiri and A. Pandey, *Appl. Microbiol. Biotechnol.*, 2007, 74, 524–534.

144 R. P. John, K. M. Nampoothiri and A. Pandey, *Process Biochem.*, 2006, **41**, 759–763.

145 R. Auras, B. Harte and S. Selke, *Macromol. Biosci.*, 2004, 4, 835–864.

146 A. C. Albertsson and I. K. Varma, *Biomacromolecules*, 2003, 4, 1466–1486.

147 S. Jacobsen, H. G. Fritz, P. Degée, P. Dubois and R. Jérôme, *Polym. Eng. Sci.*, 1999, **39**, 1311–1319.

148 R. Platel, L. Hodgson and C. Williams, *Polym. Rev.*, 2008, **48**, 11–63.

149 K. A. M. Thakur, R. T. Kean, E. S. Hall, J. J. Kolstad, T. A. Lindgren, M. A. Doscotch, J. I. Siepmann and E. J. Munson, *Macromolecules*, 1997, **30**, 2422–2428.

150 K. A. M. Thakur, R. T. Kean, M. T. Zell, B. E. Padden and E. J. Munson, *Chem. Commun.*, 1998, **0**, 1913–1914.

151 P. J. Dijkstra, H. Du and J. Feijen, *Polym. Chem.*, 2011, 2, 520–527.

152 S. M. Guillaume, E. Kirillov, Y. Sarazin and J.-F. Carpentier, *Chem. - A Eur. J.*, 2015, **21**, 7988–8003.

153 A. Sauer, J. C. Buffet, T. P. Spaniol, H. Nagae, K. Mashima and J. Okuda, *Inorg. Chem.*, 2012, **51**, 5764–5770.

154 J. C. Buffet, A. N. Martin, M. Kol and J. Okuda, *Polym. Chem.*, 2011, **2**, 2378–2384.

155 A. Pietrangelo, S. C. Knight, A. K. Gupta, L. J. Yao, M. A. Hillmyer and W. B. Tolman, *J. Am. Chem. Soc.*, 2010, **132**, 11649–11657.

156 T. M. Ovitt and G. W. Coates, *J. Am. Chem. Soc.*, 2002, **124**, 1316–1326.

157 J. M. Becker, R. J. Pounder and A. P. Dove, *Macromol. Rapid Commun.*, 2010, **31**, 1923–1937.

158 K. Madhavan Nampoothiri, N. R. Nair and R. P. John, *Bioresour. Technol.*, 2010, 101, 8493–8501.

159 J. C. Buffet and J. Okuda, *Polym. Chem.*, 2011, 2, 2758–2763.

160 N. Diteepeng, J. C. Buffet, Z. R. Turner and D. O'Hare, *Dalton Trans.*, 2019, **48**, 16099–16107.

161 N. Diteepeng, I. A. P. Wilson, J. C. Buffet, Z. R. Turner and D. O'Hare, *Polym. Chem.*, 2020, **11**, 6308–6318.

162 B. J. O'Keefe, M. A. Hillmyer and W. B. Tolman, *Dalton Trans.*, 2001, 2215–2224.

163 C. M. Thomas, *Chem. Soc. Rev.*, 2010, **39**, 165–173.

164 D. Bourissou, B. Martin-Vaca, A. Dumitrescu, M. Graullier and F. Lacombe, *Macromolecules*, 2005, **38**, 9993–9998.

165 L. Clark, G. B. Deacon, C. M. Forsyth, P. C. Junk, P. Mountford, J. P. Townley and J. Wang, *Dalton Trans.*, 2013, **42**, 9294–9312.

166 D. S. McGuinness, E. L. Marshall, V. C. Gibson and J. W. Steed, *J. Polym. Sci. Part A Polym. Chem.*, 2003, **41**, 3798–3803.

167 A. Bhaw-Luximon, D. Jhurry, N. Spassky, S. Pensec and J. Belleney, *Polymer*, 2001, **42**, 9651–9656.

168 A. P. Dove, *ACS Macro Lett.*, 2012, 1, 1409–1412.

169 M. R. Newman, S. G. Russell and D. S. W. Benoit, *RSC Adv.*, 2018, **8**, 28891–28894.

170 O. Dechy-Cabaret, B. Martin-Vaca and D. Bourissou, *Chem. Rev.*, 2004, **104**, 6147–6176.

171 W. Rao, C. Cai, J. Tang, Y. Wei, C. Gao, L. Yu and J. Ding, *Chinese J. Chem.*, 2021, **39**, cjoc.202000519.

172 M. L. McGraw and E. Y. X. Chen, *Macromolecules*, 2020, 53, 6102–6122.

173 P. Dobrzynski, J. Kasperczyk, H. Janeczek and M. Bero, *Macromolecules*, 2001, **34**, 5090–5098.

174 P. Degée, P. Dubois and R. Jérôme, *Macromol. Chem. Phys.*, 1997, **198**, 1985–1995.

175 C. Jacobs, P. Dubois, R. Jerome and P. Teyssie, *Macromolecules*, 1991, **24**, 3027–3034.

176 A. J. Nijenhuis, D. W. Grijpma and A. J. Pennings, *Macromolecules*, 1992, **25**, 6419–6424.

177 A. Kowalski, A. Duda and S. Penczek, *Macromolecules*, 2000, **33**, 689–695.

178 A. Duda and S. Penczek, *Macromol. Rapid Commun.*, 1995, **16**, 67–76.

179 G. Schwach, J. Coudane, R. Engel and M. Vert, *Polym. Int.*, 1998, **46**, 177–182.

180 G. Schwach, J. Coudane, R. Engel and M. Vert, *Polym. Bull.*, 1996, **37**, 771–776.

181 D. C. Aluthge, B. O. Patrick and P. Mehrkhodavandi, *Chem. Commun.*, 2013, **49**, 4295–4297.

182 M. Normand, E. Kirillov, T. Roisnel and J. F. Carpentier, *Organometallics*, 2012, **31**, 5511–5519.

183 C. Bakewell, T. P. A. Cao, N. Long, X. F. Le Goff, A. Auffrant and C. K. Williams, *J. Am. Chem. Soc.*, 2012, **134**, 20577–20580.

184 C. Bakewell, A. J. P. White, N. J. Long and C. K. Williams, *Inorg. Chem.*, 2015, **54**, 2204–2212.

185 C. Bakewell, A. J. P. White, N. J. Long and C. K. Williams, *Angew. Chem. Int. Ed.*, 2014, **53**, 9226–9230.

186 T. P. A. Cao, A. Buchard, X. F. Le Goff, A. Auffrant and C. K. Williams, *Inorg. Chem.*, 2012, **51**, 2157–2169.

187 D. Myers, A. J. P. White, C. M. Forsyth, M. Bown and C. K. Williams, *Angew. Chem. Int. Ed.*, 2017, **56**, 5277–5282.

188 A. J. Chmura, M. G. Davidson, C. J. Frankis, M. D. Jones and M. D. Lunn, *Chem. Commun.*, 2008, 1293–1295.

189 J. V. Lamb, University of Oxford, DPhil Thesis, 2019.

190 J. V. Lamb, J. C. Buffet, J. E. Matley, C. M. R. Wright, Z. R. Turner and D. O'Hare, *Dalton Trans.*, 2019, **48**, 2510–2520.

191 Z. R. Turner, J. V. Lamb, T. P. Robinson, D. Mandal, J.-C. Buffet and D. O'Hare, *Dalton Trans.*, 2021, **50**, 4805–4818.

192 Z. R. Turner, J.-C. Buffet and D. O'Hare, *Organometallics*, 2014, **33**, 3891–3903.

193 G. Baker, E. Vogel and M. Smith, *Polym. Rev.*, 2008, **48**, 64–84.

194 J. E. Kasperczyk, *Polym. Commun.*, 1999, **40**, 5455–5458.

195 M. T. Zell, B. E. Padden, A. J. Paterick, K. A. M. Thakur, R. T. Kean, M. A. Hillmyer and E. J. Munson, *Macromolecules*, 2002, **35**, 7700–7707.

196 K. Suganuma, K. Horiuchi, H. Matsuda, H. N. Cheng, A. Aoki and T. Asakura, *Polym. J.*, 2012, **44**, 838–844.

197 K. A. M. Thakur, R. T. Kean, E. S. Hall, M. A. Doscotch and E. J. Munson, *Anal. Chem.*, 1997, **69**, 4303–4309.

198 M. J. Stanford and A. P. Dove, *Chem. Soc. Rev.*, 2010, **39**, 486–494.

199 B. M. Chamberlain, M. Cheng, D. R. Moore, T. M. Ovitt, E. B. Lobkovsky and G. W. Coates, *J. Am. Chem. Soc.*, 2001, **123**, 3229–3238.

200 N. Diteepeng, University of Oxford, DPhil Thesis, 2018.

201 P. C. den Boer-Veenendaal and D. H. W. den Boer, *Mol. Phys.*, 1961, **4**, 33–38.

202 P. C. den Boer, D. H. W. den Boer, C. A. Coulson and T. H. Goodwin, *Tetrahedron*, 1963, **19**, 2163–2170.

203 T. Bally, S. Chai, M. Neuenschwander and Z. Zhu, *J. Am. Chem. Soc.*, 1997, **119**, 1869–1875.

204 K. Hafner, R. Dönges, E. Goedecke and R. Kaiser, *Angew. Chem. Int. Ed.*, 1973, **12**, 337–339.

205 S. M. Boyt, N. A. Jenek and U. Hintermair, *Dalton Trans.*, 2019, **48**, 5107–5124.

206 A. E. Ashley, A. R. Cowley and D. O'Hare, *European J. Org. Chem.*, 2007, **2007**, 2239–2242.

207 A. E. Ashley, University of Oxford, DPhil Thesis, 2006.

208 S. C. Jones, University of Oxford, DPhil Thesis, 2003.

209 J. M. Manriquez, D. R. McAlister, E. Rosenberg, A. M. Shiller, K. L. Williamson, S. I. Chan and J. E. Bercaw, *J. Am. Chem. Soc.*, 1978, **100**, 3078–3083.

210 H. Brintzinger and J. E. Bercaw, *J. Am. Chem. Soc.*, 1971, **93**, 2045–2046.

211 P. Jutzi and U. Meyer, *J. Organomet. Chem.*, 1987, **333**, C18–C20.

212 K. Hafner and H. U. Süss, *Angew. Chem. Int. Ed.*, 1973, **12**, 575–577.

213 E. Le Goff, *J. Am. Chem. Soc.*, 1962, **84**, 3975–3976.

214 F. G. N. Cloke, *Pure Appl. Chem.*, 2001, **73**, 233–238.

215 R. D. Shannon, *Acta Crystallogr. Sect. A*, 1976, **32**, 751–767.

216 K. Jonas, P. Kolb, G. Kollbach, B. Gabor, R. Mynott, K. Angermund, O. Heinemann and C. Krüger, *Angew. Chem. Int. Ed.*, 1997, **36**, 1714–1718.

217 F. M. Chadwick, R. T. Cooper, A. E. Ashley, J.-C. Buffet and D. M. O'Hare, *Organometallics*, 2014, **33**, 3775–3785.

218 F. M. Chadwick, A. E. Ashley, R. T. Cooper, L. A. Bennett, J. C. Green and D. M. O'Hare, *Dalton Trans.*, 2015, **44**, 20147–20153.

219 S. C. Binding, J. C. Green, Z. R. Turner, J.-C. Buffet and D. O'Hare, *Dalton Trans.*, 2019, **48**, 4263–4273.

220 T. J. Katz and N. Acton, *J. Am. Chem. Soc.*, 1972, **94**, 3281–3283.

221 T. J. Katz, N. Acton and J. McGinnis, *J. Am. Chem. Soc.*, 1972, **94**, 6205–6206.

222 A. E. Ashley, R. T. Cooper, G. G. Wildgoose, J. C. Green and D. O'Hare, *J. Am. Chem. Soc.*, 2008, **130**, 15662–15677.

223 Y. A. Ustynyuk, A. K. Shestakova, V. A. Chertkov, N. N. Zemlyansky, I. V. Borisova, A. I. Gusev, E. B. Tchuklanova and E. A. Chernyshev, *J. Organomet. Chem.*, 1987, **335**, 43–57.

224 R. T. Cooper, F. M. Chadwick, A. E. Ashley and D. O'Hare, *Organometallics*, 2013, **32**, 2228–2233.

225 T. H. Coffield, K. G. Ihrman and W. Burns, *J. Am. Chem. Soc.*, 1960, **82**, 4209–4210.

226 T. J. Katz and M. Rosenberger, *J. Am. Chem. Soc.*, 1963, **85**, 2030–2031.

227 B. Oelckers, I. Chavez, J. M. Manriquez and E. Roman, *Organometallics*, 1993, **12**, 3396–3397.

228 C. Miravitlles, E. Molins, W. Maniukiewicz, M. Mas, J. M. Manríquez, I. Chávez, B. Oelckers, A. Alvarez-Larena and J. L. Briansó, *Acta Crystallogr. Sect. C Cryst. Struct. Commun.*, 1996, **52**, 3047–3049.

229 S. C. Jones, P. Roussel, T. Hascall and D. O'Hare, *Organometallics*, 2005, **25**, 221–229.

230 C. Janiak, *Coord. Chem. Rev.*, 1997, **163**, 107–216.

231 T. J. Katz and J. J. Mrowca, *J. Am. Chem. Soc.*, 1967, **89**, 1105–1111.

232 A. Shamiri, M. Chakrabarti, S. Jahan, M. Hussain, W. Kaminsky, P. Aravind and W. Yehye, *Materials*, 2014, **7**, 5069–5108.

233 F. G. N. Cloke, J. S. Parry, WO1999007716 A1, 1999.

234 D. A. Fraser, University of Oxford, DPhil Thesis, 2018.

235 K. Jonas, P. Kolb, G. Kollbach, US 5959132 A, 1999.

236 G. J. P. Britovsek, V. C. Gibson and D. F. Wass, *Angew. Chem. Int. Ed.*, 1999, **38**, 428–447.

237 F. Helmer-Metzmann, F. Osan, M. Riedel, CA2179355 A1, 1996.

238 R. T. Cooper, University of Oxford, DPhil Thesis, 2012.

Chapter Two
Cyclopentadienyl and Permethylpentalene trichloride complexes for Olefin Polymerisations

2.1 Introduction

Styrene is an economically important monomer used in the production of polystyrene and other types of industrially prepared polymers.[1,2] Polystyrene is particularly interesting for its tunable chemical and physical properties depending on its tacticity.[3] The synthesis of syndiotactic polystyrene was first reported by Ishihara *et al.* in 1986.[4] By using $CpTiCl_3$ (Cp = cyclopentadienyl C_5H_5), in the presence of MAO, they obtained activities up to 1.55 $kg_{PS}/mol_{Ti}/h$ and good stereocontrol with 98% syndiotactic polystyrene.[5] Since then, the olefin polymerisation chemistry of the half titanocene Cp^*TiCl_3 (Cp^* = pentamethylcyclopentadienyl $C_5(CH_3)_5$) has been widely studied as well as related derivatives such as $IndTiCl_3$ (Ind = indenyl, C_9H_7).[6–9]. Adding alkyl substituents on the cyclopentadienyl ring proved to increase the olefin polymerisation activities in the presence of cocatalysts such as MAO by stabilising the active centre *via* an electron-donating effect.[10,11] Nonetheless, cyclopentadienyl derivatives have remained a reference in the literature for the polymerisation of olefins.[12–14] More recently, interest has been drawn to more complex olefin chains such as ethylene/styrene copolymers. Copolymerisations of styrene with alkenes is a way to produce polymers with new and controlled properties.[15] The field of ethylene/styrene copolymerisation emerged around

1990 as previous attempts to synthesise the copolymers failed due to the high reactivity difference between the monomers.[16] Since then, progress have been made to understand the key elements of the copolymerisation process and many catalysts such as $Cp^RTiCl_2(OAr)$ complexes have been developed for the copolymerisation of ethylene with styrene and were reported to overcome the obstacle of divergent monomer reactivity.[17–21]

This chapter aims at comparing the olefin polymerisation activity of the (hydro)permethylpentalenyl complex of $Pn^*(H)TiCl_3$ with a reference Cp^*TiCl_3 (Figure 2.1). Indeed, Cp^*TiCl_3 was one of the first examples of a catalyst developed for the syndiotactic polymerisation of styrene.[4] To date, this complex is one of the most active catalysts and remains a reference to which new compounds are compared in terms of catalytic activity.[22–24] (Hydro)pentalenyl complexes are structurally similar to cyclopentadienyl complexes as both have a piano stool conformation. Nevertheless, scarce examples of (hydro)pentalenyl complexes for polymerisation have been reported in the literature.[25]

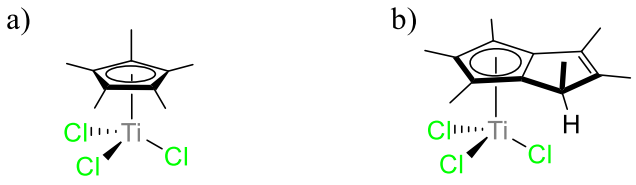

1 **2**

Figure 2.1. Structures of two piano stool complexes a) Cp^*TiCl_3 (**1**) and b) $Pn^*(H)TiCl_3$ (**2**).

This chapter describes various polymerisation studies using Cp^*TiCl_3 (**1**) and $Pn^*(H)TiCl_3$ (**2**). Firstly, the homogeneous styrene and ethylene polymerisation is investigated. The complexes were then immobilised and the slurry-phase activity for styrene and ethylene polymerisation tested. Finally, copolymerisations of ethylene with

styrene and the influence of polymerisation parameters are discussed. The polymers produced are characterised by GPC, DSC, NMR spectroscopy, XRD and SEM.

2.2 Polymerisation of styrene

Following work described by Ishihara *et al.*, two titanium trichloride complexes were tested as catalysts for the synthesis of polystyrene and different conditions such as $[Al_{MAO}]_0$:$[Ti]_0$ ratio, temperature and solvent were investigated.[4,5,26] Homogeneous polymerisation reactions were carried out using dried MAO as an initiator as widely reported in the literature for olefin polymerisation.[27–32] Slurry-phase polymerisations were performed after immobilisation of the catalysts on solid MAO (sMAO, particle size ~ 5 µm), an insoluble form of oligomeric MAO that has recently been investigated in heterogeneous catalysis.[33–36]

2.2.1 Preliminary study for the solution-phase polymerisation of styrene

Control experiments, carried out in the absence of titanium species using MAO and sMAO only, resulted in extremely low activities (Appendix A.2.1). In order to optimise the polymerisation conditions, preliminary studies were performed using $CpTiCl_3$ with various amounts of MAO in the system as well as different solvents. The polymerisations were performed at 40 °C for 10 minutes using 0.2 µmol of $CpTiCl_3$. The effect of MAO concentration on the polymerisation activity was investigated by varying the $[Al_{MAO}]_0$:$[Ti]_0$ ratio between 0 and 5000 using $CpTiCl_3$ (Figure 2.2). As expected, the activity increased with the amount of MAO added in the system. It is worth noting that the slope is steeper for $[MAO]_0$:$[Ti]_0$ ratios < 2000 and we can expect a slower rate of activity increase for higher MAO contents as reported by Pó *et al.*[37] Poisoning of the catalytically active species has been indeed reported in many occasions.[38–40] Huang and co-workers studied the effect of the $[Al]_0$:$[Ti]_0$ ratio on the synthesis of syndiotactic polystyrene with $CpTiCl_3$.[24] Increasing $[Al]_0$:$[Ti]_0$ from 100 to 1000 led to 17 times higher polymerisation activities, from 75 to 1318 $kg_{PS}/mol_{Ti}/h$. More recently. Soares and

co-workers investigated the influence of the MAO type and contents on ethylene homopolymerisation using Cp_2ZrCl_2.[41] By increasing $[Al_{MAO}]_0$:$[Zr]_0$ from 1000 to 10500 they multiplied the polymerisation activity by 1.7 (from 5600 to 9600 kg/h/atm/mol_{Zr}) and the molecular weight M_n of the polymer by 1.5 (from 25.9 to 45.8 g/mol). Figure 2.2 shows an increasing activity from 1869 to 14151 $kg_{PS}/mol_{Ti}/h$ when the ratio $[Al_{MAO}]_0$:$[Ti]_0$ is multiplied by 10 from 500 to 5000 indicating that high MAO contents will improve the monomer conversion. Due to MAO being an expensive material, low amounts will be used for the rest of this study. $[Al_{MAO}]_0$:$[Ti]_0$ ratio of 1500 in solution phase and $[Al_{sMAO}]_0$:$[Ti]_0$ of 200 in slurry-phase polymerisation resulted in acceptable activities.

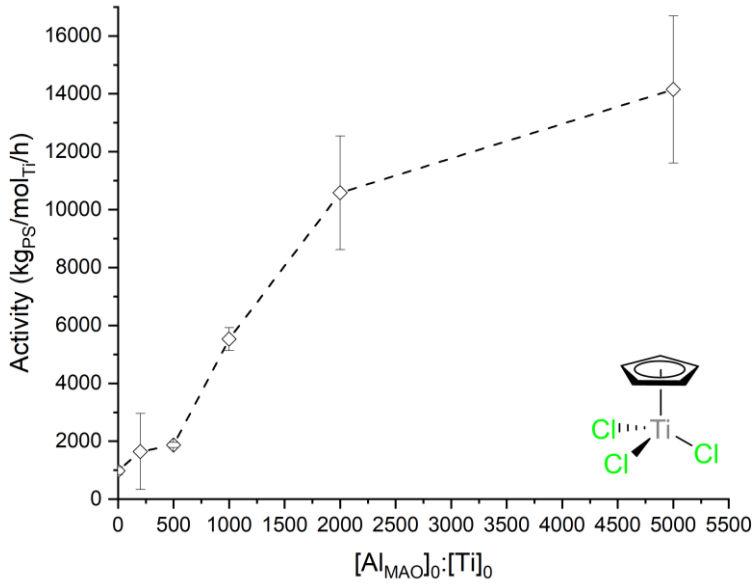

Figure 2.2. Influence of the $[Al_{MAO}]_0$:$[Ti]_0$ ratio on solution-phase polymerisation activity of $CpTiCl_3$. $[Ti]_0$ = 0.2 µmol, 2 mL solvent, T = 40 °C, 10 minutes, 1000 rpm.

As well as the amount of co-catalyst, solvent interactions with the catalyst during the polymerisation process can affect the activity and the polymer properties.[42–44] In order to determine the effects of solvent on monomer conversion, the solution polymerisation of styrene was investigated using four solvents under the same reaction conditions.

Homogeneous polymerisations were performed at 40 °C for 10 minutes using **1**/MAO system and a molar ratio $[Al_{MAO}]_0$:$[Ti]_0$ of 1500 (Figure 2.3).

The results indicated that the styrene conversion was influenced by the polymerisation solvent, following the order pentane (3800 $kg_{PS}/mol_{Ti}/h$) > toluene (3635 $kg_{PS}/mol_{Ti}/h$) > hexane (3105 $kg_{PS}/mol_{Ti}/h$) > benzene (2430 $kg_{PS}/mol_{Ti}/h$). Hexane and toluene led to similar catalytic activities, which was in accordance with previous results reported by O'Hare and co-workers using Pn* complexes,[45] and both appeared as good solvent choices for further reactions. It is advantageous that the polymer obtained in pentane and hexane directly precipitated in the reaction vessel, whereas polymer obtained in toluene or benzene required additional extraction into ethanol to yield a colourless powder. However, toluene was chosen as solvent for solution-phase polymerisations of styrene due to the better solubility of the monomer in this solvent.

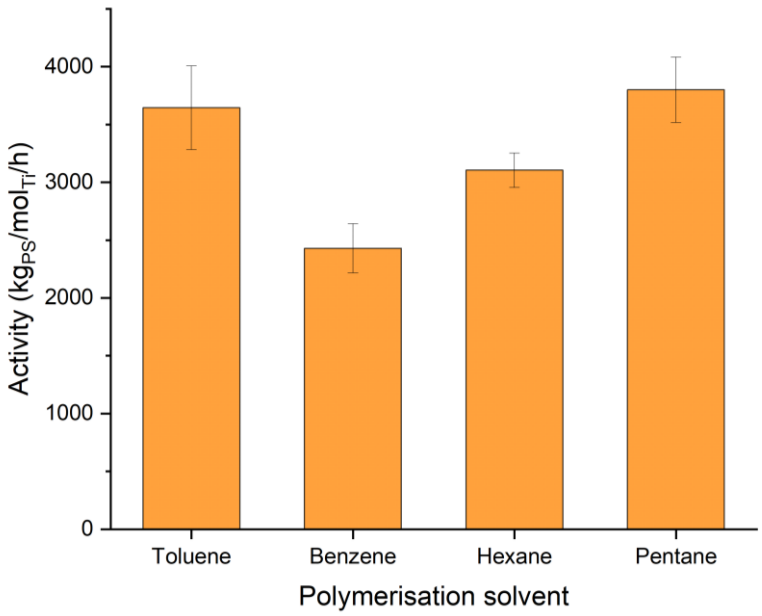

Figure 2.3. Solvent dependence of solution-phase styrene polymerisation activity of Cp^*TiCl_3 (**1**). [Ti] = 0.2 µmol, $[Al_{MAO}]_0$:$[Ti]_0$ = 1500:1, 2 mL solvent, T = 40 °C, 10 minutes, 1000 rpm.

2.2.2 Immobilisation of complexes on solid-MAO

The polymerisation activity as well as polymer properties (molecular weight, morphology) can be greatly affected by the solid-support.[46] A modified methylaluminoxane has been developed by Kaji *et al.* at Tosoh Finechem Corporation (Japan).[47] Solid polymethylaluminoxane (sMAO) is a polymerised MAO that is insoluble in many common solvents. sMAO-supported catalysts were shown to exhibit high olefin polymerisation activities and good control on the morphology of the polymers produced.[33,35,48,49]

Immobilisation of the Ti complexes on a solid support was achieved by swirling the appropriate complex and sMAO in toluene at 60 °C for 1 h. The coloured solid was let to settle and the colourless supernatant was decanted yielding the supported complexes as beige powders in good yields (67–88%).

The two polymethylaluminoxane-supported complexes, sMAO-Cp*$TiCl_3$ (**1_{sMAO}**) and sMAO-Pn*(H)$TiCl_3$ (**2_{sMAO}**), were characterised by solid state ^{13}C CPMAS and ^{27}Al DPMAS NMR spectroscopy (Figure 2.4, Figure A2.3–6). The ^{13}C CPMAS spectra of both supported complexes **1_{sMAO}** and **2_{sMAO}** exhibited a major broad resonance at -7 ppm corresponding to the methyl environment of the sMAO. As benzoic acid was employed during the synthesis of sMAO, the resonances between 120 and 130 ppm can be attributed to the aromatic environments of the benzoate group and the signal at approximately 179 ppm corresponds to the α–C(O)O. In the spectrum of sMAO-Pn*(H)$TiCl_3$, the Pn*-*Me* environments were not resolved in the solid state and appeared as a large signal at around 11 ppm. The solid state ^{27}Al DPMAS NMR spectra for the sMAO supported titanium species consisted of four major signals at around 320, 175, -95 and -240 ppm for **1_{sMAO}** and 330, 190, -85 and -235 ppm for sMAO-Pn*(H)$TiCl_3$ (Figure A2.6).

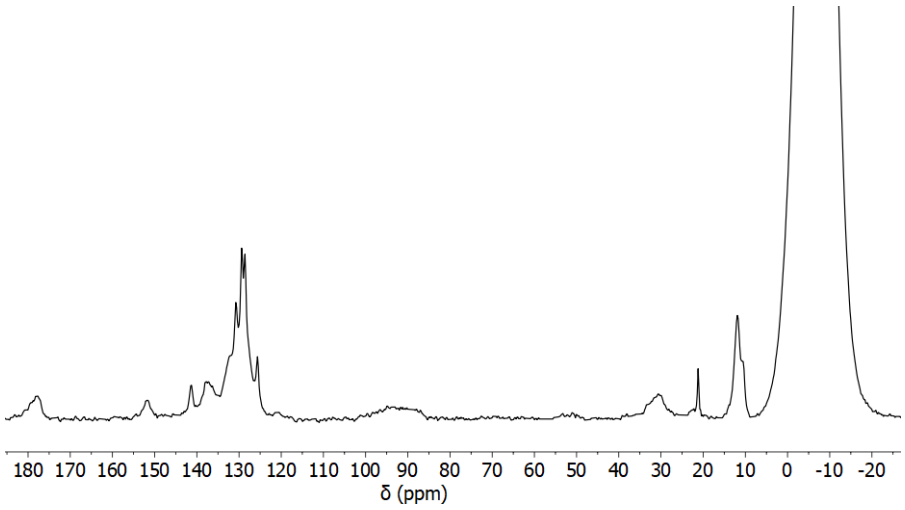

Figure 2.4. Solid state ^{13}C CPMAS NMR spectrum of sMAO-Pn*(H)$TiCl_3$ (**2$_{sMAO}$**) (100.6 kHz, 298 K).

2.2.3 Solution and slurry-phase polymerisation of styrene

Both complexes Cp*$TiCl_3$ (**1**) and Pn*(H)$TiCl_3$ (**2**) were tested for solution-phase polymerisation of styrene using MAO as a cocatalyst and were immobilised on solid polymethylaluminoxane (sMAO) for study as slurry-phase polymerisation catalysts. Three polymerisation temperatures were investigated: 40, 55 and 70 °C. Solution-phase polymerisations were performed in 2 mL of toluene with a molar ratio $[Al_{MAO}]_0$:$[Ti]_0$ of 1500 and 0.2 µmol of immobilised catalyst for 10 minutes. The slurry-phase styrene polymerisation were carried out with 50 mL of solvent for 30 minutes with 10 mg of catalyst and using $[Al_{sMAO}]_0$:$[Ti]_0$ = 200:1.

The activities were measured for the two complexes in solution-phase with MAO as a cocatalyst and in slurry-phase supported on sMAO (Figure 2.5). All catalysts showed high activity across the range of temperatures. Complex **1** displayed a slight activity increase with increasing temperature. The other systems varied little with changing temperatures, which could be attributed to the low reaction rates and formation of active species.[50] In the solution-phase, both catalysts displayed maximum activity at 55 °C

(4725 and 3435 $kg_{PS}/mol_{Ti}/h$ for **1** and **2** respectively). This trend has been reported by Ishihara *et al.* using $CpTiCl_3$ in the presence of MAO. The yields obtained with the $CpTiCl_3$/MAO system increased with temperatures to reach a maximum at 50 °C (306 $kg_{PS}/mol_{Ti}/h$ after 2 h) before decreasing between 50 and 85 °C (166 $kg_{PS}/mol_{Ti}/h$ at 85 °C).[26] The activities for both supported complexes were high and relatively constant with reaction temperature. One species stood out with really high polymerisation activity, complex $\mathbf{2_{sMAO}}$ was 2.2 times more active than $\mathbf{1_{sMAO}}$ with activities up to 7432 $kg_{PS}/mol_{Ti}/h$ at 55 °C. **1** led to higher activities than its supported analogue (values 1.4 times lower at 55 °C).

Nomura *et al.* reported lower solution-phase polymerisation activities of styrene in similar conditions and temperatures for complex **1** but described higher activity with increasing polymerisation temperature (320, 666 and 1970 $kg_{PS}/mol_{Ti}/h$ at 40, 55 and 70 °C respectively).[11] The parent cyclopentadienyl compound $CpTiCl_3$, however, achieved activities up to five times higher (15300–17500 $kg_{PS}/mol_{Ti}/h$ between 40 and 70 °C) and exhibited a maximum at 55 °C.[11]

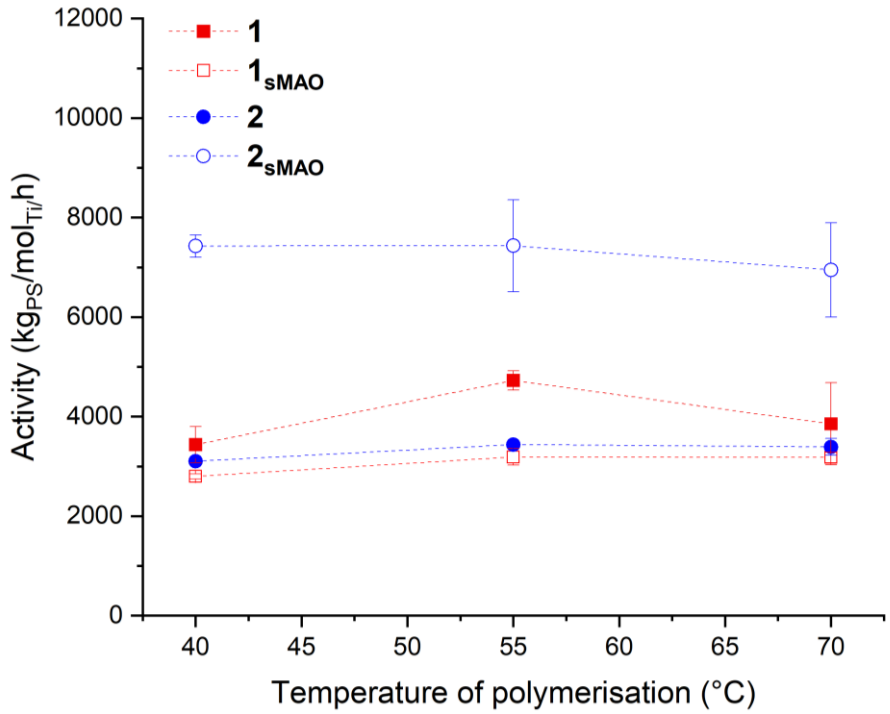

Figure 2.5. Temperature dependence of solution and slurry-phase styrene polymerisation by Cp*TiCl$_3$ (**1** and **1$_{sMAO}$**) and Pn*(H)TiCl$_3$ (**2** and **2$_{sMAO}$**). Polymerisation conditions: 10 minutes, 1000 rpm. Solution: 2 mL toluene, 2×10^{-7} mol catalyst, 1 mL styrene, $[Al_{MAO}]_0$:$[Ti]_0$ = 1500:1. Slurry: 50 mL toluene, 10 mg catalyst, 3.7 mL styrene, $[Al_{sMAO}]_0$:$[Ti]_0$ = 200:1.

2.2.4 Polymer characterisation

The polystyrene produced from the two catalysts was characterised by gel permeation chromatography (GPC) with the experimental molecular weights (M_w) and polydispersity (Đ, M_w/M_n) found to remain relatively constant across the series (Figure 2.6). The highest molecular weight observed was for **2** employed at 40 °C (M_w = 10852 g/mol). Complex **2$_{sMAO}$** yielded low molecular weight polystyrene compared to those obtained in solution-phase with lower Đ values (1.93 *vs.* 2.02 at 40 °C) which indicated that immobilising the catalyst allows for a better control of the chain termination rate. Complex **1** and the supported analogue **1$_{sMAO}$** both displayed low dispersities Đ (< 2) compared to the ones previously reported by Nomura and co-workers (2.2–2.5).[11]

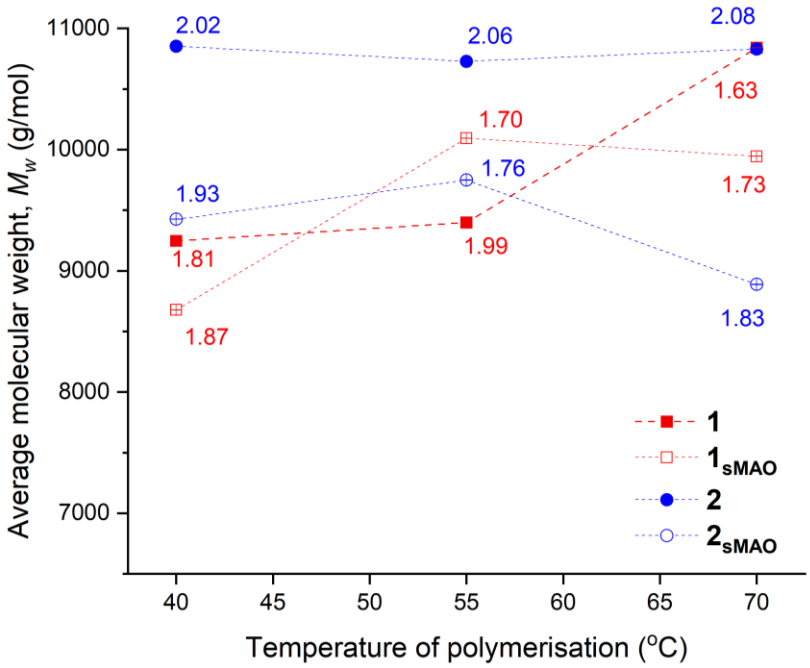

Figure 2.6. Polymer molecular weight (M_w) for solution and slurry-phase styrene polymerisation with Cp*$TiCl_3$ (**1**) and Pn*(H)$TiCl_3$ (**2**). Đ are given next to M_w. Polymerisation conditions: 10 minutes, 1000 rpm. Solution: 2 mL toluene, 2×10^{-7} mol catalyst, 1 mL styrene, $[Al_{MAO}]_0$:$[Ti]_0$ = 1500:1.. Slurry: 50 mL toluene, 10 mg catalyst, 3.7 mL styrene, $[Al_{sMAO}]_0$:$[Ti]_0$ = 200:1.

The polymers produced using complexes **1**, **2**, **1$_{sMAO}$ and 2$_{sMAO}$** exhibited a bimodal molecular weight distribution (Figure 2.7). For example, complex **2** displayed a minor peak at 6170 g/mol and a major peak at 9587 g/mol and **2$_{sMAO}$** has two maxima at 5463 and 9022 g/mol.

The thermal behaviour and crystallinity of the polymers synthesised were further characterised by differential scanning calorimetry (DSC) using 2 heating/cooling cycles between 25 and 280 °C at 5 °C/minute (Table 2.1, Figures 2.8 and 2.9). The percentage of crystallinity of the different polystyrene compounds was calculated by taking the melting heat, defined by the area under the melting peak, and dividing this by a reference value for 100% crystalline syndiotactic polystyrene.[51] This reference value has been determined by Pasztor *et al*. to be 53.2 J/g, with typical melt crystallised syndiotactic polystyrene reaching 50% crystallinity.[52]

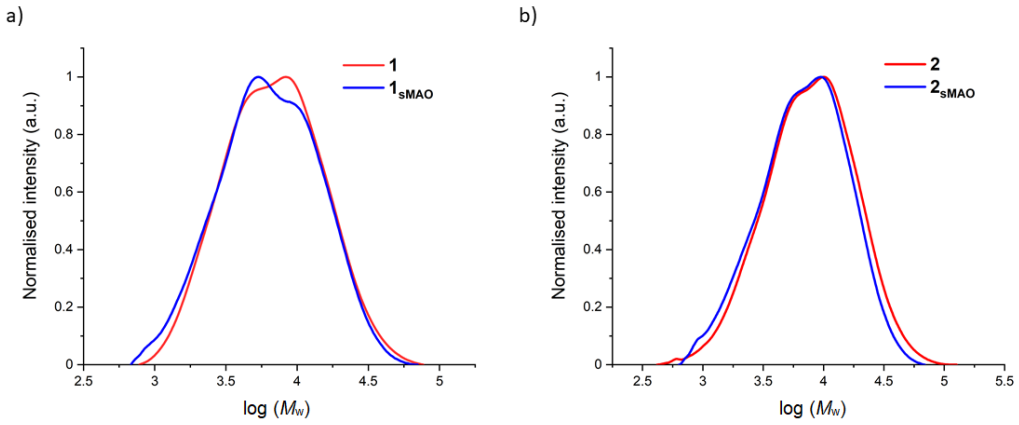

Figure 2.7. Molecular weight distributions of polymer produced in solution-phase (red) and slurry-phase (blue) by Cp*$TiCl_3$ (**1**) (a) and Pn*(H)$TiCl_3$ (**2**) (b) at 40 °C. Polymerisation conditions: 10 minutes, 1000 rpm. Solution: 2 mL toluene, 2×10^{-7} mol catalyst, 1 mL styrene, $[Al_{MAO}]_0$:$[Ti]_0$ = 1500:1. Slurry: 50 mL toluene, 10 mg catalyst, 3.7 mL styrene, $[Al_{sMAO}]_0$:$[Ti]_0$ = 200:1.

Table 2.1. DSC data for the polystyrene produced by Cp*$TiCl_3$ and Pn*(H)$TiCl_3$ in solution and slurry-phase.

T[a] (°C)	T_g (°C)	T_{m1} (°C)	T_{m2} (°C)	ΔH_m (J/g)	χ_c (%)
Cp*$TiCl_3$ (1)					
40	98.4	256.3	264.1	1.53	2.9
55	96.6	256.4	264.4	2.39	4.5
70	99.1	258.1	265.5	3.18	6.0
Pn*(H)$TiCl_3$ (2)					
40	97.3	n.s.	n.s.	-	-
55	96.1	n.s.	n.s.	-	-
70	95.5	n.s.	n.s.	-	-
sMAO-Cp*$TiCl_3$ (1_{sMAO})					
40	89.6	n.s.	n.s.	-	-
55	92.1	257.5	n.s.	0.10	0.2
70	94.7	n.s.	n.s.	-	-
sMAO-Pn*(H)$TiCl_3$ (2_{sMAO})					
40	91.7	n.s.	n.s.	-	-
55	89.0	n.s.	n.s.	-	-
70	94.3	n.s.	n.s.	-	-

n.s. = no signal. [a] Temperature of polymerisation.

All the polymer samples displayed a peak between 85 and 100 °C corresponding to the glass transition temperature of polystyrene.[53,54] When a melting peak was present, the crystallinity could be evaluated but the percentages were very low (0.2-6.0%), even for the polymers produced by complex **1**.[51,55,56] Li and co-workers reported the synthesis of

polystyrene with higher crystallinity of 52% using Cp*Ti($OCH_2C_6H_5$)$_3$/MAO at 80 °C, along with a higher melting enthalpy of 27.6 J/g.[56]

The glass transition and melting temperatures of the polystyrene produced by **1** in the solution-phase varied little with changing polymerisation temperature (Figure 2.8). A phenomenon of multi melting behaviour was observed as two peaks were obtained at high temperatures, both corresponding to melting of the polymer. Two processes could be responsible for this behaviour. Firstly, the first heating/cooling cycle created more perfect crystals that melted at a higher temperature than the original ones.[57] Secondly, polymorphism could explain the two peaks as polystyrene presents different types of units (α and β) and lamellae, which all melt at different temperatures.[24,58,59] The values of T_{m1} and T_{m2} are close to the ones reported in the literature for syndiotactic polystyrene (around 270 °C) which was the type of polymer expected to be produced by **1**.[4,14] The heat flow during the melting of the polystyrene increased with the polymerisation temperature (1.53, 2.39 and 3.18 J/g at 40, 55 and 70 °C respectively) which resulted in an increase in crystallinity from 2.9 to 6.0%.

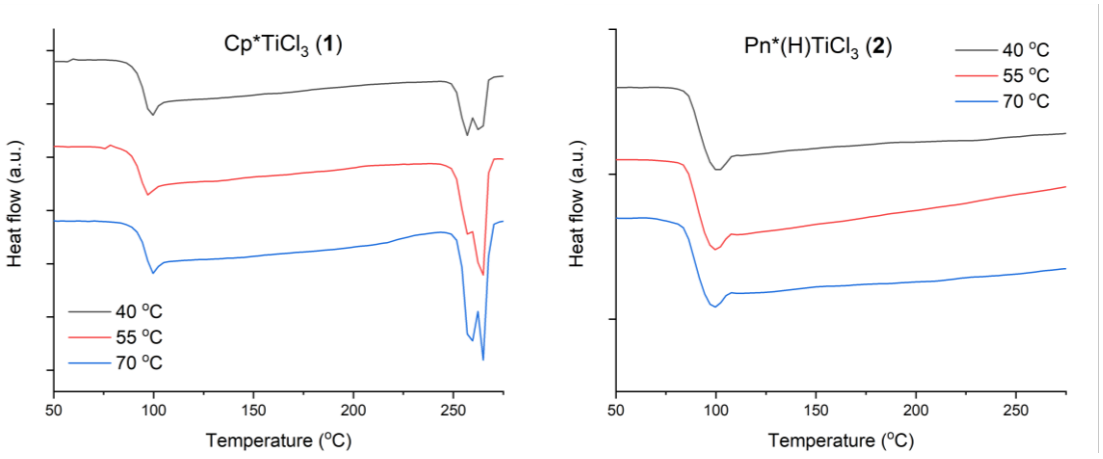

Figure 2.8. DSC of polystyrene synthesised by Cp*$TiCl_3$ (**1**) and Pn*(H)$TiCl_3$ (**2**), ramp 5 °C/minute. Polymerisation conditions: 10 minutes, 1000 rpm. 2 mL toluene, 2×10^{-7} mol catalyst, 1 mL styrene, $[Al_{MAO}]_0$:$[Ti]_0$ = 1500:1.

Compared to complex **1**, the glass transition temperature of polystyrene obtained using the (hydro)permethylpentalene **2** was lower in the two phases (99.1 *vs.* 95.5 °C at a polymerisation temperature of 70 °C for **1** and **2** respectively) (Figures 2.8 and 2.9). The T_g slightly decreased with increasing polymerisation temperature in solution-phase while very little effect is displayed in slurry-phase. No melting temperature could be observed for the polymer samples which indicated that atactic polystyrene was produced.[60–62]

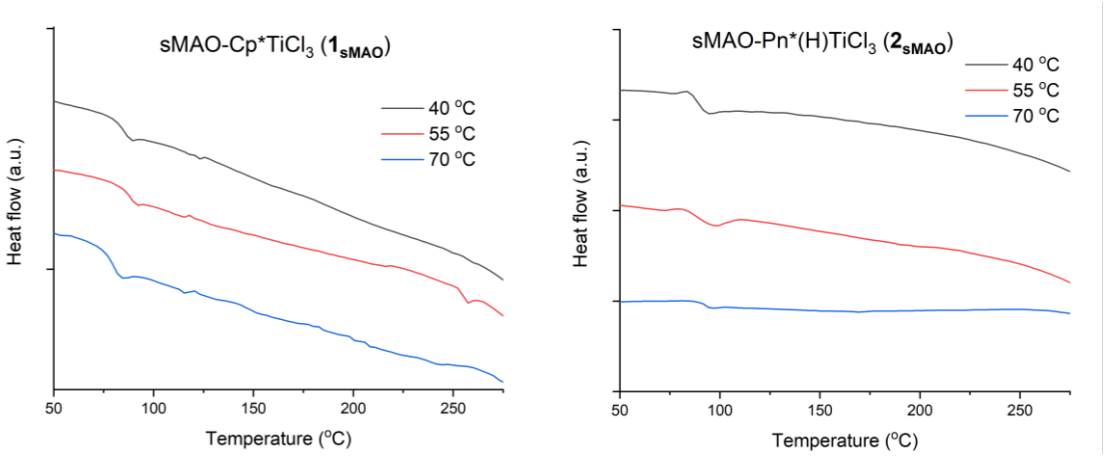

Figure 2.9. DSC of polystyrene synthesised by sMAO-Cp*$TiCl_3$ (**1_{sMAO}**) and sMAO-Pn*(H)$TiCl_3$ (**2_{sMAO}**), ramp 5 °C/minute. Polymerisation conditions: 10 minutes, 1000 rpm. 50 mL toluene, 10 mg catalyst, 3.7 mL styrene, $[Al_{sMAO}]_0$:$[Ti]_0$ = 200:1.

Crystallinity of the polymer samples can also be assessed by powder X-ray diffraction (Figures 2.10). Polystyrene obtained by **2** in solution-phase and **2_{sMAO}** in slurry-phase displayed diffractograms typical of amorphous materials. The major peak at 20° is the (211) peak and is caused by the interaction of the backbone with the side groups. For the polymer produced in slurry-phase, the shoulder between 5° and 15°, due to inter-chain interactions, possibly corresponds to the (310), (220), (300) and (210) peaks but the broadness of the signal makes the attribution difficult.[63,64] Intramolecular interactions are represented by the signal around 40°.

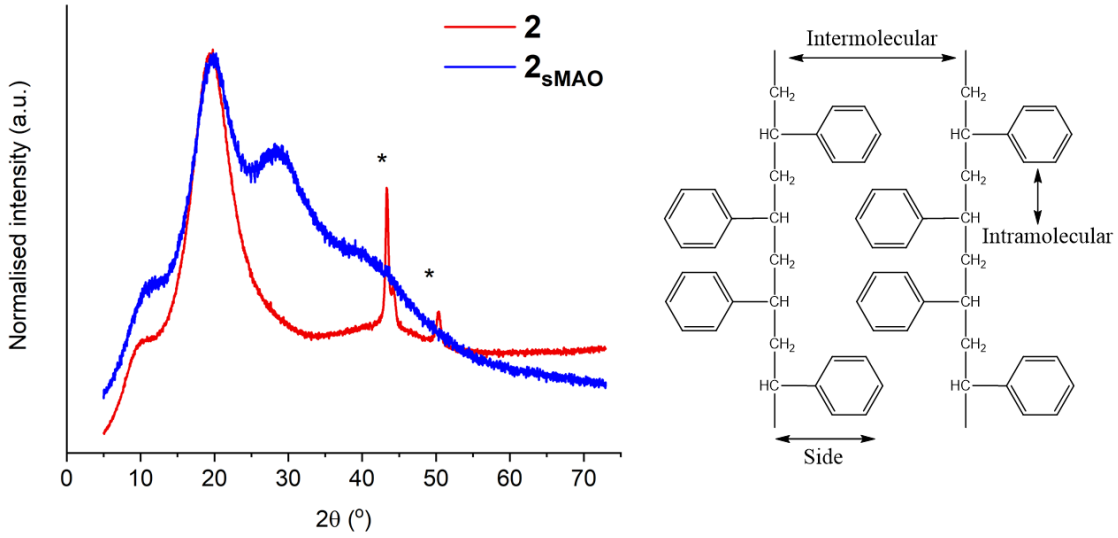

Figure 2.10. Powder X-ray diffraction pattern of polystyrene produced by Pn*(H)$TiCl_3$ (**1** and **1_{sMAO})** at 70 °C (red) and sMAO-Pn*(H)$TiCl_3$ at 55 °C (blue). * denotes sample holder.

Surprisingly, no replication of the solid support morphology could be observed in slurry-phase.[27] Nonetheless, immobilisation of the complexes on solid support allowed for an improvement in polystyrene morphology as observed by scanning electron microscopy (SEM) (Figure 2.11). The polymers synthesised in solution-phase exhibited a "glass-like" morphology whereas the slurry-phase samples adopted a "rock" shape. The polymer particles produced by **2_{sMAO}** were approximately twice the size of the ones produced by complex **1_{sMAO}** (400 vs. 200 μm) which correlates with the increase in activities.

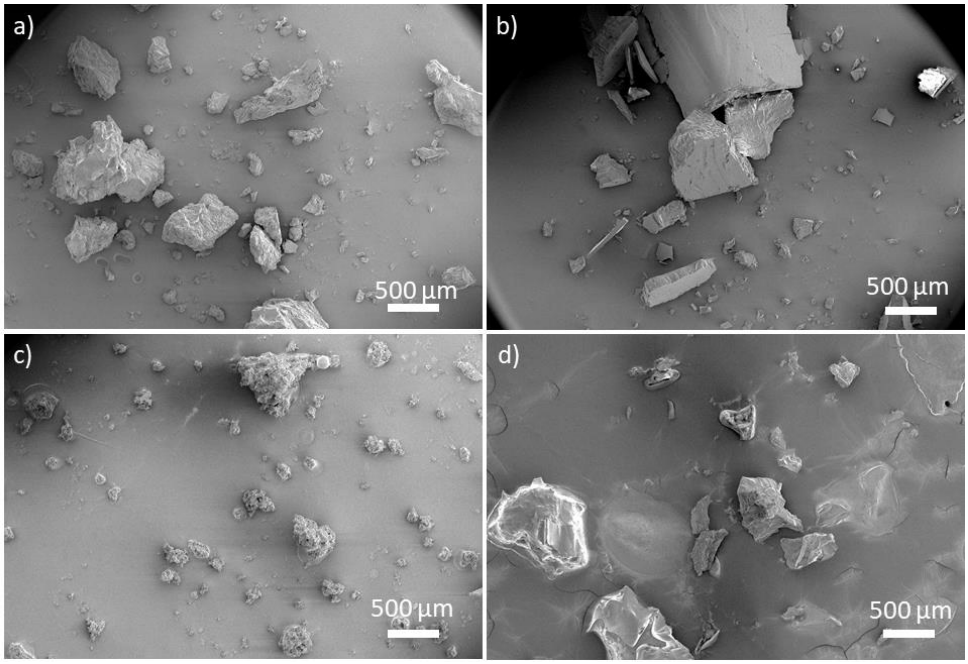

Figure 2.11. Scanning electron microscopy images of polystyrene obtained by a) Cp*$TiCl_3$ (**1**) (x27), b) Pn*(H)$TiCl_3$ (**2**) (x25), c) sMAO-Cp*$TiCl_3$ (**1$_{sMAO}$**) (x30) and d) sMAO-Pn*(H)$TiCl_3$ (**2$_{sMAO}$**) (x50).

The tacticity of the polystyrene samples was determined by $^{13}C\{^1H\}$ NMR spectroscopy in 1,1,2,2-tetrachloroethane-d_2 (Figure A2.26-33).[65–68] Deconvolution of the methine and methylene resonances allowed for the assignment of pentads and the determination of the probability of a *meso* arrangements of the pentads, P_m. The method used is illustrated using the example of polystyrene synthesised at 40 °C by complex **1** in solution-phase (Figure 2.12 and Table 2.2).

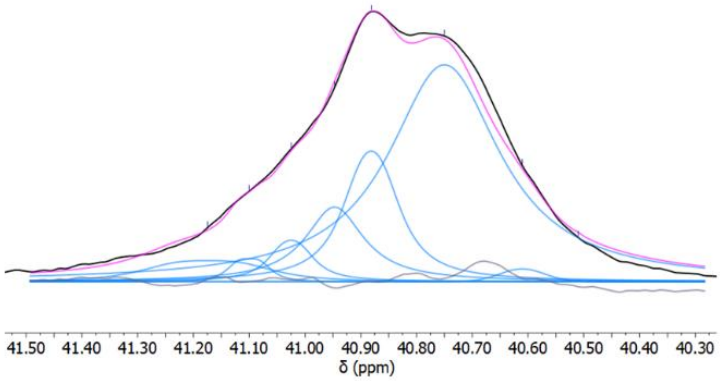

Figure 2.12. Example of deconvolution of the $^{13}C\{^1H\}$ NMR spectrum in 1,1,2,2-$C_2D_2Cl_2$ of the methine peak of the polymer produced by Cp*$TiCl_3$ (**1**) at 40 °C (393 K, 500 MHz) (blue = peak, pink = sum, grey = residue).

Table 2.2. Pentad analysis of the methine region of the polymer produced by Cp^*TiCl_3 (**1**) at 40 °C.

Peak	Shift (ppm)	Area ($\times 10^5$)	Pentad	Probability	Integration, I	Number of m in pentad, N
1	40.95	8.63	*mmrr*	$2P_m^2(1\text{-}P_m)$	1.09×10^{-1}	0.5
2	41.10	1.28	*mmrr*	$2P_m^2(1\text{-}P_m)$	$1.62\ 10^{-2}$	0.5
3	41.03	3.13	*mmmm*	P_m^3	3.95×10^{-2}	1
4	41.18	3.66	*rmrr*	$P_m(1\text{-}P_m)^2$	4.62×10^{-2}	0,25
5	40.88	12.8	*rrrr*	$(1\text{-}P_m)^3$	1.62×10^{-1}	0
6	40.75	48.0	*mmmr*	P_m^3	6.06×10^{-1}	0.75
7	40.61	0.746	*rmrm*	$P_m(1\text{-}P_m)^2$	9.42×10^{-3}	0.5
8	40.51	0.0115	*mrrm*	$P_m(1\text{-}P_m)^2$	1.45×10^{-4}	0.5

$$P_m = \sum_{i=1}^{n} I_n \times N_n \qquad \text{Equation 2.1}$$

The final probability P_m can be calculated by multiplying the integration of each peak with the number of *meso* arrangements in the pentad (Equation 2.1). For the solution-phase produced polystyrene using complex **1**, this led to $P_m = 0.58$ which indicated a slight tendency towards isotacticity with phenyl groups on the same side of the backbone. A similar method was used for the other samples leading to $P_m \geq 0.50$ in all cases indicating a slight tendency towards *meso* arrangements rather than racemic (Table 2.3). Cyclopentadienyl trichloride derivatives have been largely reported to produce polystyrene with high syndiotactic content.[8,69–71] Zhu *et al.* observed high syndiotacticity (< 95%) for polystyrene synthesised by $CpTiCl_3$/MAO in toluene.[24] Half-titanocene Cp^*TiCl_3 supported on $MgCl_2/AlEt_n(OEt)_{3-n}$ also yielded polystyrene with a high degree of syndiotacticity (74.1% for $[Al_{MAO}]$:[Ti] = 150) at 70 °C.[72]

^1H and ^{13}C NMR spectroscopy in chloroform-d_1 revealed the presence of $-CH_3$ end groups (~ 1.0 ppm) as well as unsaturated chain-end fragments (5.26 (d, ^3J = 11.0 Hz) and 5.77 (dd, ^3J = 17.6, ^4J = 0.95 Hz) integrating for 1:1).

Table 2.3. Tacticities of polystyrene produced at 55 °C calculated by pentad analysis of the polystyrene samples.

Complex	P_m
Cp^*TiCl_3 (**1**)	0.58
$Pn^*(H)TiCl_3$ (**2**)	0.52
sMAO-Cp^*TiCl_3 (**1_{sMAO}**)	0.57
sMAO-$Pn^*(H)TiCl_3$ (**2_{sMAO}**)	0.50

2.3 Ethylene homopolymerisation study

The titanium species **1**, **2** and their sMAO-immobilised analogues were used to polymerise ethylene. The influence of the polymerisation temperature on the activity was investigated in toluene and hexane using a constant pressure of 2 bar of ethylene.

2.3.1 Temperature dependence

The polymerisations were carried out at five different temperatures (40, 50, 60, 70 and 80 °C) (Figure 2.13). The two titanium species displayed very different polymerisation behaviours in solution and slurry-phase. Indeed, solution-phase activities were 1.2 to 2.5 times higher than slurry-phase values and both compounds were highly active on the Gibson scale.[73] In solution, a decrease in activity was observed with an increasing temperature when **1** was used as catalyst. This trend is mainly caused by the decrease in solubility of ethylene in hexane with increasing temperatures.[74] Complex **2** showed a slight increase in activity with temperature above 50 °C with a peak at 70 °C (885 $kg_{PE}/mol_{Ti}/bar/h$). The (hydro)permethylpentalene complex performed better than cyclopentadinyl titanium aryloxides $Cp^*TiCl_2(O^iPr)$ reported by Nomura and co-workers.[75] Under 4 bar of ethylene, the latter gave an activity of 310 $kg_{PE}/mol_{Ti}/h/bar$ which is 3 times lower than **2**.

The two immobilised complexes displayed very different profiles with lower ethylene polymerisation capacity than the non-supported species. Nevertheless both were good catalysts with activities higher than 150 $kg_{PE}/mol_{Ti}/bar/h$ (Figure 2.13). Previously reported titanium permethylpentalene complexes $Pn^*TiClCp^R$ produced very little polyethylene in solution-phase, leading to low activities (20–40 $kg_{PE}/mol_{Ti}/bar/h$).[45] Supported complex $\mathbf{1}_{\mathbf{sMAO}}$ was a better catalyst at low temperatures with a maximum of 258 $kg_{PE}/mol_{Ti}/bar/h$ at 50 °C. This was consistent with the ethylene uptake rate which

indicated that the catalyst was more active at 40 and 50 °C (Figure A2.16). For temperatures above 50 °C, the polymerisation activity dropped to 209 $kg_{PE}/mol_{Ti}/bar/h$ at 70°C and increased again at 80 °C. Complex **2**$_{sMAO}$ had a different behaviour. Polymerisation activity increased with temperature and reached its highest value at 70 °C (259 $kg_{PE}/mol_{Ti}/bar/h$) and then dropped to 206 $kg/mol_{Ti}/bar/h$ at 80 °C. The polymers formed in slurry-phase were forming a coating around the catalyst which could lead to a diffusion barrier as explained by Chien.[76] The slurry-phase activities were significantly lower than the ones observed with sMAO-Cp*$TiCl_2$(O-2,6-^{i}Pr-C_6H_3) by Nomura *et al.*; an increase from 21000 $kg_{PE}/mol_{Ti}/h/bar$ at 25 °C to 30800 $kg_{PE}/mol_{Ti}/h/bar$ at 50 °C was reported using sMAO particles of 5.6 µm.[77]

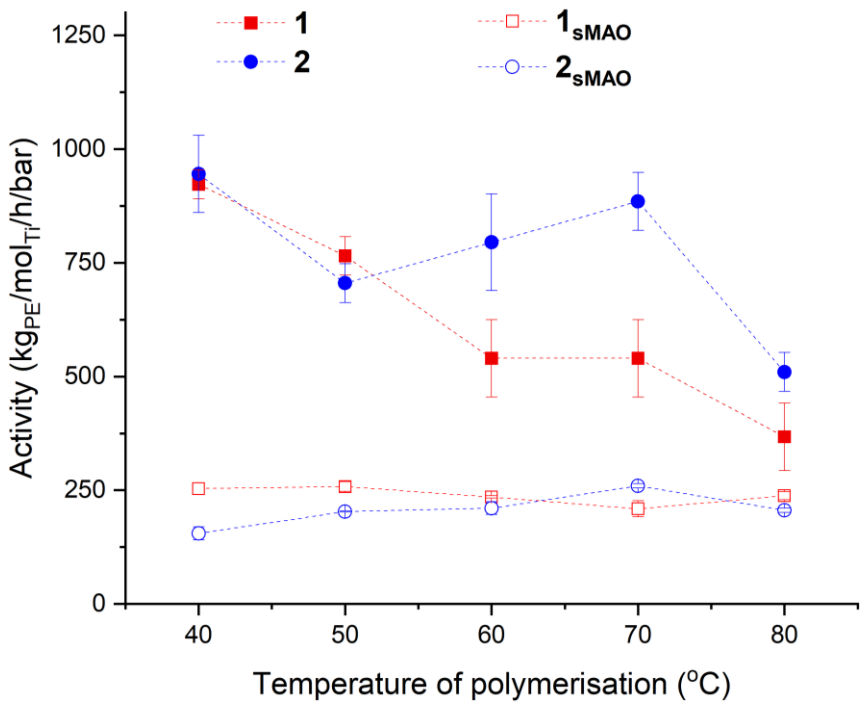

Figure 2.13. Temperature dependence of solution and slurry-phase ethylene polymerisation activity Cp*$TiCl_3$ (**1** and **1**$_{sMAO}$) and Pn*(H)$TiCl_3$ (**2** and **2**$_{sMAO}$). Polymerisation conditions: 30 minutes, 1000 rpm, 2 bar ethylene, 50 mL hexane, 150 mg TiBA. Solution: 2×10^{-7} mol catalyst, $[Al_{MAO}]_0$:$[Ti]_0$ = 1500:1. Slurry: 10 mg catalyst, $[Al_{sMAO}]_0$:$[Ti]_0$ = 200:1.

2.3.2 Polymer characterisation

The polyethylene produced in solution-phase by catalysts **1** and **2** could not be characterised by GPC. The samples were not soluble in 1,3,5-trichlorobenzene at 150 °C or gave too high pressure on the GPC instrument to be injected, suggesting that polymers with high molecular weights were generated. The molecular weights of polyethylenes synthesised in slurry phase were measured with difficulty. Indeed, samples produced with $\mathbf{1}_{\mathbf{sMAO}}$ and $\mathbf{2}_{\mathbf{sMAO}}$ achieved low mass recovery of 2.2–5.2% and 1.7–2.8% respectively. The polyethylene formed might have been retained on the column because of a molecular weight too high ($> 5\times10^6$ g/mol) thus only a small fraction corresponding to the very lowest molecular weights was analysed. Indeed, the molecular weights measured were very low (500–800 g/mol) with narrow dispersity in the range 1.5–1.7 (Figure 2.14). Catalyst $\mathbf{2}_{\mathbf{sMAO}}$ formed polymer with bimodal distribution exhibiting a major peak in the region $2.62 < \log(M_w) < 2.73$ (corresponding to M_w between 417 and 537 g/mol) and a minor peak at $2.24 < \log(M_w) < 2.28$ (M_w = 174 g/mol and 190 g/mol respectively) (Figure 2.14). Nomura and co-workers investigated different modified half-titanocenes for the homopolymerisation of ethylene. The ketimide derivative Cp*$TiCl_2$(N=C^tBu_2) yielded molecular weights of $M_w = 114\times10^4$ g/mol with a low dispersity of 2.1 at 40 °C and aryloxide compounds Cp*$TiCl_2$(O-2,6-^{i}Pr-C_6H_3) afforded polyethylene with broad dispersity (Đ= 14.8) and lower molecular weight (2.8×10^4 g/mol).[75,78]

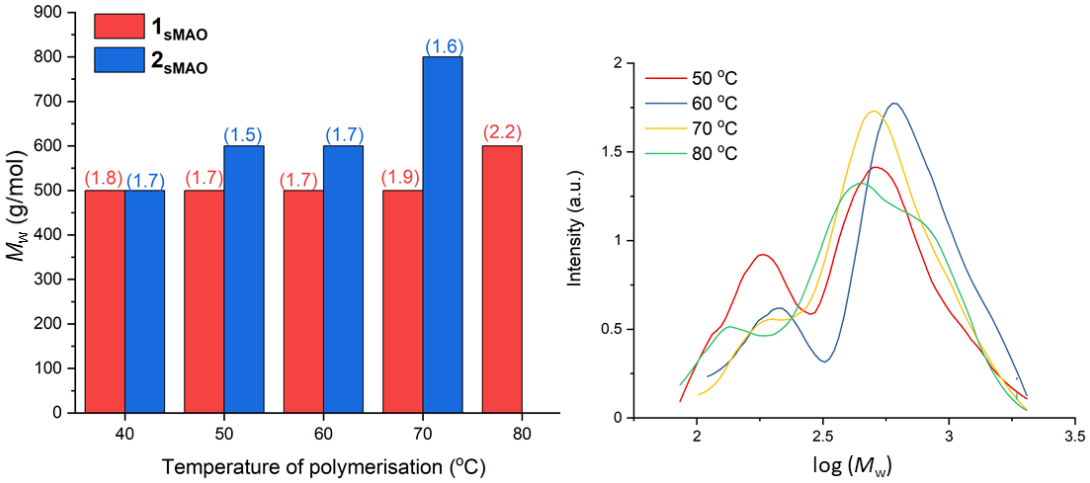

Figure 2.14. Polymer molecular weight for slurry phase ethylene polymerisation with sMAO-Cp*$TiCl_3$ (**1**$_{sMAO}$) and sMAO-Pn*(H)$TiCl_3$ (**2**$_{sMAO}$) (left) and molecular weight distrobutions of polyethylene produced by sMAO-Pn*(H)$TiCl_3$ (**2**$_{sMAO}$) between 50 °C and 80 °C. Đs are given in parentheses.

The polymer samples were analysed by DSC and melt temperature and enthalpy values were taken from the second heating cycle. All samples showed one crystallisation peak and one melting peak (Figure 2.15 and 2.16). All polymers synthesised by **1** displayed the same T_m at 132 °C as well as similar heat flows. Polyethylenes obtained with **2** had different thermal behaviours depending on the polymerisation temperature. The T_m increased following the order 40 °C (T_m = 128.1 °C) < 50 °C (133.3 °C) < 60 °C (134.4 °C) < 70 °C (134.8 °C). Similarly, the heat flows increased with the polymerisation temperature between 40 and 70 °C. The polyethylene obtained at 80 °C exhibited a singular behaviour having the minimal heat flow and a low T_m of 130.9 °C. Except at 70 °C where no DSC signal was observed, complex **1** generated polymer samples with a higher degree of crystallinity than **2** (Table 2.4).[79] The low crystallinity calculated for PE produced by **1** and **2** reflect the high molecular weight. Indeed Richards and Buckser reported that low molecular weight polyethylene exhibited higher degree of crystallinity and that the opposite was observed for high molecular weight PE.[80,81]

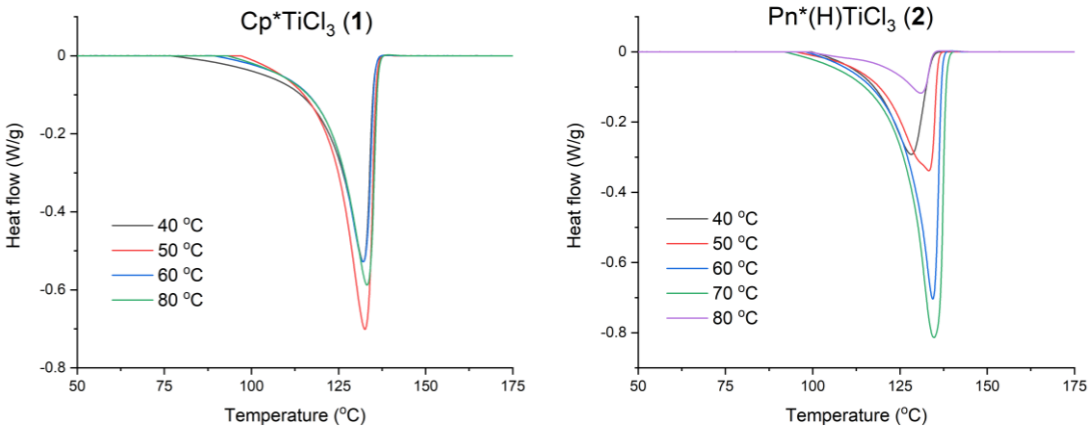

Figure 2.15. DSC of polyethylene synthesised by Cp*$TiCl_3$ (**1**) and Pn*(H)$TiCl_3$ (**2**), ramp 5 °C/minute. Polymerisation conditions: 30 minutes, 1000 rpm, 150 mg TiBA. 50 mL hexane, 2×10^{-7} mol catalyst, 2 bar ethylene, $[Al_{MAO}]_0$:$[Ti]_0$ = 1500:1.

Table 2.4. DSC analysis of the polyethylene produced by Cp*$TiCl_3$ (**1**) and Pn*(H)$TiCl_3$ (**2**). Polymerisation conditions: 30 minutes, 1000 rpm. 50 mL hexane, 150 mg TiBA, 2×10^{-7} mol catalyst, 2 bar ethylene, $[Al_{MAO}]_0$:$[Ti]_0$ = 1500:1.

Complex	T[a] (°C)	T_m (°C)	ΔH_m	χ_c (%)
Cp*$TiCl_3$ (**1**)	40	132.1	69.8	23.8
Cp*$TiCl_3$ (**1**)	50	132.6	91.8	31.3
Cp*$TiCl_3$ (**1**)	60	132.1	69.5	23.7
Cp*$TiCl_3$ (**1**)	80	133.2	79.8	27.2
Pn*(H)$TiCl_3$ (**2**)	40	128.1	44.4	15.2
Pn*(H)$TiCl_3$ (**2**)	50	133.3	51.8	17.7
Pn*(H)$TiCl_3$ (**2**)	60	134.4	87.4	29.8
Pn*(H)$TiCl_3$ (**2**)	70	134.8	103.5	35.3
Pn*(H)$TiCl_3$ (**2**)	80	130.9	16.1	5.5

[a] Temperature of polymerisation

In the slurry-phase, the melting temperature appeared to be independent of the polymerisation temperature for both complexes with a T_m = 133 °C in all cases except at 40 °C where the T_m was lower by 5 °C and 2.5 °C for **1**$_{sMAO}$ and **2**$_{sMAO}$ respectively (Table 2.5). The melting peaks observed by DSC were slightly lower than the one measured for PE generated using sMAO-Pn*ZrCpCl at 40 °C (138.6 °C); nonetheless they also corresponded to high density polyethylene.[45]

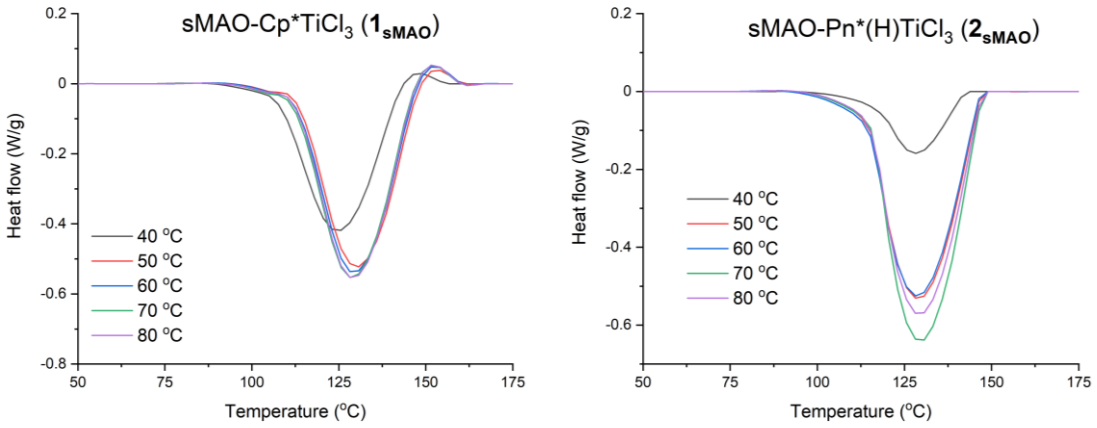

Figure 2.16. DSC of polyethylene synthesised by sMAO-Cp*$TiCl_3$ (**1_{sMAO}**) and sMAO-Pn*(H)$TiCl_3$ (**2_{sMAO}**), ramp 5 °C/minute. Polymerisation conditions: 30 minutes, 1000 rpm. 50 mL hexane, 10 mg catalyst, 2 bar ethylene, $[Al_{sMAO}]_0$:$[Ti]_0$ = 200:1, 150 mg TiBA.

Polyethylene produced by catalyst **1_{sMAO}** was between 36.6 and 46.1% crystalline (Table 2.5).[79] Following the trend observed by Hussein *et al.*, the crystallinity increased with the polymerisation temperature.[82] The same evolution was observed for the samples synthesised using **2_{sMAO}** with a lower crystallinity of 11.1% at 40 °C. Supporting the complexes on sMAO allowed for higher crystallinity relative to the polymers produced in the solution phase (17.7% *vs.* 43.2% at 50 °C for **2** and **2_{sMAO}**). The crystallinity calculated in slurry-phase for **1_{sMAO}** and **2_{sMAO}** were higher than those reported for polyethylene produced by sMAO-Pn*ZrCpCl and sMAO-Pn*ZrCp^{nBu}Cl under the same conditions (30% and 28% respectively).[45]

Table 2.5. DSC analysis of the polyethylene produced by sMAO-Cp*$TiCl_3$ (**1_{sMAO}**) and sMAO-Pn*(H)$TiCl_3$ (**2_{sMAO}**). Polymerisation conditions: 30 minutes, 1000 rpm. 50 mL hexane, 10 mg catalyst, 2 bar ethylene, $[Al_{sMAO}]_0$:$[Ti]_0$ = 200:1, 150 mg TiBA.

Complex	T[a]	T_m (°C)	ΔH_m (J/g)	χ_c (%)
sMAO-Cp*$TiCl_3$ **(1_{sMAO})**	40	128.2	107.1	36.6
sMAO-Cp*$TiCl_3$ **(1_{sMAO})**	50	133.3	123.8	42.3
sMAO-Cp*$TiCl_3$ **(1_{sMAO})**	60	133.2	131.8	45.0
sMAO-Cp*$TiCl_3$ **(1_{sMAO})**	70	133.3	130.7	44.6
sMAO-Cp*$TiCl_3$ **(1_{sMAO})**	80	133.3	135.2	46.1
sMAO-Pn*(H)$TiCl_3$ **(2_{sMAO})**	40	130.8	32.4	11.1
sMAO-Pn*(H)$TiCl_3$ **(2_{sMAO})**	50	133.2	127.3	43.2
sMAO-Pn*(H)$TiCl_3$ **(2_{sMAO})**	60	133.2	132.3	45.1
sMAO-Pn*(H)$TiCl_3$ **(2_{sMAO})**	70	133.2	157.2	53.7
sMAO-Pn*(H)$TiCl_3$ **(2_{sMAO})**	80	133.2	140.9	48.1

[a] Temperature of polymerisation

The crystallinity of the polyethylene can be further characterised by powder X-ray diffraction (Figure 2.17). The X-ray diffraction pattern of polyethylene synthesised by complexes **2** and **2_{sMAO}** corresponded to the orthorhombic crystal phase.[83] Major peaks found at 21.63 and 24.05° correspond to the (110) and (200) peaks respectively and other less intense peaks at 36.23° and 39.74° can be attributed to (020) and (011).[83,84] The lattice parameters are calculated as a = 0.73916, b=0.49548 and c = 0.22687 nm which is slightly shorter than that of linear polyethylene reported by Busing (a = 0.74069, b = 0.49491 and c = 0.25511 nm).[85,86]

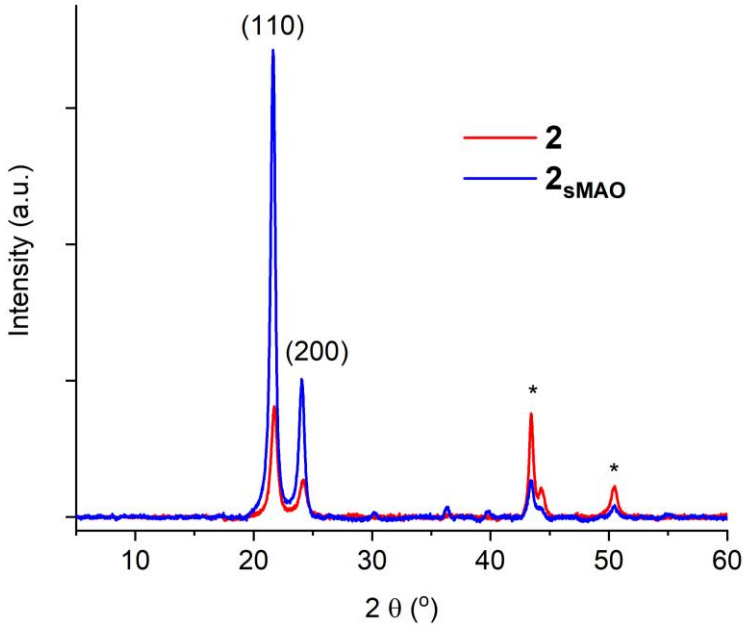

Figure 2.17. Powder X-ray diffraction pattern of polyethylene produced by **2** and $\mathbf{2_{sMAO}}$. * denotes sample holder.

The $^{13}C\{^1H\}$ NMR spectra of polyethylene samples recorded in 1,1,2,2-tetrachloroethane-d_2 were characterised by a major singlet at 29 ppm corresponding to the CH_2 groups (Figure A2.34-38). The number of methyl branches was evaluated comparably to the amount of CH_2 from the polymer backbone; the polyethylene produced by $\mathbf{2_{sMAO}}$ at 50 °C exhibited a ratio CH_3/1000 CH_2 of 0.9 which was consistent with the linear nature of the polymer determined by other characterisation techniques.[87,88]

Figure 2.18 highlights the effect of solid-support of the resulting polymer morphology. The SEM images of polyethylene produced by **1** and **2** in solution-phase show a filamentous morphology suggesting a poor control during polymerisation. The two supported complexes generated polymer with a completely different morphology relative to the solution-phase polymers. Indeed, as reported by O'Hare *et al.*, replication of the sMAO support occured and the polyethylene displayed a typical "popcorn"

morphology.[33–35] Aggregates formed by spherical particles of 10 µm were observed by SEM for samples synthesised by **1**$_{sMAO}$ and **2**$_{sMAO}$.

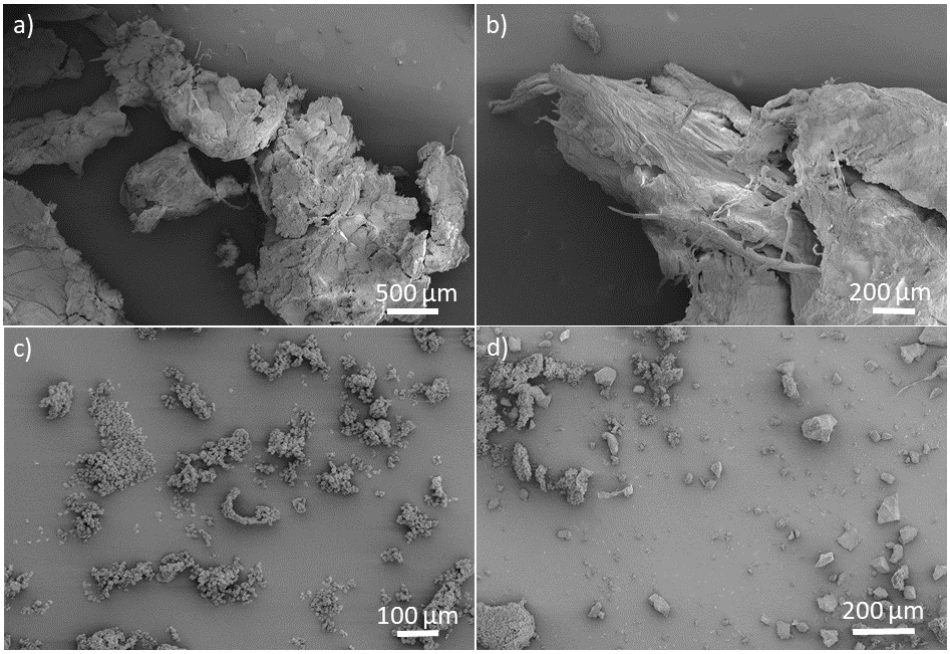

Figure 2.18. SEM images of polyethylenes produced by a) Cp*$TiCl_3$ (**1**) (x30), b) Pn*(H)$TiCl_3$ (**2**) (x60), c) sMAO-Cp*$TiCl_3$ (**1**$_{sMAO}$) (x120) and d) sMAO-Pn*(H)$TiCl_3$ (**2**$_{sMAO}$) (x85).

2.4 Copolymerisation of ethylene with styrene

The use of **1** and **2** for the copolymerisation of ethylene and styrene was studied in solution and slurry-phase. For this purpose, glass copolymerisation ampoules were used with the styrene being introduced into the system *via* the side arm in one portion (Figure 2.19). The experiments were performed at different temperatures and different volumes of styrene in order to investigate their influence on the polymer samples morphology and properties. Solution-phase polymerisations were carried out using 0.2 µmol of titanium complexes and 1500 eq. of dried MAO as cocatalyst in toluene and slurry-phase polymerisations were performed with 10 mg of supported complex ($[Al_{sMAO}]_0$:$[Ti]_0$ = 200:1).

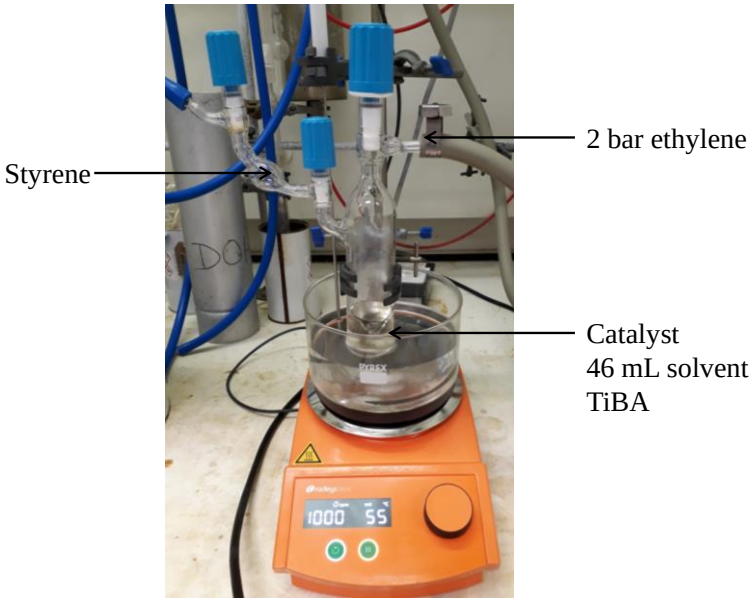

Figure 2.19. Slurry-phase copolymerisation set-up.

2.4.1 Solvent effect

Firstly, the influence of the polymerisation solvent was investigated at 40 °C with 125 µL of styrene using $\mathbf{2_{sMAO}}$ ($[Al_{sMAO}]_0$:$[Ti]_0$ = 200:1) (Figure 2.20).

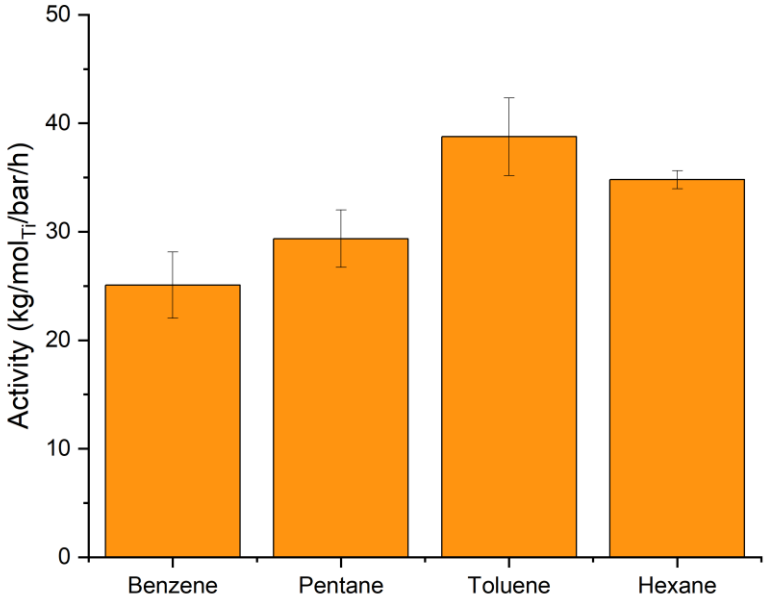

Figure 2.20 Solvent dependence of slurry-phase ethylene/styrene copolymerisation activity of sMAO-Pn*(H)TiCl$_3$ (**2$_{sMAO}$**). $[Al_{sMAO}]_0$:$[Ti]_0$ = 200:1, 10 mg catalyst, 125 µL styrene, 2 bar ethylene, 50 mL solvent, 40 °C, 30 minutes, 1000 rpm, 150 mg TiBA.

Four solvents have been tested and the resulting polymerisation activities can be ordered as follow: benzene (25 kg/mol$_{Ti}$/h/bar) < pentane (29 kg/mol$_{Ti}$/h/bar) < hexane (35 kg/mol$_{Ti}$/h/bar) < toluene (39 kg/mol$_{Ti}$/h/bar). The activities measured were lower than those of ethylene homopolymerisation (10 times lower), highlighting the negative effect of introducing styrene in the polymerisation system. Scott *et al.* also reported a decline in activity relative to ethylene homopolymerisation for the copolymerisation with styrene using zirconium salicylaldimine complexes.[89] Under 1.2 bar of ethylene, they recorded activities between 5 and 18 times lower after addition of styrene.

Under the same conditions, toluene and hexane had similar activities 1.6 and 1.4 times higher than benzene respectively using complex **2$_{sMAO}$**. Similarly to styrene homopolymerisations, benzene achieved the lowest activity. Although toluene performed slightly better as a solvent, further copolymerisation experiments were carried out in hexane for better comparison with ethylene homopolymerisation results.

From polymerisations in hexane using complex **2$_{sMAO}$**, two distinct crops of material could be afforded. The first crop precipitated in hexane and was isolated after several washings with pentane. The second crop was obtained after filtration and drying of the reaction mixture. The first crop yielded white flakes and characterisation established its polymeric type. The second crop, however, was a fine grey powder. Further characterisation were performed to determine the nature of the latter. No signal could be observed after DSC measurements suggesting that the second crop contained no or little amount of polymer. It was hypothesised that the grey crop consisted of Al residues derived from the sMAO support which was confirmed by the ^{27}Al DPMAS NMR spectrum. Figure 2.21 shows the thermogravimetric analysis (TGA) spectra for both crops. Presence of polymer in the first crop was confirmed by the drop corresponding to a degradation temperature of 483 °C. This value is consistent with degradation temperature expected for polyethylene (450–490 °C).[90,91] The analysis of the second crop displayed a degradation peak at 173 °C. No additional peak at higher temperatures were detected, supporting the hypothesis that no polymer was present in this crop. The degradation temperature was too low to be polyethylene, polystyrene or a copolymer and the product isolated probably consisted in a mixture of inorganic compounds from the MAO an the TiBA.[92,93] XRD characterisation of the second crop further confirmed the absence of polymer in the material (Figure A2.40). The flat baseline and sharp peaks indicated the presence of a highly crystalline material, incompatible with the desired copolymer. Only the first crop of polymer precipitating in the reaction vessel and filtered was used for activity calculations and further product characterisations.

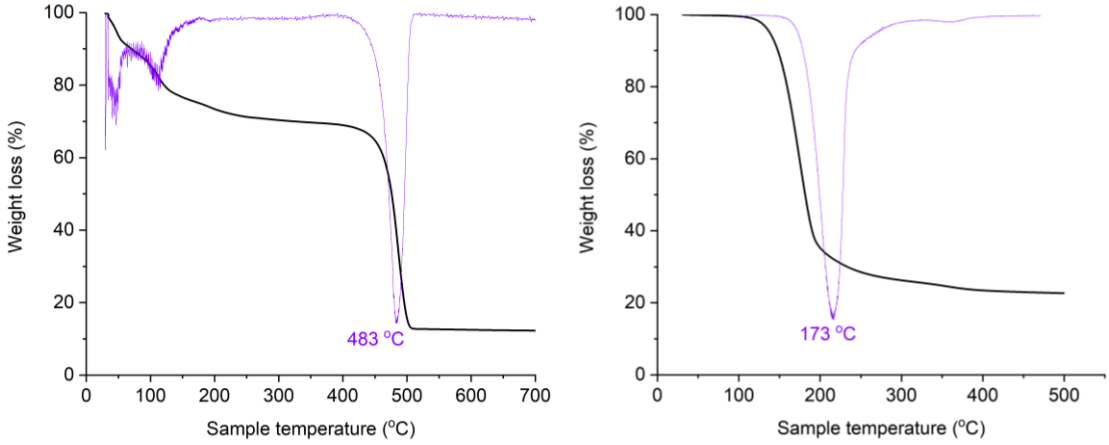

Figure 2.21. Thermogravimetric analysis (TGA) of crops 1 and 2 produced by the copolymerisation of ethylene with styrene using $\mathbf{2}_{\mathbf{sMAO}}$ at 40 °C with 125 µL of styrene. Polymerisation conditions: 30 minutes, 1000 rpm, 2 bar of ethylene, 50 mL hexane, 125 µL styrene, 150 mg TiBA. Derivative in purple.

2.4.2 Temperature effect

The influence of temperature on ethylene/styrene copolymerisation activities was studied using both unsupported and supported complexes. Polymerisations were carried out at five different temperatures (40, 50, 60, 70 and 80 °C) using a fixed amount of 125 µL styrene (Figure 2.22).

In the range of temperatures tested, solution-phase copolymerisations of ethylene with styrene led to higher activities than slurry-phase experiments (up to 17 and 21 times for **1** and **2** respectively). The activities between 40 and 80 °C can be ordered as follow: **1** > **2** > $\mathbf{1}_{\mathbf{sMAO}}$ > $\mathbf{2}_{\mathbf{sMAO}}$. The polymerisation temperature had a greater influence when the copolymerisations were performed using the unsupported complexes rather than their immobilised analogues. Indeed, while activities obtained in slurry-phase remained constant across the range of temperatures, solution-phase polymerisations exhibited two activity maxima at 60 and 80 °C (848 and 825 $kg_{polymer}/mol_{Ti}/h/bar$ with catalyst **1** respectively). Seppälä and co-workers described the same trend for ethylene/styrene copolymerisations by $CpTiCl_3$ in the presence of MAO.[94] By varying the reaction

temperature between 10 and 90 °C, they measured a maximal activity at 30 °C and a minimum at 70 °C before an increase for higher temperatures. The increase in yield from 70 °C was explained by the higher polymer solubility that revealed catalytic active sites and enabled monomers to access them.[94]

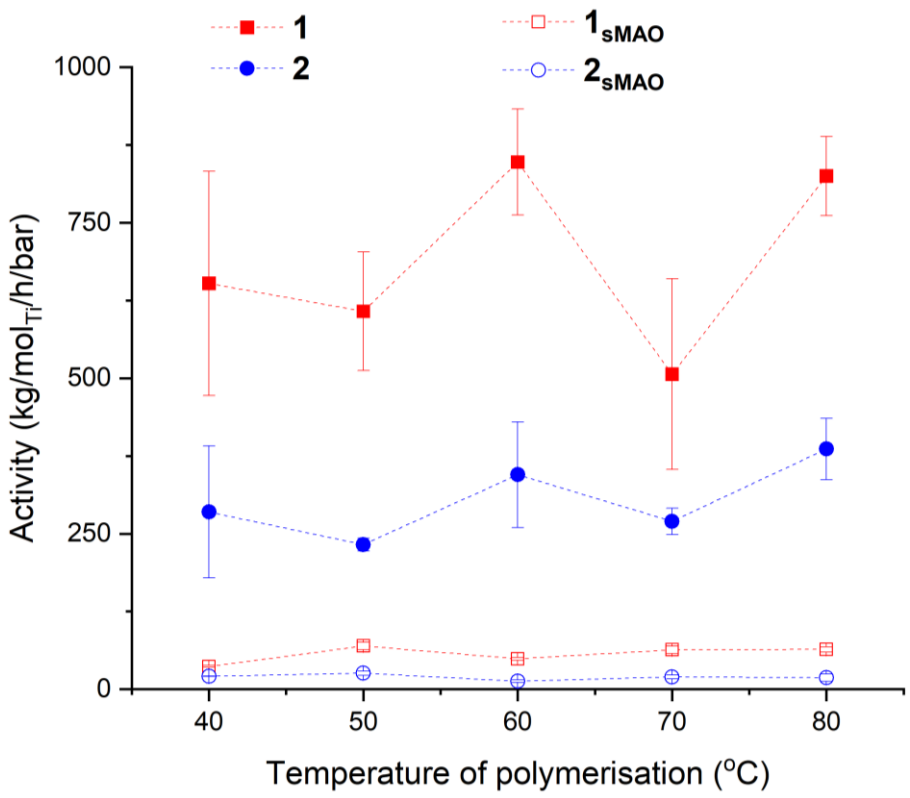

Figure 2.22. Temperature dependence of solution and slurry-phase ethylene/styrene copolymerisation activity of Cp*$TiCl_3$ (red) and Pn*(H)$TiCl_3$ (blue). Polymerisation conditions: 30 minutes, 1000 rpm, 2 bar of ethylene, 50 mL hexane, 125 µL styrene, 150 mg TiBA. Solution-phase: 2×10^{-7} mol catalyst, $[Al_{MAO}]_0$:$[Ti]_0$ = 1500:1. Slurry: 10 mg catalyst, $[Al_{sMAO}]_0$:$[Ti]_0$ = 200:1.

Catalysts **1** and **2** displayed two different activity profiles with increasing temperatures for copolymerisation relative to the results reported previously for homopolymerisation. Homopolymerisations using **2** led to better activities than ethylene/styrene copolymerisations while the homopolymerisation using **1** led to a lower activity than the copolymerisation except at 40 °C (923 *vs.* 653 $kg_{polymer}/mol_{Ti}/h/bar$).

In the slurry-phase, the copolymerisation using complex **1$_{sMAO}$** exhibited higher activities than **2$_{sMAO}$**. Both supported complexes performed the best at 50 °C (69 and 26 $kg_{polymer}/mol_{Ti}/h/bar$ for **1$_{sMAO}$** and **2$_{sMAO}$**) but the activity profiles remained relatively constant across the temperature range. Kang *et al.* reported a different trend for copolymerisation activities using $CpTiCl_3$ suported on $MgCl_2$ with MAO.[95] They measured an increase in activity between 20 and 60 °C followed by a decline from 1.07×10^3 $kg_{polymer}/mol_{Ti}/h/bar$ at 60 °C to 0.05×10^3 $kg_{polymer}/mol_{Ti}/h/bar$ at 100 °C in the presence of 0.146 mol of styrene under 2 bar of ethylene. Furthermore, they observed that the composition of the products varied significantly with polymerisation temperatures.

Polymer fouling was observed for the solution-phase copolymerisations (Figure 2.23). It may be caused by the formation of hot spots in the system as the heat generated during the exothermic polymerisation was not effectively removed from the growing polymer. This phenomenon would result in softened polymer particles and fouling.[46] No fouling happened during slurry-phase experiments which is the clear advantage of the supported systems. Many reports describe the absence of fouling when the polymerisation catalyst is immobilised on a solid support.[27,96–98]



Figure 2.23. Fouling from a solution-phase copolymerisation of ethylene with styrene.

2.4.3 Effect of the styrene comonomer concentration

Polymerisations were conducted with five different volumes of styrene at 40 °C (500, 250, 125, 62.5 and 0 µL), using complexes **1**, **2**, **1**$_{sMAO}$ and **2**$_{sMAO}$ (Figure 2.24).

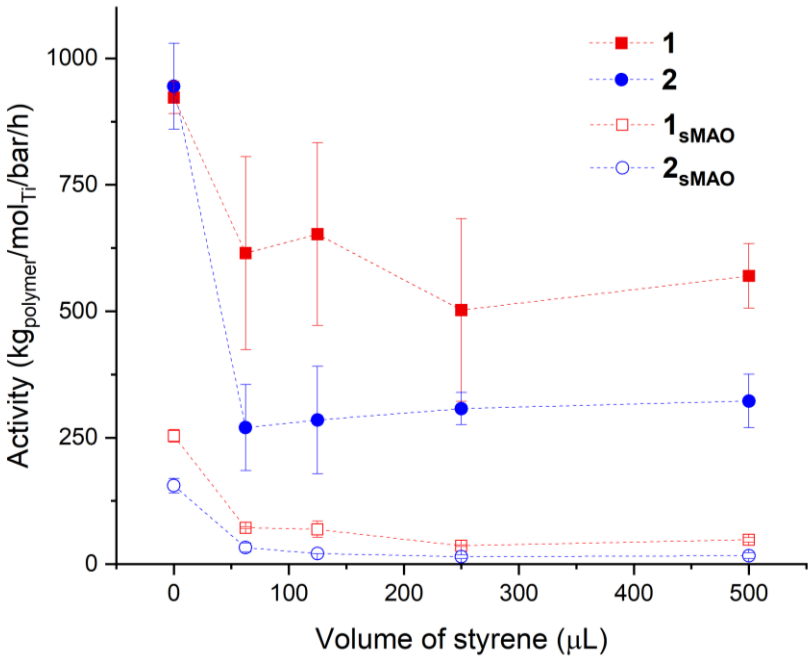

Figure 2.24. Styrene volume dependence of solution and slurry-phase ethylene/styrene copolymerisation activity of Cp*TiCl$_3$ (red) and Pn*(H)TiCl$_3$ (blue). Polymerisation conditions: 30 minutes, 1000 rpm, 2 bar of ethylene, 50 mL hexane, 40 °C, 150 mg TiBA. Solution-phase: 2×10^{-7} mol catalyst, $[Al_{MAO}]_0$:$[Ti]_0$ = 1500:1. Slurry: 10 mg catalyst, $[Al_{sMAO}]_0$:$[Ti]_0$ = 200:1.

As expected, solution-phase polymerisation activities were greater than in slurry-phase for the two complexes (12 and 19 times for **1** and **2** with 500 µL of styrene). As can be seen in Figure 2.24, as well in the ethylene uptake rate plots (Figure A2.14–17), the catalytic activity of all species was lower for copolymerisation than that for homopolymerisation of ethylene. The decrease in activity after addition of 62.5 µL of styrene was more significant in solution-phase (from 945 to 270 $kg_{polymer}/mol_{Ti}$/bar/h for **2** and from 155 to 33 $kg_{polymer}/mol_{Ti}$/bar/h for **2**$_{sMAO}$). Addition of styrene caused a negative comonomer effect. The phenomenon has been largely reported for ethylene/α-olefin copolymerisation.[99,100] Chien and co-workers observed a negative effect in the

homogeneous copolymerisation of ethylene with 1-hexene using metallocene Cp_2ZrCl_2 and MAO.[100] They suggested that the second monomer, hexene, competed against ethylene in the complexation with the catalyst, reducing the rate of polymerisation. Negative comonomer effects can also be explained by a higher energy barrier of comonomer insertion, which would reduce the activity. Theoretical studies have confirmed that the activation barrier for styrene to insert into a polyethylene-coordinated metal centre is higher than that of ethylene insertion (8 *vs.* 4.7 kcal/mol).[101,102] sMAO-supported permethylindenyl complexes also achieved a negative comonomer effect in the copolymerisation of ethylene with styrene. Decline from 4380 to 728 $kg_{polyme}/mol_{Ti}/h/bar$, an 83% decrease, was observed for the CGC catalyst sMAO-^{Me_2}SB($^{t\text{Bu}}$N,I*)Ti($CH_2Ph)_2$.[103] Conversely, Noh *et al.* described a positive comonomer effect with trichloride catalysts $CpTiCl_3$ and $IndTiCl_3$, indicating the dependence of the copolymerisation on the comonomer and the nature of the catalyst. The latter performed 6 times better after addition of 0.35 mol/L of styrene reaching 42.0 $kg_{polymer}$/molTi/h compared to 7.2 $kg_{polymer}$/molTi/h in the absence of styrene.[104]

The solution-phase activities obtained using catalysts **1** and **2** were significantly higher than those described by Waymouth *et al.* using $CpTiCl_2L$ (L = Cl or 2,2,6,6-tetramethylpiperidine-*N*-oxyl).[105] At 120 °C in toluene, they reported that $CpTiCl_3$ achieved 25 $kg_{polymer/}mol_{Ti}$/bar/h after addition of 11 mL of styrene co-monomer. Conversely, 5 mL of styrene enabled aryloxide catalyst (1,3-Me-C_5H_3)$TiCl_2$(O-2,6-^{i}Pr-C_6H_3) to copolymerise ethylene and styrene under 4 bars and reached 1070 $kg_{polymer/}mol_{Ti}$/bar/h.[21]

2.4.4 Polymer characterisation

The copolymer samples did not dissolve well in 1,2,4-trichlorobenzene at 150 °C which made characterisation by GPC difficult (Table A2.13). When measurements were possible, high molecular weights were obtained (2.13×10^6 g/mol for **1$_{sMAO}$** at 40°C with 125 µL styrene). Waymouth and Son previously observed a decrease in polymer molecular weights with increased addition of styrene with a $(C_5H_4CH_2CH_2N(CH_3)_2)TiCl_3$/MAO system under 0.34 bar of ethylene (from 118×10^3 g/mol with 20 g of styrene to 94×10^3 g/mol with 10 g of styrene).[106] In slurry-phase, CGC permethylindenyl complexes supported on sMAO achieved the same evolution; for example, sMAO-^{Me2}SB(^{tBu}N,I*)TiCl$_2$ produced copolymers of $M_w = 333\times10^3$ g/mol with 156 µL of styrene and $M_w = 178\times10^3$ g/mol with 625 µL of styrene.[103]

The polymer melt temperatures were measured by DSC for the copolymers produced and all presented only one crystallisation peak and one melting peak (Figure 2.25, Table A2.14). Variations of the polymerisation temperature had little to no effect on the T_m which were very similar to the ones obtained for ethylene homopolymerisation in section 2.3.2. Increasing the concentration of styrene decreased the melting temperatures of the polymers produced by complexes **1** and **1$_{sMAO}$** (132.5 °C *vs.* 128.0 °C with 62.5 and 500 µL styrene at 40 °C). The opposite trend was observed for **2$_{sMAO}$** with an increase from 129.0 °C to 136.3 °C with 62.5 and 500 µL of styrene respectively. It was expected that styrene incorporation would decrease the melting temperature as observed for CGC Cp* complex ^{Me2}SB(^{tBu}N,Cp*)TiCl$_2$ where addition of 625 µL of styrene resulted in 3.8% styrene incorporation and a decrease from T_m = 134 °C without styrene to 98 °C after addition of the second monomer.[103] Noh and co-workers reported significant decrease in

melting temperatures from 132 °C to 126 °C after addition of 0.35 mol/L of styrene using $CpTiCl_3$.[104] The absence of significant decrease reported for complexes **1**, **2**, $\mathbf{1}_{sMAO}$ and $\mathbf{2}_{sMAO}$ suggested that little to no styrene was incorporated in the polymer. XRD analysis confirmed the low incorporation of styrene (Figure 2.26). Signals at 21.53° and 23.94° corresponding to the (110) and the (200) peaks were observed and the pattern was very similar to the one measured for polyethylene in section 2.3.2. The absence of amorphous halo on the XRD pattern was consistent with the hypothesis of low incorporation of styrene.

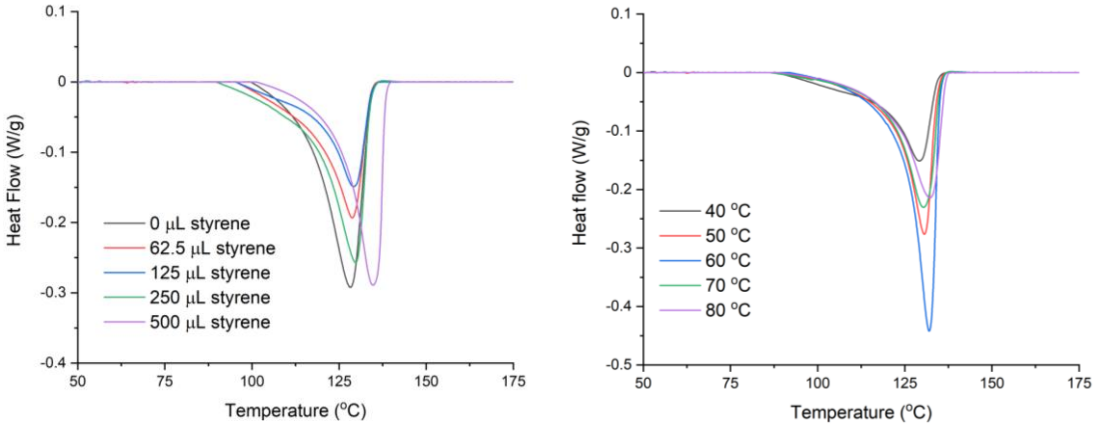

Figure 2.25. DSC plots of copolymers produced by Pn^*TiCl_3 (**2**). Polymerisation conditions: 150 mg of TiBA, 2 bar ethylene, 1000 rpm, 50 mL of hexane, 0.2 µmol of catalyst, $[Al_{MAO}]_0$:$[Ti]_0$ = 1500:1, 10 minutes. Left: 40 °C, Right: 125 µL styrene.

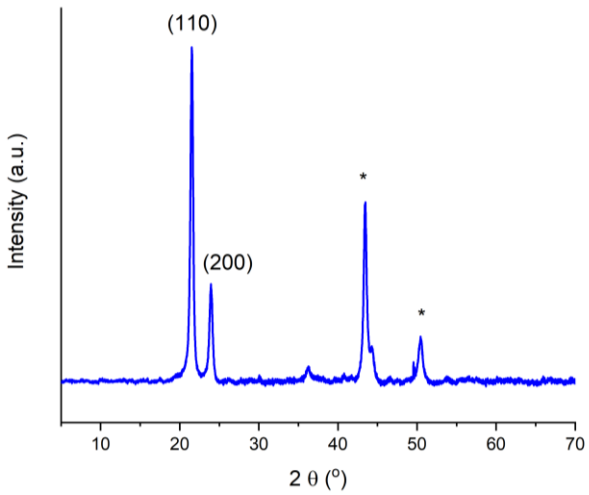

Figure 2.26. XRD pattern of the copolymer produced by **2**$_{sMAO}$ at 40 °C with 250 µL of styrene.

High temperature $^{13}C\{^{1}H\}$ NMR spectroscopy was performed to determine the levels of styrene incorporation with resonances attributed by comparison with literature values (Figure A2.39).[21,105,107] Resonances corresponding to styrene were detected at 101.1, 125.2, 129.7 and 147.2 ppm. The signal to noise ratio, however, was too low to be able to quantify the amount of styrene incorporated in the copolymer, confirming that the majority of the chains formed consisted in ethylene monomer enchainments. Known cyclopentadienyl catalysts $Cp^{R}TiCl_2(O\text{-}2,6\text{-}^{i}Pr\text{-}C_6H_3)$ (Cp^{R} = $^{t}BuC_5H_4$, 1,3-Me-C_5H_3, 1,2,3-Me-C_5H_2, 1,2,4-Me-C_5H_2) reached high styrene molar incorporation (< 24%). (1,2,4-Me-C_5H_2)$TiCl_2(O\text{-}2,6\text{-}^{i}Pr\text{-}C_6H_3)$ produced copolymers with 54.8 mol% styrene, indicating the benefit of incorporation of an aryloxide substituent.[11] Okuda *et al.* reported that styrene molar content increased with addition of increasing amount of styrene, reaching 68% after injection of 7.9 mol/L styrene for copolymers produced by bis(phenolato)titanium catalyst in the presence of MAO.[20]

SEM images showed the improvement in polymer morphology due to immobilisation of the catalyst on a solid support (Figure 2.27). In solution-phase, the copolymer formed large elongated aggregates of 500 µm width. In a similar manner to copolymerisation using CGC permethylindenyl catalysts, replication of the sMAO support was observed in slurry-phase where popcorn-shaped particles were formed with a diameter of 5 µm, which is approximately half of what was reported for polyethylene particles in section 2.3.2.[35,103] This observation correlates with the lower activity measured for copolymerisation compared to ethylene homopolymerisation using catalysts $\mathbf{1}_{\mathbf{sMAO}}$ and $\mathbf{2}_{\mathbf{sMAO}}$ (~ 8 times lower).

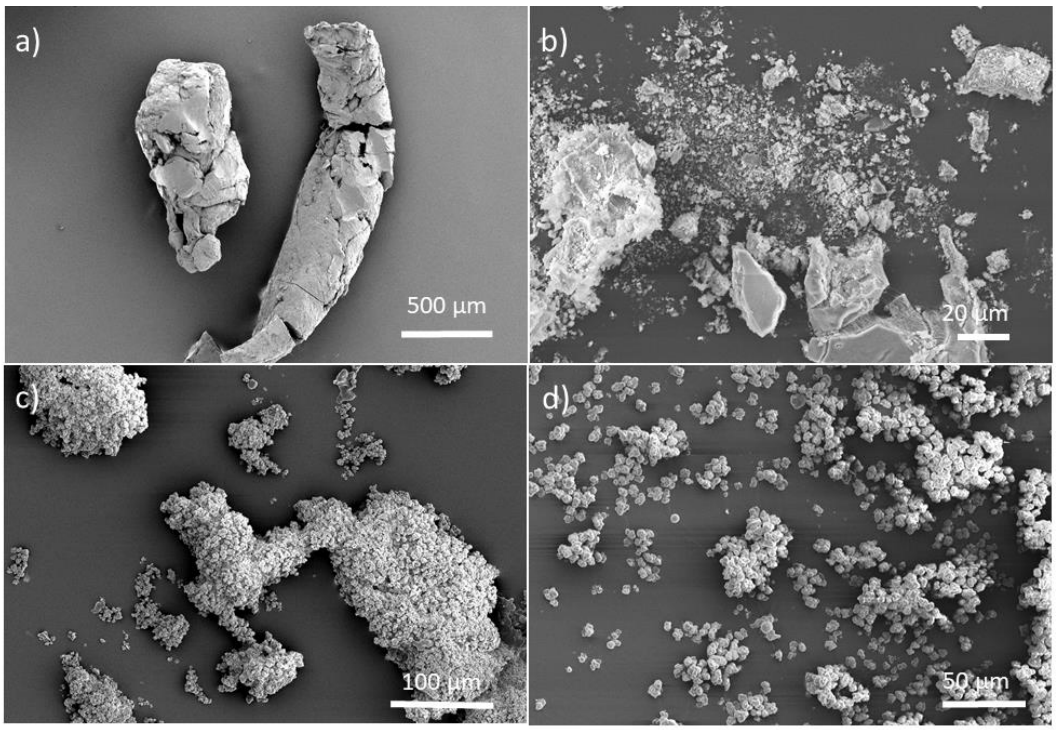

Figure 2.27. SEM images of ethylene/styrene copolymers synthesised at 40 °C using 125 µL of styrene with a) Cp*$TiCl_3$ (**1**) (x250), b) Pn*(H)$TiCl_3$ (**2**) (x400), c) sMAO-Cp*$TiCl_3$ ($\mathbf{1}_{\mathbf{sMAO}}$) (x45), d) sMAO-Pn*(H)$TiCl_3$ ($\mathbf{2}_{\mathbf{sMAO}}$) (x600).

2.5 Conclusion

Two titanium complexes Cp^*TiCl_3 and $Pn^*(H)TiCl_3$ were investigated for their olefin polymerisation properties. Investigation of the optimum $[Al_{MAO}]_0$:$[Ti]_0$ showed that high amount of MAO were necessary to obtain high styrene homopolymerisation activities. The solvent dependence has been investigated, revealing that toluene led to the highest polymerisation activities. Solution and slurry phase polymerisations of styrene have been performed using the complexes Cp^*TiCl_3 and $Pn^*(H)TiCl_3$. The latter supported of sMAO gives the highest recorded activity (up to 7432 $kg_{PS}/mol_{Ti}/h$). The two catalysts achieved high activities compared to those measured for Cp^*TiCl_3 and 1,2,4-Me-$C_5H_3TiCl_3$ in solution phase, but Nomura and co-workers reported better catalysts for the syndiotactic polymerisation of styrene, such as $CpTiCl_3$ and aryloxide 1,2,4-Me-$C_5H_3TiCl_2$(O-2,6-^{i}Pr-C_6H_3).[11] DSC profiles of the polystyrene as well as NMR spectroscopy established the atactic nature of the polymers.

The four catalysts **1**, **2**, $\mathbf{1_{sMAO}}$ and $\mathbf{2_{sMAO}}$ have been tested for the polymerisation of ethylene. Solution-phase activities were up to 4 times higher than slurry-phase activities and were shown to decrease with temperature, $Pn^*(H)TiCl_3$ achieving higher activities than the cyclopentadienyl analogue above 50 °C. The two supported complexes displayed little to no variation with polymerisation temperature.

Copolymerisations of ethylene with styrene have been performed using complexes **1**, **2**, $\mathbf{1_{sMAO}}$ and $\mathbf{2_{sMAO}}$, resulting in low activities in contrast to piano-stool aryloxide complexes developed by Nomura *et al*.[21] The solvent dependence has been investigated, revealing that toluene and hexane lead to the highest polymerisation activities. The styrene volume dependence showed that there was a negative comonomer effect, with the copolymerisation activity decreasing when the styrene content was increased. The

copolymerisaiton temperature was showed to have a significant influence on solution-phase activities with Cp^*TiCl_3 displaying a maximum of 848 $kg_{polymer}/mol_{Ti}/h/bar$ at 60 °C. Minimal incorporation of styrene were observed by NMR spectroscopy and DSC.

2.6 References

1 A. Tossavainen, *Scand. J. Work. Environ. Heal.*, 1978, **4**, 7–13.

2 M. Mobed-Miremadi, D. Grandio and J. Kunkel, in *Wound Healing Biomaterials*, Elsevier Inc., 2016, vol. 2, pp. 309–334.

3 C.-L. Huang, Y.-C. Chen, T.-J. Hsiao, J.-C. Tsai and C. Wang, *Macromolecules*, 2011, **44**, 6155–6161.

4 N. Ishihara, T. Seimiya, M. Kuramoto and M. Uoi, *Macromolecules*, 1986, **19**, 2464–2465.

5 N. Tomotsu, N. Ishihara, T. H. Newman and M. T. Malanga, *J. Mol. Catal. A Chem.*, 1998, **128**, 167–190.

6 T. E. Ready, J. C. W. Chien and M. D. Rausch, *J. Organomet. Chem.*, 1996, **519**, 21–28.

7 Y. Kim, B. H. Koo and Y. Do, *J. Organomet. Chem.*, 1997, **527**, 155–161.

8 M. Masnadi, R. Jamjah, S. Ahmadjo and M. Nekoomanesh, *Synth. React. Inorganic, Met. Nano-Metal Chem.*, 2006, **36**, 543–547.

9 G. Xu and E. Ruckenstein, *J. Polym. Sci. Part A Polym. Chem.*, 1999, **37**, 2481–2488.

10 X. Qian, J. Huang, Y. Qian and C. Wang, *Appl. Organomet. Chem.*, 2003, **17**, 277–281.

11 J. B. Doo, A. Fudo, A. Tanaka, M. Fujiki and K. Nomura, *Macromolecules*, 2004, **37**, 5520–5530.

12 K. Nomura, N. Naga, M. Miki, K. Yanagi and A. Imai, *Organometallics*, 1998, **17**, 2152–2154.

13 K. Nomura, T. Komatsu and I. Yukio, *Macromolecules*, 2000, **33**, 8122–8124.

14 K. Nomura, K. Oya, T. Komatsu and Y. Imanishi, *Macromolecules*, 2000, **33**, 3187–3189.

15 N. Galdi, A. Buonerba and L. Oliva, *Polymers*, 2016, **8**, 405–417.

16 K. Soga, D. ho Lee and H. Yanagihara, *Polym. Bull.*, 1988, **20**, 237–241.

17 L. Oliva, S. Mazza and P. Longo, *Macromol. Chem. Phys.*, 1996, **197**, 3115–3122.

18 P. Longo, A. Grassi and L. Oliva, *Die Makromol. Chemie*, 1990, **191**, 2387–2396.

19 D. H. Lamparelli, V. Speranza, I. Camurati, A. Buonerba and L. Oliva, *Polymers*,

2019, **11**, 698–709.

20 C. Capacchione, A. Proto, H. Ebeling, R. Mülhaupt and J. Okuda, *Polym. Chem.*, 2006, **44**, 1908–1913.

21 N. Kotohiro, H. Okumura, T. Komatsu and N. Naga, *Macromolecules*, 2002, **35**, 5388–5395.

22 G. Xu and D. Cheng, *Macromolecules*, 2000, **33**, 2825–2831.

23 Q. Huang, Y. Sheng and W. Yang, *J Appl Polym Sci*, 2007, **103**, 501–505.

24 B. Huang, K. Cao, B. G. Li and S. Zhu, *J. Appl. Polym. Sci.*, 2004, **94**, 1449–1455.

25 Z. R. Turner, J.-C. Buffet and D. O'Hare, *Organometallics*, 2014, **33**, 3891–3903.

26 N. Ishihara, M. Kuramoto and M. Uoi, *Macromolecules*, 1988, **21**, 3356–3360.

27 J. R. Severn and J. C. Chadwick, *Tailor-made polymers : via immobilization of alpha-olefin polymerization catalysts*, Wiley-VCH, 2008.

28 W. Kaminsky and R. Steiger, *Polyhedron*, 1988, **7**, 2375–2381.

29 W. J. Gauthier, J. F. Corrigan, N. J. Taylor and S. Collins, *Macromolecules*, 1995, **28**, 3771–3778.

30 C. Janiak, U. Versteeg, K. C. H. Lange, R. Weimann and E. Hahn, *J. Organomet. Chem.*, 1995, **501**, 219–234.

31 W. Kaminsky and H. Sinn, *Adv. Polym. Sci.*, 2013, **258**, 1–28.

32 S. Srinivasa Reddy, K. Radhakrishnan and S. Sivaram, *Polym. Bull.*, 1996, **36**, 165–171.

33 T. J. Williams, J. C. Buffet, Z. R. Turner and D. O'Hare, *Catal. Sci. Technol.*, 2018, **8**, 5454–5461.

34 J. V. Lamb, J. C. Abell, J. E. McLaren, J. C. Buffet, Z. R. Turner and D. O'Hare, *Mol. Catal.*, 2019, **484**, 110735.

35 J. C. Buffet, Z. R. Turner and D. O'Hare, *Chem. Commun.*, 2018, **54**, 10970–10973.

36 A. F. R. R. Kilpatrick, J.-C. C. Buffet, P. Nørby, N. H. Rees, N. P. Funnell, S. Sripothongnak, D. O'Hare and D. O'Hare, *Chem. Mater.*, 2016, **28**, 7444–7450.

37 L. Resconi, S. Bossi and L. Abis, *Macromolecules*, 1990, **23**, 4489–4491.

38 S. Koltzenburg, *J. Mol. Catal. A Chem.*, 1997, **116**, 355–363.

39 J. Chirinos, T. Rajmankina, A. Parada and F. Ciardelli, *Macromol. Chem. Phys.*,

2000, **201**, 2581–2585.

40 A. Morillo, J. Chirinos, T. Rajmankina, D. Ibarra, J. Arevalo and A. Parada, *J. Chem. Res.*, 2003, **2003**, 238–239.

41 D. M. Sarzotti, D. J. Marshman, W. E. Ripmeester and J. B. P. Soares, *J. Polym. Sci. Part A Polym. Chem.*, 2007, **45**, 1677–1690.

42 V. Volkis, E. Smolensky, A. Lisovskii and M. S. Eisen, *Polym. Chem.*, 2005, **43**, 4505–4516.

43 S. H. Yang, J. Huh and W. H. Jo, *Macromolecules*, 2005, **38**, 1402–1409.

44 T. Tanaka, T. Tokuzumi and K. Iwachido, *Kobunshi Kagaku*, 1969, **26**, 566–574.

45 D. A. Fraser, University of Oxford, DPhil Thesis, 2018.

46 J. R. Severn, J. C. Chadwick, R. Duchateau and N. Friederichs, *Chem. Phys. Lett.*, 2005, **105**, 4073–4147.

47 E. Kai and E. Yoshioka, WO2010055652, 2010.

48 D. A. X. Fraser, Z. R. Turner, J.-C. Buffet and D. O'Hare, *Organometallics*, 2016, **35**, 2664–2674.

49 P. Angpanitcharoen, G. Hay, J.-C. Buffet, Z. R. Turner, T. A. Q. Arnold and D. O'Hare, *Polyhedron*, 2016, **116**, 216–222.

50 J. Liu, H. Ma, J. Huang and Y. Qian, *Eur. Polym. J.*, 2000, **36**, 2055–2058.

51 M. Jaymand, *Polym. Chem.*, 2014, **5**, 2663–2690.

52 A. J. Pasztor, B. G. Landes and P. J. Karjala, *Thermochim. Acta*, 1991, **177**, 187–195.

53 J. Rieger, *J. Therm. Anal.*, 1996, **46**, 965–972.

54 L. Aras and M. J. Richardson, *Polymer*, 1989, **30**, 2246–2252.

55 J. G. Lim, J. H. Baïk, X. Q. Zhang, Y. Son, W. M. Choi and O. O. Park, *Polym. Bull.*, 2002, **48**, 397–405.

56 Y. Gao and H.-M. Li, *Polym. Int.*, 2004, **53**, 1436–1441.

57 Z. Yuan, R. Song and D. Shen, *Polym. Int.*, 2000, **49**, 1377–1382.

58 T. Liu and J. Petermann, *Polymer*, 2001, **42**, 6453–6461.

59 T. Liu, S. Yan, M. Bonnet, I. Lieberwirth, K.-D. Rogausch and J. Petermann, *J. Mater. Sci.*, 2000, **35**, 5047–5055.

60 K. Grigoriadi, J. B. H. M. Westrik, G. G. Vogiatzis, L. C. A. Van Breemen, P. D. Anderson and M. Hütter, *Macromolecules*, 2019, **52**, 5948–5954.

61 N. Brun, P. Bourson, S. Margueron and M. Duc, *AIP Conf. Proc.*, 2011, **1353**, 856–861.

62 J. Zhao and Q. Fan, *Polym. Bull.*, 2001, **47**, 91–97.

63 V. Abhilash, N. Rajender and K. Suresh, in *Spectroscopy of Polymer Nanocomposites*, Elsevier Inc., 2016, pp. 410–451.

64 W. Zhu, Y. Wu, C. Yan, C. Wang, M. Zhang and Z. Wu, *Materials*, 2013, **6**, 5625–5638.

65 H. N. Cheng and G. H. Lee, *Int. J. Polym. Anal. Charact.*, 1996, **2**, 439–455.

66 J. C. Randall, *J. Polym. Sci. Polym. Phys. Ed.*, 1975, **13**, 889–899.

67 H. Sato, Y. Tanaka and K. Hatada, *J. Polym. Sci. Polym. Phys. Ed.*, 1983, **21**, 1667–1674.

68 F. Feil and S. Harder, *Macromolecules*, 2003, **36**, 3446–3448.

69 J. H. Yim, K. J. Chu, K. W. Choi and S. K. Ihm, *Eur. Polym. J.*, 1996, **32**, 1381–1385.

70 J. Schellenberg, *Prog. Polym. Sci.*, 2009, **34**, 688–718.

71 A. Entezami, M. Agaalipour and P. N. Moghaddam, *J. Iran. Chem. Soc.*, 2005, **2**, 149–154.

72 D. Liu, S. Lin, F. Zhu, H. Gao and Q. Wu, *Polym. Bull.*, 2008, **61**, 71–80.

73 G. J. P. Britovsek, V. C. Gibson and D. F. Wass, *Angew. Chem. Int. Ed.*, 1999, **38**, 428–447.

74 T. P. Zhuze and A. S. Zhurba, *Russ. Chem. Bull.*, 1960, **9**, 335–337.

75 K. Nomura, N. Naga, M. Miki and K. Yanagi, *Macromolecules*, 1998, **31**, 7588–7597.

76 J. C. W. Chien, *J. Polym. Sci. Polym. Chem. Ed.*, 1979, **17**, 2555–2565.

77 P. Unruean, W. Apisuk, Y. Kawabata, T. Murayama, B. Kitiyanan and K. Nomura, *Mol. Catal.*, 2019, **475**, 110490.

78 K. Nomura, K. Fujita and M. Fujiki, *Catal. Commun.*, 2004, **5**, 413–417.

79 D. Li, L. Zhou, X. Wang, L. He and X. Yang, *Materials*, 2019, **12**, 1746.

80 R. B. Richards, *J. Appl. Chem.*, 2007, **1**, 370–376.

81 L. H. Tung and S. Buckser, *J. Phys. Chem.*, 1959, **62**, 1530–1534.

82 M. A. Parvez, M. Rahaman, M. A. Suleiman, J. B. P. Soares and I. A. Hussein, *Int. J. Polym. Sci.*, 2014, **2014**, 549031.

83 A. A. Alsaygh, J. Al-hamidi, F. D. Alsewailem, I. M. Al-Najjar and V. L. Kuznetsov, *Appl. Petrochemical Res.*, 2014, **4**, 79–84.

84 M. Laridjani and P. Leboucher, *PLoS One*, 2009, **4**, e6228.

85 W. R. Busing, *Macromolecules*, 1990, **23**, 4608–4610.

86 *Physical Properties of Polymers Handbook*, Springer New York, 2007.

87 P. Kenyon, M. Wörner and S. Mecking, *J. Am. Chem. Soc.*, 2018, **140**, 6685–6689.

88 T. Wiedemann, G. Voit, A. Tchernook, P. Roesle, I. Göttker-Schnetmann and S. Mecking, *J. Am. Chem. Soc.*, 2014, **136**, 2078–2085.

89 G. W. Theaker, C. Morton and P. Scott, *Dalton Trans.*, 2008, 6883–6885.

90 L. Contat-Rodrigo, A. Ribes-Greus and C. T. Imrie, *J. Appl. Polym. Sci.*, 2002, **86**, 764–772.

91 S. Kumar and R. K. Singh, *J. Pet. Eng.*, 2013, **2013**, 1–7.

92 F. Carrasco and P. Pagès, *J. Appl. Polym. Sci.*, 1996, **61**, 187–197.

93 B. V. Kokta, J. L. Valade and W. N. Martin, *J. Appl. Polym. Sci.*, 1973, **17**, 1–19.

94 P. Aaltonen and J. Seppälä, *Eur. Polym. J.*, 1995, **31**, 79–83.

95 K. K. Kang, J.-K. Oh, Y.-T. Jeong, T. Shiono and T. Ikeda, *Macromol. Chem. Phys.*, 2000, **201**, 846–850.

96 A. Entezami and P. Najafi Moghadam, *Polym. Int.*, 2005, **54**, 1326–1329.

97 J. R. Severn and J. C. Chadwick, *Macromol. Chem. Phys.*, 2004, **205**, 1987–1994.

98 G. G. Hlatky, *Chem. Rev.*, 2000, **100**, 1347–1376.

99 T. J. Williams, J. V. Lamb, J. C. Buffet, T. Khamnaen and D. O'Hare, *RSC Adv.*, 2021, **11**, 5644–5650.

100 J. C. W. W. Chien and T. Nozaki, *J. Polym. Sci. Part A Polym. Chem.*, 1993, **31**, 227–237.

101 J. Yi, N. Nakatani, N. Tomotsu, K. Nomura and M. Hada, *Organometallics*, 2021, **40**, 643–653.

102 A. Muoz-Escalona, V. Cruz, N. Mena, S. Martínez and J. Martinez-Salazar,

Polymer, 2002, **43**, 7017–7026.

103 T. J. Williams, University of Oxford, DPhil Thesis, 2020.

104 D.-H. Lee, K.-B. Yoon, H.-J. Kim, S.-S. Woo and S. K. Noh, *J. Appl. Polym. Sci.*, 1998, **67**, 2187–2198.

105 K. S. Son, F. Jöge and R. M. Waymouth, *Macromolecules*, 2008, **41**, 9663–9668.

106 K.-S. Son and R. M. Waymouth, *J. Polym. Sci. Part A Polym. Chem.*, 2010, **48**, 1579–1585.

107 H. Zhang, D.-J. Byun and K. Nomura, *Dalton Trans.*, 2007, 1802–1806.

Chapter Three
Polymerisation of Polar Styrene Monomers

3.1 Introduction

Recently, efforts have been focused on homopolymerisation and copolymerisation of substituted styrenes with the aim of improving polymer properties.[1,2] Substituents play an important role in polymerisation of vinyl monomers because the mechanism is dependent on the electronic and steric properties of the pendant groups. Indeed, the electron density of the vinyl group is modified through resonance and inductive effects.[3] The polymerisation of functionalised styrene monomers leads to new materials with different chemical and physical properties than polystyrene such as melting temperature or Young's modulus.[4] Although many examples of radical and ionic polymerisation of substituted styrene monomers are reported, the use of coordination complexes for the polymerisation of functionalised styrene remains poorly explored.[5] The incorporation of functionalised styrene in insertion-coordination copolymerisation with other α-olefins has since emerged as a promising route to improve polymer properties.

In 1996, Cardi *et al.* used $Ti(OEt)_4$ to copolymerise styrene with *para*-methylstyrene.[6] They reported lower melting and crystallisation temperatures for the copolymer compared to the styrene homopolymer (< 245 °C and 265 °C respectively). Grassi and co-workers observed that the polymerisation activity was enhanced when the ring-

substituent had an inductive donor +I effect, and they established that the polymer stereoregularity was strongly influenced by the styrene substituent.[7] More recently, Schwecke and Kaminsky have been using $CpTiF_3$/MAO systems for the copolymerisation of styrene with *para*-Me-, *para*-^{t}Bu- and *ortho*-Me-styrene.[8] They observed a reduction in melting temperature by 40 °C when small amounts of ^{t}Bu-styrene are incorporated whereas 20% of *para*-Me-styrene were needed to lower the styrene/*para*-Me-styrene copolymer melting point by 60 °C, which facilitated processing of these polymers. Rabagliati and co-workers have extensively investigated the solution phase polymerisation and copolymerisation of substituted styrenes by $CpTiCl_3$ in the presence of diphenylzinc.[9–12] They observed that the inductive effect of *para* substituents influence the polymerisation activity of $CpTiCl_3$ as well as the glass transition and melting temperatures.[13] As well as producing new materials with interesting and tunable properties, polymerisation of functionalised styrene opens the field of post-polymerisation modification and allows the synthesis of polymers which are difficult to obtain otherwise.[14–18]

This chapter describes the polymerisation of *para*-substituted styrene monomers. First, solution and slurry-phase homopolymerisations of three *para*-substituted styrene monomers were reported using Cp^*TiCl_3 and $Pn^*(H)TiCl_3$. The influence of the electronic properties of the substituents was investigated. The catalytic behaviour of the two titanium trichloride compounds towards slurry-phase copolymerisations of ethylene with *para*-substituted styrene was then studied using 4-NR_2-styrene (R = H or Me). The effect of the amino group, polymerisation temperature and concentration of polar monomer were also explored. The polymers produced were characterised by NMR and IR spectroscopy, DSC and GPC.

3.2 Homopolymerisation of substituted styrene monomers

Over the last 20 years, research has leaned towards the development of new polymers with tunable properties, such as *para*-substituted polystyrenes. While many group 3 catalysts have been reported,[19–21] example of titanium catalysts remain scarce. In 2006, Proto *et al.* described the polymerisation of alkyl- and halogeno-substituted styrene using dichloro[1,4-dithiabutanediyl-2,2′-bis(4,6-di-*tert*-butyl-phenoxy)]titanium activated by methylaluminoxane.[22] More recently, Rabagliati and co-workers extensively studied $CpTiCl_3$ and derivatives for the successful polymerisation of *para*-functionalised styrene.[9,12,23]

Improving the chemical and physical properties of polystyrene such as compatibility with other polymers and surface properties is possible by introducing functional groups.[24–26] Specific properties can be obtained by tuning the functional groups and their position on the aromatic ring. For this purpose, three *para*-substituted styrenes, 4-methoxystyrene, 4-aminostyrene and 4-bromostyrene, were investigated as monomers in solution and slurry phase polymerisation by Cp^*TiCl_3 (**1**), $Pn^*(H)TiCl_3$ (**2**) and their sMAO-immobilised analogues (**1**$_{\mathbf{sMAO}}$ and **2**$_{\mathbf{sMAO}}$).

No control experiment in the absence of titanium species has been performed. Nevertheless, homopolymerisation of styrene in the only presence of MAO and TiBA resulted in extremely low activities (< 1 $kg_{PS}/mol_{Ti}/h$) (Appendix Table A.2.1), so it is hypothesised that the titanium catalysts were responsible for the high activities described below.

3.2.1. Influence of temperature

The homopolymerisation reactions yielded polystyrenes with different appearances depending on the *para*-substituent (Figure 3.1).

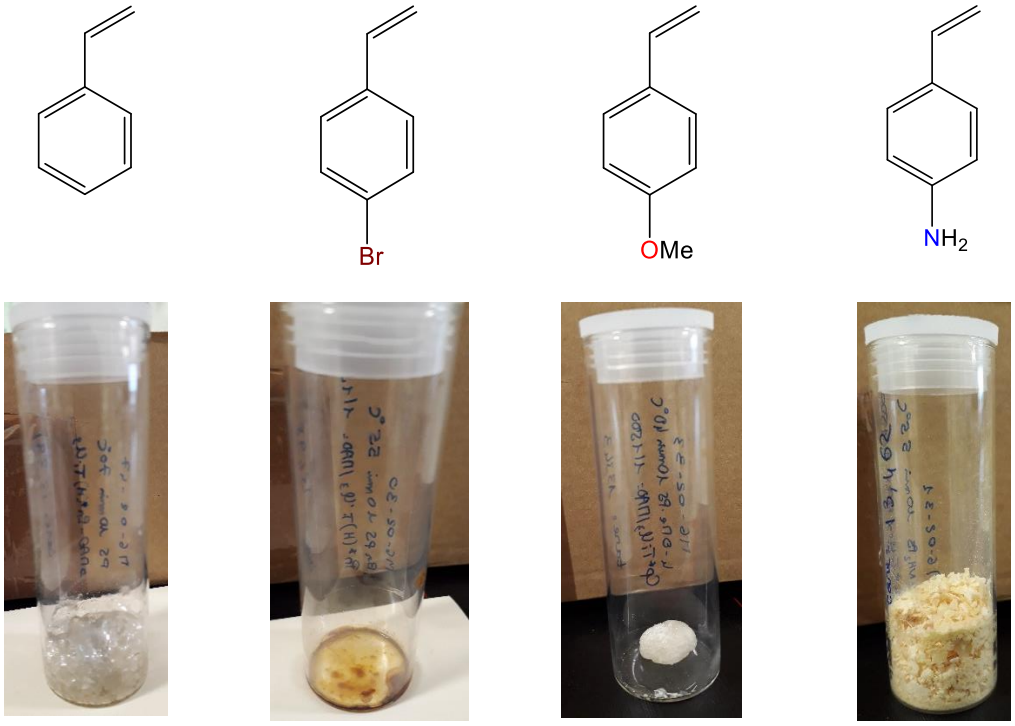

Figure 3.1. Aspects of all polystyrenes. From left to right: polystyrene, poly(4-bromo-styrene), poly(4-methoxy-styrene), poly(4-amino-styrene).

Poly(4-bromostyrene) was a brown oil and was isolated in low yields, poly(4-methoxystyrene) was synthesised as a colourless solid and poly(4-aminostyrene) as yellow flakes in high yields. Solution-phase homopolymerisations of the polar styrene monomers were carried out at 55 °C in toluene with MAO in a ratio $[Al_{MAO}]_0$:$[Ti]_0$ = 1500:1. Polymerisations using the supported catalysts were performed at the same temperature with a ratio $[Al_{sMAO}]_0$:$[Ti]_0$ = 200:1. Figure 3.2 displays the homopolymerisation activities measured in solution and slurry-phase for the substituted styrene monomers and compare them to activities achieved with styrene.

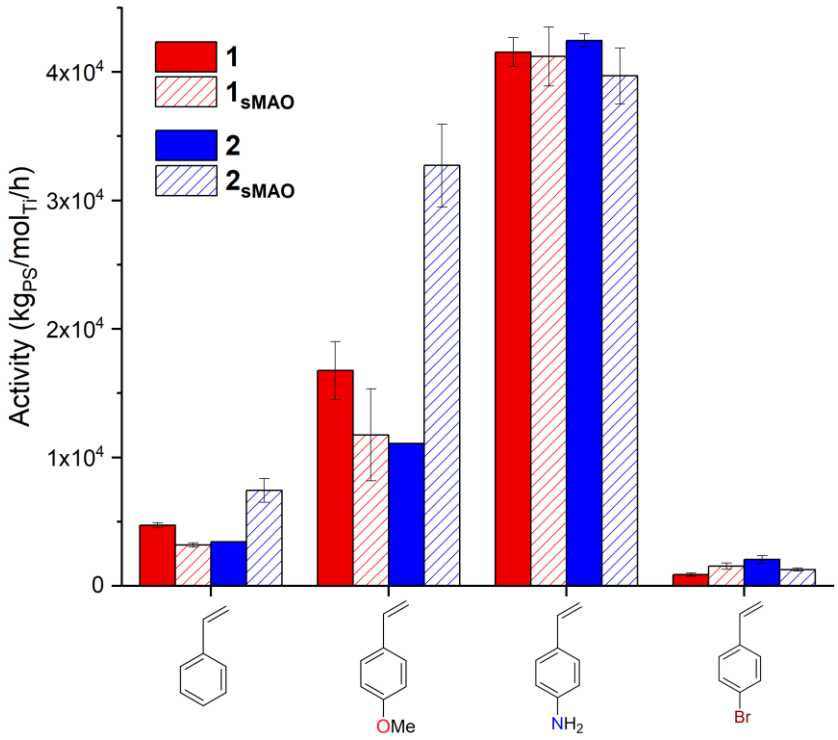

Figure 3.2. Solution and slurry phase substituted styrene polymerisation by Cp*$TiCl_3$ (**1**), Pn*(H)$TiCl_3$ (**2**), sMAO-Cp*$TiCl_3$ (**1_{sMAO}**) and sMAO-Pn*(H)$TiCl_3$ (**2_{sMAO}**) at 55 °C. Polymerisation conditions: 10 minutes, 1000 rpm. Solution: 2 mL toluene, 2 µL [Ti], 1.0 mL styrene, $[Al_{MAO}]_0$:$[Ti]_0$ = 1500:1. Slurry: 50 mL toluene, 10 mg of catalyst, 3.7 mL styrene, $[Al_{sMAO}]_0$:$[Ti]_0$ = 200:1, 150 mg TiBA.

The four catalysts **1**, **2**, **1_{sMAO}** and **2_{sMAO}** performed differently for the four styrene monomers. Complexes **1**, **2**, **1_{sMAO}** and **2_{sMAO}** successfully produced functionalised polystyrene with activities measured in the order 4-aminostyrene > 4-methoxystyrene > styrene > 4-bromostyrene. Polymerisation performed with the 4-bromostyrene resulted in the lowest activities of the series (up to 5.8 times lower than styrene for slurry phase polymerisation by **2_{sMAO}**). 4-X-styrene monomers (X= Br, Cl, F) were reported by Rabagliati *et al*. to lead to very low conversions.[13,23] They measured 6.9% conversion after 6 hours for the homopolymerisation of *para*-chlorostyrene by Ph_2Zn-$CpTiCl_3$-MAO, which is 6 times lower than for styrene. While complex **1** achieved higher

activities for the homopolymerisation of 4-methoxy- and 4-aminostyrene compared with the supported analogue **1$_{sMAO}$**, the latter performed better in the presence of 4-bromostyrene (885 and 1555 $kg_{PS}/mol_{Ti}/h$ for **1** and **1$_{sMAO}$** respectively). Pn*(H)$TiCl_3$ exhibited a different behaviour, the supported complex **2$_{sMAO}$** surpassed **2** for the polymerisation of 4-methoxystyrene (11.1×10^3 *vs.* 32.7×10^3 $kg_{PS}/mol_{Ti}/h$) but lower activities were determined for the two other substituted monomers (*e.g.* 2070 and 1281 $kg_{PS}/mol_{Ti}/h$ using 4-bromostyrene).

Polymerisation of 4-methoxystyrene and 4-aminostyrene yielded higher activities than styrene in both the solution and the slurry-phase. This is consistent with the increase in conversion reported by Rabagliati and co-workers. The methoxy substituent led to 77% conversion after 6 h using $CpTiCl_3$/MAO compared to 30% for styrene.[13] Very high homopolymerisation activities were recorded for 4-aminostyrene with the four catalysts **1**, **2**, **1$_{sMAO}$** and **2$_{sMAO}$**. Indeed, the amino-substituent multiplied the activities by 10 to 13 times compared to styrene (42450 $kg_{PS}/mol_{Ti}/h$ *vs.* 3435 $kg_{PS}/mol_{Ti}/h$ for complex **2**). Cp*$Ti(OMe)_3$ was reported to achieve lower activities for the polymerisation of 4-NR_2-styrene (R = Me or Et) (147 and 567 $kg_{PS}/mol_{Ti}/h$ for R = Me and Et respectively).[27]

The trend observed for complexes **1**, **2**, **1$_{sMAO}$** and **2$_{sMAO}$** suggested that the *para*-substituents on the styrene monomer played an important role in controlling activity. Indeed, the monomer bearing the inductive acceptor substituent (-Br) was observed to lead to very low activities and the presence of inductive donor groups (-OMe and $-NH_2$) resulted in higher activities compared to styrene.[9–11,13,28] Coordination of the monomer to the catalyst was facilitated in the presence of an electron donating substituent as the π electrons of the monomer double bond are more available compared to electron withdrawing substituents.[23] This phenomenon can be characterised with the

para-Hammett constant σ_{para}.[29–32] This constant describes how strongly a substituent donates electrons into the aromatic ring. Electron donating substituents have a negative σ_{para}. which would result in higher polymerisation activity compared to monomers with a positive Hammett constant (Figure 3.3).

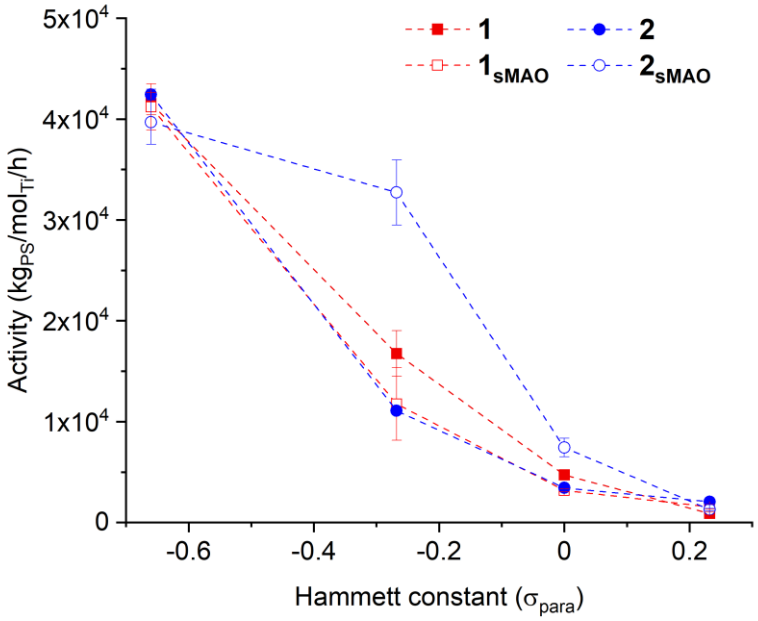

Figure 3.3. Hammet contant dependance of the substituted styrene polymerisation activity by Cp*$TiCl_3$ and Pn*(H)$TiCl_3$ in solution phase and slurry phase at 55 °C. Polymerisation conditions: 10 minutes, 1000 rpm. Solution: 2 mL toluene, 2 µL [Ti], 1 mL styrene, $[Al_{MAO}]_0$:$[Ti]_0$ = 1500:1. Slurry: 50 mL toluene, 10 mg of catalyst, 3.7 mL styrene, $[Al_{sMAO}]_0$:$[Ti]_0$ = 200:1, 150 mg TiBA.

3.2.2. Polymer characterisation

The polymers were characterised by a range of methods to determine how the *para*-substituents on the styrene affect the chemical and physical properties of the polystyrenes produced. ^{1}H NMR spectroscopy and FTIR confirmed the formation of polystyrenes for the three functionalised monomers (Figures A3.8–15). Deconvolution of the methine resonance in the $^{13}C\{^1H\}$ NMR spectra indicated a random enchainment of the monomers leading to a lack of tacticity. For example, a P_m= 0.52 was calculated for the poly(4-OMe-styrene) synthesised by complex **2** at 55 °C. This is consistent with the observations of

Rabagliati and co-workers who reported the synthesis of atactic poly(4-OMe-styrene) with $IndTiCl_3$ in the presence of MAO.[9] Conversely, Do *et al.* achieved the formation of syndiotactic poly(4-NR_2-styrene) (R = Me or Et) using $Cp^*Ti(OMe)_3$.[27]

The molecular weight of the functionalised polystyrenes, analysed by GPC, were very different from those measured for unsubstituted styrene (Figure 3.4 and Table 3.1). Except for the polymerisation of 4-OMe-styrene with **2** and $\mathbf{2_{sMAO}}$, immobilising the complex on a solid support yielded lower M_w compared to homogeneous catalysts. The polymerisation of 4-NH_2-styrene using **1** led to a molecular weight of 2.0×10^3 g/mol whereas slurry-phase polymerisation generated polystyrene of $M_w = 1.3\times10^3$ g/mol.

Polymerisation of 4-OMe-styrene generated high molecular weights using the cyclopentadienyl catalyst **1**. The M_n (1.5×10^5 g/mol at 55 °C) is almost twice as high as that reported by Cui *et al*. for an yttrium catalyst (5.5×10^4 g/mol).[33] Very low molecular weights were measured for **2** and $\mathbf{2_{sMAO}}$, corresponding to oligomers (3-4 repeat units). Similar results were observed for 4-Br-styrene using the two supported catalysts $\mathbf{1_{sMAO}}$ and $\mathbf{2_{sMAO}}$. The homogeneous polymerisations produced poly(4-Br-styrene) with higher molecular weight ($M_w = 1.5\times10^5$ and 7.6×10^4 g/mol for **1** and **2** respectively), similar as that reported by Hou *et al.* using a half-sandwich scandium catalyst (7.8×10^4 g/mol).[34] The molecular weights of poly(4-Br-styrene) and poly(4-OMe-styrene) varied little with polymerisation temperatures which is consistent with results reported in Chapter 2 for styrene (Figure 3.5). The measured molecular weight distributions were, however, broader than those observed for styrene, indicating a less controlled polymerisation.

Table 3.1. Molecular weight and dispersity of substituted polystyrenes produced by **1**, **2**, **1$_{sMAO}$** and **2$_{sMAO}$** at 55 °C. Polymerisation conditions: 10 minutes, 1000 rpm. Solution: 2 mL toluene, 2 µL [Ti], 1.0 mL styrene, $[Al_{MAO}]_0$:$[Ti]_0$ = 1500:1. Slurry: 50 mL toluene, 10 mg of catalyst, 3.7 mL styrene, $[Al_{sMAO}]_0$:$[Ti]_0$ = 200:1, 150 mg TiBA.

	1		**1$_{sMAO}$**		**2**		**2$_{sMAO}$**	
	M_w[a]	Đ	M_w	Đ	M_w	Đ	M_w	Đ
Styrene	9.4×10^3	1.99	1.0×10^4	1.70	1.1×10^4	2.06	9.7×10^3	1.76
4-OMe-styrene	3.2×10^5	2.14	1.3×10^3	1.53	474	1.12	494	1.11
4-NH_2-styrene	1.7×10^3	1.28	1.3×10^3	1.24	2.0×10^3	1.30	1.3×10^3	1.17
4-Br-styrene	1.5×10^5	3.35	511	1.04	7.6×10^4	2.09	526	1.06

[a] g/mol

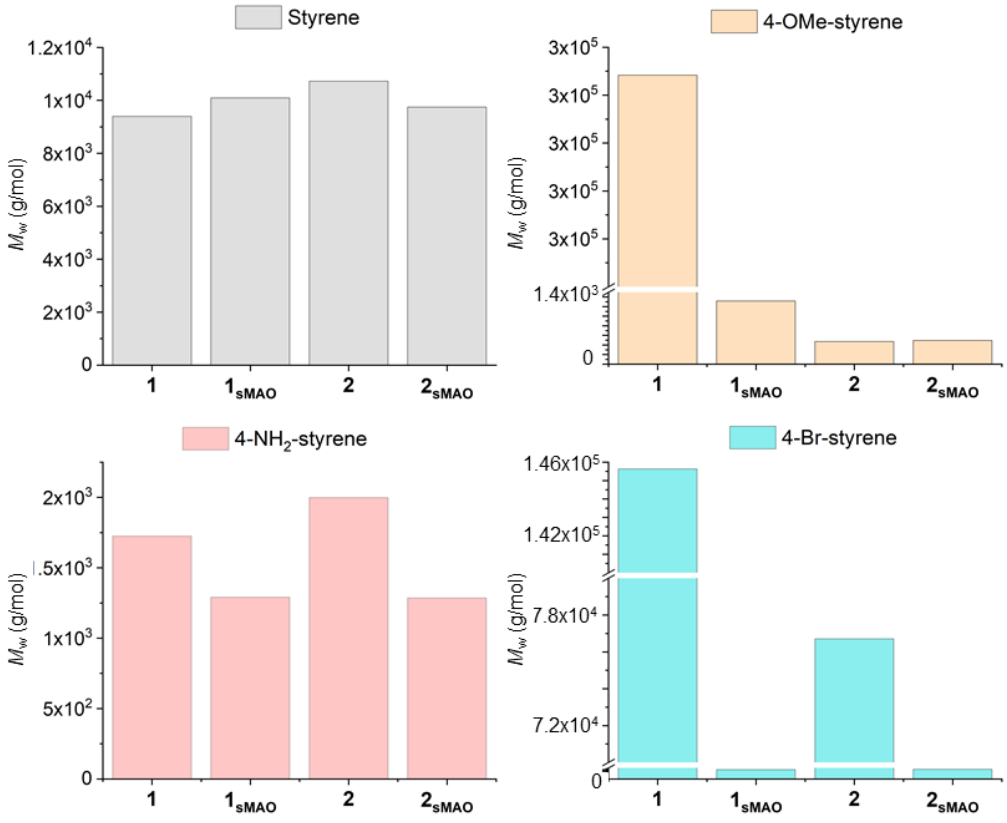

Figure 3.4. Comparison of the molecular weights (M_w) of poly(4-R-styrene) (R= H, OMe, NH_2 and Br) produced by **1**, **2**, **1$_{sMAO}$** and **2$_{sMAO}$**. Polymerisation conditions: 55 °C, 10 minutes, 1000 rpm. Solution: 2 mL toluene, 2 µL [Ti], 1.0 mL styrene, $[Al_{MAO}]_0$:$[Ti]_0$ = 1500:1. Slurry: 50 mL toluene, 10 mg of catalyst, 3.7 mL styrene, $[Al_{sMAO}]_0$:$[Ti]_0$ = 200:1, 150 mg TiBA.

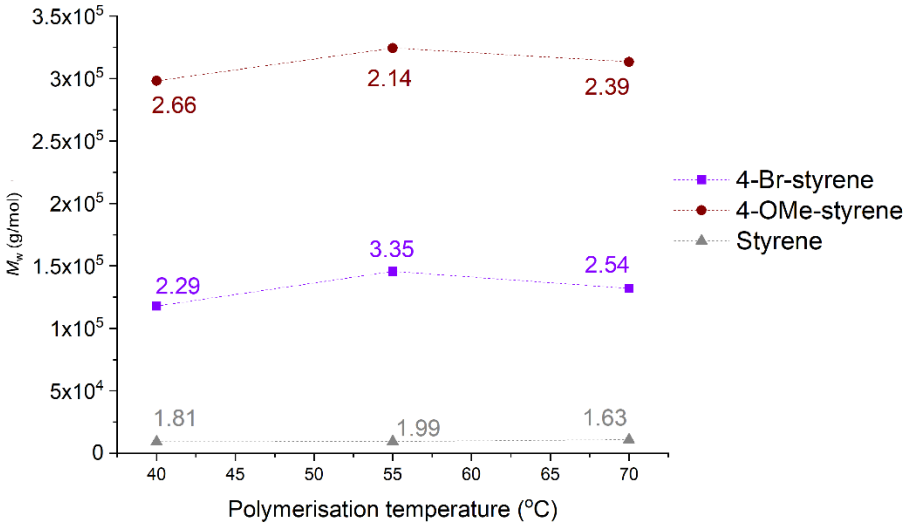

Figure 3.5. Molecular weights (M_w) of poly(4-R-styrene) (R = H, OMe, and Br) produced by **1** at three different temperatures. Polymerisation conditions: 10 minutes, 1000 rpm. Solution: 2 mL toluene, 2 µL [Ti], 1.0 mL styrene, $[Al_{MAO}]_0$:$[Ti]_0$ = 1500:1. Slurry: 50 mL toluene, 10 mg of catalyst, 3.7 mL styrene, $[Al_{sMAO}]_0$:$[Ti]_0$ = 200:1, 150 mg TiBA. Dipersities Đ are given next to datapoint.

The thermal behaviour of the functionalised polymers was characterised by DSC. The poly(4-Br-styrene) produced by complex **1** displayed a glass transition temperature at temperatures higher than those observed for styrene in chapter 2 (144.8 < T_g < 150.2 °C for poly(4-Br-styrene)) (Figure 3.6), which is consistent with the increase in T_g observed by Hou and co-workers for the polymerisation of 4-X-styrene (X = F, Cl, Br, I) using scandium complexes.[34] Similarly, Rabagliati *et al.* reported a T_g of 127.5 °C for poly(4-Br-styrene) produced by the system Ph_2Zn-$CpTiCl_3$-MAO.[12] At 40 and 55 °C, the glass transition temperatures of poly(4-OMe-styrene) were similar to those measured for the unsubstituted monomer. Figure 3.6 however shows an increase to 107.4 °C for a polymerisation temperature of 70 °C. Complexes Cp_2TiCl_2 and $IndTiCl_3$ were described to yield poly(4-OMe-styrene) with T_g of 113 and 112 °C respectively.[9] The polymerisation temperature had opposite effects for poly(4-X-styrene) (X= Br or OMe): increasing the temperature resulted in a decrease in T_g for X = Br and an increase by 13 °C for X = OMe. Adding an NH_2 group in *para*-position also influenced the glass

transition temperature; the poly(4-NH_2-styrene) synthesised by supported complex $\mathbf{1}_{sMAO}$ exhibited a T_g of 117.3 °C (Figure A3.4).

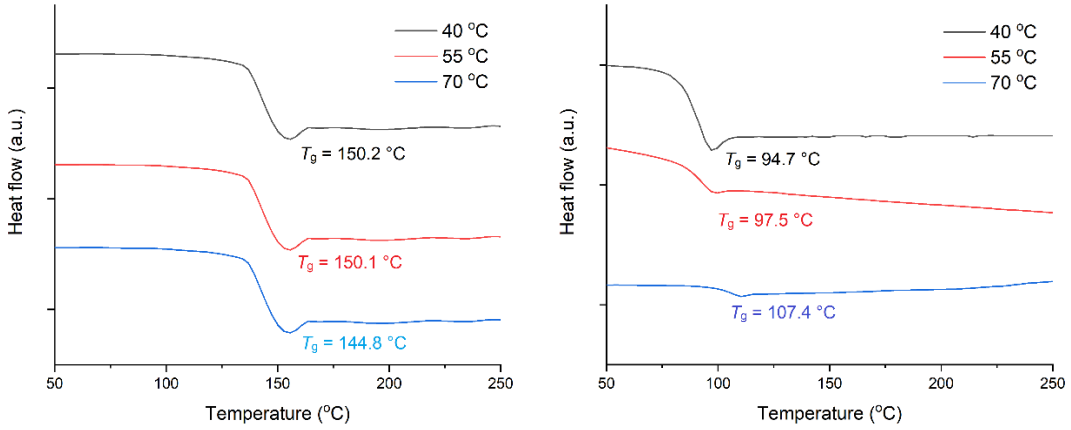

Figure 3.6. DSC of poly(4-Br-styrene) (left) and poly(4-OMe-styrene) (right) synthesised by **1**, ramp 10 °C/min.

The poly(4-NH_2-styrene) samples were further characterised by SEM (Figure 3.7). Different morphologies were observed for the four catalysts. Complex **1** led to aggregates of 300-500 µm in size composed of needles-like particles. A replication of the solid-support morphology can be observed when 4-NH_2-styrene is polymerised by $\mathbf{1}_{sMAO}$. This reflected the typical morphologies reported by O'Hare *et al.* for slurry-phase ethylene polymerisation.[35–37] Conversely, the SEM images indicated no replication for the permethylpentalene catalyst; while solution-phase polymerisation with **2** led to aggregates of various sizes, $\mathbf{2}_{sMAO}$ produced poly(4-NH_2-styrene) as needles.

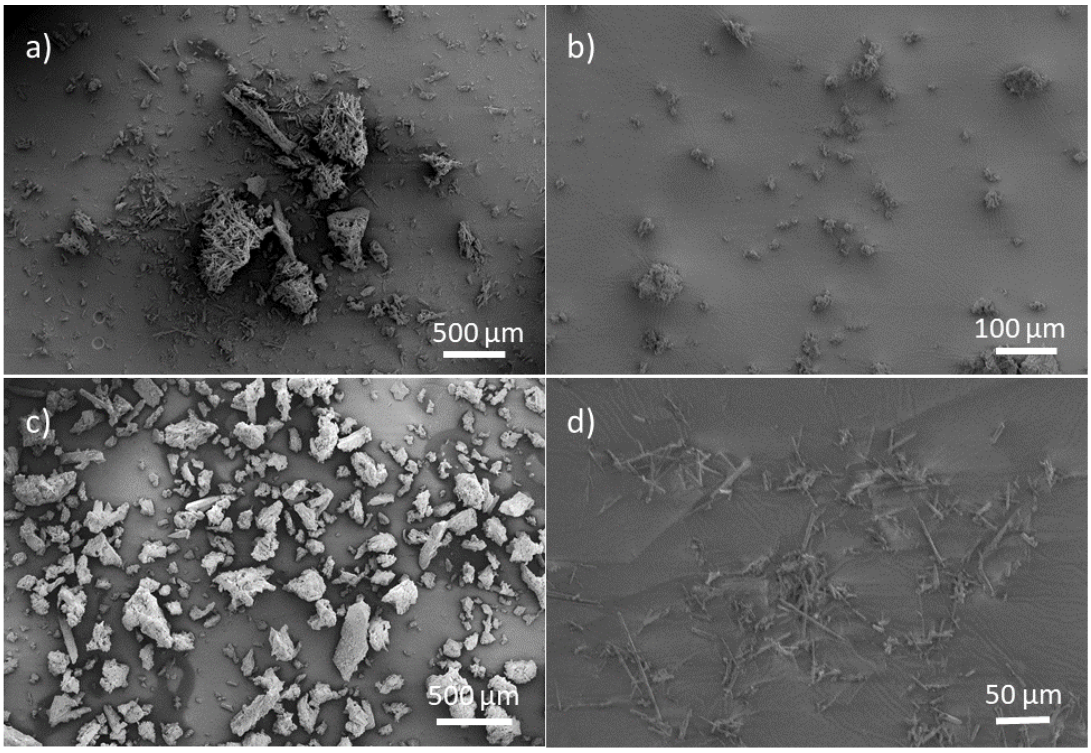

Figure 3.7. SEM images of poly(4-NH_2-styrene) synthesised at 55 °C by a) **1** (x30), b) **1s$_{MAO}$** (x37), c) **2** (x100) and d) **2$_{sMAO}$** (x270).

3.3 Copolymerisation of ethylene with 4-NR_2-styrene (R = H, Me)

The four titanium catalysts **1**, **2**, **1$_{sMAO}$** and **2$_{sMAO}$** exhibited efficient catalytic activity for the homopolymerisation of 4-NH_2-styrene, yielding a large amounts of poly(4-NH_2-styrene).

Do and co-workers also observed high activities for the homopolymerisation of *para*-*N*,*N*-dimethylamino- and *para*-*N*,*N*-diethylaminostyrene using Cp*$TiCl_3$ and Cp*$Ti(OMe)_3$ in the presence of modified methylaluminoxane (MMAO).[27] They observed that 4-NMe_2-styrene yielded less polymer than the diethyl analogue under the same polymerisation conditions (0.7×10^4 *vs.* 2.8×10^4 $kg_{PS}/mol_{Ti}/mol_{styrene}/h$). Copolymerisation of ethylene with polar monomers is a challenge due to reported poisoning of the catalyst by the Lewis basic comonomer.[38,39] Recently however, Cui *et al.* found that polar groups do not always poison the catalysts and successfully developed fluorenyl scandium and yttrium complexes for the copolymerisation of ethylene with polar styrene monomers.[40,41] They described high activities for the copolymerisation of ethylene with *para*-NR_2-styrenes (2.11×10^5 *versus* 3.99×10^5 $kg_{polymer}/mol_{Sc}/h$ for R=Me and Et respectively) using a scandium catalyst.[41] Complexes **1**, **2**, **1$_{sMAO}$** and **2$_{sMAO}$** were used to investigate the effect of the substituent on copolymerisation of ethylene with *para*-NR_2-styrene (R= H, Me) and the resulting polymer properties (Figure 3.8).

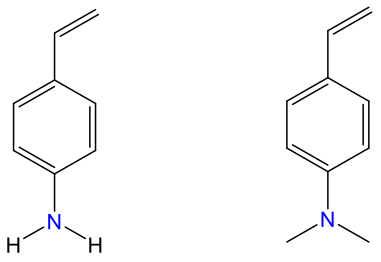

Figure 3.8. Structure of the two 4-NR_2-styrene comonomer, R = H and Me.

3.3.1. Preliminary studies

As a preliminary study, the homopolymerisation of 4-NMe_2-styrene using complex **2_{sMAO}** was carried out at 55 °C in toluene. The activity measured was very similar to that obtained for 4-NH_2-styrene (39.8×10^3 vs. 39.7×10^3 $kg_{PS}/mol_{Ti}/h$ for R= Me and R= H respectively) (Figure 3.9). The NMe_2-substituted monomer was expected to generate higher activities according to the *para*-Hammett constant (–0.83 for NMe_2). The poor performance observed may be caused by steric protection of the nitrogen by the two methyl groups as discussed by Chung *et al.*.[42] Despite this, the activity with the NMe_2 monomer was much larger than the ones reported by Do *et al.* using $Cp^*Ti(OMe)_3$ in the presence of MMAO (147 $kg_{polymer}/mol_{Ti}/h$).[27]

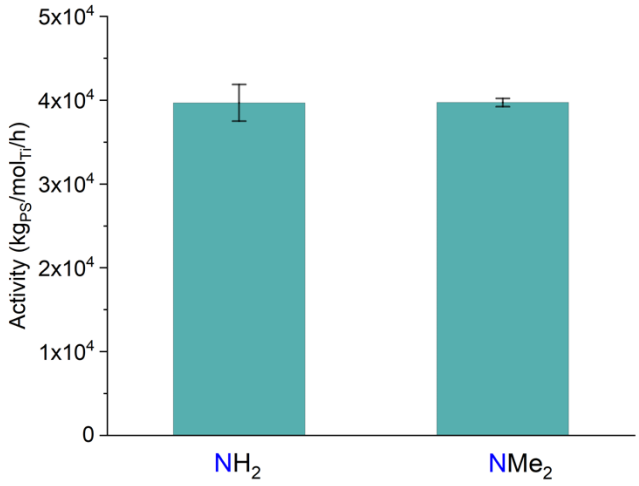

Figure 3.9. Slurry phase 4-(NR_2-styrene) (R = H or Me) polymerisation using sMAO-Pn*(H)$TiCl_3$ (**2_{sMAO}**) at 55 °C. Polymerisation conditions: 10 minutes, 1000 rpm, 50 mL toluene, 10 mg of catalyst, 3.7 mL styrene, $[Al_{sMAO}]_0$:$[Ti]_0$ = 200:1, 150 mg TiBA.

The analysis of the material produced by GPC indicated the formation of an oligomer with low molecular weight. Further characterisation was performed to solve the structure of the product formed. ESI mass spectrometry revealed a peak at *m/z* = 295.21 in the positive mode and NMR spectroscopy confirmed the formation of a small molecule and the absence of polymer chains. The compound formed by the attempted

homopolymerisation of 4-NMe_2-styrene by catalyst **2$_{sMAO}$** was determined to be a dimer, 4,4'-[(1E)-3-methyl-1-propene-1,3-diyl]bis[N,N-dimethylbenzenamine] (Figure 3.10).[43] The formation of dimeric compounds has already been observed by Bercaw *et al.*; [(Me_2SiCpN^tBu)ScCl] was not able to polymerise styrene but a double insertion resulted in the dimer 1,4-diphenylbutane. The ^1H NMR spectrum of 4,4'-[(1E)-3-methyl-1-propene-1,3-diyl]bis[N,N-dimethylbenzenamine] displayed two singlets at 3.0 ppm corresponding to the six methyl groups of the amino substituents (Figure 3.10). The multiplet at 3.6 ppm and the doublet at 1.5 ppm were attributed to the $CHCH_3$ fragment. The allyl protons appeared as a doublet of doublets at 6.2 ppm and a doublet at 3.4 ppm. The $^{13}C\{^1H\}$ NMR spectrum showed resonances at 46.4 ppm for the 6 methyl groups and the aromatic quaternary carbons appeared at 139.3, 141.3, 141.7 and 147.5 ppm.

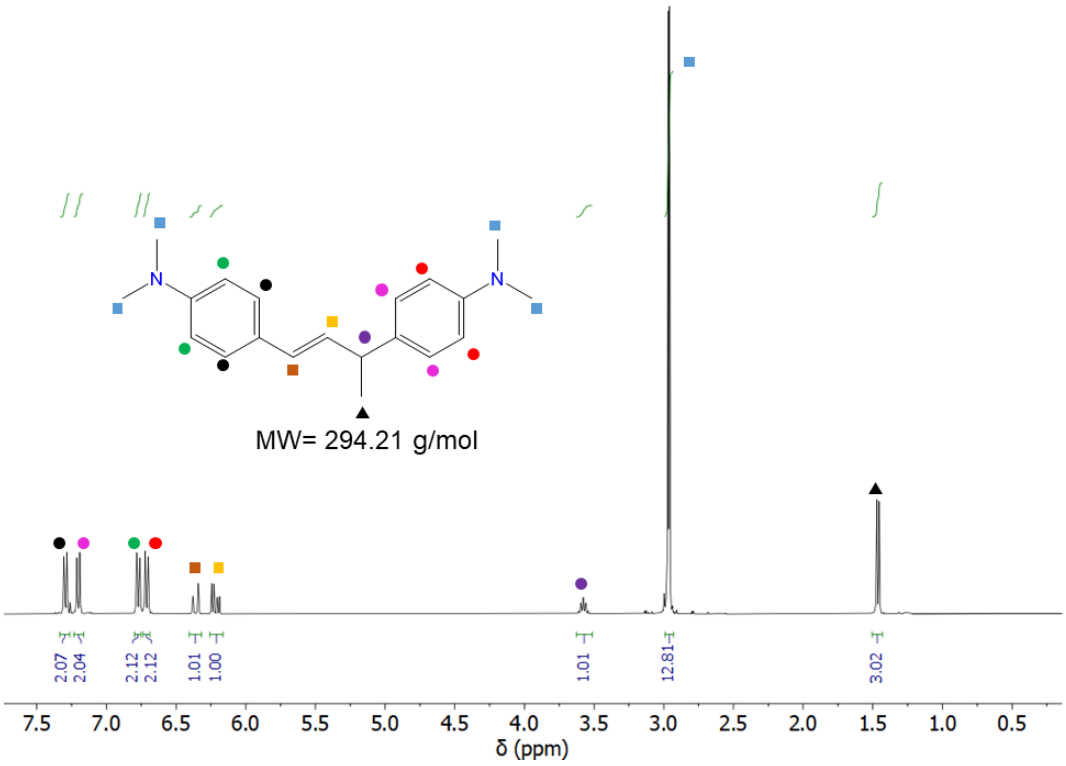

Figure 3.10. ^1H NMR spectrum of 4,4'-[(1E)-3-methyl-1-propene-1,3-diyl]bis[N,N-dimethylbenzenamine] (chloroform-d_1, 298 K, 400 MHz).

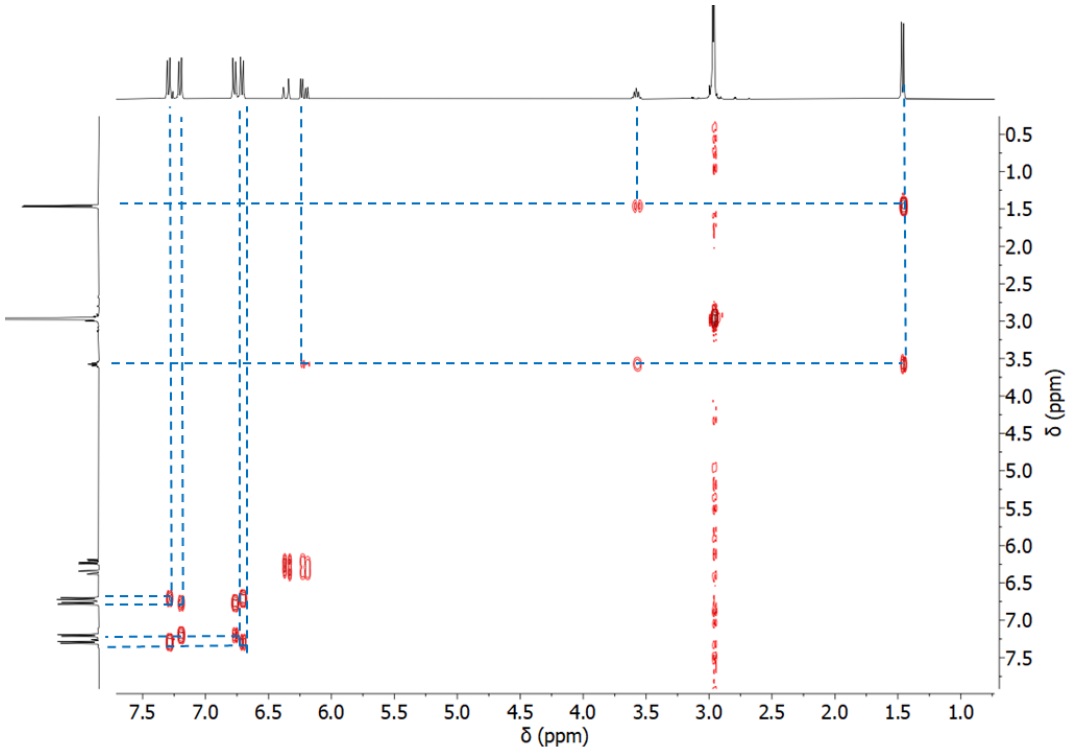

Figure 3.11. COSY ^{1}H-^{1}H NMR spectrum 4,4'-[(1E)-3-methyl-1-propene-1,3-diyl]bis[N,N-dimethylbenzenamine] (chloroform-d_1, 298 K, 400 MHz).

It is proposed that the dimer was formed by the coordination-insertion of two monomeric units with a Ti hydride active species. Many reports suggest that the Ti-H species is formed in the presence of aluminium alkyls such as MAO.[44–47] Bueschges observed the formation of an hydride after mixing $CpZrCl_3$ and MAO and explained the formation of the hydride by complexation of two MAO molecules to the zirconium complex.[46] They described that dissociation and rearrangement led to the final hydride, which was later confirmed by Grassi and co-workers (Scheme 3.1).[48]

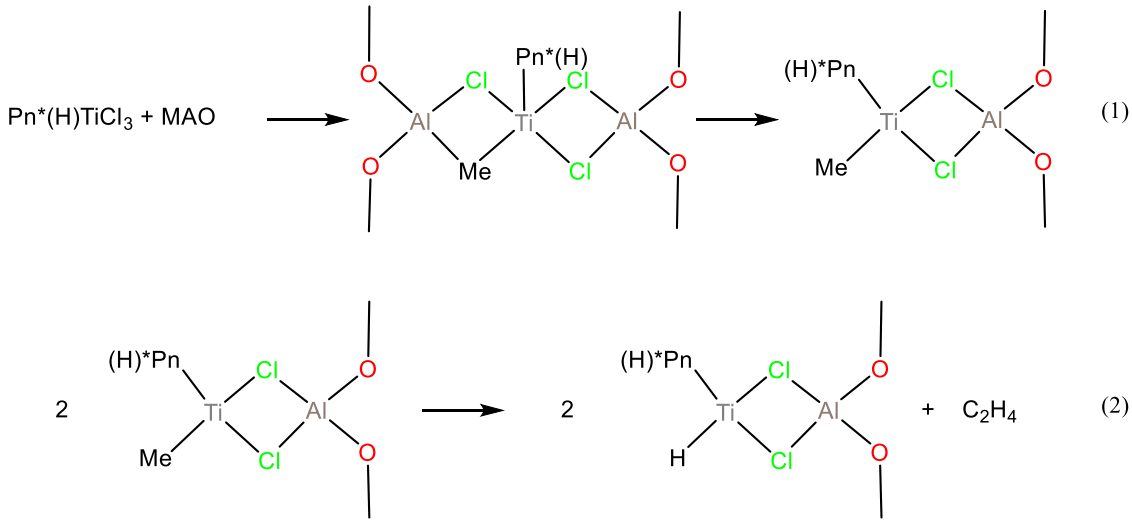

Scheme 3.1. Proposed mechanism of formation of Pn*(H)Ti-hydride species adapted from Bueschghes *et al.*.[46]

Grassi *et al.* investigated the formation of hydride species and confirmed that Ti^{III}-H species are able to polymerise styrene in the presence of MAO.[48] Subsequently, it is proposed that the permethylpentalene supported complex **2$_{sMAO}$** was able to dimerise 4-NMe_2-styrene following the mechanism presented in Scheme 3.2. First, a styrene molecule coordinates to the metal centre, followed by a 1,2-insertion into the Ti-H bond. The opposite regioselectivity was described by Oliva *et al.* using $Me_2Si(Ind)_2Zr$-based zirconocene.[49] They studied the effects of *para*-substituents on styrene insertion and revealed that electron-donating groups shift monomer insertion toward 2,1-insertion. Conversely, Nomura and co-workers reported that polymerisation of styrene using Cp* titanium compounds was ruled by 1,2-insertions of the monomer.[50] Chain termination proceeds *via* β-hydride elimination to afford the dimer and regenerate the Ti-hydride species.[48,51]

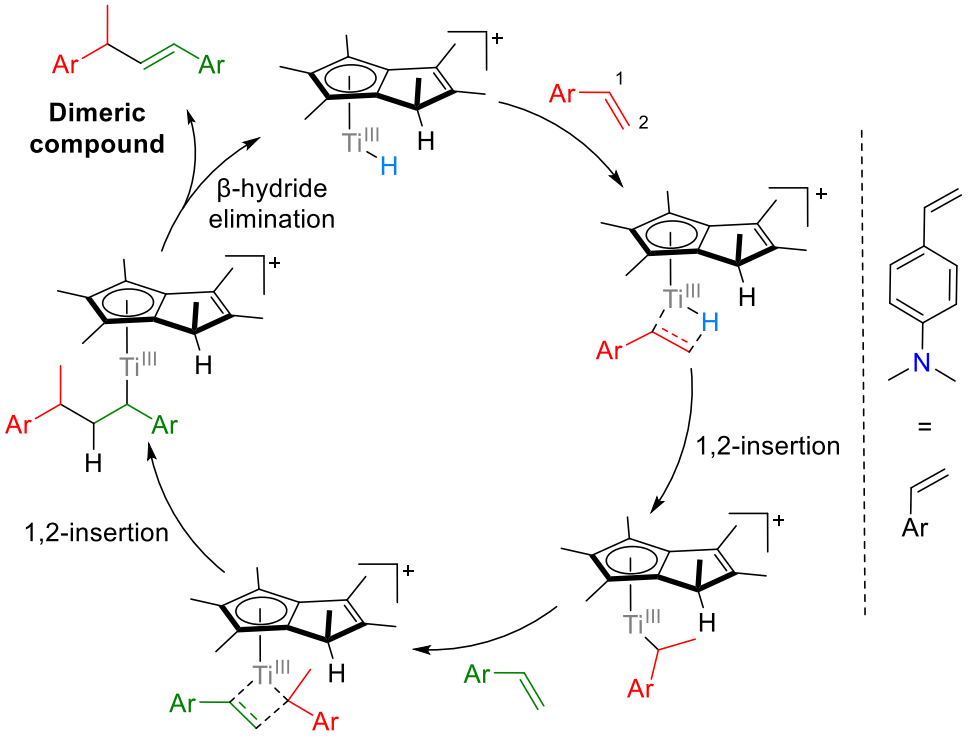

Scheme 3.2. Proposed catalytic cycle for the formation of 4,4'-[(1E)-3-methyl-1-propene-1,3-diyl]bis[N,N-dimethylbenzenamine] using $\mathbf{2}_{\mathbf{sMAO}}$. The $sMAO^{-}$ counter anion has been omitted for clarity.

3.3.2. Influence of the amount of 4-NR_2-styrene (R= H and Me)

Following the high activities observed for 4-NR_2-styrene (R= H or Me), slurry-phase copolymerisations with ethylene were carried out under the same conditions as in Chapter 2 using Y-shaped ampoules to incorporate the substituted styrene comonomer *via* a side arm. The two titanium complexes **1** and **2** were supported on sMAO in a ratio $[Al_{sMAO}]_0$:$[Ti]_0$ = 200 and toluene was used as the solvent. Copolymerisations were performed at 40 °C using 62.5, 125, 250 and 500 µL of 4-NR_2-styrene (R = H or Me).

3.3.2.1. 4-NH_2-styrene

The amount of 4-NH_2-styrene introduced in the system greatly affected the polymerisation. Copolymerisations with 62.5 µL of comonomer achieved different results than reactions performed with higher volumes of 125, 250 and 500 µL.

When 62.5 µL of for 4-NH_2-styrene were added in the polymerisation vessel, two crops were obtained, in a similar manner to ethylene/styrene copolymerisations described in Chapter 2. Crop 1 precipitated in the ampoule and was collected by filtration and crop 2 was obtained after removing the solvent *in vacuo*. TGA and DSC analysis allowed for the determination of the nature of the crops. The TGA curves for the first crops showed a characteristic weight loss corresponding to polyethylene at temperatures of 465 and 478 °C for polymers produced using $\mathbf{1}_{\mathbf{sMAO}}$ and $\mathbf{2}_{\mathbf{sMAO}}$ respectively (Figure 3.12).[52–54] The curves corresponding to the second crops displayed a weight loss as well, but at a temperature too low to correspond to polymer. While DSC characterisation of crops 1 produced by $\mathbf{1}_{\mathbf{sMAO}}$ and $\mathbf{2}_{\mathbf{sMAO}}$ exhibited a melting peak (T_m = 133.4 and 135.7 °C respectively)[52,55], no heat flow were recorded for the second crops (Figure 3.13). These results were consistent with the observations reported in Chapter 2 stating that only the first crop contained polymer, in this case polyethylene, and the second isolated crop consisted of Al residues.

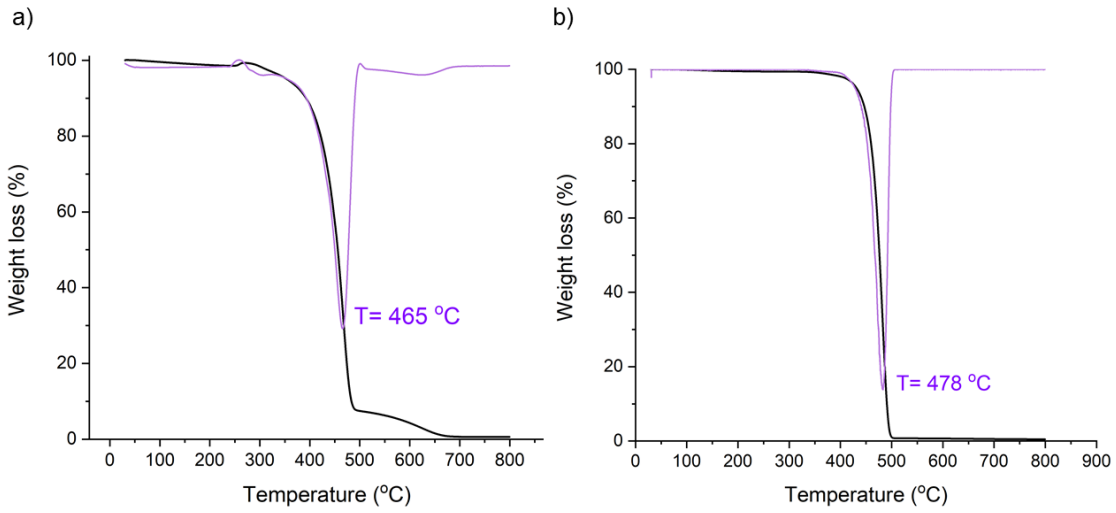

Figure 3.12. TGA curves of the polymers collected in the first crop of the attempted copolymerisation of ethylene with 65.2 µL of 4-NH_2-styrene at 40 °C using a) sMAO-Cp*$TiCl_3$ ($\mathbf{1}_{\mathbf{sMAO}}$) and b) sMAO-Pn*(H)$TiCl_3$ ($\mathbf{2}_{\mathbf{sMAO}}$). The derivatives are shown in purple.

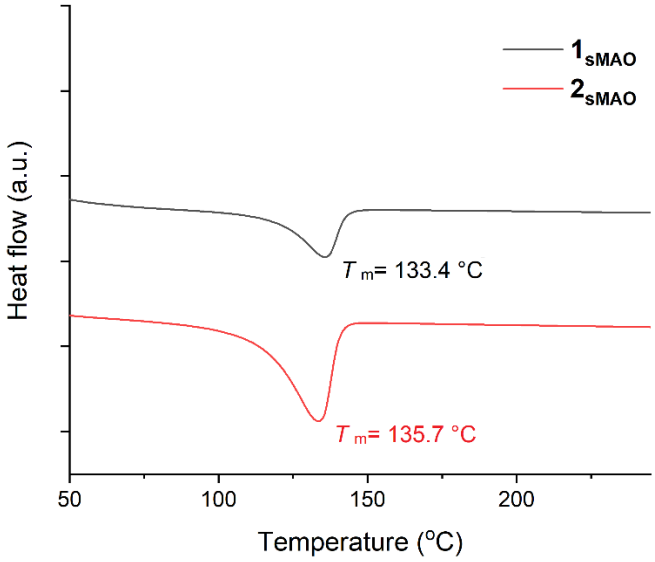

Figure 3.13. DSC curves of for the polymers collected in the first crop of the attempted copolymerisation of ethylene with 65.2 μL of 4-NH_2-styrene at 40 °C. Ramp 10 °C/min

These experiments revealed that polyethylene was synthesised rather than ethylene/styrene copolymer. The determination of the polymerisation activity for complexes **1**$_{sMAO}$ and **2**$_{sMAO}$ indicated that the permethylpentalene complex was less efficient than the cyclopentadienyl derivative (Table 3.2). The activities measured were in the same range as those described for unsubstituted styrene in Chapter 2 (14-75 $kg_{PS}/mol_{Ti}/h$). Similarly, they were lower than activities obtained for homopolymerisations of ethylene (203 $kg_{polymer}/mol_{Ti}/h/bar$ using **2**$_{sMAO}$ at 50 °C). This could be due to a negative comonomer effect after coordination of NH_2 preventing ethylene coordination.[20,56,57]

Table 3.2. Data for the copolymerisation ethylene with 65.2 μL of 4-NH_2-styrene at 40 °C.

Catalyst	Activity ($kg_{polymer}/mol_{Ti}/h/bar$)	Degradation temperature (°C)	T_m (°C)
sMAO-Cp*$TiCl_3$ (**1**$_{sMAO}$)	39 ± 1	465	133.4
sMAO-Pn*(H)$TiCl_3$ (**2**$_{sMAO}$)	26 ± 3	478	135.7

Addition of larger volumes of 4-NH_2-styrene (125, 250 and 500 μL) resulted in no polymerisation. Only one crop of material was isolated after solvent removal, which was revealed to be Al residues after TGA analysis (Figures A3.5 and A3.6). The absence of polymerisation suggested that the polar monomer poisoned the Lewis acidic catalyst, making it inactive for further reactions.[58–60]

3.3.2.2. 4-NMe_2-styrene

Copolymerisation of ethylene with 4-NMe_2-styrene were attempted under the same reaction conditions as 3.2.2.1. Various amounts of styrene comonomer and temperatures between 40 and 80 °C were studied. TGA analysis of the material produced revealed little to no polymer was formed which was consistent with the results using 4-NH_2-styrene (Figure A3.7). ^{1}H NMR spectroscopy confirmed that no polymerisation took place and that 4-NMe_2-styrene was unable to form a dimer.

The use of polar monomers poisoned the titanium catalyst. Indeed, 4-NR_2-styrene (R = H or Me) strongly bound to the highly oxophilic metal centre and formed a complex that was too stable for further reactions.[57,61,62] There are however examples of copolymerisations with polar monomers using particular substrates.[63–67] Cui *et al.* achieved activities between 528 and 998 $kg_{polymer}/mol_{Sc}/h/bar$ for the copolymerisation of ethylene with 4-NR_2-styrene (R = Me or Et) under 4 bar of pressure using a scandium catalyst.[41]

3.4 Conclusion

Cyclopentadienyl and permethylpentalene compounds **1**, **2**, $\mathbf{1}_{\mathbf{sMAO}}$ and $\mathbf{2}_{\mathbf{sMAO}}$ were studied for the polymerisation of *para*-substituted styrene monomers. Four substituent were investigated, -Br, -OMe, $-NH_2$ and $-NMe_2$, and the solution and slurry phase homopolymerisations resulted in very different activities depending on the group. Electron withdrawing substituent -Br achieved lower activities than styrene but the poly(4-Br-styrene) synthesised using complex **1** exhibited molecular weights ten times higher (~ 3×10^5 g/mol). Polymerisation of monomers bearing electron-donating groups, -OMe, $-NH_2$ and NMe_2, resulted in very high activities (~ 4×10^4 $kg_{PS}/mol_{Ti}/h$ for $–NH_2$). The Cp^*TiCl_3 and $Pn^*(H)TiCl_3$ and their immobilised analogues were among the most active systems reported for the homopolymerisation of 4-NR_2-styrene (R = H or Me). Supported catalysts $\mathbf{1}_{\mathbf{sMAO}}$ and $\mathbf{2}_{\mathbf{sMAO}}$ produced low molecular weight polymers. Homopolymerisation of 4-NMe_2-styrene unexpectedly produced a dimer in high yield and was rationalised through the catalysis with a Ti^{III} hydride species.

Copolymerisations of ethylene with 4-NR_2-styrene (R = H, Me) comonomer were carried out at different temperatures and volumes of comonomer. The reaction under 2 bar of ethylene and with 62.5 μL of 4-NH_2-styrene only produced polyethylene. Catalytic activities for copolymerisations were lower than those measured for the homopolymerisation of ethylene indicating a negative comonomer effect. Addition of higher volumes of 4-NH_2-styrene poisoned the catalyst and inhibited polymerisation. Copolymerisation of ethylene with 4-NMe_2-styrene were then attempted but TGA analysis indicated the absence of polymer, confirming the poisoning of the catalyst by the polar monomer.

Nevertheless, the high activities reported for homopolymerisation of 4-OMe and 4-NH_2-styrene created valuable polymers for post-polymerisation modifications.[68]

3.5 References

1 H. Yoshioka, K. Yamaguchi and M. Kobayashi, *Polym. J.*, 2019, **51**, 627–636.

2 S. Pal, P. K. Ghorai and P. De, *Polymer*, 2012, **53**, 3687–3694.

3 J. Qiu and K. Matyjaszewski, *Macromolecules*, 1997, **30**, 5643–5648.

4 T. C. M. Chung, *Functionalization of Polyolefins*, Elsevier., 2002.

5 J. M. Nasrullah, S. Raja, K. Vijayakumaran and R. Dhamodharan, *J. Polym. Sci. Part A Polym. Chem.*, 2000, **38**, 453–461.

6 N. Cardi, R. Po', L. Abbondanza, L. Abis and G. Conti, *Macromol. Symp.*, 1996, **102**, 123–130.

7 A. Grassi, P. Longo, A. Proto and A. Zambelli, *Macromolecules*, 1989, **22**, 104–108.

8 C. Schwecke and W. Kaminsky, *Macromol. Rapid Commun.*, 2001, **22**, 508–512.

9 F. M. Rabagliati, G. V Mardones, H. E. Muñoz and F. J. Rodríguez, *Polym. Int.*, 2008, **57**, 744–749.

10 F. M. Rabagliati, F. J. Rodríguez, A. Alla and S. Muñoz-Guerra, *Polym. Int.*, 2006, **55**, 910–915.

11 F. M. Rabagliati, F. J. Rodríguez, A. Alla, A. Martínez de Ilarduya and S. Muñoz-Guerra, *Polymer*, 2007, **48**, 4646–4652.

12 F. M. Rabagliati, M. A. Pérez, F. J. Rodríguez, R. A. Cancino, N. Crispel, G. A. Mardones, H. E. Muñoz, M. A. Saavedra, M. Vidal and L. A. Muñoz, *Macromol. Symp.*, 2011, **304**, 33–39.

13 F. M. Rabagliati, M. A. Pérez, F. J. Rodríguez, C. J. Caro and N. Crispel, *Polym. Int.*, 2005, **54**, 437–441.

14 R. Kakuchi and P. Theato, *ACS Macro Lett.*, 2013, **2**, 419–422.

15 J. S. Oakdale, L. Kwisnek and V. V. Fokin, *Macromolecules*, 2016, **49**, 4473–4479.

16 M. Jaymand, *Polym. Chem.*, 2014, **5**, 2663–2690.

17 M. Ciftci, D. Wang, M. Buchmeiser and Y. Yagci, *Macromol. Chem. Phys.*, 2017, **218**, 1700279.

18 M. A. Gauthier, M. I. Gibson and H.-A. Klok, *Angew. Chem. Int. Ed.*, 2009, **48**, 48–58.

19 B. Liu, K. Qiao, J. Fang, T. Wang, Z. Wang, D. Liu, Z. Xie, L. Maron and D. Cui, *Angew. Chem. Int. Ed.*, 2018, **130**, 15112–15117.

20 D. Liu, C. Yao, R. Wang, M. Wang, Z. Wang, C. Wu, F. Lin, S. Li, X. Wan and D. Cui, *Angew. Chem. Int. Ed.*, 2015, **54**, 5205–5209.

21 Z. Zhang, Y. Dou, Z. Cai, D. Liu, S. Li and D. Cui, *Macromolecules*, 2020, **53**, 5895–5902.

22 F. De Carlo, C. Capacchione, V. Schiavo and A. Proto, *J. Polym. Sci. Part A Polym. Chem.*, 2006, **44**, 1486–1491.

23 F. M. Rabagliati, M. A. Pérez, R. A. Cancino, F. J. Rodríguez and C. J. Caro, *Macromol. Symp.*, 2003, **195**, 81–88.

24 R. Kurbanova, A. Okudan, R. Mirzaoğlu, S. Kurbanov, Karataş, M. Ersöz, E. Özcan, G. Ahmedova and V. Pamuk, *J. Adhes. Sci. Technol.*, 1998, **12**, 947–955.

25 F. M. Rabagliati, R. A. Cancino and F. J. Rodríguez, *Polym. Bull.*, 2001, **46**, 427–434.

26 Z. Wang, D. Liu and D. Cui, *Macromolecules*, 2016, **49**, 781–787.

27 Y. Kim, S. Park, Y. Han and Y. Do, *Bull. Korean Chem. Soc.*, 2004, **25**, 1648–1652.

28 F. M. Rabagliati, R. A. Cancino, M. A. Pérez and F. J. Rodríguez, *Macromol. Symp.*, 2004, **216**, 55–64.

29 J. D. Roberts and M. C. Caserio, *Basic principles of organic chemistry*, W.A. Benjamin, 1977.

30 C. Hansch, A. Leo and R. W. Taft, *Chem. Rev.*, 1991, **91**, 165–195.

31 M. Lewis, C. Bagwill, L. K. E. Hardebeck and S. Wireduaah, *Comput. Struct. Biotechnol. J.*, 2012, **1**, e201204004.

32 C. D. Johnson, *The Hammett equation*, University Press, 1973.

33 D. Liu, R. Wang, M. Wang, C. Wu, Z. Wang, C. Yao, B. Liu, X. Wan and D. Cui, *Chem. Commun.*, 2015, **51**, 4685–4688.

34 F. Guo, N. Jiao, L. Jiang, Y. Li and Z. Hou, *Macromolecules*, 2017, **50**, 8398–8405.

35 J. C. Buffet, Z. R. Turner and D. O'Hare, *Chem. Commun.*, 2018, **54**, 10970–10973.

36 J. V. Lamb, J. C. Abell, J. E. McLaren, J. C. Buffet, Z. R. Turner and D. O'Hare, *Mol. Catal.*, 2019, **484**, 110735.

37 D. A. X. Fraser, Z. R. Turner, J.-C. Buffet and D. O'Hare, *Organometallics*, 2016, **35**, 2664–2674.

38 N. M. G. Franssen, J. N. H. Reek and B. de Bruin, *Chem. Soc. Rev.*, 2013, **42**, 5809.

39 L. S. Boffa and B. M. Novak, *Chem. Rev.*, 2000, **100**, 1479–1493.

40 D. Liu, M. Wang, Z. Wang, C. Wu, Y. Pan and D. Cui, *Angew. Chem. Int. Ed.*, 2017, **56**, 2714–2719.

41 S. Li, D. Liu, Z. Wang and D. Cui, *ACS Catal.*, 2018, **8**, 6086–6093.

42 G. Xu and T. C. Chung, *Macromolecules*, 2000, **33**, 5803–5809.

43 K. Troshin, C. Schindele and H. Mayr, *J. Org. Chem.*, 2011, **76**, 9391–9408.

44 L. Bonoldi, L. Abis, L. Fiocca, R. Fusco, L. Longo, F. Simone and S. Spera, *J. Mol. Catal. A Chem.*, 2004, **219**, 47–56.

45 K. P. Bryliakov, N. V. Semikolenova, V. A. Zakharov and E. P. Talsi, *J. Organomet. Chem.*, 2003, **683**, 23–28.

46 U. Bueschges and J. C. W. Chien, *J. Polym. Sci. Part A Polym. Chem.*, 1989, **27**, 1525–1538.

47 J. C. W. Chien, Z. Salajka and S. Dong, *Macromolecules*, 1992, **25**, 3199–3203.

48 E. Salvadori, M. Chiesa, A. Buonerba and A. Grassi, *Chem. Sci.*, 2020, **11**, 12436–12445.

49 A. Correa, N. Galdi, L. Izzo, L. Cavallo and L. Oliva, *Organometallics*, 2008, **27**, 1028–1029.

50 J. Yi, N. Nakatani, N. Tomotsu, K. Nomura and M. Hada, *Organometallics*, 2021, **40**, 643–653.

51 K. Osakada, Ed., *Organometallic Reactions and Polymerization*, Springer, 2014.

52 L. Contat-Rodrigo, A. Ribes-Greus and C. T. Imrie, *J. Appl. Polym. Sci.*, 2002, **86**, 764–772.

53 I. Dubdub and M. Al-Yaari, *Polymers*, 2020, **12**, 891.

54 A. H. Awad, A. Aly Abd El-Wahab, R. El-Gamsy and M. H. Abdel-latif, *Ain Shams Eng. J.*, 2019, **10**, 353–358.

55 K. Menard and N. Menard, in *Handbook of Industrial Polyethylene and Technology*, John Wiley & Sons, Inc., Hoboken, NJ, USA, 2017, pp. 217–238.

56 J. C. W. W. Chien and T. Nozaki, *J. Polym. Sci. Part A Polym. Chem.*, 1993, **31**, 227–237.

57 C. Chen, *Nat. Rev. Chem.*, 2018, **2**, 6–14.

58 Y. Chai, C. Wu, D. Liu, M. Run and D. Cui, *Sci. China Chem.*, 2019, **62**, 761–766.

59 L. Guo, W. Liu and C. Chen, *Mater. Chem. Front.*, 2017, 1, 2487–2494.

60 J. Chen, Y. Gao and T. J. Marks, *Angew. Chem. Int. Ed.*, 2020, **132**, 14834–14843.

61 M. Srebro, M. Mitoraj and A. Michalak, *Can. J. Chem.*, 2009, **87**, 1039–1054.

62 S. D. Ittel, L. K. Johnson and M. Brookhart, *Chem. Rev.*, 2000, **100**, 1169–1203.

63 T. C. Chung, *Macromolecules*, 1988, **21**, 865–869.

64 P. Aaltonen and B. Löfgren, *Macromolecules*, 1995, **28**, 5353–5357.

65 M. R. Kesti, G. W. Coates and R. M. Waymouth, *J. Am. Chem. Soc.*, 1992, 114, 9679–9680.

66 P. Aaltonen, G. Fink, B. Löfgren and J. Seppälä, *Macromolecules*, 1996, **29**, 5255–5260.

67 M. Galimberti, U. Giannini, E. Albizzati, S. Caldari and L. Abis, *J. Mol. Catal. A. Chem.*, 1995, **101**, 1–10.

68 K. Suzuki, K. Yamaguchi, A. Hirao and S. Nakahama, *Macromolecules*, 1989, **22**, 2607–2611.

Chapter Four
(Hydro)permethylpentalene complexes as Olefin Polymerisation catalysts

4.1 Introduction

Piano-stool titanium complexes Cp^RTiX_3 (*e.g.* Cp^R = Cp, Cp*; X = halide, alkyls, alkoxides, aryloxides) have been shown to be efficient catalysts for the formation of syndiotactically-enriched polystyrene in the presence of an alkylaluminium activator such as methylaluminoxane (MAO) (Figure 4.1).[1–5] The nature of the cyclopentadienyl-base and X ligands have significant effects on both the catalytic activity and physical properties of the resulting polystyrene.[6–9] Notably, when the X ligand is a halide, the activity for styrene polymerisation is good but only low activities have been achieved for the copolymerisation of ethylene and styrene. Undesirable mixtures of polyethylene, polystyrene and poly(ethylene-*co*-styrene) are often obtained.[10–12] In contrast, when aryloxide ligands were incorporated into complexes of the form $Cp^RTiCl_2(OAr)$, both styrene homopolymerisation and ethylene/styrene copolymerisation activities were excellent (4140 $kg/mol_{Ti}/h$ using $(1,3\text{-}Me_2C_5H_3)TiCl_2(O\text{-}2,6\text{-}^iPr\text{-}C_6H_3)$ under 4 bar of ethylene) with the latter affording exclusively poly(ethylene-*co*-styrene).[13–16]

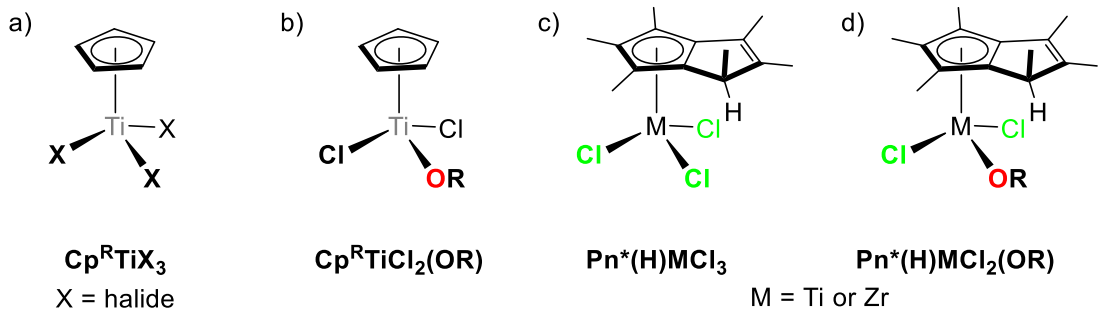

Figure 4.1. a) Cp^RTiX_3 b) $Cp^RTiCl(OAr)$ pre-catalysts for styrene polymerisation, and c) $Pn^*(H)TiCl_3$ and d) $Pn^*(H)TiCl_2(OAr)$ complexes used in this study.

In 1998, Nomura *et al.* reported that half-titanocene aryloxide complexes such as $Cp^RTiCl_2(OAr)$ (OAr= aryloxide group) were highly active for olefin polymerisation.[17] Titanium complexes bearing the ligand O-2,6-^{i}Pr-C_6H_3 exhibited good catalytic activities for the copolymerisation of ethylene with 1-butadiene. They later expanded the range of olefin comonomers as well as half-titanocenes achieving good polymerisation activities.[18–20]

In light of the high catalytic activity for styrene polymerisation and the ability to copolymerise ethylene and styrene demonstrated by $Cp^RTiCl_2(OAr)$, this chapter investigates the use of new (hydro)permethylpentalene analogues $Pn^*(H)TiCl_2(OR)$ as pre-catalysts for solution and slurry-phase olefin polymerisation and the influence of the R group on polymerisation activities (Figure 4.1). Three new $Pn^*(H)TiCl_2(OR)$ complexes were prepared and their resulting catalytic activity was investigated in solution and slurry-phase homopolymerisations of ethylene and styrene as well as their copolymerisation.

4.2 Synthesis and characterisation of new Pn*(H)MCl$_2$(OR) (M = Ti and Zr) complexes

4.2.1 Complex synthesis

The titanium complexes Pn*(H)TiCl$_2$(OR) (R = 2,6-^{i}Pr-C$_6$H$_3$ (**3**), 2,4-^{t}Bu-C$_6$H$_3$ (**4**), SiMe$_2$^{t}Bu (**5**)) were prepared by the reaction of 1 eq. [Pn*TiCl(μ-Cl)]$_2$ with 2 eq. of the appropriate alcohol.[21] Synthesis of the aryloxide complexes (**3** and **4**) required heating to 85 °C for 24 h whereas **5** was synthesised at 25 °C after 1 h. All three complexes were formed in good yields (Scheme 4.1).

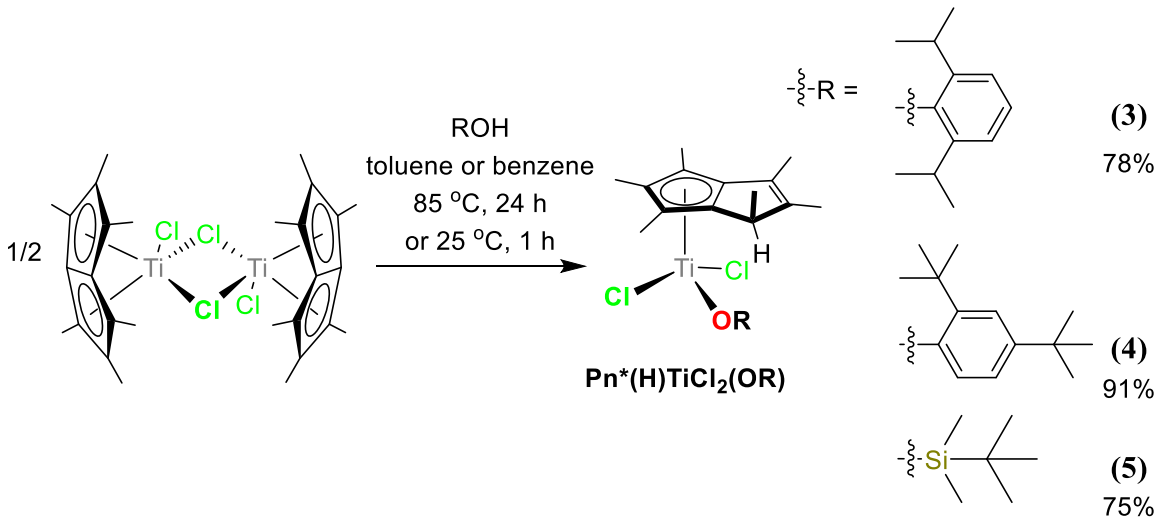

Scheme 4.1. Synthesis of Pn*(H)TiCl$_2$(OR) complexes (R = 2,6-^{i}Pr-C$_6$H$_3$ (**3**), 2,4-^{t}Bu-C$_6$H$_3$ (**4**), SiMe$_2$^{t}Bu (**5**)).

A different series of starting alcohols were also used but led to intractable mixtures of products (Table 4.1). The target product was identified but in the majority of cases, the reaction did not go to completion. Attempts of fractional crystallisation to separate the desired complexes from other species were unsuccessful due to the similar solubilities of the compounds.

Table 4.1. Summary of Pn*(H)$TiCl_2$(OR) complexes synthesis attempted.

R group	Reaction results
2,6-Me-C_6H_3	Reference, O'Hare *et al.*[21]
2,6-^{i}Pr-C_6H_3	Successful reaction, 78% yield.
2,6-^{t}Bu-C_6H_3	No reaction. Ligand too bulky.
2,4-^{t}Bu-C_6H_3	Successful reaction, 97% yield.
$SiMe_2{}^t$Bu	Successful reaction, 90% yield.[a]
Me	Mixture of Pn*(H)$TiCl_2$(OMe) and unreacted starting materials. Decomposition on large scale.
^{t}Bu	Successfully formed on spectroscopic scale.
^{i}Pr	Mixture of Pn*(H)$TiCl_2$(O^{i}Pr) and unreacted starting materials.
$CH_2CH_2NMe_2$	Mixture of Pn*(H)$TiCl_2$($OCH_2CH_2NMe_2$) and by-products.

[a] spectroscopic yield.

The zirconium analogues Pn*(H)$ZrCl_2$(OR) (R = 2,6-^{i}Pr-C_6H_3 and 2,4-^{t}Bu-C_6H_3) were prepared on NMR scale by reaction of 1 eq. of [Pn*Zr(μ−Cl)$_{3/2}$)]$_2$(μ−Cl)$_2$Li(thf)$_2$ with 2 eq. of the corresponding alcohol (Scheme 4.2). Scale-up reactions generated a mixture of the desired zirconium aryloxide complexes and by-products and quick decomposition was observed. It was decided the zirconium complexes did not warrant further investigation as literature reports on related complexes reported poor productivities and atactic polymers.[22]

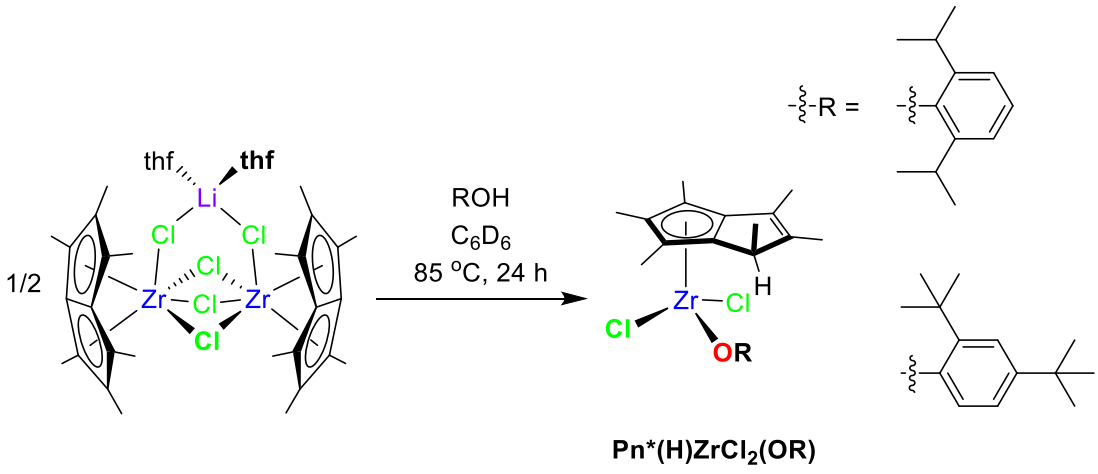

Scheme 4.2. Synthesis of Pn*(H)$ZrCl_2$(OR) complexes (R = 2,6-^{i}Pr-C_6H_3, 2,4-^{t}Bu-C_6H_3).

4.2.2 Complex characterisation

The ^{1}H NMR spectra of the Pn*(H)TiCl$_2$(OR) complexes (Figures 4.2 and 4.3) have common diagnostic features relating to the (hydro)permethylpentalene ligand. There are 5 singlets between 1.2 and 2.5 ppm which correspond to the 2,3,5,6,7-*Me*-Pn*(H) protons. A doublet in the range 0.2-0.9 ppm defines the 1-*Me*-Pn* protons and this is coupled to a quartet at ~3.5 ppm which is attributed to the Pn*(*H*) ring proton. Each complex also contains the resonances associated with the -OR ligand. For example, in Pn*(H)TiCl$_2$(O-2,6-^{i}Pr-C$_6$H$_3$) (**3**), two doublets and a septet integrating to 12 H and 2 H respectively correspond to the isopropyl substituents on the aryloxide ligand (Figures 4.2). In Pn*(H)TiCl$_2$(O-SiMe$_2$^{t}Bu) (**5**), two singlets at 1.01 and 1.03 ppm integrating to 6 H and 9H represent the silyl methyl and *tert*-butyl protons respectively (Figure 4.3). The ^{1}H NMR spectrum of Pn*(H)TiCl$_2$(O-2,4-^{t}Bu-C$_6$H$_3$) (**4**) (Figure A4.2) reveals the formation of a mixture of two isomers in a 1:1 ratio, probably due to the position of the Pn* ring to the aryloxide ligand.

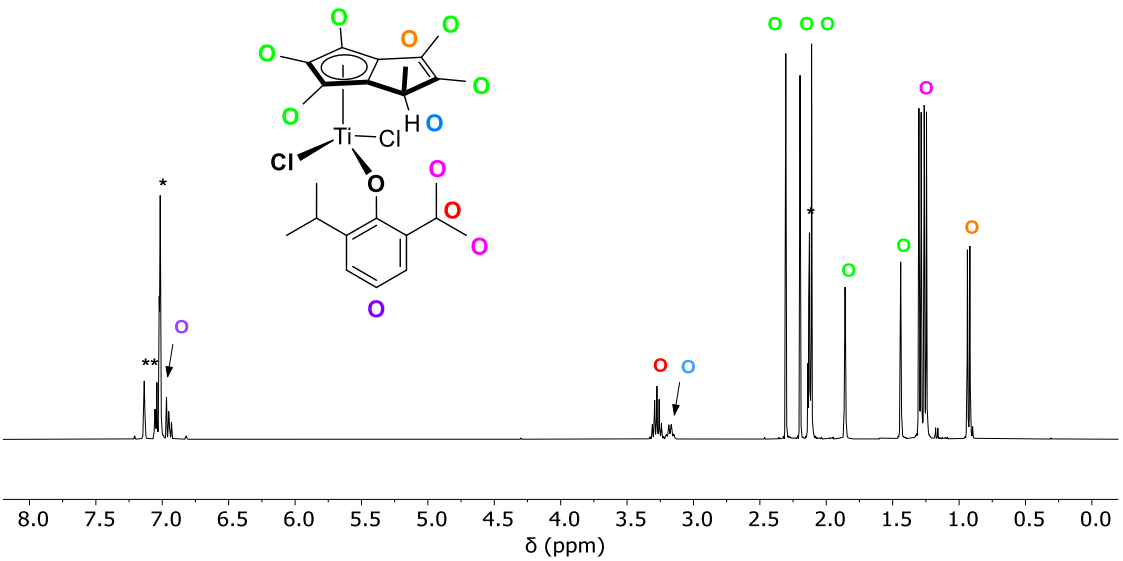

Figure 4.2. ^{1}H NMR spectrum of Pn*(H)TiCl$_2$(O-2,6-^{i}Pr-C$_6$H$_3$) (**3**) (C$_7$D$_8$, 298 K, 400 MHz). * denotes residual protio solvent.

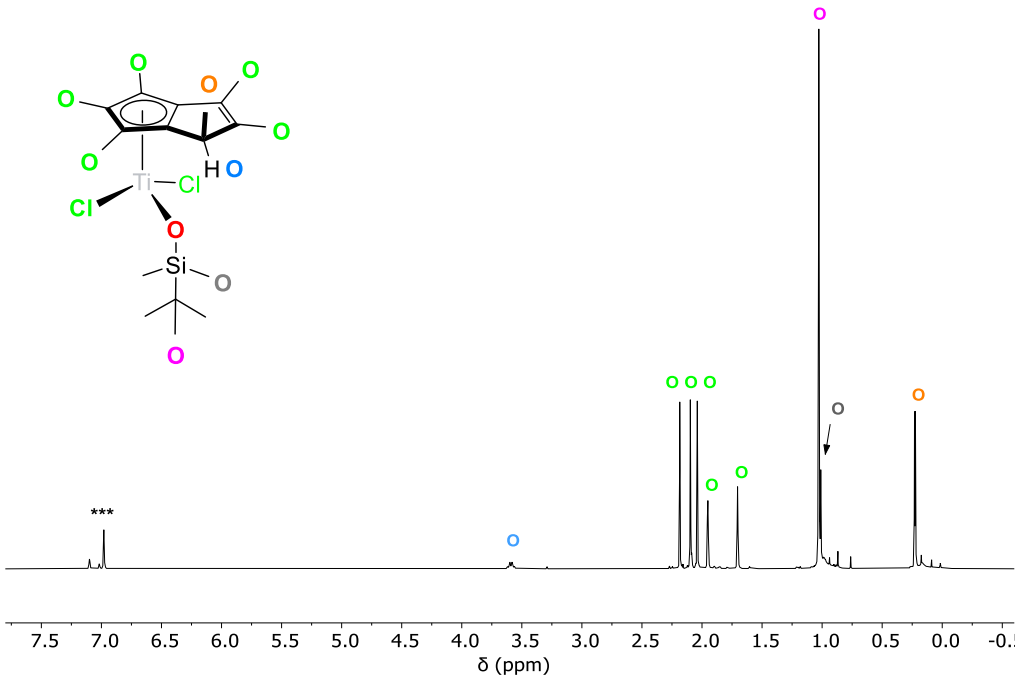

Figure 4.3. ^{1}H NMR spectrum of Pn*(H)TiCl$_2$(O-Si(CH$_3$)$_2$^{t}Bu) (**5**) (C$_7$D$_8$, 298 K, 400 MHz). * denotes residual protio solvent.

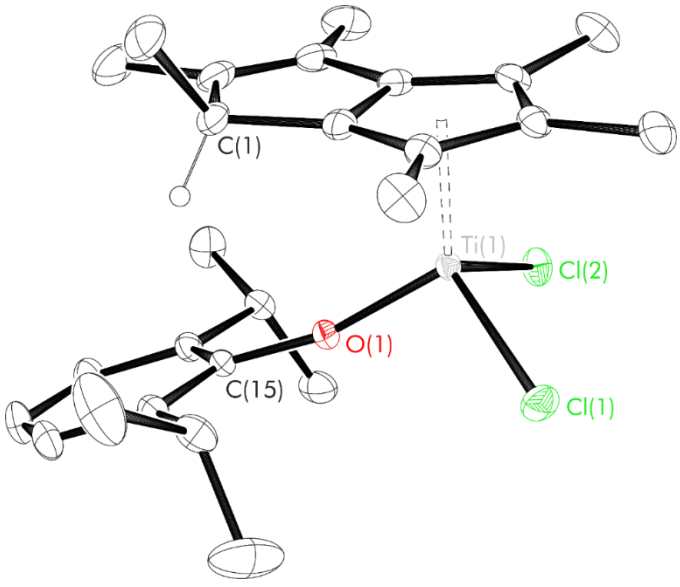

Figure 4.4. Thermal displacement ellipsoid drawing (30% probability) of Pn*(H)TiCl$_2$(O-2,6-^{i}Pr-C$_6$H$_3$) (**3**). All hydrogen atoms apart from that bound to C(1) have been omitted for clarity.

Single crystals of **3** suitable for X-ray single crystal structure determination were grown at room temperature from a pentane solution (Figure 4.4 and Table 4.2). The coordination geometry of titanium is distorted tetrahedral (*e.g.* Cl(1)-Ti(1)-Cl(2) = 104.591(16)°, O(1)-Ti(1)-Cl(1) = 101.94(3)°, O(1)-Ti(1)-Cl(2) = 101.28(3)° and Cl(1)-Ti(1)-C_t = 112.96°) and the complex adopts a structure similar to that of the classic piano stool arrangement exhibited by many cyclopentadienyl complexes.[21,23–25] The Ti-O distance of Pn*(H)$TiCl_2$(O-2,6-Me-C_6H_3) reported by O'Hare *et al.* (1.7925(17) Å) is shorter than the distance observed in **3** (1.7892(9) Å) and the two angles Cl(1)-Ti-Ct (112.96°) and Cl(2)-Ti-Ct (114.05°) are bigger (112.96° and 114.05° for complex **3** and 112.38° and 113.80° for the methyl analogue).[21] Compared with the cyclopentadienyl compound Cp*$TiCl_2$(O-2,6-Me-C_6H_3),[15] the O-Ti-Ct angle is very similar (120.10° for Pn* an 120.5° for Cp*) but the O-Ti-Cl angles (101.94(3) and 101.28(3)°) are very different from the Cp* analogue (99.1(2) and 104.1(2)°). According to previously synthesised (hydro)permethylpentalene complexes, the methyl group attached to C1 is oriented in the *exo*-position to the titanium centre to reduce steric hindrance.[21] This stereochemistry results from the coordination of the alcohol to the metal centre followed by an intramolecular protonation of the Pn* ring.[21] The Ti(1)-O(1)-C(15) angle is 164.85(8)° indicating that, while there is likely some contribution to bonding from overlap of the Ti d_π and O p_π orbitals, the significant steric bulk of the aryloxide group results in a deviation from linearity.

Table 4.2. Selected bond lengths (Å) and angles (°) for Pn*(H)$TiCl_2$(O-2,6-^{i}Pr-C_6H_3) (**3**).

Ti(1)-C_t	2.8088(1)	C(2)-C(1)-C(8)	101.18(13)
Ti(1)-	2.2794(4)	Cl(1)-Ti(1)-Cl(2)	104.591(16
Ti(1)-	2.2619(4)	O(1)-Ti(1)-Cl(1)	101.94(3)
Ti(1)-	1.7892(9)	O(1)-Ti(1)-Cl(2)	101.28(3)
C(1)-C(2)	1.518(3)	Cl(1)-Ti(1)-C_t	112.96
C(1)-C(8)	1.508(2)	Cl(2)-Ti(1)-C_t	114.05
C(5)-C(6)	1.416(2)	O(1)-Ti(1)-C_t	120.10
C(6)-C(7)	1.437(2)	Ti(1)-O(1)-C(15)	164.85(8)
C(7)-C(8)	1.406(2)	C(2)-C(1)-C(8)	101.18(13)
		Cl(1)-Ti(1)-Cl(2)	104.591(16
		O(1)-Ti(1)-Cl(1)	101.94(3)

4.2.3 Alternative synthetic routes

Turner *et al.* reported an alternative synthetic route, salt metathesis, for the synthesis of Pn*(H)$TiCl_2$(OAr) complexes using potassium aryloxides (Scheme 4.3).[26] Using the same reaction conditions, attempt syntheses of Pn*(H)$TiCl_2$(O^{t}Bu), Pn*(H)$TiCl_2$(O-2,6-^{i}Pr-C_6H_3) and Pn*(H)$TiCl_2$(O-2,6-Me-C_6H_3) were carried out in benzene. While the alkoxide derivative decomposed quickly, the formation of the two aryloxide analogues proceeded at 80 °C but a mixture of the target complexes, unreacted materials and multi-subtituted Pn* titanium species were obtained. The protonolysis route using alcohols gave cleaner reactions and was preferred for the synthesis of Pn*(H)$TiCl_2$(OR) complexes.

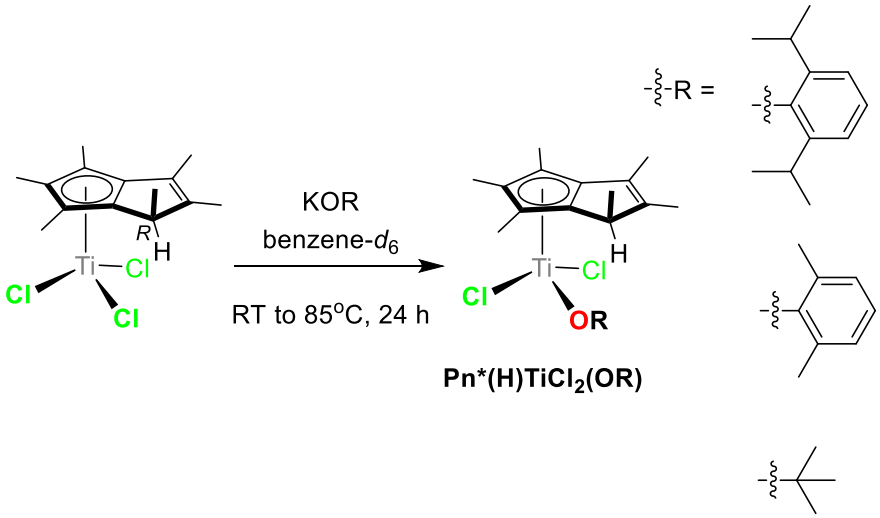

Scheme 4.3. Attempted synthesis of Pn*(H)$TiCl_2$(OR) complexes using potassium salts.

4.3 Homopolymerisation of styrene

To determine the effect of the aryloxide/alkoxide substituent on catalytic performances, the three titanium complexes Pn*(H)$TiCl_2$(O-2,6-^{i}Pr-C_6H_3) (**3**), Pn*(H)$TiCl_2$(O-2,4-^{t}Bu-C_6H_3) (**4**) and Pn*(H)$TiCl_2$(O-Si$(CH_3)_2{}^t$Bu) (**5**) were tested for homopolymerisation of styrene with MAO as co-catalyst.

4.3.1 Solution phase styrene polymerisation

Solution phase polymerisations of styrene were carried out in 2 mL of toluene using MAO as a co-catalyst in a molar ratio of $[Al_{MAO}]_0$:$[Ti]_0$ = 1500:1. The trichloride complex Pn*(H)$TiCl_3$ (**2**) from Chapter 2 was used as a reference. As expected, the three complexes behaved differently regarding the polymerisation of styrene (Figure 4.5). The aryloxide complexes **3** and **4** displayed lower catalytic activities than **2** across the same range of temperatures. The activities obtained with **4** showed little variation with polymerisation temperature, similarly to the trichloride complex **2**. Complex **3** was observed to have increasing activity from 1365 $kg_{PS}/mol_{Ti}/h$ at 40 °C to 3090 $kg_{PS}/mol_{Ti}/h$ at 55 °C. This trend is consistent with the reports by Nomura *et al.* using Cp*$TiCl_2$(O-2,6-^{i}Pr-C_6H_3). The activities increased by 13 times from 285 to 1640 and 3600 $kg_{PS}/mol_{Ti}/h$ at 40, 55 and 70 °C under similar conditions.[3,9] The siloxide derivative exhibited high polymerisation activities between 5400 and 5790 $kg_{PS}/mol_{Ti}/h$ which are up to 1.8 times higher than Pn*(H)$TiCl_3$. This increase compared to the trichloride analogue is consistent with results observed by Chan *et al.*, where $CpTiCl_2$(OR) compounds (R = Me, Et, ^{i}Pr) perform 58% better than $CpTiCl_3$.[4,27] Complex **5** performed better than aryloxide complexes **3** and **4** due to the smaller size of the ligand that facilitates the approach of styrene to the active site. As reported by Nomura and co-workers, at temperatures lower than 70 °C the steric effect was more important

than electronic effect and complexes with large substituents perform poorly compared to smaller ones.[9] Chan *et al*. also showed that $CpTiCl_2(OR)$ catalysts performed in the order R = Me (90 $kg_{PS}/mol_{Ti}/h$) > Et (77 $kg_{PS}/mol_{Ti}/h$) > ^{i}Pr (76 $kg_{PS}/mol_{Ti}/h$) suggesting that steric hinderance reduced polymerisation activities.[27] At 40 and 55 °C, **5** showed higher activities than aryloxide compounds Cp^*TiCl_2OR (R = C_6H_5, 4-Me-C_6H_4, 2,6-Me-C_6H_3 and 2,6-^{t}Bu-C_6H_3).[3] Qian and co-workers successfully polymerised styrene with alkoxides $CpTiCl_2(OR)$ along with MAO, however they reported low activities compared to the Pn*(H) siloxide.[28] At 50 °C, $CpTiCl_2(O^{i}Pr)$ and $CpTiCl_2(OCH_2CH_2OCH_3)$ exhibited activities of 60 and 74 $kg_{PS}/mol_{Ti}/h$ respectively.[29]

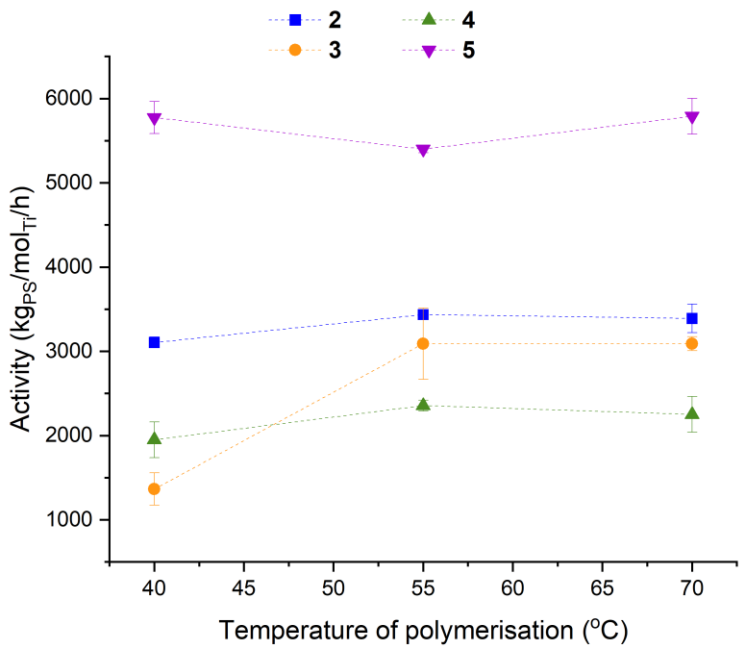

Figure 4.5. Temperature dependence of solution phase styrene polymerisation by $Pn^*(H)TiCl_2(OR)$. Polymerisation conditions: 10 minutes, 1000 rpm. 2 mL toluene, 2×10^{-7} mol catalyst, 1 mL styrene, $[Al_{MAO}]_0$:$[Ti]_0$ = 1500:1.

The polystyrenes obtained were characterised by gel permeation chromatography and were shown to possess multimodal molecular weight distributions with the low molecular weight fraction being 5 times more intense than the high molecular weight fraction (Figure 4.6).

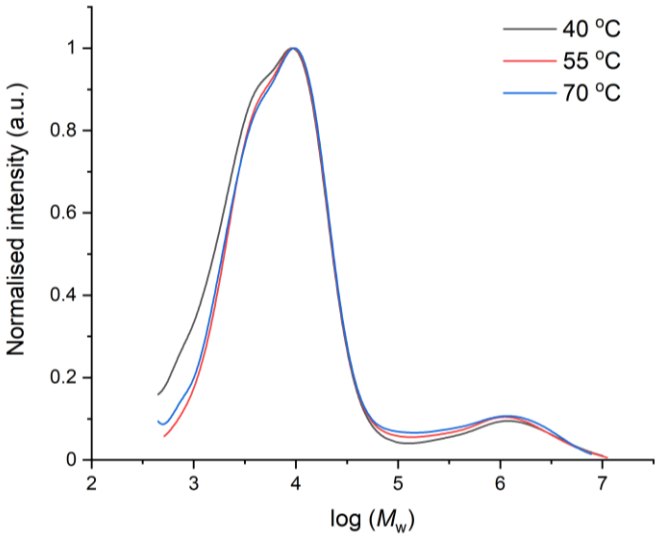

Figure 4.6. Molecular weight distribution of the polystyrene produced by Pn*(H)$TiCl_2$(O-2,6-^{i}Pr-C_6H_3) (**3**). Polymerisation conditions: 10 minutes, 1000 rpm. 2 mL toluene, 2×10^{-7} mol catalyst, 1 mL styrene, $[Al_{MAO}]_0$:$[Ti]_0$ = 1500:1.

A likely explanation for the presence of two fractions could be the coexistence of two active species. In Ti catalysed styrene polymerisation, it is thought that the major active species is Ti^{III+} moiety,[30–33] however the presence of neutral Ti^{III} or cationic Ti^{IV} active species might be responsible for the formation of a second fraction. The mechanism remains unclear but Nomura and co-workers suggested that neutral Ti^{III} or cationic Ti^{IV} could have a role in styrene polymerisation using this titanocene-type complexes.[3,30]

In the GPC trace, the molecular weight high fraction comprised molecular weights between 1.3×10^6 and 5×10^6 g/mol, the GPC traces show almost no variation with polymerisation temperature (Figure 4.7). Polystyrenes with lower molecular weights were also obtained, with values between 0.9×10^4 and 1.4×10^4 g/mol. The polydispersities (Đ, M_w/M_n) of the high polystyrene weight fraction were narrow (1.7–3.6) with **5** displaying the lowest values. For both fractions, **3** yielded polymer with the lowest M_w of the series (9325 g/mol at 40 °C). The M_w of polymers produced by **3** followed a different evolution than those observed for Cp*$TiCl_2$(O-2,6-^{i}Pr-C_6H_3). Even though the dispersities were in the same range, Nomura *et al*. observed monomodal molecular

weight distributions with molecular weights (M_w) one order of magnitude lower than those obtained with the Pn* derivative (26.8×10^4 g/mol, Đ= 2.6 at 40 °C).[3] Cp*$TiCl_2$(O-2,6-^{t}Bu-C_6H_3) produced higher M_w than Cp*$TiCl_2$(O-2,6-^{t}Bu-C_6H_3) (49.0×10^4 vs 20.5×10^4 g/mol at 70 °C) implying that the steric bulk of the anionic ligand affects M_w.[9] However, polystyrene with higher M_w were achieved with **4** compared to **3**. This result suggested that opening the aromatic ring on C6 allowed for a better monomer approach yielded longer chains.

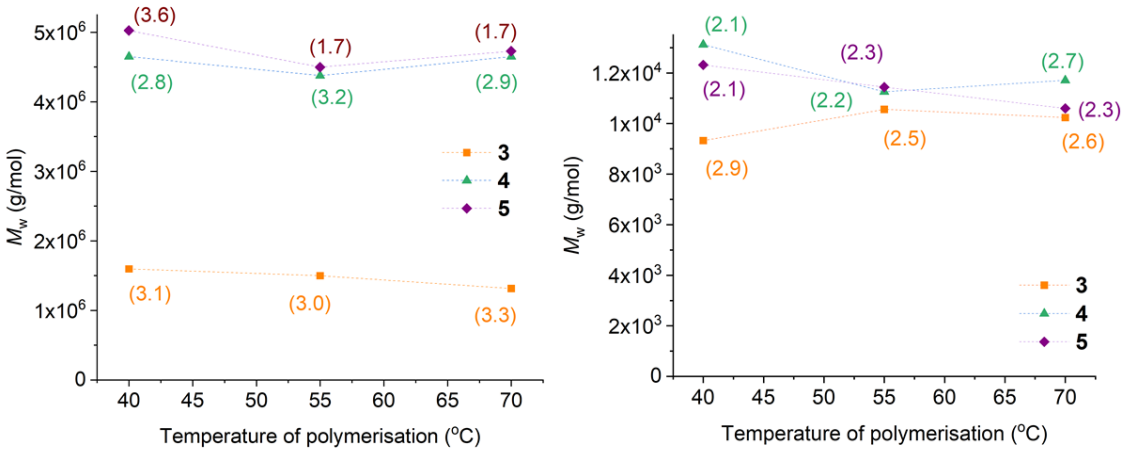

Figure 4.7. Polystyrenes molecular weights (M_w) and dispersities (in brackets) for solution phase polymerisations by Pn*(H)$TiCl_2$(OR). Polymerisation conditions: 10 minutes, 1000 rpm. 2 mL toluene, 2×10^{-7} mol catalyst, 1 mL styrene, $[Al_{MAO}]_0$:$[Ti]_0$ = 1500:1.

^{1}H and ^{13}C{^{1}H} NMR spectroscopy confirmed the formation of polystyrene (Figure A4.19–31). The deconvolution of the methine peak signal around 40 ppm suggested the formation of atactic polystyrene with a trend towards *meso* arrangments. The probability to obtain syndiotactic polymers were calculated between 0.57 and 0.62.[34–37]

The tacticity of the polystyrene was confirmed by DSC where no melting peak was observed (Figure 4.8).The glass transition temperature of the polystyrenes varied with the catalyst used meaning that the anionic -OR ligand influence the physical properties of the polystyrene produced. Syndiotacticity was observed by Qian and co-workers using

$CpTiCl_2(OR)$ complexes. Polystyrenes synthesised using the alkoxide and aryloxide half-titanocenes displayed melting peaks around 257-260 °C confirming the formation of syndiotactic polystyrene (*e.g.* T_m = 259 °C for $CpTiCl_2(O^iPr)$).[28,29]

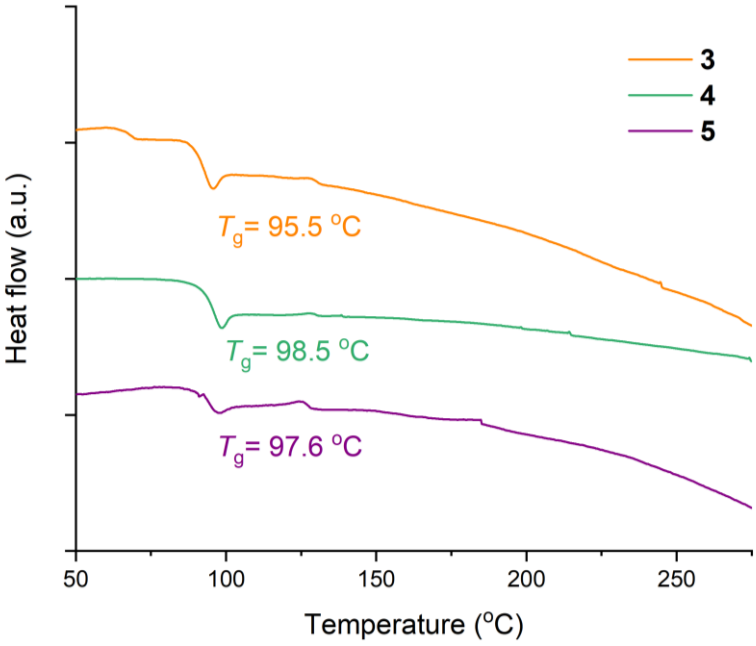

Figure 4.8. DSC plots of polystyrene produced by $Pn^*(H)TiCl_2(OR)$. Polymerisation conditions: 10 minutes, 1000 rpm. 2 mL toluene, 2×10^{-7} mol catalyst, 1 mL styrene, $[Al_{MAO}]_0$:$[Ti]_0$ = 1500:1.

The morphology of the polystyrene varied greatly depending on the titanium catalyst (Figure 4.9). The two aryloxide complexes yielded a colourless powder formed by small aggregates of various sizes, similar to the morphology observed by Entezami *et al*. with indenyl compounds.[38,39] **5** produced a very brittle glass-like polystyrene sheets of 40 µm width. The lack of control over the morphology using **5** might explain the lower enthalpy highlighted by DSC (Figure 4.8).

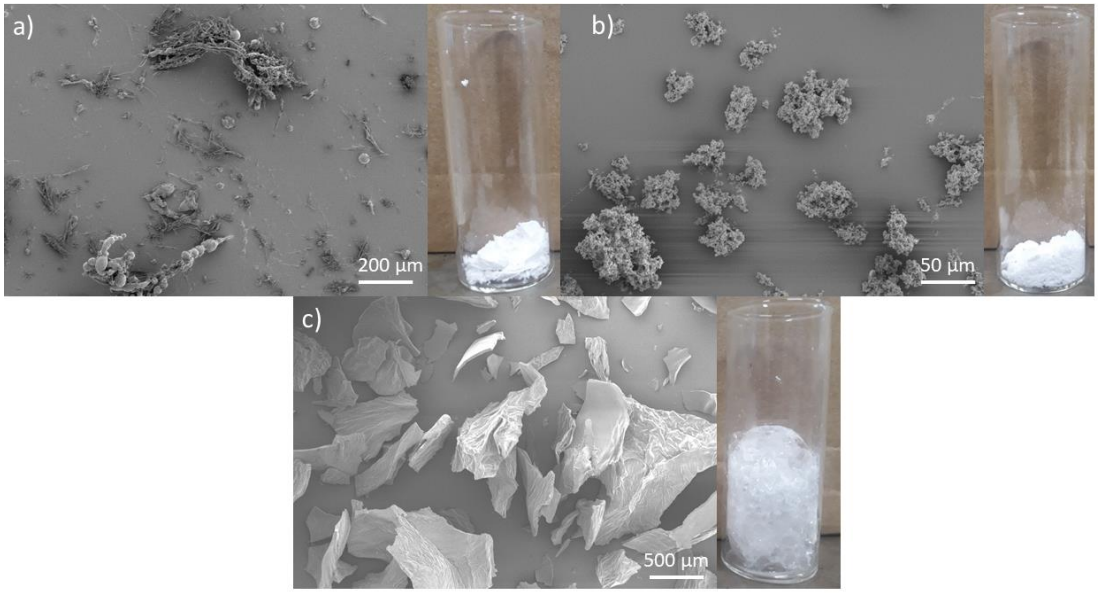

Figure 4.9. SEM images and pictures of polystyrene produced by a) Pn*(H)$TiCl_2$(O-2,6-^{i}Pr-C_6H_3) (**3**) (x80), b) Pn*(H)$TiCl_2$(O-2,4-^{t}Bu-C_6H_3) (**4**) (x300) and c) Pn*(H)$TiCl_2$(O-Si$(CH_3)_2{}^{t}$Bu) (**5**) (x30) at 40 °C.

4.3.2 Slurry-phase styrene polymerisation

Similarly to Chapter 2, the three Pn* complexes were immobilised on sMAO in a molar ratio of $[Al_{sMAO}]_0$:$[Ti]_0$ = 200:1 and tested as slurry-phase styrene polymerisation catalysts in toluene dispersion (Figure 4.10). The addition of an aryloxide/alkoxide group significantly reduced polymerisation activities compared to the parent trichloride compound. These three catalyst systems perform better than the $CpTiCl_3$/MAO/SiO_2 system described by Kaminsky.[2] At 30 °C, the supported cyclopentadienyl complex achieved 5.0 $kg_{PS}/mol_{Ti}/h$ using TiBA as a scavenger. The two supported aryloxide catalysts display similar activities with little to no variation in activity with polymerisation temperature (1143 and 1221 $kg_{PS}/mol_{Ti}/h$ for $\mathbf{3_{sMAO}}$ and $\mathbf{4_{sMAO}}$ at 55 °C respectively). O'Hare and co-workers observed interactions between the MAO support and the aryloxide ligands for ethylene polymerisation, resulting in low activities.[40] It is hypothesised that the aryloxide groups become bound to the solid support during immobilisation and may therefore hinder styrene coordination.[40,41] Once again, $\mathbf{5_{sMAO}}$

stands out with higher activities. The polymerisation activity increased from 1938 $kg_{PS}/mol_{Ti}/h$ at 40 °C to 3442 $kg_{PS}/mol_{Ti}/h$ at 55 °C. The activities measured in slurry-phase using Pn*(H)$TiCl_2$(OR) were up to 3 times lower compared to solution phase. This result was consistent with the decline in activity observed by Ihm *et al.* for the homopolymerisation of styrene using $CpTiCl_3$ supported on MAO-treated silica.[42,43] The use of the heterogeneous catalyst caused a 58% decrease in activity compare to the homogeneous $CpTiCl_3$ (39.2 *vs.* 16.6 $kg_{PS}/mol_{Ti}/h$ at 50 °C).

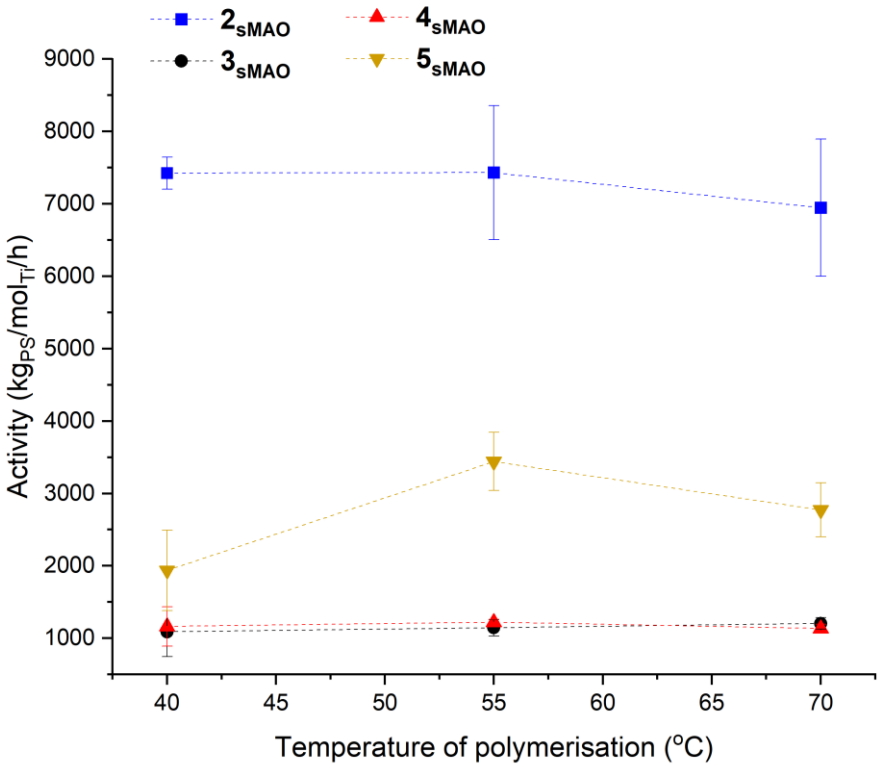

Figure 4.10. Temperature dependence of slurry-phase styrene polymerisation by sMAO-Pn*(H)$TiCl_2$(OR). Polymerisation conditions: 10 minutes, 1000 rpm. 50 mL toluene, 10 mg catalyst, 3.7 mL styrene, $[Al_{sMAO}]_0$:$[Ti]_0$ = 200:1.

Similar to solution-phase polymerisation, polymers produced in slurry-phase possessed a multimodal distribution (Figures 4.11 and 4.12). While only **3$_{sMAO}$** displayed M_w inferior to solution phase for the high fraction, the lower fraction showed that all three titanium species have higher M_w compared to solution phase (Figure 4.11). Noteworthy

is the increase from 1.9×10^6 to 4.5×10^6 g/mol displayed by $\mathbf{5}_{\mathbf{sMAO}}$. $\mathbf{3}_{\mathbf{sMAO}}$ exhibited two maxima at 2.2×10^6 and 10.1×10^3 g/mol for a polymerisation temperature of 55 °C. The M_w of polymers produced by $\mathbf{4}_{\mathbf{sMAO}}$ were mostly independent of the temperature for the two fractions. The M_w obtained with the three supported complexes were notably higher than values described for other supported titanium complexes.[2,42–44] Ihm and co-workers observed that $CpTiCl_3$ supported on MAO treated silica yielded lower M_w than when supported on silica only (38.6×10^3 vs 44.6×10^3 g/mol) along with a broader dispersity (4.4 vs 5.7).[42] Later on they also stated that titanium trichlorides such as Cp^*TiCl_3 and $IndTiCl_3$ supported on SiO_2 generated molecular weights 39% and 20% higher than their homogeneous analogues with similar dispersities.[43] At 50 °C, the homogeneous polymerisation of styrene with Cp^*TiCl_3 produced polymer with 116.2×10^3 g/mol while the heterogeneous catalysis produced polystyrene with 161.3×10^3 g/mol.[43]

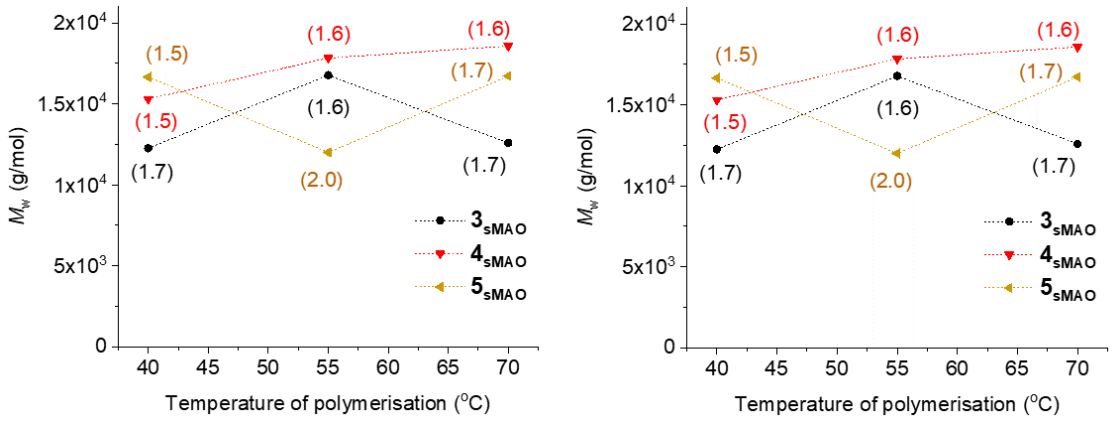

Figure 4.11. Molecular weight of high-molecular weight (left) and low-molecular weight (right) polystyrene produced by sMAO-Pn*(H)$TiCl_2$(OR). Polymerisation conditions: 10 minutes, 1000 rpm. 50 mL toluene, 10 mg catalyst, 3.7 mL styrene, $[Al_{sMAO}]_0$:$[Ti]_0$ = 200:1.

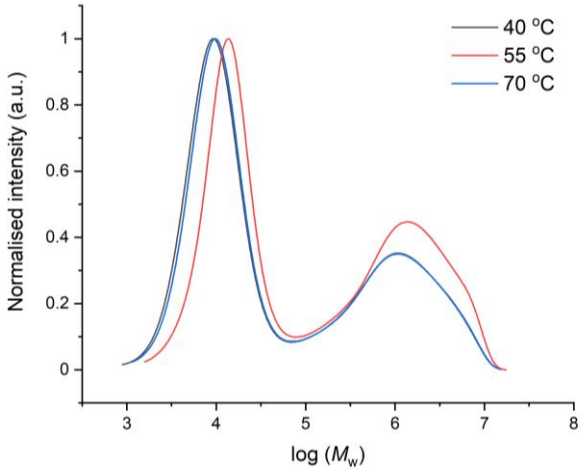

Figure 4.12. Molecular weight distribution of polystyrene produced by sMAO-Pn*(H)$TiCl_2$(O-2,6-^{i}Pr-C_6H_3) (**3$_{sMAO}$**).

The determination of the polystyrene tacticity was achieved by NMR spectroscopy. Analysis of the $^{13}C\{^1H\}$ NMR spectra revealed atactic polystyrene (P_m = 0.56–0.60, Table A4.10). DSC confirmed the amorphous nature of the polymers by the absence of melting heat flow in the region 240-280 °C (Figure 4.13). Conversely, Kaminsky and co-workers have reported melting temperatures between 246 and 258 °C for polystyrene synthesised using $CpTiCl_3$ supported on MAO-treated silica.[2] Their thermal analysis of two half-sandwich complexes $CpTiCl_3$ and $CpTiF_3$ supported on MAO/SiO_2 revealed glass transition temperature between 98 and 102 °C depending on the ratio $Al_{support}$:Ti, which is consistent with the T_g measured for the three Pn* compounds (Figure 4.13).

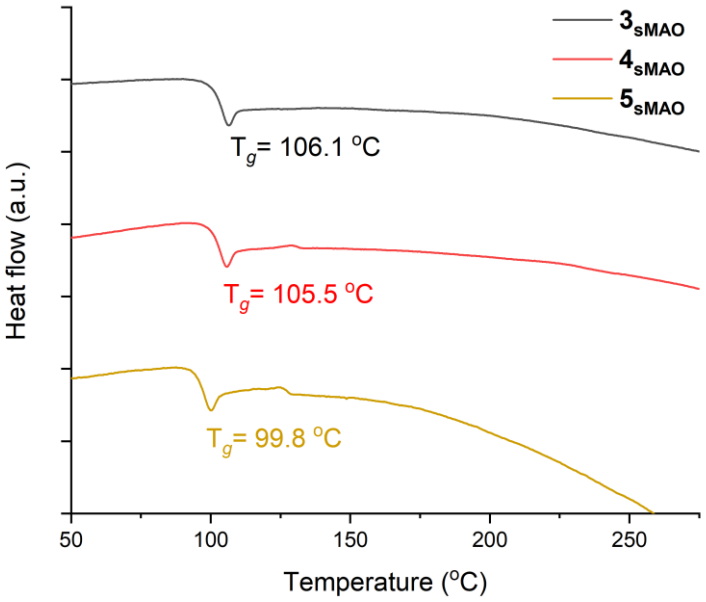

Figure 4.13. DSC plots of polystyrene produced by sMAO-Pn*(H)$TiCl_2$(OR). Polymerisation conditions: 10 minutes, 1000 rpm. 50 mL toluene, 10 mg catalyst, 3.7 mL styrene, $[Al_{sMAO}]_0$:$[Ti]_0$ = 200:1.

Unlike in solution phase, the polymer samples synthesised using **3$_{sMAO}$** and **4$_{sMAO}$** were brittle materials formed by very thin sheets, similar to those produced by **5$_{sMAO}$** in both homogeneous and heterogeneous polymerisations (Figure 4.14). The morphology obtained was unexpected for sMAO-supported catalysts. Indeed, O'Hare *et al.* described the formation of popcorn-shaped polymers using sMAO-supported catalysts due to replication of the solid support morphology.[45,46] Entezami and co-workers also observed replication for silica-supported indenyl catalysts.[38,39] This result may be a consequence of catalysts leaching from the support. Indeed, desorption from the solid MAO can occur in the presence of MAO and TiBA and the catalysts then behave similar to solution phase, in this case leading to comparable morphologies.[47–51]

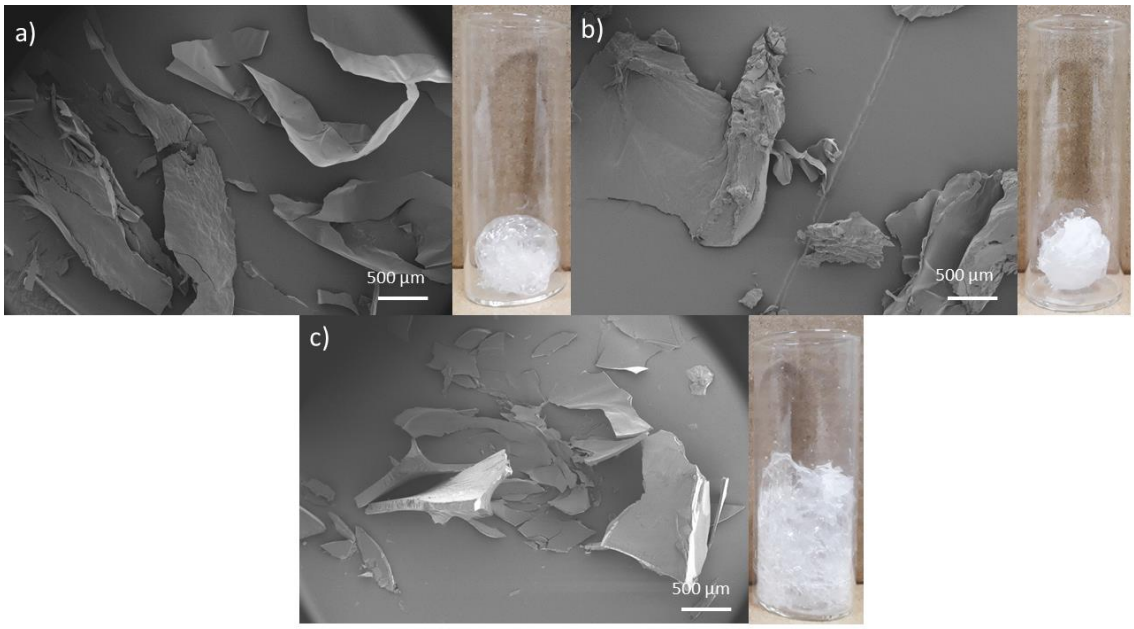

Figure 4.14. SEM images and pictures of polystyrene produced by a) sMAO-Pn*(H)$TiCl_2$(O-2,6-^{i}Pr-C_6H_3) (**3$_{sMAO}$**) (x25), b) sMAO-Pn*(H)$TiCl_2$(O-2,4-^{t}Bu-C_6H_3) (**4$_{sMAO}$**) (x30) and c) sMAO-Pn*(H)$TiCl_2$(O-Si$(CH_3)_2{}^t$Bu) (**5$_{sMAO}$**) (x25).

4.4 Homopolymerisation of ethylene

The same three titanium complexes, Pn*(H)$TiCl_2$(OR) (R = 2,6-^{i}Pr-C_6H_3 (**3**), 2,4-^{t}Bu-C_6H_3 (**4**), $SiMe_2{}^t$Bu (**5**)) were then tested as catalysts for solution and slurry-phase polymerisation of ethylene.

4.4.1 Solution phase ethylene polymerisations

Homogeneous ethylene polymerisations were carried out in hexane between 40-80 °C in the presence of MAO as co-catalyst (Figure 4.15). The polymerisation activities for the Pn*(H)$TiCl_2$(OR)-MAO system were observed to be lower than those or the trichloride analogue. At 40 °C, the substitution by O-2,6-^{i}Pr-C_6H_3 led to a 93% decrease in activity. Nomura *et al.* reported drastically higher catalytic activities for Cp*$TiCl_2$(OAr) with Cp*$TiCl_2$(O-2,6-^{i}Pr-C_6H_3) exhibiting high activity of 1240 $kg_{PE}/mol_{Ti}/h$ at 60 °C while 35 $kg_{PE}/mol_{Ti}/h$ was obtained under similar reaction conditions with **3**.[15,52] The activities obtained with the latter are lower than Cp$TiCl_2$(O-2,6-^{i}Pr-C_6H_3) (87 $kg_{PE}/mol_{Ti}/h$ at 25 °C).[53] Firth *et al.* described a 66% increase in activity as a result of the inclusion of a second Cp ring in the catalyst precursor.[53] The activity of Pn*(H)$TiCl_2$(OR) decreased in the order R = $Si(Me)_2{}^t$Bu > 2,4-^{t}Bu-C_6H_3 > 2,6-^{i}Pr-C_6H_3 suggesting that steric hindrance affects the catalyst performance. The three Pn*(H)$TiCl_2$(OR) complexes generated activities in the range of those reported for aryloxide and alkoxide half-titanocenes. Wu *et al.* investigated the effect of different substituents on the Cp ring of Cp'$TiCl_2$(O-2,6-^{i}Pr-C_6H_3) and they obtained activities between 130 and 336 $kg_{PE}/mol_{Ti}/h$ by varying the polymerisation temperature.[54]

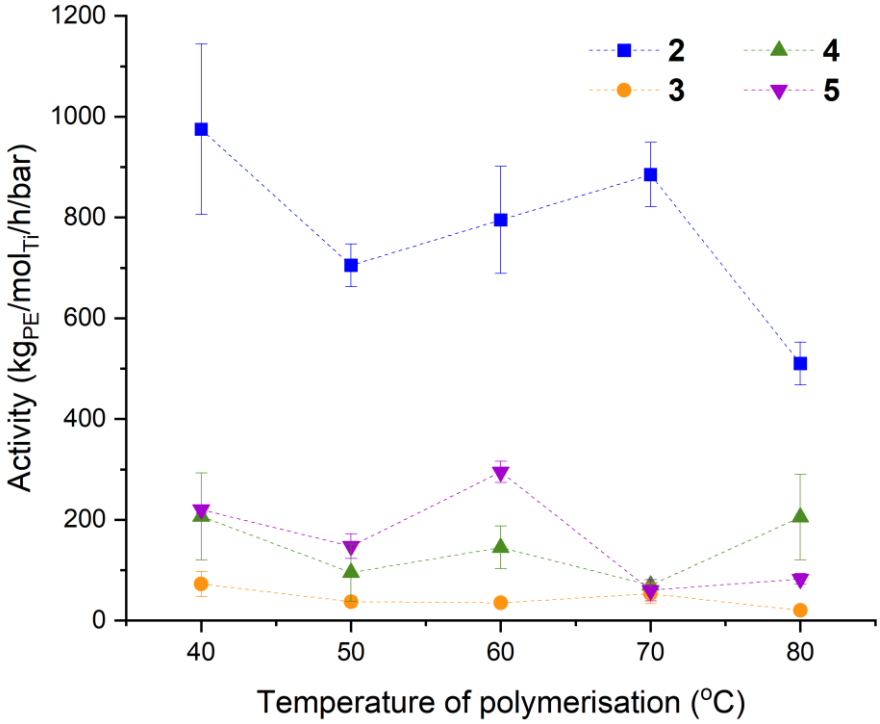

Figure 4.15. Temperature dependence of ethylene polymerisation activities by Pn*(H)TiCl$_2$(OR). Polymerisation conditions: 30 minutes, 1000 rpm. 50 mL hexane, 2×10^{-7} mol catalyst, 2 bar ethylene, 150 mg TiBA, $[Al_{MAO}]_0$:$[Ti]_0$ = 1500:1.

The molecular weights of the polymers synthesised by Pn*(H)TiCl$_2$(O-2,6-^{i}Pr-C$_6$H$_3$) and Pn*(H)TiCl$_2$(O-2,4-^{t}Bu-C$_6$H$_3$) at 40 °C could be analysed by GPC (Figure 4.16). Both catalysts generated multimodal distributions. The morphology observed by SEM was however irregular. The polyethylene produced by Pn*(H)TiCl$_2$(O-Si(CH$_3$)$_2$^{t}Bu) could not be dissolved after several days and therefore was not characterised. High molecular weights of 1.43×10^6 and 1.78×10^6 g/mol were obtained using the two aryloxide complexes which was one to two orders of magnitude higher than polyethylene synthesised using cylopentadienyl aryloxides.[15,52–54] For example, Cp*TiCl$_2$(O-2,6-^{i}Pr-C$_6$H$_3$) yielded polyethylene with M_w of 1.38×10^5 g/mol and a broad molecular weight dispersity of 4.7 due to the bimodality.[52] In the case of the CpTiCl$_2$(O-2,6-^{i}Pr-C$_6$H$_3$), Wu and co-workers observed M_w of 8×10^4 g/mol when Ph$_3$C$^+$[B(C$_6$F$_5$)$_4$]$^-$ was used as an activator.[54] Molecular weights of the polyethylene produced appeared to decrease in the

order Pn*(H) > Cp* > Cp for the (2,6-^{i}Pr-C_6H_3) aryloxide, revealing the effect of the cyclopentadienyl moiety. The stabilisation of the active species by more electron-donating substituents is an important factor to obtain high molecular weights. Similar effects were described by Nomura *et al.* with $Cp^{R}TiCl_2$(O-2,6-^{i}Pr-C_6H_3) in the presence of Al$^{i}Bu_3$/$Ph_3CB(C_6F_5)_4$. The molecular weights of polyethylene followed the order 1,3-$^{t}Bu_2C_5H_3$ (9.54×10^4 g/mol) ~ Cp* (9.17×10^4 g/mol) > $^{t}BuC_5H_4$ (2.85×10^4 g/mol) > 1,3-$Me_2C_5H_3$ (0.75×10^4 g/mol).[52]

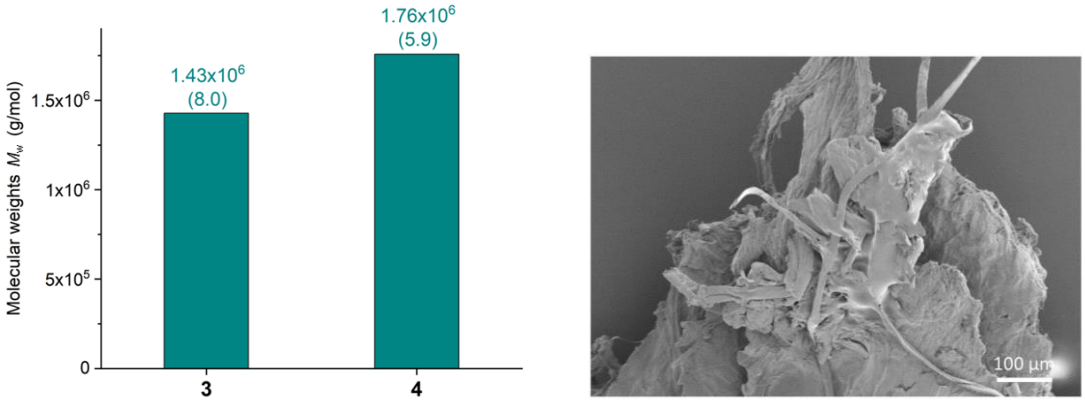

Figure 4.16. Molecular weights of the polyethylenes produced by Pn*(H)$TiCl_2$(O-2,6-^{i}Pr-C_6H_3) (**3**) and Pn*(H)$TiCl_2$(O-2,4-^{t}Bu-C_6H_3) (**4**) at 40 °C, Đ in parentheses and SEM image of polyethylene produced by Pn*(H)$TiCl_2$(O-2,6-^{i}Pr-C_6H_3), (x150).

The polyethylenes obtained in solution phase have a melting temperature between 132.8 and 135.5 °C which is typical of high density polyethylene (Table 4.3, Figure A4.15–18). There was little to no variation of the T_m with the aryloxide/alkoxide ligand although a slight increase was displayed with higher polymerisation temperatures (Table 4.3).

Table 4.3. Peak melting temperatures (T_m), enthalpy and crystallinity of polyethylene produced by Pn*(H)$TiCl_2$(OR).

Complex	T_p (°C)	T_m (°C)	ΔH_m (J/g)	χ_c%
Pn*(H)$TiCl_2$(O-2,6-^{i}Pr-C_6H_3) (**3**)	40	133.8	92.9	32
Pn*(H)$TiCl_2$(O-2,6-^{i}Pr-C_6H_3) (**3**)	50	133.5	78.1	27
Pn*(H)$TiCl_2$(O-2,6-^{i}Pr-C_6H_3) (**3**)	60	133.5	85.8	29
Pn*(H)$TiCl_2$(O-2,6-^{i}Pr-C_6H_3) (**3**)	70	134.6	136.3	47
Pn*(H)$TiCl_2$(O-2,6-^{i}Pr-C_6H_3) (**3**)	80	135.5	103.5	35
Pn*(H)$TiCl_2$(O-2,4-^{t}Bu-C_6H_3) (**4**)	40	133.8	110.1	38
Pn*(H)$TiCl_2$(O-Si$(CH_3)_2{}^t$Bu) (**5**)	40	132.8	100.7	34

4.4.2 Slurry-phase ethylene polymerisation

Heterogeneous polymerisations of ethylene were then performed with complexes supported on sMAO in a molar ratio of $[Al_{sMAO}]_0$:$[Ti]_0$ =200:1 using TiBA acting as scavenger (Figure 4.17). Complexes **3$_{sMAO}$**, **4$_{sMAO}$** and **5$_{sMAO}$** all displayed decreasing activities with an increase in polymerisation temperature. Above 50 °C, the activities were lower than those obtained using **2$_{sMAO}$**. O'Hare *et al.* also observed a reduction in polymerisation activities with the addition of an aryloxide group using *ansa*-bridged permethylindenyl catalysts supported on sMAO. At 80 °C, ^{Me2}SB(Cp,I*)ZrCl(O-2,6-^{i}Pr-C_6H_3) the activity was 9 times less than the parent dichloride compound (549 *vs.* 5144 $kg_{PE}/mol_{Ti}/h/bar$).[45] Activities for sMAO-Pn*(H)$TiCl_2$(OR) greatly depended on the R substituent in the order of Si$(CH_3)_2{}^t$Bu > 2,4-^{t}Bu-C_6H_3 > 2,6-^{i}Pr-C_6H_3 suggesting that the size of the ligand as well as the open area around it played a role in the ability to coordinate an ethylene molecule. Catalytic activities with **5$_{sMAO}$** reached a maximum of 354 $kg_{PE}/mol_{Ti}/h/bar$ at 40 °C before declining to 115 $kg_{PE}/mol_{Ti}/h/bar$ at 80 °C. Except at 60 °C, the catalyst was more active in slurry than in solution-phase.

Supporting the aryloxide catalysts resulted in an increase in activity of up to 62% for **3** at 50 °C. **4_{sMAO}** displayed a very different behaviour than for homogeneous polymerisations and its activity decreased constantly following the same trend as the other aryloxide catalyst. The three supported sMAO-Pn*(H)$TiCl_2$(OR) exhibited a significantly lower catalytic performance compared to other reported group 4 complexes immobilised on solid MAO. Permethylindenyl zirconium complexes ^{Me2}SB(Cp,I*)ZrCl(O-2,6-Me-C_6H_3) and ^{Me2}SB(Cp,I*)ZrCl(O-2,6-^{i}Pr-C_6H_3) catalysed the homopolymerisation of ethylene with high activities of 2262 and 549 $kg_{PE}/mol_{Ti}/h/bar$ at 80 °C.[40] The introduction of an aryloxide group reduced polymerisation activities compared to **2_{sMAO}**. Recently, Nomura and co-workers studied the homopolymerisation of ethylene by Cp*$TiCl_2$(O-2,6-^{i}Pr-C_6H_3) supported on sMAO . They observed very high activities using particles of sMAO of 5.6 µm of diameter. For example, the supported cyclopentadienyl catalyst exhibited an activity of 31×10^3 $kg/mol_{Ti}/h/bar$ at 50 ° C under 6 bar of ethylene which represents a 300-fold increase compared to the permethylpentalene compound.[55] This result also implies that the Cp ring is crucial to achieving high activities using aryloxides and alkoxides in slurry-phase polymerisations. Similar to styrene homopolymerisations discussed in 4.3, the two aryloxide compounds led to similar activities due to interactions between the solid support and the ligand.[40,41]

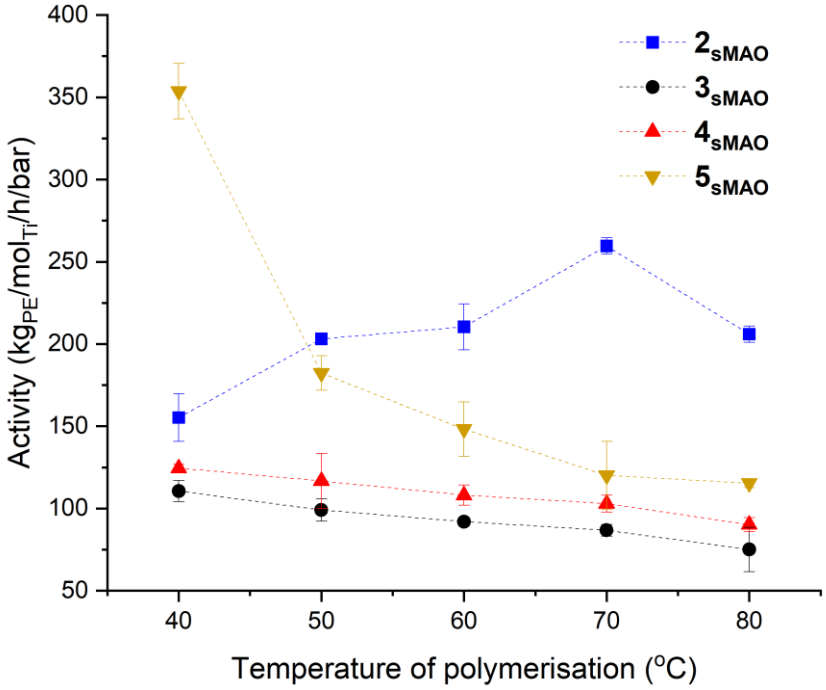

Figure 4.17. Temperature dependence of ethylene polymerisation activities by sMAO-Pn*(H)TiCl$_2$(OR). Polymerisation conditions: 30 minutes, 1000 rpm. 50 mL hexane, 10 mg catalyst, 2 bar ethylene, 150 mg TiBA, [Al$_{sMAO}$]$_0$:[Ti]$_0$ = 200:1.

The polyethylenes produced by **3$_{sMAO}$** and **4$_{sMAO}$** presented bimodal molecular weight distributions suggesting the formation of two active species (probably cationic Ti^{IV} and Ti^{III}) (Figure 4.18 and Table 4.4)[56,57]. Unsurprisingly, for the two fractions, **4$_{sMAO}$** generated polymer with higher M_w than **3$_{sMAO}$**. It is expected that catalysts with bulkier ligands produce polyethylene with higher M_w. Indeed, bulkier coordination environments slow down the process of hydride elimination and chain transfer termination.[40,58]

Polymer molecular weights were shown to decrease with an increase in polymerisation temperatures (Table 4.4). The same trend was observed for other permethylpentalene and permethylindenyl compounds supported on sMAO.[40,59] This decline was expected as higher temperatures induce an increase in termination reaction rates resulting in shorter polymer chains.[60,61] At 40 °C, the molecular weights are slightly higher compared to

homogeneous polymerisations. The molecular weight distributions of all the polymers were found to be relatively narrow over the temperature range (Table 4.4). The polydispersities were narrower than those measured in solution phase (2.6 and 1.8 in slurry-phase *vs.* 5.9 in solution phase).

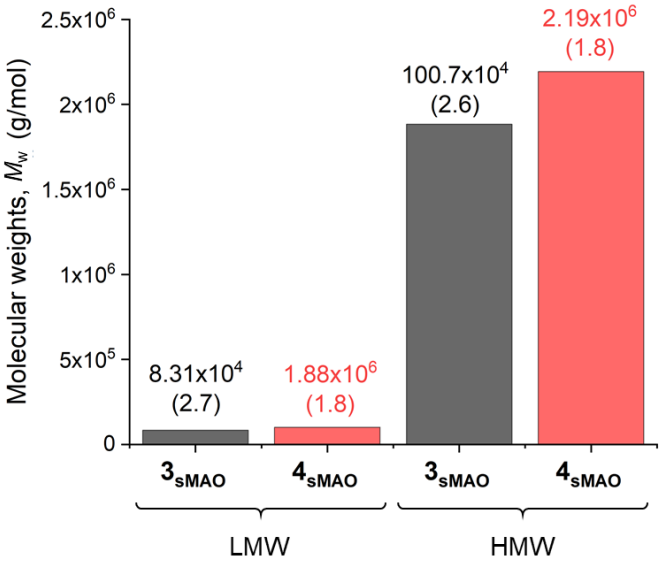

Figure 4.18. Molecular weights of polyethylenes produced by sMAO-Pn*(H)$TiCl_2$(OR) at 40 °C, Đ in parentheses. Polymerisation conditions: 30 minutes, 1000 rpm. 50 mL hexane, 10 mg catalyst, 2 bar ethylene, $[Al_{sMAO}]_0$:$[Ti]_0$ = 200:1.

Table 4.4. Molecular weights and dispersities of the two polyethylene fractions produced by sMAO-Pn*(H)$TiCl_2$(O-2,6-^{i}Pr-C_6H_3) (**3$_{sMAO}$**) and sMAO-Pn*(H)$TiCl_2$(O-2,4-^{t}Bu-C_6H_3) (**4$_{sMAO}$**).

Complex	T_p[a] (°C)	LMW		HMW	
		$M_w\times10^{-4}$ (g/mol)	Đ	$M_w\times10^{-6}$ (g/mol)	Đ
sMAO-Pn*(H)$TiCl_2$(O-2,6-^{i}Pr-C_6H_3) (**3$_{sMAO}$**)	40	8.31	2.7	1.88	1.8
sMAO-Pn*(H)$TiCl_2$(O-2,6-^{i}Pr-C_6H_3) (**3$_{sMAO}$**)	50	7.69	3.0	1.84	1.7
sMAO-Pn*(H)$TiCl_2$(O-2,6-^{i}Pr-C_6H_3) (**3$_{sMAO}$**)	60	5.62	5.0	1.51	1.7
sMAO-Pn*(H)$TiCl_2$(O-2,6-^{i}Pr-C_6H_3) (**3$_{sMAO}$**)	70	5.81	4.5	1.36	1.8
sMAO-Pn*(H)$TiCl_2$(O-2,6-^{i}Pr-C_6H_3) (**3$_{sMAO}$**)	80	4.25	3.9	1.14	1.8
sMAO-Pn*(H)$TiCl_2$(O-2,4-^{t}Bu-C_6H_3) (**4$_{sMAO}$**)	40	100.7	2.5	2.19	1.7

[a] Polymerisation temperature, LMW = low molecular weight fraction, HMW = high molecular weight fraction.

The polymers melting temperatures were measured between 130 and 134.5 °C corresponding to high density polyethylene which is consistent with Wu *et al.* (Table 4.5).[54] DSC characterisation revealed that the T_m slightly decreased from 132.8 to 130.2 °C when the polymerisation temperature increased from 40 to 70 °C. **5$_{sMAO}$** produced polyethylene with the highest melting point of the series (134.2 °C when polymerised at 40 °C).

Table 4.5. Melting temperature, melting enthalpy and degree of crystallinity of polyethylene produced by sMAO-Pn*(H)$TiCl_2$(OR).

Complex	T_p[a] (°C)	T_m (°C)	ΔH_m (J/g)	χ_c (%)
sMAO-Pn*(H)$TiCl_2$(O-2,6-^{i}Pr-C_6H_3) (**3$_{sMAO}$**)	40	132.8	130.4	45
sMAO-Pn*(H)$TiCl_2$(O-2,6-^{i}Pr-C_6H_3) (**3$_{sMAO}$**)	50	131.9	119.6	41
sMAO-Pn*(H)$TiCl_2$(O-2,6-^{i}Pr-C_6H_3) (**3$_{sMAO}$**)	60	131.3	117.0	40
sMAO-Pn*(H)$TiCl_2$(O-2,6-^{i}Pr-C_6H_3) (**3$_{sMAO}$**)	70	130.2	119.4	41
sMAO-Pn*(H)$TiCl_2$(O-2,6-^{i}Pr-C_6H_3) (**3$_{sMAO}$**)	80	133.8	129.4	44
sMAO-Pn*(H)$TiCl_2$(O-2,4-^{t}Bu-C_6H_3) (**4$_{sMAO}$**)	40	133.5	112.0	38
sMAO-Pn*(H)$TiCl_2$(O-Si$(CH_3)_2$^{t}Bu) (**5$_{sMAO}$**)	40	134.2	111.4	38

[a] Polymerisation temperature

The morphologies of the polyethylenes produced using sMAO-Pn*(H)$TiCl_2$(OR) at 40 °C were analysed by SEM (Figure 4.19). The catalysts were shown to replicate the solid support morphology and exhibit a typical "popcorn" shape and a monodisperse morphology. This morphology is typical of polyethylene produced by sMAO-supported catalysts and has been widely reported by O'Hare *et al.*[45,46,59] The particles were uniform in size (~10 μm) and aggregated, confirming that immobilising the complexes on a support significantly improved the polymers morphology.

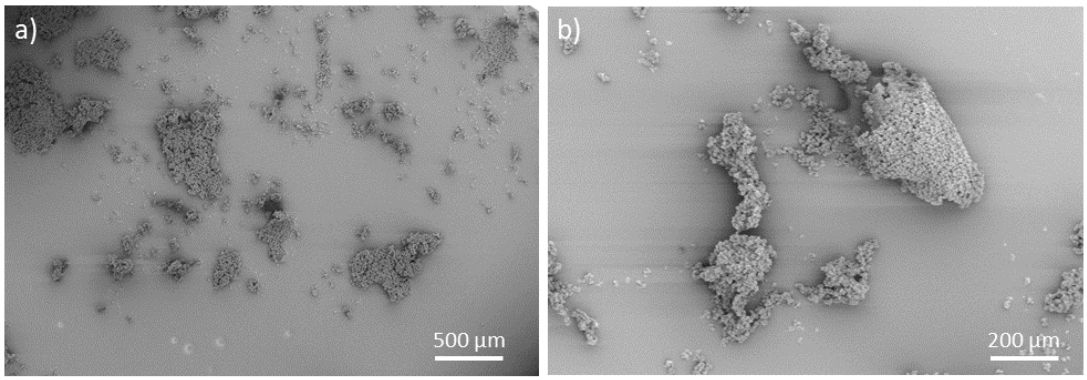

Figure 4.19. SEM images of polyethylene produced by sMAO-Pn*(H)$TiCl_2$(O-2,6-^{i}Pr-C_6H_3) (**3$_{sMAO}$**), a) x33, b) x95.

4.5 Copolymerisation of ethylene and styrene

Nomura and co-workers have been pioneers in the study of copolymerisations of ethylene with α-olefins using cyclopentadienyl half-titanocenes.[13,14,19,52,62,63] Substitution of a chloride ligand by an aryloxide proved to be efficient in the exclusive synthesis of copolymers and prevented the synthesis of a mixture of homopolymers. The three permethylpentalene complexes (**3**, **4** and **5**) were investigated for their copolymerisation properties in homogeneous and heterogeneous phases. Copolymerisations of ethylene with styrene were performed at 40 °C using a fixed volume of 125 µL of styrene (Figure 4.20).

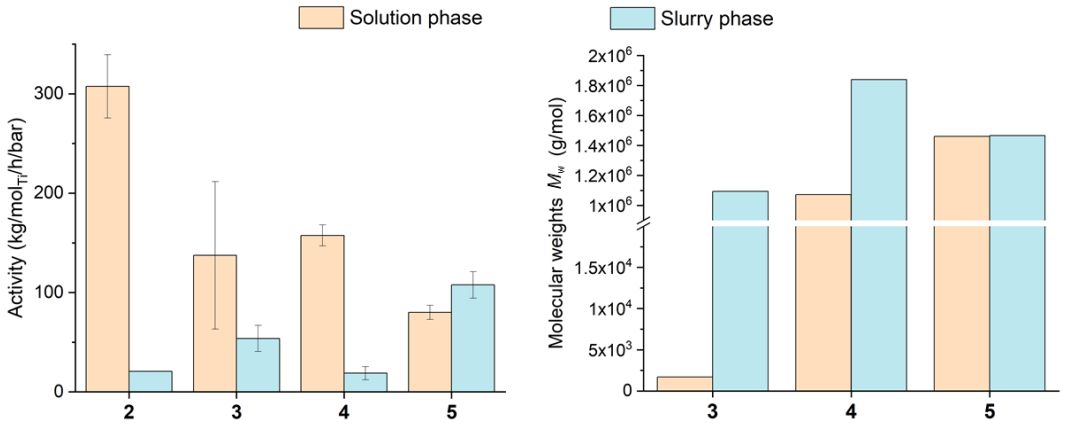

Figure 4.20. Activities and molecular weights of polymers produced by the copolymerisation of ethylene with 125 µL of styrene at 40 °C. Polymerisation conditions: solution: Polymerisation conditions: solution 30 minutes, 1000 rpm. 50 mL hexane, 2×10^{-7} mol catalyst, 2 bar ethylene, 150 mg TiBA, $[Al_{MAO}]_0$:$[Ti]_0$ = 1500:1. Slurry: 30 minutes, 1000 rpm. 50 mL hexane, 10 mg catalyst, 2 bar ethylene, 150 mg TiBA, $[Al_{sMAO}]_0$:$[Ti]_0$ = 200:1.

In a similar manner to Pn*(H)$TiCl_3$ and Cp*$TiCl_3$ in Chapter 2, the copolymerisation reactions yielded two crops. The majority of the polymer was collected in the first crop and the second one contained significant amounts of Al residues. Figure 4.20 shows the activity and the molecular weights obtained in solution and slurry-phase. In solution phase, the three Pn*(H)$TiCl_2$(OR) displayed lower activities than Pn*(H)$TiCl_3$ used as a

reference. The highest activities were measured for **4** (158 kg/mol$_{Ti}$/h/bar) followed by **3$_{sMAO}$** (138 kg/mol$_{Ti}$/h/bar) and **5** (80 kg/mol$_{Ti}$/h/bar). Nomura *et al.* reported activities up to 9 times higher using $Cp^{Me2}TiCl_2$(O-2,6-^{i}Pr-C_6H_3) under 8 bar of ethylene (1483 kg/molTi/h/bar).[13] They also reported higher activities for $Cp^{R}TiCl_2$(O-2,6-^{i}Pr-C_6H_3) confirming the important role of the Cp ring to obtain high activities and stereospecificity.[19]

In the slurry-phase, the activity followed a different trend than for homogeneous polymerisations. Except for **4$_{sMAO}$** which exhibited an activity similar to **2$_{sMAO}$** (19 kg/mol$_{Ti}$/h/bar), the two other modified complexes showed higher activity (54 and 108 kg/mol$_{Ti}$/h/bar for **3$_{sMAO}$** and **5$_{sMAO}$** respectively). Noteworthy is the differentiation in activity for the two aryloxides which behaved identically for the homopolymerisation of ethylene. Furthermore, the three (hydro)permethylpentalene sMAO-Pn*(H)$TiCl_2$(OR) had lower activities compared to slurry-phase ethylene polymerisation (19 *vs.* 125 kg/mol$_{Ti}$/h/bar for **4$_{sMAO}$** at 40 °C). Conversely, the opposite trend was observed by Nomura in the copolymerisation of ethylene with 1-hexene.[55]

As expected, the molecular weights obtained in slurry-phase were higher than those in solution (Table 4.6). The immobilisation of the titanium compounds on sMAO allowed for a better reaction control and reduced the rate of termination to chain propagation. Except for **3** which showed very low molecular weights, the (hydro)permethylpentalene compounds all produced high molecular weights, one order of magnitude greater than copolymers reported in the literature.[9,13,19,62–64] Nomura *et al*. reported molecular weights of 17×10^4 g/mol using (1,2,4-Me_3-C_5H_2)$TiCl_2$(O-2,6-^{i}Pr-C_6H_3) under 4 bar of ethylene.[19]

The melting temperatures measured by DSC (e.g. 132.3 °C for **4$_{sMAO}$** after addition of 125 µL styrene) were very similar to those of homopolyethylene (133.5 °C for **4$_{sMAO}$** at 40 °C) suggesting that little to no incorporation of styrene occurred (Table 4.6 and Figure 4.21). By contrast, high styrene incorporation was shown using half-titanocene aryloxides.[19,63,65] 56.6% of styrene incorporation were reached using (1,3-Me_2-C_5H_3)$TiCl_2$(O-2,6-^{i}Pr-C_6H_3) as catalyst in solution phase.[13] Likewise, between 36.6 and 40.0% of 1-hexene incorporation could be achieved using Cp* $TiCl_2$(O-2,6-^{i}Pr-C_6H_3) supported on different types of solid MAO.[55] The absence of melting peak between 150 and 280 °C implied that the copolymers synthesised have no stereoregularity and are atactic. It is worth noting that solution phase reactions lead to lower T_m than slurry-phase polymerisations. Solid-state ^{13}C CPMAS NMR spectroscopy of the resulting polymers showed a resonance at 32.1 ppm corresponding to the ethylene chain. Resonances corresponding to styrene can be observed but to a very low intensity, confirming that little incorporation occurred (Figure A4.32).

Table 4.6. Molecular weights, dispersities, melting temperatures and melting enthalpies of polymers produced by the copolymerisation of ethylene with 125 µL of styrene at 40 °C. Polymerisation conditions: 30 minutes, 1000 rpm. 50 mL hexane, 10 mg catalyst, 2 bar ethylene, $[Al_{sMAO}]_0$:$[Ti]_0$ = 200:1.

Complex	M_w (×10^4 g/mol)	Đ	T_m (°C)	ΔH_m (J/g)
Pn*(H)$TiCl_2$(O-2,6-^{i}Pr-C_6H_3) (**3**)	0.17	3.1	n.s.[a]	-
Pn*(H)$TiCl_2$(O-2,4-^{t}Bu-C_6H_3) (**4**)	107.2	3.3	126.8	19.1
Pn*(H)$TiCl_2$(O-Si$(CH_3)_2{}^t$Bu) (**5**)	146.1	3.3	128.3	96.3
sMAO-Pn*(H)$TiCl_2$(O-2,6-^{i}Pr-C_6H_3) (**3$_{sMAO}$**)	109.4	4.9	128.5	32.9
sMAO-Pn*(H)$TiCl_2$(O-2,4-^{t}Bu-C_6H_3) (**4$_{sMAO}$**)	183.9	4.9	132.3	81.5
sMAO-Pn*(H)$TiCl_2$(O-Si$(CH_3)_2{}^t$Bu) (**5$_{sMAO}$**)	146.6	2.7	131.5	83.0

[a] no signal.

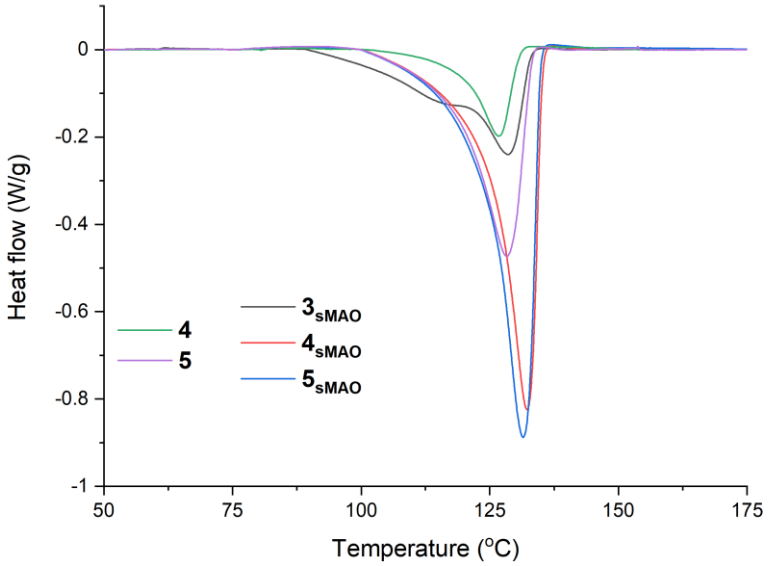

Figure 4.21. DSC plots with melting peaks of polymers produced by the copolymerisation of ethylene with 125 µL of styrene at 40 °C.

4.6 Conclusion

Three (hydro)permethylpentalene half-sandwich titanium complexes, Pn*(H)$TiCl_2$(OR) (R = 2,6-^{i}Pr-C_6H_3 (**3**), 2,4-^{t}Bu-C_6H_3 (**4**), $SiMe_2{}^{t}Bu$ (**5**)) were synthesised and tested for their ethylene and styrene polymerisation both in solution and slurry-phase.

The two aryloxide compounds displayed low styrene polymerisation activities in both solution and slurry-phase. The siloxide derivative **5** exhibited the highest activities in solution phase, performing better than the trichloride parent and reaching a maximum of 5790 $kg_{PS}/mol_{Ti}/h$. A decline in activities was observed when the three catalysts were supported on solid-MAO, consistent with literature reports.[42,43] The two aryloxides display low slurry-phase activities probably due to interaction with the solid support as described by O'Hare *et al.*[40,41]

All three Pn*(H)$TiCl_2$OR catalysts polymerised ethylene in the presence of MAO or immobilised on solid-MAO. They could however not reach the activities of the trichloride complex $\mathbf{2_{sMAO}}$ except for $5_{\mathbf{sMAO}}$ at 40 °C (354 $kg_{PS}/mol_{Zr}/h/bar$). High molecular weights were obtained by all complexes with **4** producing polyethylene of 1.8×10^6 g/mol. Immobilising the catalysts on a solid support yielded better control of the polymerisation leading to lower dispersities and better morphology.

Finally, copolymerisation of ethylene with styrene was carried out. Surprisingly, NMR spectroscopy highlighted a very low incorporation of styrene which was opposite to results reported by Nomura *et al.* for aryloxides Cp*$TiCl_2$OR.[22] The addition of the comonomer resulted in a decline in polymerisation activities suggesting a negative comonomer effect.[66]

4.7 References

1 X. Qian, J. Huang and Y. Qian, *J. Organomet. Chem.*, 2004, **689**, 1503–1510.

2 W. Kaminsky, D. Arrowsmith and C. Strübel, *J. Polym. Sci. Part A Polym. Chem.*, 1999, **37**, 2959–2968.

3 J. B. Doo, A. Fudo, A. Tanaka, M. Fujiki and K. Nomura, *Macromolecules*, 2004, **37**, 5520–5530.

4 J. Liu, J. Huang, Y. Qian, F. Wang and A. S. C. Chan, *Polym. Bull.*, 1996, **37**, 719–721.

5 J. Schellenberg, *Prog. Polym. Sci.*, 2009, **34**, 688–718.

6 M. Y. R. Blom, A. Follestad, E. Rytter, M. Tilset, Ed., *Organometallic Catalysts and Olefin Polymerization. Catalysts for a New Millennium.*, Springer, 2001.

7 Y. Kissin, *Alkene Polymerization Reactions with Transition Metal Catalysts*, Elsevier, vol. 173.

8 K. Nomura, K. Fujita and M. Fujiki, *Catal. Commun.*, 2004, **5**, 413–417.

9 K. Nomura and J. Liu, *Dalton Trans.*, 2011, **40**, 7666–7682.

10 C. Pellecchia, D. Pappalardo, M. D'Arc and A. Zambelli, *Macromolecules*, 1996, **29**, 1158–1162.

11 L. Oliva, S. Mazza and P. Longo, *Macromol. Chem. Phys.*, 1996, **197**, 3115–3122.

12 P. Longo, A. Grassi and L. Oliva, *Die Makromol. Chemie*, 1990, **191**, 2387–2396.

13 K. Nomura, T. Komatsu and I. Yukio, *Macromolecules*, 2000, **33**, 8122–8124.

14 Z. Hao, K. Nomura, H. Zhang and K. Nomura, *Macromolecules*, 2005, **39**, 5266–5274.

15 K. Nomura, N. Naga, M. Miki, K. Yanagi and A. Imai, *Organometallics*, 1998, **17**, 2152–2154.

16 K. Nomura, H. Okumura, T. Komatsu and N. Naga, *Macromolecules*, 2002, **35**, 5388–5395.

17 K. Nomuram N. Naga, JPH11166010A, 1999.

18 K. Nomura, T. Komatsu and Y. Imanishi, *J. Mol. Catal. A Chem.*, 2000, **152**, 249–252.

19 N. Kotohiro, H. Okumura, T. Komatsu and N. Naga, *Macromolecules*, 2002, **35**,

5388–5395.

20 K. Nomura, J. Yamada, W. Wang and J. Liu, *J. Organomet. Chem.*, 2007, **692**, 4675–4682.

21 D. D. Clement, S. C. Binding, T. A. Q. Arnold, F. M. Chadwick, I. J. Casely, Z. R. Turner, J.-C. Buffet and D. O'Hare, *Polyhedron*, 2019, **157**, 146–151.

22 K. Osakada, Ed., *Organometallic Reactions and Polymerization*, Springer, 2014.

23 F. Amor, S. Fokken, T. Kleinhenn, T. P. Spaniol and J. Okuda, *J. Organomet. Chem.*, 2001, **621**, 3–9.

24 P. Gómez-Sal, A. Martín, M. Mena, P. Royo and R. Serrano, *J. Organomet. Chem.*, 1991, **419**, 77–84.

25 M. D. Bala and M. I. Ikhile, *J. Mol. Catal. A Chem.*, 2014, **385**, 98–105.

26 Z. R. Turner, J.-C. Buffet and D. O'Hare, *Organometallics*, 2014, **33**, 3891–3903.

27 J. Liu, J. Huang, Y. Qian, F. Wang and A. S. C. Chan, *Polym. J.*, 1997, **29**, 182–183.

28 J. Liu, H. Ma, J. Huang and Y. Qian, *Eur. Polym. J.*, 2000, **36**, 2055–2058.

29 H. Ma, Y. Zhang, B. Chen, J. Huang and Y. Qian, *J. Polym. Sci. Part A Polym. Chem.*, 2001, **39**, 1817–1824.

30 K. Nomura, I. Izawa, J. Yi, N. Nakatani, H. Aoki, H. Harakawa, T. Ina, T. Mitsudome, N. Tomotsu and S. Yamazoe, *Organometallics*, 2019, **38**, 4497–4507.

31 J. Yi, N. Nakatani and K. Nomura, *Dalton Trans.*, 2020, **49**, 8008–8028.

32 T. E. Ready, R. Gurge, J. C. W. Chien and M. D. Rausch, *Organometallics*, 1998, **17**, 5236–5239.

33 Q. H. Zhou, H. Q. Liang, Y. J. Long, Q. Wu, H. Y. Gao, G. D. Liang and F. M. Zhu, *J. Organomet. Chem.*, 2015, **798**, 347–353.

34 H. Sato, Y. Tanaka and K. Hatada, *J. Polym. Sci. Polym. Phys. Ed.*, 1983, **21**, 1667–1674.

35 J. C. Randall, *J. Polym. Sci. Polym. Phys. Ed.*, 1975, **13**, 889–899.

36 J. Xu, J. Ouyang, Z. Fan, D. Chen, L. Feng and Y. Yang, *Polym. J.*, 1998, **30**, 720–722.

37 H. N. Cheng and G. H. Lee, *Int. J. Polym. Anal. Charact.*, 1996, **2**, 439–455.

38 S. Rahmani, R. Mohammadi and A. A. Entezami, *Macromol. Symp.*, 2008, **274**,

43–48.

39 A. Entezami, M. Agaalipour and P. N. Moghaddam, *J. Iran. Chem. Soc.*, 2005, **2**, 149–154.

40 J. V. Lamb, University of Oxford, DPhil Thesis, 2019.

41 C. M. R. Wright, Z. R. Turner, J. C. Buffet and D. O'Hare, *Chem. Commun.*, 2016, **52**, 2850–2853.

42 J. H. Yim, K. J. Chu, K. W. Choi and S. K. Ihm, *Eur. Polym. J.*, 1996, **32**, 1381–1385.

43 J.-H. Yim and S.-K. Ihm, *J. Appl. Polym. Sci.*, 2006, **102**, 2293–2298.

44 T. Dall'Occo, F. Sartori, G. Vecellio, U. Zucchini and A. Maldotti, *Die Makromol. Chemie*, 1993, **194**, 151–161.

45 J. V. Lamb, J. C. Abell, J. E. McLaren, J. C. Buffet, Z. R. Turner and D. O'Hare, *Mol. Catal.*, 2019, **484**, 110735.

46 J. C. Buffet, Z. R. Turner and D. O'Hare, *Chem. Commun.*, 2018, **54**, 10970–10973.

47 N. V. Semikolenova and V. A. Zakharov, *Macromol. Chem. Phys.*, 1997, **198**, 2889–2897.

48 H. Liu, C. W. M. Bastiaansen, J. G. P. Goossens, A. P. H. J. Schenning and J. R. Severn, *Macromol. Chem. Phys.*, 2017, **218**, 1600490.

49 M. A. Bashir, V. Monteil, C. Boisson and T. F. L. McKenna, *React. Chem. Eng.*, 2017, **2**, 521–530.

50 M. C. Sacchi, D. Zucchi, I. Tritto, P. Locatelli and T. Dall'Occo, *Macromol. Rapid Commun.*, 1995, **16**, 581–590.

51 J. P. J. Turunen and T. T. Pakkanen, *J. Appl. Polym. Sci.*, 2006, **100**, 4632–4635.

52 K. Nomura, N. Naga, M. Miki and K. Yanagi, *Macromolecules*, 1998, **31**, 7588–7597.

53 A. V. Firth, J. C. Stewart, A. J. Hoskin and D. W. Stephan, *J. Organomet. Chem.*, 1999, **591**, 185–193.

54 Q. Wu, C. Wu, Q. Su and L. Ye, *Inorganica Chim. Acta*, 2014, **423**, 263–267.

55 P. Unruean, W. Apisuk, Y. Kawabata, T. Murayama, B. Kitiyanan and K. Nomura, *Mol. Catal.*, 2019, **475**, 110490.

56 J. Yi, N. Nakatani, N. Tomotsu, K. Nomura and M. Hada, *Organometallics*, 2021,

40, 643–653.

57 A. Ashuiev, F. Allouche, N. Wili, K. Searles, D. Klose, C. Copéret and G. Jeschke, *Chem. Sci.*, 2021, **12**, 780–792.

58 K. Liu, Q. Wu, X. Mu, W. Gao and Y. Mu, *Polyhedron*, 2013, **52**, 222–226.

59 D. A. Fraser, University of Oxford, DPhil Thesis, 2018.

60 L. D'Agnillo, J. B. P. Soares and A. Penlidis, *Macromol. Chem. Phys.*, 1998, **199**, 955–962.

61 M. Eskelinen and J. V. Seppälä, *Eur. Polym. J.*, 1996, **32**, 331–335.

62 K. Nomura, K. Oya and Y. Imanishi, *J. Mol. Catal. A Chem.*, 2001, **174**, 127–140.

63 H. Zhang, D.-J. Byun and K. Nomura, *Dalton Trans.*, 2007, 1802–1806.

64 K. S. Son, F. Jöge and R. M. Waymouth, *Macromolecules*, 2008, **41**, 9663–9668.

65 H. H. Brintzinger, D. Fischer, R. Mülhaupt, B. Rieger and R. M. Waymouth, *Angew. Chem. Int. Ed.*, 1995, **34**, 1143–1170.

66 J. C. W. W. Chien and T. Nozaki, *J. Polym. Sci. Part A Polym. Chem.*, 1993, **31**, 227–237.

Chapter Five

Ring Opening Polymerisation of Lactide

5.1. Introduction

Polylactic acid (PLA) has emerged as an alternative to traditional polyolefin materials. These biodegradable polymers, issued from renewable sources, are produced from the ring-opening polymerisation (ROP) of lactide (LA).[1–4] As the lactide monomer exists with various stereochemistry, polymers with different tacticity can be produced.[5,6] Therefore, interest is particularly focused on the development of single-site catalysts with the ability to control polymer properties.

Group 4 metal complexes have not been widely investigated as ROP initiators, however, Okuda *et al.* reported successful ROP using phenolate complexes.[7–9] (Hydro)permethylpentalene complexes have been reported to successfully promote the ROP of *L*-and *rac*-lactide.[10] Benzyl alkoxide initiators Pn*(H)Zr[OCH(CH_3)C_6H_5]$_3$ demonstrated very high rates of propagation at 100 °C ($1.885 < k_{obs} < 3.442\ h^{-1}$). Recently, O'Hare *et al*. described the ROP of lactide using η^8-Pn* aryloxides.[11]

This chapter aims to investigate the catalytic activity of (hydro)permethylpentalene titanium complexes developed in Chapter 4 as catalysts for the ROP of lactide. Different

polymerisation conditions were tested to study the polymer properties as well as the kinetics of polymerisation.

5.2. Ring-Opening Polymerisation of lactide

Pn*(H)$TiCl_2$(O-2,6-^{i}Pr-C_6H_3) (**3**), Pn*(H)$TiCl_2$(O-2,4-^{t}Bu-C_6H_3) (**4**) and Pn*(H)$TiCl_2$(O-Si$(CH_3)_2{}^t$Bu) (**5**) were tested as initiators for the ROP of *L*-, *D*-, *rac*- and *meso*-lactide (Figure 5.1). The effect of monomer stereochemistry, temperature, catalyst concentration, solvent and co-initiator were studied.

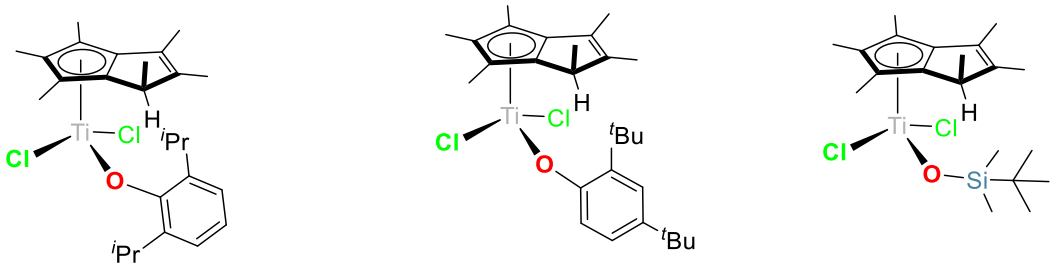

3 **4** **5**

Figure 5.1. (Hydro)permethylpentalene titanium complexes used in this study.

The polymerisations were performed in J. Young's tap NMR tubes with an initial lactide monomer concentration ($[LA]_0$) of 0.5 M. The reactions were halted by submerging the NMR tubes in cold water. Conversion was monitored by ^{1}H NMR spectroscopy. After an initial induction period, the polymerisations were stopped between 80 and 90% monomer conversion to avoid side reactions such as epimerisation. On completion, the reaction mixture was decanted into diethyl ether. Compound **4** was used as a mixture of isomers.

5.2.1 ROP of *L*-lactide

5.2.1.1 Effect of the alkoxide/aryloxide

The polymerisations were conducted at 120 °C in toluene-d_8 with a 50:1 ratio of $[LA]_0$:$[Ti]_0$. Plots of $\ln([LA]_0/[LA]_t)$ *vs.* time revealed linear relationships (Figure 5.2) indicating first-order dependence with respect to monomer concentration which is consistent with what Turner and co-workers described for zirconium and hafnium (hydro)permethylpentalene.[10] The three initiators were much slower than titanium amidinate complexes $[(N')_2CR']TiCl_3$ reported by Grisi *et al.* (74% conversion after 2 h at 130 °C using $[(SiMe_3)_2CPh]TiCl_3$).[12]

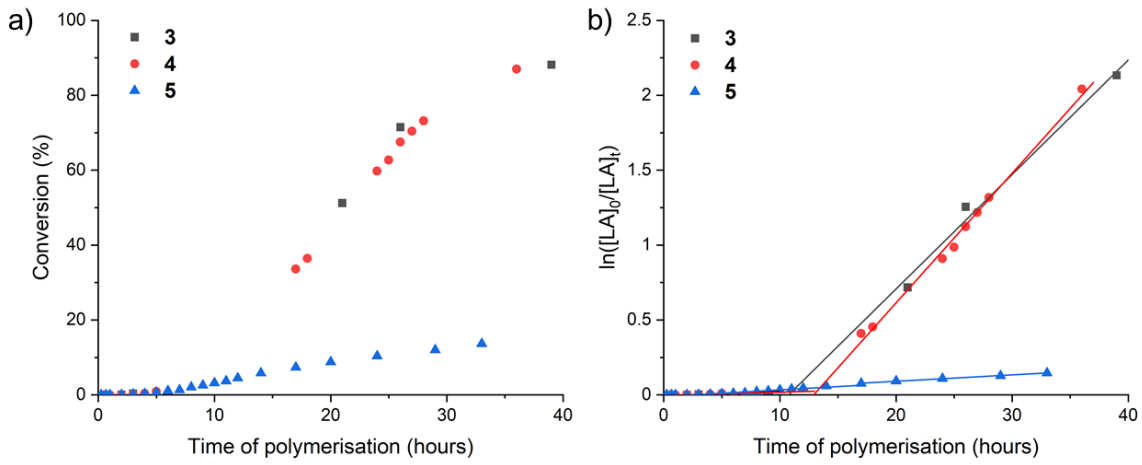

Figure 5.2. a) percentage conversion to PLA and b) $\ln([LA]_0/[LA]_t)$ as a function of time of the polymerisation for the ROP of *L*-lactide using Pn*(H)$TiCl_2$(O-2,6-^{i}Pr-C_6H_3) (**3**) (k_{obs} = 0.076 ± 0.009 h^{-1}), Pn*(H)$TiCl_2$(O-2,4-^{t}Bu-C_6H_3) (**4**) (k_{obs} = 0.087 ± 0.003 h^{-1}) and Pn*(H)$TiCl_2$(O-Si$(CH_3)_2{}^t$Bu) (**5**) ($k_{obs\ s}$ = 00.0043 ± 0.0002 h^{-1}). Polymerisation conditions: toluene-d_8, 120 °C, $[LA]_0$:$[Ti]_0$ = 50 and $[LA]_0$ = 0.5 M.

The observed first order rate constants, k_{obs}, were afforded by the gradients of the $\ln([LA]_0/[LA]_t)$ *vs.* time plots (Table 5.1). The rate of polymerisation followed the order **4** (k_{obs} = 0.087 h^{-1}) > **3** (k_{obs} = 0.076 h^{-1}) > **5** (k_{obs} = 0.0043 h^{-1}). All three complexes required an initiation period of 10 h. Solubility of the lactide monomer in the solvent may be responsible for the induction period as well as the difference in reactivity between the

initiating species and the propagating chain end. Indeed, once the initiator opened the lactide ring and formed the propagating species, it has more open space at the metal centre for the primary alcohol to coordinate and be inserted. Hence, the initiator required an initiation period corresponding to the slow conversion of the aryloxide to an alkoxide. Compounds **3** and **4** reached 87 and 88% conversions after 39 and 36 h respectively while siloxide **5** only reached 14% conversion after 33 h before decomposition was observed in the NMR tube (Table 5.1). The rates are in the same range as those reported by Turner *et al.* for group 4 (hydro)permethylpentalene initiators Pn*(H)MCl_2(O-2,6-^{t}Bu-C_6H_3) (k_{obs} = 0.043 and 0.086 h^{-1} for M = Zr and Hf respectively).[10] They also described that titanium tris(aryloxide), Pn*(H)Ti(O-2,6-Me-C_6H_3)$_3$, had a k_{obs} of 0.113 h^{-1}, one order of magnitude higher than complexes **3** and **4**.[10] This result can be explained by assuming that **3** and **4** have one growing polymer chain per initiator compared to three growing chains for the tris(aryloxide) compound. k_{obs} for **3–5** were around 2 times lower than that reported by O'Hare and co-workers for the η^8 derivative Pn*TiCp(O-2,6-Me-C_6H_3).[11]

Table 5.1. Polymerisation of *L*-lactide using Pn*(H)$TiCl_2$(O-2,6-^{i}Pr-C_6H_3) (**3**), Pn*(H)$TiCl_2$(O-2,4-^{t}Bu-C_6H_3) (**4**) and Pn*(H)$TiCl_2$(O-Si$(CH_3)_2{}^t$Bu) (**5**). Polymerisation conditions: toluene-d_8, 120 °C, $[LA]_0$:$[Ti]_0$= 50 and $[LA]_0$= 0.5 M.

Initiators	Time (h)	Conversion (%)	k_{obs} (h^{-1})	M_n [a] (g/mol)	M_n^{calcd} [b] (g/mol)	Đ
3	39	88	0.076 ± 0.009	29580	6510	1.77
4	36	87	0.087 ± 0.003	42350	6470	1.40
5	33	14	0.0043 ± 0.0002	1750	1140	1.26

[a] determined by GPC in thf. [b] $M_n^{calcd} = (M_{LA} \times \%conversion/100 \times [LA]_0/[Ti]_0) + M_{end\ group}$.

The experimental molecular weights (M_n) of the poly-*L*-lactide (PLLA) produced using **3** and **4** were higher than those reported for group 4 (hydro)permethylpentalene complexes (2000-17000 g/mol) (Figure 5.3 a and Table 5.1).[10] The theoretical molecular

weights, M_n^{calcd} were calculated using Equation 5.1 assuming one growing polymer chain per initiator. It was hypothesised that the end groups consisted of a proton and an aryloxide or siloxide fragment as observed by Turner *et al.*.[10]

$$M_n^{calcd} = \left(M_{\mathrm{LA}} \times \frac{[\mathrm{LA}]_0}{[\mathrm{Ti}]_0} \times \frac{\mathrm{conversion}}{100}\right) + M_{\mathrm{end\ group}} \qquad \text{Equation 5.1.}$$

Values of 6510, 6470 and 1140 g/mol were determined for the M_n^{calcd} using initiators **3**, **4** and **5** respectively. The experimental M_n measured for aryloxide compounds **3** and **4** are 5.5 and 6.5 times higher than those calculated, suggesting that only a portion of the complexes initiate polymerisation at this concentration. This was confirmed by the molecular weight distribution (Đ) being relatively large (1.26-1.77) indicating that transesterification may be occurring during the ROP.[11] Conversely, a good fit between measured M_n and calculated values M_n^{calcd} was observed by Milione *et al.* for the ROP of *L*-lactide using [(NSSN-^{i}Pr)Zr(NMe$_2$)$_2$ (M_n = 8.7 kg/mol and and M_n^{calcd} = 9.9 kg/mol at 80 °C in toluene).[13]

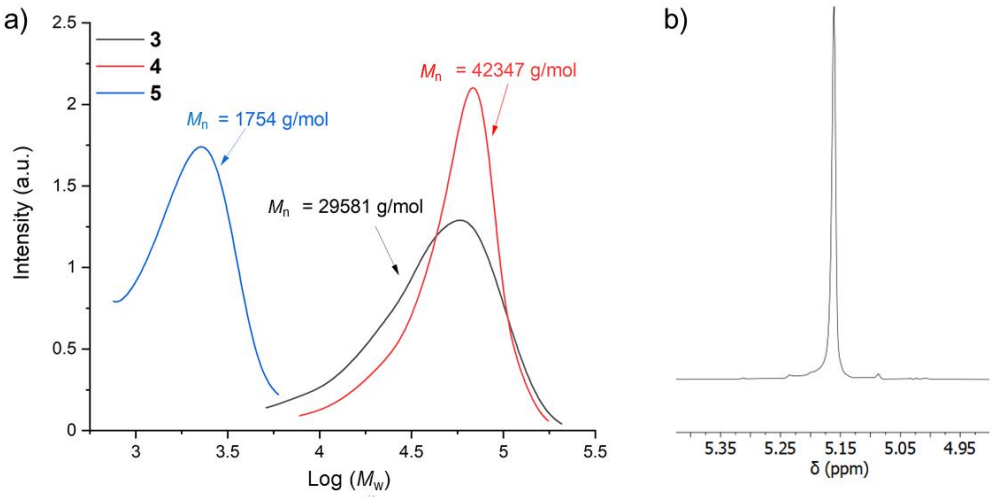

Figure 5.3. a) GPC traces of the PLLA produced using Pn*(H)TiCl$_2$(O-2,6-^{i}Pr-C$_6$H$_3$) (**3**), Pn*(H)TiCl$_2$(O-2,4-^{t}Bu-C$_6$H$_3$) (**4**) and Pn*(H)TiCl$_2$(O-Si(CH$_3$)$_2$^{t}Bu) (**5**). b) ^{1}H{^{1}H} NMR spectrum (chloroform-d_1, 500 MHz, 298 K) of the PLLA produced using Pn*(H)TiCl$_2$(O-2,6-^{i}Pr-C$_6$H$_3$) (**3**). Polymerisation conditions: toluene-d_8, 120 °C, [LA]$_0$:[Ti]$_0$= 50 and [LA]$_0$= 0.5 M.

To determine the end groups of the polymer, matrix-assisted laser desorption/ionisation time of flight (MALDI-TOF) mass spectrometry was used. The molecular weights of the PLLA produced was, however, too high to generate a spectrum.

The homodecoupled $^{1}H\{^{1}H\}$ NMR spectra of the PLLA synthesised by the ROP of *L*-lactide by **3**, **4** and **5** indicated that no epimerisation had occurred (Figure 5.3 b). As expected, only one resonance corresponding to the *mmm* tetrad was observed, highlighting the formation of isotactic PLA. (Figure A5.8).[14]

5.2.1.2 Initiator concentration dependency

The effect of initiator concentration on the rates of polymerisations was investigated. The ROP of *L*-lactide using compounds **3** and **4** were performed at four catalyst loadings ($[LA]_0$:$[Ti]_0$ = 20, 50, 100 and 100) at 120 °C in toluene-d_8. The initial concentration of lactide was fixed at $[LA]_0$ = 0.5 M (Figures A5.1 and A5.2).

No linear relation was observed for the plot of $-\ln(k_{obs})$ *vs.* $-\ln([Ti]_0)$ for catalyst **3** (Figure A5.3). This could be due to the ratios $[LA]_0$:$[Ti]_0$ being too similar to observe significant difference in polymerisation rate (Table 5.2). To overcome this limitation, ROP with higher $[LA]_0$:$[Ti]_0$, such as 300 to 1000, could be carried out and should allow for a linear trend to be observed. Conversely, O'Hare *et al.* reported an increase in k_{obs} with increasing initiator concentration for $Pn^*Zr(OR)_2$.[11] The same trend was highlighted by Li and co-workers for salen-Ti initiators; k_{obs} increased from 0.76 to 3.73 $mol^{-1}\,h^{-1}$ upon increasing $[Ti]_0$ from 0.05 to 0.25 mmol L^{-1}.[15] For complex **4**, ratios $[LA]_0$:$[Ti]_0$ = 50, 100 and 200 revealed a linear trend between $-\ln(k_{obs})$ and $-\ln([Ti]_0)$ (Figure 5.4). The observed rate of propagation demonstrated pseudo first-order kinetics as a function of the initiator.

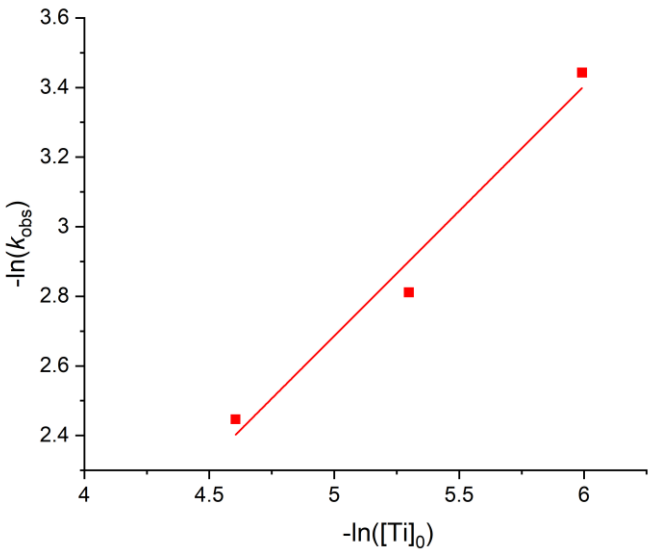

Figure 5.4. Plot of $-\ln(k_{obs})$ vs. $-\ln([Ti]_0)$ using Pn*(H)TiCl$_2$(O-2,4-^{t}Bu-C$_6$H$_3$) (**4**), slope 0.72 with R^2 = 0.98. Polymerisation conditions: toluene-d_8, 120 °C and $[LA]_0$ = 0.5 M.

The propagation rate constant for complex **4**, k_p was calculated to be 7.0 M^{-1} h^{-1} using Equation 5.2. The overall rate law was determined as Equation 5.3. The value of k_p was consistent with those reported for Pn*Zr(O-2,6-^{i}Pr-C$_6$H$_3$) (k_p = 7.2 M^{-1} h^{-1}) and Pn*ZrCl(O-2,6-^{t}Bu-4-Me-C$_6$H$_2$) (k_p = 6.4 M^{-1} h^{-1}).[11] Schiff-based titanium initiators were described by Chen *et al.* to exhibit much higher k_p (242 M^{-1} h^{-1} for the unsubstituted hydrazine-bridged compound).[16]

$$k_{obs} = k_p[\mathrm{Ti}]_0 \qquad \text{Equation 5.2.}$$

$$\frac{-\mathrm{d[LA]}}{\mathrm{dt}} = k_p[\mathrm{LA}][\mathrm{Ti}] \qquad \text{Equation 5.3.}$$

Table 5.2. Polymerisation of *L*-lactide using Pn*(H)TiCl$_2$(O-2,6-^{i}Pr-C$_6$H$_3$) (**3**) and Pn*(H)TiCl$_2$(O-2,4-^{t}Bu-C$_6$H$_3$) (**4**) at different [LA]$_0$:[Ti]$_0$ ratios. Polymerisation conditions: toluene-d_8, 120 °C and [LA]$_0$= 0.5 M.

Initiators	[LA]$_0$:[Ti]$_0$	Time (h)	Conversion (%)	k_{obs} (h^{-1})	M_n[a] (g/mol)	M_n^{calcd} [b] (g/mol)	Đ
3	20	50	82	0.0060 ± 0.001	32880	2540	1.37
3	50	39	88	0.076 ± 0.009	29580	6510	1.77
3	100	87	83	0.027 ± 0.001	67690	12130	1.26
3	200	88	85	0.032 ± 0.001	64620	24660	1.39
4	20	37	89	0.084 ± 0.005	24930	2770	1.41
4	50	36	87	0.087 ± 0.003	42350	6470	1.40
4	100	43	87	0.060 ± 0.005	58840	12730	1.55
4	200	75	84	0.032 ± 0.001	64620	24400	1.49

[a] determined by GPC in thf. [b] $M_n^{calcd} = (M_{LA} \times \%conversion/100 \times [LA]_0/[Ti]_0) + M_{end\ group}$.

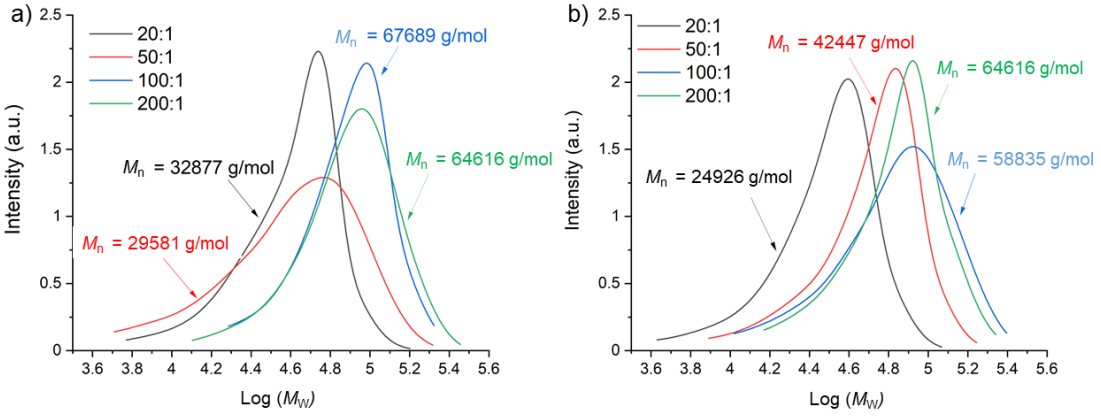

Figure 5.5. GPC traces of the PLLA produced using a) Pn*(H)TiCl$_2$(O-2,6-^{i}Pr-C$_6$H$_3$) (**3**) and b) Pn*(H)TiCl$_2$(O-2,4-^{t}Bu-C$_6$H$_3$) (**4**). Polymerisation conditions: toluene-d_8, 120 °C and [LA]$_0$ = 0.5 M.

The molecular weights of the PLLA produced using **4** increased with increasing [LA]$_0$:[Ti]$_0$ ratios as expected (M_n = 24930 and 58840 g/mol for [LA]$_0$:[Ti]$_0$ of 20 and 200 respectively) (Figure 5.5 b) and Table 5.2). Indeed, increasing the amount of lactide

monomer relative to the amount of catalyst improved the probability of propagation occurring.[10,17] The same trend was observed for compound **3** with higher M_n measured for low initiator concentrations (Figure 5.5 a) and Table 5.2). Chen *et al.* described the same trend using Schiff-based titanium complexes; PLLA produced by an unsubstituted hydrazine-bridging titanium initiator exhibited M_n of 1600, 3500 and 6100 g/mol for $[LA]_0$:$[Ti]_0$ of 50, 133 and 200 respectively.[16] Modifying the initiator concentration did not affect the tacticity of the PLLA produced and the homodecoupled $^1H\{^1H\}$ NMR spectra indicated the formation of isotactic PLA (Figure A5.9).[14]

5.2.1.3 Temperature variation

ROP of *L*-lactide were carried out at different temperatures to determine the enthalpy ($\Delta H^{\ddagger}$) and entropy ($\Delta S^{\ddagger}$) of activation with a fixed initiator concentration such as $[LA]_0$:$[Ti]_0$ = 50. Three temperatures were studied: 80, 100 and 120 °C (Table A5.1). For both initiators **3** and **4**, an increase in temperature resulted in higher k_{obs} (from 0.0063 h^{-1} at 80 °C to 0.076 h^{-1} at 120 °C for complex **3**, Figure 5.6). At higher temperatures, the catalysts disposed of more energy to overcome the activation barriers for polymerisation. Slow rates of polymerisation were observed at 80 °C with **3** requiring 344 h to reach 84% conversion and **4** reaching 83% in 174 h (Figure A5.4). Nonetheless, catalyst **4** was faster than **3** for the three temperatures studied which is due to the monomer approach facilitated by the absence of aromatic substituent on C6. The evolution of conversion with polymerisation temperature was studied by Grisi *et al.* using the amidinate complex $[(NSiMe_3)_2CPh]TiCl_3$.[12] At 100 °C, the initiator reached 95% conversion in 9 h while it required 24 h at 25 °C to reach 51%. O'Hare *et al.* also reported the increase of k_{obs} with polymerisation temperature using a permethylindenyl scandium complex at 60, 80 and 100 °C (k_{obs} = 0.34, 1.35 and 2.68 h^{-1} respectively).[18] Similarly, an increase in

temperature from 140 to 180 °C resulted in k_{obs} 10 times faster for salen-type titanium complexes (k_{obs} = 0.76 and 7.54 $mol^{-1}\,h^{-1}$ at 140 and 180 °C respectively).[15]

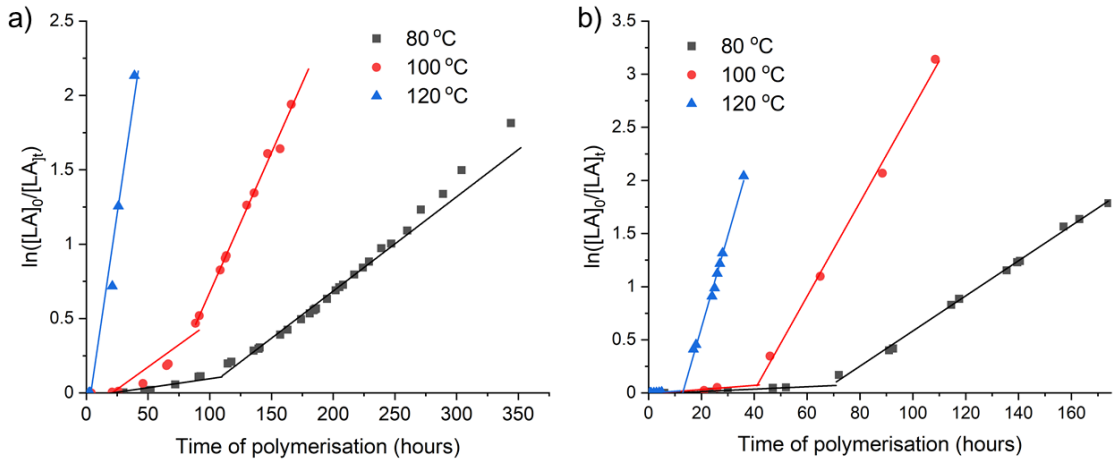

Figure 5.6. $\ln([LA]_0/[LA]_t)$ as a function of time of the polymerisation for the ROP of *L*-lactide using a) Pn*(H)$TiCl_2$(O-2,6-^{i}Pr-C_6H_3) (**3**) (k_{obs} = 0.0063 ± 0.001, 0.019 ± 0.001, 0.076 ± 0.009 h^{-1} at 80, 100 and 120 °C) and b) Pn*(H)$TiCl_2$(O-2,4-^{t}Bu-C_6H_3) (**4**) (k_{obs} = 0.017 ± 0.001, 0.044 ± 0.002, 0.087 ± 0.003 h^{-1} at 80, 100 and 120 °C). Polymerisation conditions: toluene-d_8, $[LA]_0$:$[Ti]_0$ = 50, $[LA]_0$ = 0.5 M.

The enthalpy and entropy of activation were determined from Eyring plots of $\ln(k_{obs}/T)$ *vs.* (1/T) (Figure 5.7). For the ROP of *L*-lactide using **3**, $\Delta H^{\ddagger}$ = 69 ± 7 kJ/mol and $\Delta S^{\ddagger}$ = –95 ± 20 J/mol/K, using **4** $\Delta H^{\ddagger}$ = 45 ± 4 kJ/mol and $\Delta S^{\ddagger}$ = –153 ± 10 J/mol/K. The values of $\Delta H^{\ddagger}$ are in the same range as those reported for Pn*(H)$Zr(OR)_3$ ($30.4 < \Delta H^{\ddagger} < 75.9$ kJ/mol).[10] An activation energy of propagation of 70.9 ± 1.5 kJ/mol was measured for the ROP of *L*-lactide using tin(II) ethylhexanoate.[19] The entropy values are similar to those obtained when using η^8-Pn* alkoxides and aryloxides, *e.g.* –270 J/mol/K for the ROP of *L*-lactide using Pn*Zr(O^{i}Pr)$_2$.[11] O'Hare and co-workers reported comparable values when using zirconium permethylindenyl initiators; $\Delta H^{\ddagger}$ = 96 kJ/mol and $\Delta S^{\ddagger}$ = –40 J/mol/K for ^{Me2}SB(Cp,I*)$ZrCl_2$ and $\Delta H^{\ddagger}$ = 65 kJ/mol and $\Delta S^{\ddagger}$ = –129 J/mol/K for ^{Me2}SB(Cp^{Me},I*)$ZrCl_2$.[20] The ROP of *L*-lactide using

organotin alkoxide (4-OMe-C_6H_4)$_2$Sn(O^{i}Pr)$_2$ resulting in $\Delta H^{\ddagger}$ and $\Delta S^{\ddagger}$ in the same range as those obtained for compounds **3** and **4**: $\Delta H^{\ddagger}$ = 51 kJ/mol and $\Delta S^{\ddagger}$ = –53 J/mol/K.[21]

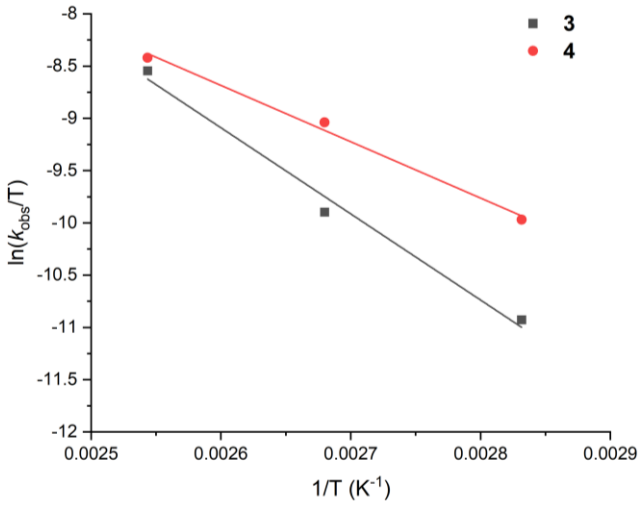

Figure 5.7. Eyring plot of ln(k_{obs}/T) as a function of (1/T) using Pn*(H)TiCl$_2$(O-2,6-^{i}Pr-C_6H_3) (**3**) ($\Delta H^{\ddagger}$ = 69 ± 7 kJ mol^{-1} and $\Delta S^{\ddagger}$ = –95 ± 20 J mol^{-1} K^{-1}) and Pn*(H)TiCl$_2$(O-2,4-^{t}Bu-C_6H_3) (**4**) ($\Delta H^{\ddagger}$ = 45 ± 4 kJ mol^{-1} and $\Delta S^{\ddagger}$ = –153 ± 10 J mol^{-1} K^{-1}) as initiators for the ROP of *L*-lactide. Polymerisation conditions: toluene-d_8, [LA]$_0$:[Ti]$_0$ = 50, [LA]$_0$ = 0.5 M.

For both aryloxide complexes **3** and **4**, the molecular weight of the PLLA produced was observed to decrease with increasing polymerisation temperature indicating that high temperatures resulted in a higher rate of chain termination and transesterification reaction (Figure 5.8). The molecular weight distributions increased from 80 to 120 °C demonstrating that polymerisation was less controlled at higher temperatures (Đ = 1.36, 1.45 and 1.77 at 80, 100 and 120 °C respectively for **3**).

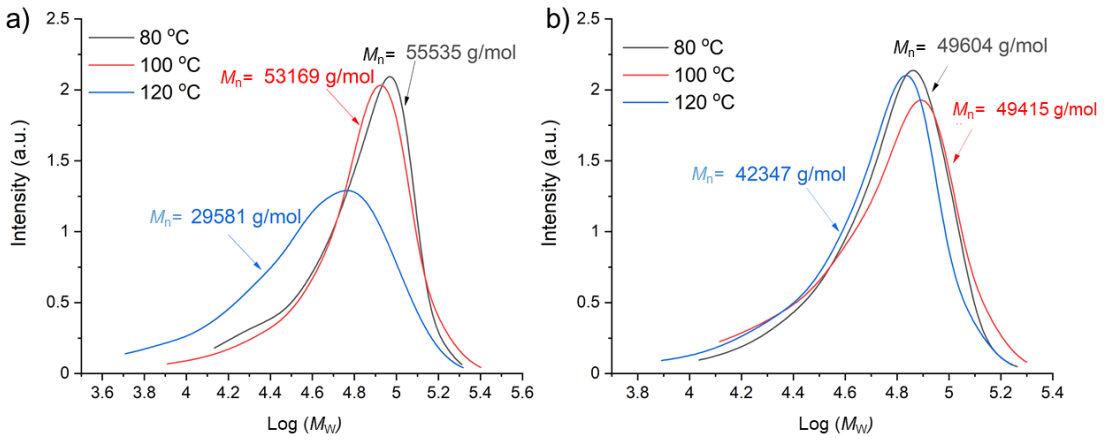

Figure 5.8. GPC traces of the PLLA produced using a) Pn*(H)$TiCl_2$(O-2,6-^{i}Pr-C_6H_3) (**3**) and b) Pn*(H)$TiCl_2$(O-2,4-^{t}Bu-C_6H_3) (**4**). Polymerisation conditions: toluene-d_8, $[LA]_0$:$[Ti]_0$= 50 and $[LA]_0$= 0.5 M.

5.2.1.4 Co-initiator dependency

Addition of an alcohol co-initiator has been widely reported to increase rates and to improve control on the polymerisation.[5,20,22,23] A co-initiator, benzyl alcohol (BnOH), was introduced in the system to investigate the effect on the rate of polymerisation. ROP of *L*-lactide using catalyst **4** was carried out at 120 °C with $[LA]_0$:$[Ti]_0$ = 50 and $[LA]_0$ = 0.5 M. 2 eq. of BnOH were added to the reaction mixture. In the presence of BnOH, no induction period was observed and the polymerisation proceeded faster than those without the co-initiator (Figure 5.9). This phenomenon is consistent with the greater reactivity of a primary compared with a secondary alcohol due to steric hindrance and limited access to the coordination sphere. Addition of BnOH resulted in the same effects on rates using permethylindenyl zirconocenes ^{Me_2}SB(Cp,I*)$ZrCl_2$ and ^{Me_2}SB(Cp^{Me},I*)$ZrCl_2$.[24] The ROP of *L*-lactide performed without BnOH required a 10 hour initiation period and only 46 and 43% conversion were achieved after 4 days.

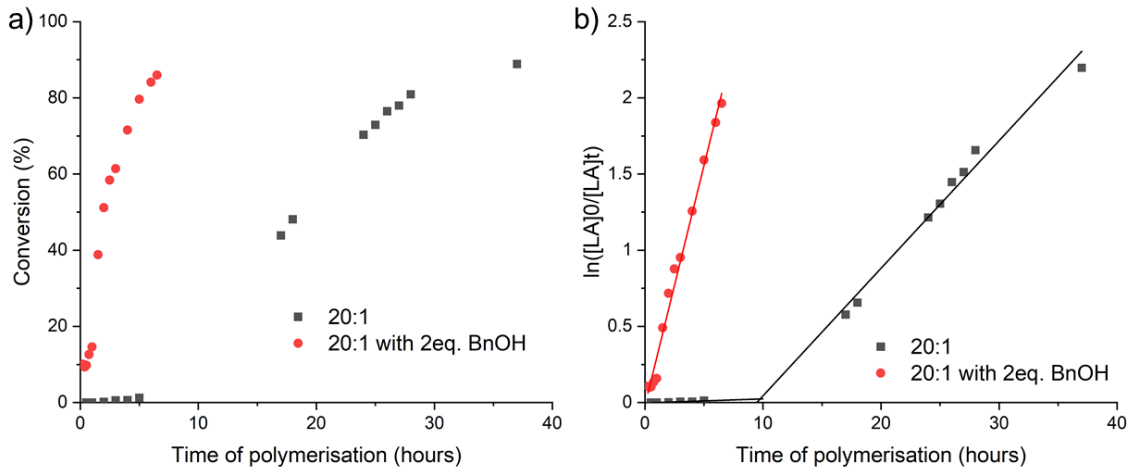

Figure 5.9. a) percentage conversion to PLA and b) $\ln([LA]_0/[LA]_t)$ as a function of time of the polymerisation for the ROP of *L*-lactide using Pn*(H)TiCl$_2$(O-2,4-^{t}Bu-C$_6$H$_3$) (**4**) in the absence of co-initiator (k_{obs} = 0.084 ± 0.005 h^{-1}) and with 2 eq. of BnOH (k_{obs} = 0.31 ± 0.010 h^{-1}). Polymerisation conditions: toluene-d_8, 120 °C, $[LA]_0$:$[Ti]_0$ = 50 and $[LA]_0$ = 0.5 M.

For complex **4**, k_{obs} was 3.7 times faster with addition of benzyl alcohol (0.31 ± 0.010 h^{-1}) (Figure 5.9 b). The addition of 2 eq. of BnOH allowed for the activation of two other initiating sites by substitution of the chloride ligands by benzyl alkoxide. This was verified by measuring the PLLA molecular weight by GPC. The M_n measured with the BnOH co-initiator was one order of magnitude lower than those measured without, confirming that the addition of the alcohol created more chain propagating sites and that three polymer chains were growing per metal centre (Table 5.3 and Figure A5.5). The value was however twice lower than the theoretical M_n^{calcd} which suggested that a slight excess of benzyl alcohol was added into the system, acting as a chain transfer agent responsible for a lower M_n.[25,26] The molecular weight distribution obtained with BnOH was narrower than that determined with no co-initiator. This suggested that the addition of BnOH achieved a more controlled polymerisation.[24] Likewise, the molecular weight of PLLA produced using Cp$_2$ZrMe(O-2,6-Me-C$_6$H$_3$) decreased when BnOH was introduced in the system and narrower molecular weight distributions were measured (M_n = 13810 g mol^{-1} and Đ = 1.12 without BnOH *vs.* M_n = 9070 g mol^{-1} and Đ = 1.09 with BnOH).[27]

Table 5.3. Polymerisation of *L*-lactide using Pn*(H)TiCl$_2$(O-2,4-^{t}Bu-C$_6$H$_3$) (**4**) in the absence of BnOH and with 2 eq. of BnOH. Polymerisation conditions: toluene-d_8, 120 °C, [LA]$_0$:[Ti]$_0$= 50 and [LA]$_0$= 0.5 M.

Initiating system	M_n (g/mol)[a]	M_n^{calcd} (g/mol)[b]	Đ
Pn*(H)TiCl$_2$(O-2,4-^{t}Bu-C$_6$H$_3$) (**4**)	24930	2770	1.41
Pn*(H)TiCl$_2$(O-2,4-^{t}Bu-C$_6$H$_3$) (**4**) and+ 2 eq. BnOH	1270	2590	1.17

[a] determined by GPC in thf. [b] $M_n^{calcd} = (M_{LA} \times \%conversion/100 \times [LA]_0/[Ti]_0) + M_{end\ group.}$

MALDI-TOF mass spectrometry analysis of the PLLA produced by **4** and 2 eq. BnOH confirmed the formation of PLLA terminated with -OCH$_2$Ph on one end and –OH end group on another end (Figure A5.6 and Table A5.2).[28] The spectrum also showed a series of peaks with a shift of Δ*m*/*z* values of 72.0, indicating inter molecular transesterification.[29,30] ^{13}C{^{1}H} NMR spectroscopy also established the presence of the -OCH$_2$Ph and -OH fragments.

5.2.1.5 Solvent variation

The effect of solvent on *L*-lactide polymerisation was investigated using complexes **3** and **4** at 80 °C with [LA]$_0$:[Ti]$_0$ = 50 and [LA]$_0$ = 0.5 M. Three different solvents were studied: toluene-d_8, chloroform-d_1 and thf-d_8.

While the polymerisation proceeded in toluene-d_8, little to no conversion was observed for chloroform-d_1 and thf-d_8. Indeed, when chloroform-d_1 was used as solvent, ^{1}H NMR spectroscopy showed no evidence of the formation of PLA and decomposition of the complexes in the NMR tube was observed by ^{1}H NMR spectroscopy. Polymerisation attempts in thf-d_8 resulted in a very low conversion; 0.4 and 10.6% were reached by compounds **3** and **4** after 174 h, respectively. The polymerisation rates were much lower than those measured in toluene-d_8. It is hypothesised that thf-d_8, the most polar solvent, coordinated to the metal centres, inhibiting their ability to proceed to the ROP through

competition between the thf and the lactide monomer.[31–34] The same phenomenon was observed for permethylindenyl complexes.[24] The rates of polymerisation decreased in solvent order benzene-d_6 > toluene-d_8 > chloroform-d_1 > thf-d_8. The opposite effect was observed in calcium Schiff base complexes was ROP performed in thf were faster than those performed in chloroform.[35]

5.2.2 ROP of *D*-lactide

Complexes **3**, **4** and **5** were used for the ROP of *D*-lactide under the same conditions of section 5.2.2.1. Plots of $\ln([LA]_0/[LA]_t)$ *vs.* time revealed a first-order dependency on monomer concentration with k_{obs} of 0.024, 0.073 and 0.023 h^{-1} for **3**,**4** and **5** respectively (Figure 5.10).

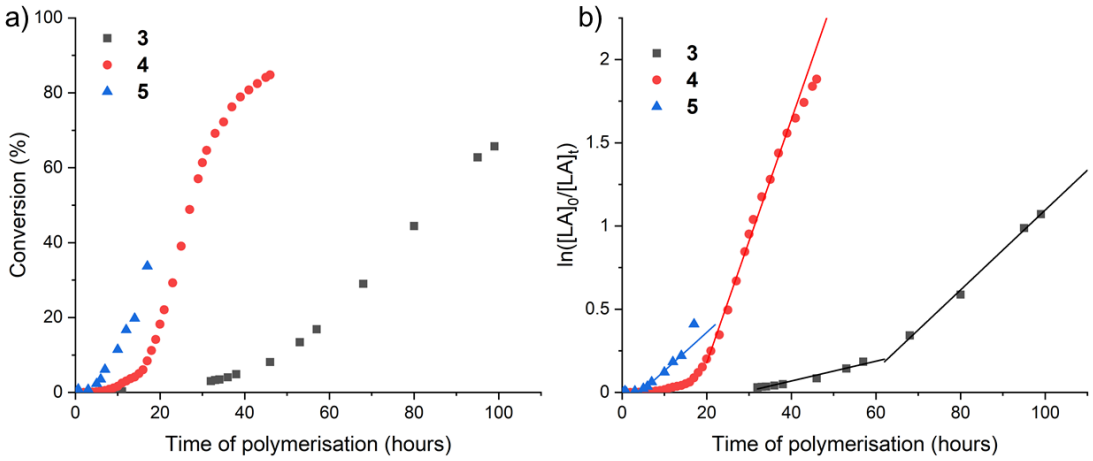

Figure 5.10. a) percentage conversion to PLA and b) $\ln([LA]_0/[LA]_t)$ as a function of time of the polymerisation for the ROP of *D*-lactide using Pn*(H)$TiCl_2$(O-2,6-^{i}Pr-C_6H_3) (**3**) (k_{obs} = 0.024± 0.001 h^{-1}), Pn*(H)$TiCl_2$(O-2,4-^{t}Bu-C_6H_3) (**4**) (k_{obs} = 0.073 ± 0.002 h^{-1}) and Pn*(H)$TiCl_2$(O-Si$(CH_3)_2{}^t$Bu) (**5**) (k_{obs} = 0.023 ± 0.002 h^{-1}). Polymerisation conditions: toluene-d_8, 120 °C, $[LA]_0$:$[Ti]_0$ = 50 and $[LA]_0$ = 0.5 M.

The siloxide **5** was observed to decompose after 17 h with 34% monomer conversion and a similar phenomenon occurred after 99 h for **3**. An initiation period of 61 and 16 h were observed for **3** and **4**. The rate of polymerisations of the two aryloxides **3** and **4** were slower than those recorded for the ROP of *L*-lactide with a ratio k_L/k_D = 3.2 and 1.2

respectively, indicating a preference of the ligand environment for *L*-lactide (Table 5.4). The opposite preference was reported by Darensbourg *et al.* for the ROP of *L*-and *D*-lactide using amino-acid based zinc initiators ($0.86 < k_L/k_D < 0.97$ at room temperature with $[LA]_0:[Zn]_0 = 49$).[36] Zhong and co-workers found higher k_L/k_D ratios than those calculated for aryloxides **3** and **4**. At 70 °C, they reported $k_L/k_D = 14$ with $k_p = 0.038$ and 0.003 h^{-1} for the ROP of *L*- and *D*-lactide respectively using the aluminium complex (cyclohexylsalen)AlO^iPr with $[LA]_0:[Al]_0 = 62$.[37]

Table 5.4. Polymerisation of *D*-lactide using Pn*(H)$TiCl_2$(O-2,6-^{i}Pr-C_6H_3) (**3**), Pn*(H)$TiCl_2$(O-2,4-^{t}Bu-C_6H_3) (**4**) and Pn*(H)$TiCl_2$(O-Si$(CH_3)_2{}^t$Bu) (**5**). Polymerisation conditions: toluene-d_8, 120 °C, $[LA]_0:[Ti]_0$= 50 and $[LA]_0$= 0.5 M.

Initiators	t (h)	Conversion (%)	k_{obs} (h^{-1})	$M_n{}^{calcd}$ (g/mol)[a]	M_n[b] (g/mol)	Đ
3	99	66	0.076 ± 0.009	4930	5940	1.30
4	46	85	0.087 ± 0.003	3520	19570	1.26
5	17	34	0.0043 ± 0.0002	2580	7430	1.31

[a] $M_n{}^{calcd} = (M_{LA}\times\%conversion/100\times[LA]_0/[Ti]_0)+M_{end\ group.}$ [b] determined by GPC in thf..

Similarly to *L*-lactide, the molecular weights of the poly-*D*-lactide (PDLA) produced were higher than the theoretical values indicating that only a portion of the active sites participated in the polymerisation (Figure 5.11 a and Table 5.4). Complex **4** led to the highest M_n amongst the initiators series measured like for the ROP of *L*-lactide. Except for the siloxide compound **5**, the M_n were lower for *D*-lactide monomer compared to *L*-lactide.

The homodecoupled $^1H\{^1H\}$ NMR spectra of the PDLA synthesised highlighted the formation of isotactic PDLA (Figure 5.11b and Figure A5.12).

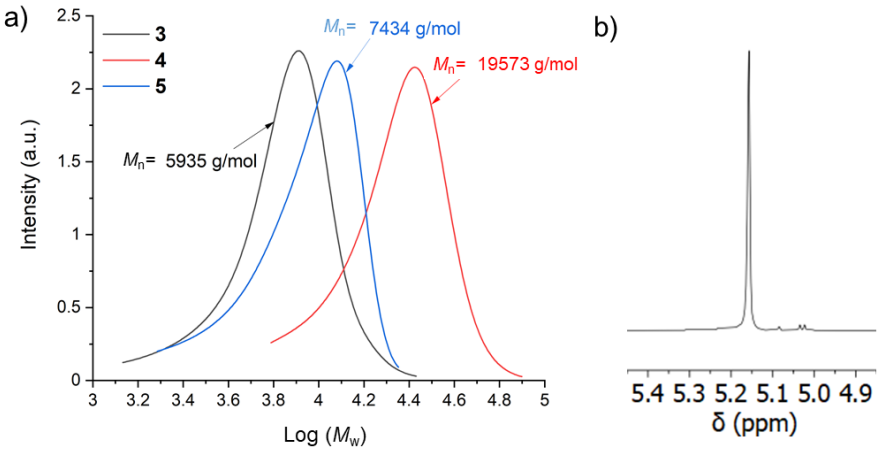

Figure 5.11. a) GPC traces for the PDLA produced using Pn*(H)$TiCl_2$(O-2,6-^{i}Pr-C_6H_3) (**3**), Pn*(H)$TiCl_2$(O-2,4-^{t}Bu-C_6H_3) (**4**) and Pn*(H)$TiCl_2$(O-Si$(CH_3)_2{}^t$Bu) (**5**) and b) $^1H\{^1H\}$ NMR spectrum (chloroform-d_1, 500 MHz, 298K) of the PDLA produced using Pn*(H)$TiCl_2$(O-2,6-^{i}Pr-C_6H_3) (**3**). Polymerisation conditions: toluene-d_8, 120 °C, $[LA]_0$:$[Ti]_0$ = 50 and $[LA]_0$ = 0.5M.

5.2.3 ROP of *meso*-lactide

meso-Lactide was used as monomer for the ROP of lactide by permethylpentalene complexes **3**, **4** and **5**. Surprisingly, siloxide complex **5** remained active until completion of the polymerisation, achieving 87% conversion in 43 h (Figure 5.12). The aryloxide compound **4** was observed to have the fastest polymerisation rate (k_{obs} = 0.15 h^{-1}) reaching 84% conversion in 17 h (Table 5.5). All three initiators required an initiation period, the longest one for **3** (around 10 h). After this period, the k_{obs} measured for **3** and **5** were very similar (k_{obs} = 0.045 and 0.050 h^{-1} respectively). The polymerisations using permethylpentalene compounds were much slower than ROP of *meso*-lactide reported by Okuda *et al.* using scandium compounds bearing OSSO ligands (< 99% conversion after 30 minutes at 25 °C with $[LA]_0$:$[Sc]_0$ = 100).[38] Complexes **3**, **4** and **5**, however, performed faster than (OSSO)-based titanium complexes (55% conversion after 72 h at 100 °C with $[LA]_0$:$[Ti]_0$ = 100).[8]

The constants of polymerisation k_{obs} increased in the order *D*- < *meso*- < *L*-lactide for **3**, *D*- < *L*- < *meso*-lactide for **4** and *L*- < *D*- < *meso*-lactide for **5**, suggesting a ligand

preference for *meso*-lactide compared to *D*-lactide for the three catalysts. Chisholm *et al.* analysed the structure of *meso*-lactide and its polymerisation by single-site catalysts. They calculated that the ground state of the *meso* monomer was higher in energy than for *L*- and *D*-lactide, reducing the activation barrier and increasing the rates.[39,40] Okuda *et al.* also reported faster polymerisation rates for the ROP of *meso*-lactide using(OSSO)-based group 4 complexes compared with *L*- and *rac*-lactide; the titanium derivative proceeded with a ratio k_{meso}/k_L = 5.3 with polymerisation rate constants k_{obs} = 0.016 and 0.003 h^{-1} for *meso*- and *L*-lactide respectively at 100 °C with $[LA]_0:[M]_0$ = 100.[8]

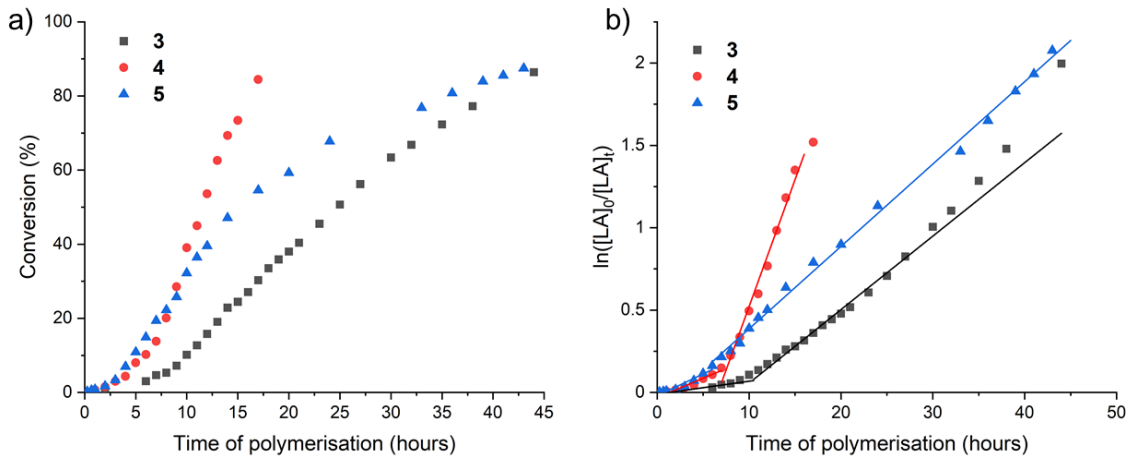

Figure 5.12. a) percentage conversion to PLA and b) $\ln([LA]_0/[LA]_t)$ as a function of time of the polymerisation for the ROP of *meso*-lactide using Pn*(H)$TiCl_2$(O-2,6-^{i}Pr-C_6H_3) (**3**) (k_{obs} = 0.045 ± 0.001 h^{-1}), Pn*(H)$TiCl_2$(O-2,4-^{t}Bu-C_6H_3) (**4**) (k_{obs} = 0.15 ± 0.009 h^{-1}) and Pn*(H)$TiCl_2$(O-Si$(CH_3)_2{}^t$Bu) (**5**) (k_{obs} = 0.050 ± 0.0007 h^{-1}). Polymerisation conditions: toluene-d_8, 120 °C, $[LA]_0:[Ti]_0$ = 50 and $[LA]_0$= 0.5 M.

Table 5.5. Polymerisation of *meso*-lactide using Pn*(H)$TiCl_2$(O-2,6-^{i}Pr-C_6H_3) (**3**), Pn*(H)$TiCl_2$(O-2,4-^{t}Bu-C_6H_3) (**4**) and Pn*(H)$TiCl_2$(O-Si$(CH_3)_2{}^t$Bu) (**5**). Polymerisation conditions: toluene-d_8, 120 °C, $[LA]_0:[Ti]_0$= 50 and $[LA]_0$= 0.5 M.

Initiators	Time (h)	Conversion (%)	k_{obs} (h^{-1})	$M_n{}^{calcd}$ (g/mol)	$M_n{}^b$ (g/mol)	Đ
3	44	86	0.045 ± 0.001	6370	20160	1.39
4	17	84	0.15 ± 0.009	6250	20850	1.27
5	43	87	0.005 ± 0.001	6400	7960	1.32

[a] $M_n{}^{calcd}$ = (M_{LA}×%conversion/100×$[LA]_0/[Ti]_0$) + $M_{end\ group}$. [b] determined by GPC in thf.

The molecular weight of the PLA were measured by GPC, revealing that PLAs produced by aryloxides **3** and **4** had very similar M_n (20160 and 20850 g/mol for **3** and **4** respectively) (Figure 5.13 a). The M_n were higher than the theoretical values, like for the other lactide monomers, indicating that only a portion of the active species were taking part in the polymerisation process. Bimodality was observed for catalysts **3** and **4**, which suggested that several active species were responsible for the ROP. The M_n were in the same range as those measured for zirconium and hafnium complexes containing two bis(phenolate) ligands reported by Okuda *et al.* (M_n = 17000–25500 g/mol).[7]

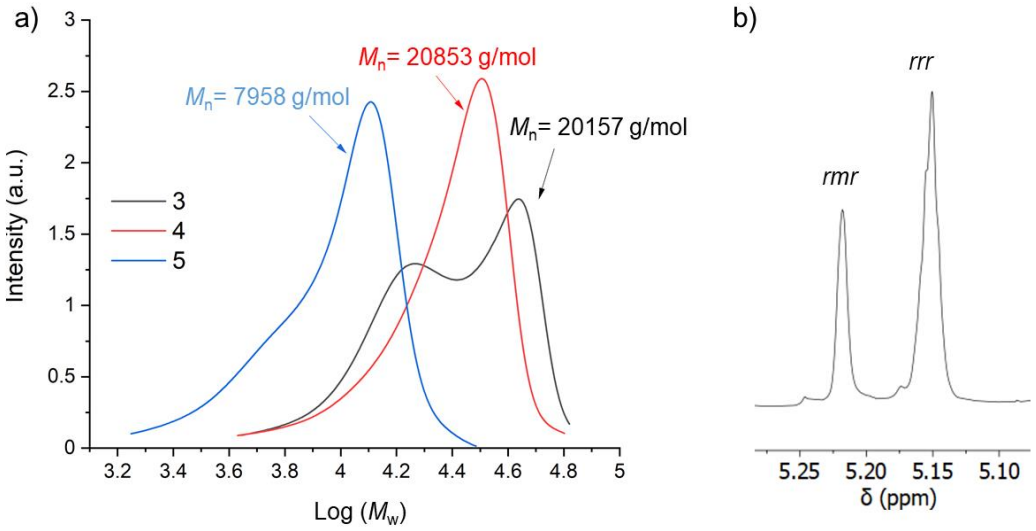

Figure 5.13. a) GPC traces for the PLA produced using Pn*(H)$TiCl_2$(O-2,6-^{i}Pr-C_6H_3) (**3**), Pn*(H)$TiCl_2$(O-2,4-^{t}Bu-C_6H_3) (**4**) and Pn*(H)$TiCl_2$(O-Si$(CH_3)_2{}^t$Bu) (**5**) b) $^1H\{^1H\}$ NMR spectrum (chloroform-d_1, 500 MHz, 298K) of the PLA produced using Pn*(H)$TiCl_2$(O-2,4-^{t}Bu-C_6H_3) (**4**). Polymerisation conditions: toluene-d_8, 120 °C, $[LA]_0$:$[Ti]_0$ = 50 and $[LA]_0$ = 0.5 M.

The homodecoupled $^1H\{^1H\}$ NMR spectra of the PLA showed two resonances corresponding to the *rmr* and *rrr* tetrads (Figure 5.13 b and A5.13).[38,41] Probabilities P_r and P_m were determined by deconvolution of the resonances (Table 5.6). The calculated P_r were very similar for the three permethylpentalene complexes and revealed the formation of syndiotactically-enriched PLA. Okuda and co-workers reported the

formation of highly syndiotactic PLA using scandium initiators ($0.88 < P_r < 0.93$) and moderately syndioctactic polymers using aluminium catalysts ($0.53 < P_r < 0.70$).[38,40]

Table 5.6. Tacticity probabilities calculated by $^1H\{^1H\}$ NMR spectroscopy for PLA produced by the ROP of *meso*-lactide using Pn*(H)$TiCl_2$(O-2,6-^{i}Pr-C_6H_3) (**3**), Pn*(H)$TiCl_2$(O-2,4-^{t}Bu-C_6H_3) (**4**) and Pn*(H)$TiCl_2$(O-Si$(CH_3)_2{}^t$Bu) (**5**).

Initiators	P_m	P_r
Pn*(H)$TiCl_2$(O-2,6-^{i}Pr-C_6H_3) (**3**)	0.28	0.72
Pn*(H)$TiCl_2$(O-2,4-^{t}Bu-C_6H_3) (**4**)	0.32	0.68
Pn*(H)$TiCl_2$(O-Si$(CH_3)_2{}^t$Bu) (**5**)	0.33	0.67

5.2.4 ROP of *rac*-lactide

Complexes **3** and **4** were employed as initiators for the ROP of *rac*-lactide under the same condition of section 5.2.2.1. Plots of $\ln([LA]_0/[LA]_t)$ *vs.* time revealed a first-order dependency on monomer concentration with k_{obs} of 0.012 and 0.088 h^{-1} for **3** and **4** respectively (Table 5.7 and Figure A5.7). Similar to the ROP of *L*- and *D*- lactide, compound **4** was faster than **3** (by a factor 7). Indeed, the former achieved 84% conversion after 52 h compared with 74% after 123 h for **3**. Pn* zirconium aryloxides were observed to have faster polymerisation rates (k_{obs} = 0.18 h^{-1} for Pn*Zr(O-2,6-^{i}Pr-$C_6H_3)_2$ and Pn*ZrCl(O-2,6-^{t}Bu-4-Me-C_6H_2) at 80 °C with $[LA]_0:[Zr]_0 = 50$).[11] Complexes **3** and **4** were much slower than unsymmetrical ONNO salalen titanium compounds reported by Jones and co-workers, which achieved between 89 and 95% conversion after 15 min in the melt state.[42] The monomers can be ordered in terms of rate of polymerisation in the order *rac* < *D* < *L* for **3** and *D* < *L* ≤ *rac* for **4**. Turner *et al.* reported 2 times faster ROP of *L*-lactide compared to *rac*-lactide using Pn*(H)Zr(OCH$(CH_3)C_6H_5)_3$.[10]

Table 5.7. Polymerisation of *rac*-lactide using Pn*(H)TiCl$_2$(O-2,6-^{i}Pr-C$_6$H$_3$) (**3**) and Pn*(H)TiCl$_2$(O-2,4-^{t}Bu-C$_6$H$_3$) (**4**). Polymerisation conditions: toluene-d_8, 120 °C, $[LA]_0$:$[Ti]_0$= 50 and $[LA]_0$= 0.5 M.

Initiators	Time (h)	Conversion (%)	k_{obs} (h^{-1})	M_n^{calcd} [b](g/mol)	M_n[b] (g/mol)	Đ
3	123	74	0.012 ± 0.001	5510	5430	1.83
4	52	84	0.088 ± 0.014	6250	7330	1.42

[a] $M_n^{calcd} = (M_{LA} \times \%conversion/100 \times [LA]_0/[Ti]_0) + M_{end\ group.}$ [b] determined by GPC in thf.

The molecular weight distribution of PLA formed from **3** (1.83) is higher than those from **4** (1.42) as a result of its bimodality displayed on the GPC trace (Figure 5.14 a). This may be due to the presence of several active species. The molecular weights measured are lower than those reported by Turner *et al*. for Pn*(H)Zr(OCH(CH$_3$)C$_6$H$_5$)$_3$ (2690 and 3060 g/mol at 100 °C with $[LA]_0$:$[Zr]_0$ = 50).[10] Using higher $[LA]_0$:$[M]_0$ ratios (200-300), Verkade and co-workers observed molecular weights in the same range as those measured for **3** and **4** for titanium alkoxides Ti(O^{i}Pr)$_4$ and TiCl(O^{i}Pr)$_3$ (4200 and 5200 g/mol respectively).[43] The decoupled ^{1}H{^{1}H} NMR spectra highlighted the presence of *rmr*, *rmm*, *mmr*, *mmm* and *mrm* tetrads (Figure 5.14 b and A5.14).[41,44] P_r = 0.52 and 0.56 for complexes **3** and **4** respectively, which indicated the formation of atactic PLA. Heterotacticity was achieved by other permethylpentalene compounds reported in the literature.[10,11] Pn*ZrCp(O^{t}Bu) was found to produce heterotactic PLA with a P_r of 0.68.

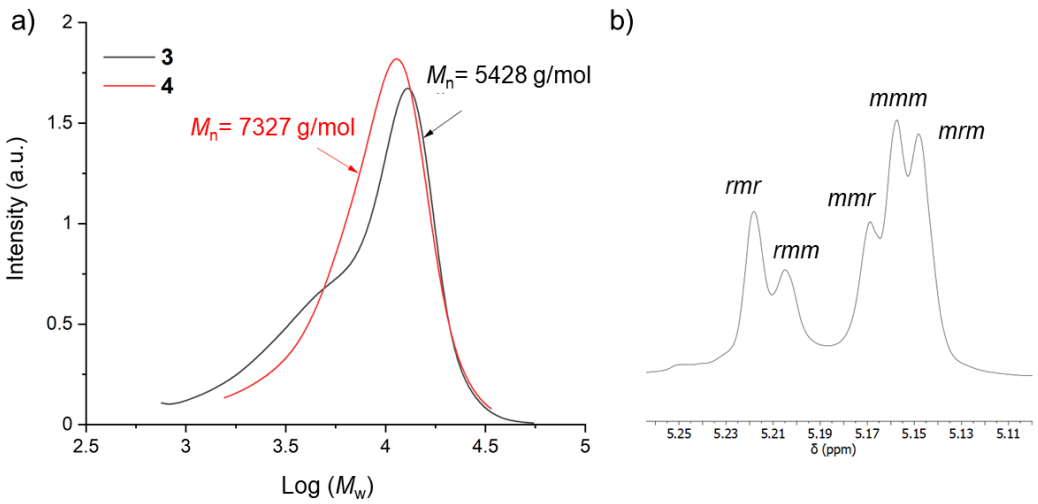

Figure 5.14. a) GPC traces for the PLA produced using Pn*(H)$TiCl_2$(O-2,6-^{i}Pr-C_6H_3) (**3**) and Pn*(H)$TiCl_2$(O-2,4-^{t}Bu-C_6H_3) (**4**) and b) $^1H\{^1H\}$ NMR spectrum (chloroform-d_1, 500 MHz, 298 K) of the PLA produced using Pn*(H)$TiCl_2$(O-2,4-^{t}Bu-C_6H_3) (**4**). Polymerisation conditions: toluene-d_8, 120 °C, $[LA]_0$:$[Ti]_0$ = 50 and $[LA]_0$ = 0.5 M.

5.3. Conclusion

Three (hydro)permethylpentalene titanium complexes Pn*(H)$TiCl_2$(O-2,6-^{i}Pr-C_6H_3) (**3**), Pn*(H)$TiCl_2$(O-2,4-^{t}Bu-C_6H_3) (**4**) and Pn*(H)$TiCl_2$(O-Si$(CH_3)_2{}^t$Bu) (**5**) were investigated as initiators for the ROP of *L*-, *D*-, *rac*- and *meso*-lactide. They all displayed first-order dependency on monomer concentration. The complexes required an initiation period and exhibited slow polymerisation rate compared to reported group 4 catalysts.[10,11] Compound **4** was found to have the fastest rate of polymerisation of the series towards *L*-, *D*-, *rac*- and *meso*-lactide (k_{obs} = 0.087, 0.073, 0.088 and 0.15 h^{-1} respectively). Siloxide titanium catalyst **5** was observed to decompose at 120 °C except in the presence of *meso*-lactide, resulting in faster rate than aryloxide **3** (k_{obs} = 0.050 *vs*. 0.045 h^{-1}).

The polymers produced showed molecular weights (M_n) higher than theoretical values, indicating that only a portion of the active sites were taking part in the ROP. The initiators were found to produce isotactic PLA for the ROP of *L*- and *D*- lactide, and syndiotactically-enriched PLA for the ROP of *meso*- (P_r = 0.68-0.72) and atactic PLA from the ROP of *rac*-lactide (P_r = 0.52-0.56).

Further studies into the kinetics of the ROP of *L*-lactide using **4** indicated a first-order dependency on catalyst concentration. The overall polymerisation equation can be described by Equation 5.4. When $[LA]_0$ = 0.5 M, an investigation of the effect of the initiator concentration found that k_p = 7.0 M^{-1} h^{-1} using aryloxide **4**.

$$\frac{-d[LA]}{dT} = k_p[LA]_0[Ti]_0 \qquad \text{Equation 5.4}$$

Addition of 2 eq. of benzyl alcohol (BnOH) as co-initiator in the polymerisation mixture resulted in polymerisation rate 3.7 times faster and no initiation period was observed. The co-initiator activated two more active sites and allowed for three polymer chain per metal

centre to grow simultaneously, thus reducing the M_n compared to ROP performed without alcohol and allowing for a better polymerisation control on molecular weight and molecular weight distribution.

5.4. References

1 K. Madhavan Nampoothiri, N. R. Nair and R. P. John, *Bioresour. Technol.*, 2010, 101, 8493–8501.

2 J. Ahmed and S. K. Varshney, *Int. J. Food Prop.*, 2011, **14**, 37–58.

3 J. M. Becker, R. J. Pounder and A. P. Dove, *Macromol. Rapid Commun.*, 2010, **31**, 1923–1937.

4 S. Jacobsen, H. G. Fritz, P. Degée, P. Dubois and R. Jérôme, *Polym. Eng. Sci.*, 1999, **39**, 1311–1319.

5 N. Diteepeng, J. C. Buffet, Z. R. Turner and D. O'Hare, *Dalton Trans.*, 2019, **48**, 16099–16107.

6 P. J. Dijkstra, H. Du and J. Feijen, *Polym. Chem.*, 2011, 2, 520–527.

7 A. Sauer, J. C. Buffet, T. P. Spaniol, H. Nagae, K. Mashima and J. Okuda, *Inorg. Chem.*, 2012, **51**, 5764–5770.

8 J. C. Buffet, A. N. Martin, M. Kol and J. Okuda, *Polym. Chem.*, 2011, **2**, 2378–2384.

9 A. Sauer, A. Kapelski, C. Fliedel, S. Dagorne, M. Kol and J. Okuda, *Dalton Trans.*, 2013, 42, 9007–9023.

10 Z. R. Turner, J.-C. Buffet and D. O'Hare, *Organometallics*, 2014, **33**, 3891–3903.

11 Z. R. Turner, J. V. Lamb, T. P. Robinson, D. Mandal, J.-C. Buffet and D. O′Hare, *Dalton Trans.*, 2021, **50**, 4805–4818.

12 R. Lapenta, M. Mazzeo and F. Grisi, *RSC Adv.*, 2015, **5**, 87635–87644.

13 S. Impemba, G. Roviello, S. Milione and C. Capacchione, *Inorg. Chem.*, 2021, **60**, 7561–7572.

14 M. T. Zell, B. E. Padden, A. J. Paterick, K. A. M. Thakur, R. T. Kean, M. A. Hillmyer and E. J. Munson, *Macromolecules*, 2002, **35**, 7700–7707.

15 X. Li, B. Yang, H. Zheng, P. Wu and G. Zeng, *PLoS One*, 2018, **13**, e0201054.

16 H. C. Tseng, H. Y. Chen, Y. T. Huang, W. Y. Lu, Y. L. Chang, M. Y. Chiang, Y. C. Lai and H. Y. Chen, *Inorg. Chem.*, 2016, **55**, 1642–1650.

17 J. V. Lamb, J. C. Abell, J. E. McLaren, J. C. Buffet, Z. R. Turner and D. O'Hare, *Mol. Catal.*, 2019, **484**, 110735.

18 N. Diteepeng, I. A. P. Wilson, J. C. Buffet, Z. R. Turner and D. O'Hare, *Polym.*

Chem., 2020, **11**, 6308–6318.

19 D. R. Witzke, R. Narayan and J. J. Kolstad, *Macromolecules*, 1997, **30**, 7075–7085.

20 J. V. Lamb, J. C. Buffet, J. E. Matley, C. M. R. Wright, Z. R. Turner and D. O'Hare, *Dalton Trans.*, 2019, **48**, 2510–2520.

21 M. H. Chisholm, J. C. Gallucci and C. Krempner, *Polyhedron*, 2007, **26**, 4436–4444.

22 M. W. Hsiao and C. C. Lin, *Dalton Trans.*, 2013, **42**, 2041–2051.

23 L. Clark, G. B. Deacon, C. M. Forsyth, P. C. Junk, P. Mountford, J. P. Townley and J. Wang, *Dalton Trans.*, 2013, **42**, 9294–9312.

24 J. V. Lamb, University of Oxford, DPhil Thesis, 2019.

25 V. Katiyar and H. Nanavati, *Polym. Chem.*, 2010, **1**, 1491–1500.

26 M. Helou, G. Moriceau, Z. W. Huang, S. Cammas-Marion and S. M. Guillaume, *Polym. Chem.*, 2011, **2**, 840–850.

27 J. C. Buffet, G. R. Harris, J. J. Coward, T. A. Q. Arnold, Z. R. Turner and D. O'Hare, *J. Organomet. Chem.*, 2016, **801**, 87–95.

28 M. Florczak, A. Michalski, A. Kacprzak, M. Brzeziński, T. Biedroń, A. Pajak, P. Kubisa and T. Biela, *React. Funct. Polym.*, 2016, **104**, 71–77.

29 S. M. Weidner and H. R. Kricheldorf, *Macromol. Chem. Phys.*, 2018, **219**, 1800445.

30 S. M. Weidner and H. R. Kricheldorf, *Rapid Commun. Mass Spectrom.*, 2020, **34**, e8673.

31 S. Bian, S. Abbina, Z. Lu, E. Kolodka and G. Du, *Organometallics*, 2014, **33**, 2489–2495.

32 B. Liu, T. Roisnel, J.-P. Guégan, J.-F. Carpentier and Y. Sarazin, *Chem. - A Eur. J.*, 2012, **18**, 6289–6301.

33 N. Ikpo, C. Hoffmann, L. N. Dawe and F. M. Kerton, *Dalton Trans.*, 2012, **41**, 6651–6660.

34 D. Alhashmialameer, N. Ikpo, J. Collins, L. N. Dawe, K. Hattenhauer and F. M. Kerton, *Dalton Trans.*, 2015, **44**, 20216–20231.

35 D. J. Darensbourg, W. Choi, O. Karroonnirun and N. Bhuvanesh, *Macromolecules*, 2008, **41**, 3493–3502.

36 D. J. Darensbourg and O. Karroonnirun, *Inorg. Chem.*, 2010, **49**, 2360–2371.

37 Z. Zhong, P. J. Dijkstra and J. Feijen, *J. Am. Chem. Soc.*, 2003, **125**, 11291–11298.

38 J. C. Buffet, A. Kapelski and J. Okuda, *Macromolecules*, 2010, **43**, 10201–10203.

39 M. Chisholm, N. W. Eilerts, J. C. Huffman, S. S. Iyer, M. Pacold and K. Phomphrai, *J. Am. Chem. Soc.*, 2000, **122**, 11845–11854.

40 J. C. Buffet and J. Okuda, *Polym. Chem.*, 2011, 2, 2758–2763.

41 J. E. Kasperczyk, *Polym. Commun.*, 1999, **40**, 5455–5458.

42 E. L. Whitelaw, M. D. Jones and M. F. Mahon, *Inorg. Chem.*, 2010, **49**, 7176–7181.

43 Y. Kim, G. K. Jnaneshwara and J. G. Verkade, *Inorg. Chem.*, 2003, **42**, 1437–1447.

44 K. A. M. Thakur, R. T. Kean, E. S. Hall, J. J. Kolstad, T. A. Lindgren, M. A. Doscotch, J. I. Siepmann and E. J. Munson, *Macromolecules*, 1997, **30**, 2422–2428.

Chapter Six

Permethylpentalene Zirconium Amidinate complexes for Olefin Polymerisation

6.1. Introduction

Higher polymerisation activities as well as different polymer properties can often be achieved by varying the ligand environment around the metal centre of the catalysts used. Generally, the greatest changes result from modifications to the ancillary ligand and the initiating group. Highly versatile and readily accessible, amidinate anions emerged as alternatives to cyclopentadienyl ligands in coordination chemistry.[1,2] The most common bonding modes are κ^1 and κ^2. In the κ^2 binding mode, the negative charge of the ligand is delocalised across the C and N atoms stabilising the coordination complex (Figure 6.1).[3–6]

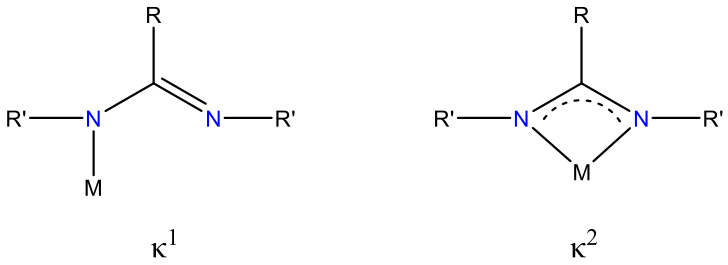

Figure 6.1. κ^1 and κ^2 binding modes of the amidinate ligand.

Group 4 metal amidinate complexes are known to promote the polymerisation of a variety of olefins such as ethylene, propylene and styrene in the presence of methylaluminoxane (MAO).[7–12] For example, κ^2 complex $[(N^iPr)_2C(C_6F_5)]TiCl_3$ polymerises propene and 1,3-butadiene in the presence of MAO.[7] As well as being an efficient catalyst for the polymerisation of ethylene, bis(amidinate) titanium and zirconium complexes $[(NR')(NR'')CR]_2MCl_2$ (M = Zr and Ti) catalyse the polymerisation of propylene with a tacticity controlled by the monomer concentration.[13–17] Polymerisation of styrene with high syndiotacticity can be achieved by using titanium monoamidinates $[(NR')(NR'')CR]TiCl_3$ with MAO at high temperature. For example, the complex $[(N^iC_3H_7)_2C(CH_2C_6H_5)]TiCl_3$ forms syndiotactic polystyrene in the presence of MAO at 50 °C whereas only atactic polymer is obtained at –60 °C in absence of co-catalyst.[7] While amidinate complexes have been widely studied for homogeneous catalysis, examples of solid-supported amidinate catalysts for olefin polymerisations are very scarce.[18–23] Sita *et al*. successfully developed a Cp*ZrMe[(NEt)(N^tBu)CMe] initiator immobilised on a polymer support to polymerise α-olefins.[18]

This chapter describes the preparation of Pn*MX[(NR')(NR")CR]] (M = Zr and Ti) complexes to explore their capacity to polymerise ethylene and styrene (Figure 6.2). The synthesis and characterisation of 4 new formamidine and amidine derivatives are described. New ligands were synthesised and used for the synthesis of new group 4

complexes. Their ethylene and styrene polymerisation activities were studied in order to determine the effect of steric and electronic properties of the ligand substituents on their catalytic capability.

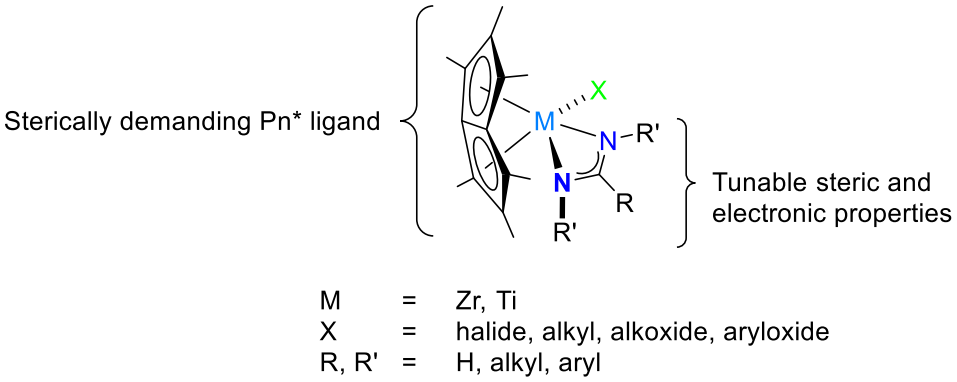

M = Zr, Ti
X = halide, alkyl, alkoxide, aryloxide
R, R' = H, alkyl, aryl

Figure 6.2. Targeted amidinate group 4 complexes.

6.2. Synthesis of formamidine/amidine ligands and complexes

Three new formamidinate ligands Li[(N^{i}Pr)$_2$C(4-OMe-C$_6$H$_4$)], Li[(N^{i}Pr)$_2$C(4-CF$_3$-C$_6$H$_4$)] and Li[(N^{i}Pr)$_2$C(4-^{t}Bu-C$_6$H$_4$)] were obtained by initial Li-halide exchange of 1-Br-4-R-C$_6$H$_4$ (R = OMe, CF$_3$ and ^{t}Bu) and ^{n}BuLi in thf at -78 °C for 1 hour, followed by addition of di*iso*propylcarbodiimide *in situ*. The reaction mixture was stirred for another hour at 0 °C before work up to yield Li[(N^{i}Pr)$_2$C(4-R-C$_6$H$_4$)] as colourless solids (R = OMe, 50%; R = CF$_3$, 41% and R = ^{t}Bu, 84%) (Scheme 6.1).

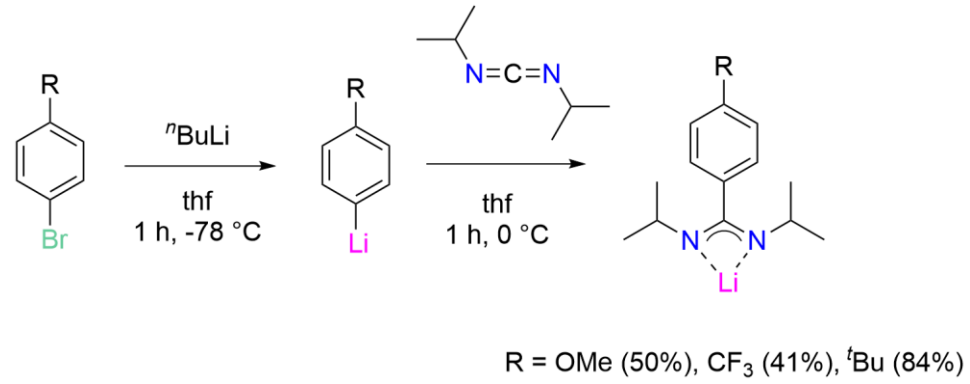

Scheme 6.1. Synthesis of Li[(N^{i}Pr)$_2$C(4-OMe-C$_6$H$_4$)], Li[(N^{i}Pr)$_2$C(4-CF$_3$-C$_6$H$_4$)] and Li[(N^{i}Pr)$_2$C(4-^{t}Bu-C$_6$H$_4$)].

The formamidinate salt K[(NMes)$_2$CH] (Mes = 2,4,6-Me-C$_6$H$_2$)was synthesised by deprotonation of H[(NMes)$_2$CH] with KH in thf (Scheme 6.2). Filtration led to a white powder in 30% yield.[24]

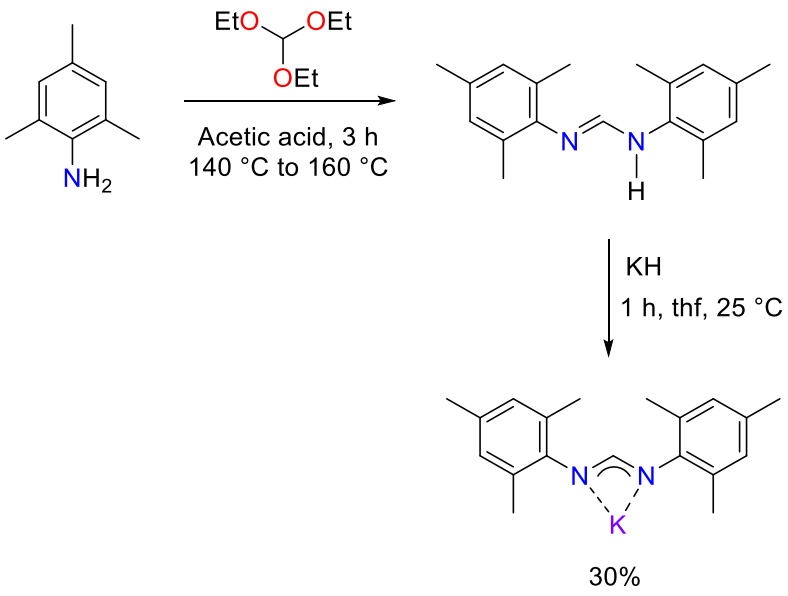

Scheme 6.2. Synthesis of K[(NMes)$_2$CH].

Amidinate zirconium complexes Pn*ZrCl[(NR′)$_2$CR] (R′ = ^{i}Pr, R = 4-OMe-C$_6$H$_4$, **6**; 4-CF$_3$-C$_6$H$_4$, **7**; 4-^{t}Bu -C$_6$H$_4$, **8**; R′ = Mes, R = H, **9**) as shown on Scheme 6.3 were prepared by reactions of [Pn*ZrCl(μ-Cl)$_{3/2}$]$_2$(μ-Cl)$_2$Li(thf)$_2$ with the appropriate amidinate alkali metal salts in benzene-d_6 at 25 °C for 1 hour and were obtained in spectroscopic yields superior to 90% (Scheme 6.3).

Following a similar procedure, the zirconium complex Pn*ZrCl[(N^{i}Pr)$_2$C(N^{i}Pr$_2$)] was synthesised from Li[(N^{i}Pr)$_2$C(N^{i}Pr$_2$)] and [Pn*ZrCl(μ-Cl)$_{3/2}$]$_2$(μ-Cl)$_2$Li(thf)$_2$ but decomposed upon purification of the material and thus was not further investigated (Scheme 6.3).[25]

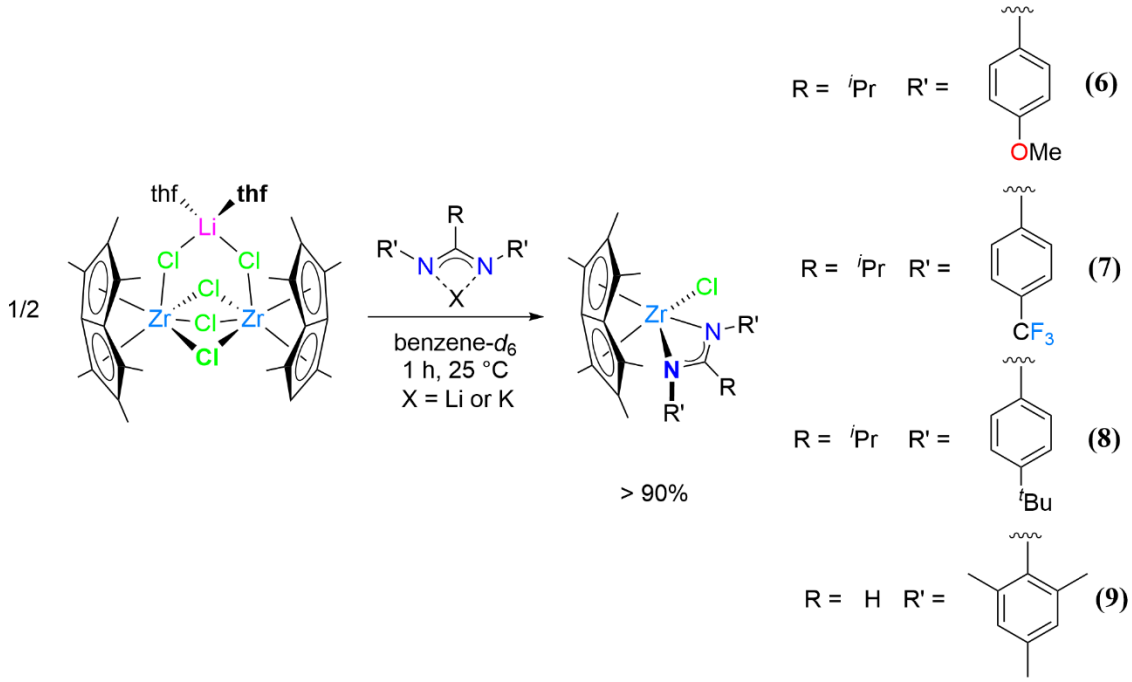

Scheme 6.3. Synthesis of Pn*ZrCl[(NR′)$_2$CR] complexes.

Synthesis of the analogous titanium complexes by reaction of [Pn*TiCl(μ-Cl)]$_2$[16] with corresponding amidinate or formamidinate potassium salts in benzene at 25 °C for 1 hour afforded Pn*TiCl[RNC(R')NR] complexes and conversions greater than 90% were observed by NMR spectroscopy (Scheme 6.4.). Titanium complexes were however not further studied as the purification and extraction of the complexes on a larger scale led to their decomposition.

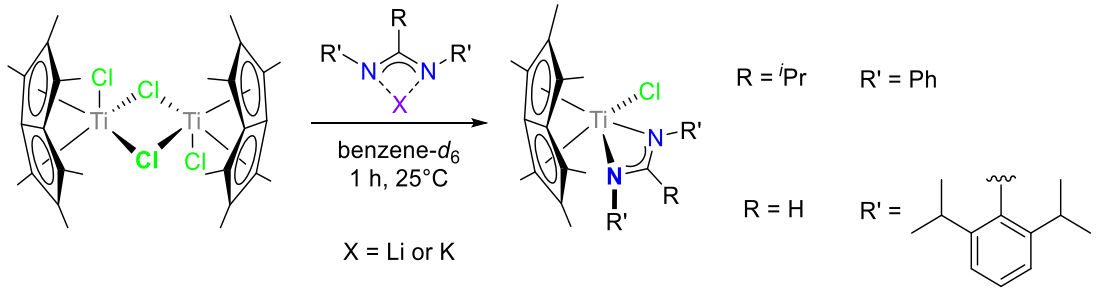

Scheme 6.4. Synthesis of Pn*TiCl[(NR′)$_2$CR] complexes.

The ^{1}H NMR spectrum of Pn*ZrCl[(N^{i}Pr)$_2$C(4-OMe-C$_6$H$_4$)] (**6**) is shown in Figure 6.3 as a representative example for this class of complexes. All ^{1}H NMR spectra displayed

two singlets at 2.05 and 2.16 ppm in a 12:6 ratio corresponding to the six methyl groups on the Pn* rings, one singlet corresponding to the non-wingtip (NWT) protons and the other singlet observed for the wingtip (WT) positions. The ^{1}H NMR spectra of Pn*ZrCl[(N^{i}Pr)$_2$C(4-R-C$_6$H$_4$)] (R = OMe, CF$_3$ and ^{t}Bu) were very similar, only distinguishing themselves by the protons from the methoxy and *tert*-butyl groups, appearing as singlets at 3.22 and 1.15 ppm respectively. Complexes with ^{i}Pr groups showed two doublets corresponding to the six methyl groups from the ^{i}Pr at 0.92 and 1.19 ppm. The steric bulk of both the Pn* and amidinate ligands hindered N-C bond rotation making the protons chemically inequivalent. The ^{1}H NMR spectrum of Pn*M[(NMes)$_2$CH](Cl) (**9**) presented differences in the chemical shifts relative to the Pn*-Me substituents with all methyl groups appearing as one singlet around 2.16 ppm.

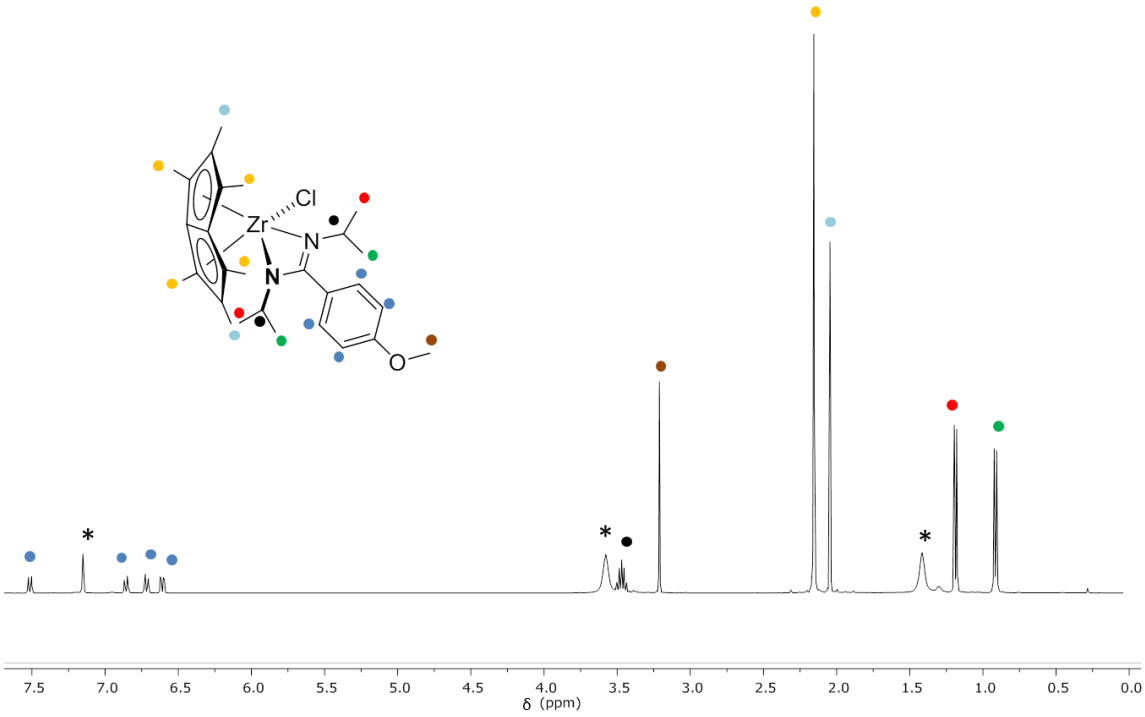

Figure 6.3. ^{1}H NMR spectrum of Pn*ZrCl[(N^{i}Pr)$_2$C(4-OMe-C$_6$H$_4$)] (benzene-d_6, 298 K, 400 MHz). * represents residual protio solvent and thf.

6.3. Homopolymerisation of olefins

Previously reported complexes Pn*ZrClCp^{R} (R = alkyl) showed high activities for the homopolymerisation of olefins.[26,27] The amidinate complexes possess the same number of electrons and were tested for ethylene and styrene polymerisations to investigate the effect of the amidinate ligands and compare them with Cp. In addition to the list of four zirconium complexes described in section 6.2, four related complexes (**10**, 1**1**, **12**, **13**) synthesised by Dr. Thomas Robinson were also used (Figure 6.4). All complexes were immobilised *in situ* on sMAO in a molar ratio of $[Al_{sMAO}]_0$:$[Zr]_0$ = 200:1 and tested for the homopolymerisations of styrene and ethylene and the copolymerisations of ethylene with styrene and ethylene with 4-NH_2-styrene in the slurry-phase.

Liu *et al.* reported the rearrangement from κ^1 to κ^2 amidinate after activation of a catalyst by MAO resulting from the cleavage of metal-nitrogen bond.[28] Likewise, Eisen and coworkers revealed by NMR spectroscopy the existence of two bis(amidinate) titanium complexes species in solution corresponding to the two coordination modes of the bidentate ligand.[29] It is hypothesised that the dynamic nature of the amidinate ligand in the Pn*MX[(NR')(NR")CR]] allows for a rearrangement and formation of a vacant site, crucial for the coordination of an olefin monomer.

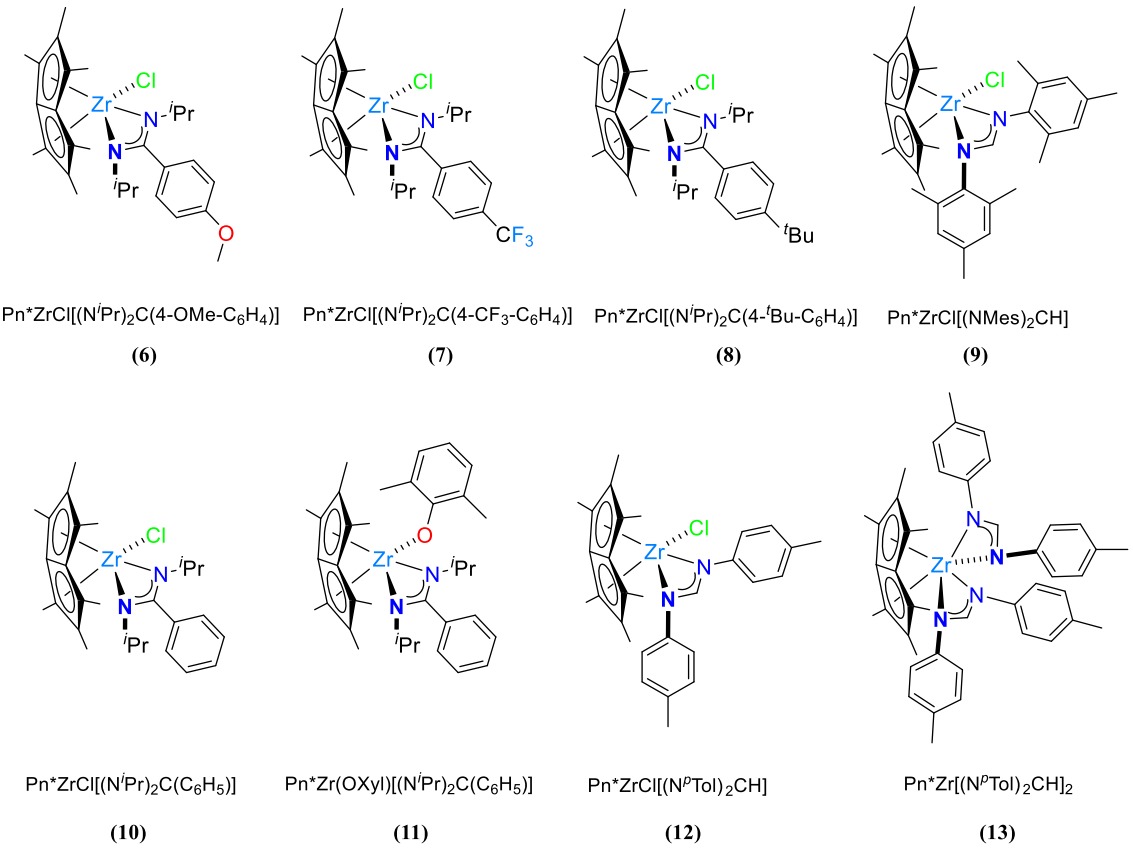

Figure 6.4. Amidinate and formamidinate complexes **6**–**13** studied for their polymerisation properties in this chapter. ^{p}Tol = 4-Me-C$_6$H$_4$, Mes = 2,4,6-Me-C$_6$H$_2$, Xyl = 2,6-Me-C$_6$H$_3$.

6.3.1 Slurry-phase homopolymerisation of styrene

Homopolymerisation activities for the eight complexes were determined in toluene at various temperatures (Figures 6.5 and 6.6). Figure 6.5 displays the polymerisation activities at three different temperatures: 40, 55 and 70 °C. The temperature appeared to have little to no effect on the activities except for **8$_{sMAO}$**: the activity increaseed dramatically from 1072 at 40 °C to 4061 $kg_{PS}/mol_{Zr}/h$ at 55 °C respectively. It was the highest activity of any complex in the polymerisation series measured at 55 °C as shown on Figure 6.6.

Three different *para*-substituents were investigated in immobilised complexes Pn*ZrCl[(N^{i}Pr)$_2$C(4-R-C$_6$H$_4$)] (**6**–**8$_{sMAO}$**) and compared with the unsubstituted Pn*ZrCl[(N^{i}Pr)$_2$C(C$_6$H$_5$)] (**10$_{sMAO}$**). Their activities can be ranked in the order ^{t}Bu (σ_{tBu} = –0.20) > OMe (σ_{OMe} = –0.27) > CF_3 (σ_{CF_3} = 0.54) > Ø.[30] Electron donating groups on the *para*-position led to greater activities compared with the equivalent complexes without *para* substitution. Skupiński *et al.* described the same trend when using $CpTiCl_2$(O-4-X-C$_6$H$_4$)/MAO (X = NO_2, Cl, CH_3); they reported the lowest activity for the NO_2 substituted catalyst and the highest for the compound bearing the CH_3 group at 30 °C.[31] In the case of the Pn* catalysts, the Hammett constants alone are not sufficient to rationalise the order observed. A possible explanation is an interaction between the -OMe and -CF_3 groups of complexes **6$_{sMAO}$** and **7$_{sMAO}$** and the Al from the solid MAO support that may therefore hinder monomer coordination.

The two mono-formamidinate complexes have very distinct styrene polymerisation activities. Complex **9$_{sMAO}$** reaches 2977 $kg_{PS}/mol_{Zr}/h$ at 70 °C which is 2.5 times higher than **12$_{sMAO}$**. This can be rationalised by the greater stabilisation of the active species by the methyl substituents on the mesityl group compared to the tolyl group.

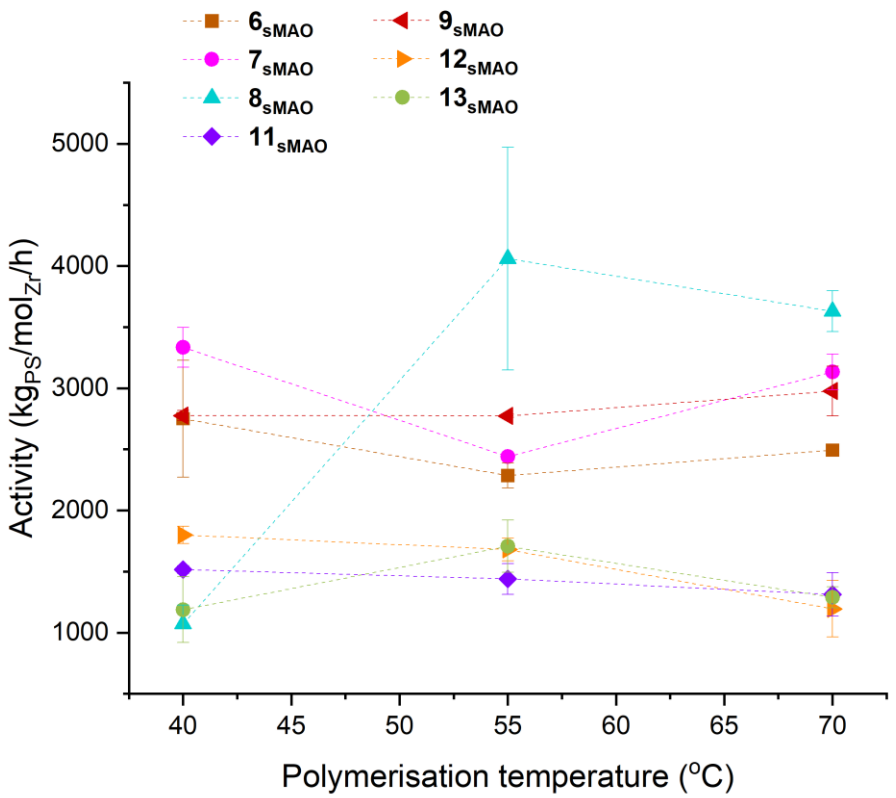

Figure 6.5. Temperature dependence of slurry-phase styrene homopolymerisation by Pn*ZrCl[RNC(R')NR]. Polymerisation conditions: 10 minutes, 1000 rpm. 50 mL toluene, 10 mg catalyst, 3.7 mL styrene, $[Al_{sMAO}]_0$:$[Zr]_0$ = 200:1.

When investigating the effect of a chloride ancillary ligand, Figure 6.5 highlights an increase in activity at 55 °C from 654 to 1440 $kg_{PS}/mol_{Zr}/h$ for complexes **10**$_{sMAO}$ and **11**$_{sMAO}$ respectively. The presence of the additional oxygen from the -OXyl ligand is hypothesised to stabilise the active species more effectively. The oxygen coordinates with the electron deficient aluminium from the solid support thus increasing the active species stability and the polymerisation activities.[32,33] The opposite phenomenon was described by O'Hare and co-workers for ethylene polymerisation using sMAO supported catalysts;[34,35] however, the presence of the zirconium metal as well as the amidinate ligand modifies the properties of the catalysts that could interact differently with the support. Comparing the mono- and di-formamidinate ^{p}Tol complexes **12**$_{sMAO}$ and **13**$_{sMAO}$, no significant difference in polymerisation activities was observed along the range of temperatures suggesting that the steric bulk of the amidinate ligand has little

impact on the monomer coordination and polymer chain growth. The steric congestion caused by the formamidinate ligands might result in a rearrangement of the species, explaining the similar activities measured for complexes **11$_{sMAO}$-13$_{sMAO}$**.

All permethylpentalene complexes tested except **10$_{sMAO}$** showed higher activities than Cp*$ZrCl_3$ after 15 hours at 80 °C (1467 $kg_{PS}/mol_{Zr}/h$).[36] Though complexes **6**–**13$_{sMAO}$** remained less active than the recently developed bis(phenolate) zirconium complexes that exhibited high activity up to 7700 $kg_{PS}/mol_{Zr}/h$,[37] they were considerably more active than previously reported amidinate complexes which repeatedly exhibited low catalytic activities.[8,10,11] For example, the permethylpentalene containing amidinate systems had activities greater than complexes such as $TiCl_3[(N^iPr)_2C(CH_2Ph)]$ (2 $kg_{PS}/mol_{Ti}/h$ at 50 °C).[7]

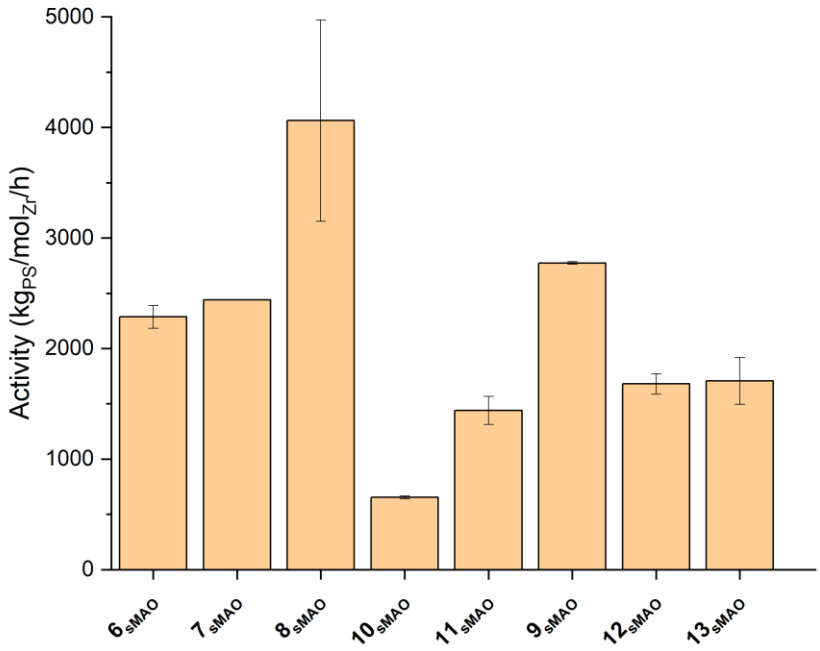

Figure 6.6. Slurry-phase styrene polymerisation activities at 55 °C. Polymerisation conditions: 10 minutes, 1000 rpm. 50 mL toluene, 10 mg catalyst, 3.7 mL styrene, $[Al_{sMAO}]_0$:$[Zr]_0$ = 200:1.

All polymer samples were characterised by GPC to determine the effect of the temperature on the molecular weights (Figures 6.7 and 6.8). Multimodal molecular

weight distributions were obtained possibly due to the presence of Zr^{III} and Zr^{IV} active species.[38,39] By analogy with mechanisms reported by Nomura and co-workers for titanium complexes, the Zr^{III} species is the main catalytic species but other species such as cationic Zr^{IV+} might form and could polymerise styrene. The GPC traces reveal two distinct fractions: high molecular weight (HMW) with dispersities between 3–3.5 and low molecular weight (LMW) with narrower dispersities between 1.5–2 (Figures 6.7, 6.8 and A6.23–29). The M_w evolution with polymerisation temperature varies with the type of complex used. For the high molecular weight range, the amidinate complexes display a minimum at 55 °C. The drop in M_w is more significant for **6**$_{sMAO}$ and **7**$_{sMAO}$ than the two other amidinates where distributions remain between 2.2×10^6 and 2.6×10^6 g/mol. These values are one order of magnitude higher than those observed by Zambelli *et al.* using $TiCl_3[(N^iPr)_2C(CH_2Ph)]$ (M_w = 1.9×10^5 g/mol at 50 °C).[40] An increase in temperature led to a decrease in molecular weights of the low fraction with the lowest value obtained using complex **8**$_{sMAO}$ at 70 °C (8978 g/mol). The polymers synthesised using the three formamidinate complexes displayed little to no variation in molecular weights with the polymerisation temperature for both the high and the low fractions. While complex **9**$_{sMAO}$ gave the highest M_w of the series at 55 °C (2.3×10^6 g/mol), it also led to the lowest values in the formamidinate series for the second fraction with 9299 g/mol which was around half the M_w of the *para*-tolyl analogue.

The ratio of high molecular weights to low molecular weights depended on each complex as well as the polymerisation temperature. At a polymerisation temperature of 55 °C, the high M_w fraction of polystyrene produced by **6**$_{sMAO}$ was predominant. When the temperature reached 70 °C, the opposite trend can be observed (Figure 6.9).

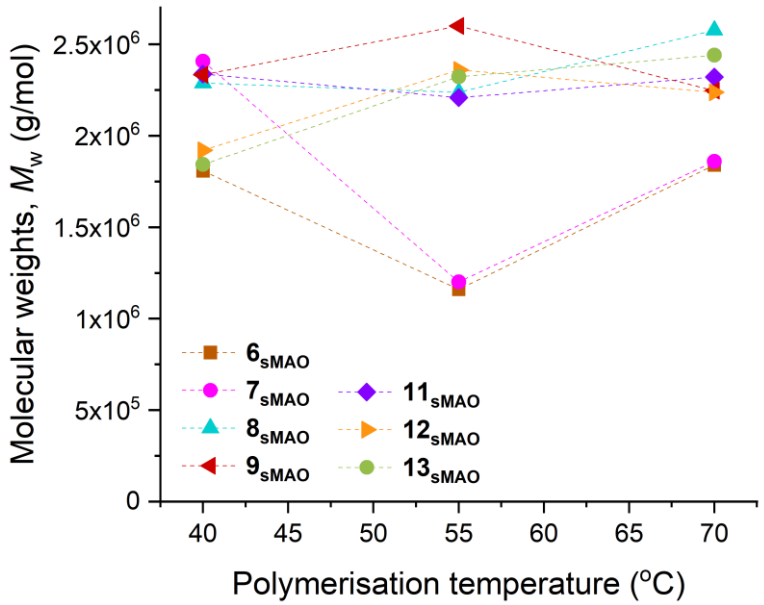

Figure 6.7. Temperature dependence of the high fraction molecular weights, M_w, of the polystyrenes synthesised with Pn*ZrCl[RNC(R')NR]. Polymerisation conditions: 10 minutes, 1000 rpm. 50 mL toluene, 10 mg catalyst, 3.7 mL styrene, $[Al_{sMAO}]_0$:$[Zr]_0$ = 200:1.

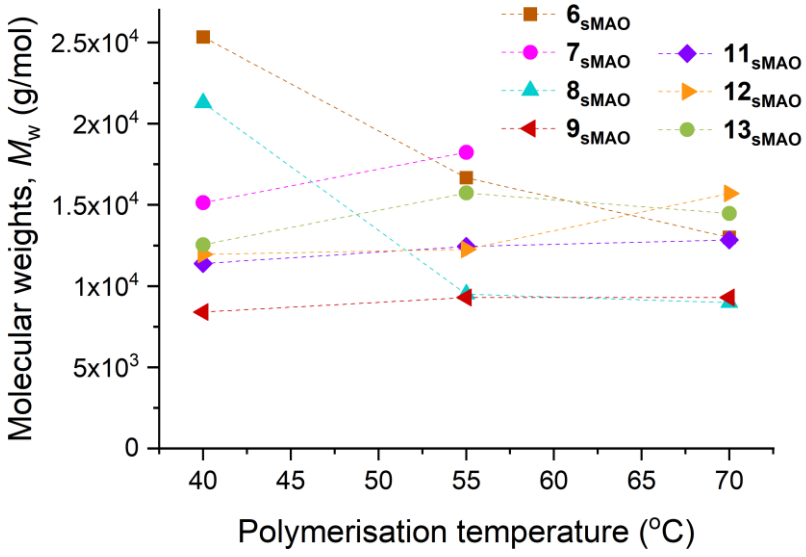

Figure 6.8. Temperature dependence of the low fraction molecular weights, M_w, of the polystyrenes synthesised with Pn*ZrCl[RNC(R')NR]. Polymerisation conditions: 10 minutes, 1000 rpm. 50 mL toluene, 10 mg catalyst, 3.7 mL styrene, $[Al_{sMAO}]_0$:$[Zr]_0$ = 200:1.

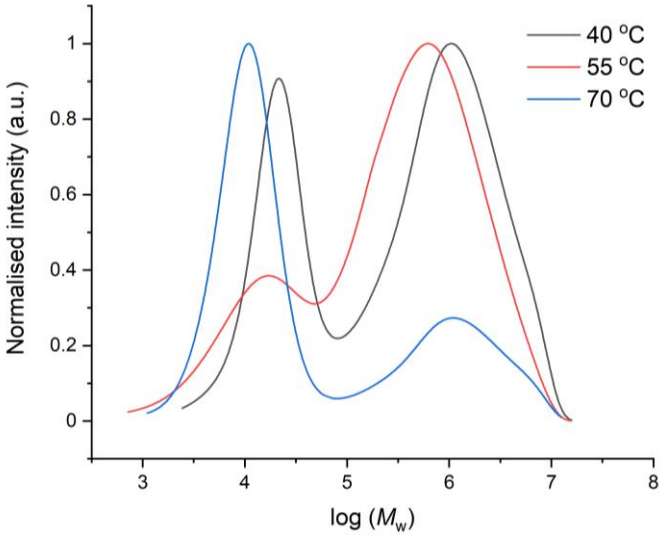

Figure 6.9. Molecular weights traces of polystyrenes synthesised with Pn*ZrCl[(N^iPr)$_2$C(4-OMe-C_6H_4)] (**6$_{sMAO}$**) between 40 and 70 °C. Polymerisation conditions: 10 minutes, 1000 rpm. 50 mL toluene, 10 mg catalyst, 3.7 mL styrene, $[Al_{sMAO}]_0$:$[Zr]_0$ = 200:1.

SEM was performed in order to further characterise the polymer samples (Figure 6.10). The materials present themselves are thin sheets of 15-20 µm width with a smooth surface. Different morphologies of polystyrene are reported in the literature with supported catalysts.[41–43] Using 2-Me-IndTiCl_3 supported on silica, Entezami *et al.* observed a porous material with soft small particles compared to dense polystyrene produced by the same homogeneous catalyst.[42] O'Hare and co-workers previously reported olefin polymerisations using sMAO-supported indenyl and permethylpentalene complexes. All polymer samples exhibited replication of the sMAO support morphology with a typical "popcorn" shape.[26,44–46] The absence of replication for the supported amidinate and formamidinate complexes may result from leaching from the support.[47]

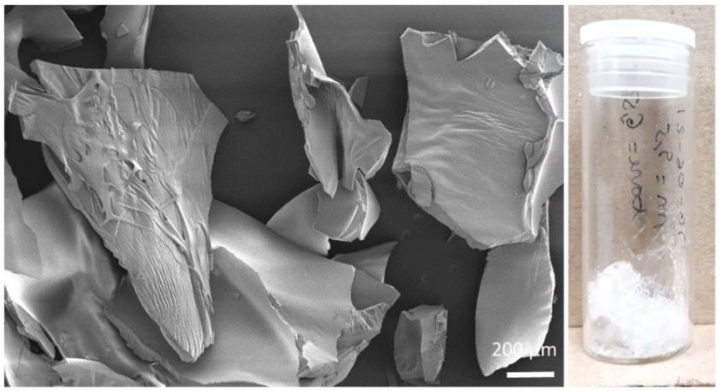

Figure 6.10. SEM images of polystyrene synthesised using Pn*ZrCl[(N^iPr)$_2$C(4-OMe-C_6H_4)] (**6$_{sMAO}$**) at 55 °C and picture of the polymer sample.

$^{13}C\{^1H\}$ NMR spectroscopy of the polystyrenes show several resonances in the region 40-50 ppm, revealing the atactic nature of the polymers with P_m between 0.45 and 0.69 (Table A6.8).[48–51] This is confirmed by DSC measurements showing no heat flow peak on heating above 150 °C and the absence of crystallinity (Figure 6.11 and Table 6.1).[52,53] The lack of tacticity was expected with these zirconium complexes as discussed in Chapter 2.[54] The thermal behaviour of the polymer samples reveal that the glass transition temperature can be tuned by changing the supported complex and the polymerisation temperature. Figure 6.11. compares the DSC profiles of all polystyrenes synthesised at 55 °C. While most of the complexes exhibit a heat flow peak in the DSC between 103 and 106 °C, two complexes have lower glass transition temperatures at this polymerisation temperature**: 8$_{sMAO}$** and **9$_{sMAO}$** with T_g of 95.6 and 96.1 °C respectively. It is worth noting that the glass transition temperature of the polystyrenes do not vary with the polymerisation temperature. For example, the polymers synthesised by the methoxy derivative **6$_{sMAO}$** exhibited a T_g at 107–108 °C (Figure 6.12).

Table 6.1. Polymer glass transition temperatures (T_g) for supported Pn*ZrCl[RNC(R')NR]; 10 mg catalyst ($[Al]_0$:$[Zr]_0$ = 200:1), 2 bar ethylene, 125 µL of styrene, 50 mL hexanes, 150 mg TiBA, 40 °C and 30 minutes.

Supported complex	T_g (°C)
Pn*ZrCl[(N^{i}Pr)$_2$C(4-OMe-C$_6$H$_4$)] (**6$_{sMAO}$**)	107.9
Pn*ZrCl[(N^{i}Pr)$_2$C(4-CF$_3$-C$_6$H$_4$)] (**7$_{sMAO}$**)	104.4
Pn*ZrCl[(N^{i}Pr)$_2$C(4-^{t}Bu-C$_6$H$_4$)] (**8$_{sMAO}$**)	95.6
Pn*Zr(OXyl)[(N^{i}Pr)$_2$C(C$_6$H$_5$)] (**11$_{sMAO}$**)	103.9
Pn*ZrCl[(NMes)$_2$CH] (**9$_{sMAO}$**)	96.2
Pn*ZrCl[(N^{p}Tol)$_2$CH] (**12$_{sMAO}$**)	103.0
Pn*Zr[(N^{p}Tol)$_2$CH]$_2$ (**13$_{sMAO}$**)	105.8

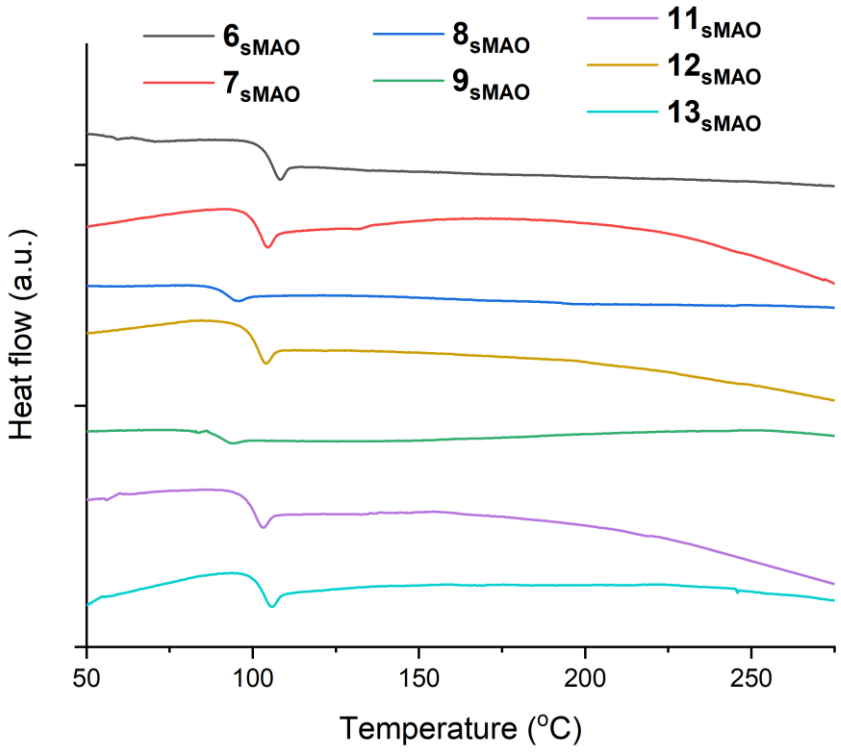

Figure 6.11. Glass transition temperature (T_g) of polystyrene synthesised by Pn*ZrCl[RNC(R')NR] at 55 °C, ramp 5 °C/minute. Polymerisation conditions: 10 minutes, 1000 rpm. 50 mL toluene, 10 mg catalyst, 3.7 mL styrene, $[Al_{sMAO}]_0$:$[Zr]_0$ = 200:1.

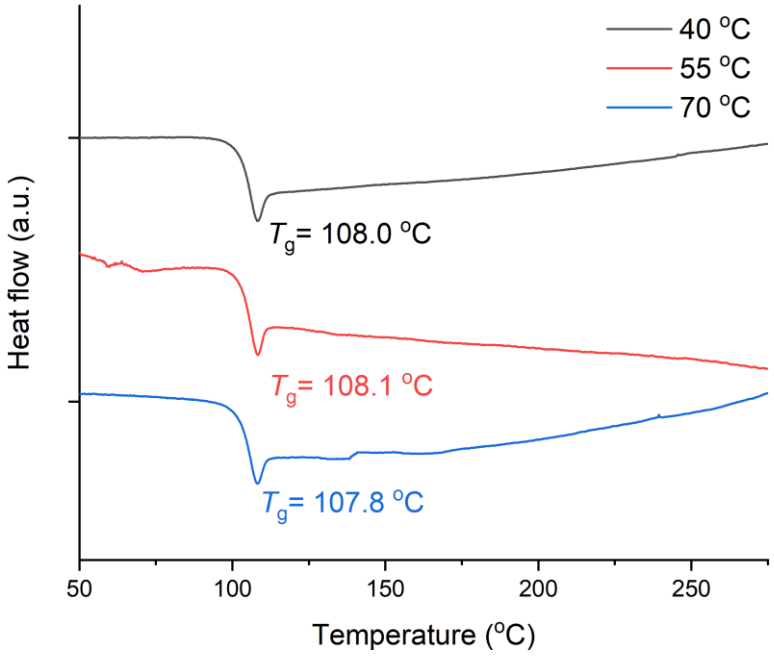

Figure 6.12. DSC of polystyrene synthesised by Pn*ZrCl[(N^{i}Pr)$_2$C(4-OMe-C$_6$H$_4$)] (**6$_{sMAO}$**), ramp 5 °C/minute. Polymerisation conditions: 10 minutes, 1000 rpm. 50 mL toluene, 10 mg catalyst, 3.7 mL styrene, [Al$_{sMAO}$]$_0$:[Zr]$_0$ = 200:1.

6.3.2 Slurry-phase homopolymerisation of ethylene

Similarly to styrene, the eight supported zirconium complexes were tested as ethylene homopolymerisation catalysts in a hexane slurry. Using a pressure of 2 bar of ethylene, fine white flakes of polymers were obtained and the catalytic activities of the amidinate complexes were determined at five different temperatures (Figures 6.13 and 6.14).

Activities between 28 and 175 kg$_{PE}$/mol$_{Zr}$/bar/h were obtained for the Pn* amidinate series (Figure 6.13). Except for **8$_{sMAO}$**, all amidinate complexes exhibited an increased polymerisation activity with temperature. The former led to a drop in activity above 60 °C which may be caused by the catalyst deactivation above this temperature.

All Pn* (form)amidinate complexes performed poorly in terms of catalytic activities compared with sMAO-supported Pn* cyclopentadienyl. At 60 °C, the highest activity, measured for the unsubstituted **10$_{sMAO}$**, is 26 times lower than that of sMAO-Pn*ZrCpCl under similar reaction conditions (163 *vs.* 4209 kg$_{PE}$/mol$_{Zr}$/bar/h).[26,27] Hessen and co-

workers observed catalytic activities 1 to 2 orders of magnitude higher using yttrium amidinate complexes in solution phase.[23] In the presence of a boron activator, $Y(CH_2SiMe_3)_2[(N\text{-}2,6\text{-}^iPr\text{-}C_6H_3)_2C(C_6H_5)]$ and $Y(CH_2SiMe_3)_2[(N\text{-}2,6\text{-}^iPr\text{-}C_6H_3)_2C(C_6F_5)]$ led to high activities of 1146 and 1252 $kg_{PE}/mol_Y/bar/h$ at 50 °C under 5 bar of ethylene.

Nonetheless, the amidinate complexes **6**$_{sMAO}$, **7**$_{sMAO}$, **8**$_{sMAO}$, **10**$_{sMAO}$ and **11**$_{sMAO}$ achieved greater activities than reported for $[\eta^4\text{-}4\text{-}RC_6H_4C(NSiMe_3)_2]_2ZrCl_2$. by Eisen *et al.*[9] The benzamidinate reaches activities up to 32 $kg_{PE}/mol_{Zr}/bar/h$ for the polymerisation of ethylene under 1 bar of pressure at 25 °C.

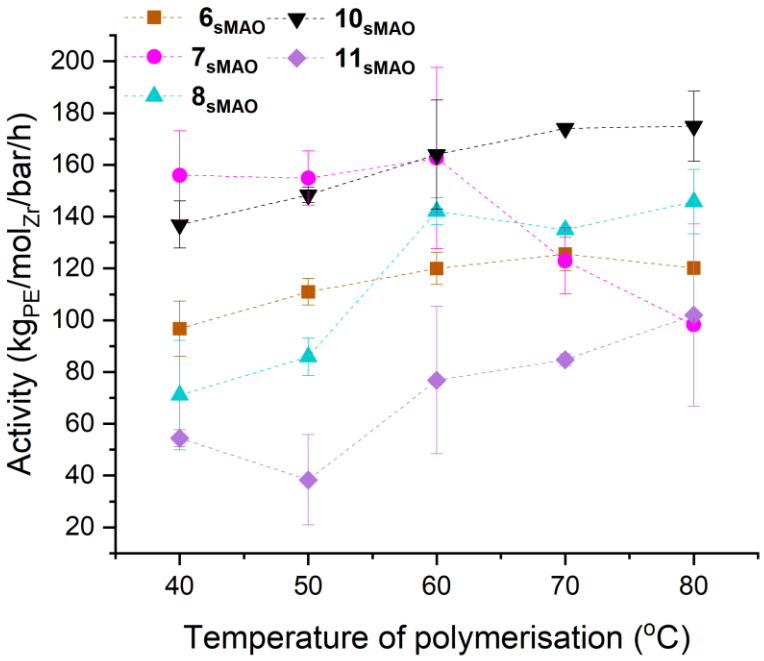

Figure 6.13. Temperature dependence of slurry-phase ethylene polymerisation activity using Pn* zirconium amidinates. Polymerisation conditions: 30 minutes, 1000 rpm, 2 bar ethylene, 50 mL hexane, 10 mg catalyst, $[Al_{sMAO}]_0:[Zr]_0$ = 200:1.

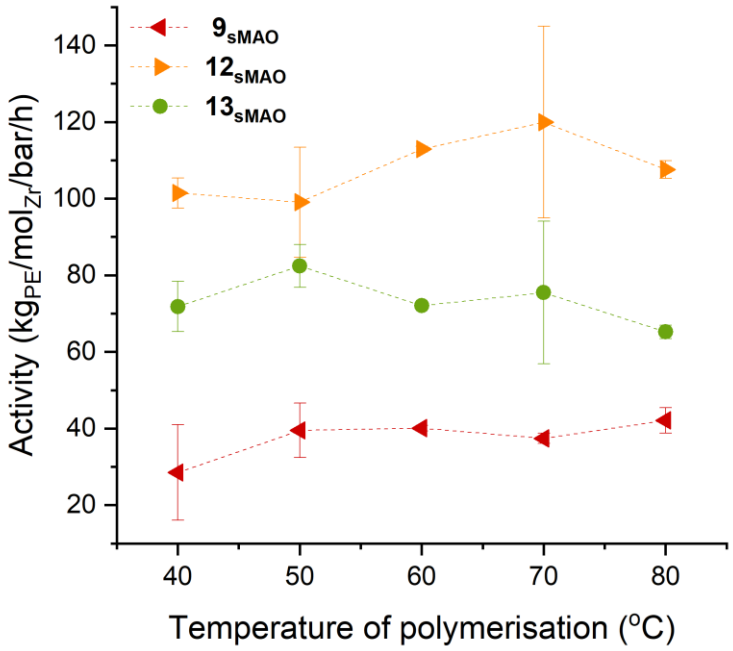

Figure 6.14. Temperature dependence of slurry-phase ethylene polymerisation activity using Pn* zirconium formamidinates **9**$_{sMAO}$, **12**$_{sMAO}$ and **13**$_{sMAO}$. Polymerisation conditions: 30 minutes, 1000 rpm, 2 bar ethylene, 50 mL hexane, 10 mg catalyst, $[Al_{sMAO}]_0$:$[Zr]_0$ = 200:1.

The highest activities were obtained using compound **10**$_{sMAO}$ at 80 °C (175 $kg_{PE}/mol_{Zr}/bar/h$) which is more than ten times lower than activities observed by Scharmann *et al.* who reported activities of 1900 $kg_{PE}/mol_{Zr}/bar/h$ using $CpZrCl_2[(NSiMe_3)_2CPh]$ under 5 bar of ethylene at 80 °C.[55] At this temperature, the Pn* complexes performance can be ranked in the order H > ^{t}Bu > OMe > CF_3 regarding the aromatic substituent. The bulkiness of the aromatic ring as well as the electronic effects of the *para*-substituents affect the catalyst behaviour. Electron donating substituents achieved higher activities as previously described for $CpTiCl_2(O\text{-}4\text{-}X\text{-}C_6H_5)$ (X = OMe, CH3, Cl, NO_2).[56] Skupiński and Wasilewski reported the successful polymerisation of ethylene in the presence of Et_2AlCl with the methoxy-substituted catalyst performing 2 times better than the nitro analogue. Replacing the chloride ligand by an aryloxide such as -O-2,6-Me-C_6H_3 reduced the catalytic activity of the zirconocene by up to 4 times (148 and 38 $kg_{PE}/mol_{Zr}/bar/h$ for complexes **10**$_{sMAO}$ and **11**$_{sMAO}$ respectively at 50 °C). The

latter displayed the lowest range of activities of the amidinate series. Similarly to styrene polymerisation, it is proposed that this behaviour was due to interactions between the active species and the solid support reducing the activity of the complex.[34,35]

The three formamidinate complexes showed very different performances between 40 and 80 °C (Figure 6.14). At high temperatures, the formamidinate catalysts generally behaved less effectively than the amidinate complexes, resulting in lower activities. The polymerisation temperature had little to no effect on their performance. The sterically-demanding mesityl groups in complex **9$_{sMAO}$** prevented the ethylene monomer from approaching the active sites resulting in low activities between 28 and 42 $kg_{PE}/mol_{Zr}/bar/h$. The less hindered *para*-tolyl analogue exhibited activities 2.5 to 3.6 times higher. As expected, increasing steric bulk by swapping the chloride for another formamidine reduced the catalytic ability of the supported species. At 70 °C, **13$_{sMAO}$** afforded 1.6 times less polyethylene than the mono-substituted **12$_{sMAO}$** (75 and 120 $kg_{PE}/mol_{Zr}/bar/h$ respectively). Rausch and co-workers observed the same trend while using $TiCl_2[(NSiMe_3)_2CPh]_2$ and $TiCl_3[(NSiMe_3)_2CPh]$ with $[Al]_0:[Ti]_0 = 2000$.[12] At 20 °C, the mono(amidinate) reached activities of 2.4 $kg_{PE}/mol_{Ti}/bar/h$ while 0.7 $kg_{PE}/mol_{Ti}/bar/h$ were achieved with the titanium bis(amidinate). The reverse trend followed by Pn* compounds was anticipated and believed to be caused by the large size of the permethylpentalene ligand causing steric hindrance around the metal centre. This hypothesis is supported by the low polymerisation activities obtained with large tris(amidinate) complexes.[57–59]

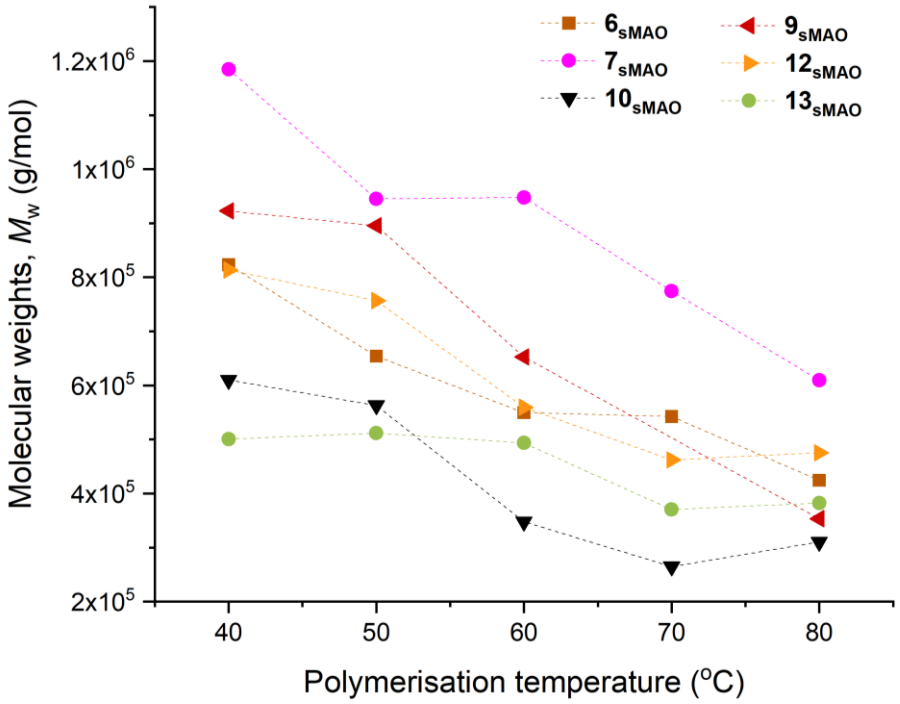

Figure 6.15. Polyethylene molecular weights, M_w, of sMAO-supported Pn*ZrCl[RNC(R')NR] across the temperature range 40–80 °C. Polymerisation conditions: 30 minutes, 1000 rpm, 2 bar ethylene, 50 mL hexane, 10 mg catalyst, $[Al_{sMAO}]_0$:$[Zr]_0$ = 200:1.

The molecular weights of the polymers were measured by GPC in 1,2,3-$C_6H_3Cl_3$ at 160 °C and are shown in Figure 6.15. The values were between 3.1×10^5 at 80 °C and 1.2×10^6 g/mol at 40 °C for **10**$_{sMAO}$ and **7**$_{sMAO}$ respectively. Other permethylpentalene zirconium complexes studied by O'Hare and co-workers, Pn*ZrCpCl and Pn*$ZrCp_2$, yielded polymers with molecular weights one order of magnitude lower (M_w = 7.64×10^6 g/mol for Pn*$ZrCp_2$ at 40 °C) highlighting the effect of the amidinate ligands.[60] All the zirconium complexes exhibited a comparable behaviour with M_w significantly decreasing when the polymerisation temperature increases as expected.[11] The same trend was described for Pn*ZrCpCl and Pn*$ZrCp_2$ between 40 and 100 °C.[60] This phenomenon can be explained by the difference in activation energy between chain termination and chain propagation. As the temperature of polymerisation increases, the ratio of transfer to propagation increases leading to shorter chains.[61,62] The two complexes **7**$_{sMAO}$ and **9**$_{sMAO}$ showed a significant decrease in polymer molecular weight over the range of

temperatures studied. **7$_{sMAO}$** exhibited a two-fold decrease from 1.2×10^6 to 6.1×10^5 g/mol and the formamidinate **9$_{sMAO}$** displayed a decrease from 9.2×10^5 to 3.5×10^5 g/mol between 40 and 80 °C. The M_w distributions were much larger than those observed for polystyrenes (9.6–103.1) with some catalysts leading to multimodality (Figure 6.16.). At low temperatures, the polyethylene coats the catalyst and renders the system heterogeneous; the catalytic species is not single-site anymore resulting in broadened molecular weight distributions.[62] Noteworthy is the shape of the M_w distributions displayed in Figures 6.16 and 6.17. They show a tail for all complexes except **11$_{sMAO}$** for log (M_w) between 2.5 and 4 indicating the synthesis of short polyethylene chains and reflecting the broad dispersities.

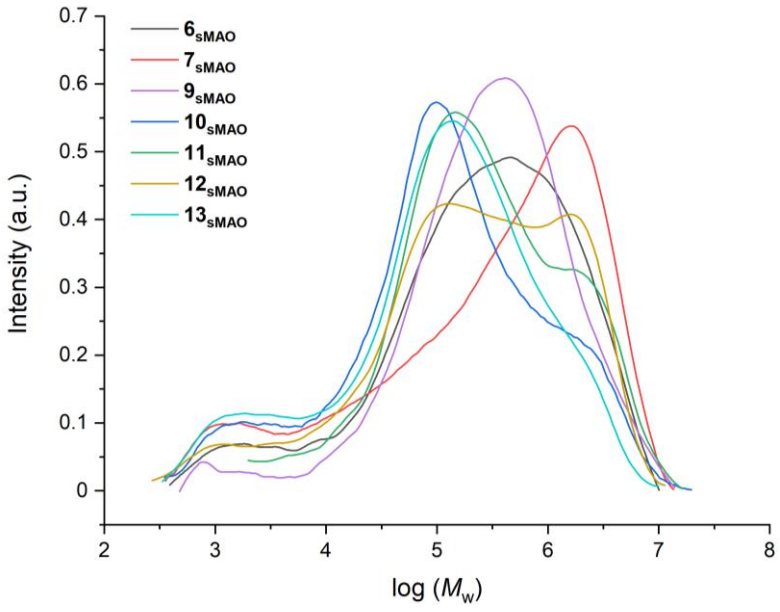

Figure 6.16. Molecular weight distribution for polyethylene synthesised at 40 °C using Pn*ZrCl[RNC(R')NR]. Polymerisation conditions: 30 minutes, 1000 rpm, 2 bar ethylene, 50 mL hexane, 10 mg catalyst, $[Al_{sMAO}]_0$: $[Zr]_0$ = 200:1.

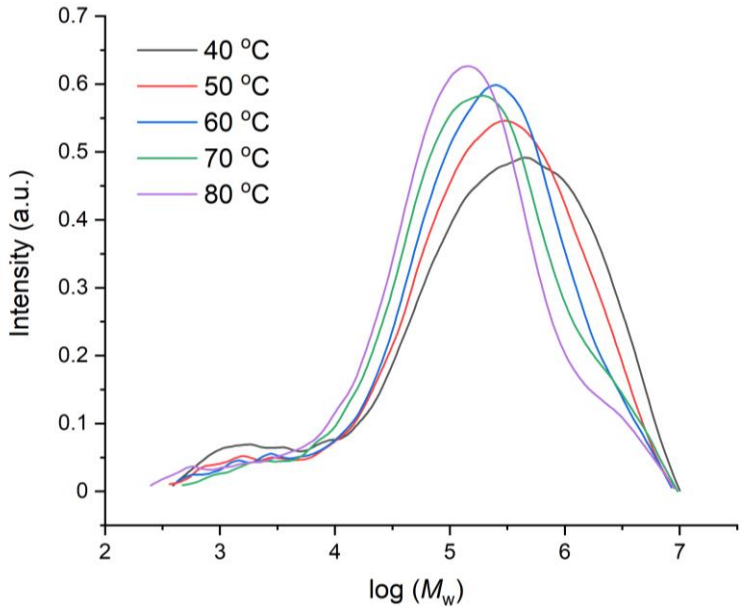

Figure 6.17. Molecular weight distribution for polyethylene synthesised using Pn*ZrCl[(N^{i}Pr)$_2$C(4-OMe-C$_6$H$_4$)] supported on sMAO (**6$_{sMAO}$**) across the range of temperature 40–80 °C. Polymerisation conditions: 30 minutes, 1000 rpm, 2 bar ethylene, 50 mL hexane, 10 mg catalyst, [Al$_{sMAO}$]$_0$: [Zr]$_0$ = 200:1.

Analysis of the polyethylenes by differential scanning calorimetry allowed for the characterisation of their thermal behaviour and crystallinity (Table 6.2). The melting peak temperatures were slightly lower than those previously reported by O'Hare *et al.* for polyethylene produced by Pn* zirconium complexes supported on sMAO (138.8 °C for Pn*ZrCpCl).[26,27] For complex **6$_{sMAO}$**, the melting temperature slightly increased with the polymerisation temperature as shown in Figure 6.18. (T_m = 132.6 °C at 40 °C and 133.9 °C at 80 °C). The values were consistent with high molecular weight and high density polyethylene (Table 6.2). The crystallinity values (χ_c), calculated using the area underneath the melting endotherm, were very similar for all polymerisation temperatures between 43–49%. Varying the polymerisation catalyst allowed for tuning of the melting temperature of the polymer produced (Figure 6.19). Complex **9$_{sMAO}$** differentiated itself from other formamidinate derivatives by a higher T_m of 136.0 °C while polyethylene afforded by **12$_{sMAO}$** displays a T_m at 131.1 °C. The bis(formamidinate) **13$_{sMAO}$** exhibited two melting peaks (128.3 and 133.6 °C). This implied that linear low density

polyethylene (LLDPE) was produced along HDPE. $^{13}C\{^{1}H\}$ NMR spectroscopy in 1,1,2,2-tetrachloroethane-d_2 revealed only one resonance around 30 ppm but the solubility of the polymers at 130 °C made it difficult to characterise them by NMR spectroscopy. Amidinate complexes Pn*ZrCl[(N^{i}Pr)$_2$C(4-R-C$_6$H$_4$)] influenced the T_m following the order: CF_3 > Ø >OMe> ^{t}Bu indicating that electron withdrawing groups lead to an increase of T_m and electron donating groups result in a decrease of T_m.

Table 6.2. Crystallinity of the polyethylenes produced by Pn*ZrCl[(NR′)$_2$CR].

Supported complex	T_p (°C)[a]	T_m (°C)	ΔH_m (mJ)	χ_c% [b]
Pn*ZrCl[(N^{i}Pr)$_2$C(4-OMe-C$_6$H$_4$)] (**6$_{sMAO}$**)	40	132.6	134.7	46
Pn*ZrCl[(N^{i}Pr)$_2$C(4-OMe-C$_6$H$_4$)] (**6$_{sMAO}$**)	50	133.4	124.8	43
Pn*ZrCl[(N^{i}Pr)$_2$C(4-OMe-C$_6$H$_4$)] (**6$_{sMAO}$**)	60	133.4	136.1	46
Pn*ZrCl[(N^{i}Pr)$_2$C(4-OMe-C$_6$H$_4$)] (**6$_{sMAO}$**)	70	134.1	141.7	48
Pn*ZrCl[(N^{i}Pr)$_2$C(4-OMe-C$_6$H$_4$)] (**6$_{sMAO}$**)	80	133.9	143.1	49
Pn*ZrCl[(N^{i}Pr)$_2$C(4-CF$_3$-C$_6$H$_4$)] (**7$_{sMAO}$**)	40	133.9	54.6	19
Pn*ZrCl[(N^{i}Pr)$_2$C(4-^{t}Bu-C$_6$H$_4$)] (**8$_{sMAO}$**)	40	131.5	51.2	13
Pn*ZrCl[(N^{i}Pr)$_2$C(C$_6$H$_5$)] (**10$_{sMAO}$**)	40	133.2	70.0	17
Pn*Zr(OXyl)[(N^{i}Pr)$_2$C(C$_6$H$_5$)] (**11$_{sMAO}$**)	40	135.1	70.3	24
Pn*ZrCl[(NMes)$_2$CH] (**9$_{sMAO}$**)	40	136.0	38.6	20
Pn*ZrCl[(N^{p}Tol)$_2$CH] (**12$_{sMAO}$**)	40	131.1	57.2	24
Pn*Zr[(N^{p}Tol)$_2$CH]$_2$(**13$_{sMAO}$**)	40	128.3/133.6	47.0	16

a. Polymerisation temperature, *b.* calculated using 293 J/g as reference.

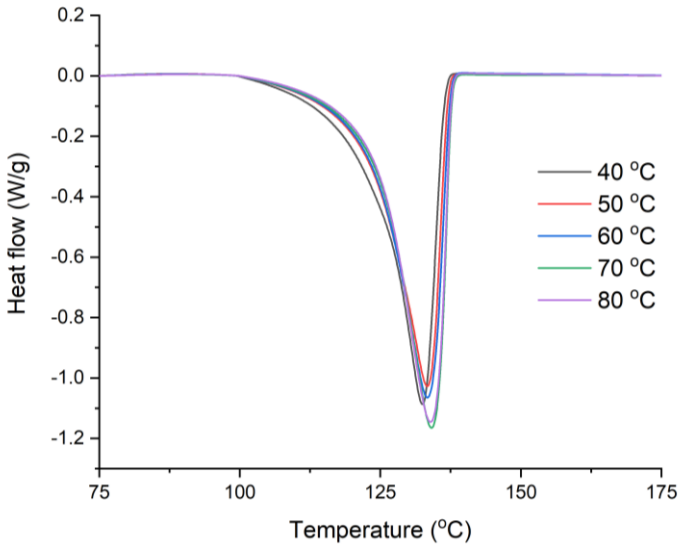

Figure 6.18. DSC heating plot of polyethylene produced by Pn*ZrCl[($N^{i}Pr$)$_2$C(4-OMe-C_6H_4)] supported on sMAO (**6_{sMAO}**) between 40 and 80 °C. Polymerisation conditions: 30 minutes, 1000 rpm, 2 bar ethylene, 50 mL hexane, 10 mg catalyst, $[Al_{sMAO}]_0$: $[Zr]_0$ = 200:1.

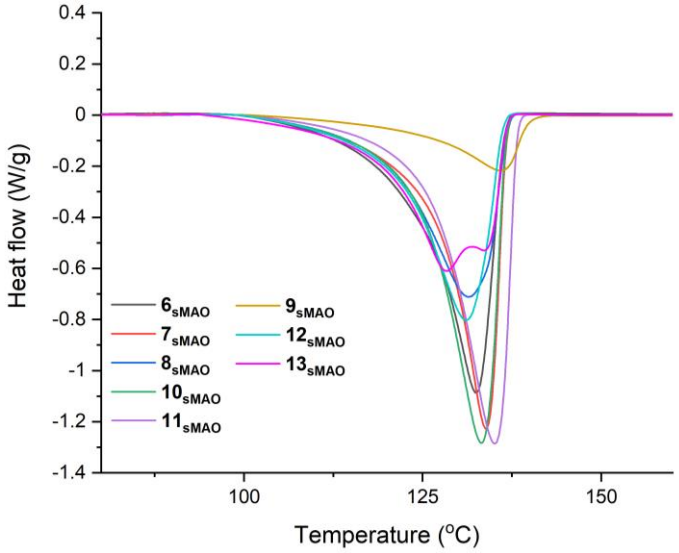

Figure 6.19. DSC heating plot of polyethylenes produced by Pn*ZrCl[RNC(R')NR] at 40 °C.

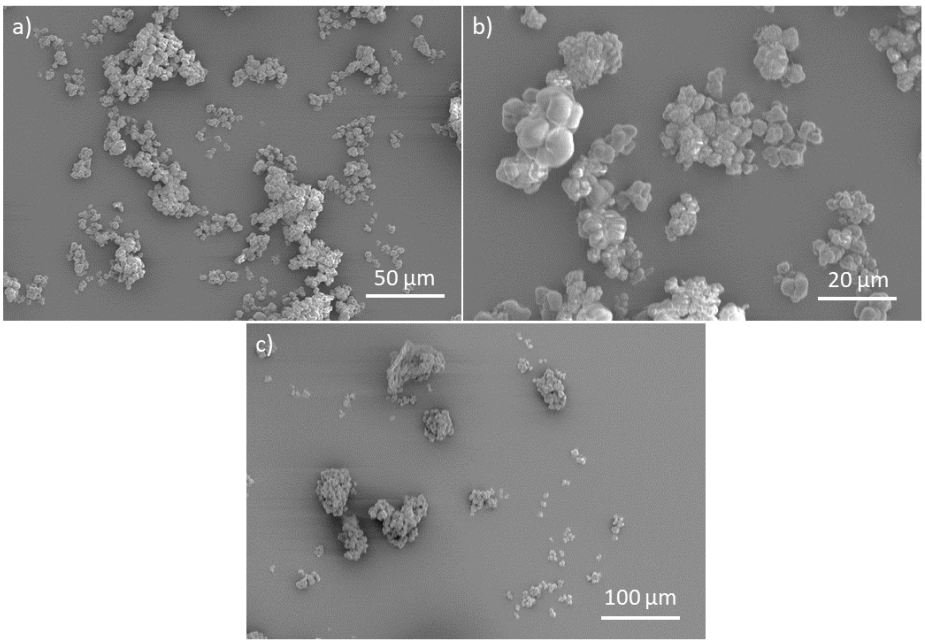

Figure 6.20. SEM images of polyethylenes produced by a) Pn*ZrCl[(N^{i}Pr)$_2$C(4-OMe-C$_6$H$_4$)] (**6$_{sMAO}$**) (x270), b) Pn*ZrCl[(N^{i}Pr)$_2$C(4-CF$_3$-C$_6$H$_4$)] (**7$_{sMAO}$**) (x850) and c) Pn*ZrCl[(NMes)$_2$CH] (**9$_{sMAO}$**) (x500). Polymerisation conditions: 30 minutes, 1000 rpm, 2 bar ethylene, 50 mL hexane, 10 mg catalyst, [Al$_{sMAO}$]$_0$: [Zr]$_0$ = 200:1.

As expected, scanning electron microscopy (SEM) images of the polymers showed "popcorn" morphology which is characteristic of sMAO-supported ethylene polymerisations.[63] Replication of the solid-support morphology explains this typical aspect. The particles possessed similar diameter for all complexes used around 5 µm (Figure 6.20).

6.4. Copolymerisations of ethylene with α-olefins

Amidinate catalysts for olefin homopolymerisation have been widely investigated, however few examples of olefin copolymerisations were reported.[64] Efficient copolymerisation of ethylene, propylene and dienes for forming EP and EPDM were described with mono and bimetallic κ^1-amidinate catalysts by Mountford *et al.*.[21,22,65,66] Examples of κ^2-amidinate complexes for copolymerisations are, however, rare and limited to polar monomers.[67]

6.4.1 Ethylene/styrene copolymerisations

The same eight solid supported catalysts have been tested for the slurry-phase copolymerisations of ethylene with styrene under the same conditions of section 6.3.2. For five catalysts, while the pressure of ethylene was kept constant at 2 bars, the molar ratio of styrene to catalyst was varied at 779, 1558, 3117 and 6234 with addition of 62.5, 125, 250 and 500 µL of styrene respectively. Similarly to Chapter 2, two crops were produced: the first crop precipitated in the reaction vessel while the second crop was obtained after drying the reaction mixture. Characterisation of the second crop revealed a low percentage of polymer thus only the materials precipitated and filtered was used for the following discussion.

Copolymerisation activities were first measured at 40 °C using a fixed volume of 125 µL of styrene (Figure 6.21). The three formamidinate complexes **9$_{sMAO}$**, **12$_{sMAO}$** and **13$_{sMAO}$** exhibited lower activities than the amidinates Pn*ZrCl[(N^{i}Pr)$_2$C(4-R-C$_6$H$_4$)] (R = OMe, CF$_3$, ^{t}Bu, H).

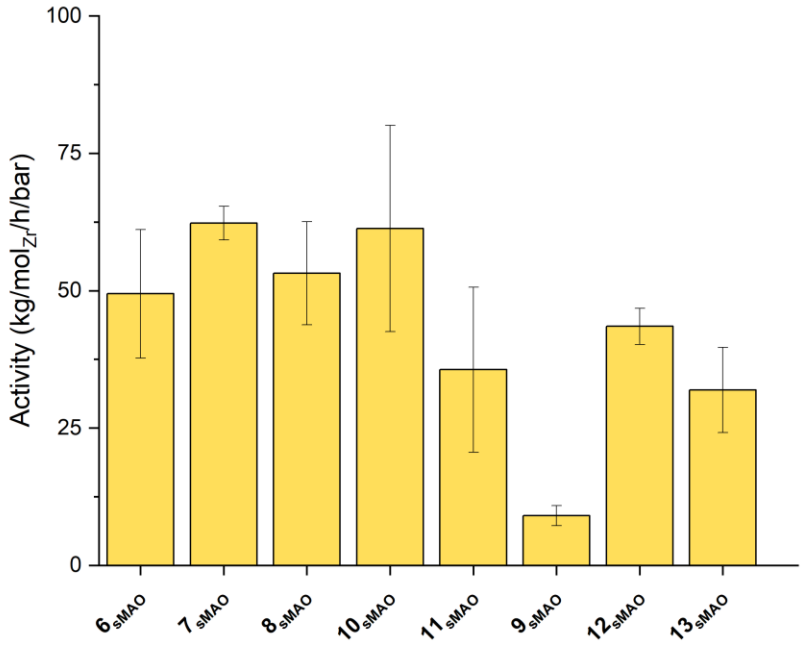

Figure 6.21. Ethylene/styrene copolymerisation activities for Pn*ZrCl[RNC(R')NR] at 40 °C using 125 µL of styrene. Polymerisation conditions: 30 minutes, 1000 rpm, 2 bar ethylene, 50 mL hexane, 10 mg catalyst, $[Al_{sMAO}]_0$: $[Zr]_0$ = 200:1, 150 mg TiBA.

The amidinate complexes **6$_{sMAO}$**, **7$_{sMAO}$** and **8$_{sMAO}$** can be ordered in terms of activity as following: CF_3 > ^{t}Bu > OMe suggesting that substituents with increasing electron donation lead to lower activity. Similarly to copolymerisation attempts in previous chapters, the presence of the two monomers in the system might lead to interactions decreasing the performance. As expected, replacing the chloride ligand by either an aryloxide or a formamidinate ligand resulted in a decrease in activity. The mesityl compounds **9$_{sMAO}$** exhibited the lowest activity at 9 kg$_{polymer}$/mol$_{Ti}$/h/bar. Systems with amidinate ligands have previously shown poor copolymerisation performance as described by Klosin *et al.* for the copolymerisation of ethylene with 1-octene. They observed a decrease from 55500 to 588 kg$_{polymer}$/mol$_{Zr}$ after substituting one methyl group by [N(^{i}Pr)$_2$CMe] in their zirconium trimethyl guanidinate catalysts.[68]

Significant reductions in activity were observed after addition of styrene compared to ethylene homopolymerisation; *e.g.* 97 and 53 kg$_{polymer}$/mol$_{Ti}$/h/bar for **6$_{sMAO}$** at 40 °C with

0 and 125 µL of styrene respectively. This indicates that the negative comonomer effect outweighs the positive effect. Indeed, as the insertion rate into the Zr-polymer bond is slower for styrene than for ethylene the rate of polymerisation might be negatively impacted by the introduction of the comonomer in the system.[69,70] Okuda and co-workers calculated an ethylene/styrene copolymerisation parameter ratio (r_E/r_S), comparing the rate of insertion of the monomers into the a growing polymer chain, and obtained r_E/r_S = 38.7 for a linked bis(phenolato)titanium catalyst using the Fineman-Ross equation.[71] They calculated the same r_E/r_S ratios for other catalysts including constrained geometry complexes $Me_2Si(Cp^{Me_4})(N\text{-}^tBu)TiCl_2$ and $Ti(tbmp)(O^iPr)_2$ (tbmp = 2,2'-thiobis(6-tert-butyl-4-methylphenolato)).[72,73] All catalysts show a polymerisation rate for the insertion of ethylene much higher than those for the insertion of styrene. The same phenomenon might explain that the addition of styrene resulted in a negative comonomer effect for the Pn* amidinate complexes. The rate of styrene insertion was very slow due to the high insertion barrier of styrene into a secondary alkyl Zr-CHPh-polymer and steric hindrance for the insertion into Zr-CH_2-CHPh-Polymer.

The influence of the amount of styrene used in the polymerisation system was then investigated (Figure 6.22). Fouling was observed for **9_{sMAO}** under all conditions, making it difficult to weight the exact amount of polymer produced. The evolution of activities with volumes of styrene was similar for all the supported catalysts used. All catalysts showed a decline in activity with the addition of styrene followed by an increase when 250 µL of styrene are added, except **6_{sMAO}** which exhibited an increase for 500 µL of co-monomer. O'Hare *et al.* have previously reported similar results using constrained geometry complexes supported on solid MAO.[70]

Using a fixed volume of 125 µL of styrene, the polymerisation temperature has been varied between 40 and 80 °C to determine the effect of temperature on the polymerisation

activities and the polymer properties (Figure 6.23). All the supported zirconium complexes tested behave differently with temperature variation. The copolymerisation activities of **6$_{sMAO}$** remained constant between 47 and 61 $kg_{polymer}/mol_{Zr}/h/bar$ across the range of temperatures. The fluorinated-analogue **7$_{sMAO}$** also showed little to no variation with temperature except an increase from 55 to 71 $kg_{polymer}/mol_{Zr}/h/bar$ at 60 °C. A very different behaviour was observed by complex **8$_{sMAO}$**. The two formamidinate complexes reacted differently to ethylene/styrene copolymerisations. While the *para*-tolyl complex **12$_{sMAO}$** showed the highest activities at 50 and 80 °C (106 $kg_{polymer}/mol_{Zr}/h/bar$ for both temperatures), the mesityl compound **9$_{sMAO}$** possessed very low activities between 9 $kg_{polymer}/mol_{Zr}/h/bar$ at 40 °C and 33 $kg_{polymer}/mol_{Zr}/h/bar$ at 70 °C.

Unsurprisingly, at a constant volume of styrene comonomer, molecular weights were decreasing with the increasing polymerisation temperature (Figure 6.24, Table 6.3.). At 40 °C, **7$_{sMAO}$** afforded the highest values followed by the unsubstituted complex **10$_{sMAO}$**, the formamidinate **12$_{sMAO}$** and the mesityl analogue **9$_{sMAO}$** (1265, 1216, 845 and 714 kg/mol). The large size of the latter probably hindered chain growth and comonomer insertion, resulting in M_w up to 5 times lower than **7$_{sMAO}$** at 80 °C (162 and 829 kg/mol respectively). The dispersities measured were broad but they were shown to decrease at high temperatures (Figure 6.25).

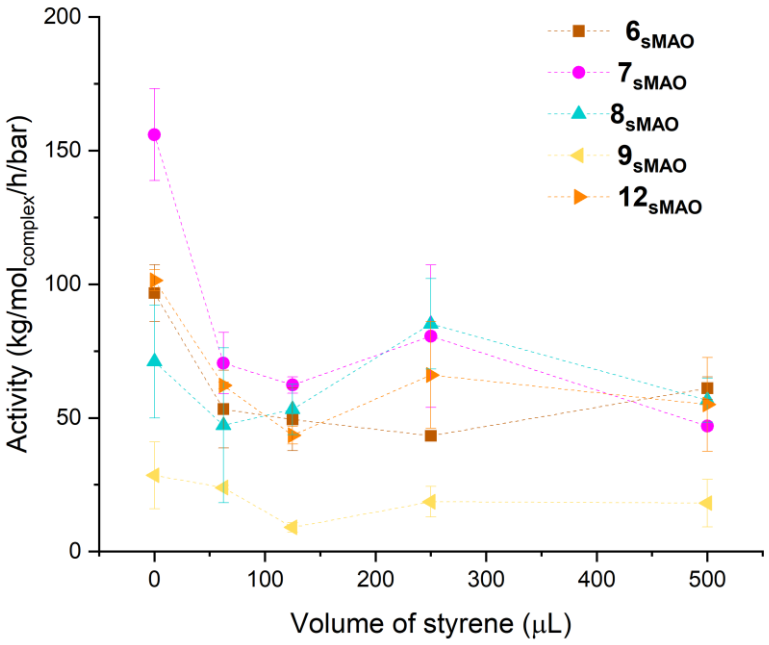

Figure 6.22. Copolymerisation activities of supported Pn*ZrCl[RNC(R')NR] at 40 °C. Polymerisation conditions: 30 minutes, 1000 rpm, 2 bar ethylene, 50 mL hexane, 10 mg catalyst, $[Al_{sMAO}]_0$: $[Zr]_0$ = 200:1, 150 mg TiBA.

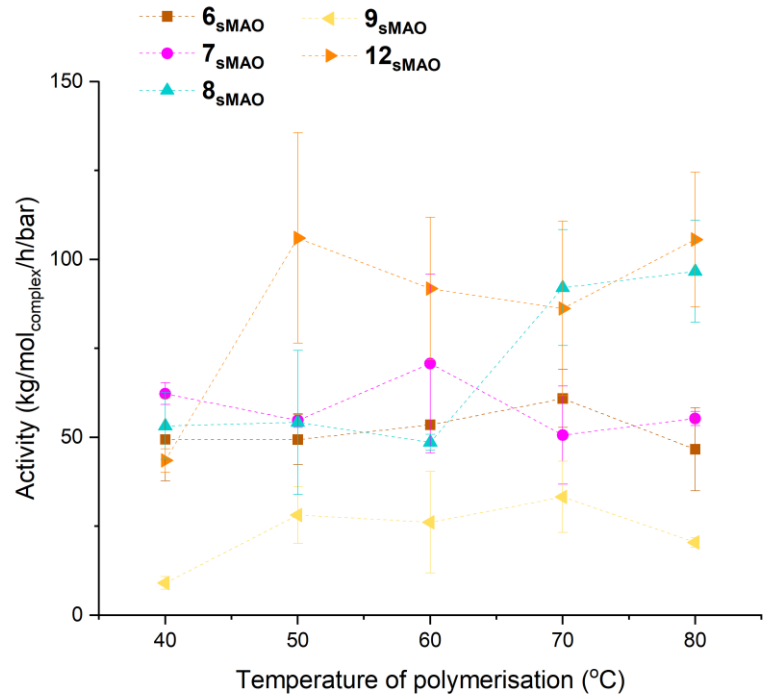

Figure 6.23. Temperature dependence of copolymerisation activities of supported Pn*ZrCl[RNC(R')NR] using 125µL of styrene. Polymerisation conditions: 30 minutes, 1000 rpm, 2 bar ethylene, 50 mL hexane, 10 mg catalyst, $[Al_{sMAO}]_0$: $[Zr]_0$ = 200:1, 150 mg TiBA.

Addition of 500 µL of comonomer resulted in a decrease in polymer molecular weight compared to homopolymerisation of ethylene (1185 *vs.* 953 kg/mol at 40 °C for **7**$_{\mathbf{sMAO}}$) as previously observed by O'Hare and co-workers (Table 6.3).[70,74] The formamidinate complex **12**$_{\mathbf{sMAO}}$ produced polymer with decreasing dispersities upon increasing addition of styrene. The reason for the narrower distribution is unclear, but this decline suggests a better degree of control in the copolymerisation compared to homopolymerisation of ethylene.

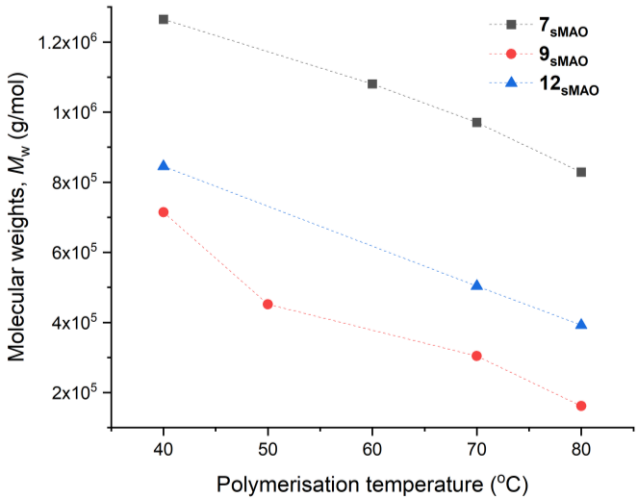

Figure 6.24. Temperature influence on molecular weights (M_w) of polymers produced by Pn*ZrCl[(N^{i}Pr)$_2$C(4-CF$_3$-C$_6$H$_4$)] (**7**$_{\mathbf{sMAO}}$), Pn*ZrCl[(NMes)$_2$CH] (**9**$_{\mathbf{sMAO}}$) and Pn*ZrCl[(N^{p}Tol)$_2$CH] (**12**$_{\mathbf{sMAO}}$). Polymerisation conditions: 125 µL of styrene, 40–80 °C, 30 minutes, 1000 rpm, 2 bar ethylene, 50 mL hexane, 10 mg catalyst, [Al$_{sMAO}$]$_0$: [Zr]$_0$ = 200:1, 150 mg TiBA.

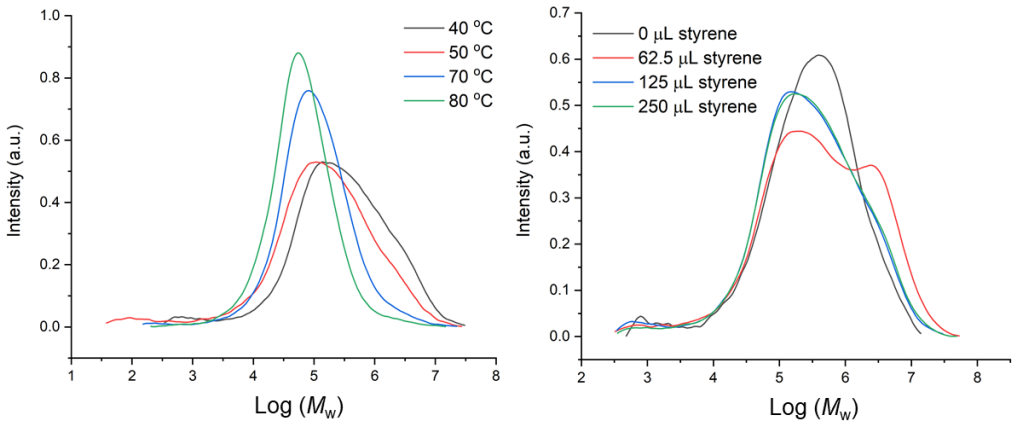

Figure 6.25. Influence of polymerisation temperature (left) and styrene volume (right) on the molecular weights distributions of polymers produced by Pn*ZrCl[(NMes)$_2$CH] (**9**$_{\mathbf{sMAO}}$). Polymerisation conditions: 30 minutes, 1000 rpm, 2 bar ethylene, 50 mL hexane, 10 mg catalyst, [Al$_{sMAO}$]$_0$:[Zr]$_0$ = 200:1, 125 µL styrene, 150 mg TiBA.

Table 6.3. Polymer molecular weights (M_w) and molecular weight distributions (Đ); 10 mg catalyst ($[Al]_0$: $[Zr]_0$ = 200:1), 2 bar ethylene, 62.5, 125, 250 and 500 µL styrene, 50 mL hexane, 150 mg TiBA, 40 °C, 30 minutes, 150 mg TiBA.

Volume of styrene (µL)	0		62.5		125		250		500	
Supported Complex	M_w[a]	Đ	M_w[a]	Đ	M_w[a]	Đ	M_w[a]	Đ	M_w[a]	Đ
Pn*ZrCl[(N^{i}Pr)$_2$C(4-CF$_3$-C$_6$H$_4$)] (**7$_{sMAO}$**)	1185	101	1028	107	1265	178	1170	102	953	125
Pn*ZrCl[(NMes)$_2$CH] (**9$_{sMAO}$**)	829	25	1216	64	714	47	796	18	-	-
Pn*ZrCl[(N^{i}Pr)$_2$C(C$_6$H$_5$)] (**10$_{sMAO}$**)	610	52	-	-	1216	26	-	-	-	-
Pn*ZrCl[(N^{p}Tol)$_2$CH] (**11$_{sMAO}$**)	813	63	985	30	845	19	891	17	701	17

[a] kg/mol

As observed in previous chapters, the DSC plots of the polymers only showed one melting peak between 132 and 136 °C (Figure 6.26., Table 6.4.). The melting temperatures were however different from those obtained for ethylene homopolymerisation. The introduction of the second monomer in the system resulted in an increase in all T_m by 1 to 4 °C. Addition of 250 µL of styrene allowed an increase of almost 2 °C for polymers produced by **6$_{sMAO}$** at 40 °C. Previous work by O'Hare and co-workers highlighted a decline in melting temperature with incorporation of styrene (from 138 to 119 °C at 0 and 156 µL styrene respectively using sMAO-^{Me_2}SB(^{tBu}N,I*)TiCl$_2$).[70] Using zirconium diamine-bis(phenolate) complexes, Fryga et al. observed melting temperatures as low as 111 °C for ethylene/styrene copolymers produced in the presence of MMAO.[75] Likewise, a drop in melting temperature by 13 °C (from 138 °C to 125 °C) was reported for copolymers generated using scandium complexes.[76] The melting temperatures observed using the amidinate compounds suggest that no styrene was incorporated during the reactions and only polyethylene is produced. Noteworthy is the lower melting enthalpy of the polymer synthesised using the bis-formamidinate **13$_{sMAO}$** which indicates that the catalyst produces a less crystalline material compared to the other Pn* amidinate compounds.[77]

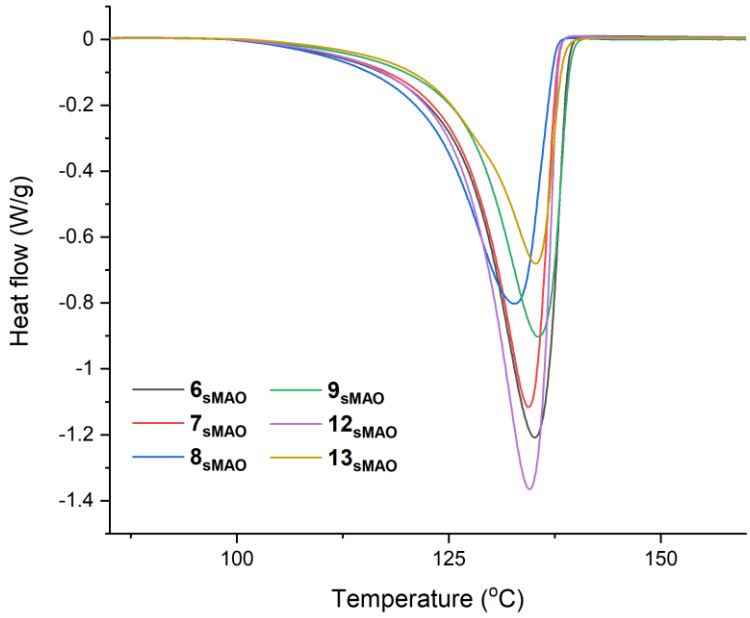

Figure 6.26. DSC plots for polymers produced by supported Pn*ZrCl[RNC(R')NR] using 125µL of styrene at 40 °C.

Table 6.4. Polymer melt temperatures (T_m) and enthalpy ΔH_m for supported Pn*ZrCl[RNC(R')NR]; 10 mg catalyst ($[Al]_0$:$[Zr]_0$ = 200:1), 2 bar ethylene, 125 µL of styrene, 50 mL hexanes, 150 mg TiBA, 40 °C and 30 minutes, 150 mg TiBA.

Supported complex	T_m (°C)	ΔH_m (J/g)
Pn*ZrCl[(N^{i}Pr)$_2$C(4-OMe-C$_6$H$_4$)] (**6$_{sMAO}$**)	135.1	142.8
Pn*ZrCl[(N^{i}Pr)$_2$C(4-CF$_3$-C$_6$H$_4$)] (**7$_{sMAO}$**)	134.4	115.8
Pn*ZrCl[(N^{i}Pr)$_2$C(4-^{t}Bu-C$_6$H$_4$)] (**8$_{sMAO}$**)	132.8	108.3
Pn*ZrCl[(NMes)$_2$CH] (**9$_{sMAO}$**)	135.5	101.1
Pn*ZrCl[(N^{p}Tol)$_2$CH] (**12$_{sMAO}$**)	134.5	134.3
Pn*Zr[(N^{p}Tol)$_2$CH]$_2$(**13$_{sMAO}$**)	135.2	69.4

Further measurements reveal that the temperature of polymerisation did not affect the thermal properties of the polymers produced by **6$_{sMAO}$** (Table 6.5). The melting temperature was also independent of the amount of styrene present in the reaction vessel. Addition of an increasing amount of comonomer resulted in an increase in melting enthalpy from 99.9 J/g to 146.1 J/g for 0 and 250 µL of styrene respectively. This effect

translated into an increase in polymer crystallinity from 34% in the absence of styrene to 36%, 49% and 50% with 62.5, 125 and 250 μL.

Table 6.5. Polymer melt temperatures (T_m) and enthalpy ΔH_m for supported Pn*ZrCl[$(N^iPr)_2C$(4-OMe-C_6H_4)] (**6_{sMAO}**); 10 mg catalyst ($[Al]_0$:$[Zr]_0$ = 200:1), 2 bar ethylene, 50 mL hexanes, 150 mg TiBA, and 30 minutes, 150 mg TiBA.

Polymerisation temperature (°C)	Styrene volume (μL)	T_m (°C)	ΔH_m (J/g)	χ_c%
40	125	135.1	142.8	49
50	125	133.7	126.3	43
60	125	135.2	172.3	59
70	125	135.1	146.7	50
80	125	135.1	147.0	50
40	0	132.5	99.9	34
40	62.5	132.5	106.8	36
40	250	135.4	146.1	50
40	500	135.2	115.8	40

6.4.2 Ethylene/4-NH_2-styrene copolymerisations

Ethylene/4-NH_2-styrene copolymerisation studies were carried out for 30 minutes in a 150 mL ampoule with a sidearm. 125 µL of 4-NH_2-styrene ($mol_{4\text{-}NH_2\text{-}styrene}/mol_{Zr}$ = 1524) in 5 mL of toluene that was added at the start of the polymerisation. Other polymerisation conditions were identical to 6.3.3 and the reactions were performed at 40 °C. In the same manner as Chapter 3, the reaction mixture was dried *in vacuo* leading to a fine powder.

Characterisation of the powders obtained proved to be difficult. GPC could not be performed as they were insoluble in trichlorobenzene at high temperature after several days. DSC measurements showed no signal between 25-280 °C. ^{1}H NMR characterisation of the material produced confirmed that no copolymerisation occurred (Figure A6.51). The absence of GPC and DSC signals suggested that ethylene was not or only minimally polymerised. The material produced was characterised by IR (Figure 6.27). Styrene signals can be observed at 1500 cm^{-1} (C-C stretches in the aromatic ring). The large signal between 3400 and 2700 cm^{-1} includes the C-H aromatic stretches above 3000 cm^{-1}, as well as the N-H stretches (3440-3360 cm^{-1}). Compared to observations from Chapter 3, the absence of polymerisation reaction can be explained by poisoning of the catalyst by the 4-NH_2-styrene monomer. The Lewis acidic catalysts are deactivated by the Lewis basic NH_2 functional groups of the comonomer.[78–80]

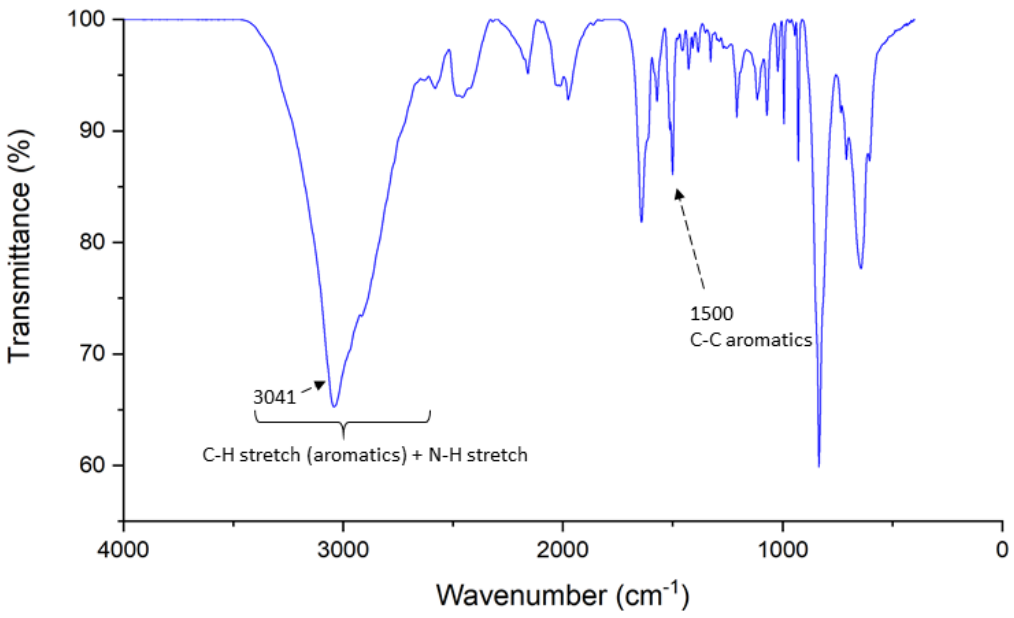

Figure 6.27. Infrared spectrum of the material produced by the attempted copolymerisation of ethylene/4-NH_2-styrene by Pn*ZrCl[(N^iPr)$_2$C(4-^{t}Bu-C_6H_4)] (**8$_{sMAO}$**) at 40 °C.

6.5. Conclusion

Eight new permethylpentalene zirconium amidinate complexes have been studied as olefin polymerisation catalysts. These catalysts were immobilised on solid MAO and used for the homopolymerisation of styrene and ethylene as well as ethylene/styrene copolymerisations.

The catalysts were able to produce polystyrene in good activities with the *tert*-butyl **8$_{sMAO}$** showing a high polymerisation activity of 4061 kg_{PS}/mol/h at 55 °C. The polystyrene produced was characterised by a range of different techniques: GPC, SEM, DSC, NMR spectroscopy confirming the atactic nature of the polymers.

The immobilised complexes were also investigated for the homopolymerisation of ethylene in slurry-phase. Amidinates derivatives performed better than the formamidinate catalysts, even though all activities reported were low compared with other η^8-Pn* catalysts.[26] The activities were shown to slightly increase with polymerisation temperature, **10$_{sMAO}$** giving the highest at 80 °C (175 kg_{PE}/mol_{Zr}/bar/h) which is 10 times better than what Yap and co-workers reported for solution phase polymerisations.[81] Previously reported Pn*ZrCpCl gave activities two orders of magnitude higher for slurry-phase homopolymerisation of ethylene. Although the Pn* amidinates compounds possess the same number of electrons, the amidinate ligands behave differently from a Cp ring and achieve significantly lower activities.

Selected catalysts were tested as potential catalysts for ethylene copolymerisation with styrene and 4-NH_2-styrene. With the unsubstituted comonomer, no incorporation was observed using different volumes of styrene and across a range of temperatures conversely to what O'Hare *et al.* previously described for group 4 constrained geometry

permethylindenyl complexes.[70] The copolymerisation attempts using 4-NH_2-stryrene resulting in no reaction due to poisoning of the catalyst by the polar monomer.[78–80]

6.6. References

1 F. T. Edelmann, *Adv. Organomet. Chem.*, 2008, **57**, 183–352.

2 F. T. Edelmann, *Struct. Bond.*, 2010, **137**, 109–163.

3 M. Allen, H. C. Aspinall, S. R. Moore, M. B. Hursthouse and A. I. Karvalov, *Polyhedron*, 1992, **11**, 409–413.

4 H. C. Aspinall, S. R. Moore and A. K. Smith, *Dalton Trans.*, 1992, 153–156.

5 H. C. Aspinall, D. C. Bradley, M. B. Hursthouse, K. D. Sales, N. P. C. Walker and B. Hussain, *Dalton Trans.*, 1989, 623–626.

6 C. J. Schaverien, J. H. G. Frijns, H. J. Heeres, J. R. van den Hende, J. H. Teuben and A. L. Spek, *Chem. Commun.*, 1991, 642–644.

7 D. Liguori, F. Grisi, I. Sessa and A. Zambelli, *Macromol. Chem. Phys.*, 2003, **204**, 164–170.

8 Claudia Averbuj, A. Edith Tish, M. S. Eisen, C. Averbuj, E. Tish and M. S. Eisen, *J. Am. Chem. Soc.*, 1998, **120**, 8640–8646.

9 D. Herskovics-Korine and M. S. Eisen, *J. Organomet. Chem.*, 1995, **503**, 307–314.

10 D. Liguori, R. Centore, A. Tuzi, F. Grisi, A. Irene Sessa and A. Zambelli, *Macromolecules*, 2003, **36**, 5451–5458.

11 J. C. Flores, J. C. W. Chien and M. D. Rausch, *Organometallics*, 1995, **14**, 2106–2108.

12 J. C. Flores, J. C. W. Chien and M. D. Rausch, *Organometallics*, 1995, **14**, 1827–1833.

13 V. Volkis, E. Nelkenbaum, A. Lisovskii, G. Hasson, R. Semiat, M. Kapon, M. Botoshansky, Y. E. And and M. S. Eisen, *J. Am. Chem. Soc.*, 2003, **125**, 2179–2194.

14 J. Richter, F. T. Edelmann, M. Noltemeyer, H.-G. Schmidt, M. Shmulinson and M. S. Eisen, *J. Mol. Catal. A Chem.*, 1998, **130**, 149–162.

15 N. V. Kulkarni, T. Elkin, B. Tumaniskii, M. Botoshansky, L. J. W. Shimon and M. S. Eisen, *Organometallics*, 2014, **33**, 3119–3136.

16 R. T. Cooper, F. M. Chadwick, A. E. Ashley and D. O'Hare, *Organometallics*, 2013, **32**, 2228–2233.

17 T. Elkin, N. V. Kulkarni, B. Tumanskii, M. Botoshansky, L. J. W. Shimon and M.

S. Eisen, *Organometallics*, 2013, **32**, 6337–6352.

18 Y. Zhang and L. R. Sita, *Chem. Commun.*, 2003, **3**, 2358–2359.

19 T. Elkin and M. S. Eisen, *Catal. Sci. Technol.*, 2015, **5**, 82–95.

20 H. Tsurugi, K. Yamamoto, R. Rochat and K. Mashima, *Polym. J.*, 2015, 47, 2–17.

21 Richard T W Scott, University of Oxford, DPhil Thesis, 2016.

22 R. A. Collins, A. F. Russell, R. T. W. Scott, R. Bernardo, G. H. J. Van Doremaele, A. Berthoud and P. Mountford, *Organometallics*, 2017, **36**, 2167–2181.

23 S. Bambirra, E. Otten, D. van Leusen, A. Meetsma and B. Hessen, *Zeitschrift für Anorg. und Allg. Chemie*, 2006, **632**, 1950–1952.

24 G. A. Chesnokov, M. A. Topchiy, P. B. Dzhevakov, P. S. Gribanov, A. A. Tukov, V. N. Khrustalev, A. F. Asachenko and M. S. Nechaev, *Dalton Trans.*, 2017, **46**, 4331–4345.

25 T. M. Cameron, C. Xu, A. G. Dipasquale and A. L. Rheingold, *Organometallics*, 2008, **27**, 1596–1604.

26 D. A. X. Fraser, Z. R. Turner, J.-C. Buffet and D. O'Hare, *Organometallics*, 2016, **35**, 2664–2674.

27 D. A. Fraser, University of Oxford, DPhil Thesis, 2018.

28 W. Li, F. Su, S. Yuan, X. Duan, S. Bai and D. Liu, *RSC Adv.*, 2016, **6**, 40741–40749.

29 T. Elkin, S. Aharonovich, M. Botoshansky and M. S. Eisen, *Organometallics*, 2012, **31**, 7404–7414.

30 C. Hansch, A. Leo and R. W. Taft, *Chem. Rev.*, 1991, **91**, 165–195.

31 W. Skupi?ski and K. Nici?ski, *Appl. Organomet. Chem.*, 2001, **15**, 635–638.

32 H. Ma, Y. Zhang, B. Chen, J. Huang and Y. Qian, *J. Polym. Sci. Part A Polym. Chem.*, 2001, **39**, 1817–1824.

33 J. Liu, H. Ma, J. Huang and Y. Qian, *Eur. Polym. J.*, 2000, **36**, 2055–2058.

34 C. M. R. Wright, Z. R. Turner, J. C. Buffet and D. O'Hare, *Chem. Commun.*, 2016, **52**, 2850–2853.

35 J. V. Lamb, University of Oxford, DPhil Thesis, 2019.

36 P. Longo, A. Proto and L. Oliva, *Macromol. Rapid Commun.*, 1994, **15**, 151–154.

37 N. Nakata, T. Toda, Y. Saito, T. Watanabe, A. Ishii, N. Nakata, T. Toda, Y. Saito,

T. Watanabe and A. Ishii, *Polymers*, 2016, **8**, 31.

38 J. Yi, N. Nakatani, N. Tomotsu, K. Nomura and M. Hada, *Organometallics*, 2021, **40**, 643–653.

39 K. Nomura, I. Izawa, J. Yi, N. Nakatani, H. Aoki, H. Harakawa, T. Ina, T. Mitsudome, N. Tomotsu and S. Yamazoe, *Organometallics*, 2019, **38**, 4497–4507.

40 D. Liguori, R. Centore, A. Tuzi, F. Grisi, I. Sessa and A. Zambelli, *Macromolecules*, 2003, **36**, 5451–5458.

41 S. Rahmani and A. A. Entezami, *J. Mol. Catal. A Chem.*, 2010, **320**, 27–33.

42 S. Rahmani, R. Mohammadi and A. A. Entezami, *Macromol. Symp.*, 2008, **274**, 43–48.

43 A. Entezami, M. Agaalipour and P. N. Moghaddam, *J. Iran. Chem. Soc.*, 2005, **2**, 149–154.

44 J. C. Buffet, Z. R. Turner and D. O'Hare, *Chem. Commun.*, 2018, **54**, 10970–10973.

45 J. V. Lamb, J. C. Abell, J. E. McLaren, J. C. Buffet, Z. R. Turner and D. O'Hare, *Mol. Catal.*, 2019, **484**, 110735.

46 T. J. Williams, J. C. Buffet, Z. R. Turner and D. O'Hare, *Catal. Sci. Technol.*, 2018, **8**, 5454–5461.

47 M. A. Bashir, V. Monteil, C. Boisson and T. F. L. McKenna, *React. Chem. Eng.*, 2017, **2**, 521–530.

48 H. N. Cheng and G. H. Lee, *Int. J. Polym. Anal. Charact.*, 1996, **2**, 439–455.

49 H. Sato, Y. Tanaka and K. Hatada, *J. Polym. Sci. Polym. Phys. Ed.*, 1983, **21**, 1667–1674.

50 J. C. Randall, *J. Polym. Sci. Polym. Phys. Ed.*, 1975, **13**, 889–899.

51 T. Kawamura, N. Toshima and K. Matsuzaki, *Macromol. Rapid Commun.*, 1994, **15**, 479–486.

52 N. Brun, P. Bourson, S. Margueron and M. Duc, *AIP Conf. Proc.*, 2011, **1353**, 856–861.

53 J. Schellenberg, *Syndiotactic polystyrene : synthesis, characterization, processing, and applications*, Wiley, 2010.

54 N. Tomotsu, N. Ishihara, T. H. Newman and M. T. Malanga, *J. Mol. Catal. A Chem.*, 1998, **128**, 167–190.

55 C. Janiak, K. C. H. Lange and T. G. Scharmann, *Appl. Organomet. Chem.*, 2000, **14**, 316–324.

56 W. Skupiński and A. Wasilewski, *J. Organomet. Chem.*, 1985, **282**, 69–74.

57 D. Walther, R. Fischer, H. Görls, J. Koch and B. Schweder, *J. Organomet. Chem.*, 1996, **508**, 13–22.

58 P. B. Hitchcock, M. F. Lappert and P. G. Merle, *Dalton Trans.*, 2007, 585–594.

59 M. Zhou, H. Tong, X. Wei and D. Liu, *J. Organomet. Chem.*, 2007, **692**, 5195–5202.

60 F. M. Chadwick, R. T. Cooper, A. E. Ashley, J.-C. Buffet and D. M. O'Hare, *Organometallics*, 2014, **33**, 3775–3785.

61 L. D'Agnillo, J. B. P. Soares and A. Penlidis, *Macromol. Chem. Phys.*, 1998, **199**, 955–962.

62 M. Eskelinen and J. V. Seppälä, *Eur. Polym. J.*, 1996, **32**, 331–335.

63 A. F. R. R. Kilpatrick, J.-C. C. Buffet, P. Nørby, N. H. Rees, N. P. Funnell, S. Sripothongnak, D. O'Hare and D. O'Hare, *Chem. Mater.*, 2016, **28**, 7444–7450.

64 S. Collins, *Coord. Chem. Rev.*, 2011, 255, 118–138.

65 R. A. Collins, University of Oxford, 2016.

66 M. T. Scharbert, University of Oxford, 2018.

67 D. Osorio Meléndez, J. A. Castro-Osma, A. Lara-Sánchez, R. S. Rojas and A. Otero, *J. Polym. Sci. Part A Polym. Chem.*, 2017, **55**, 2397–2407.

68 J. Klosin, P. P. Fontaine, R. Figueroa, S. D. McCann and D. Mort, *Organometallics*, 2013, **32**, 6488–6499.

69 J. C. W. W. Chien and T. Nozaki, *J. Polym. Sci. Part A Polym. Chem.*, 1993, **31**, 227–237.

70 T. J. Williams, A. D. H. Smith, J. C. Buffet, Z. R. Turner and D. O'Hare, *Mol. Catal.*, 2020, **486**, 110872.

71 C. Capacchione, A. Proto, H. Ebeling, R. Mülhaupt and J. Okuda, *Polym. Chem.*, 2006, **44**, 1908–1913.

72 F. G. Sernetz, R. Mülhaupt, S. Fokken and J. Okuda, *Macromolecules*, 1997, **30**, 1562–1569.

73 F. G. Sernetz, R. Mülhaupt, F. Amor, T. Eberle and J. Okuda, *J. Polym. Sci. Part A Polym. Chem.*, 1997, **35**, 1571–1578.

74 T. J. Williams, J. V. Lamb, J. C. Buffet, T. Khamnaen and D. O'Hare, *RSC Adv.*, 2021, **11**, 5644–5650.

75 M. Białek and J. Fryga, *J. Appl. Polym. Sci.*, 2020, **137**, 49349.

76 B. Liu, L. Wang, C. Wu and D. Cui, *Polym. Chem.*, 2019, **10**, 235–243.

77 Y. Kong and J. N. Hay, *Eur. Polym. J.*, 2003, **39**, 1721–1727.

78 Y. Chai, C. Wu, D. Liu, M. Run and D. Cui, *Sci. China Chem.*, 2019, **62**, 761–766.

79 J. Chen, Y. Gao and T. J. Marks, *Angew. Chem. Int. Ed.*, 2020, **132**, 14834–14843.

80 L. Guo, W. Liu and C. Chen, *Mater. Chem. Front.*, 2017, 1, 2487–2494.

81 A. Littke, N. Sleiman, C. Bensimon, D. S. Richeson, G. P. A. Yap and S. J. Brown, *Organometallics*, 1998, **17**, 446–451.

Concluding Remarks and Perspectives

Conclusions

The results discussed in this thesis describes the synthesis of new group 4 permethylpentalene complexes and study of their catalytic activity for the polymerisation of ethylene and styrene. In addition, (hydro)permethylpentalene titanium initiators were investigated for the ring-opening polymerisation (ROP) of lactide monomers. Details of the key highlights and conclusions of the thesis are presented below.

1) New permethylpentalene titanium and zirconium complexes

Three new (hydro)permethylpentalene complexes Pn*(H)$TiCl_2$(OR) (R = 2,6-^{i}Pr-C_6H_3, 2,4-^{t}Bu-C_6H_3 and Si(Me)$_2$^{t}Bu) and four new permethylpentalene amidinate complexes Pn*ZrCl[$(NR)_2$CR'] (R = ^{i}Pr, 2,4,6-Me-C_6H_2; R' = 4-OMe-C_6H_4, 4-CF_3-C_6H_4, 4-^{t}Bu-C_6H_4, H) have been synthesised and characterised. The complexes have been immobilised on a solid support, sMAO, for use in slurry-phase olefin polymerisation catalysis.

2) Efficient olefin polymerisation catalysts

A study of styrene and ethylene polymerisation using Cp*$TiCl_3$, Pn*(H)$TiCl_3$, (hydro)permethylpentalene compounds Pn*(H)$TiCl_2$(OR) and amidinate complexes Pn*ZrCl[$(NR)_2$CR'] in both solution and slurry-phase. The supported sMAO-Pn*(H)$TiCl_3$ exhibited very high activities (up to 7432 $kg_{PS}/mol_{Ti}/h$) surpassing the analogous cyclopentadienyl complex. Characterisation of the polystyrene produced by the two trichloride compounds and their sMAO-immobilised analogues revealed the formation of atactic polystyrene. Cp*$TiCl_3$ and Pn*(H)$TiCl_3$, sMAO-Cp*$TiCl_3$ and

sMAO-Pn*(H)$TiCl_3$ were then used as ethylene homopolymerisation catalysts. It was found that the homogeneous reactions resulted in better activities than slurry-phase polymerisation. Homopolymerisation of *para*-functionalised styrene monomers was investigated, the results revealed that electron-donating substituents give higher activities. The polymerisation of 4-NH_2-styrene using Cp*$TiCl_3$ and Pn*(H)$TiCl_3$ resulted in very high activities (> 40000 $kg_{PS}/mol_{Ti}/h$). The two aryloxide compounds Pn*(H)$TiCl_2$(O-2,6-^{i}Pr-C_6H_3) and Pn*(H)$TiCl_2$(O-2,4-^{t}Bu-C_6H_3) displayed low styrene polymerisation activities in both solution and slurry-phase. In solution phase, the siloxide derivative, Pn*(H)$TiCl_2$(O-Si(Me)$_2$^{t}Bu) exhibited the highest activities of the series, performing better than the trichloride parent and reaching a maximum of 5790 $kg_{PS}/mol_{Ti}/h$. All three Pn*(H)$TiCl_2$OR catalysts exhibited low ethylene homopolymerisation activities. The amidinate catalysts Pn*ZrCl[(NR)$_2$CR'] were able to produce polystyrene with good performance with the *tert*-butyl derivative Pn*ZrCl[(N^{i}Pr)2C(4-^{t}Bu-C_6H_4)]showing a high polymerisation activity of 4061 kg_{PS}/mol/h at 55 °C. The immobilised complexes were also investigated for the homopolymerisation of ethylene in slurry-phase but low activities were observed.

Copolymerisation of ethylene with styrene were performed at various temperatures and with various amounts of styrene using the permethylpentalene complexes. The addition of increasing volumes of styrene caused a negative comonomer effect and little to no styrene incorporation was observed. Attempts to copolymerise ethylene with *para*-NH_2-styrene failed as the polar comonomer poisoned the catalyst.

3) Active initiators for the ROP of *L*-, *D*-, *meso*- and *rac*-lactide

Pn*(H)$TiCl_2$(O-2,6-^{i}Pr-C_6H_3) (**3**), Pn*(H)$TiCl_2$(O-2,4-^{t}Bu-C_6H_3) (**4**) and Pn*(H)$TiCl_2$(O-Si(CH_3)$_2$^{t}Bu) (5) were found to be active initiators for the ROP of *L*-, *D*-, *meso*- and *rac*-lactide. The complexes required an initiation period and displayed first-

order dependency on monomer concentration; k_{obs} = 0.087, 0.073, 0.15 and 0.088 h^{-1} for the ROP of *L*-, *D*-, *meso*- and *rac*-lactide using Pn*(H)$TiCl_2$(O-2,4-^{t}Bu-C_6H_3) (**4**). The latter exhibited the fastest polymerisation rates of the series but remained less active than tris(alkoxide)Pn* zirconium catalysts reported in the literature. ROP of *L*-lactide in the presence of benzyl alcohol co-initiator revealed faster polymerisation constants and better control on the molecular weight and molecular weight distribution.

Further kinetics studies indicated that polymerisation proceeded with an order of one in respect to catalyst concentration and followed the law:

$$\frac{-\mathrm{d[LA]}}{\mathrm{dt}} = k_p[\mathrm{LA}][\mathrm{Ti}]$$

Characterisation of the polymers revealed that the (hydro)permethylpentalene initiators produced isotactic PLA for the ROP of *L*- and *D*-lactide, syndiotactic PLA for the ROP of *meso*- and atactic PLA for the ROP of *rac*-lactide (P_r ~ 0.30 and 0.52 respectively).

Perspectives

The results described in this thesis open various research avenues. Many amidinate complexes were reported to be efficient at the ROP of lactide but group 4 amidinate initiators have not been widely investigated.[1–4] Preliminary research carried out showed that zirconium Pn* amidinate complexes were efficient catalysts for the ROP of lactide with high rate constants. Polymerisation catalysis is reorienting towards circular economy. Therefore, expanding the range of monomers by testing lactones and cyclic carbonates would benefit the field. Copolymerisations of CO_2 with epoxides or anhydride with epoxides could be performed.[5]

Producing high molecular weight functionalised polystyrene and copolymers with high degree of functionalised styrene incorporation would result in valuable materials with diverse applications.[6]

The formation of substituted polystyrene is closely linked to the area of post-polymerisation modifications. Indeed, the polymer can further react to form modified polymers with tuneable properties.[7–9] Different *para*-substituents such as –OH, -Cl or SO_2H could be investigated regarding homopolymerisation for various post-polymerisation modifications. Furthermore, preliminary studies were carried out where poly(4-NH_2-styrene) was reacted with benzoyl chloride and trimethylacetyl chloride to form amide bonds.

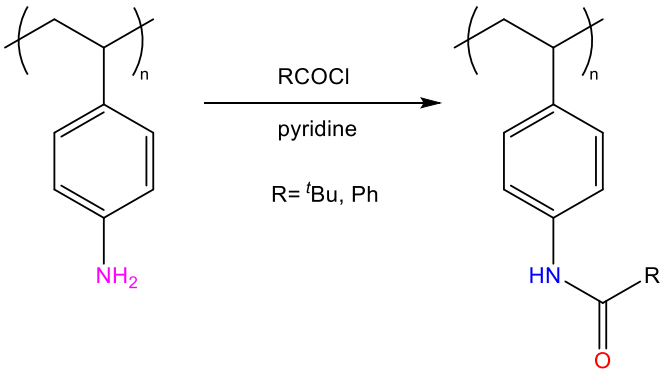

Figure 1. Post-polymerisation modification of poly(4-NH_2-styrene).

Other transformation such as the reaction with sulfonyl chlorides could be investigated. Likewise, if successful polymerisations of allylstyrene were achieved, the polymer produced could undergo further reactions with other polymers (with halogen groups for example), and form hyper branched polymers that have several industrial applications, notably in the domain of cargo transport.

Post-polymerisation modification of substituted polystyrenes has already been showed to produce polymers with interesting chemical and physical properties; in 2015, the post-

polymerisation reaction of poly(4-NH_2-styrene) with glycidol formed a resin able to remove boron from water.[10]

References

1 F. Qian, K. Liu and H. Ma, *Dalton Trans.*, 2010, **39**, 8071–8083.

2 C. Chen, J. Jiang, X. Mao, Y. Cong, Y. Cui, X. Pan and J. Wu, *Inorg. Chem.*, 2018, **57**, 3158–3168.

3 Y. Luo, P. Xu, Y. Lei, Y. Zhang and Y. Wang, *Inorganica Chim. Acta*, 2010, **363**, 3597–3601.

4 D. Osorio Meléndez, J. A. Castro-Osma, A. Lara-Sánchez, R. S. Rojas and A. Otero, *J. Polym. Sci. Part A Polym. Chem.*, 2017, **55**, 2397–2407.

5 C. K. Williams and A. Plajer, *Angew. Chem. Int. Ed.*, 2021, anie.202104495.

6 P. L. Ku, *Adv. Polym. Technol.*, 1988, **8**, 177–196.

7 M. A. Gauthier, M. I. Gibson and H.-A. Klok, *Angew. Chem. Int. Ed.*, 2009, **48**, 48–58.

8 M. Ciftci, D. Wang, M. Buchmeiser and Y. Yagci, *Macromol. Chem. Phys.*, 2017, **218**, 1700279.

9 W. Wang, Y. Shi, X. Wang, A. Qin, J. Z. Sun and B. Z. Tang, *Polym. Chem.*, 2017, **8**, 2630–2639.

10 J. Kluczka, T. Korolewicz, M. Zołotajkin and J. Adamek, *Water Resour. Ind.*, 2015, **11**, 46–57.

Chapter Seven
Experimental details

7.1 General methods

7.1.1 Air- and moisture-sensitive techniques

Air- and moisture-sensitive techniques were performed under an inert nitrogen atmosphere using standing Schlenk line techniques, or an MBraun UNIlab glovebox.

7.1.2 Solvent preparation

Pentane, hexane, benzene and toluene were dried using an MBraun SPS-800 solvent purification system, stored over potassium mirror and degassed prior to use. Tetrahydrofuran (thf) was distilled from purple Na/benzophenone and stored over 4 Å molecular sieves. Et_2O was distilled from purple Na/K and stored over a potassium mirror.

Deuterated solvents were dried over K (benzene-d_6-, toluene-d_8) or CaH_2 (tetrahydrofuran-d_8, pyridine-d_5, chloroform-d_1), freeze-pump-thaw degassed, vacuum transferred and stored over pre-activated 4 Å molecular sieves.

7.1.3 Commercially supplied reagents

Titanium tetrachloride (Sigma Aldrich), *n*-butyllithium (1.6 M in hexanes, Sigma Aldrich), tri*iso*butylaluminium (Sigma Aldrich), (pentamethylcyclopentadienyl)titanium(IV) trichloride (TCI), *D*-lactide (Purac) were used as supplied. Prior to use, zirconium tetrachloride (Sigma Aldrich) was dried under vacuum (15 h, 25 °C), styrene (Sigma Aldrich), 4-bromostyrene (Alfa Aesar), 4-methoxystyrene (Alfa Aesar), 4-NH_2-styrene (Alfa Aesar) and 4-NMe_2-styrene (Fluorochem) were dried for 3 days over calcium hydride, styrene was freeze-thaw degassed and stored over pre-activated 4 Å molecular sieves; 4-bromoanisole, 4-bromobenzotrifluoride and N,N'-di*iso*propylcarbodiimide (Alfa Aesar) were dried over 3 Å molecular sieves; solid polymethylaluminoxane (sMAO, Tosoh Finechem Corporation) and methylaluminoxane (MAO, Chemtura) were supplied as slurries in toluene which were dried under vacuum. Ethylene, CONCOA regulators and flashback arrestors were supplied by CK Gas Products Limited. *L*- and *rac*-lactide (Alfa Aesar) were recrystallised from toluene and dried under vacuum.

7.1.4 Synthesis of literature compounds

The following compounds were synthesised according to the literature procedure: $TiCl_4.2thf$,[1] $Li{\cdot}(NiPr)_2CN(^iPr)_2$,[2] $H[N(2,4,6\text{-}Me\text{-}C_6H_2)]_2CH$,[3] $[Pn^*TiCl(\mu\text{–}Cl)]_2$,[4] $[ZrPn^*(\mu\text{–}Cl)_{3/2}]_2(\mu\text{–}Cl)_2Li.Et_2O_{(X)}$,[4] $Pn^*(H)TiCl_3$.[5], $K(O\text{-}2,6\text{-}Me\text{-}C_6H_3)$ and $K(O\text{-}2,6\text{-}^iPr\text{-}C_6H_3)$.[6]

7.1.5 Solution NMR spectroscopy

Solution phase NMR spectra were recorded either on a Bruker Avance III HD nanobay 400 MHz NMR spectrometer, or a Bruker Avance III 500 MHz NMR spectrometer and

were referenced to the residual protio-solvent peak. Unless otherwise stated, ^{1}H and $^{13}C\{^{1}H\}$ spectra were recorded at 25 °C. Air sensitive samples were prepared in a glovebox under an inert atmosphere, using dried deuterated solvents in J. Young's NMR tubes.

For polymer samples, unless otherwise stated, NMR spectra were recorded in 1,1,2,2-tetrachloroethane-d_2 at 393 K with chromium (III) acetylacetonate as a relaxation agent (0.5 wt%).

7.1.6 Solid-state NMR spectroscopy

Solid-state NMR spectroscopy experiments were carried out by Dr. Nicholas Rees (University of Oxford). Air-sensitive compounds were prepared in a glovebox under a nitrogen atmosphere and sealed in 5 mm zirconia rotors. Spectra were recorded on a Bruker Avance III HD NanoBay 400.2 MHz solid-state NMR spectrometer, samples were spun at the magic angle (54.71°) at spin rates of 10 kHz for ^{13}C CP-MAS and 15 kHz for ^{27}Al DP-MAS. ^{13}C NMR spectra were referenced to adamantane and ^{27}Al to $Al(NO_3)_3$.

7.1.7 Differential scanning calorimetry

Differential scanning calorimetry (DSC) samples were run on a DSC3+ (Mettler Toledo, Ltd) using 5 mg of polymer in a sealed aluminium 100 μL crucible. An empty crucible was used as a reference, and the DSC was calibrated using indium. Samples were heated from 25 to 280 °C and cooled back again at a rate of 5 °C per minute unless otherwise stated, a total of two cycles were run. Polymer melt temperature and enthalpy values were taken from the second heating cycle.

7.1.8 Scanning electron microscopy

Scanning electron microscopy (SEM) analyses were performed by Dr. Philip Kenyon and Mr Clement Collins Rice on a JOEL JSM 6610LV scanning electron microscope with an accelerating voltage of 3.0 kV. Polymer samples were spread on carbon tape adhered to an SEM stage. Before imaging, the samples were coated with a thin platinum layer (20 nm) to prevent charging and improve image quality.

7.1.9 Gel permeation chromatography

Polyethylene and copolymer samples:

Gel Permeation Chromatography (GPC) samples were collected by Ms Liv Thobru at Norner AS (Norway) on a high temperature gel permeation chromatograph with an IR5 infrared detector (GPC-IR5). Samples were dissolved in 1,2,4-trichlorobenzene (TCB) containing 300 ppm of 3,5-di*tert*butyl-4-hydroxytoluene (BHT) at 160 °C for 90 minutes and then filtered with a 10 μm SS filter before being passed through the GPC column. The samples were run under a flow rate of 0.5 mL/minute using TCB containing 300 ppm of BHT as mobile phase with 1 mg/mL BHT added as a flow rate marker. The GPC column and detector temperature were set at 145 and 160 °C respectively.

Polystyrene and polylactide samples:

Polymer molecular weights were determined by GPC using an Agilent 1260 Infinity II GPC/SEC instrument equipped with an Agilent PLgel Mixed-D column (300 mm length, 7.5 mm diameter) and a refractive index (RI) detector. Thf (Sigma-Aldrich, HPLC grade containing 250 ppm BHT as inhibitor) was used as an eluent at 35 °C with a flow rate of 1.0 mL min^{-1}. Samples were dissolved in thf at a concentration of 1.0 mg mL^{-1} and

filtered before injection. Linear polystyrenes were used as primary calibration standards and the appropriate Mark-Houwink corrections were applied to calculate the experimental molecular weights.[7]

7.1.10 Mass spectrometry

Mass spectrometry samples were run as electron impact (EI) mass spectra on an Agilent GC-TOF-MS by Dr. James Wickens or Dr. Victor Mikhailov (University of Oxford).

Matrix-assisted laser desorption/ionisation time of flight spectra were collected Dr. Victor Mikhailov (University of Oxford) using a Bruker MALDI Autoflex TOF MS. Samples were run using either a DHB or DCTB matrix. The DHB matrix was prepared by mixing the sample with DHB (10 mg mL^{-1} in 70:30 H_2O:CH_3CN) in a 1:1 volume ratio. The DCTB matrix was prepared by mixing 10 µL of sample with 10 µL DCTB (40 mg mL^{-1} in thf) and 2.5 µL KTFA (5 mg mL^{-1} in thf). 1.5 µL of the mixed solutions were spotted on the MALDI plate and dried prior to the run.

7.1.11 Single crystal X-ray diffraction

Single crystal X-ray diffraction data collection and structure determinations were performed by Dr. Zoë Turner (University of Oxford). Crystals were mounted on MiTeGen MicroMounts using perfluoropolyether oil and rapidly transferred to a goniometer head on a diffractometer fitted with an Oxford Cryosystems Cryostream open-flow nitrogen cooling device.[8] Data collections were carried out at 150 K using an Oxford Diffraction Supernova diffractometer with mirror-monochromated Cu Kα radiation (λ = 1.54178 Å) and the data processed using CrysalisPro.[9] The structures were solved using direct methods (SIR-92)[10] or a charge flipping algorithm (SUPERFLIP)[11] and refined by full-matrix least-squares procedures using the Win-GX software suite.[12,13]

Molecular structures were depicted utilising Ortep,[13] with ellipsoids shown at 30% probability. Molecular bond lengths and angles were calculated using Platon.[14]

7.1.12 Powder X-ray diffraction (PXRD)

PXRD was carried out on a PANAnalytical X'Pert Pro Diffractometer in scanning mode using Cu Kα radiation (λ= 1.542 Å) into a steel sample holders. The samples were analysed from 2 to 70 °, with a step size 0.0334 ° and scan speed 0.0354 ° s^{-1} by Mr Justin (Doy) Leung.

7.1.13 Elemental analysis

Elemental analysis samples were prepared in a glove box under a nitrogen atmosphere and sealed in glass vials. CHN analyses were carried out in duplicate by Miss Orla McCullough (London Metropolitan University).

7.1.14 Fourier transform infrared (FTIR) spectroscopy

FTIR spectra were collected on a ThermoScientific Nicolet iS5 spectrometer with a iD3 ATR stage. The spectrometer was set to record 50 scans between 600 and 4000 cm^{-1} with a resolution on 4 cm^{-1}.

7.1.15 General procedure for immobilising catalysts on solid support.

200 equivalents of solid polymethylaluminoxane (sMAO) were mixed with the pre-catalyst in toluene (40 mL). The slurry was heated to 60 °C for 1 h, during which time the content was swirled every 5 minutes. After 1 h, the product was allowed to settle leaving a coloured solid and a colourless solution. The supernatant was removed *via* cannula and the solid dried under vacuum at room temperature.

7.1.16 General procedure for solution phase polymerisation of styrene

The precatalyst was dissolved in toluene. An ampoule was charged with dried MAO and toluene (5 mL) before 500 µL of the precatalyst solution was added. The reaction mixture was placed in an oil bath at the desired temperature and let to equilibrate for 5 minutes. Styrene (1 mL, 8.7 mmol) was injected into the mixture *via* syringe. The mixture was stirred at 1000 rpm for the duration of the experiment. The polymerisation was quenched by adding acidified MeOH (ca. 1.5 mL). The mixture was then poured into MeOH (15 mL) and the polymer was allowed to settle. If precipitated, the polystyrene was filtered and washed with 3×10 mL MeOH. If still in suspension, the solution was concentrated then the polymer was filtered and washed. The final polystyrene was dried in a vacuum oven at 30 °C for 18 h. All polymerisations were carried out in duplicate.

7.1.17 General procedure for solution phase polymerisation of ethylene

1500 equivalents of MAO were added to a 150 mL ampoule. A stock solution of 2 µmol/mL of complex in 10 mL of toluene was prepared and 0.1 mL of stock solution was added to the ampoule followed by 50 mL of hexanes. The ampoule was allowed to warm to the desired temperature in an oil bath and the headspace degassed. The flask was opened to ethylene (2 bar) and stirred at 1000 rpm for the duration of the experiment. The ampoule was then degassed and the mixture filtered. The polyethylene was then washed with pentane, dried and weighed. All polymerisations were carried out in duplicate.

7.1.18 General procedure for slurry-phase polymerisation of styrene

An ampoule was charged with the supported complex (10 mg), TiBA (150 mg) and toluene (50 mL). The mixture was placed in an oil bath at the desired temperature and let to equilibrate for 5 minutes. Styrene (3.7 mL, 32.3 mmol) was injected into the mixture *via* syringe. The mixture was stirred at 1000 rpm for the duration of the experiment. The polymerisation was quenched by adding acidified EtOH (ca. 7 mL). The mixture was then poured into MeOH (15 mL) and the polymer was allowed to settle. If precipitated, the polystyrene was filtered and washed with 3×10 mL MeOH. If still in suspension, the solution was concentrated then the polymer was filtered and washed. The final polystyrene was dried in a vacuum oven at 30 °C for 18 h. All polymerisations were carried out in duplicate.

7.1.19 General procedure for slurry-phase polymerisation of ethylene

An ampoule was charged with TiBA (150 mg, 0.756 mmol), toluene (50 mL) and the supported catalyst (10 mg). The contents were placed in an oil bath at the required temperature and allowed to equilibrate for 5 minutes while the headspace is degassed. The flask was opened to ethylene (2 bar) and stirred at 1000 rpm for the duration of the experiment. The polymer was then filtered, washed with pentane (2×20 mL) and dried at 5 mbar for 18 h. All polymerisations were carried out in duplicate.

7.1.20 General procedure for slurry-phase copolymerisation

In an ampoule were mixed 10 mg of supported catalyst, 150 mg of TiBA and 46 mL of solvent. In a sidearm, the desired amount of comonomer was added in 4 mL of solvent. The contents were placed in an oil bath at the required temperature and allowed to

equilibrate for 5 minutes while the headspace was degassed. The flask was opened to ethylene (2 bar) then the sidearm was opened and stirred at 1000 rpm for the duration of the experiment. The ampoule was then degassed and the polymerisation was quenched by adding acidified EtOH (ca. 7 mL). The polymer was then filtered and dried yielding a first crop. A second crop was obtained by removing the solvent from the filtrate under vacuum. All polymerisations were carried out in duplicate.

7.1.21 General procedure for solution phase copolymerisation

In an ampoule were mixed 2×10^{-7} mol of catalyst 150 mg of TiBA and 46 mL of solvent. In a sidearm, the desired amount of comonomer was added in 4 mL of solvent. The contents were placed in an oil bath at the required temperature and allowed to equilibrate for 5 minutes while the headspace is degassed. The flask was opened to ethylene (2 bar) then the sidearm was opened and stirred at 1000 rpm for the duration of the experiment. The ampoule was then degassed and the polymerisation was quenched by adding acidified EtOH (ca. 7 mL). The polymer was then filtered and dried yielding a first crop. A second crop was obtained by removing the solvent from the filtrate under vacuum. All polymerisations were carried out in duplicate.

7.2 Experimental details for Chapter 2

7.2.1 sMAO-Cp*TiCl$_3$ (1$_{sMAO}$)

Isolated in 80% yield.

^{13}C CPMAS (10 kHz) δ (ppm): −7.9 (sMAO−*C*H$_3$), 12.3 (Cp*−*C*H$_3$), 128.6(sMAO−benzoate), 178.0 (sMAO−benzoate α-*C*(O)O).

^{27}Al DPMAS (15 kHz) δ (ppm): –255.7, –96.8, 62.0, 170.7, 322.9.

7.2.2 sMAO-Pn*(H)TiCl$_3$ (2$_{sMAO}$)

Isolated in 79% yield.

^{13}C CPMAS (10 kHz) δ (ppm): −7.4 (sMAO−*C*H$_3$), 11.2 (Pn*−*C*H$_3$), 128.3 (sMAO−benzoate), 177.1(sMAO−benzoate α-*C*(O)O).

^{27}Al DPMAS (15 kHz) δ (ppm): –239.2, –84.3, 81.9, 185.8, 329.3.

7.2.3 Typical NMR spectroscopy data of polystyrene samples

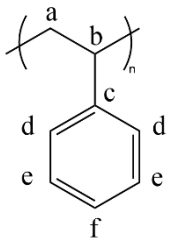

PS produced using Pn*(H)TiCl$_3$ ([Al$_{MAO}$]$_0$:[Ti]$_0$ = 1500, 40 °C, 10 minutes): ^{1}H NMR (chloroform-*d*$_1$, 400 MHz, 298 K) δ (ppm): 6.86-7.25 (br, C$_6$*H*$_{5d/f}$), 6.29-6.86 (br, C$_6$*H*$_{5d}$), 1.70-2.05 (br, C*H*$_b$), 1.24-1.65 (br, C*H*$_{2a}$).

^{13}C{^{1}H} NMR (chloroform-*d*$_1$, 125 MHz, 393 K) δ (ppm): 145.0-146.6 (br, *C*$_{6c}$H$_5$), 127.4-128.6 (br, *C*$_{6d/e}$H$_5$), 125.8 (br, *C*$_{6f}$H$_5$), 44.4(br, *C*$_b$H), 40.5 (br, *C*$_a$H$_2$).

7.2.4 Typical NMR spectroscopy data of polyethylene samples

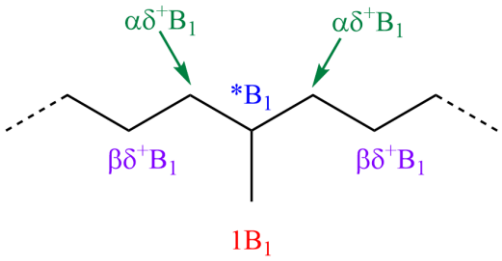

Resonances were attributed according to literature assignments.[15,16] PE produced using sMAO-Pn*(H)$TiCl_3$ (**2$_{sMAO}$**) ($[Al_{MAO}]_0$:$[Ti]_0$ = 200, 50 °C, 30 minutes): $^{13}C\{^1H\}$ NMR (1,2-dichloroethane-d_4, 125 MHz, 393 K) δ (ppm): 37.7 ($\alpha\delta^+B_1$), 35.4 ($^*B_1$), 29.4 (CH_2 backbone), 25.2 ($\beta\delta^+B_1$), 21.1 ($1B_1$).

7.3 Experimental details for Chapter 3

7.3.1 Typical NMR spectroscopy data of poly(4-methoxy-styrene)

Resonances were attributed according to literature assignments.[17]

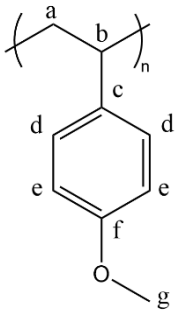

Poly(4-methoxy-styrene) produced using Pn*(H)$TiCl_3$ (**2**) ($[Al_{MAO}]_0$:$[Ti]_0$ = 1500, 55 °C, 10 minutes): ^{1}H NMR (chloroform-d_1, 500 MHz, 298 K) δ (ppm): 6.4-7.0 (br, 4H, $C_6H_{4d/e}$), 3.7-3.9 (br, 3H, O-CH_3), 1.7-2.5 (br, 1H, CH_b), 1.36-1.74 (br, 2H, CH_{2a}).

$^{13}C\{^1H\}$ NMR (chloroform-d_1, 125 MHz, 298 K) δ (ppm): 157.8 (br, $C_{6f}H_4$), 137.7 (br, $C_{6c}H_4$), 127.6 ($C_{6e}H_4$), 113.9 ($C_{6d}H_4$), 55.4 (O-CH_3), 45.1 (C_aH_2), 39.8 (C_bH).

IR (cm^{-1}): 3002, 2926 (C-H stretch aromatics), 2837 (C-H stretch backbone), 1508 (C-C stretch aromatics), 1243 (C-O), 1033 (C-H bending).

7.3.2 Typical NMR spectroscopy data of poly(4-amino-styrene)

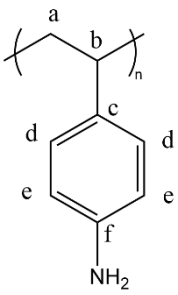

After quenching the polymerisation, the polymer was dissolved in a minimum volume of pyridine then dried *in vacuo*. The polymer was extracted in 10 mL of dichloromethane and washed with water (3×10 mL) before being dried with $MgSO_4$. The filtrate was dried under reduced pressure to yield the polystyrene derivative. Poly(4-amino-styrene) produced using Pn*(H)$TiCl_3$ (**2**) ($[Al_{MAO}]_0$:$[Ti]_0$ = 1500, 55 °C, 10 minutes): ^{1}H NMR (chloroform-d_1, 500 MHz, 298 K) δ (ppm): 7.1 (2H, C_6H_{4d}), 6.5 (2H, C_6H_{4e}), 4.3 (1H, NH_2), 3.8 (1H, br, NH_2), 1.45 (3H, CH_2CH).

$^{13}C\{^1H\}$ NMR (chloroform-d_1, 125 MHz, 298 K) δ (ppm): 145.5 ($C_{6f}H_4$), 132.7 ($C_{6c}H_4$), 126.1 ($C_{6d}H_4$), 113.1 ($C_{6e}H_4$), 52.4 (C_aH_2), 26.2 (C_bH).

IR (cm^{-1}): 2964 (C-H stretch aromatics), 2925 (C-H stretch backbone), 1612 (N-H bend), 1515 (C-C stretch aromatics). 1178 (C-N stretch), 1022 (C-H bend).

7.3.3 Typical NMR spectroscopy data for poly(4-bromo-styrene)

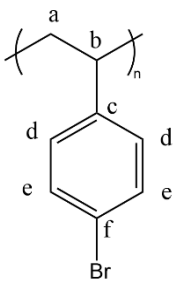

Poly(4-amino-styrene) produced using Cp^*TiCl_3 (**1**) ($[Al_{MAO}]_0/[Ti]_0$ = 1500, 55 °C, 10 minutes): ^1H NMR (chloroform-d_1, 500 MHz, 298 K) δ (ppm): 7.4-7.0 (2H, br, C_6H_{4e}), 6.5-6.1 (2H, br, C_6H_{4d}), 1.8-1.5 (1H, br, C*H*), 1.5-1.1 (2H, br, CH_2). $^{13}C\{^1H\}$ NMR (chloroform-d_1, 125 MHz, 298 K) δ (ppm): 143.3 ($C_{6f}H_4$), 131.6 ($C_{6c}H_4$), 129.3 ($C_{6d}H_4$), 120.0 ($C_{6e}H_4$), 40.2 (C_aH_2), 21.8 (C_bH).

IR (cm^{-1}): 3028 (C-H stretch aromatics/backbone), 1089, 1047 (C-H bend), 646 (C-Br stretch).

7.3.4 Typical NMR spectroscopy data for 4-dimethylaminostyrene dimer

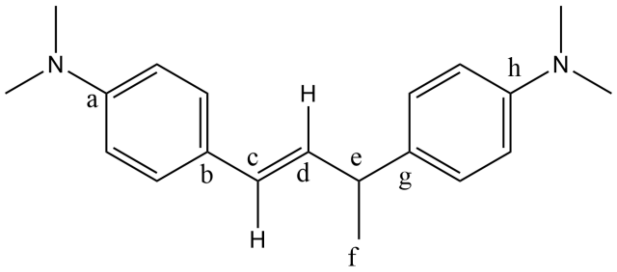

After quenching the polymerisation, the product was dissolved in minimum pyridine then dried *in vacuo*. The polymer was extracted in dichloromethane and washed with water (3×10 mL) before being dried with $MgSO_4$. The filtrate was dried under reduced pressure yielded the polystyrene derivative. Poly(4-amino-styrene) produced using sMAO-$Pn^*(H)TiCl_3$ (**2_{sMAO}**) ($[Al_{MAO}]_0$:$[Ti]_0$ = 200, 55 °C, 10 minutes): ^1H NMR (chloroform-d_1, 500 MHz, 298 K) δ (ppm): 7.30 (d, ^3J = 8.7 Hz, 2H, C*H*-Ar), 7.20 (d, ^3J = 8.8 Hz, 2H,

C*H*-Ar), 6.77 (d, ^{3}J = 8.8 Hz, 2H, C*H*-Ar), 6.71 (d, ^{3}J = 8.7 Hz, 2H, C*H*-Ar), 6.36 (d, ^{3}J = 15.9 Hz, 1H, C_c*H*=CH) 6.22 (dd, ^{3}J = 15.9 Hz, ^{4}J = 6.7 Hz, 2H, C*H*=C_d*H*), 3.58 (p, 1H, C_e*H*), 2.97 (s, 6H, N(CH_3)), 2.96 (s, 6H, N(CH_3)), 1.46 (d, ^{3}J = 7.1 Hz, 3H, $C_f$$H_3$).

^{13}C{^{1}H} NMR (chloroform-d_1, 125 MHz, 298 K) δ (ppm): 147.5 (*C*$_g$-Ar)), 141.7 (*C*$_h$-Ar), 141.3 (*C*$_a$-Ar), 139.3 (*C*$_b$-Ar), 136.9 (*C*$_d$H), 129.44 (*C*H-Ar), 128.1 (*C*H-Ar), 127.7 (*C*$_c$H), 121.2 (*C*H-Ar), 46.7 (*C*$_e$H), 42.3 (N(*C*H_3)$_2$), 21.0 (*C*$_f$$H_3$).

ESI/MS (positive mode): 295.2165 $[MH]^+$.

7.4 Experimental details for Chapter 4

7.4.1 Pn*(H)TiCl$_2$(O-2,6-^{i}Pr-C$_6$H$_3$) (3)

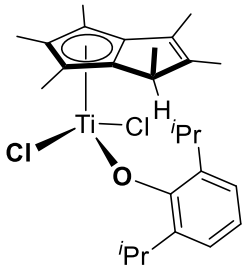

[Pn*TiCl(μ–Cl)]$_2$ (268 mg, 0.44 mmol) was dissolved in toluene (50 mL) and 2,6-^{i}Pr-phenol (163 μL, 0.88 mmol) was added. The mixture which turned dark orange was stirred for 15 h at 85 °C. A precipitate was filtered off *via* cannula and solvent was removed *in vacuo*. Recrystallisation from hexane at -30 °C yielded Pn*(H)TiCl$_2$(O-2,6-^{i}Pr-C$_6$H$_3$) as a purple solid (271 mg, 78%).

^{1}H NMR (toluene-d_8, 298 K, 400 MHz): δ 6.99(d, ^3J = 1.2 Hz, 1H, 3,4,5-C$_6$*H*$_3$), 6.92 (s, 1H, 3,4,5-C$_6$*H*$_3$), 6.90 (d, ^3J = 1.8 Hz, 1H, 3,4,5-C$_6$*H*$_3$), 3.23 (sept, ^3J = 6.8 Hz, 2H, C*H*(CH$_3$)$_2$*H*), 3.14 (m, 1H, Pn*(*H*)), 2.26 (s, 3H, Pn*(H)-C*H*$_3$), 2.15 (s, 3H, Pn*(H)-C*H*$_3$), 2.06 (s, 3H, Pn*(H)-C*H*$_3$), 1.81 (s, 3H, Pn*(H)-C*H*$_3$), 1.39 (s, 3H, Pn*(H)-C*H*$_3$), 1.25 (d, ^3J = 7.0 Hz, 6H, CH(C*H*$_3$)$_2$), 1.21 (d, ^3J = 6.8 Hz, 6H, CH(C*H*$_3$)$_2$), 0.88 (d, ^3J = 7.5 Hz, 3H, Pn*(H)-C*H*$_3$).

^{13}C{^{1}H} NMR (toluene-d_8, 298 K, 125 MHz): δ 160.07 (1-*C*$_6$H$_3$), 150.40 (3-*C*$_6$H$_3$), 147.99 (5-*C*$_6$H$_3$), 140.40 (Pn*(H)-bridge), 139.42 (2-*C*$_6$H$_3$), 136.41 (Pn*(H)), 129.53 (Pn*(H)), 123.75 (Pn*(H)-bridge), 123.34 (4-*C*$_6$H$_3$), 43.90 (Pn*(H)), 27.22 (*C*H(CH$_3$)$_2$), 24.23 (CH(*C*H$_3$)$_2$), 23.97 (CH(*C*H$_3$)$_2$), 15.23 (Pn*(H)-*C*H$_3$), 13.94 (Pn*(H)-*C*H$_3$), 13.53 (Pn*(H)-*C*H$_3$), 12.93 (Pn*(H)-*C*H$_3$), 11.78 (Pn*(H)-*C*H$_3$), 11.47 (Pn*(H)-*C*H$_3$).

CHN analysis (%): expected C 65.07, H 7.89; observed C 62.89, H 7.29. Solvent or moisture trapped in the sample affect the accuracy and might explain the difference between the expected and observed values.

7.4.2 Pn*(H)TiCl$_2$(O-2,4-^{t}Bu-C$_6$H$_3$) (4)

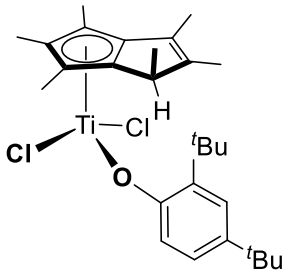

[Pn*TiCl(μ–Cl)]$_2$ (225 mg, 0.37 mmol) was dissolved in toluene (50 mL) and 2,4-^{t}Bu-phenol (152 mg, 0.74 mmol) was added. The mixture, which turned dark purple, was stirred for 15 h at 85 °C. A precipitate was filtered off *via* cannula and the solid was washed with toluene (3×5 mL). The solvent was removed *in vacuo*. Recrystallisation from hexane at -30 °C yielded Pn*(H)TiCl$_2$(O-2,4-^{t}Bu-C$_6$H$_3$) as a purple solid (188 mg, 91%).

^{1}H NMR (toluene-d_8, 298 K, 400 MHz): δ 7.40 (d, ^3J = 2.4 Hz, 1H, 6-C$_6$*H*$_3$), 7.04 (dd, ^4J = 8.2, ^3J = 2.4 Hz, 1H, 5-C$_6$*H*$_3$), 6.89 (d, ^4J = 8.4 Hz, 1H, 3-C$_6$*H*$_3$), 3.38 (q, ^3J = 7.0 Hz, 1H, Pn*(*H*)), 2.25 (s, 3H, Pn*(H)-C*H*$_3$), 2.17 (s, 3H, Pn*(H)-C*H*$_3$), 2.10 (s, 3H, Pn*(H)-C*H*$_3$), 1.92 (s, 3H, Pn*(H)-C*H*$_3$), 1.55 (s, 3H, Pn*(H)-C*H*$_3$), 1.47 (s, 9H, ^{t}Bu-*H*), 1.26 (s, 9H, ^{t}Bu-*H*), 0.92 (d, ^3J = 7.5 Hz, 3H, Pn*(H)-C*H*$_3$).

^{13}C{^{1}H} NMR (toluene-d_8, 298 K, 125 MHz): δ 162.35 (1-C$_6$H$_3$), 150.70 (Pn*(H)), 148.22 (Pn*(H)), 145.63 (Pn*(H)), 141.36 (Pn*(H)), 136.69 (Pn*(H)), 130.01 (Pn*(H)), 124.25 (3-*C*$_6$H$_3$), 124.01 (*C*$_6$H$_3$), 123.45 (6-*C*$_6$H$_3$), 44.76 (Pn*(H)), 35.42 (^{t}Bu-*C*$_{quat}$), 34.71 (^{t}Bu-*C*$_{quat}$), 31.67 (^{t}Bu), 30.32 (^{t}Bu), 15.14 (Pn*(H)-*C*H$_3$), 13.87 (Pn*(H)-*C*H$_3$), 13.32 (Pn*(H)-*C*H$_3$), 13.17 (Pn*(H)-*C*H$_3$), 11.98 (Pn*(H)-*C*H$_3$), 11.62 (Pn*(H)-*C*H$_3$).

CHN analysis (%): expected C 66.17, H 8.23; observed C 65.20, H 7.99. Solvent or moisture trapped in the sample affect the accuracy.

7.4.3 Pn*(H)TiCl$_2$(O-Si(Me)$_2$^{t}Bu) (5)

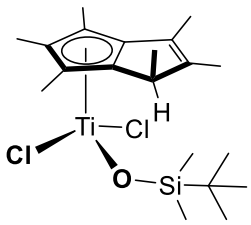

[Pn*TiCl(μ–Cl)]$_2$ (221 mg, 0.36 mmol) was dissolved in toluene (50 mL) and Si(Me)$_2$^{t}BuOH (114.3 μL, 0.72 mmol) was added. The mixture which turned dark purple was stirred for 1 h at 25 °C. A precipitate was filtered off *via* cannula and solvent removed *in vacuo* yielding Pn*(H)TiCl$_2$(O-Si(Me)$_2$^{t}Bu) as a dark red oil (338 mg, 75%).

^{1}H NMR (toluene-d_8, 298 K, 400 MHz): δ 3.58 (q, ^3J = 7.6 Hz, 1H, Pn*(*H*)), 2.18 (s, 3H, Pn*(H)-C*H*$_3$), 2.09 (s, 3H, Pn*(H)-C*H*$_3$), 2.03 (s, 3H, Pn*(H)-C*H*$_3$), 1.94 (s, 3H, Pn*(H)-C*H*$_3$), 1.69 (s, 3H, Pn*(H)-C*H*$_3$), 1.02 (s, 9H, ^{t}Bu), 1.00 (s, 6H, Si(C*H*$_3$)$_2$), 0.22 (d, ^3J = 7.4 Hz, 3H, Pn*(H)-C*H*$_3$).

^{13}C{^{1}H} NMR (toluene-d_8, 298 K, 125 MHz): δ 149.72 (Pn*(H)), 147.43 (Pn*(H)), 143.05 (Pn*(H)), 135.21 (Pn*(H)), 130.17 (Pn*(H)), 127.11 (Pn*(H)), 122.10 (Pn*(H)), 45.51 (Pn*(H)), 26.27 (^{t}Bu), 15.22(Pn*(H)-*C*H$_3$), 13.54 (Pn*(H)-*C*H$_3$), 13.23 (Pn*(H)-*C*H$_3$), 13.19 (Pn*(H)-*C*H$_3$), 11.99 (Pn*(H)-*C*H$_3$), 11.78 (Pn*(H)-*C*H$_3$), -2.78 (Si(*C*H$_3$)$_2$).

7.4.4 sMAO-Pn*(H)TiCl$_2$(O-2,6-^{i}Pr-C$_6$H$_3$) (3$_{sMAO}$)

Isolated in 91% yield.

^{13}C CPMAS (10 kHz) δ (ppm): −8.4 (sMAO−*C*H$_3$), 11.8, 20.7, 25.6, 51.4, 128.5 (sMAO−benzoate).

^{27}Al DPMAS (15 kHz) δ (ppm): –249.4, –99.9, 132.7, 287.8.

7.4.5 sMAO-Pn*(H)TiCl$_2$(O-2,4-^{t}Bu-C$_6$H$_3$) (4$_{sMAO}$)

Isolated in 91% yield.

^{13}C CPMAS (10 kHz) δ (ppm): −8.0 (sMAO−*C*H$_3$), 11.4, 20.3, 30.1, 51.4, 128.5 (sMAO−benzoate), 177.4.

^{27}Al DPMAS (15 kHz) δ (ppm): –255.0, –99.9, 138.4, 293.5.

7.4.6 sMAO-Pn*(H)TiCl$_2$(O-Si(Me)$_2$^{t}Bu) (5$_{sMAO}$)

Isolated in 93% yield.

^{13}C CPMAS (10 kHz) δ (ppm): −7.9 (sMAO−*C*H$_3$), 11.1, 20.4, 25.6, 51.4, 128.2 (sMAO−benzoate), 176.7 (sMAO−benzoate α-*C*(O)O).

^{27}Al hanhecho (20 kHz) δ (ppm): –339.1, –136.2, –62.5, 38.9,239.3, 424.8.

7.5 Experimental details for Chapter 5

7.5.1 Lactide polymerisation

L-, *D*-, *meso*- or *rac*-Lactide (40 mg, 0.278 mmol) was weighed into a J. Young's tap NMR spectroscopy tube. Stock solutions of complex (and benzyl alcohol when required) in an amount of deuterated solvent corresponding to an initial lactide concentration ($[LA]_0$) of 0.5 M were prepared and the desired quantity added to the NMR tube. Polymerisations were run at 80–120 °C and halted by submerging the NMR tubes in an ice bath. Conversion was monitored by ^{1}H NMR spectroscopy. On completion, the reaction mixture was decanted into −5 °C pentane (10 mL), the solution allowed to settle and the solvent removed. The polymer was then washed pentane (2×10 mL) and dried under vacuum at 30 °C for 18 hours.

7.6 Experimental details for chapter 6

7.6.1 Li[(N^{i}Pr)$_2$C(4-OMe-C$_6$H$_4$)]

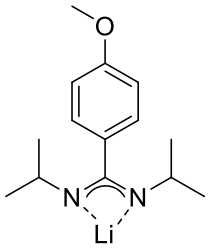

4-Bromoanisole (2.24 g, 12 mmol) was dissolved in thf (100 mL) and cooled to -78 °C. To this, a solution of *n*-BuLi in hexanes (5.3 mL, 12 mmol, 1.6 M) was added dropwise. The mixture was stirred for 1 h. N,N'-di*iso*propylcarbodiimide (1.86 mL, 12 mmol) was then added at 0 °C. The reaction mixture was stirred for another 1 h at room temperature. Volatiles were removed *in vacuo* and the product was washed with hexane (3×10 mL), filtered and dried again. Recrystallisation from thf at -30 °C yielded Li[(N^{i}Pr)$_2$C(4-OMe-C$_6$H$_4$)] as a colourless solid (1.64 g, 50%).

^{1}H NMR (C$_4$D$_8$O, 298 K, 400 MHz): δ 6.92 (d, ^3J = 7.6 Hz, 2H, 2,6-C$_6$*H*$_4$), 6.82 (d, ^3J = 7.6 Hz, 2H, 3,5-C$_6$*H*$_4$), 3.75 (s, 3H, OC*H*$_3$, 2.95 (s, 2H, C*H*(CH$_3$)$_2$), 0.83 (s, 12H, CH(C*H*$_3$)$_2$).

^{13}C{^{1}H} NMR (C$_4$D$_8$O, 298 K, 125 MHz): δ 158.7 (N*C*HN), 133.6 (4-*C*$_6$H$_4$), 128.7 (1-*C*$_6$H$_4$), 113.4 (2,3,5,6-*C*$_6$H$_4$), 54.94 (O*C*H$_3$), 47.8 (*C*H(CH$_3$)$_2$), 27.4 (br, CH(*C*H$_3$)$_2$), 26.2 (CH(*C*H$_3$)$_2$).

^{7}Li NMR (C$_4$D$_8$O, 298 K, 155.5 MHz): δ 1.54.

CHN analysis (%): expected C 69.34, H 9.31, N 9.70; observed C 65.14, H 10.19, N 8.88. Solvent or moisture trapped in the sample affect the accuracy and can explain the difference between the expected and observed values.

7.6.2 Li[(N^{i}Pr)$_2$C(4-CF$_3$-C$_6$H$_4$)]

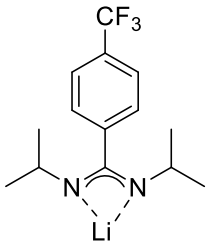

4-Bromobenzotrifluoride (1.50 mL, 10.7 mmol) was dissolved in thf (100 mL) and cooled to -78 °C. To this, a solution of *n*-BuLi in hexanes (4.7 mL, 10.7 mmol, 1.6 M,) was added dropwise. The mixture was stirred for 1 h. N,N'-di*iso*propylcarbodiimide (1.66 mL, 10.7 mmol) was then added at 0 °C. The reaction mixture was stirred for another 1 h at room temperature. Volatiles were removed *in vacuo*, the product was washed with hexane (3×10 mL), filtered off and dried again. Recrystallisation from thf/hexane (90/10) at -30 °C yielded Li[(N^{i}Pr)$_2$C(4-CF$_3$-C$_6$H$_4$)] as a colourless solid (1.35 g, 41%).

^{1}H NMR (C$_4$D$_8$O, 298 K, 400 MHz): δ 7.60 (d, ^3J = 7.6 Hz, 2H, 2,6-C$_6$*H*$_4$), 7.19 (d, ^3J = 6.9 Hz, 2H, 3,5-C$_6$*H*$_4$), 2.82 (s, 2H, C*H*(CH$_3$)$_2$), 0.82 (s, 12H, CH(C*H*$_3$)$_2$).

^{13}C{^{1}H} NMR (C$_4$D$_8$O, 298 K, 125 MHz): δ 170.8 (N*C*N), 145.7 (*C*F$_3$), 128.4 (2,6-*C*$_6$H$_4$), 126.6 (3,5-*C*$_6$H$_4$), 125.0 (*C*$_6$H$_4$), 47.7 (C*H*(CH$_3$)$_2$), 27.4 (br, CH(*C*H$_3$)$_2$), 26.2 (CH(*C*H3)$_2$).

^{7}Li NMR (C$_4$D$_8$O, 298 K, 155.5MHz): δ 1.52.

^{19}F NMR (C$_4$D$_8$O, 298 K, 376.5 MHz): δ -62.9.

CHN analysis (%): expected C 61.29, H 7.31, N 8.57; observed C 53.41, H 6.47, N 7.87. Solvent or moisture trapped in the sample affect the accuracy hence the difference between the calculated and observed values.

7.6.3 Li[(N^{i}Pr)$_2$C(4-^{t}Bu-C$_6$H$_4$)]

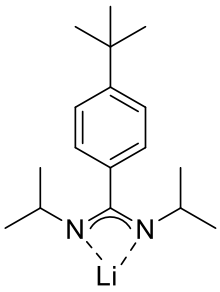

1-Bromo-4-*tert*-butylbenzene (2.0 mL, 11.5 mmol) was dissolved in thf (100 mL) and cooled to -78 °C. To this, a solution of *n*-BuLi in hexanes (7.2 mL, 11.5 mmol, 1.6 M,) was added dropwise. The mixture was stirred for 1 h. N,N'-di*iso*propylcarbodiimide (1.86 mL, 10.7 mmol) was then added at 0 °C. The reaction mixture was stirred for another 1 h at room temperature. Volatiles were removed *in vacuo*, the product was washed with hexane (3×10 mL), filtered off and dried again yielding Li[(N^{i}Pr)$_2$C(4-^{t}Bu-C$_6$H$_4$)] as a colourless solid (2.98 g, 84%).

^{1}H NMR (C$_4$D$_8$O, 298 K, 400 MHz): δ 7.30 (d, ^{3}J = 7.6 Hz, 2H, 2,3,5,6-C$_6$*H*$_4$), 6.94 (d, ^{3}J = 7.7 Hz, 2H, 2,3,5,6-C$_6$*H*$_4$), 2.92 (s, 2H, C*H*(CH$_3$)$_2$), 0.86 (s, 12H, CH(C*H*$_3$)$_2$).

^{13}C{^{1}H} NMR (C$_4$D$_8$O, 298 K, 125 MHz): δ 174.0 (N*C*N), 149.2 (2,3,5,6-*C*$_6$H$_4$), 138.8 (*C*^{t}Bu), 128.4 (2,3,5,6-*C*$_6$H$_4$), 127.8 (2,3,5,6-*C*$_6$H$_4$), 125.3 (2,3,5,6-*C*$_6$H$_4$), 48.4 (*C*H(CH$_3$)$_2$), 35.2 (^{t}Bu), 27.6 (br, CH(C*H*$_3$)$_2$), 26.5 (CH(C*H*$_3$)$_2$).

^{7}Li NMR (C$_4$D$_8$O, 298 K, 155.5 MHz): δ 1.53.

CHN analysis (%): expected C 75.21, H 10.47, N 9.10; observed C 67.16, H 9.64, N 8.93. Solvent or moisture trapped in the sample affect the accuracy and explain the difference between the expected and the observed values.

7.6.4 K{[N(2,4,6-Me-C_6H_2)]$_2$CH}

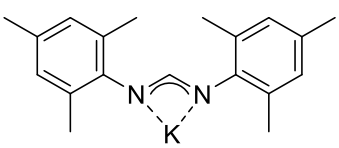

H{[N(2,4,6-Me-C_6H_2)]$_2$CH} (268 mg, 0.96 mmol) and KH (46.2 mg, 1.15 mol) were mixed in thf (5 mL). The reaction mixture was stirred at 25 °C for 1 h. The product was filtered off *via* cannula and dried *in vacuo* affording K{[N(2,4,6-Me-C_6H_2)]$_2$CH} as a colourless powder (177 mg, 50%).

^{1}H NMR (C_4D_8O, 298 K, 400 MHz): δ 7.57 (s, 1H, NC*H*), 6.62 (s, 4H, 3,5-C_6H_2), 2.12 (s, 18H, CH_3).

^{13}C{^{1}H} NMR (C_4D_8O, 298 K, 125 MHz): δ 163.4 (N*C*HN), 153.4 (*C*$_6$H$_2$, 130.5 (3,5-*C*$_6$H$_2$), 128.6 (3,5-*C*$_6$H$_2$), 126.67 (3,5-*C*$_6$H$_2$), 20.7 (*C*$_6$H$_2$-*C*H$_3$), 19.9 (*C*$_6$H$_2$-*C*H$_3$).

CHN analysis (%): expected C 71.42, H 7.57, N 8.77; observed C 68.65, H 7.68, N 8.25. Solvent and moisture trapped in the sample might explain the difference between the calculated and observed values.

7.6.5 General procedure for the synthesis of Pn*ZrCl[(NR′)$_2$CR]

[Pn*Zr(μ–Cl)$_{3/2}$]$_2$(μ–Cl)$_2$Li.thf$_{(1.88)}$ and M[(NR′)$_2$CR] (M = Li or K)were dissolved in benzene-d_6 (0.5 mL) in a J. Youngs tap NMR tube. The reaction was left for 1 h at 25 °C and after this time Pn*Zr{(NR′)$_2$CR}(Cl) was formed in a spectroscopic yields superior to 90% as determined by ^{1}H NMR spectroscopy.

7.6.6 Pn*ZrCl[(N^{i}Pr)$_2$C(4-OMe-C$_6$H$_4$)] (6)

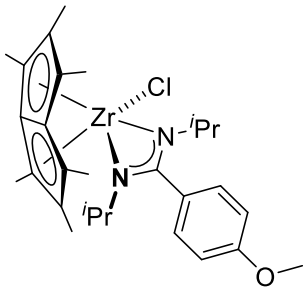

^{1}H NMR (benzene-d_6, 298 K, 400 MHz): δ 7.52 (dd, ^3J = 8.4 Hz, ^4J = 2.0 Hz, 1H, 3,5-C$_6$*H*$_4$), 6.86 (dd, ^3J = 8.3 Hz, ^4J = 2.0 Hz, 1H, 3,5-C$_6$*H*$_4$), 6.73 (dd, ^3J = 8.3 Hz, ^4J = 2.6 Hz, 1H, 2,6-C$_6$*H*$_4$), 6.62 (dd, ^3J = 8.4 Hz, ^4J = 2.6 Hz, 1H, 2,6-C$_6$*H*$_4$), 3.48 (sept, ^3J = 6.6 Hz, 2H, C*H*(CH$_3$)$_2$), 3.22 (s, 3H, OC*H*$_3$), 2.16 (s, 12H, 2,6-C*H*$_3$-Pn*), 2.05 (s, 6H, 1,3,5,7-C*H*$_3$-Pn*), 1.20 (d, ^3J = 6.7 Hz, 6H, CH(C*H*$_3$)$_2$), 0.92 (d, ^3J = 6.5 Hz, 6H, CH(C*H*$_3$)$_2$).

^{13}C{^{1}H} NMR (benzene-d_6, 298 K, 125 MHz): δ 175.6 (N*C*N), 156.0 (4-*C*$_6$H$_4$), 134.0 (2,6- Pn*), 131.6 (4,8-Pn*), 128.8 (1-*C*$_6$H$_4$), 126.7 (3,5-*C*$_6$H$_4$), 114.4 (2,6-*C*$_6$H$_4$), 109.2 (br, 1,3,5,7-Pn*), 54.7 (O*C*H$_3$), 50.0 (*C*H(CH$_3$)$_2$), 26.2 (CH(*C*H$_3$)$_2$), 24.3 (CH(*C*H$_3$)$_2$), 12.6 (1,3,5,7-*C*H$_3$-Pn*), 12.1 (2,6-*C*H$_3$-Pn*).

7.6.7 Pn*ZrCl[(N^{i}Pr)$_2$C(4-CF$_3$-C$_6$H$_4$)] (7)

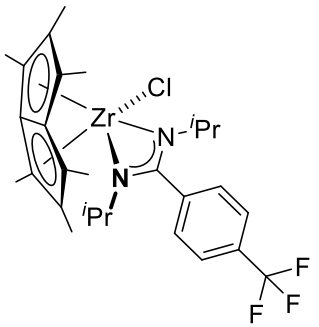

^{1}H NMR (benzene-d_6, 298 K, 400 MHz): δ 7.55 (d, ^3J = 8.0 Hz, 1H, 3,5-C$_6$*H*$_4$), 7.29 (d, ^3J = 7.9 Hz, 1H, 3,5-C$_6$*H*$_4$), 7.24 (d, ^3J = 8.0 Hz, 1H, 2,6-C$_6$*H*$_4$), 6.79 (d, ^3J = 7.9 Hz, 1H, 2,6-C$_6$*H*$_4$), 3.14 (p, ^3J = 6.6 Hz, 2H, C*H*(CH$_3$)$_2$), 2.12 (s, 12H, 1,3,5,7-C*H*$_3$-Pn*), 2.02 (s, 6H, 2,6-C*H*$_3$-Pn*), 1.10 (d, ^3J = 6.6 Hz, 6H, CH(C*H*$_3$)$_2$), 0.79 (d, ^3J = 6.5 Hz, 6H, CH(C*H*$_3$)$_2$).

^{13}C{^{1}H} NMR (benzene-d_6, 298 K, 125 MHz): δ 173.3 (N*C*N), 134.2 (1,3,5,7 -Pn*), 131.9 (4,8-Pn*), 130.8 (4-*C*$_6$H$_4$), 130.6 (1-*C*$_6$H$_4$), 127.2 (2,3,5,6-*C*$_6$H$_4$), 126.0 (2,3,5,6-

C$_6$H$_4$), 125.7 (2,3,5,6-*C*$_6$H$_4$), 125.4 (2,3,5,6-*C*$_6$H$_4$), 109.5 (br, 2,6-*Pn**), 50.1 (*C*H(CH$_3$)$_2$), 26.0 (CH(*C*H$_3$)$_2$), 24.2 (CH(*C*H$_3$)$_2$), 12.6 (1,3,5,7-*C*H$_3$-Pn*), 12.1 (2,6-*C*H$_3$-Pn*).

7.6.8 Pn*ZrCl[(N^{i}Pr)$_2$C(4-^{t}Bu-C$_6$H$_4$)] (8)

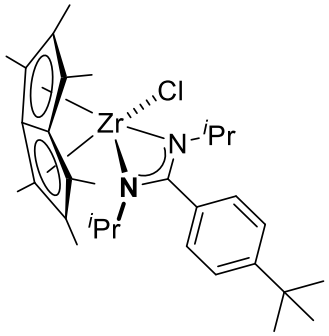

^{1}H NMR (benzene-d_6, 298 K, 400 MHz): δ 7.64 (d, ^3J = 8.0 Hz, 1H, 3,5-C$_6$*H*$_4$), 7.27 (d, ^3J = 8 Hz, 1H, 3,5-C$_6$*H*$_4$), 7.20 (d, ^3J = 8.0 Hz, 1H, 2,6-C$_6$*H*$_4$), 7.02 (d, ^3J = 7.8 Hz, 1H, 2,6-C$_6$*H*$_4$), 3.45 (p, ^3J = 6.2 Hz, 2H, C*H*(CH$_3$)$_2$), 2.16 (s, 12H, 1,3,5,7-C*H*$_3$-Pn*), 2.05 (s, 6H, 2,6-C*H*$_3$-Pn*), 1.16 (m, 15H, C(C*H*$_3$)$_3$ and CH(C*H*$_3$)$_2$), 0.90 (d, ^3J = 6.5 Hz, 6H, CH(C*H*$_3$)$_2$).

^{13}C{^{1}H} NMR (benzene-d_6, 298 K, 125 MHz): δ 175.8 (N*C*N), 151.8 (4-*C*$_6$H$_4$), 134.3 (1,3,5,7-*Pn**), 132.2 (4,8-*Pn**), 132.0 (1-*C*$_6$H$_4$), 127.6 (3,5-*C*$_6$H$_4$), 126.8 (3,5-*C*$_6$H$_4$), 126.4 (2,6-*C*$_6$H$_4$), 125.6 (2,6-*C*$_6$H$_4$), 109.5 (br, 2,6-*Pn**), 50.5 (*C*H(CH$_3$)$_2$), 35.0 (*C*(CH$_3$)$_3$), 31.7 (C(*C*H$_3$)$_3$), 26.6 (CH(*C*H$_3$)$_2$), 26.2 (CH(*C*H$_3$)$_2$), 13.0 (1,3,5,7-*C*H$_3$-Pn*), 12.4 (2,6-*C*H$_3$-Pn*).

7.6.9 Pn*ZrCl[[N(2,4,6-Me-C$_6$H$_2$)$_2$]CH] (9)

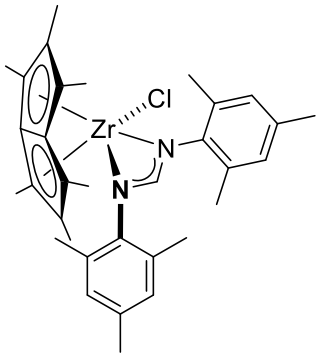

^{1}H NMR (benzene-d_6, 298 K, 400 MHz): δ 7.31 (s, 1H, NC*H*), 6.77 (s, 4H, C$_6$*H*$_2$), 2.36 (s, 12H, 1,3,5,7-C*H*$_3$-Pn*), 2.17 (s, 12H, 2,6-C*H*$_3$-C$_6$*H*$_2$), 1.80 (s, 6H, 2,6-C*H*$_3$-Pn*), 1.59 (s, 6H, 4-C*H*$_3$-C$_6$*H*$_2$).

^{13}C{^{1}H} NMR (benzene-d_6, 298 K, 125 MHz): δ 171.4 (N*C*N), 142.8 (1-C$_6$*H*$_2$), 133.4 (2,6-*Pn**), 133.3 (2,6-*Pn**), 129.7 (4,8-*Pn**), 112.8

(3,5-C_6H_2), 108.8 (1,3,5,7-*Pn**), 21.6 (2-C_6H_2), 20.8 (6-C_6H_2), 11.97 (1,3,5,7-*C*H_3-Pn*), 11.6 (2,6-*C*H_3-Pn*), 10.5 (4-C_6H_2).

7.6.10 General procedure for the synthesis of Pn*TiCl[(NR')$_2$CR]

[Pn*TiCl(μ–Cl)]$_2$ and K[(NR′)$_2$CH] were dissolved in benzene-d_6 (0.5 mL) in a J. Young's tap NMR tube. The reaction was left for 1 h at 25 °C and after this time Pn*Ti(Cl)[(NR′)$_2$CH] was formed in a spectroscopic yield superior to 90% as determined by ^{1}H NMR spectroscopy.

7.6.11 Pn*TiCl[[N(2,4,6-Me-C$_6$H$_2$)$_2$]CH]

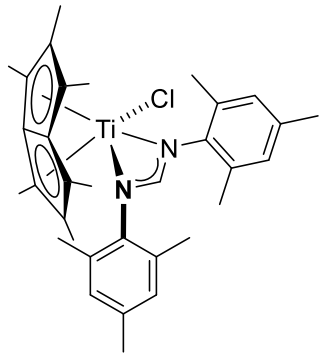

^{1}H NMR (benzene-d_6, 298 K, 400 MHz): δ 7.34 (s, 1H, NC*H*), 6.75 (s, 4H, 3,5-C_6H_2), 2.16 (s, 6H, 2,6-C*H*$_3$-C_6H_2), 2.03 (s, 6H, 1,3-C*H*$_3$-Pn*), 1.85 (s, 6H, 5,7-C*H*$_3$-Pn*), 1.74 (s, 6H, 2,6-C*H*$_3$-Pn*), 1.38 (s, 12H, 4-C*H*$_3$-C_6H_2).

^{13}C{^{1}H} NMR (benzene-d_6, 298 K, 125 MHz): δ 168.7 (N*C*N), 144.1 (1-C_6H_2), 134.2 (2,6-*Pn**), 133.2 (br, 4,8-*Pn**), 129.8 (br, 3,5-*C*$_6$H$_2$), 20.8 (2,6-*C*H_3-C_6H_2), 13.0 (1,3-*C*H_3-Pn*), 12.4 (5,7-*C*H_3-Pn*), 12.0 (2,6-*C*H_3-Pn*), 10.4 (4-*C*H_3-C_6H_2).

7.6.12 Pn*TiCl[[N(2,6-^{i}Pr-C$_6$H$_3$)$_2$]CH]

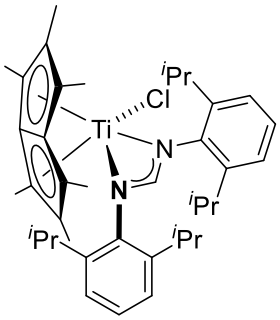

^{1}H NMR (benzene-d_6, 298 K, 400 MHz): δ 7.96 (s, 1H, NC*H*), 7.33 – 6.78 (m, 6H, 3,4,5-C$_6$H$_3$), 4.54 (p, 2H, C*H*(CH$_3$)$_2$), 3.04 (p, ^{3}J = 6.6 Hz, 2H, C*H*(CH$_3$)$_2$), 1.95 (s, 6H, 1,3-C*H*$_3$-Pn*), 1.82 (s, 6H, 5,7-C*H*$_3$-Pn*), 1.45 (d, ^{3}J = 6.6 Hz, 6H, CH(C*H*$_3$)$_2$), 1.42 (s, 6H, 2,6-C*H*$_3$-Pn*), 1.36 (d, ^{3}J = 6.7 Hz, 6H, CH(C*H*$_3$)$_2$), 1.23 (d, ^{3}J = 6.7 Hz, 6H, CH(C*H*$_3$)$_2$), 0.98 (d, ^{3}J = 6.6 Hz, 6H, CH(C*H*$_3$)$_2$).

^{13}C{^{1}H} NMR (benzene-d_6, 298 K, 125 MHz): δ 166.8 (N*C*N), 145.7 (1-*C*$_6$H$_3$), 144.0 (2-*C*$_6$H$_3$), 143.9 (6-*C*$_6$H$_3$), 141.4 (2,6-*Pn**), 137.4 (4,8-*Pn**), 134.0 (1,3,5,7-*Pn**), 125.7 (3-*C*$_6$H$_3$), 124.3 (5-*C*$_6$H$_3$), 123.6 (4-*C*$_6$H$_3$), 28.8 (*C*H(CH$_3$)$_2$), 28.5 (*C*H(CH$_3$)$_2$), 27.7 (CH(*C*H$_3$)$_2$), 27.5 (CH(*C*H$_3$)$_2$), 23.5 (CH(*C*H$_3$)$_2$), 23.4 (CH(*C*H$_3$)$_2$), 12.5 (1,3,5,7-*C*H$_3$-Pn*), 12.3 (2,6-*C*H$_3$-Pn*).

7.6.13 sMAO-Pn*ZrCl[(N^{i}Pr)$_2$C(4-OMe-C$_6$H$_4$)] (6$_{sMAO}$)

Isolated in 80% yield.

^{13}C CPMAS (10 kHz) δ (ppm): −7.6 (sMAO−*C*H$_3$), 11.7, 24.3, 73.4, 128.6 (sMAO−benzoate), 176.9 (sMAO−benzoate α-*C*(O)O).

^{27}Al DPMAS (15 kHz) δ (ppm): –241.7, –81.3, 88.5, 182.9, 326.3.

7.6.14 sMAO-Pn*Zr[(N^{i}Pr)$_2$C(4-CF$_3$-C$_6$H$_4$)] (7$_{sMAO}$)

Isolated in 89% yield.

^{13}C CPMAS (10 kHz) δ (ppm): −7.6 (sMAO−*C*H$_3$), 11.9, 24.5, 49.9, 73.5, 127.6 (sMAO−benzoate), 176.6 (sMAO−benzoate α-*C*(O)O).

^{27}Al DPMAS (15 kHz) δ (ppm): –241.7, –75.6, 79.1, 177.2, 331.9.

7.6.15 sMAO-Pn*ZrCl[(N^{i}Pr)$_2$C(4-^{t}Bu-C$_6$H$_4$)] (8$_{sMAO}$)

Isolated in 89% yield.

^{13}C CPMAS (10 kHz) δ (ppm): −8.0 (sMAO−*C*H$_3$), 11.4, 24.6, 50.0, 73.7, 127.7 (sMAO−benzoate), 177.2 (sMAO−benzoate α-*C*(O)O).

^{27}Al DPMAS (15 kHz) δ (ppm): –240.5, –91.3, 125.9, 269.4.

7.6.16 sMAO-Pn*ZrCl[(NMes)$_2$CH] (9$_{sMAO}$)

Isolated in 80% yield.

^{13}C CPMAS (10 kHz) δ (ppm): −7.3 (sMAO−*C*H$_3$), 10.6, 19.6, 24.9, 73.0, 128.8 (sMAO−benzoate), 177.3 (sMAO−benzoate α-*C*(O)O).

^{27}Al DPMAS (15 kHz) δ (ppm): –257.5, –97.0, 129.6, 290.1.

7.6.17 sMAO-Pn*Zr(OXyl)[(N^{i}Pr)$_2$C(C$_6$H$_5$)] (11$_{sMAO}$)

Isolated in 97% yield.

^{13}C CPMAS (10 kHz) δ (ppm): −7.7 (sMAO−*C*H$_3$), 10.6, 20.2, 50.5, 73.0, 91.1, 128.5 (sMAO−benzoate), 177.3 (sMAO−benzoate α-*C*(O)O).

^{27}Al DPMAS (15 kHz) δ (ppm): –355.6, –240.5, –91.3, 114.5, 275.0.

7.6.18 sMAO-Pn*ZrCl[(N^{p}Tol)$_2$CH] (12$_{sMAO}$)

Isolated in 95% yield.

^{13}C CPMAS (10 kHz) δ (ppm): −7.6 (sMAO *C*H$_3$), 10.3, 20.3, 128.5 (sMAO−benzoate), 136.7, 177.3 (sMAO−benzoate α-*C*(O)O).

^{27}Al DPMAS (15 kHz) δ (ppm): –361.3, –234.6, –90.8, 121.0, 253.4.

7.6.19 sMAO-Pn*Zr[(N^{p}Tol)$_2$CH]$_2$ (13$_{sMAO}$)

Isolated in 93% yield.

^{13}C CPMAS (10 kHz) δ (ppm): −8.2 (sMAO−*C*H$_3$), 10.0, 18.3, 90.4, 127.7 (sMAO−benzoate), 135.7, 176.3 (sMAO−benzoate α-*C*(O)O).

^{27}Al DPMAS (15 kHz) δ (ppm): –358.0, –220.3, –75.0, 157.0, 317.4.

7.7 References

1 J. P. Fackler, *Inorganic Syntheses*, Hoboken, NJ, USA, John Wiley., 1982.

2 T. M. Cameron, C. Xu, A. G. Dipasquale and A. L. Rheingold, *Organometallics*, 2008, **27**, 1596–1604.

3 G. A. Chesnokov, M. A. Topchiy, P. B. Dzhevakov, P. S. Gribanov, A. A. Tukov, V. N. Khrustalev, A. F. Asachenko and M. S. Nechaev, *Dalton Trans.*, 2017, **46**, 4331–4345.

4 R. T. Cooper, F. M. Chadwick, A. E. Ashley and D. O'Hare, *Organometallics*, 2013, **32**, 2228–2233.

5 Z. R. Turner, J.-C. Buffet and D. O'Hare, *Organometallics*, 2014, **33**, 3891–3903.

6 M. J. Monreal, R. K. Thomson, T. Cantat, N. E. Travia, B. L. Scott and J. L. Kiplinger, *Organometallics*, 2011, **30**, 2031–2038.

7 J. R. Dorgan, J. Janzen, D. M. Knauss, S. B. Hait, B. R. Limoges and M. H. Hutchinson, *J. Polym. Sci. Part B Polym. Phys.*, 2005, **43**, 3100–3111.

8 B. J. Cosier and A. M. Glazer, *J. Appl. Crystallogr.*, 1986, **19**, 105–107.

9 *CrysAlisPRO*, Oxford Diffraction /Agilent Technologies UK Ltd, Yarnton, England.

10 A. Altomare, G. Cascarano, C. Giacovazzo and A. Guagliardi, *J. Appl. Crystallogr.*, 1993, **26**, 343–350.

11 L. Palatinus and G. Chapuis, *J. Appl. Crystallogr.*, 2007, **40**, 786–790.

12 L. J. Farrugia, *J. Appl. Crystallogr.*, 1999, **32**, 837–838.

13 L. J. Farrugia, *J. Appl. Crystallogr.*, 2012, **45**, 849–854.

14 A. L. Spek, *J. Appl. Crystallogr.*, 2003, **36**, 7–13.

15 T. Wiedemann, G. Voit, A. Tchernook, P. Roesle, I. Göttker-Schnetmann and S. Mecking, *J. Am. Chem. Soc.*, 2014, **136**, 2078–2085.

16 P. Kenyon, M. Wörner and S. Mecking, *J. Am. Chem. Soc.*, 2018, **140**, 6685–6689.

17 F. M. Rabagliati, G. V Mardones, H. E. Muñoz and F. J. Rodríguez, *Polym. Int.*, 2008, **57**, 744–749.

APPENDIX

Supplementary Data for Chapters 2-6

Chapter 2

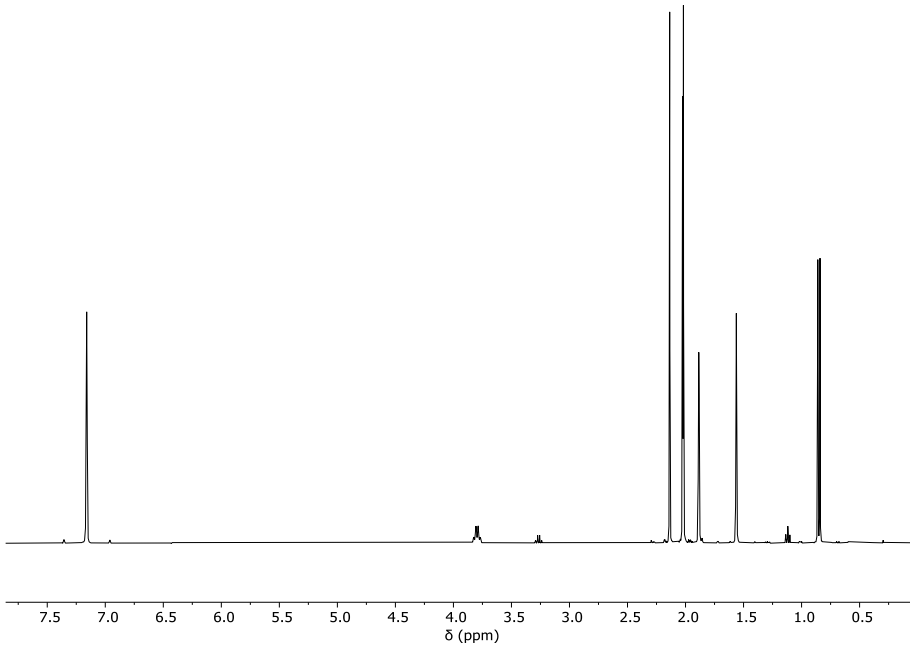

Figure A2.1. ^{1}H NMR spectrum of Pn*(H)TiCl$_3$ (**2**) (benzene-d_6, 298 K and 400 MHz).

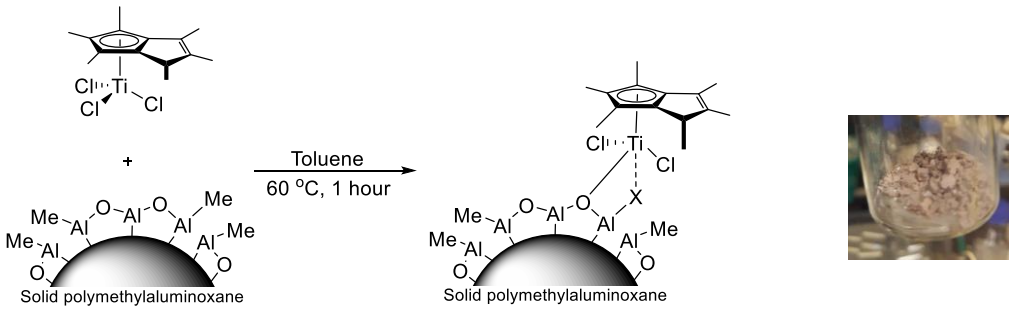

Figure A2.2. Complex immobilisation for solid catalyst based on solid methylaluminoxane (sMAO) and Pn*(H)TiCl$_3$ (**2**), sMAO- Pn*(H)TiCl$_3$ (**2$_{sMAO}$**).

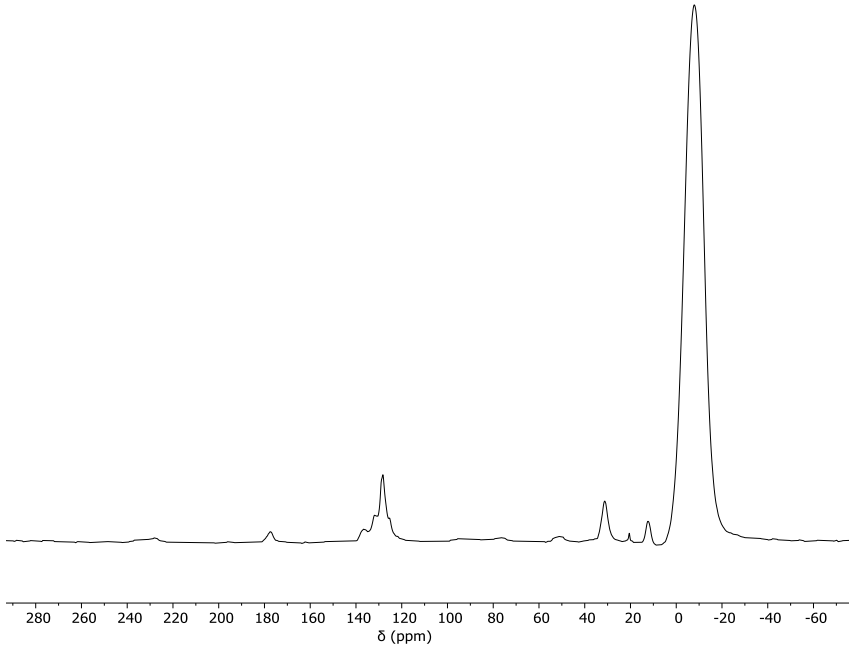

Figure A2.3 ^{13}C CP-MAS (10 kHz) NMR spectrum of sMAO-Cp*$TiCl_3$ (**1_{sMAO}**).

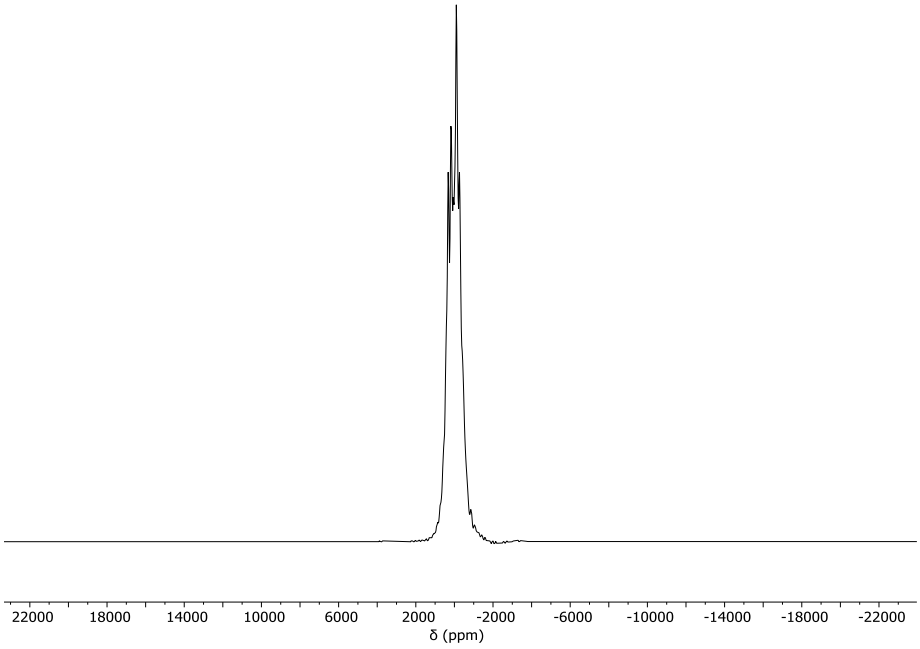

Figure A2.4. ^{27}Al DP-MAS (15 kHz) NMR spectrum of sMAO-Cp*$TiCl_3$ (**1_{sMAO}**).

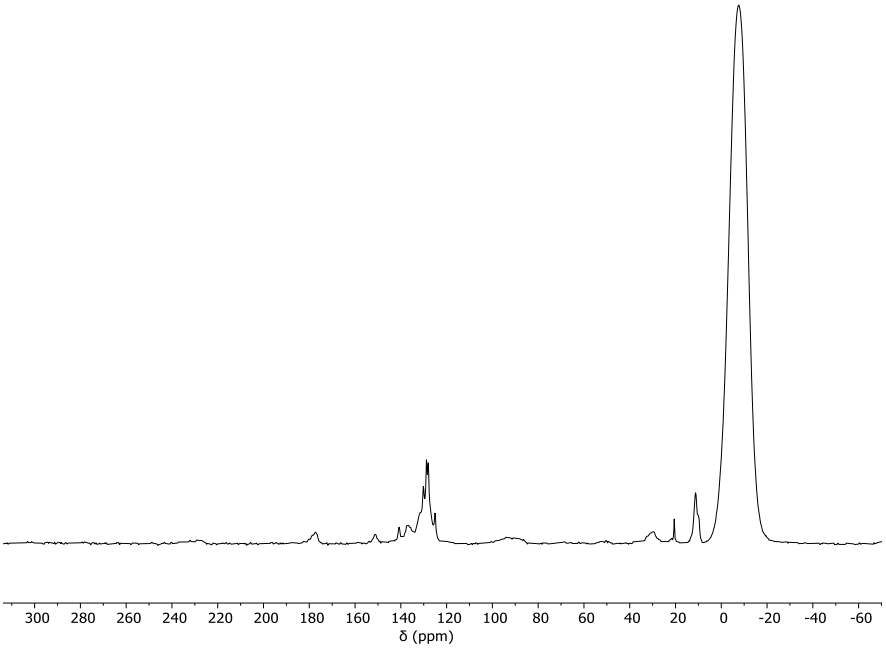

Figure A2.5. ^{13}C CP-MAS (10 kHz) NMR spectrum of sMAO-Pn*(H)$TiCl_3$ (**2$_{sMAO}$**).

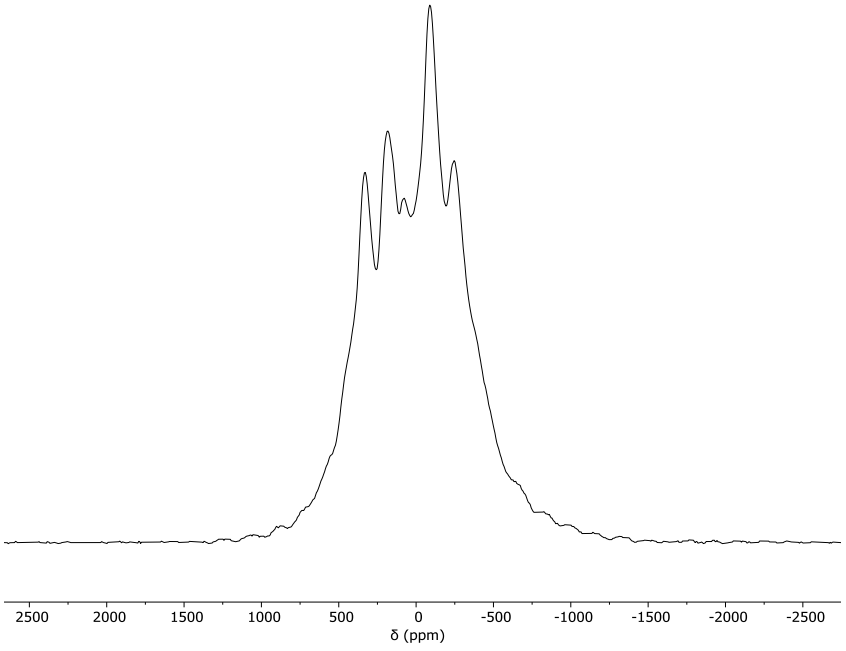

Figure A2.6. ^{27}Al DP-MAS (15 kHz) NMR spectrum of sMAO-Pn*(H)$TiCl_3$ (**2$_{sMAO}$**).

Table A2.1. Styrene homopolymerisation activities, temperature and mass of polymer with methylaluminoxane (MAO). Polymerisation conditions : 1 mL styrene, 5 mL of toluene, 1 hour, 1000 rpm 150 mg TiBA.

Temperature (°C)	Mass MAO (mg)		Mass polymer (mg)		Activity (kg_{PS}/mol/h)		Average activity (kg_{PS}/mol/h)
	1	2	1	2	1	2	
Dried MAO							
20	10	10.3	46	52	0.66	0.73	0.70
40	9.6	10.6	41	32	0.62	0.44	0.53
60	10.5	10.8	176	209	2.4	2.8	2.6
70	9.6	10.3	59	45	0.89	0.63	0.76
Solid MAO							
20	10.8	11.8	45	53	0.11	0.12	0.12
40	10.5	10.2	81	56	0.21	0.15	0.18
60	10	10.4	74	63	0.20	0.16	0.18
70	9.7	9.9	58	50	0.16	0.14	0.15

Table A2.2. Solution phase styrene homopolymerisation activities, temperature and mass of polymer using $CpTiCl_3$. Polymerisation conditions: 1 mL of toluene, 0.7 µmol of catalyst, 5 ml of toluene, 40 °C, 5 minutes, 1000 rpm.

MAO eq.	Catalyst (mg)	Mass polymer (mg)		Activity (kg_{PS}/mol_{Ti}/h)		Average activity (kg_{PS}/mol_{Ti}/h)
		1	2	1	2	
0	1.5	109	3	1912	53	983
200	1.5	88	99	1544	1737	1641
500	1.5	110	103	1930	1807	1869
1000	1.5	299	331	5246	5808	5527
2000	1.5	682	524	11966	9194	10580
5000	1.5	704	909	12352	15949	14151

Table A2.3. Solution phase styrene homopolymerisation activities, temperature and mass of polymer using Cp^*TiCl_3 (**1**). Polymerisation conditions: 10 minutes, 1000 rpm. 2 mL toluene, 2×10^{-7} mol catalyst, 1 mL styrene, $[Al_{MAO}]_0$:$[Ti]_0$ = 1500:1.

Solvent	Catalyst (mol)	Mass polymer (mg)		Activity (kg_{PS}/mol_{Ti}/h)		Average activity (kg_{PS}/mol_{Ti}/h)
		1	2	1	2	
Toluene	$0.2.10^{-6}$	141	102	4230	3060	3645
Benzene	$0.2.10^{-6}$	86	76	2580	2280	2430
Hexane	$0.2.10^{-6}$	100	107	3000	3210	3105
Pentane	$0.2.10^{-6}$	120	134	3600	4000	3800

Table A2.4. Solution phase styrene homopolymerisation activities, temperature and mass of polymer. Polymerisation conditions: 10 minutes, 1000 rpm. 2 mL toluene, 2×10^{-7} mol catalyst, 1 mL styrene, $[Al_{MAO}]_0$:$[Ti]_0$ = 1500:1.

Temperature (°C)	Catalyst (mol)	Mass polymer (mg)		Activity ($kg_{PS}/mol_{Ti}/h$)		Average activity ($kg_{PS}/mol_{Ti}/h$)
		1	2	1	2	
		Cp*TiCl$_3$ (1)				
40	$0.2.10^{-6}$	123	106	3690	3180	3435
55	$0.2.10^{-6}$	153	162	4590	4860	4725
70	$0.2.10^{-6}$	148	109	4440	3270	3855
		Pn*(H)TiCl$_3$ (2)				
40	$0.2.10^{-6}$	102	105	3060	3150	3105
55	$0.2.10^{-6}$	115	114	3450	3420	3435
70	$0.2.10^{-6}$	117	109	3510	3270	3390

Table A2.5. Slurry-phase styrene homopolymerisation activities, temperature, mass of catalyst and mass of polymer. Polymerisation conditions: 10 minutes, 1000 rpm. 50 mL toluene, 10 mg catalyst, 3.7 mL styrene, $[Al_{sMAO}]_0$:$[Ti]_0$ = 200:1, 150 mg TiBA.

Temperature (°C)	Mass catalyst (mg)		Mass polymer (mg)		Activity ($kg_{PS}/mol_{Ti}/h$)		Average activity ($kg_{PS}/mol_{Ti}/h$)
	1	2	1	2	1	2	
			sMAO-Cp*TiCl$_3$ (1$_{sMAO}$)				
40	10.1	10.3	342	340	2831	2762	2797
55	9.8	9.9	388	364	3307	3072	3189
70	10.4	10.1	404	375	3252	3104	3178
			sMAO-Pn*(H)TiCl$_3$ (1$_{sMAO}$)				
40	10	10	394	411	7268	7582	7425
55	10.3	10.3	378	451	6778	8087	7432
70	10.3	9.8	350	405	6276	7618	6947

Table A2.6. Solution phase ethylene homopolymerisation activities, temperature and mass of polymer. Polymerisation conditions: 30 minutes, 1000 rpm. 50 mL hexane, 2×10^{-7} mol catalyst, 2 bar ethylene, 150 mg TiBA, $[Al_{MAO}]_0$:$[Ti]_0$ = 1500:1.

Temperature (°C)	Catalyst (mol)	Mass polymer (mg)		Activity ($kg_{PE}/mol_{Ti}/h/bar$)		Average activity ($kg_{PE}/mol_{Ti}/h/bar$)
		1	2	1	2	
		Cp*TiCl$_3$ (1)				
40	$0.2.10^{-6}$	63	60	945	900	923
50	$0.2.10^{-6}$	49	53	735	795	765
60	$0.2.10^{-6}$	40	32	600	480	540
70	$0.2.10^{-6}$	32	40	480	600	540
80	$0.2.10^{-6}$	21	28	315	420	368
		Pn*(H)TiCl$_3$ (2)				
40	$0.2.10^{-6}$	67	59	1005	885	945
50	$0.2.10^{-6}$	49	45	735	75	705
60	$0.2.10^{-6}$	48	58	720	870	795
70	$0.2.10^{-6}$	56	62	840	930	885
80	$0.2.10^{-6}$	32	36	480	540	510

Table A2.7. Slurry-phase ethylene homopolymerisation activities, temperature, mass of catalyst and mas of polymer. Polymerisation conditions: 50 mL of hexane, $[Al_{sMAO}]_0$:$[Ti]_0$ = 200:1, 150 mg of TiBA, 2 bar ethylene, 30 minutes, 1000 rpm.

Temperature (°C)	Mass catalyst (mg)		Mass polymer (mg)		Activity ($kg_{PE}/mol_{Ti}/h/bar$)		Average activity ($kg_{PE}/mol_{Ti}/h/bar$)
	1	2	1	2	1	2	
sMAO-Cp*TiCl$_3$ (1_{sMAO})							
40	10.3	10.6	194	186	262	245	254
50	9.8	10	187	180	265	251	258
60	10.2	10.6	171	180	234	237	235
70	9.9	9.6	140	153	197	221	209
80	9.9	9.6	157	161	232	244	238
sMAO-Pn*(H)TiCl$_3$ (2_{sMAO})							
40	10.8	10.2	112	121	145	166	155
50	9.5	9.9	138	145	202	204	203
60	10.3	10	148	158	200	220	210
70	9.6	9.8	170	178	256	263	260
80	9.8	10.5	137	151	203	209	206

Table A2.8. Slurry-phase activities of copolymerisation of ethylene with styrene, solvent, mass of catalyst, volume of styrene and mass of polymer. Polymerisation conditions: 50 mL of hexane, 150 mg TiBA, $[Al_{sMAO}]_0$:$[Ti]_0$ = 200:1, 30 minutes, 1000 rpm, 40 °C.

Solvent	Mass catalyst (mg)		Styrene (µL)	Mass polymer (mg)		Activity ($kg_{polymer}/mol_{Ti}/h/bar$)		Average activity ($kg_{Polymer}/mol_{Ti}/h/bar$)
	1	2		1	2	1	2	
sMAO-Pn*(H)TiCl$_3$ (2_{sMAO})								
Benzene	9.9	10	125	15	18	22.9	27.2	25.1
Pentane	10.2	9.9	125	21	18	31.2	27.5	29.4
Toluene	10.1	10.3	125	28	25	41.3	36.2	38.8
Hexane	10.3	10.2	125	24	23	35.4	34.2	34.8

Table A2.9. Solution phase activities of copolymerisation of ethylene with styrene, temperature, volume of styrene and mass of polymer. Polymerisation conditions: 50 mL of toluene, 0.2 µmol of catalyst, $[Al_{MAO}]_0$:$[Ti]_0$ = 1500:1, 10 minutes, 1000 rpm, 150 mg TiBA.

Temperature (°C)	Catalyst (mol)	Styrene (µL)	Mass polymer (mg)		Activity ($kg_{polymer}/mol_{Ti}/h/bar$)		Average activity ($kg_{Polymer}/mol_{Ti}/h/bar$)
			1	2	1	2	
Cp*TiCl$_3$ (1)							
40	$0.2.10^{-6}$	125	52	35	780	525	653
50	$0.2.10^{-6}$	125	45	36	675	540	608
60	$0.2.10^{-6}$	125	44	69	660	1035	848
70	$0.2.10^{-6}$	125	23	41	398	615	507
80	$0.2.10^{-6}$	125	52	58	780	870	825
40	$0.2.10^{-6}$	62.5	32	50	480	750	615
40	$0.2.10^{-6}$	250	42	25	630	375	503
40	$0.2.10^{-6}$	500	41	35	615	525	570

Pn*(H)TiCl$_3$ (2)							
40	0.2.10^{-6}	125	24	14	360	210	285
50	0.2.10^{-6}	125	15	16	225	240	233
60	0.2.10^{-6}	125	19	27	285	405	345
70	0.2.10^{-6}	125	19	17	285	255	270
80	0.2.10^{-6}	125	29	25	421	351	386
40	0.2.10^{-6}	62.5	22	17	330	210	270
40	0.2.10^{-6}	250	22	19	330	285	308
40	0.2.10^{-6}	500	24	19	360	285	323

Table A2.10. Slurry-phase activities of copolymerisation of ethylene with styrene, temperature, mass of catalyst, volume of styrene and mass of polymer. Polymerisation conditions: 50 mL of hexane, $[Al_{sMAO}]_0$:$[Ti]_0$ = 200:1, 150 mg TiBA, 30 minutes, 1000 rpm.

Temperature (°C)	Mass catalyst (mg)		Styrene (µL)	Mass polymer (mg)		Activity ($kg_{polymer}/mol_{Ti}/h/bar$)		Average activity ($kg_{Polymer}/mol_{Ti}/h/bar$)
	1	2		1	2	1	2	
sMAO-Cp*TiCl$_3$ (1$_{sMAO}$)								
40	10.0	9.8	125	27	25	37.6	35.5	36.5
50	9.6	9.8	125	45	52	65.1	73.8	69.5
60	10.3	9.5	125	35	33	47.4	50.5	48.9
70	9.7	12.4	125	45	51	67.6	59.1	63.3
80	9.8	9.8	125	41	45	61.0	67.0	64.0
40	9.6	10.1	62.5	49	53	70.9	73.1	72.0
40	10.0	9.8	250	27	25	37.6	35.5	36.5
40	10.4	10.9	500	43	35	51.3	44.9	48.1
sMAO-Pn*(H)TiCl$_3$ (2$_{sMAO}$)								
40	10.3	10.2	125	14	14	20.6	20.8	20.7
50	9.9	9.6	125	20	16	28.2	23.2	25.7
60	9.6	9.9	125	8	10	11.6	14.1	12.8
70	9.5	9.5	125	12	15	17.6	22.0	19.8
80	9.9	9.9	125	16	10	22.5	14.1	18.3
40	10.4	10.1	62.5	29	19	38.9	26.2	32.6
40	10.4	9.7	250	9	12	12.1	17.2	14.7
40	10.1	11.1	500	15	10	20.7	12.6	16.7

Table A2.11. Styrene homopolymerisation molecular weights. Polymerisation conditions: solution phase: 2 mL of toluene, 0.2 µmol of catalyst, $[Al_{MAO}]_0$:$[Ti]_0$ = 1500:1, 10 minutes. Slurry-phase: 10 mg of catalyst, 50 mL of toluene, $[Al_{sMAO}]_0$:$[Ti]_0$ = 200:1, 150 mg TiBA, 10 minutes.

Temperature (°C)	M_w (g/mol)	Đ
Cp*TiCl$_3$ (1)		
40	9247	1.81
55	9398	1.99
70	10839	1.63
Pn*(H)TiCl$_3$ (2)		
40	10852	2.02
55	10728	2.06
70	10830	2.08

sMAO-Cp*TiCl$_3$ (1$_{sMAO}$)		
40	8677	1.87
55	10093	1.70
70	9945	1.73
sMAO-Pn*(H)TiCl$_3$ (2$_{sMAO}$)		
40	9425	1.93
55	9748	1.76
70	8887	1.83

Table A2.12. Ethylene homopolymerisation molecular weights. Polymerisation conditions: 150 mg of TiBA, 2 bar ethylene, 30 minutes, 1000 rpm. Solution phase: 50 mL of hexane, 0.2 µmol of catalyst, $[Al_{MAO}]_0$:$[Ti]_0$ = 1500:1. Slurry-phase: 10 mg of catalyst, 50 mL of hexane, $[Al_{sMAO}]_0$:$[Ti]_0$ = 200:1.

Temperature (°C)	M_w (g/mol)		M_n (g/mol)		Đ	
sMAO-Cp*TiCl$_3$ (1$_{sMAO}$)						
40	500	500	300	300	1.9	1.8
50	500	500	300	300	1.8	1.7
60	500	500	300	300	1.6	1.8
70	500	500	300	300	1.9	1.9
80	600	600	300	300	2.2	2.2
sMAO-Pn*(H)TiCl$_3$ (2$_{sMAO}$)						
50	500	500	300	300	1.7	1.7
60	700	600	400	400	1.9	1.5
70	600	600	300	400	1.7	1.5
80	800	800	500	500	1.6	1.7

Table A2.13. Ethylene/styrene copolymerisation molecular weights. Polymerisation conditions: 150 mg of TiBA, 2 bar ethylene, 30 minutes, 1000 rpm. Solution phase: 50 mL of hexane, 0.2 µmol of catalyst, $[Al_{MAO}]_0$:$[Ti]_0$ = 1500:1. Slurry-phase: 10 mg of catalyst, 50 mL of hexane, $[Al_{sMAO}]_0$:$[Ti]_0$ = 200:1.

Temperature (°C)	Styrene (µL)	M_w (×10^6 g/mol)		M_n (×10^3 g/mol)		Đ	
Cp*TiCl$_3$ (1)							
40	500	2.06	2.13	723.5	731.0	2.9	2.9
Pn*(H)TiCl$_3$ (2)							
60	125	1.72	1.86	307.9	303.8	5.6	6.1
sMAO-Cp*TiCl$_3$ (1$_{sMAO}$)							
40	125	2.18	2.08	14.8	15.1	148	138

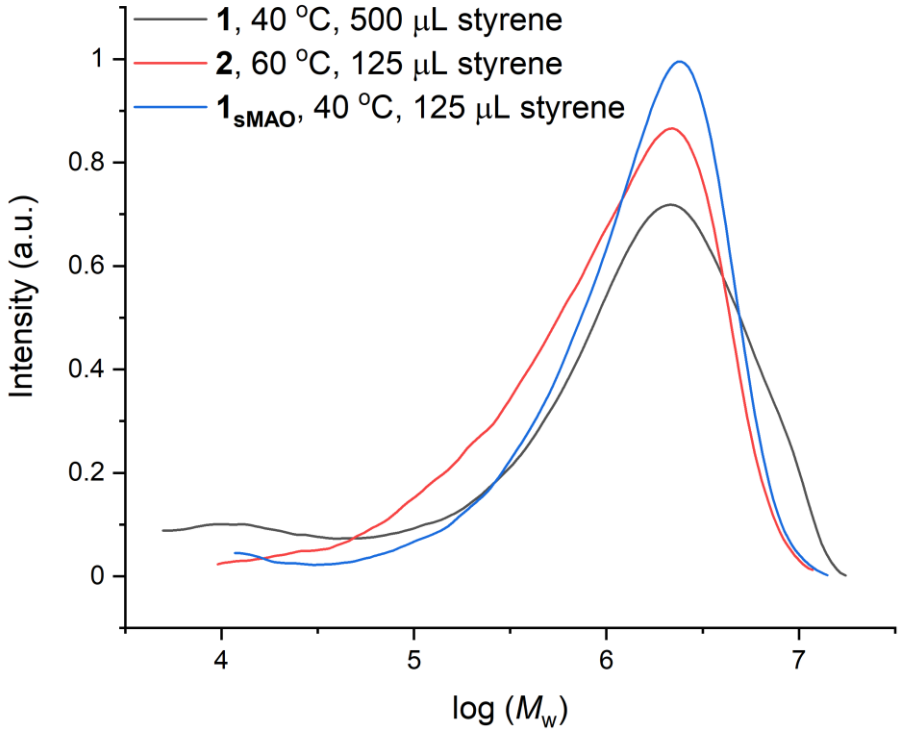

Figure A2.7. Molecular weight distributions for copolymerisation of ethylene with styrene. Polymerisation conditions: 150 mg of TiBA, 2 bar ethylene, 30 minutes, 1000 rpm. Solution phase: 50 mL of hexane, 0.2 μmol of catalyst, $[Al_{MAO}]_0$:$[Ti]_0$ = 1500:1. Slurry-phase: 10 mg of catalyst, 50 mL of hexane, $[Al_{sMAO}]_0$:$[Ti]_0$ = 200:1.

Table A2.14. Ethylene/styrene copolymerisation melting temperature and enthalpy. Polymerisation conditions: 30 minutes, 1000 rpm. 50 mL hexane. Solution: 2×10^{-7} mol catalyst, 2 bar ethylene, 150 mg TiBA, $[Al_{MAO}]_0$:$[Ti]_0$ = 1500:1. Slurry: 10 mg catalyst, 2 bar ethylene, 150 mg TiBA, $[Al_{sMAO}]_0$:$[Ti]_0$ = 200:1.

Temperature (°C)	Styrene (µL)	T_m (°C)	ΔH_m (J/g)
Cp^*TiCl_3 (1)			
40	125	131.9	80.5
50	125	130.6	68.3
60	125	134.0	121.5
70	125	131.0	61.2
80	125	131.6	71.7
40	62.5	131.9	68.0
40	250	129.9	58.2
40	500	128.5	60.3
$Pn^*(H)TiCl_3$ (2)			
40	125	129.2	16.4
50	125	130.6	34.1
60	125	131.9	50.6
70	125	130.5	32.5
80	125	132.2	32.5
40	62.5	128.7	29.7
40	250	129.8	35.8
40	500	129.8	45.0
sMAO-Cp^*TiCl_3 (1_{sMAO})			
40	125	130.8	73.2
50	125	131.3	83.5
60	125	132.5	111.4
70	125	131.3	82.2
80	125	131.8	64.3
40	62.5	132.5	94.5
40	250	130.7	102.1
40	500	128.0	71.1
sMAO-$Pn^*(H)TiCl_3$ (2_{sMAO})			
40	125	134.8	127.3
50	125	133.2	94.4
60	125	133.0	144.0
70	125	132.8	78.6
80	125	134.1	126.8
40	62.5	129.0	45.6
40	250	131.1	12.2
40	500	136.3	167.6

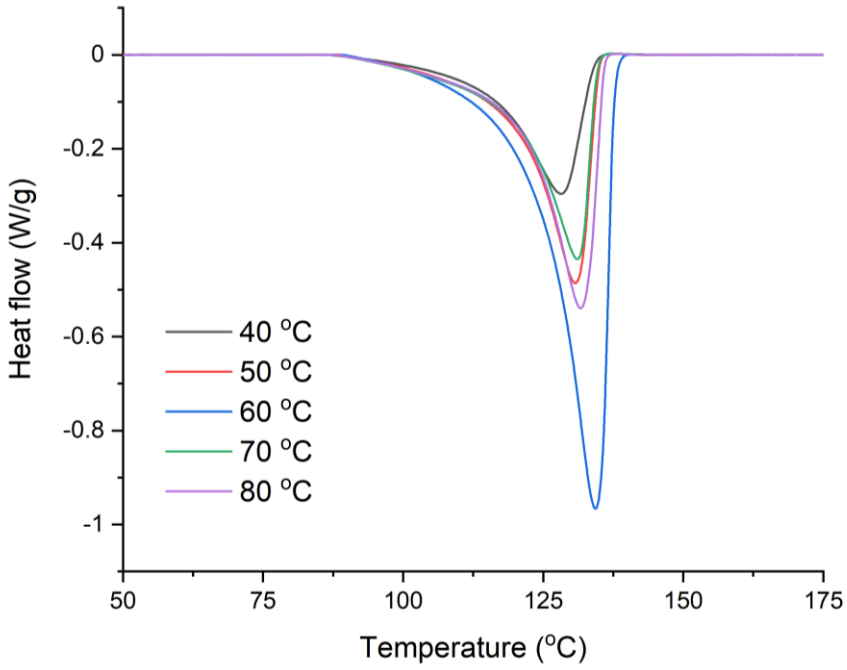

Figure A2.8. DSC plots of ethylene/styrene copolymers produced by Cp*$TiCl_3$ (**1**). Polymerisation conditions: 30 minutes, 1000 rpm. 50 mL hexane, 2×10^{-7} mol catalyst, 2 bar ethylene, 150 mg TiBA, $[Al_{MAO}]_0$:$[Ti]_0$ = 1500:1, 125 µL styrene.

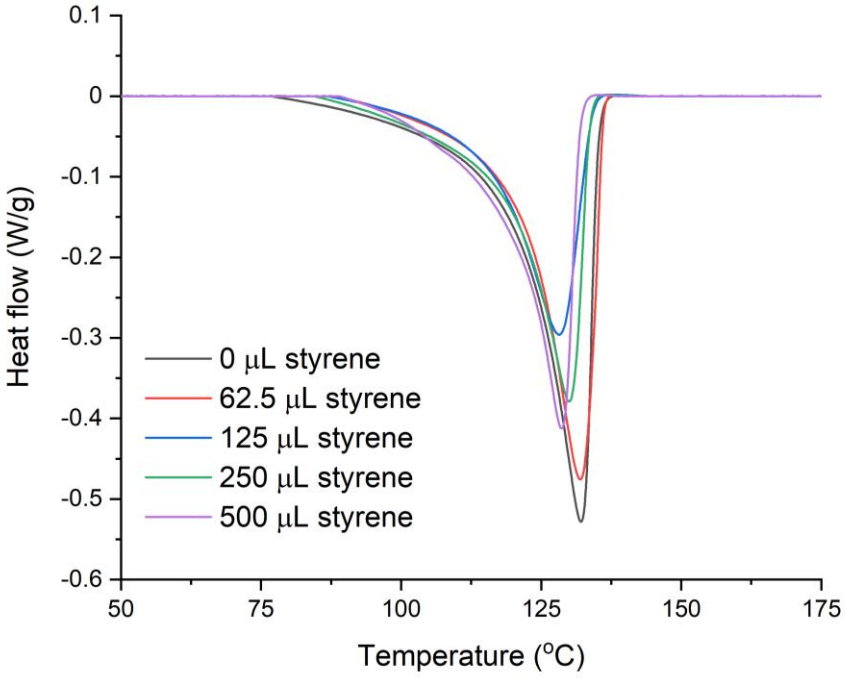

Figure A2.9. DSC plots of ethylene/styrene copolymers produced by Cp*$TiCl_3$ (**1**). Polymerisation conditions: 30 minutes, 1000 rpm. 50 mL hexane, 2×10^{-7} mol catalyst, 2 bar ethylene, 150 mg TiBA, $[Al_{MAO}]_0$:$[Ti]_0$ = 1500:1, 40 °C.

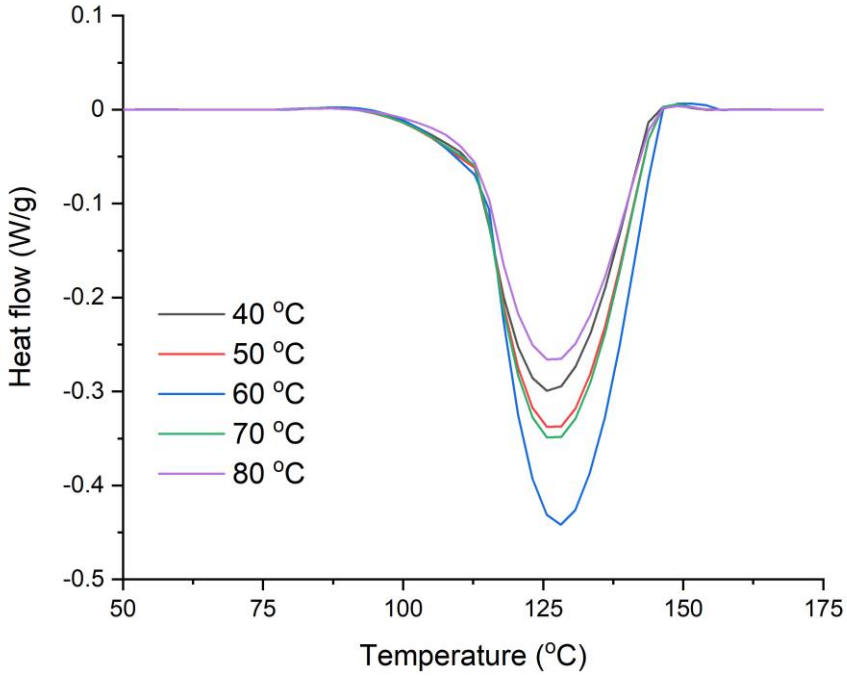

Figure A2.10. DSC plots of ethylene/styrene copolymers produced by sMAO-Cp*(H)$TiCl_3$ (**1$_{sMAO}$**). Polymerisation conditions: 30 minutes, 1000 rpm. 50 mL hexane, 10 mg catalyst, 2 bar ethylene, 150 mg TiBA, $[Al_{sMAO}]_0$:$[Ti]_0$ = 200:1, 125 µL styrene.

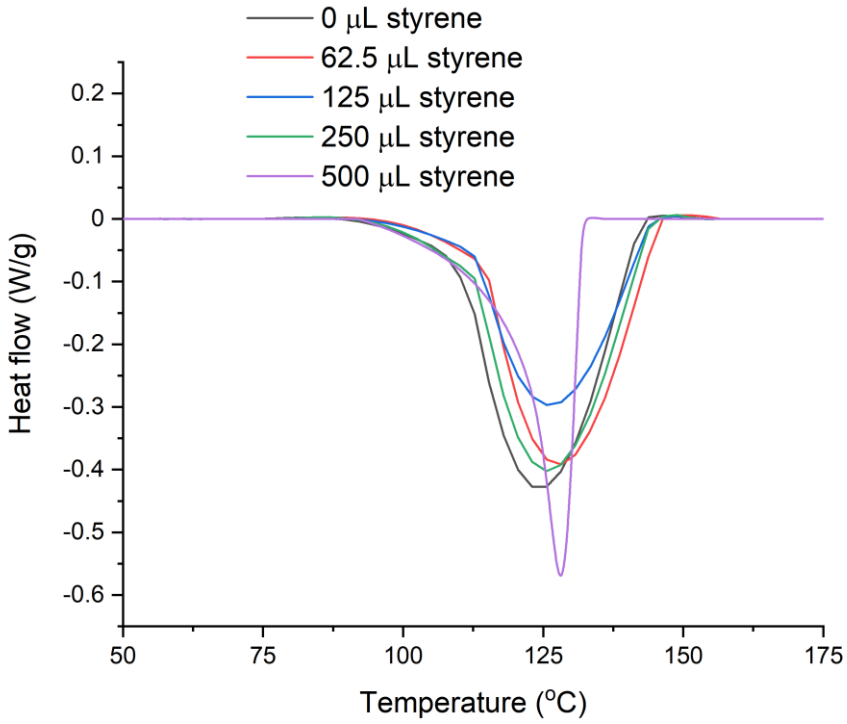

Figure A2.11. DSC plots of ethylene/styrene copolymers produced by sMAO-Cp*(H)$TiCl_3$ (**1$_{sMAO}$**). Polymerisation conditions: 30 minutes, 1000 rpm. 50 mL hexane, 10 mg catalyst, 2 bar ethylene, 150 mg TiBA, $[Al_{sMAO}]_0$:$[Ti]_0$ = 200:1, 40 °C.

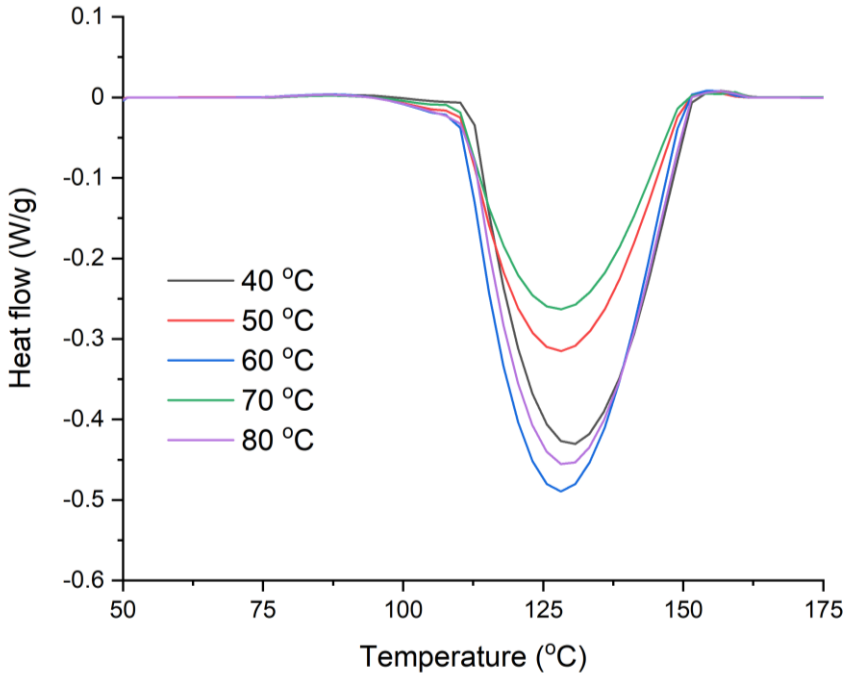

Figure A2.12. DSC plots of ethylene/styrene copolymers produced by sMAO-Pn*(H)$TiCl_3$ (**2$_{sMAO}$**). Polymerisation conditions: 30 minutes, 1000 rpm. 50 mL hexane, 10 mg catalyst, 2 bar ethylene, 150 mg TiBA, $[Al_{sMAO}]_0$:$[Ti]_0$ = 200:1, 125 µL styrene.

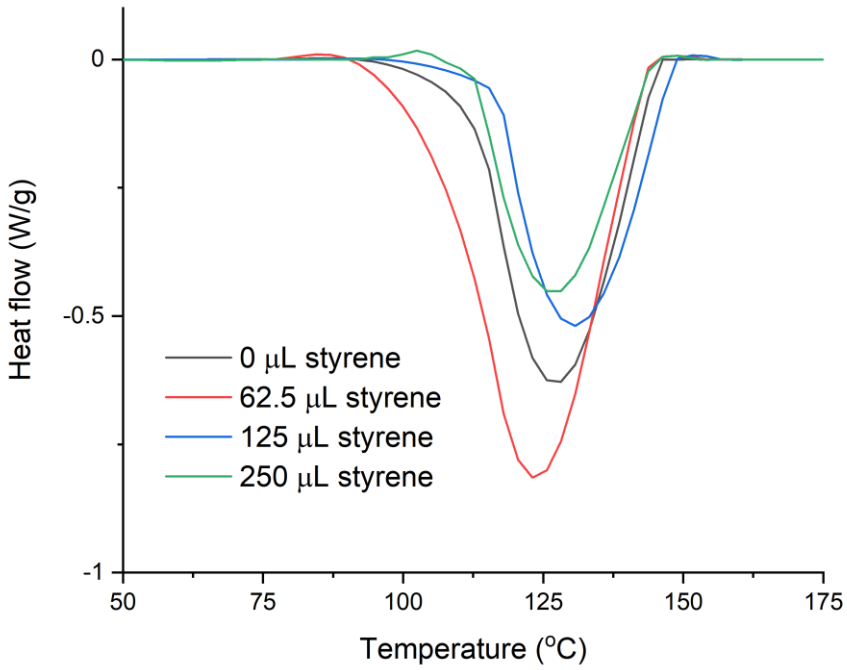

Figure A2.13. DSC plots of ethylene/styrene copolymers produced by sMAO-Pn*(H)$TiCl_3$ (**2$_{sMAO}$**). Polymerisation conditions: 30 minutes, 1000 rpm. 50 mL hexane, 10 mg catalyst, 2 bar ethylene, 150 mg TiBA, $[Al_{sMAO}]_0$:$[Ti]_0$ = 200:1, 40 °C.

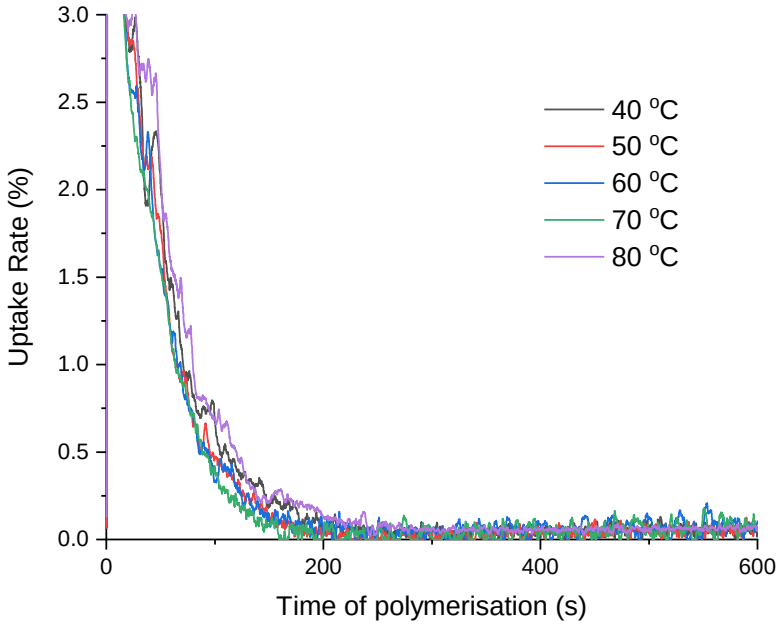

Figure A2.14. Homopolymerisation ethylene uptake rate plots for Cp*$TiCl_3$ (**1**); 50 mL of hexane, 0.2 µmol of catalyst, $[Al_{MAO}]_0$:$[Ti]_0$ = 1500:1, 150 mg of TiBA, 2 bar ethylene, 10 minutes, 1000 rpm.

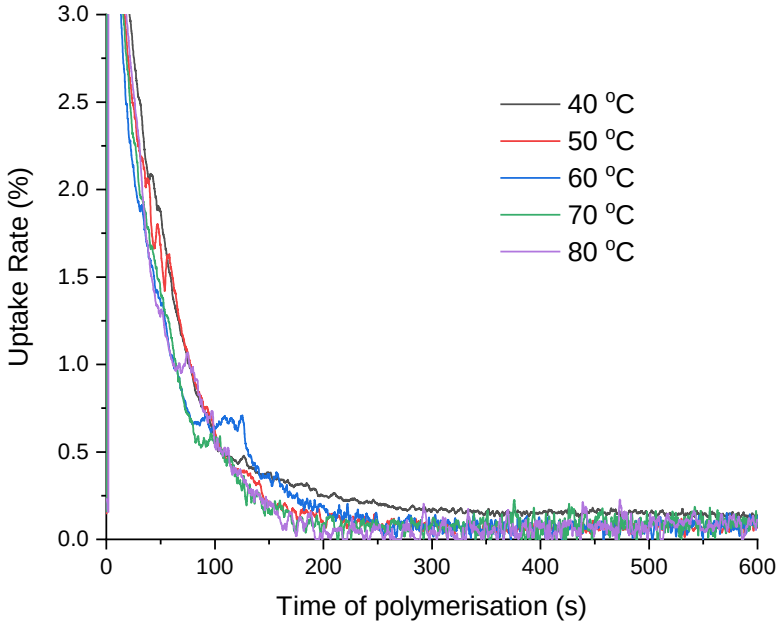

Figure A2.15. Homopolymerisation ethylene uptake rate plots for Pn*(H)$TiCl_3$ (**2**); 50 mL of hexane, 0.2 µmol of catalyst, $[Al_{MAO}]_0$:$[Ti]_0$ = 1500:1, 150 mg of TiBA, 2 bar ethylene, 10 minutes, 1000 rpm.

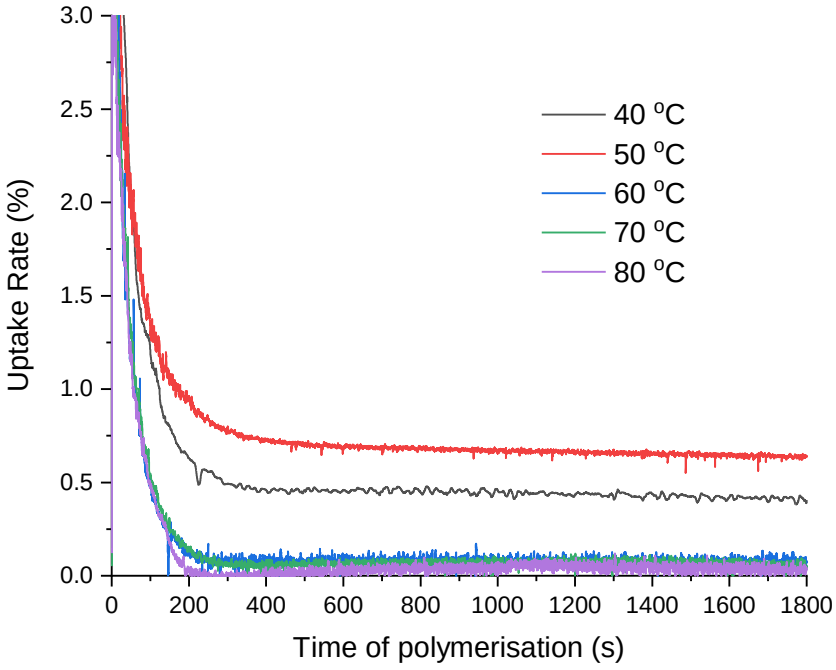

Figure A2.16. Homopolymerisation ethylene uptake rate plots for sMAO-Cp*$TiCl_3$ (**1_{sMAO}**); 10 mg of catalyst, 50 mL of hexane, $[Al_{sMAO}]_0$:$[Ti]_0$ = 200:1, 150 mg of TiBA, 2 bar ethylene, 30 minutes, 1000 rpm.

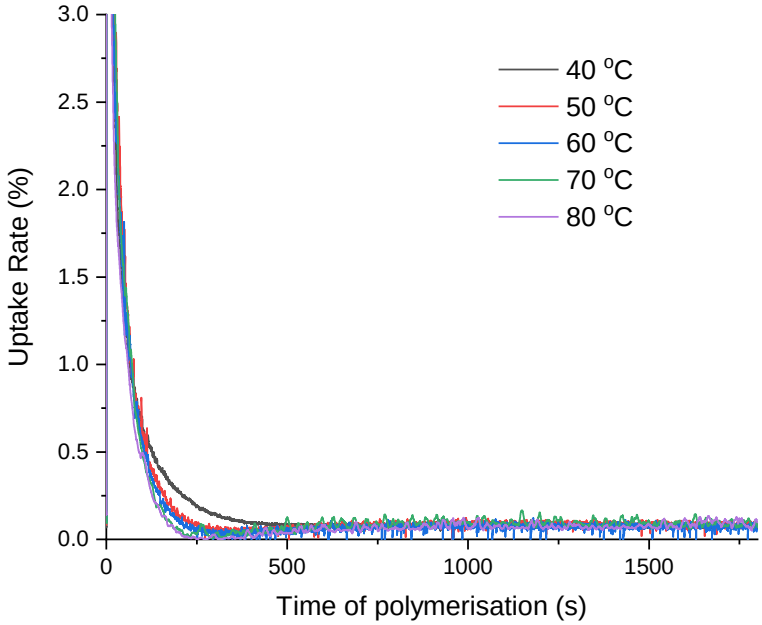

Figure A2.17. Homopolymerisation ethylene uptake rate plots for sMAO-Pn*(H)$TiCl_3$ (**2_{sMAO}**); 10 mg of catalyst, 50 mL of hexane, $[Al_{sMAO}]_0$:$[Ti]_0$ = 200:1, 150 mg of TiBA, 2 bar ethylene, 30 minutes, 1000 rpm.

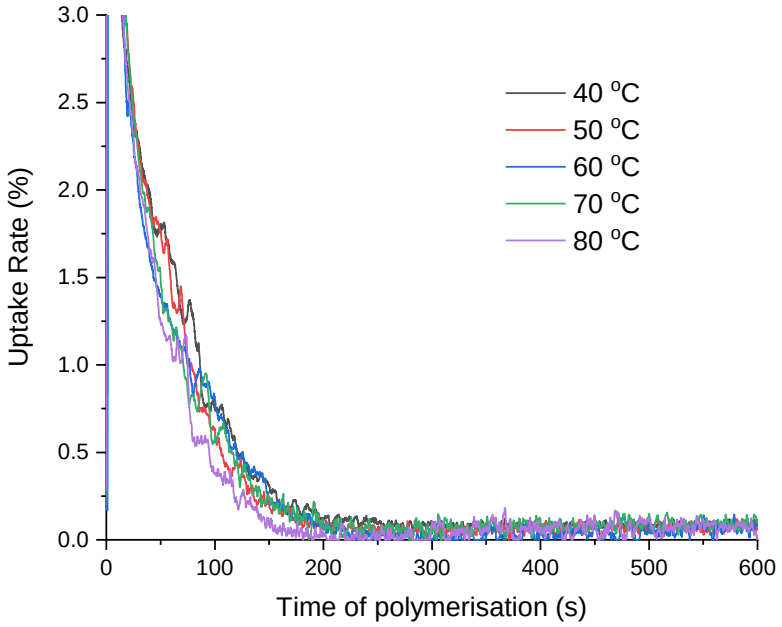

Figure A2.18. Copolymerisation ethylene uptake rate plots for Cp*$TiCl_3$ (**1**); 50 mL of hexane, 0.2 µmol of catalyst, 125 µL of styrene, $[Al_{MAO}]_0$:$[Ti]_0$ = 1500:1, 150 mg of TiBA, 2 bar ethylene, 10 minutes, 1000 rpm.

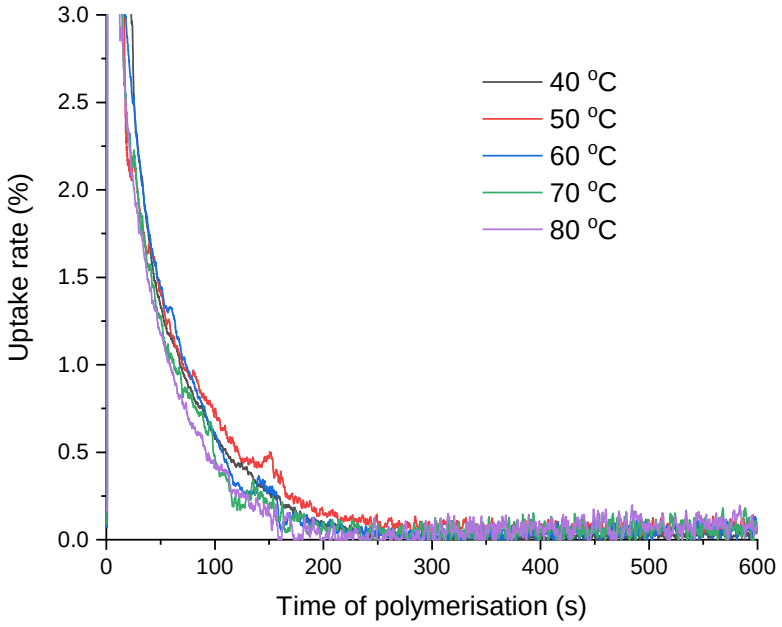

Figure A2.19. Copolymerisation ethylene uptake rate plots for Pn*(H)$TiCl_3$ (**2**); 50 mL of hexane, 0.2 µmol of catalyst, 125 µL of styrene, $[Al_{MAO}]_0$:$[Ti]_0$ = 1500:1, 150 mg of TiBA, 2 bar ethylene, 10 minutes, 1000 rpm.

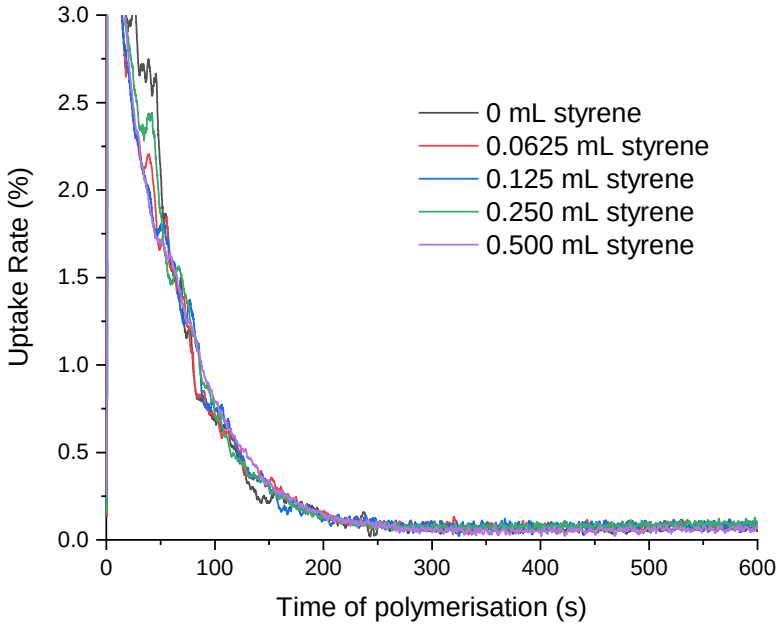

Figure A2.20. Copolymerisation ethylene uptake rate plots for Cp*$TiCl_3$ (**1**); 50 mL of hexane, 0.2 µmol of catalyst, 40 °C, $[Al_{MAO}]_0$:$[Ti]_0$ = 1500:1, 150 mg of TiBA, 2 bar ethylene, 10 minutes, 1000 rpm.

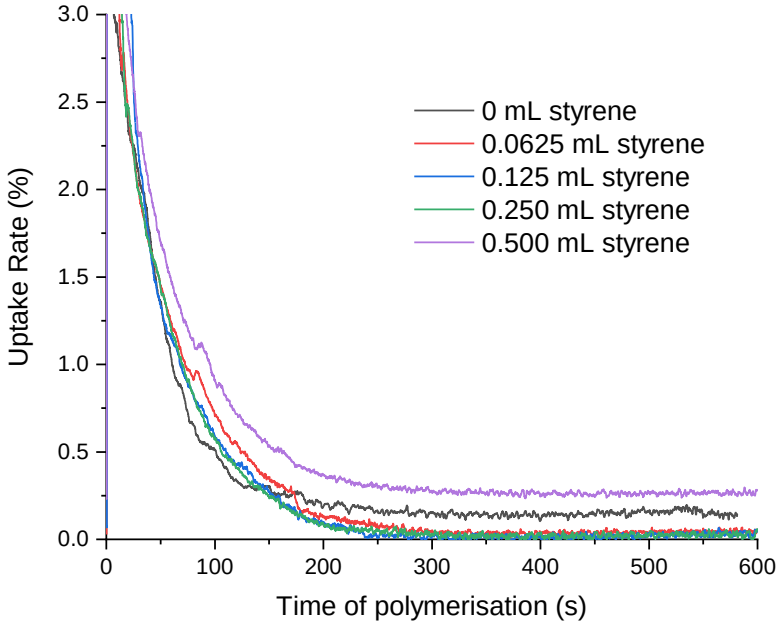

Figure A2.21. Copolymerisation ethylene uptake rate plots for Pn*(H)$TiCl_3$ (**2**); 50 mL of hexane, 0.2 µmol of catalyst, 40 °C, $[Al_{MAO}]_0$:$[Ti]_0$ = 1500:1, 150 mg of TiBA, 2 bar ethylene, 10 minutes, 1000 rpm.

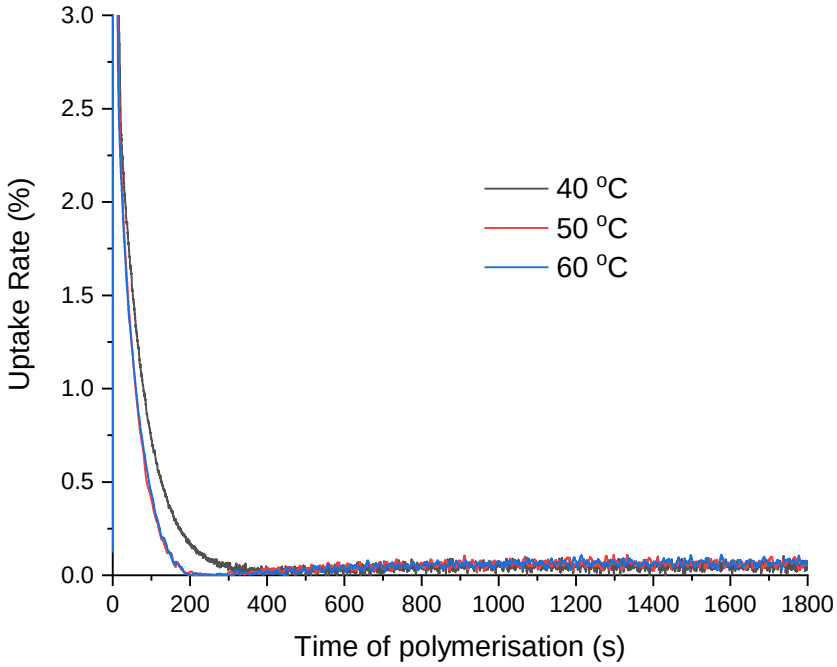

Figure A2.22. Copolymerisation ethylene uptake rate plots for sMAO-Cp*TiCl$_3$ (**1$_{sMAO}$**); 10 mg of catalyst, 125 µL styrene, 50 mL of hexane, [Al$_{sMAO}$]$_0$:[Ti]$_0$ = 200:1, 150 mg of TiBA, 2 bar ethylene, 30 minutes, 1000 rpm.

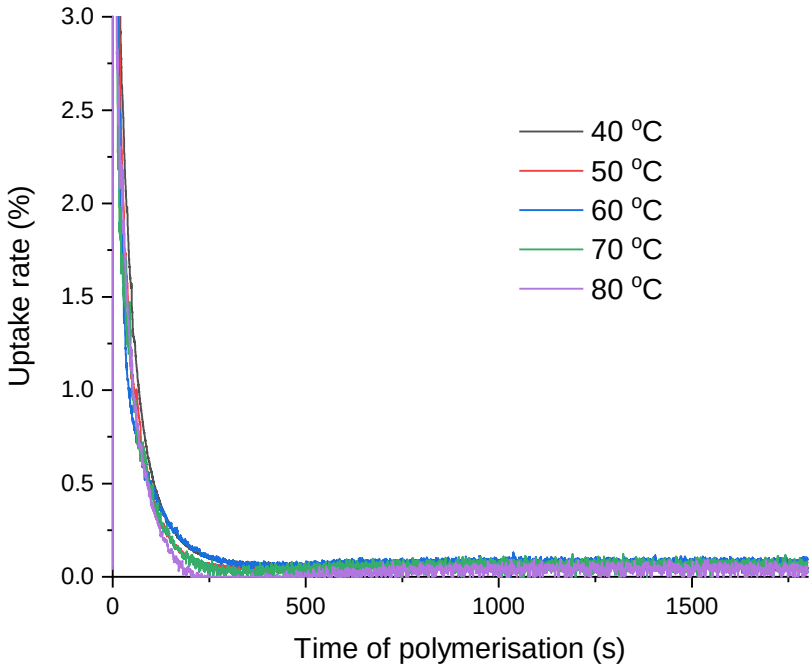

Figure A2.23. Copolymerisation ethylene uptake rate plots for sMAO-Pn*(H)TiCl$_3$ (**2$_{sMAO}$**); 10 mg of catalyst, 125 µL styrene, 50 mL of hexane, [Al$_{sMAO}$]$_0$:[Ti]$_0$ = 200:1, 150 mg of TiBA, 2 bar ethylene, 30 minutes, 1000 rpm.

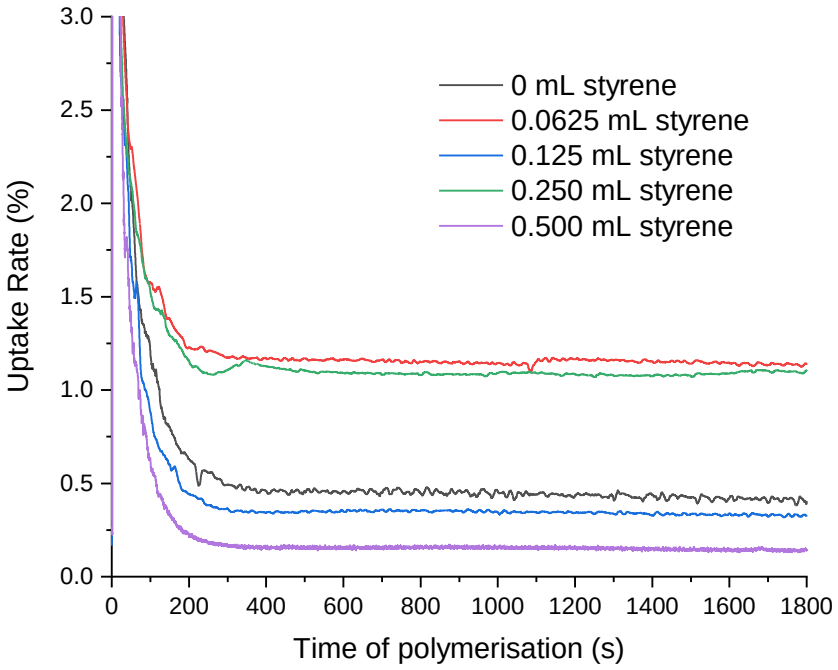

Figure A2.243. Copolymerisation ethylene uptake rate plots for sMAO-Cp*$TiCl_3$ (**1_{sMAO}**); 10 mg of catalyst, 50 mL of hexane, $[Al_{sMAO}]_0$:$[Ti]_0$ = 200:1, 150 mg of TiBA, 2 bar ethylene, 40 °C, 30 minutes, 1000 rpm.

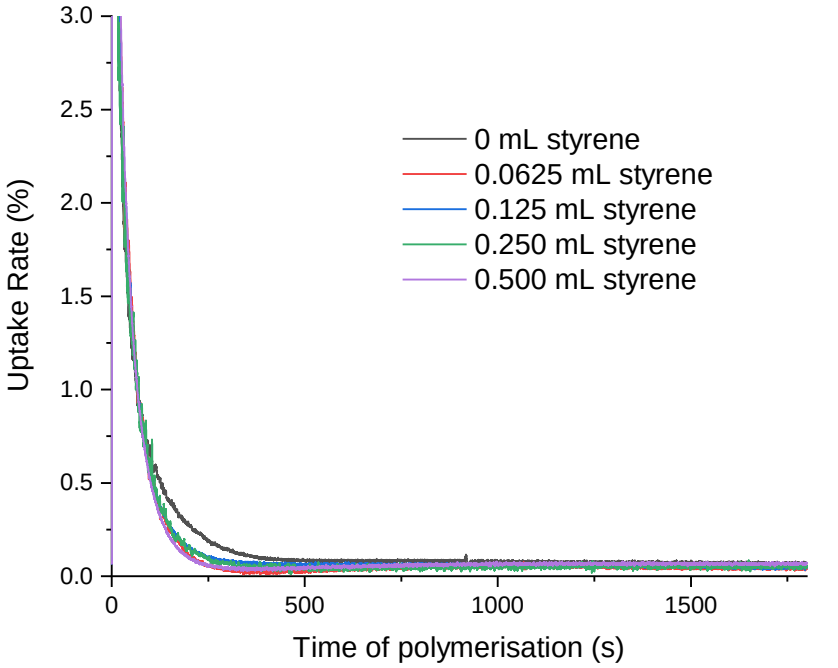

Figure A2.25. Copolymerisation ethylene uptake rate plots for sMAO-Pn*(H)$TiCl_3$ (**2_{sMAO}**); 10 mg of catalyst, 50 mL of hexane, $[Al_{sMAO}]_0$:$[Ti]_0$ = 200:1, 150 mg of TiBA, 2 bar ethylene, 40 °C, 30 minutes, 1000 rpm.

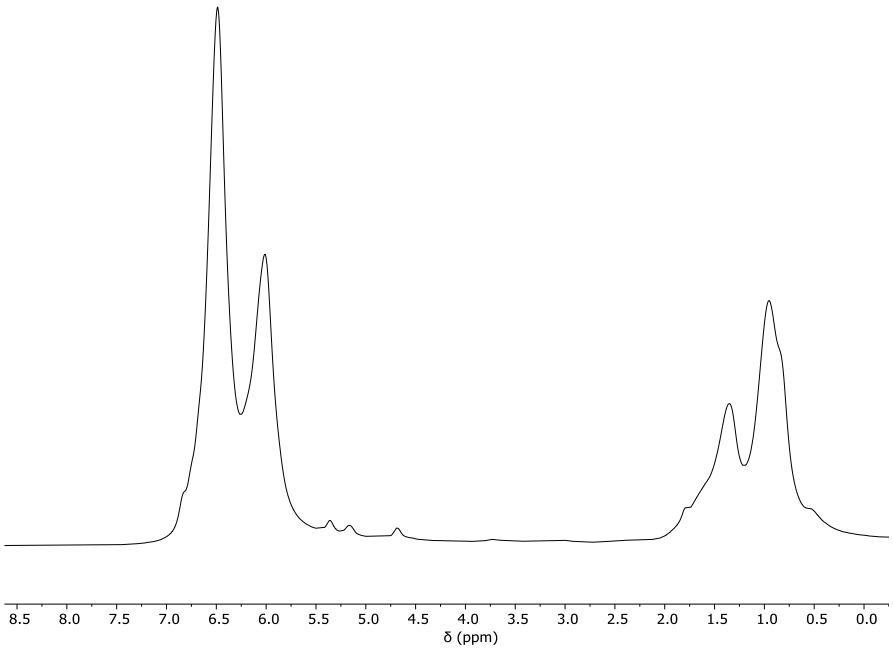

Figure A2.26. ^{1}H NMR spectrum of the polystyrene produced by Cp*TiCl$_3$ (**1**), 1 mL of styrene, 0.7 µmol of catalyst, 2 ml of toluene, 40 °C, 10 minutes, 1000 rpm (chloroform-*d*$_1$, 400 MHz, 298 K).

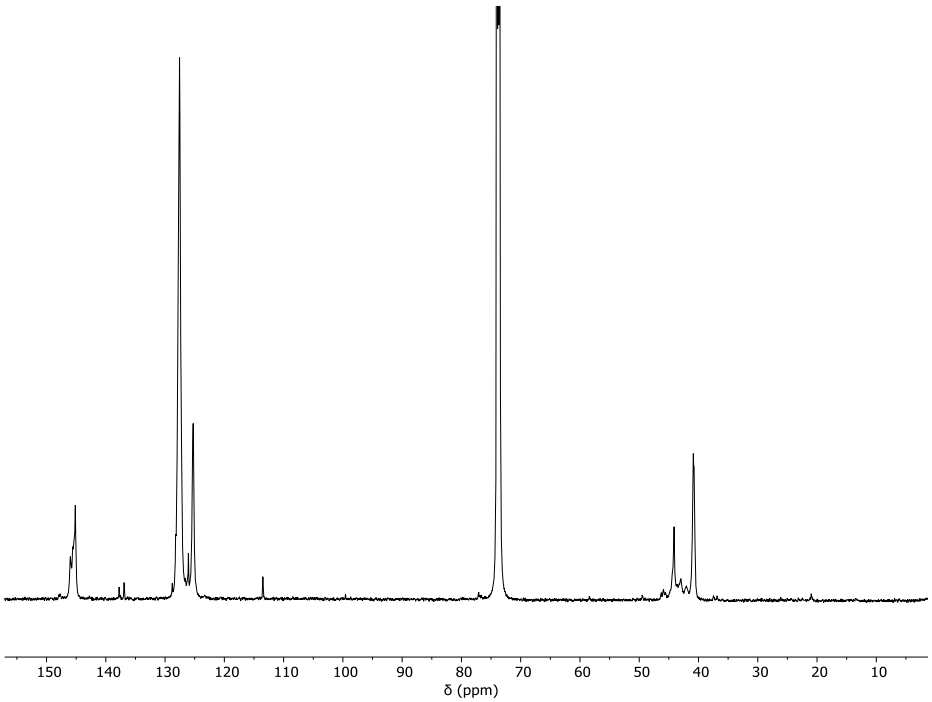

Figure A2.27. ^{13}C{^{1}H} NMR spectrum of the polystyrene produced by Cp*TiCl$_3$ (**1**), 1 mL of styrene, 0.7 µmol of catalyst, 2 ml of toluene, 40 °C, 10 minutes, 1000 rpm (chloroform-*d*$_1$, 125 MHz, 298 K).

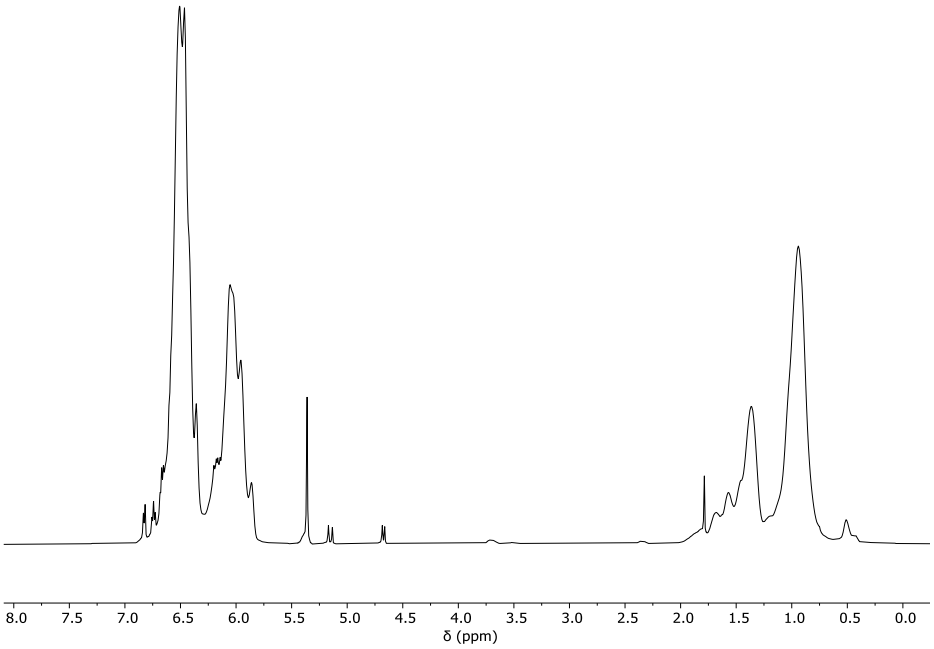

Figure A2.28. ^{1}H NMR spectrum of the polystyrene produced by Pn*(H)$TiCl_3$ (**2**), 1 mL of styrene, 0.7 µmol of catalyst, 2 ml of toluene, 40 °C, 10 minutes, 1000 rpm (chloroform-d_1, 400 MHz, 298 K).

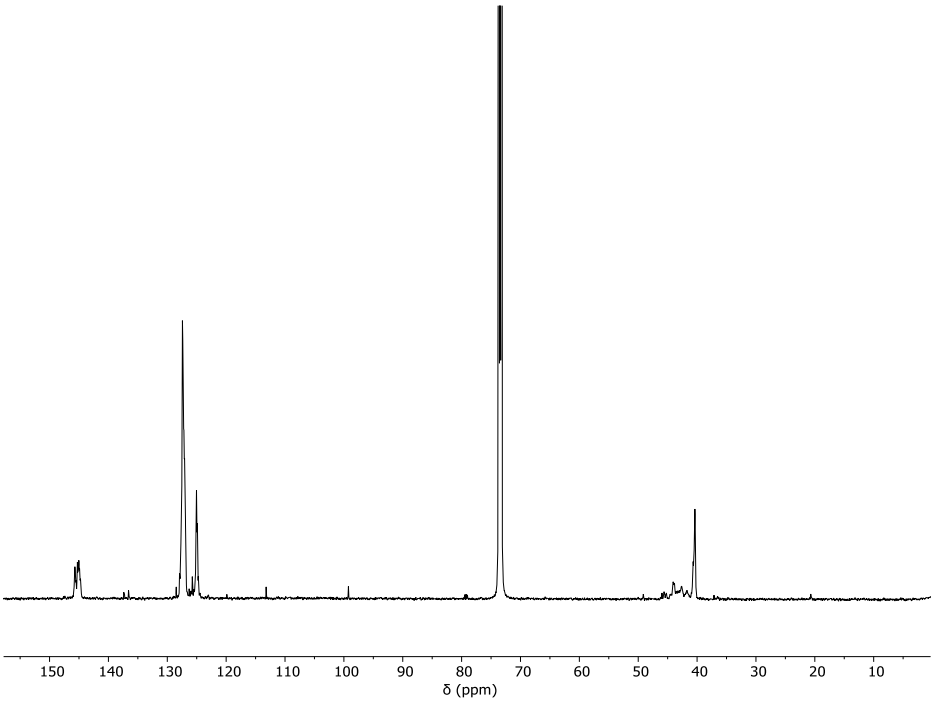

Figure A2.29. ^{13}C{^{1}H} NMR spectrum of the polystyrene produced by Pn*(H)$TiCl_3$ (**2**), 1 mL of styrene, 0.7 µmol of catalyst, 2 ml of toluene, 40 °C, 10 minutes, 1000 rpm (chloroform-d_1, 125 MHz, 298 K).

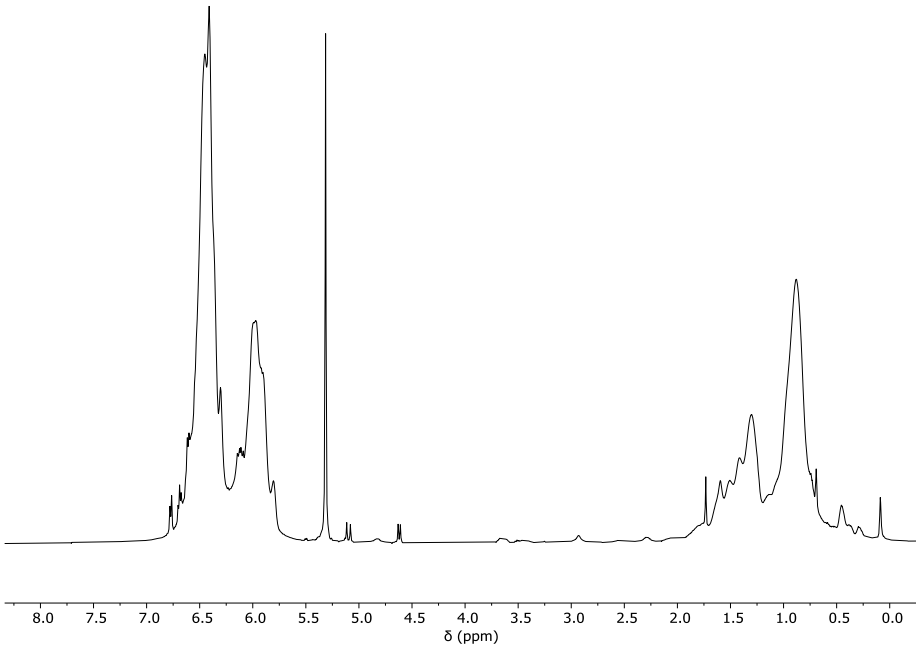

Figure A2.30. ^{1}H NMR spectrum of the polystyrene produced by sMAO-Cp*$TiCl_3$ (**1_{sMAO}**), 3.7 mL styrene 50 mL of toluene, $[Al_{sMAO}]_0$:$[Ti]_0$ = 200:1, 10 minutes, 1000 rpm (chloroform-d_1, 400 MHz, 298 K).

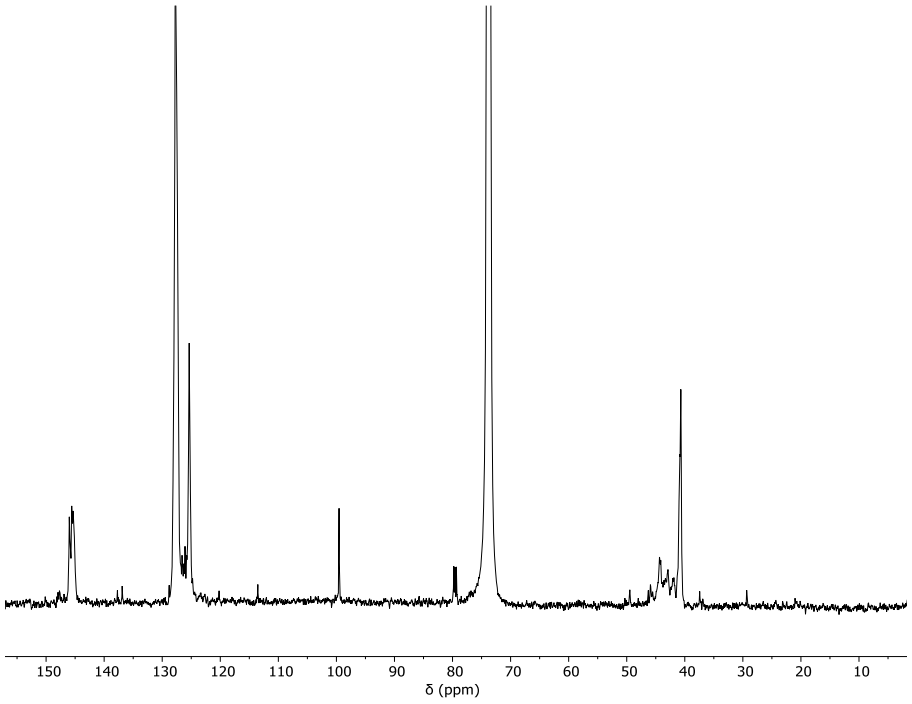

Figure A2.31. $^{13}C\{^{1}H\}$ NMR spectrum of the polystyrene produced by sMAO-Cp*$TiCl_3$ (**1_{sMAO}**), 3.7 ml styrene, 50 mL of toluene, $[Al_{sMAO}]_0$:$[Ti]_0$ = 200:1, 10 minutes, 1000 rpm (chloroform-d_1, 125 MHz, 298 K).

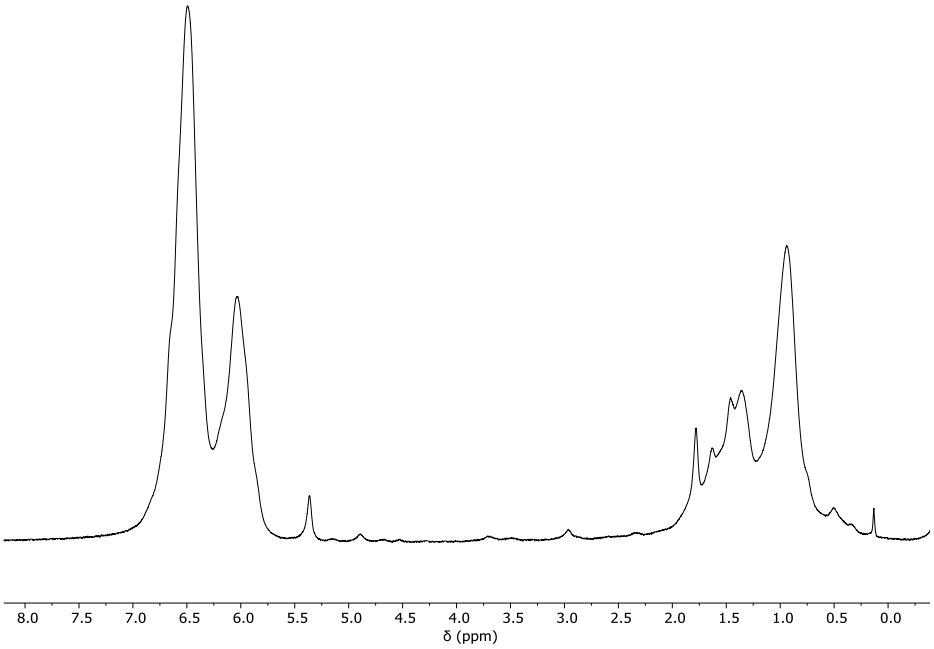

Figure A2.32. ^{1}H NMR spectrum of the polystyrene produced by sMAO-Pn*(H)TiCl$_3$ (**2$_{sMAO}$**), 3.7 mL styrene, 50 mL of toluene, $[Al_{sMAO}]_0$:$[Ti]_0$ = 200:1, 10 minutes, 1000 rpm (chloroform-*d$_1$*, 400 MHz, 298 K).

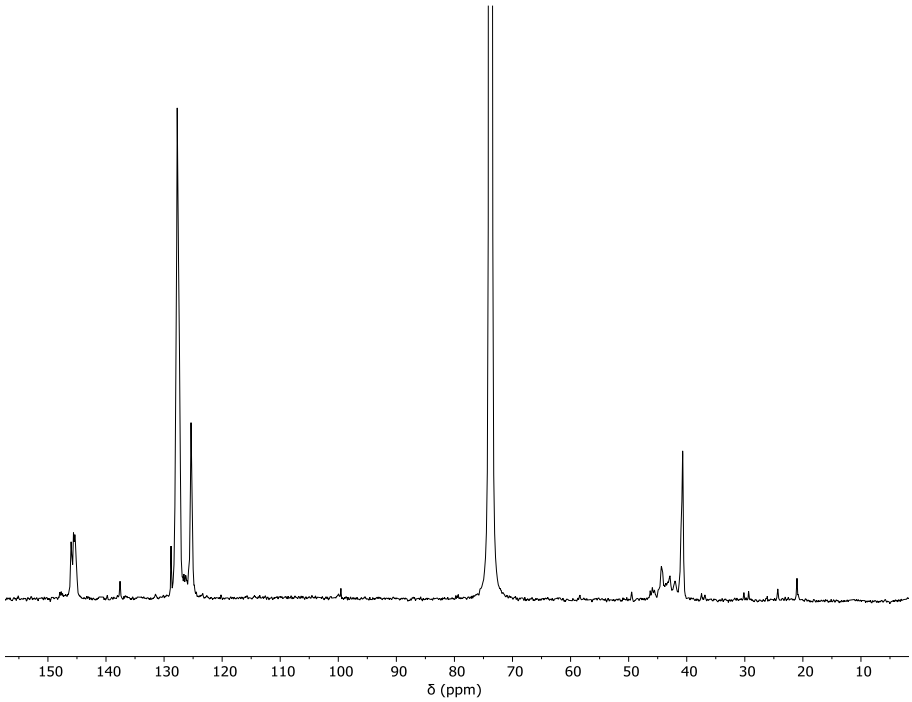

Figure A2.33. {^{1}H}^{13}C NMR spectrum of the polystyrene produced by sMAO-Pn*(H)TiCl$_3$ (**2$_{sMAO}$**), 3.7 mL styrene, 50 mL of toluene, $[Al_{sMAO}]_0$:$[Ti]_0$ = 200:1, 10 minutes, 1000 rpm (chloroform-*d$_1$*, 125 MHz, 298 K).

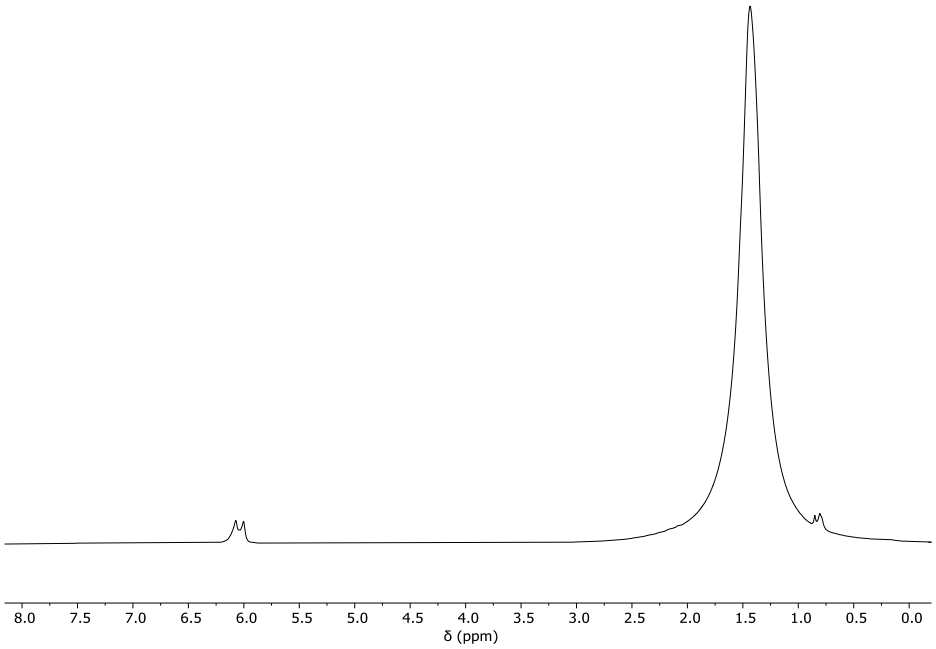

Figure A2.34. ^{1}H NMR spectrum of the polyethylene produced by Pn*(H)TiCl$_3$ (**2**) at 40 °C (1,1,2,2-tetrachloroethane-d_2, 500 MHz, 393 K).

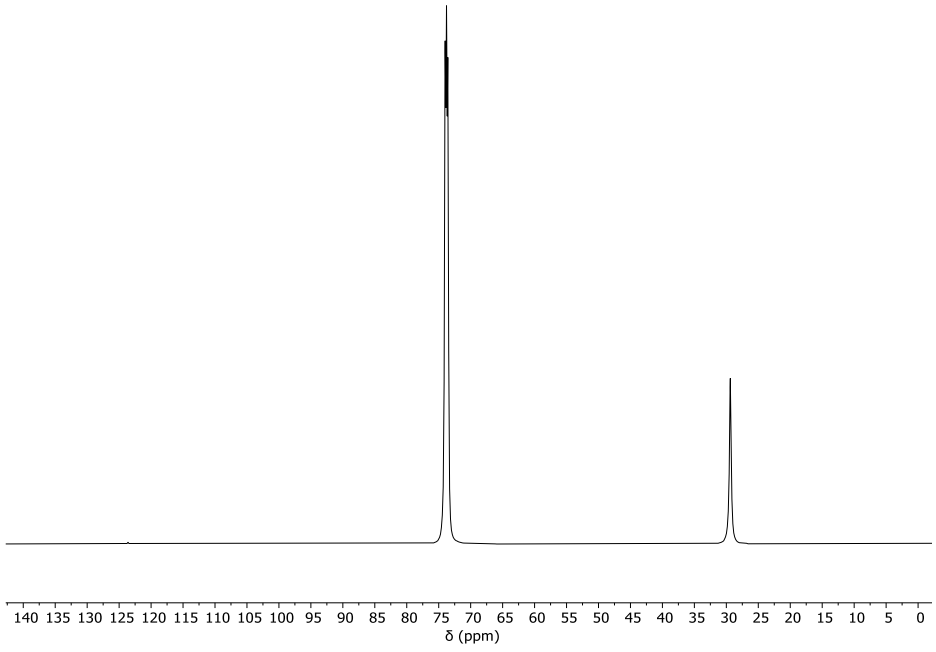

Figure A2.35. ^{13}C{^{1}H} NMR spectrum of the polyethylene produced by Pn*(H)TiCl$_3$ (**2**) at 40 °C (1,1,2,2-tetrachloroethane-d_2, 125.7 MHz, 393 K).

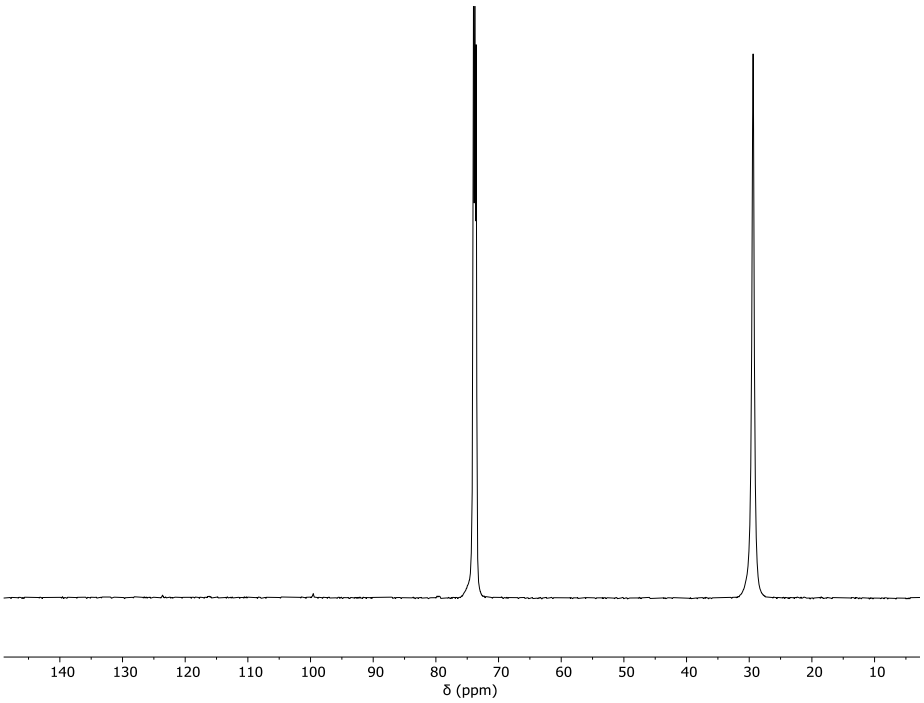

Figure A2.36. $^{13}C\{^{1}H\}$ NMR spectrum of the polyethylene produced by sMAO-Cp*(H)$TiCl_3$ (**1$_{sMAO}$**) at 50 °C (1,1,2,2-tetrachloroethane-d_2, 125.7 MHz, 393 K).

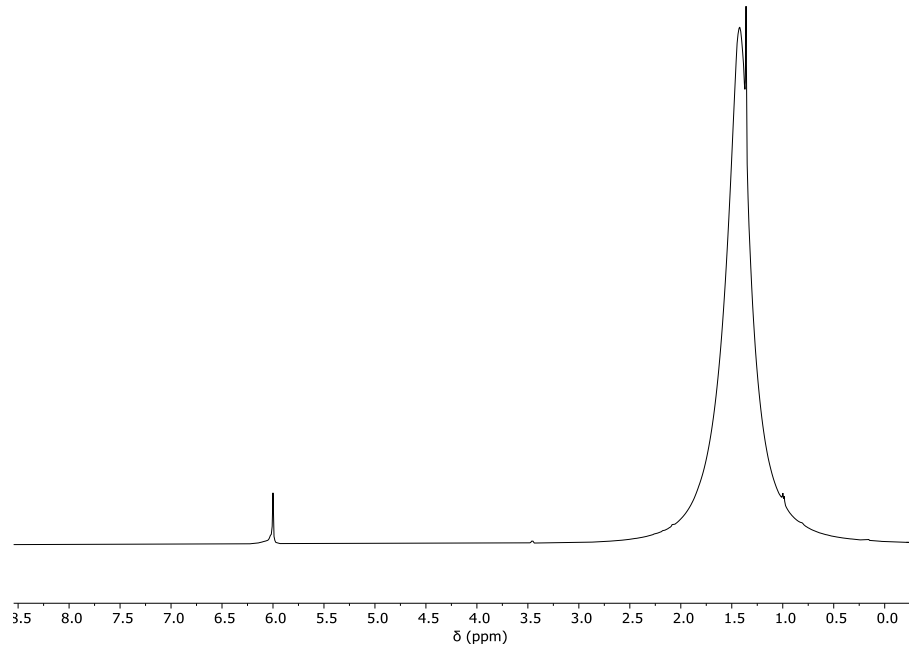

Figure A2.37. ^{1}H NMR spectrum of the polyethylene produced by sMAO-Pn*(H)$TiCl_3$ (**2$_{sMAO}$**) at 50 °C (1,1,2,2-tetrachloroethane-d_2, 500 MHz, 393 K).

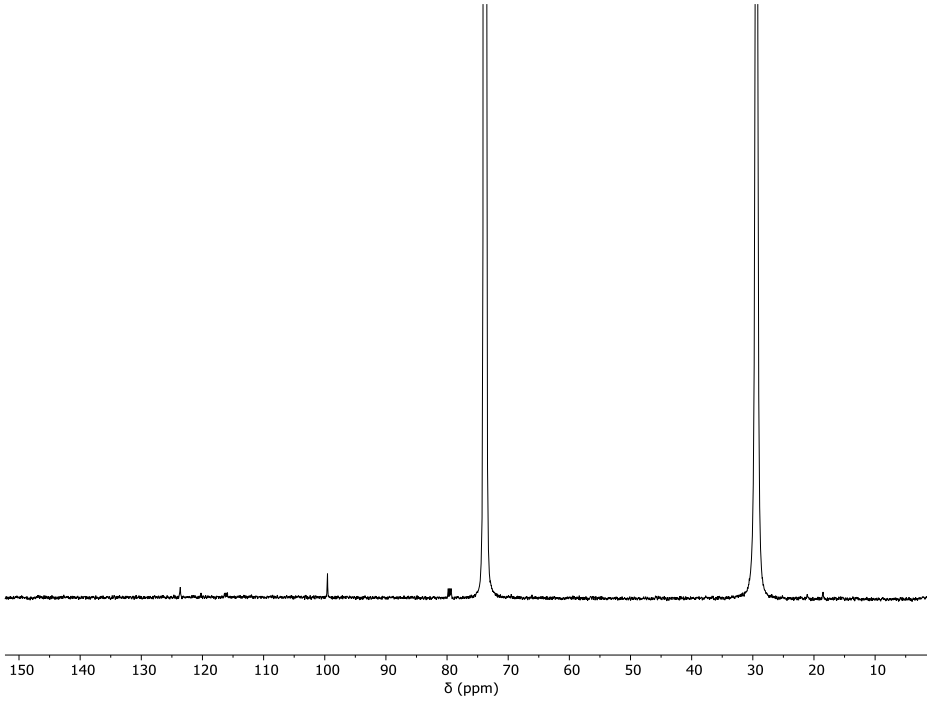

Figure A2.38. $^{13}C\{^{1}H\}$ NMR spectrum of the polyethylene produced by sMAO-Pn*(H)$TiCl_3$ (**2**$_{sMAO}$) at 50 °C (1,1,2,2-tetrachloroethane-*d*2, 125.7 MHz, 393 K).

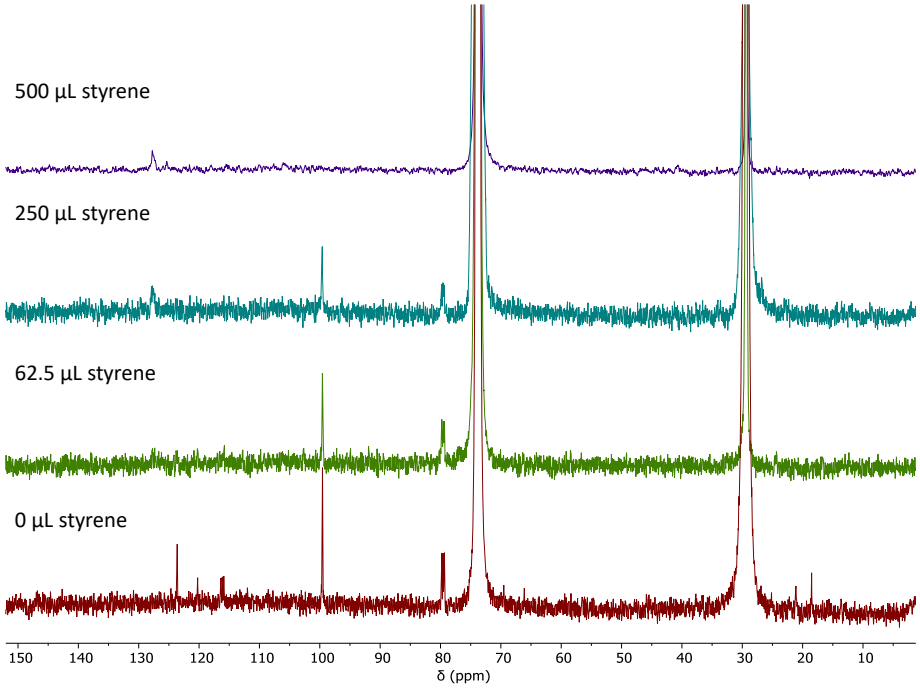

Figure A2.39. $^{13}C\{^{1}H\}$ NMR spectrum of the ethylene/styrene copolymer produced by sMAO-Pn*(H)$TiCl_3$ (**2**$_{sMAO}$) at 40 °C (1,1,2,2-tetrachloroethane-d_2, 125.7 MHz, 393 K). Red : 0 µL styrene, green : 62.5 µL styrene, blue : 250 µL styrene, purple : 500 µL styrene.

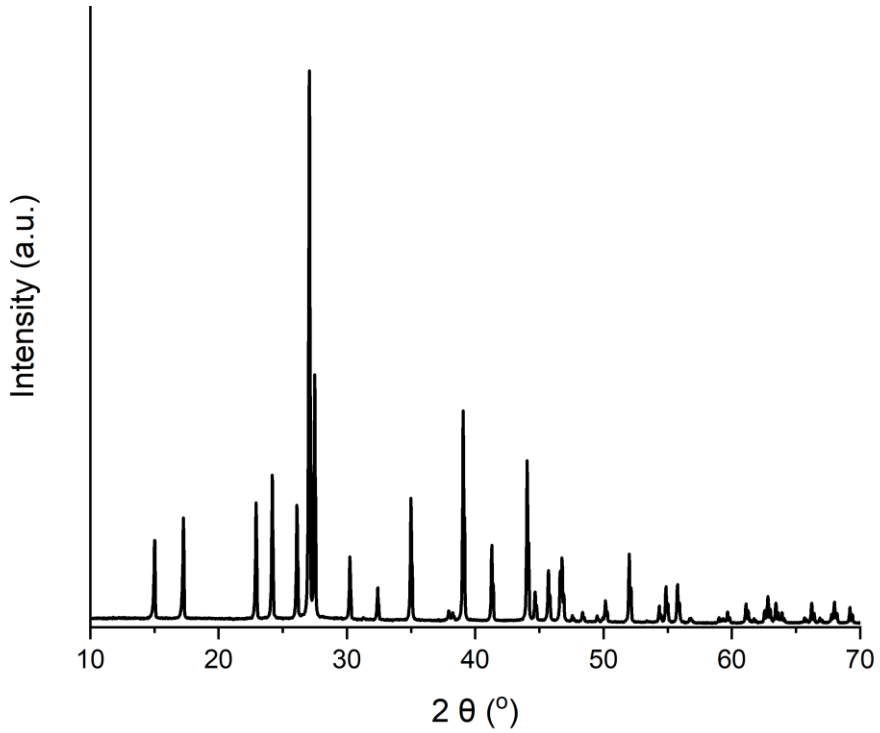

Figure A2.40. XRD pattern of the material formed after attempted copolymerisation of ethylene with styrene using using **2$_{sMAO}$**, crop 2. Reaction conditions : 40 °C, 50 mL of hexane, $[Al_{sMAO}]_0$:$[Ti]_0$ = 200:1, 30 minutes, 1000 rpm, 10 mg catalyst, 150 mg TiBA.

Chapter 3

Table A3.1. *Para*-Hammett constants.

Substituent	**σ_{para}**
NH_2	-0.66
OMe	-0.268
Br	0.232
NMe_2	-0.83

Table A3.2. Solution phase *para*-substituted styrene homopolymerisation activities, temperature and mass of polymer. Polymerisation conditions: 2 mL of toluene, 0.2 µmol of catalyst, 1 mL of styrene, $[Al_{MAO}]_0$:$[Ti]_0$ = 1500:1, 10 minutes, 55°C.

Substituent	Catalyst (mol)	Mass polymer (mg)		Activity ($kg_{PS}/mol_{Ti}/h$)		Average activity ($kg_{PS}/mol_{Ti}/h$)
		1	2	1	2	
Cp^*TiCl_3 (1_{sMAO})						
Br	$0.2.10^{-6}$	33	26	990	780	885
OMe	$0.2.10^{-6}$	505	612	15150	18360	1675
NH_2	$0.2.10^{-6}$	1411	1359	42332	40770	41550
$Pn^*(H)TiCl_3$ (2_{sMAO})						
Br	$0.2.10^{-6}$	62	76	1860	2280	2070
OMe	$0.2.10^{-6}$	370	369	11100	11070	11085
NH_2	$0.2.10^{-6}$	1403	1427	42090	42810	42450

Table A3.3. Slurry-phase substituted *para*-styrene homopolymerisation activities, temperature, mass of catalyst and mas of polymer. Polymerisation conditions: 50 mL of toluene,3.7 mL of styrene,$[Al_{sMAO}]_0$:$[Ti]_0$ = 200:1, 10 minutes, 55°C, 150 mg TiBA.

Substituent	Mass catalyst (mg)		Mass polymer (mg)		Activity ($kg_{PS}/mol_{Ti}/h$)		Average activity ($kg_{PS}/mol_{Ti}/h$)
	1	2	1	2	1	2	
sMAO-Cp^*TiCl_3 (1_{sMAO})							
Br	10.2	10	211	165	1730	1379	1555
OMe	10.1	10.1	1726	1109	14289	9218	11753
NH_2	10.1	10.1	5152	4762	42822	39581	41202
sMAO-$Pn^*(H)TiCl_3$ (2_{sMAO})							
Br	10.1	9.8	165	140	1368	1195	1281
OMe	10.3	10.6	3838	4419	30444	34997	32721
NH_2	9.8	10.1	4583	5101	38138	41234	39686
NMe_2	12.1	11.7	5739	5653	39376	40070	39773

Table A3.4. Molecular weights of substituted polystyrenes produced using Cp*$TiCl_3$ (**1**). Polymerisation conditions: 10 minutes, 1000 rpm, 2 mL toluene, 2 µL [Ti], 1.0 mL styrene, $[Al_{MAO}]_0$:$[Ti]_0$ = 1500:1.

T (°C)	M_w (kg/mol)	Đ
4-Br-polystyrene		
40	118	2.3
55	146	3.3
70	132	2.5
4-OMe-polystyrene		
40	298	2.7
55	324	2.1
70	313	2.4

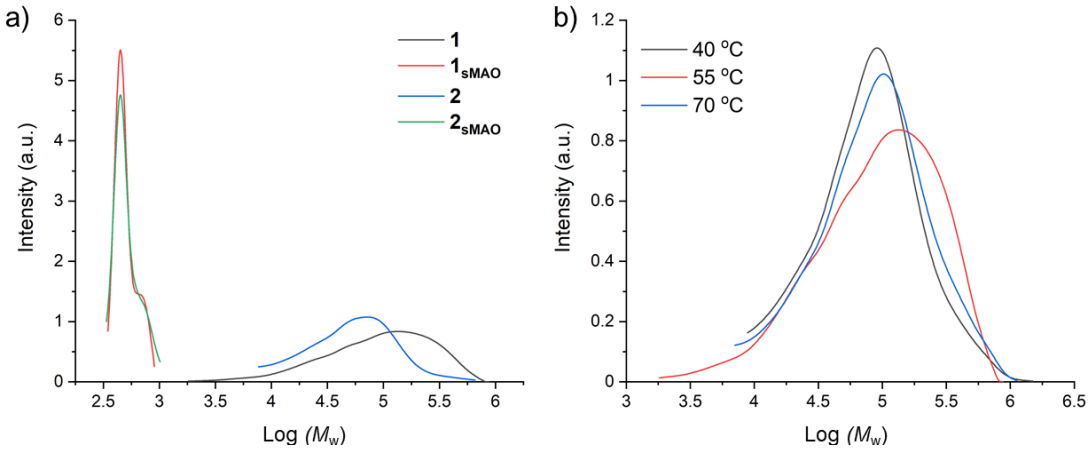

Figure A3.1. Molecular weight distribution for poly(4-Br-styrene) produced a) using Cp*$TiCl_3$ (**1**) Pn*(H)$TiCl_3$ (**2**), sMAO-Cp*$TiCl_3$ (**1$_{sMAO}$**) and sMAO-Pn*(H)$TiCl_3$ (**2$_{sMAO}$**) at 55 °C, b) using Cp*$TiCl_3$ (**1**) between 40 and 70 °C. Polymerisation conditions: 10 minutes, 1000 rpm. Solution: 2 mL toluene, 2 µL [Ti], 1.0 mL styrene, $[Al_{MAO}]_0$:$[Ti]_0$ = 1500:1. Slurry: 50 mL toluene, 10 mg of catalyst, 3.7 mL styrene, $[Al_{sMAO}]_0$:$[Ti]_0$ = 200:1, 150 mg TiBA.

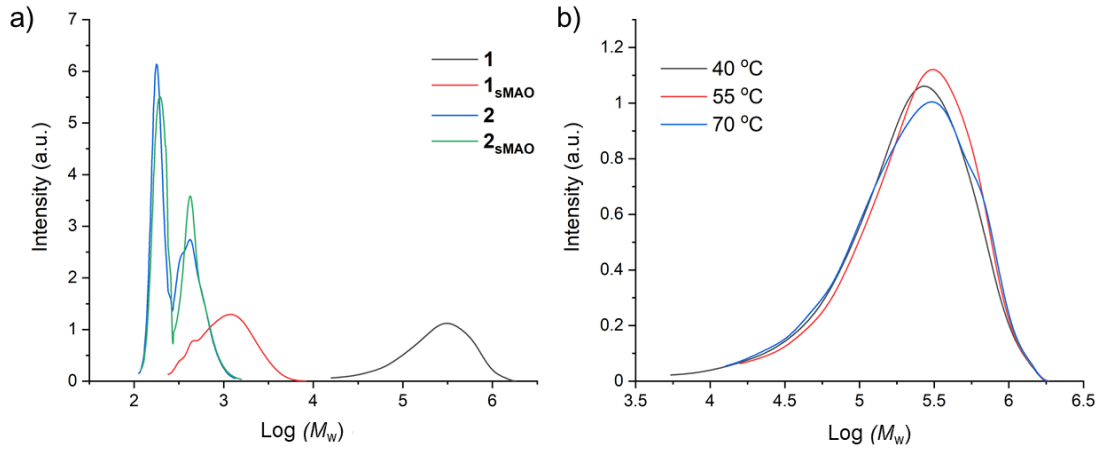

Figure A3.2. Molecular weight distribution for poly(4-OMe-styrene) produced a) using Cp*$TiCl_3$ (**1**) Pn*(H)$TiCl_3$ (**2**), sMAO-Cp*$TiCl_3$ (**1$_{sMAO}$**) and sMAO-Pn*(H)$TiCl_3$ (**2$_{sMAO}$**) at 55 °C, b) using Cp*$TiCl_3$ (**1**) between 40 and 70 °C. Polymerisation conditions: 10 minutes, 1000 rpm. Solution: 2 mL toluene, 2 µL [Ti], 1.0 mL styrene, $[Al_{MAO}]_0$:$[Ti]_0$ = 1500:1. Slurry: 50 mL toluene, 10 mg of catalyst, 3.7 mL styrene, $[Al_{sMAO}]_0$:$[Ti]_0$ = 200:1, 150 mg TiBA.

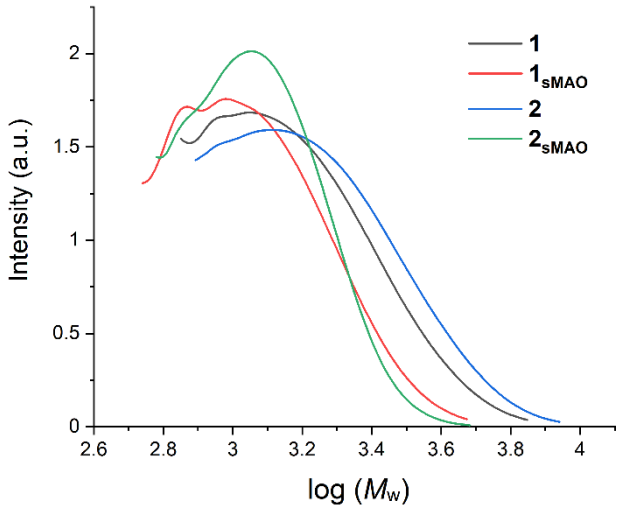

Figure A3.3. Molecular weight distribution for poly(4-NH_2-styrene) produced a) using Cp*$TiCl_3$ (**1**) Pn*(H)$TiCl_3$ (**2**), sMAO-Cp*$TiCl_3$ (**1_{sMAO}**) and sMAO-Pn*(H)$TiCl_3$ (**2_{sMAO}**) at 55 °C. Polymerisation conditions: 10 minutes, 1000 rpm. Solution: 2 mL toluene, 2 µL [Ti], 1.0 mL styrene, $[Al_{MAO}]_0$:$[Ti]_0$ = 1500:1. Slurry: 50 mL toluene, 10 mg of catalyst, 3.7 mL styrene, $[Al_{sMAO}]_0$:$[Ti]_0$ = 200:1, 150 mg TiBA.

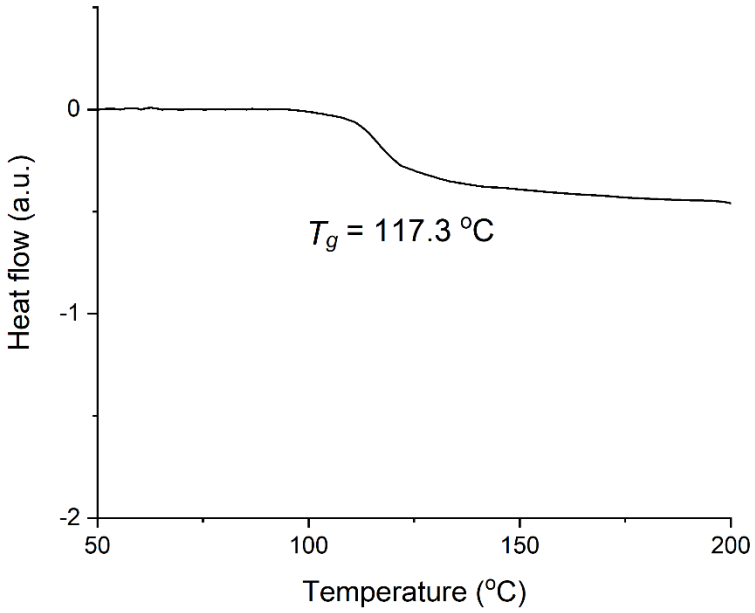

Figure A3.4. DSC curve of the poly(4-NH_2-styrene) produced using sMAO-Cp*$TiCl_3$ (**1_{sMAO}**) at 55 °C, ramp 10 °C/min.

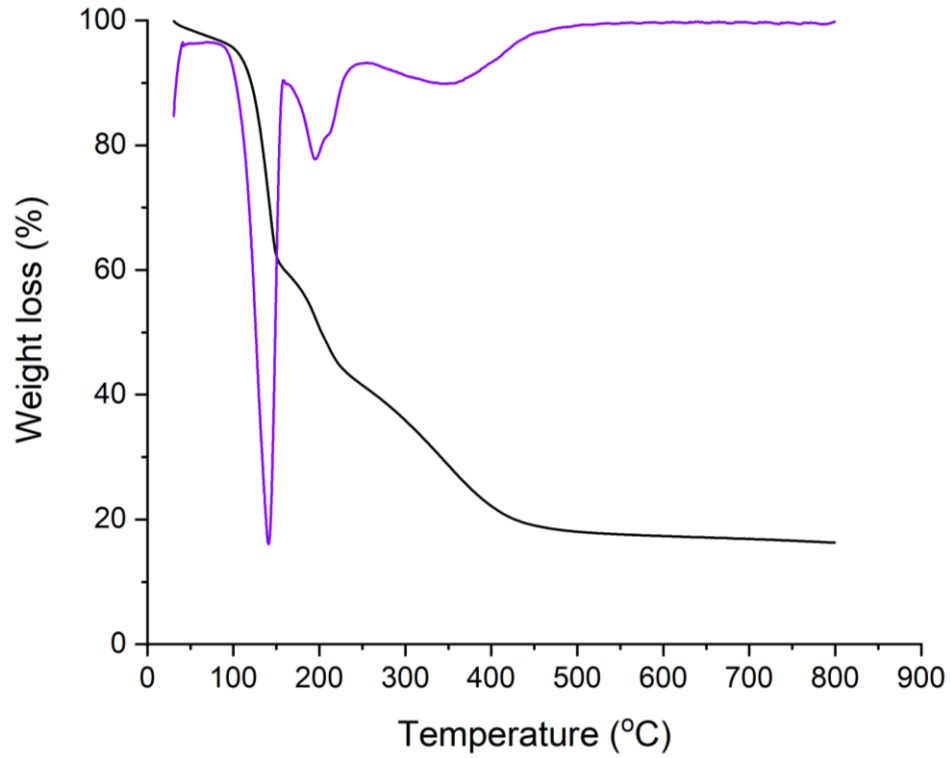

Figure A3.5. TGA curve of material produced by the copolymerisation of 125 µL of 4-NH_2-styrene with ethylene at 55 °C using sMAO-Cp*$TiCl_3$ (**1_{sMAO}**) (black) and derivative of the TGA curve (purple).

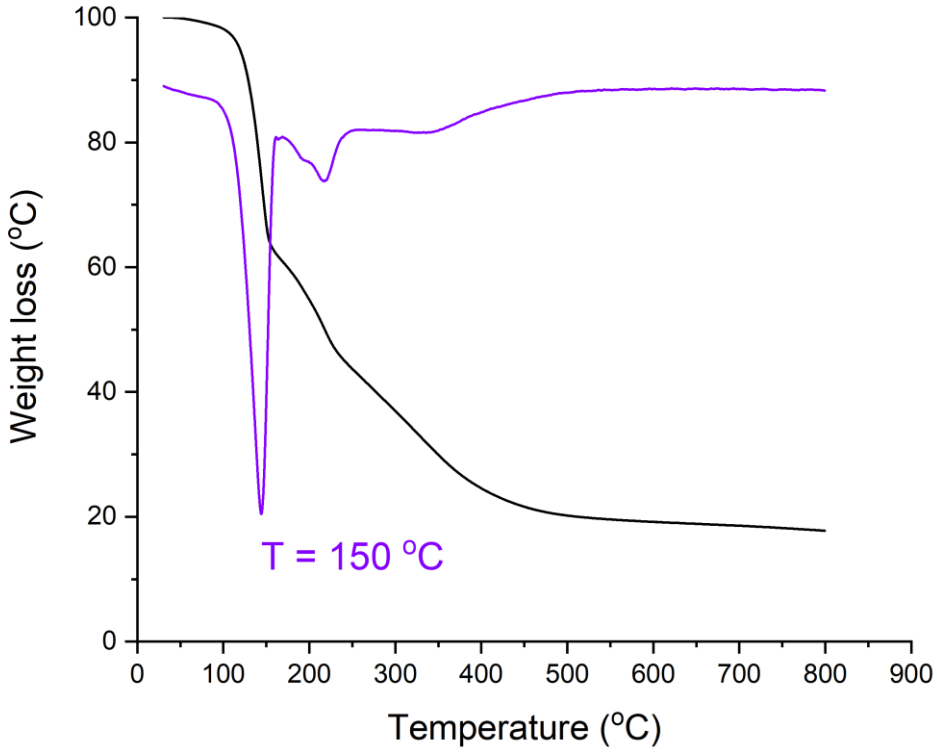

Figure A3.6. TGA curve of material produced by the copolymerisation of 125 µL of 4-NH_2-styrene with ethylene at 55 °C using sMAO-Pn*(H)$TiCl_3$ (**2_{sMAO}**) (black) and derivative of the TGA curve (purple).

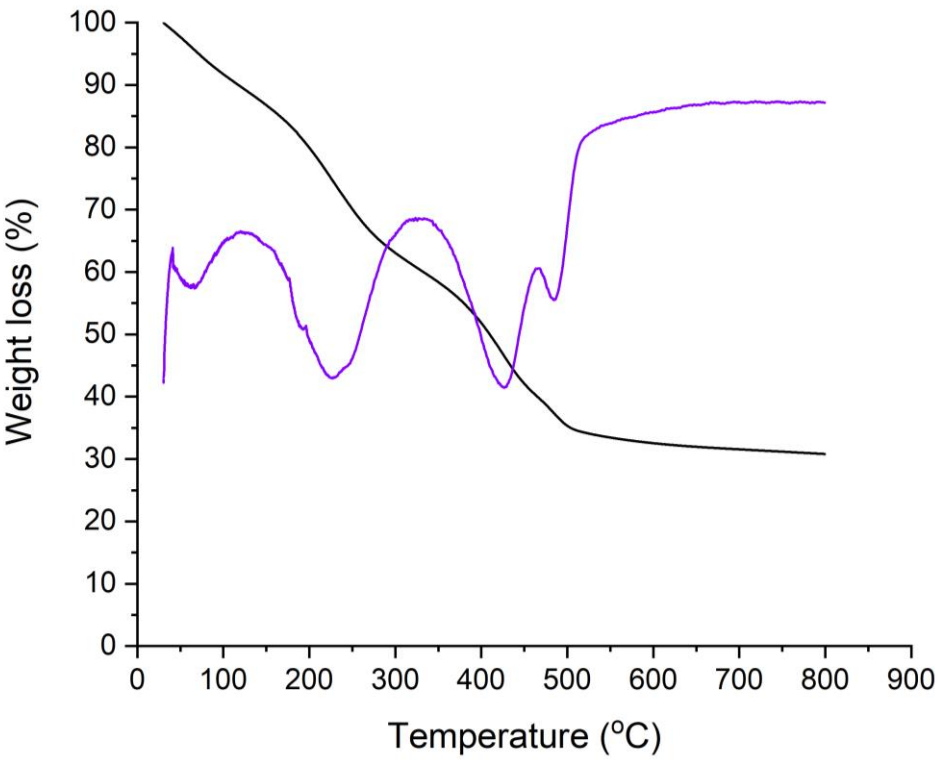

Figure A3.7. TGA curve of material produced by the copolymerisation of 125 μL of 4-NMe_2-styrene with ethylene at 55 °C using sMAO-Pn*(H)$TiCl_3$ (**2**$_{sMAO}$) (black) and derivative of the TGA curve (purple).

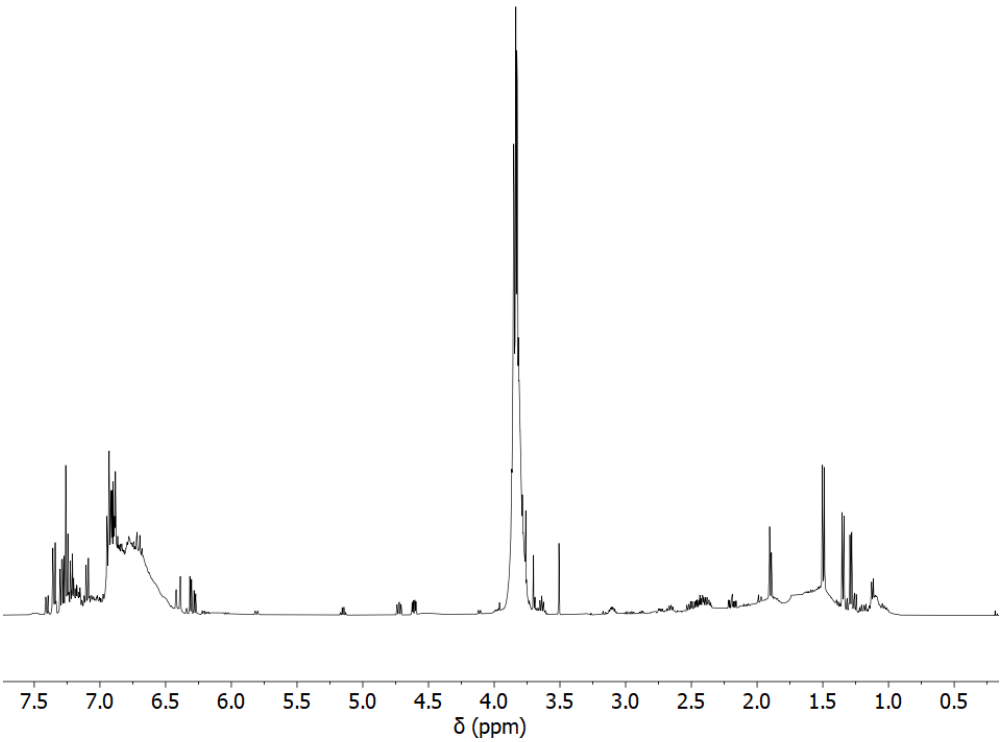

Figure A3.8. ^{1}H NMR spectrum of poly(4-methoxy-styrene) produced using Pn*(H)$TiCl_3$ (**2**) ($[Al_{MAO}]_0$:$[Ti]_0$ = 1500, 55 °C, 10 minutes) (chloroform-d_1, 500 MHz, 298 K).

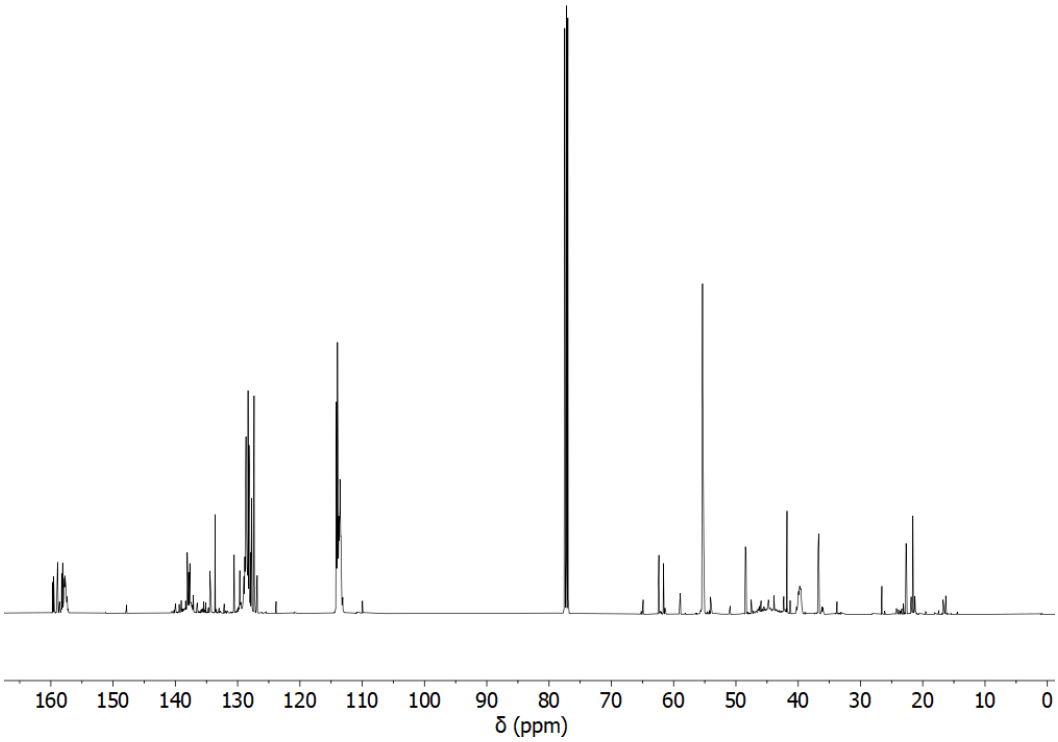

Figure A3.9. $^{13}C\{^{1}H\}$ NMR spectrum of poly(4-methoxy-styrene) produced using Pn*(H)$TiCl_3$ (**2**) ($[Al_{MAO}]_0$:$[Ti]_0$ = 1500, 55 °C, 10 minutes) (chloroform-d_1, 500 MHz, 298 K).

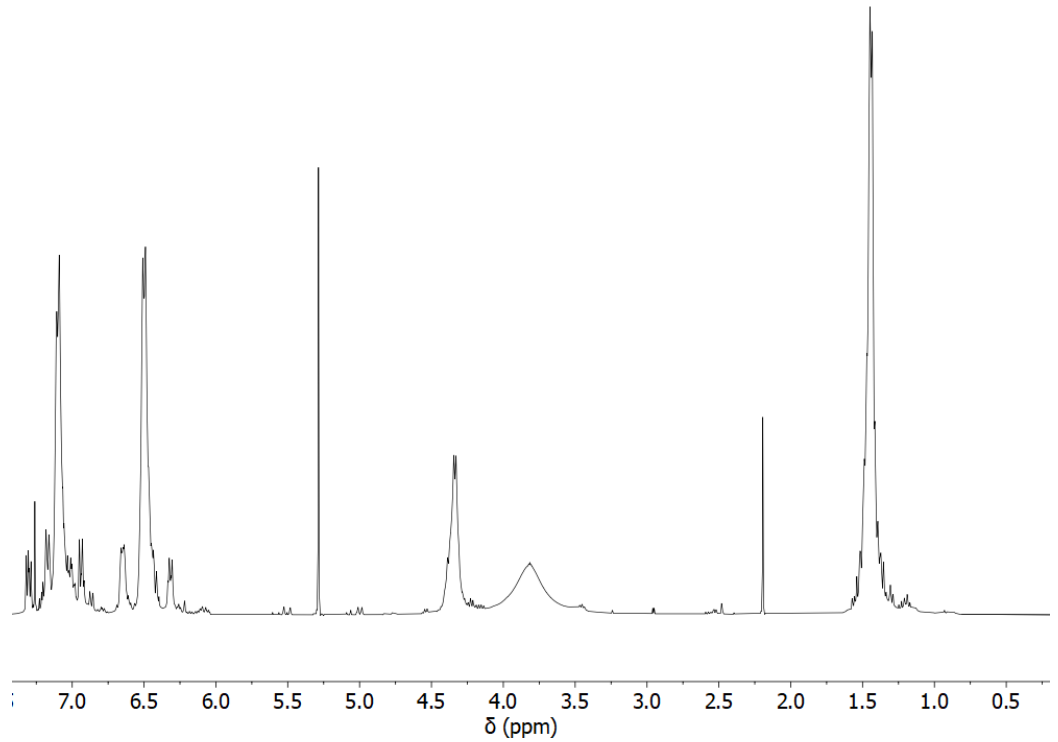

Figure A3.10. ^{1}H NMR spectrum of poly(4-NH_2-styrene) produced using Pn*(H)$TiCl_3$ (**2**) ($[Al_{MAO}]_0$:$[Ti]_0$ = 1500, 55 °C, 10 minutes) (chloroform-d_1, 500 MHz, 298 K).

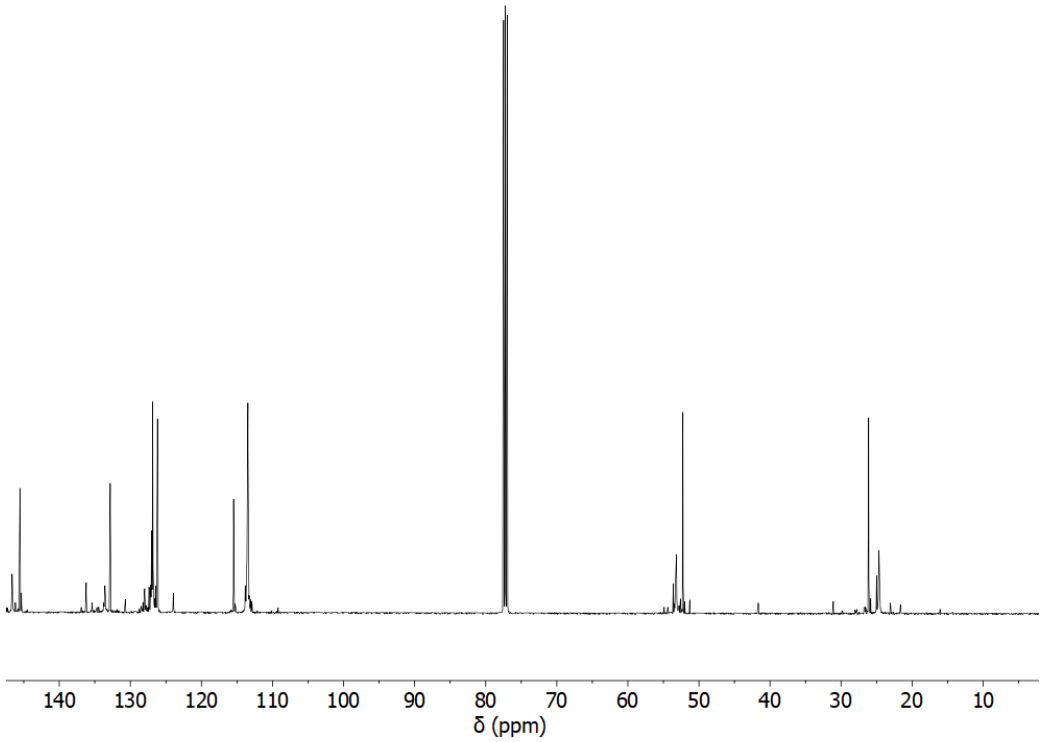

Figure A3.11. $^{13}C\{^{1}H\}$ NMR spectrum of poly(4-NH_2-styrene) produced using Pn*(H)$TiCl_3$ (**2**) ($[Al_{MAO}]_0$:$[Ti]_0$ = 1500, 55 °C, 10 minutes) (chloroform-d_1, 500 MHz, 298 K).

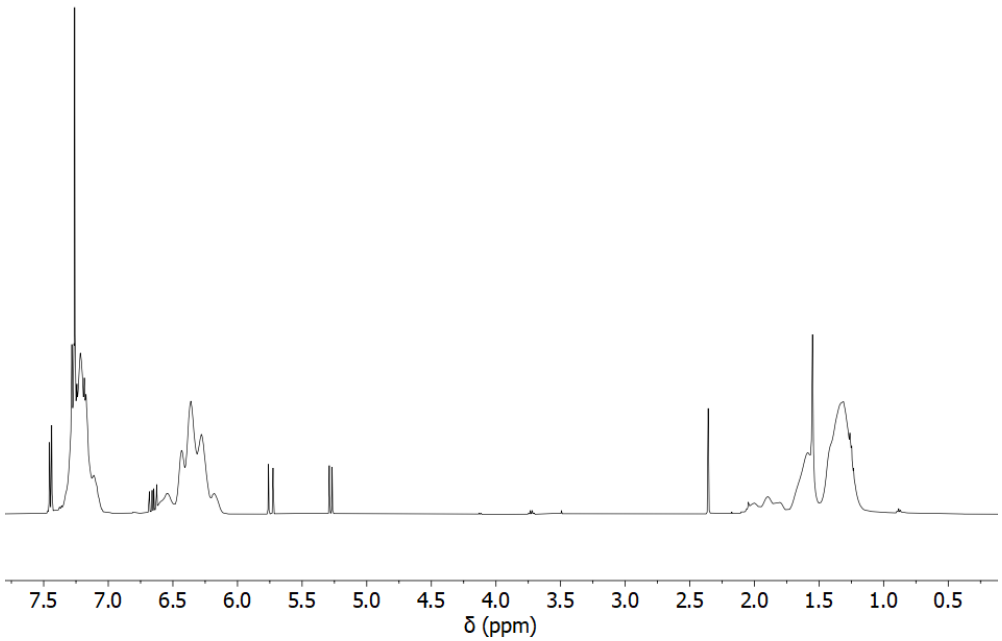

Figure A3.12. ^{1}H NMR spectrum of poly(4-bromo-styrene) produced using Cp*$TiCl_3$ (**1**) ($[Al_{MAO}]_0$:$[Ti]_0$ = 1500, 55 °C, 10 minutes) (chloroform-d_1, 500 MHz, 298 K).

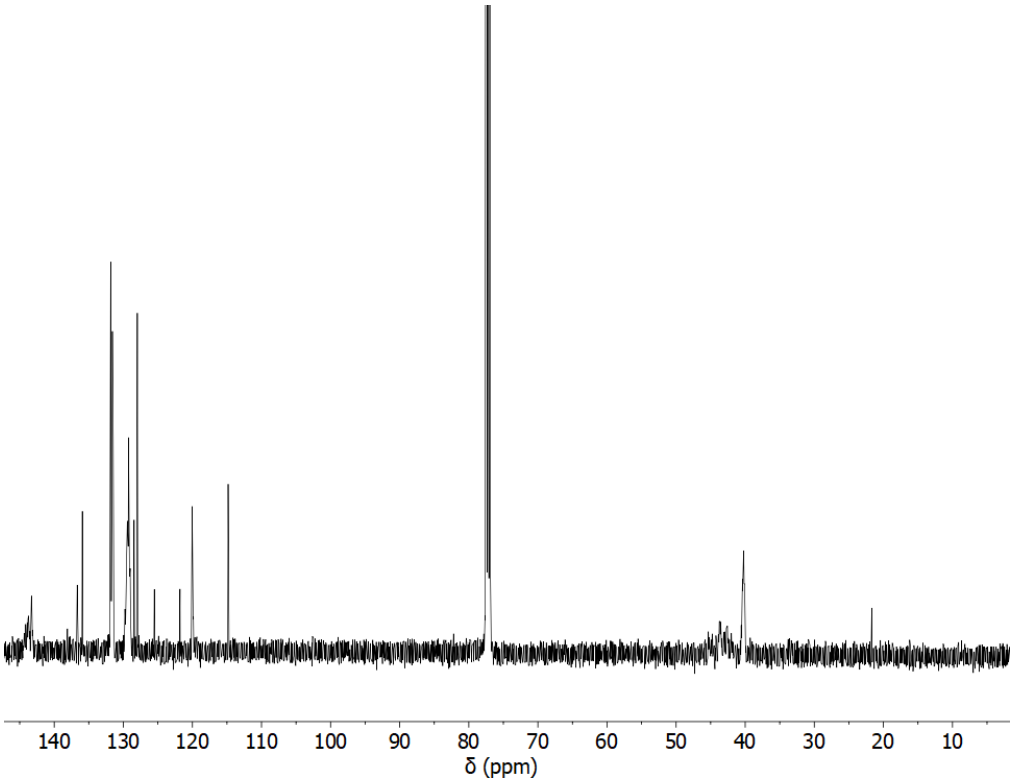

Figure A3.13. $^{13}C\{^{1}H\}$ NMR spectrum of poly(4-bromo-styrene) produced using Cp*$TiCl_3$ (**1**) ($[Al_{MAO}]_0$:$[Ti]_0$ = 1500, 55 °C, 10 minutes) (chloroform-d_1, 500 MHz, 298 K).

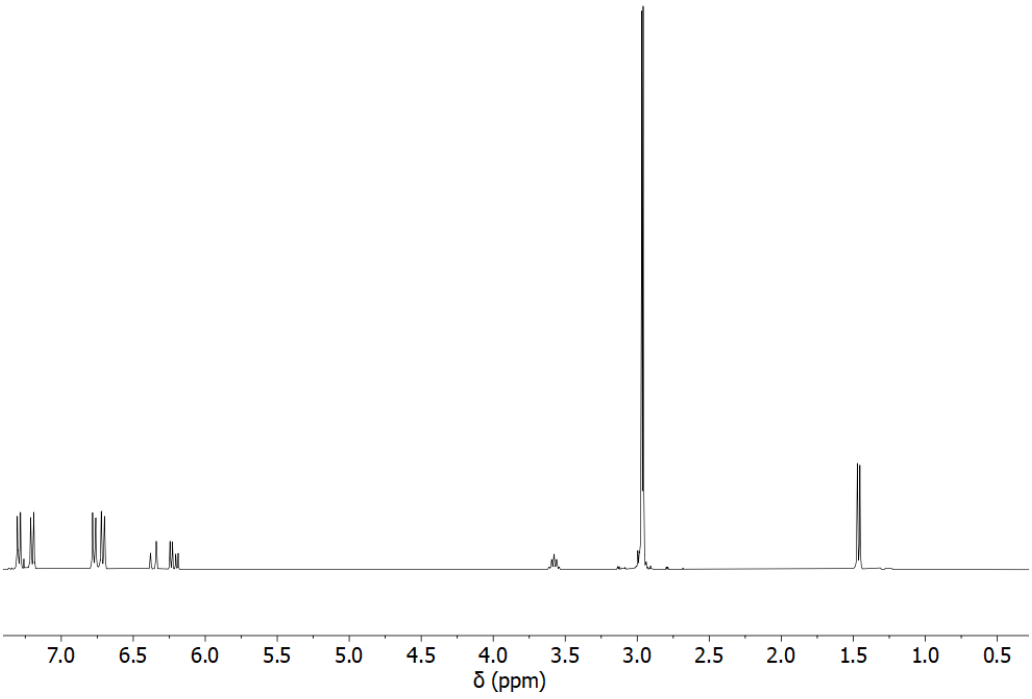

Figure A3.14. ^{1}H NMR spectrum of 4,4'-[(1E)-3-methyl-1-propene-1,3-diyl]bis[N,N-dimethylbenzenamine] produced using sMAO-Pn*(H)$TiCl_3$ (**2$_{sMAO}$**) ($[Al_{MAO}]_0$:$[Ti]_0$ = 200, 55 °C, 10 minutes) (chloroform-d_1, 500 MHz, 298 K).

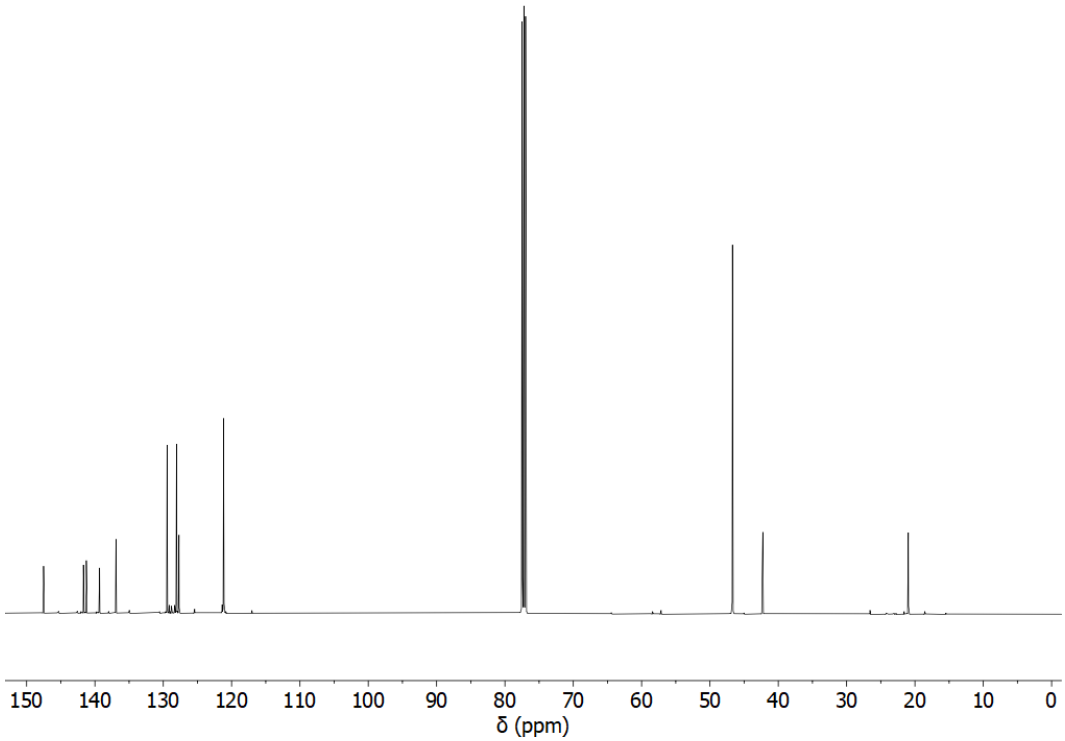

Figure A3.15. $^{13}C\{^{1}H\}$ NMR spectrum of 4,4'-[(1E)-3-methyl-1-propene-1,3-diyl]bis[N,N-dimethylbenzenamine] produced using sMAO-Pn*(H)$TiCl_3$ (**2$_{sMAO}$**) ($[Al_{MAO}]_0$:$[Ti]_0$ = 200, 55 °C, 10 minutes) (chloroform-d_1, 500 MHz, 298 K).

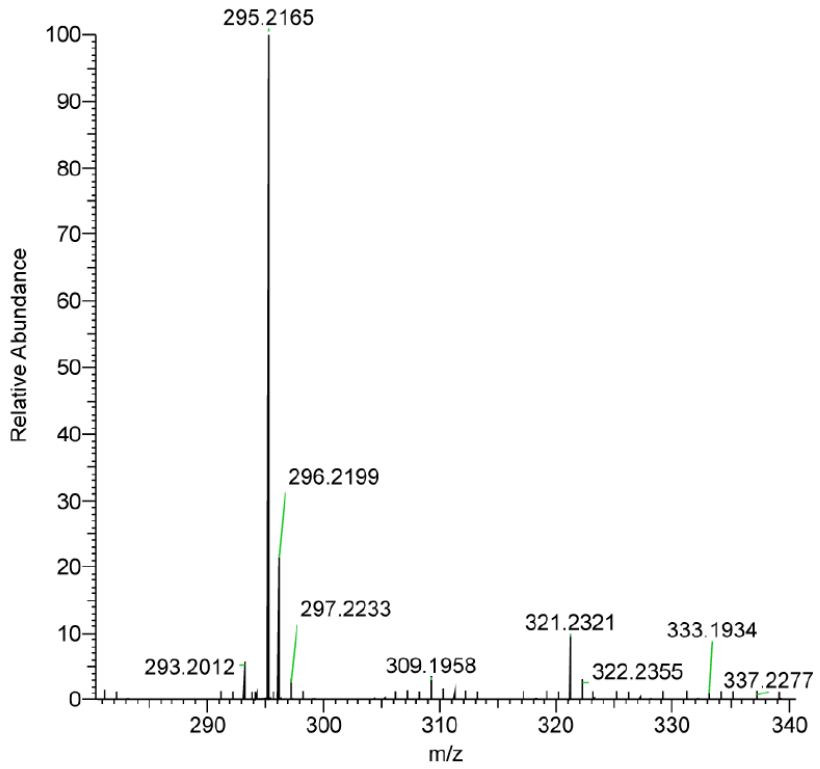

Figure A3.16. Electrospray ionisation/mass spectrometry (ESI/MS) analysis in the positive mode of 4,4'-[(1E)-3-methyl-1-propene-1,3-diyl]bis[N,N-dimethylbenzenamine].

Chapter 4

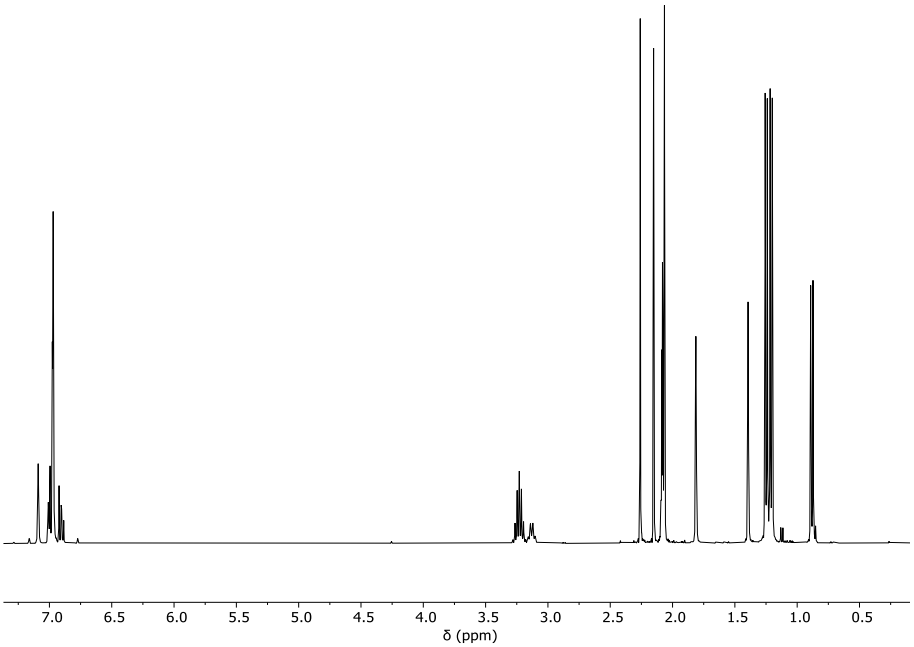

Figure A4.1. ^{1}H NMR spectrum of Pn*(H)TiCl$_2$(O-2,6-^{i}Pr-C$_6$H$_3$) (**3**) (toluene-d_8, 298 K and 499.9 MHz).

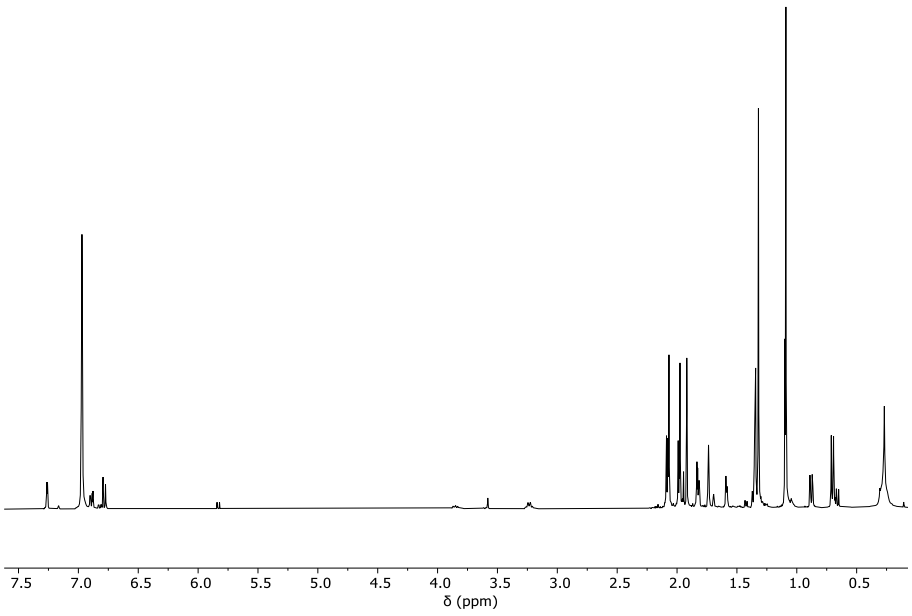

Figure A4.2. ^{1}H NMR spectrum of Pn*(H)TiCl$_2$(O-2,4-^{t}Bu-C$_6$H$_3$) (**4**) (toluene-d_8, 298 K and 499.9 MHz).

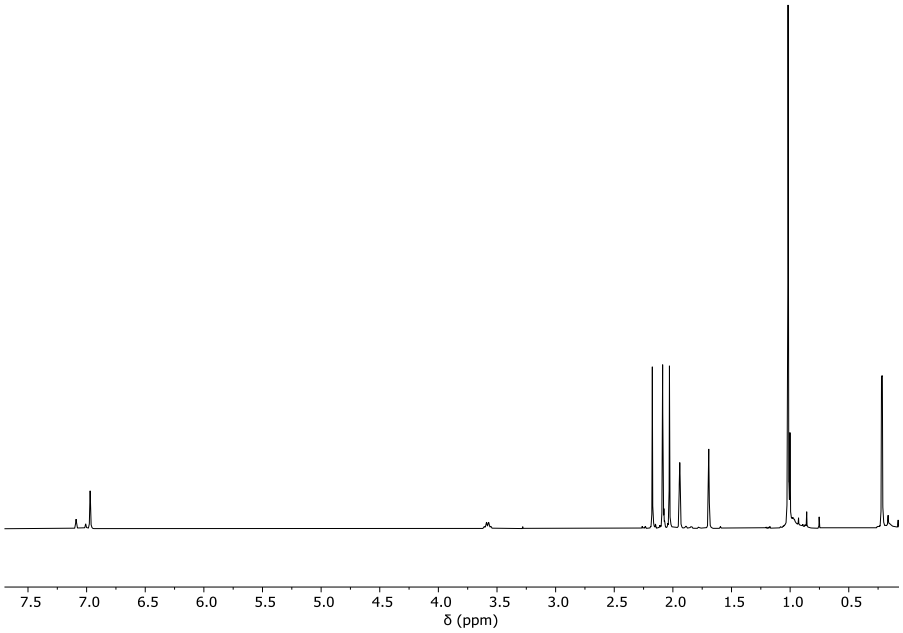

Figure A4.3. ^{1}H NMR spectrum of Pn*(H)TiCl$_2$(O-Si(Me)$_2$^{t}Bu) (**5**) (toluene-d_8, 298 K and 499.9 MHz).

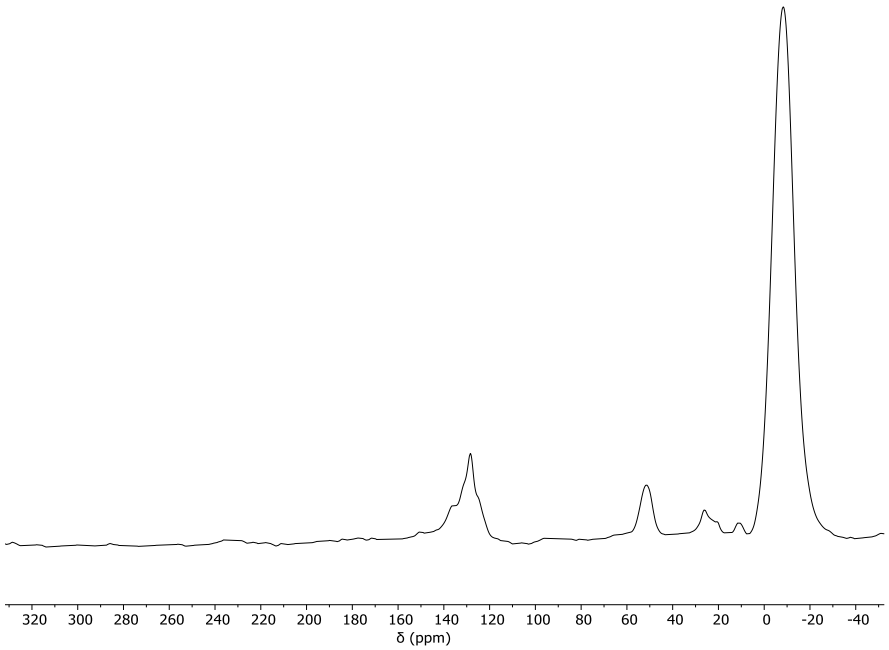

Figure A4.4. ^{13}C CP-MAS (10 kHz) NMR spectrum of sMAO- Pn*(H)TiCl$_2$(O-2,6-^{i}Pr-C$_6$H$_3$) (**3$_{sMAO}$**).

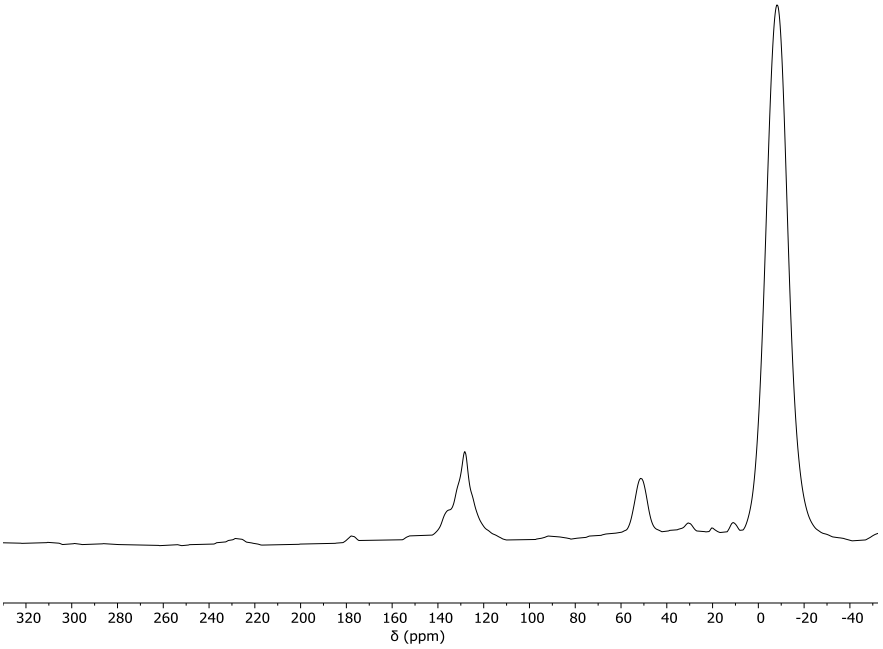

Figure A4.5. ^{13}C CP-MAS (10 kHz) NMR spectrum of sMAO-Pn*(H)$TiCl_2$(O-2,4-^{t}Bu-C_6H_3) (**4$_{sMAO}$**).

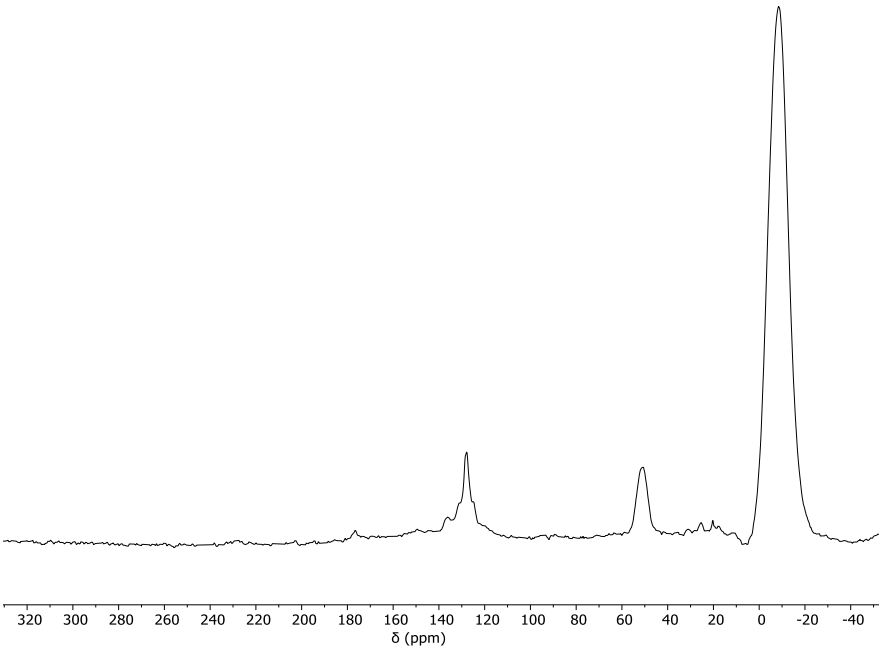

Figure A4.6. ^{13}C CP-MAS (10 kHz) NMR spectrum of sMAO-Pn*(H)$TiCl_2$(O-Si(Me)$_2$^{t}Bu) (**5$_{sMAO}$**).

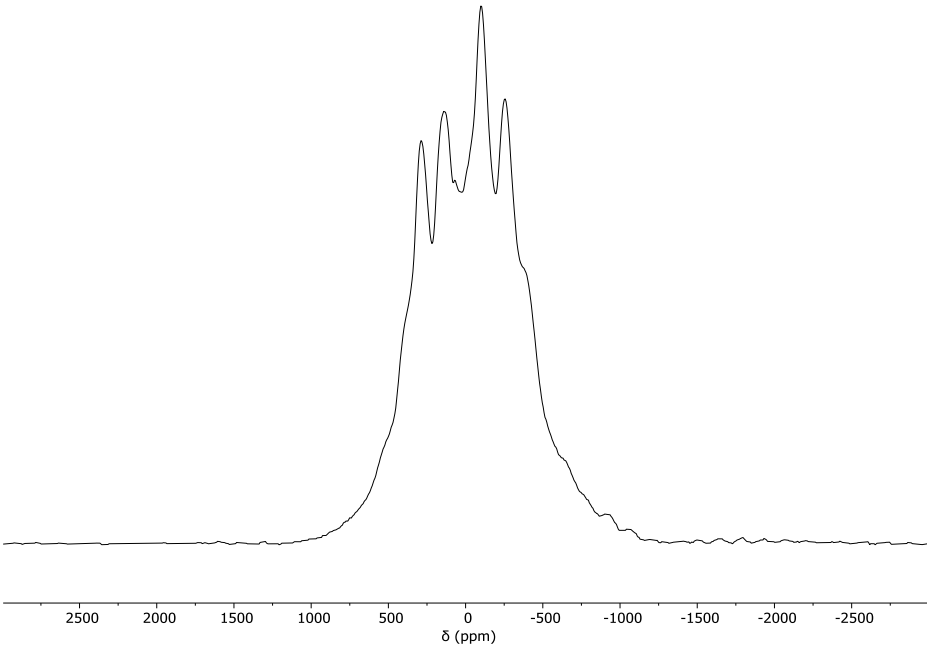

Figure A4.7. ^{27}Al DP-MAS (15 kHz) NMR spectrum of sMAO- Pn*(H)TiCl$_2$(O-2,6-^{i}Pr-C$_6$H$_3$) (**3$_{sMAO}$**).

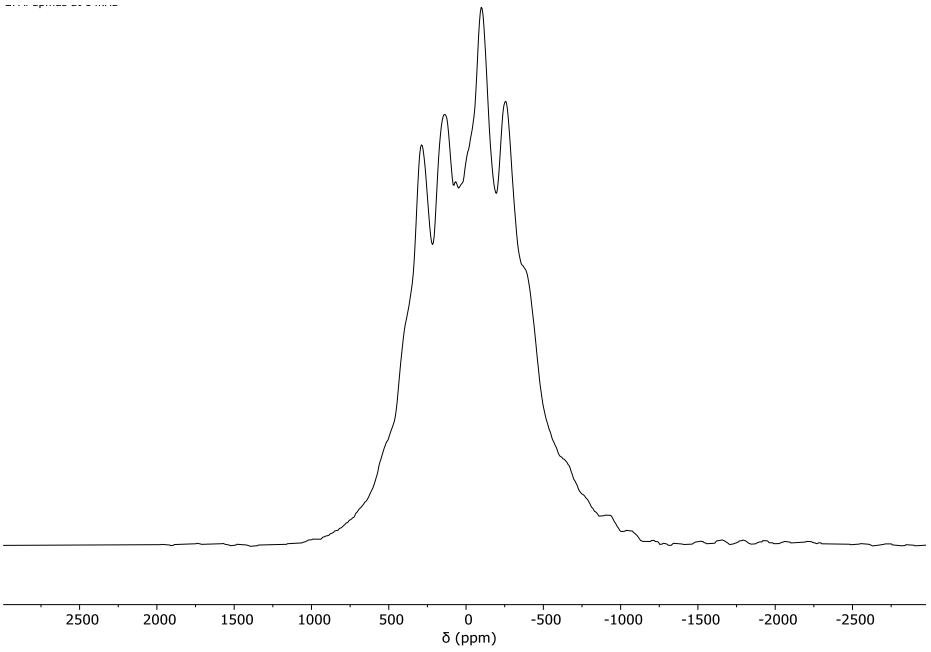

Figure A4.8. ^{27}Al DP-MAS (15 kHz) NMR spectrum of sMAO-Pn*(H)TiCl$_2$(O-2,4-^{t}Bu-C$_6$H$_3$) (**4$_{sMAO}$**).

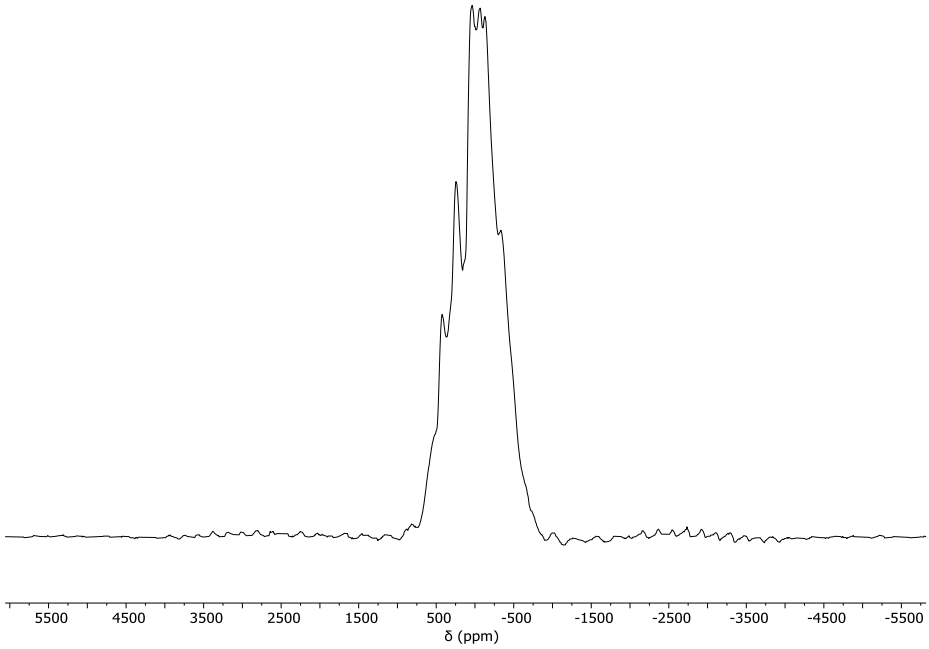

Figure A4.9. ^{27}Al hahnecho (20 kHz) NMR spectrum of sMAO-Pn*(H)TiCl$_2$(O-Si(Me)$_2$^{t}Bu) (**5$_{sMAO}$**).

Table A4.1. Solution phase styrene homopolymerisation activities, temperature and mass of polymer. Polymerisation conditions: 10 minutes, 1000 rpm. 2 mL toluene, 2×10^{-7} mol catalyst, 1 mL styrene, $[Al_{MAO}]_0$:$[Ti]_0$ = 1500:1.

Temperature (°C)	Catalyst (mol)	Mass polymer (mg)		Activity ($kg_{PS}/mol_{Ti}/h$)		Average activity ($kg_{PS}/mol_{Ti}/h$)
		1	2	1	2	
Pn*(H)TiCl2(O-2,6-^{i}Pr-C$_6$H$_3$) (3$_{sMAO}$)						
40	$0.2.10^{-6}$	41	50	1230	1500	1365
55	$0.2.10^{-6}$	113	93	3390	2790	3090
70	$0.2.10^{-6}$	101	105	3030	3150	3090
Pn*(H)TiCl$_2$(O-2,4-^{t}Bu-C$_6$H$_3$) (4$_{sMAO}$)						
40	$0.2.10^{-6}$	60	70	1800	2100	1950
55	$0.2.10^{-6}$	80	77	2400	2310	2355
70	$0.2.10^{-6}$	80	70	2400	2100	2250
Pn*(H)TiCl$_2$(O-Si(Me)$_2$^{t}Bu) (5$_{sMAO}$)						
40	$0.2.10^{-6}$	188	197	564	5910	5775
55	$0.2.10^{-6}$	181	179	5430	5370	5400
70	$0.2.10^{-6}$	198	188	5940	5640	5790

Table A4.2. Slurry-phase styrene homopolymerisation activities, temperature, mass of catalyst and mass of polymer. Polymerisation conditions: 10 minutes, 1000 rpm. 2 mL toluene, 10 mg catalyst, 3.7 mL styrene, $[Al_{MAO}]_0$:$[Ti]_0$ = 200:1, 150 mg TiBA.

Temperature (°C)	Mass catalyst (mg)		Mass polymer (mg)		Activity ($kg_{PS}/mol_{Ti}/h$)		Average activity ($kg_{PS}/mol_{Ti}/h$)
	1	2	1	2	1	2	
sMAO-Pn*(H)TiCl$_2$(O-2,6-^{i}Pr-C$_6$H$_3$) (3$_{sMAO}$)							
40	9.8	10.1	105	170	848	1332	1090
55	10.5	10.8	162	145	1222	1064	1143
70	101	10.9	161	152	1262	1149	1205
sMAO-Pn*(H)TiCl$_2$(O-2,4-^{t}Bu-C$_6$H$_3$) (4$_{sMAO}$)							
40	10.0	10.2	118	168	970	1355	1163
55	10.6	9.8	161	142	1251	1191	1221
70	10.0	10.2	133	146	1094	1178	1136
sMAO-Pn*(H)TiCl$_2$(O-Si(Me)$_2$^{t}Bu) (5$_{sMAO}$)							
40	9.9	10.2	280	191	2332	1545	1938
55	11.6	10.4	522	398	3726	2159	3442
70	10.9	11.3	331	415	2510	3038	2774

Table A4.3. Solution phase ethylene homopolymerisation activities, temperature and mass of polymer. Polymerisation conditions: 30 minutes, 1000 rpm. 50 mL hexane, 2×10^{-7} mol catalyst, 2 bar ethylene, 150 mg TiBA, $[Al_{MAO}]_0$:$[Ti]_0$ = 1500:1.

Temperature (°C)	Catalyst (mol)	Mass polymer (mg)		Activity ($kg_{PE}/mol_{Ti}/h/bar$)		Average activity ($kg_{PE}/mol_{Ti}/h/bar$)
		1	2	1	2	
Pn*(H)TiCl$_2$(O-2,6-^{i}Pr-C$_6$H$_3$) (3)						
40	$0.2.10^{-6}$	11	18	55	90	73
50	$0.2.10^{-6}$	8	7	40	35	38
60	$0.2.10^{-6}$	7	7	35	35	35
70	$0.2.10^{-6}$	10	11	50	55	53
80	$0.2.10^{-6}$	3	5	15	25	20
Pn*(H)TiCl$_2$(O-2,4-^{t}Bu-C$_6$H$_3$) (4)						
40	$0.2.10^{-6}$	47	36	235	180	207
50	$0.2.10^{-6}$	17	11	85	55	70
60	$0.2.10^{-6}$	35	23	175	115	145
70	$0.2.10^{-6}$	14	14	70	70	70
80	$0.2.10^{-6}$	53	29	265	145	205
Pn*(H)TiCl$_2$(O-Si(Me)$_2$^{t}Bu) (5)						
40	$0.2.10^{-6}$	43	45	215	225	220
50	$0.2.10^{-6}$	33	26	165	130	148
60	$0.2.10^{-6}$	56	62	280	310	295
70	$0.2.10^{-6}$	15	9	75	45	60
80	$0.2.10^{-6}$	15	18	75	90	83

Table A4.4. Slurry-phase ethylene homopolymerisation activities, temperature, mass of catalyst and mas of polymer. Polymerisation conditions: 30 minutes, 1000 rpm. 50 mL hexane, 10 mg catalyst, 2 bar ethylene, 150 mg TiBA, $[Al_{sMAO}]_0$:$[Ti]_0$ = 200:1.

Temperature (°C)	Mass catalyst (mg)		Mass polymer (mg)		Activity ($kg_{PE}/mol_{Ti}/h/bar$)		Average activity ($kg_{PE}/mol_{Ti}/h/bar$)
	1	2	1	2	1	2	
sMAO-Pn*(H)TiCl$_2$(O-2,6-^{i}Pr-C$_6$H$_3$) (3$_{sMAO}$)							
40	10.2	10.2	89	82	115	106	111
50	9.9	10.5	78	75	104	94	99
60	9.8	9.7	67	69	90	94	92
70	9.7	9.9	62	67	84	89	87
80	10.7	9.5	53	61	65	85	75
sMAO-Pn*(H)TiCl$_2$(O-2,4-^{t}Bu-C$_6$H$_3$) (4$_{sMAO}$)							
40	10.6	11.1	95	102	123	126	125
50	109	11.4	102	87	129	105	117
60	95	99	78	75	112	104	108
70	10.5	9.5	76	74	99	107	103
80	10.7	10.6	68	72	87	93	90
sMAO-Pn*(H)TiCl$_2$(O-Si(Me)$_2$^{t}Bu) (5$_{sMAO}$)							
40	10.0	10.8	266	268	366	342	354
50	9.9	9.7	126	134	175	190	182
60	11.1	10.5	110	122	137	160	148
70	10.1	9.9	99	76	135	105	120
80	10.8	110.8	92	97	117	113	115

Table A4.5. Solution phase activities of copolymerisation of ethylene with styrene and mass of polymer. Polymerisation conditions: 50 mL of toluene, 0.2 µmol of catalyst, $[Al_{MAO}]_0$:$[Ti]_0$ = 1500:1, 30 minutes, 150 mg TiBA, 1000 rpm, 40 °C, 125 µL styrene.

Complex	Catalyst (mol)	Mass polymer (mg)		Activity ($kg_{polymer}/mol_{Ti}$ /h/bar)		Average activity ($kg_{Polymer}/mol_{Ti}$ /h/bar)
		1	2	1	2	
Pn*(H)TiCl$_2$(O-2,6-^{i}Pr-C$_6$H$_3$) (**3**)	$0.2.10^{-6}$	38	17	190	85	138
Pn*(H)TiCl$_2$(O-2,4-^{t}Bu-C$_6$H$_3$) (**4**)	$0.2.10^{-6}$	40	33	200	165	183
Pn*(H)TiCl$_2$(O-Si(Me)$_2$^{t}Bu) (**5**)	$0.2.10^{-6}$	17	15	85	75	80

Table A4.6. Slurry-phase activities of copolymerisation of ethylene with styrene, mass of catalyst and mass of polymer. Polymerisation conditions: 50 mL of hexane, $[Al_{sMAO}]_0$:$[Ti]_0$ = 200:1, 30 minutes, 1000 rpm, 150 mg TiBA, 40 °C, 125 µL.

Complex	Mass catalyst (mg)		Mass polymer (mg)		Activity ($kg_{polymer}/mol_{Ti}/h/bar$)		Average activity ($kg_{Polymer}/mol_{Ti}/h/bar$)
	1	2	1	2	1	2	
sMAO-Pn*(H)$TiCl_2$(O-2,6-^{i}Pr-C_6H_3) **(3_{sMAO})**	10.9	10.7	52	36	63	44	54
sMAO-Pn*(H)$TiCl_2$(O-2,4-^{t}Bu-C_6H_3) **(4_{sMAO})**	9.9	9.7	17	10	24	14	19
sMAO-Pn*(H)$TiCl_2$(O-Si(Me)$_2{}^t$Bu) **(5_{sMAO})**	9.5	10.7	68	91	98	117	108

Table A4.7. Polystyrene molecular weights. Polymerisation conditions: solution : 10 minutes, 1000 rpm. 2 mL toluene, 2×10^{-7} mol catalyst, 1 mL styrene, $[Al_{MAO}]_0$:$[Ti]_0$ = 1500:1. Slurry : 10 minutes, 1000 rpm. 50 mL toluene, 10 mg catalyst, 3.7 mL styrene, $[Al_{sMAO}]_0$:$[Ti]_0$ = 200:1.

Temperature (°C)	Low M_w ($\times10^3$ g/mol)	Đ	High M_w ($\times10^6$ g/mol)	Đ
	Pn*(H)$TiCl_2$(O-2,6-^{i}Pr-C_6H_3) (3)			
40	9.3	2.9	1.59	3.1
55	10.6	2.5	1.50	3.0
70	10.2	2.6	1.31	3.3
	Pn*(H)$TiCl_2$(O-2,4-^{t}Bu-C_6H_3) (4)			
40	13.1	2.1	2.23	2.8
55	11.3	2.2	1.98	3.2
70	11.7	2.7	2.21	2.9
	Pn*(H)$TiCl_2$(O-Si(Me)$_2{}^t$Bu) (5)			
40	12.3	2.1	5.02	1.7
55	11.4	2.3	4.50	1.6
70	10.6	2.3	4.73	2.0
	sMAO-Pn*(H)$TiCl_2$(O-2,6-^{i}Pr-C_6H_3) (3_{sMAO})			
40	12.3	1.7	1.82	3.4
55	16.8	1.6	2.18	3.3
70	12.6	1.7	1.84	3.4
	sMAO-Pn*(H)$TiCl_2$(O-2,4-^{t}Bu-C_6H_3) (4_{sMAO})			
40	15.3	1.5	2.49	3.6
55	11.4	1.6	2.50	3.3
70	18.6	1.6	2.44	3.6
	sMAO-Pn*(H)$TiCl_2$(O-Si(Me)$_2{}^t$Bu) (5_{sMAO})			
40	16.7	1.5	0.70	1.3
55	12.0	2.0	3.42	1.7
70	16.7	1.7	4.53	1.7

Table A4.8. Polyethylene molecular weights. Polymerisation conditions: solution : 30 minutes, 1000 rpm. 50 mL hexane, 2×10^{-7} mol catalyst, 2 bar ethylene, 150 mg TiBA, $[Al_{MAO}]_0$:$[Ti]_0$ = 1500:1. Slurry : 30 minutes, 1000 rpm. 50 mL hexane, 10 mg catalyst, 2 bar ethylene, 150 mg TiBA, $[Al_{sMAO}]_0$:$[Ti]_0$ = 200:1.

Temperature (°C)	Low M_w ($\times10^3$ g/mol)	Đ	High M_w ($\times10^6$ g/mol)	Đ
		Pn*(H)TiCl$_2$(O-2,6-^{i}Pr-C$_6$H$_3$)		
40	-	-	1.43	8.0
		Pn*(H)TiCl$_2$(O-2,4-^{t}Bu-C$_6$H$_3$)		
40	-	-	1.76	5.9
		sMAO-Pn*(H)TiCl$_2$(O-2,6-^{i}Pr-C$_6$H$_3$)		
40	83.1	2.7	1.88	1.8
50	76.9	3.0	1.84	1.7
60	56.2	5.0	1.51	1.7
70	58.1	4.5	1.36	1.8
80	42.5	3.9	1.13	1.8
		sMAO- Pn*(H)TiCl$_2$(O-2,4-^{t}Bu-C$_6$H$_3$)		
40	100.7	2.5	2.19	1.7

Table A4.9. Molecular weights of polymer produced by the copolymerisation of ethylene with 125 µL of styrene at 40 °C. Polymerisation conditions: solution : 30 minutes, 1000 rpm. 50 mL hexane, 2×10^{-7} mol catalyst, 2 bar ethylene, 150 mg TiBA, $[Al_{MAO}]_0$:$[Ti]_0$ = 1500:1. Slurry : 30 minutes, 1000 rpm. 50 mL hexane, 10 mg catalyst, 2 bar ethylene, 150 mg TiBA, $[Al_{sMAO}]_0$:$[Ti]_0$ = 200:1.

Complex	M_w ($\times10^6$ g/mol)	Đ
Pn*(H)TiCl$_2$(O-2,6-^{i}Pr-C$_6$H$_3$) (**3**)	1.7×10^{-3}	3.1
Pn*(H)TiCl$_2$(O-2,4-^{t}Bu-C$_6$H$_3$) (**4**)	1.07	3.3
Pn*(H)TiCl$_2$(O-Si(Me)$_2$^{t}Bu) (**5**)	1.46	3.3
sMAO-Pn*(H)TiCl$_2$(O-2,6-^{i}Pr-C$_6$H$_3$) (**3$_{sMAO}$**)	1.09	4.9
sMAO-Pn*(H)TiCl$_2$(O-2,4-^{t}Bu-C$_6$H$_3$)	1.84	4.9
sMAO-Pn*(H)TiCl$_2$(O-Si(Me)$_2$^{t}Bu) (**4$_{sMAO}$**)	1.47	2.7

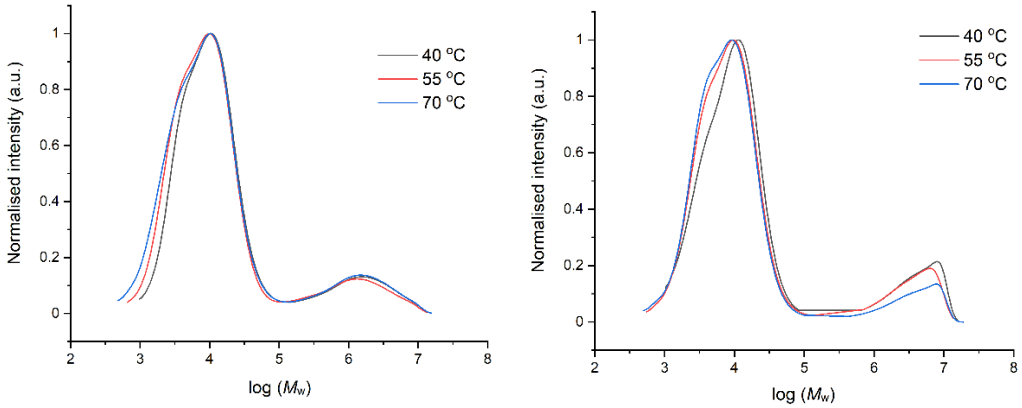

Figure A4.10. Molecular weights distribution for polystyrene synthesised using Pn*(H)TiCl$_2$(O-2,4-^{t}Bu-C$_6$H$_3$) (**4**) (left) and Pn*(H)TiCl$_2$(O-Si(Me)$_2$^{t}Bu) (**5**) (right). Polymerisation conditions: 10 minutes, 1000 rpm. 2 mL toluene, 2×10^{-7} mol catalyst, 1 mL styrene, $[Al_{MAO}]_0$:$[Ti]_0$ = 1500:1.

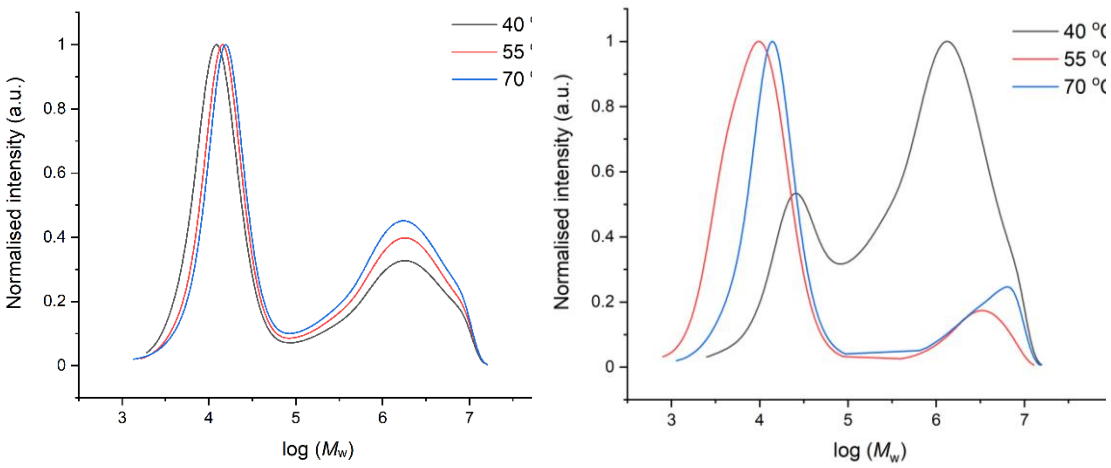

Figure A4.11. Molecular weights distribution for polystyrene synthesised using sMAO-Pn*(H)$TiCl_2$(O-2,4-^{t}Bu-C_6H_3) (**4$_{sMAO}$**) (left) and sMAO-Pn*(H)$TiCl_2$(O-Si(Me)$_2$^{t}Bu) (**5$_{sMAO}$**) (right). Polymerisation conditions: 10 minutes, 1000 rpm. 50 mL toluene, 10 mg catalyst, 3.7 mL styrene, $[Al_{sMAO}]_0$:$[Ti]_0$ = 200:1.

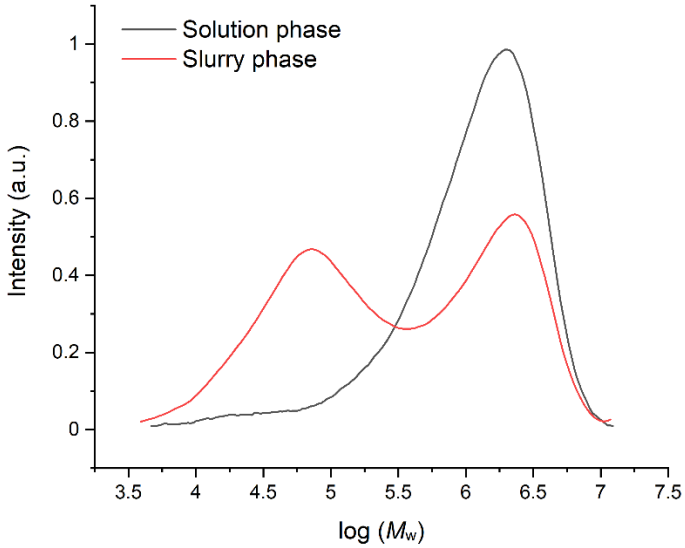

Figure A4.12. Molecular weights distribution for polyethylene synthesised using Pn*(H)$TiCl_2$(O-2,4-^{t}Bu-C_6H_3) (**4** and **4$_{sMAO}$**) at 40 °C. Polymerisation conditions: solution : 30 minutes, 1000 rpm. 50 mL hexane, 2×10^{-7} mol catalyst, 2 bar ethylene, 150 mg TiBA, $[Al_{MAO}]_0$:$[Ti]_0$ = 1500:1. Slurry : 30 minutes, 1000 rpm. 50 mL hexane, 10 mg catalyst, 2 bar ethylene, 150 mg TiBA, $[Al_{sMAO}]_0$:$[Ti]_0$ = 200:1.

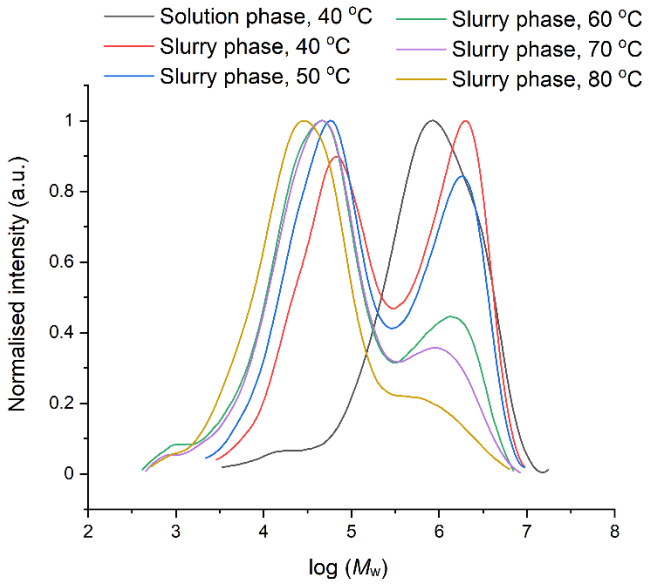

Figure A4.13. Molecular weights distribution for polyethylene synthesised using Pn*(H)$TiCl_2$(O-2,6-^{i}Pr-C_6H_3) (**3** and **3$_{sMAO}$**). Polymerisation conditions: solution : 30 minutes, 1000 rpm. 50 mL hexane, 2×10^{-7} mol catalyst, 2 bar ethylene, 150 mg TiBA, $[Al_{MAO}]_0$:$[Ti]_0$ = 1500:1. Slurry : 30 minutes, 1000 rpm. 50 mL hexane, 10 mg catalyst, 2 bar ethylene, 150 mg TiBA, $[Al_{sMAO}]_0$:$[Ti]_0$ = 200:1.

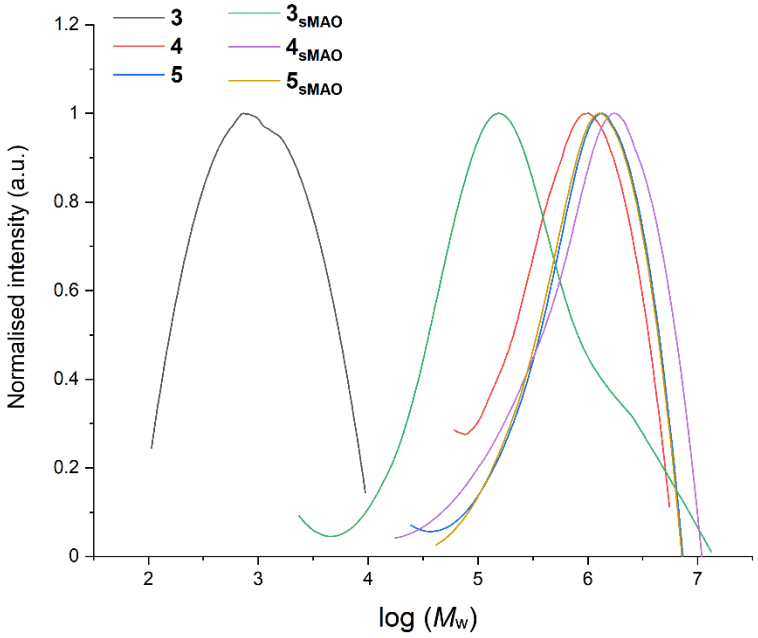

Figure A4.14. Molecular weights distribution for polymers produced by the copolymerisation of ethylene with 125 µL of styrene using Pn*(H)$TiCl_2$(OR) at 40 °C. Polymerisation conditions: solution : 30 minutes, 1000 rpm. 50 mL hexane, 2×10^{-7} mol catalyst, 2 bar ethylene, 150 mg TiBA, $[Al_{MAO}]_0$:$[Ti]_0$ = 1500:1. Slurry : 30 minutes, 1000 rpm. 50 mL hexane, 10 mg catalyst, 2 bar ethylene, 150 mg TiBA, $[Al_{sMAO}]_0$:$[Ti]_0$ = 200:1.

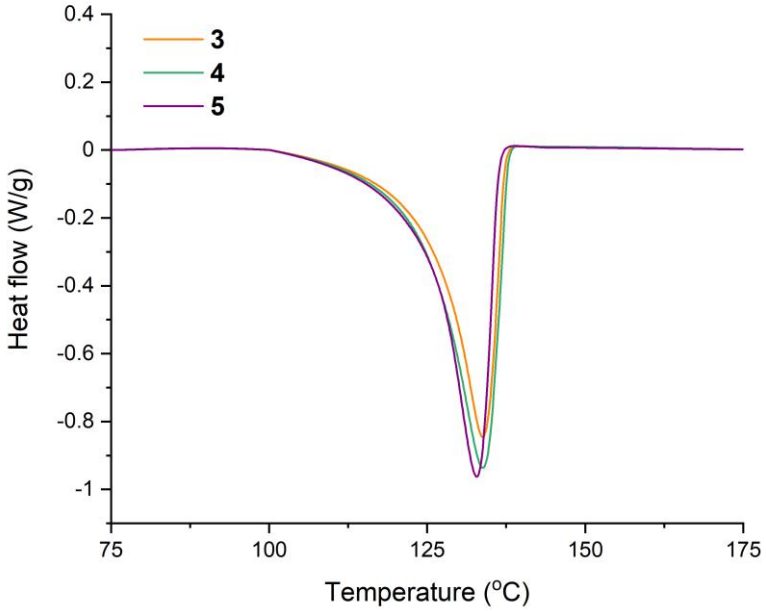

Figure A4.15 DSC curves of polyethylenes produced by Pn*(H)$TiCl_2$(OR) at 40 °C. Polymerisation conditions: 30 minutes, 1000 rpm. 50 mL hexane, 2×10^{-7} mol catalyst, 2 bar ethylene, 150 mg TiBA, $[Al_{MAO}]_0$:$[Ti]_0$ = 1500:1.

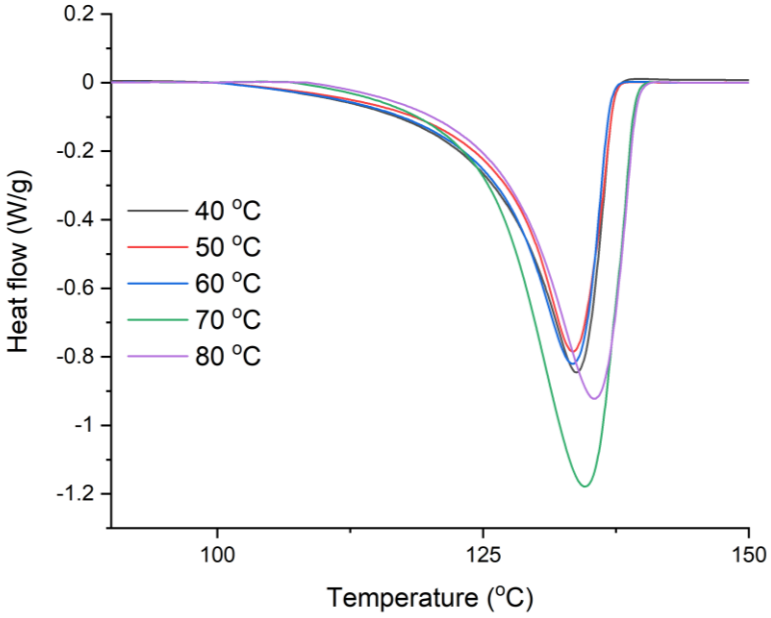

Figure A4.16. DSC curves of polyethylenes produced by Pn*(H)$TiCl_2$(O-2,6-^{i}Pr-C_6H_3) (**3**). Polymerisation conditions: 30 minutes, 1000 rpm. 50 mL hexane, 2×10^{-7} mol catalyst, 2 bar ethylene, 150 mg TiBA, $[Al_{MAO}]_0$:$[Ti]_0$ = 1500:1.

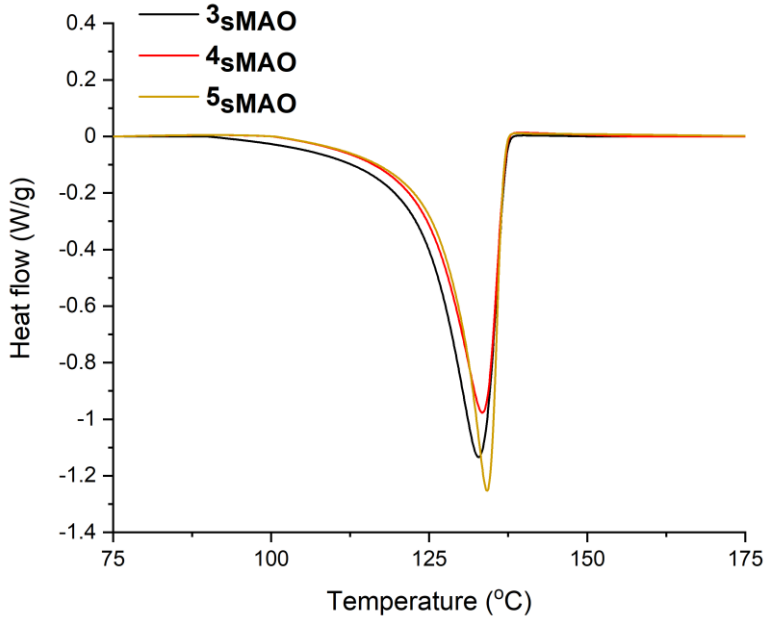

Figure A4.17. DSC curves of polyethylenes produced by sMAO-Pn*(H)$TiCl_2$(OR) at 40 °C. Polymerisation conditions: 30 minutes, 1000 rpm. 50 mL hexane, 10 mg catalyst, 2 bar ethylene, 150 mg TiBA, $[Al_{sMAO}]_0$:$[Ti]_0$ = 200:1.

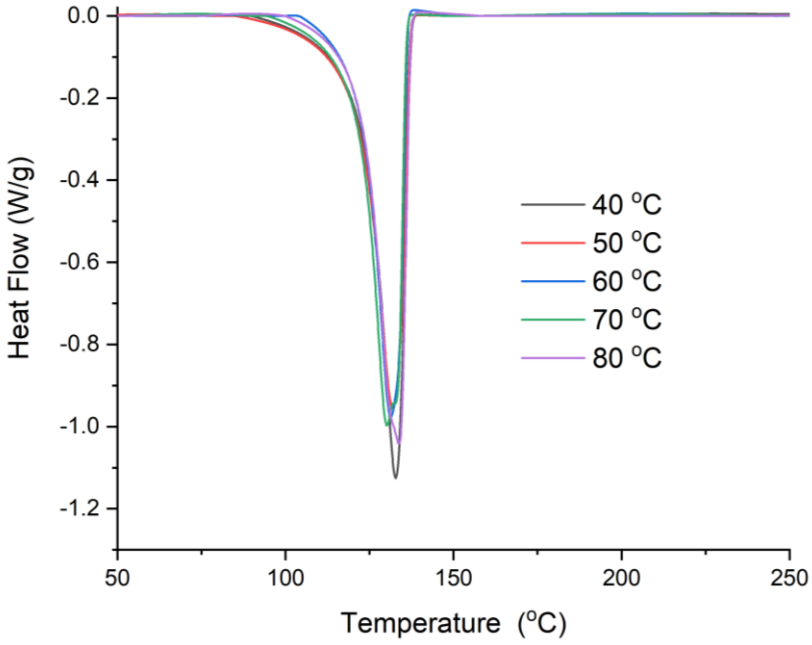

Figure A4.18. DSC curves of polyethylenes produced by sMAO-Pn*(H)$TiCl_2$(O-2,6-^{i}Pr-C_6H_3) (**3$_{sMAO}$**). Polymerisation conditions: 30 minutes, 1000 rpm. 50 mL hexane, 10 mg catalyst, 2 bar ethylene, 150 mg TiBA, $[Al_{sMAO}]_0$:$[Ti]_0$ = 200:1.

Table A4.10. *Meso* probabilities calculated for the polystyrenes synthesised by Pn*(H)$TiCl_2$(OR) at 55 °C.

Complex	P_m (calculated by $^{13}C\{^1H\}$ NMR)
Pn*(H)$TiCl_2$(O-2,6-^{i}Pr-C_6H_3) (**3**)	0.62
Pn*(H)$TiCl_2$(O-2,4-^{t}Bu-C_6H_3) (**4**)	0.58
Pn*(H)$TiCl_2$(O-Si(Me)$_2$^{t}Bu) (**5**)	0.59
sMAO-Pn*(H)$TiCl_2$(O-2,6-^{i}Pr-C_6H_3) (**3$_{sMAO}$**)	0.59
sMAO-Pn*(H)$TiCl_2$(O-2,4-^{t}Bu-C_6H_3) (**4$_{sMAO}$**)	0.59
sMAO-Pn*(H)$TiCl_2$(O-Si(Me)$_2$^{t}Bu) (**5$_{sMAO}$**)	0.57

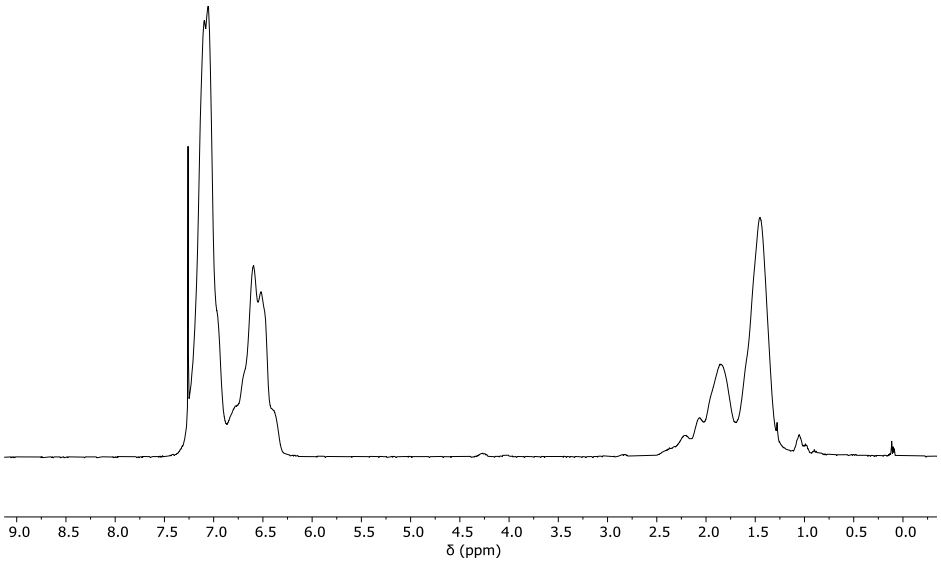

Figure A4.19. ^{1}H NMR spectrum of polystyrene produced by Pn*(H)$TiCl_2$(O-2,6-^{i}Pr-C_6H_3) (**3**) (chloroform-d_1, 298 K, 500 MHz).

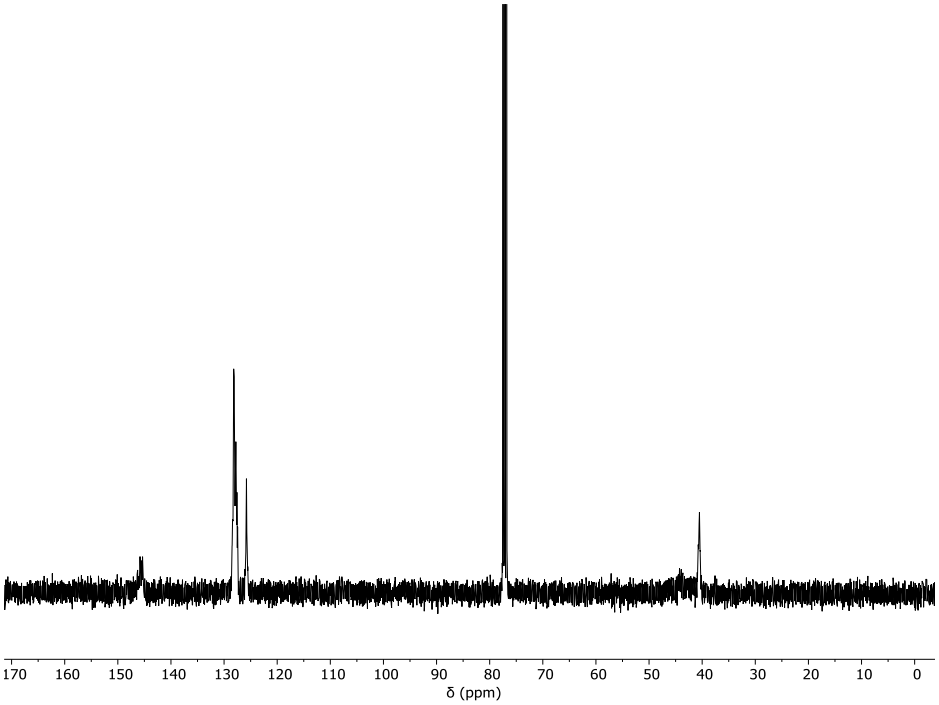

Figure A4.20. $^{13}C\{^{1}H\}$ NMR spectrum of polystyrene produced by Pn*(H)$TiCl_2$(O-2,6-^{i}Pr-C_6H_3) (**3**) (chloroform-d_1, 298 K, 125 MHz).

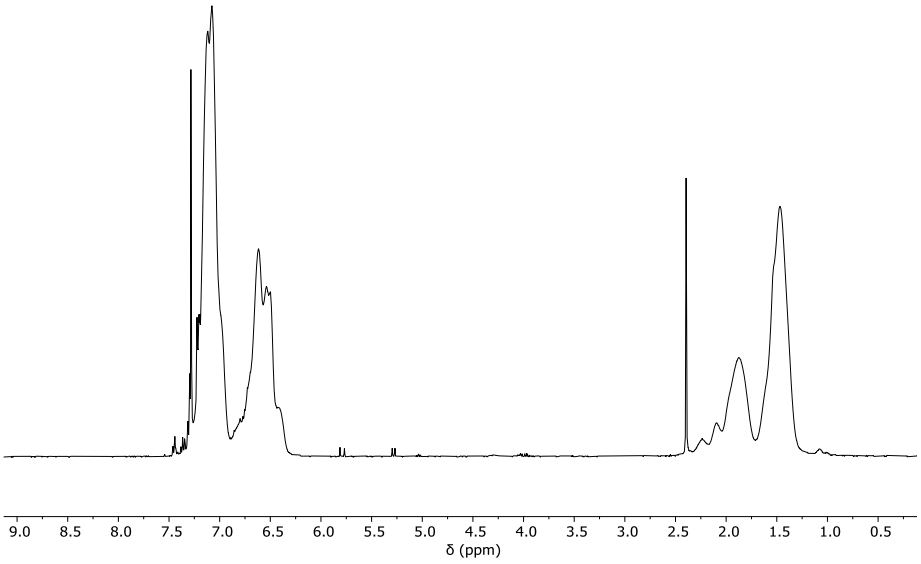

Figure A4.21. ^{1}H NMR spectrum of polystyrene produced by sMAO-Pn*(H)$TiCl_2$(O-2,6-^{i}Pr-C_6H_3) (**3_{sMAO}**) (chloroform-d_1, 298 K, 500 MHz).

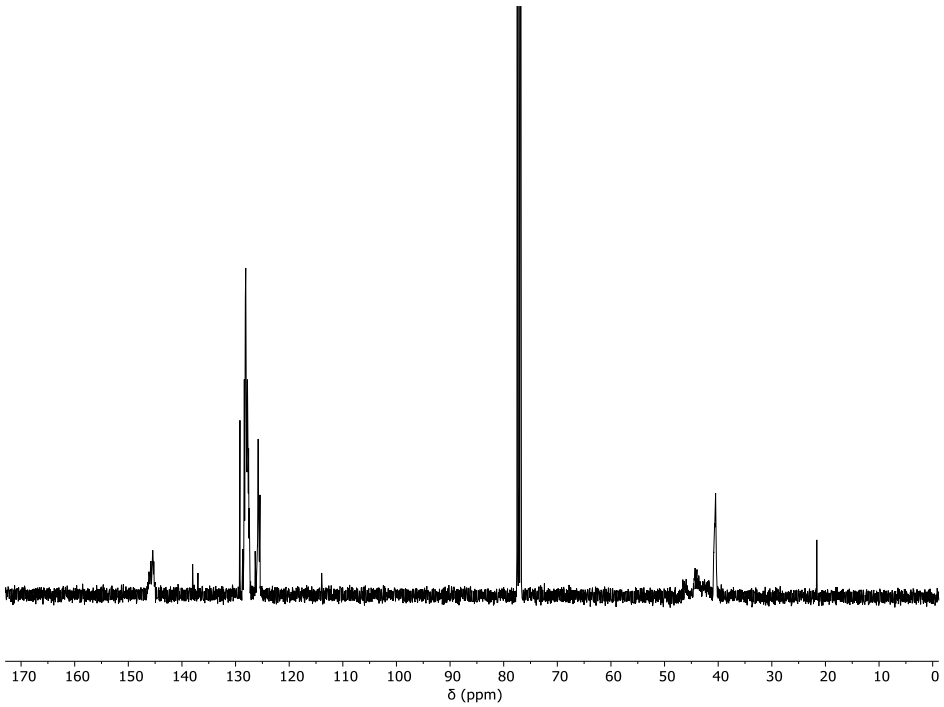

Figure A4.22. $^{13}C\{^{1}H\}$ NMR spectrum of polystyrene produced by sMAO-Pn*(H)$TiCl_2$(O-2,6-^{i}Pr-C_6H_3) (**3$_{sMAO}$**) (chloroform-d_1, 298 K, 125 MHz).

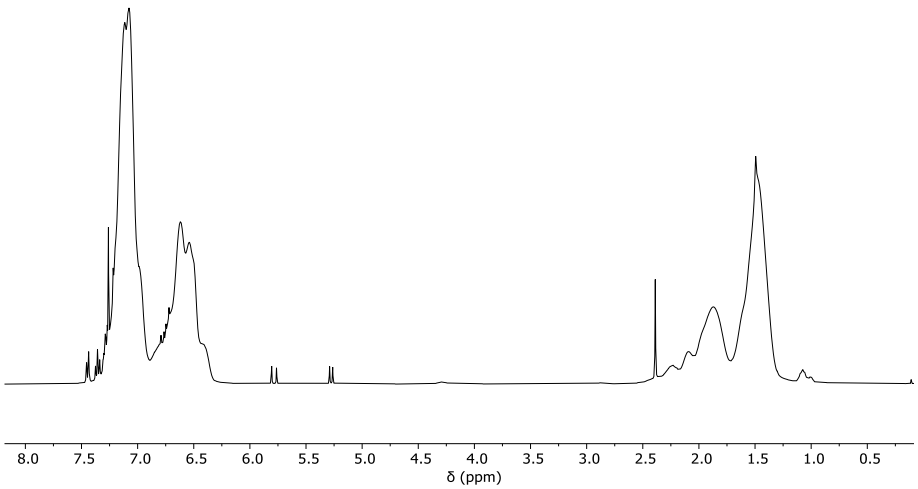

Figure A4.23. ^{1}H NMR spectrum of polystyrene produced by Pn*(H)$TiCl_2$(O-2,4-^{t}Bu-C_6H_3) (**4**) (chloroform-d_1, 298 K, 400 MHz).

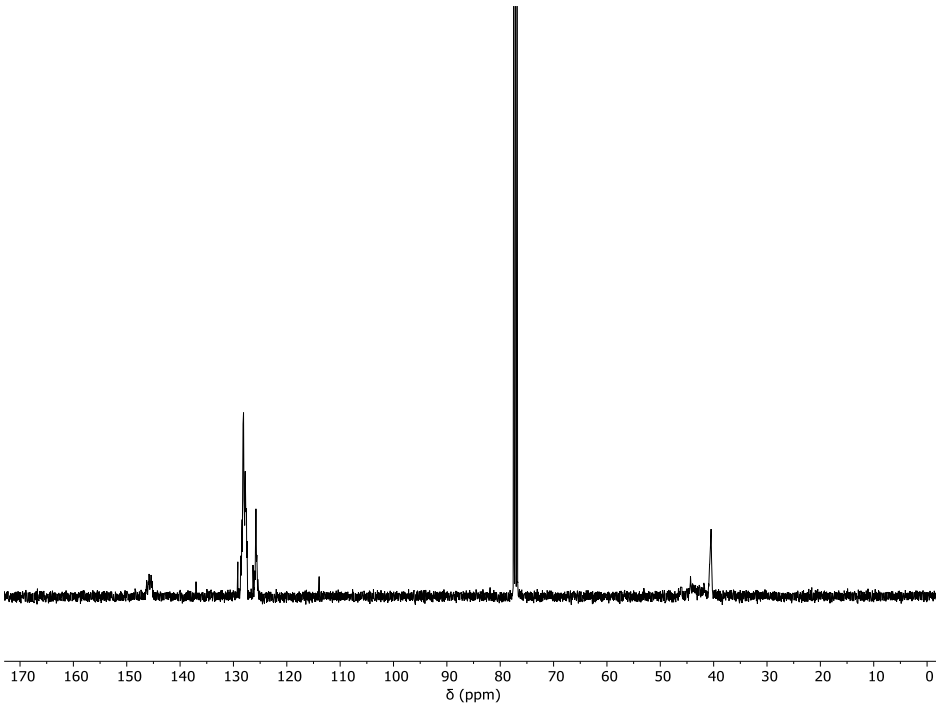

Figure A4.24. $^{13}C\{^{1}H\}$ NMR spectrum of polystyrene produced by Pn*(H)$TiCl_2$(O-2,4-^{t}Bu-C_6H_3) (**4**) (chloroform-d_1, 298 K, 125 MHz).

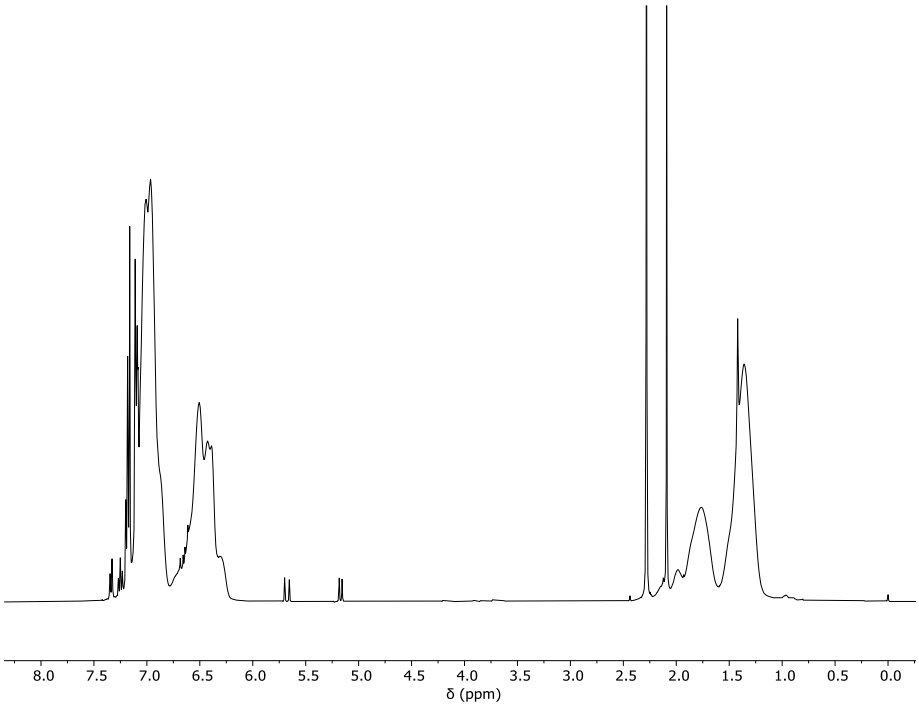

Figure A4.25. ^{1}H NMR spectrum of polystyrene produced by sMAO-Pn*(H)$TiCl_2$(O-2,4-^{t}Bu-C_6H_3) (**4_{sMAO}**) (chloroform-d_1, 298 K, 400 MHz).

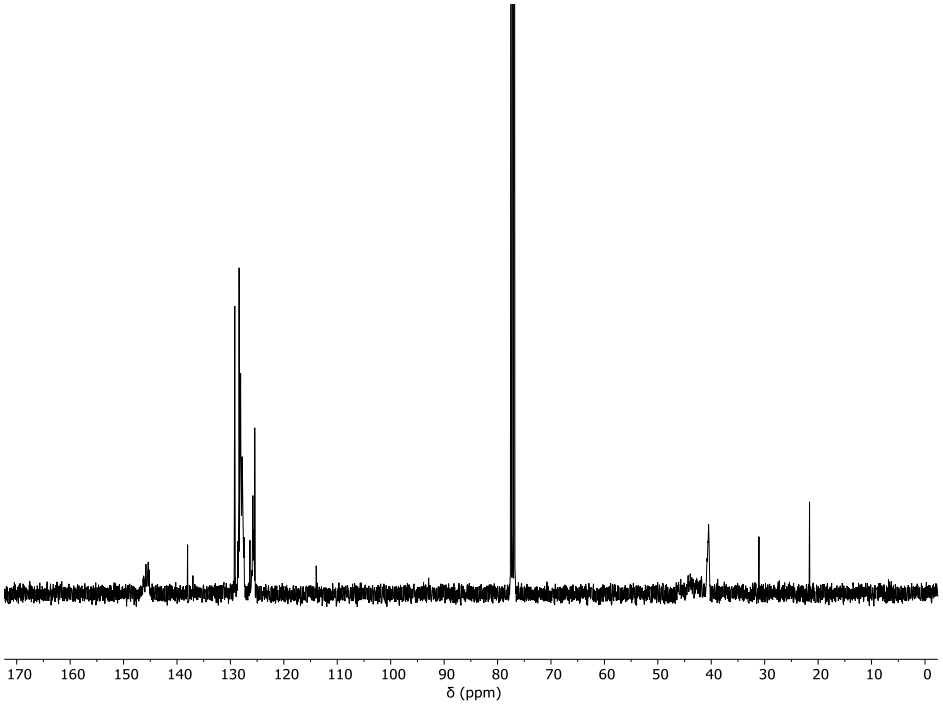

Figure A4.26. $^{13}C\{^{1}H\}$ NMR spectrum of polystyrene produced by sMAO-Pn*(H)$TiCl_2$(O-2,4-^{t}Bu-C_6H_3) (**4$_{sMAO}$**) (chloroform-d_1, 298 K, 125 MHz).

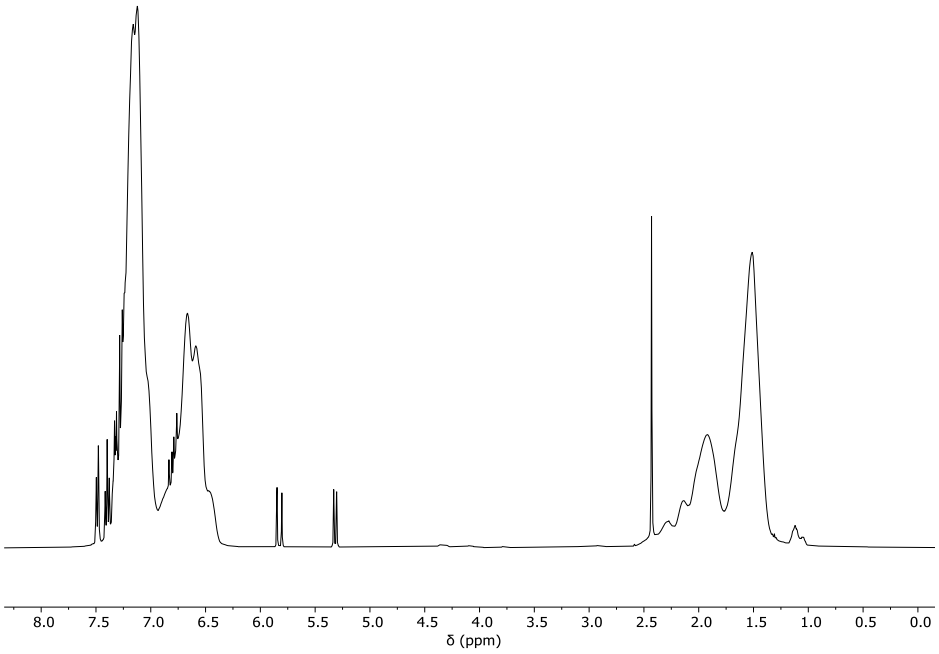

Figure A4.27. ^{1}H NMR spectrum of polystyrene produced by Pn*(H)$TiCl_2$(O-Si(Me)$_2$^{t}Bu) (**5**) (chloroform-d_1, 298 K, 400 MHz).

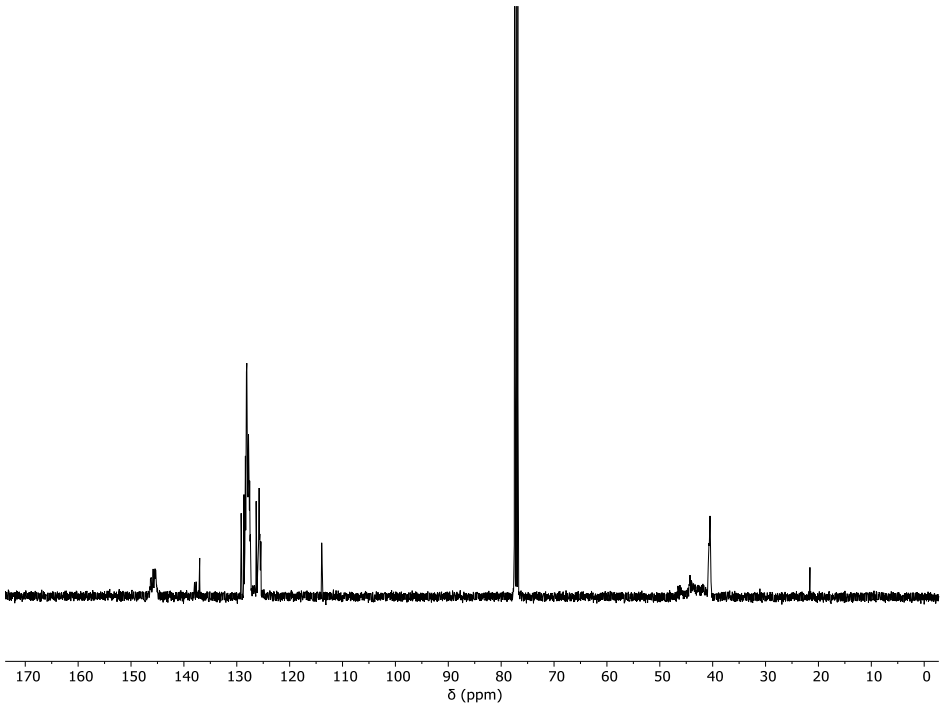

Figure A4.28. $^{13}C\{^{1}H\}$ NMR spectrum of polystyrene produced by Pn*(H)$TiCl_2$(O-Si(Me)$_2$^{t}Bu) (**5**) (chloroform-d_1, 298 K, 125 MHz).

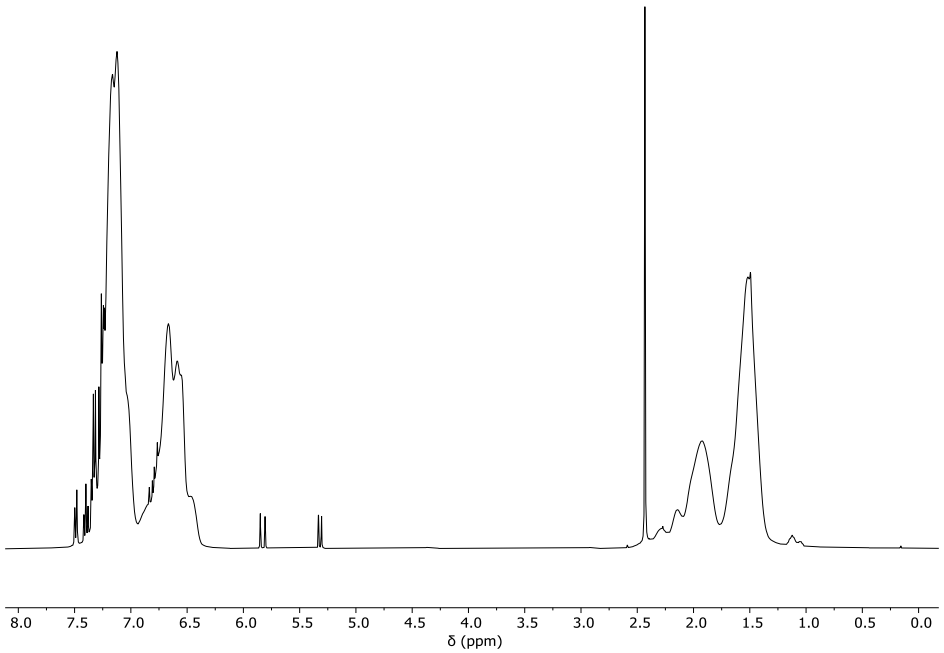

Figure A4.29. ^{1}H NMR spectrum of polystyrene produced by sMAO-Pn*(H)$TiCl_2$(O-Si(Me)$_2$^{t}Bu) (**5$_{sMAO}$**) (chloroform-d_1, 298 K, 400 MHz).

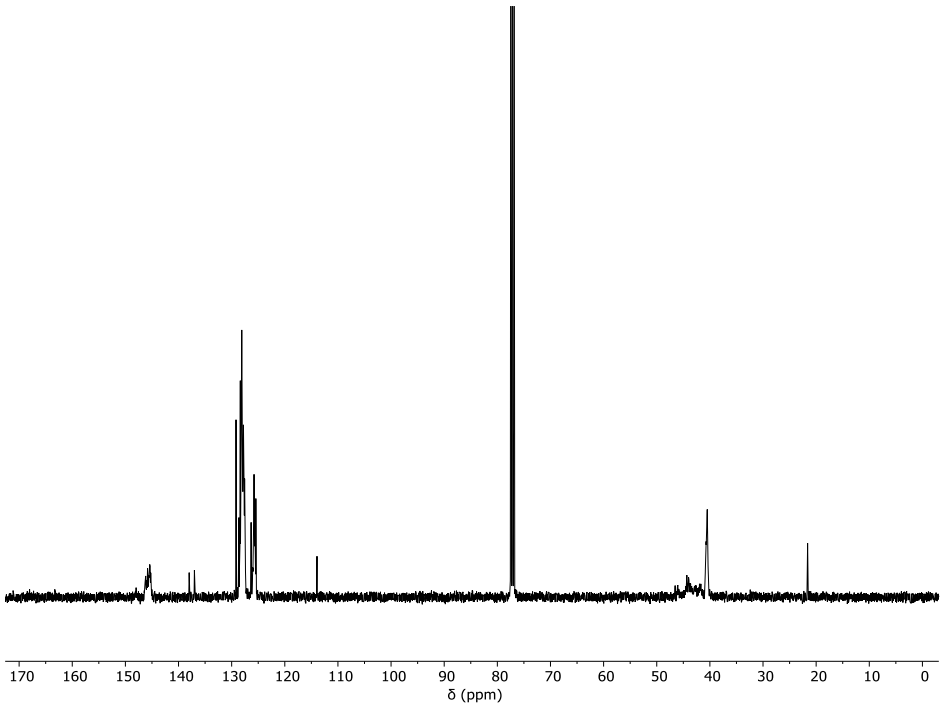

Figure A4.30. $^{13}C\{^{1}H\}$ NMR spectrum of polystyrene produced by sMAO-Pn*(H)$TiCl_2$(O-Si(Me)$_2$^{t}Bu) (**5$_{sMAO}$**) (chloroform-d_1, 298 K, 125 MHz).

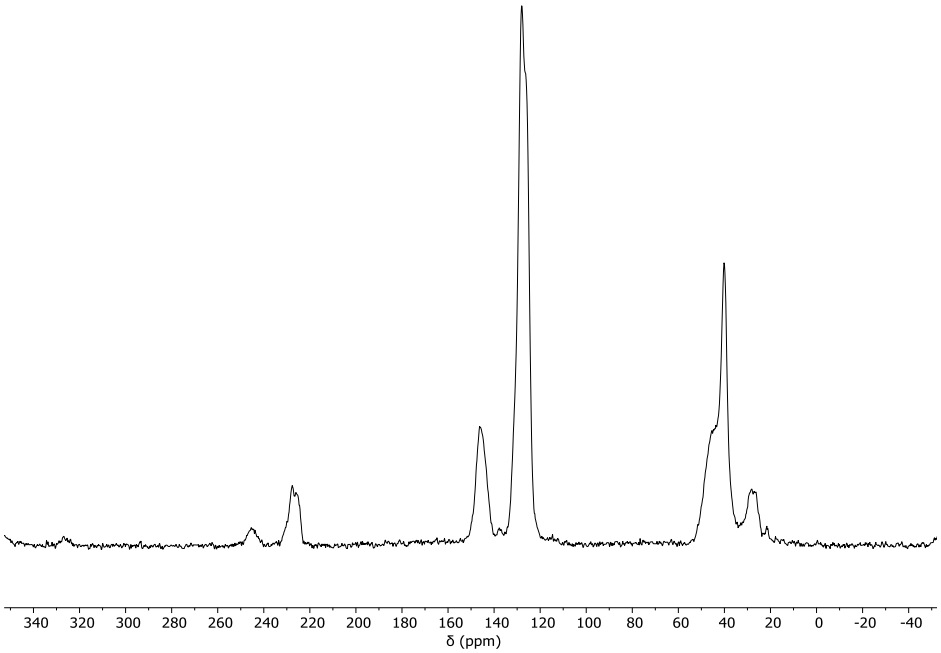

Figure A4.31. ^{13}C CPMAS NMR spectrum of polystyrene produced by sMAO-Pn*(H)$TiCl_2$(O-2,6-^{i}Pr-C_6H_3) (**5$_{sMAO}$**) (10 MHz).

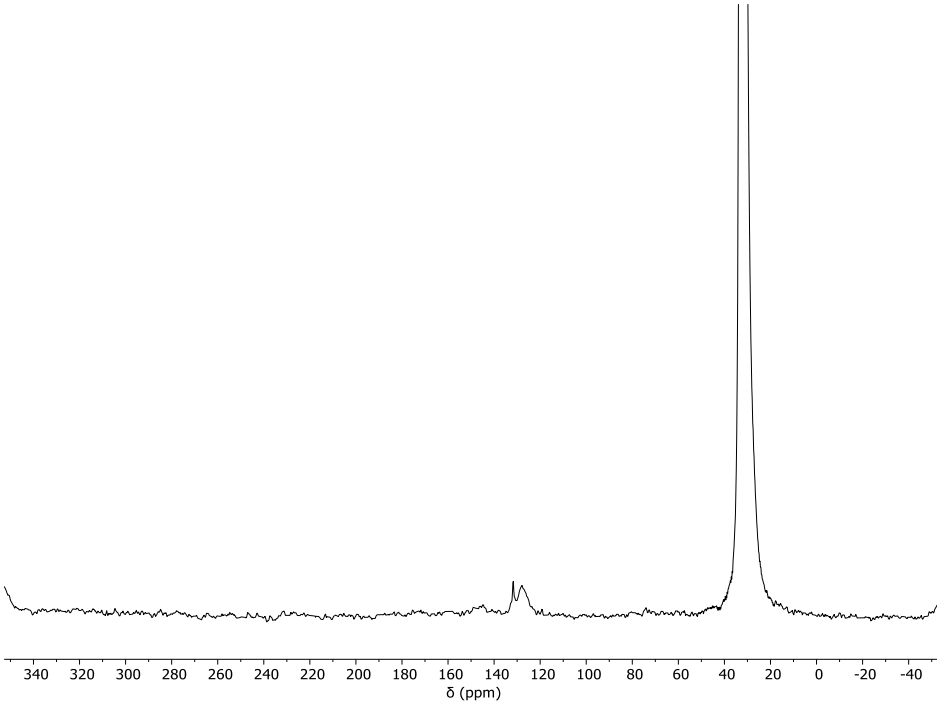

Figure A4.32. ^{13}C CPMAS NMR spectrum of polymer produced by the copolymerisation of ethylene with 125 µL styrene at 40 °C using sMAO-Pn*(H)$TiCl_2$(O-2,6-^{i}Pr-C_6H_3) (**3$_{sMAO}$**) (10 MHz).

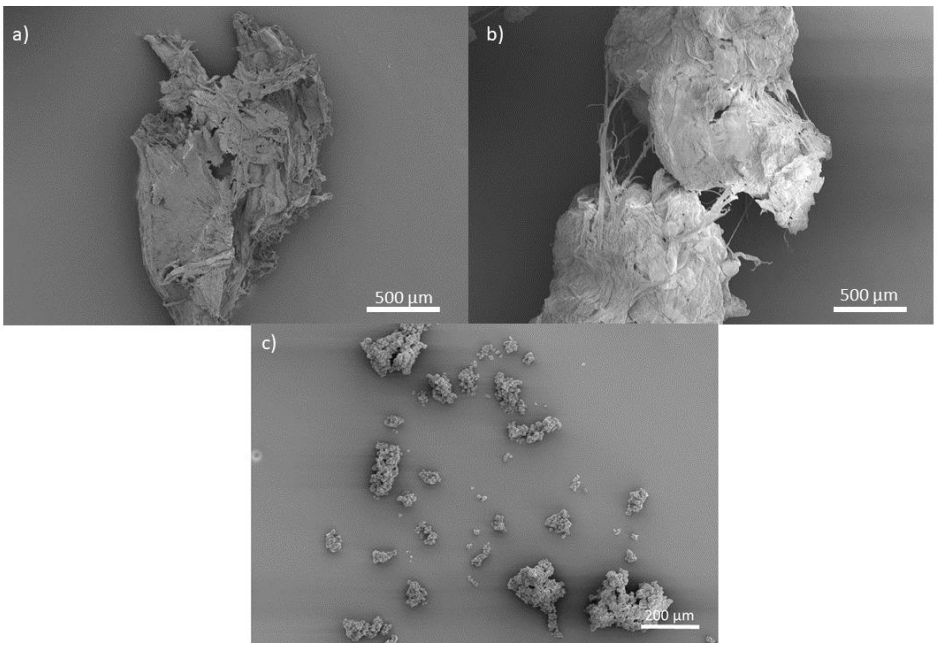

Figure A4.33. SEM images of polyethylenes produced by a) Pn*(H)$TiCl_2$(O-2,4-^{t}Bu-C_6H_3) (**4**) (x40), b) Pn*(H)$TiCl_2$(O-Si(Me)$_2$^{t}Bu) (**5**) (x35) and c) sMAO-Pn*(H)$TiCl_2$(O-Si(Me)$_2$^{t}Bu) (**5$_{sMAO}$**) (x80) at 40 °C.

Chapter 5

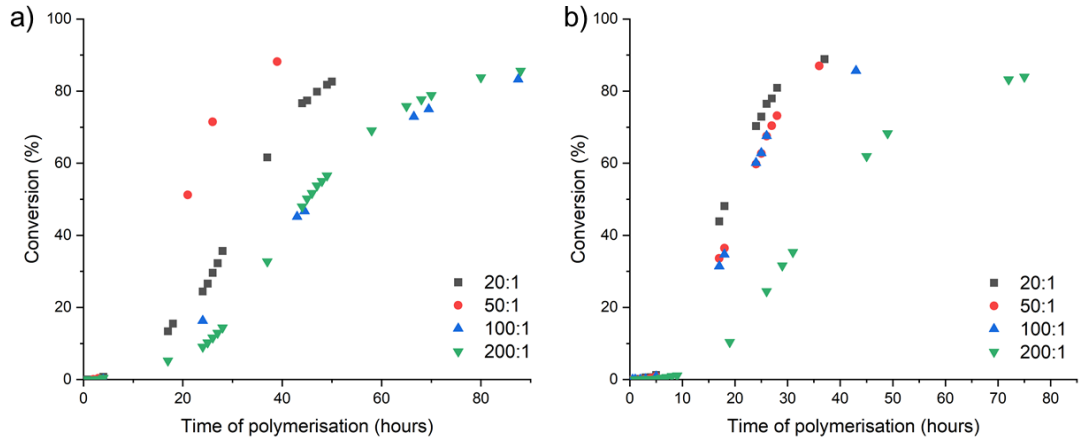

Figure A5.1. Percentage conversion to PLA for the ROP of *L*-lactide using a) Pn*(H)TiCl$_2$(O-2,6-^{i}Pr-C$_6$H$_3$) (**3**) and b) Pn*(H)TiCl$_2$(O-2,4-^{t}Bu-C$_6$H$_3$) (**4**). Polymerisation conditions: toluene-d_8, 120 °C and [LA]$_0$= 0.5M.

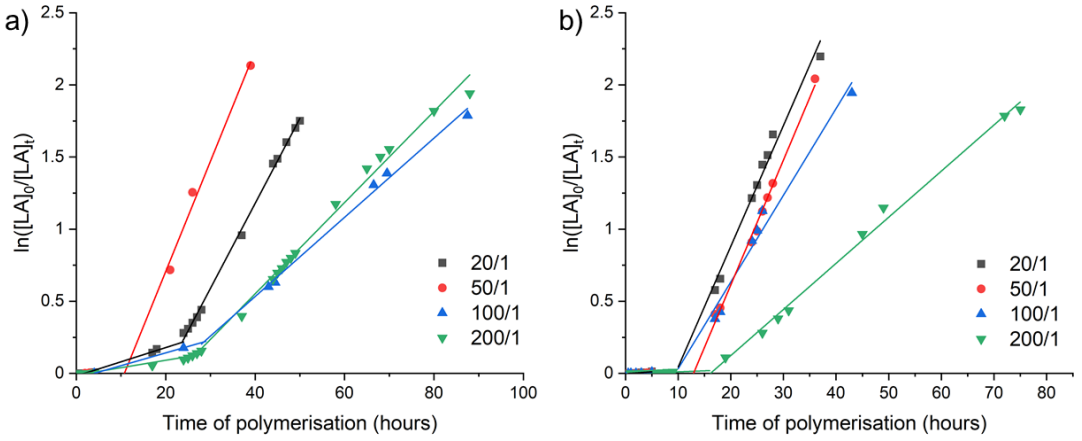

Figure A5.2. ln([LA]$_0$/[LA]$_t$) as a function of time of the polymerisation for the ROP of *L*-lactide using a) Pn*(H)TiCl$_2$(O-2,6-^{i}Pr-C$_6$H$_3$) (**3**) and b) Pn*(H)TiCl$_2$(O-2,4-^{t}Bu-C$_6$H$_3$) (**4**). Polymerisation conditions: toluene-d_8, 120 °C and [LA]$_0$= 0.5M.

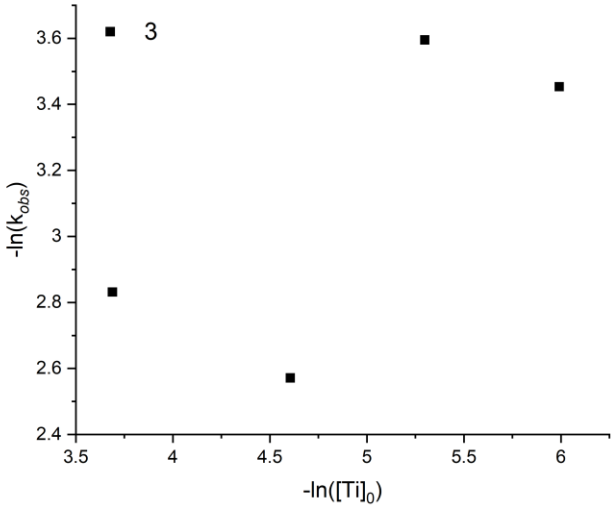

Figure A5.3. Plot of $-\ln(k_{obs})$ vs. $-\ln([Ti]_0)$ for the ROP of *L*-lactide using Pn*(H)TiCl$_2$(O-2,6-^{i}Pr-C$_6$H$_3$) (**3**). Polymerisation conditions: toluene-d_8, 120 °C and $[LA]_0$= 0.5M.

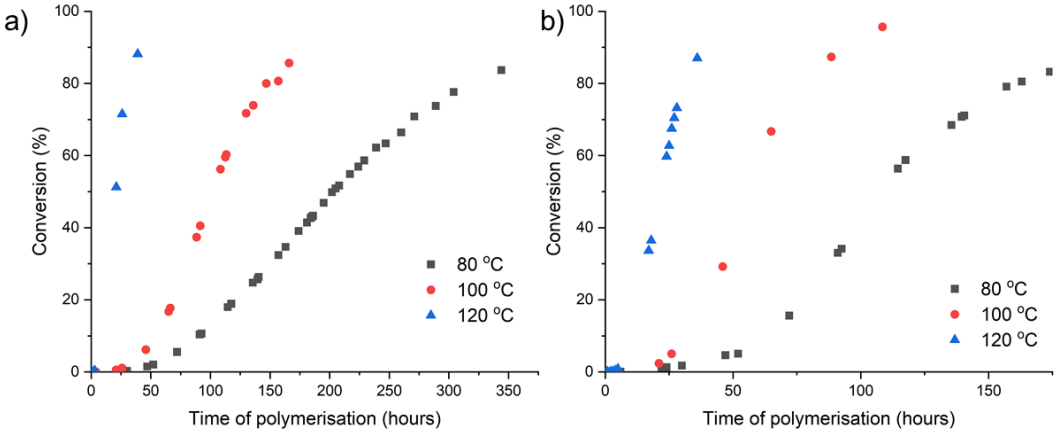

Figure A5.4. Percentage conversion to PLA for the ROP of *L*-lactide using a) Pn*(H)TiCl$_2$(O-2,6-^{i}Pr-C$_6$H$_3$) (**3**) and b) Pn*(H)TiCl$_2$(O-2,4-^{t}Bu-C$_6$H$_3$) (**4**). Polymerisation conditions: toluene-d_8, $[LA]_0$:$[Ti]_0$=50 and $[LA]_0$= 0.5M.

Table A5.1. Polymerisation of *L*-lactide using Pn*(H)TiCl$_2$(O-2,6-^{i}Pr-C$_6$H$_3$) (**3**) and Pn*(H)TiCl$_2$(O-2,4-^{t}Bu-C$_6$H$_3$) (**4**). Polymerisation conditions: toluene-d_8, 120 °C, [LA]$_0$:[Ti]$_0$= 50 and [LA]$_0$= 0.5M.

Initiators	T (°C)	Time (h)	Conversion (%)	k_{obs} (h^{-1})	M_n[a] (g/mol)	Đ
Pn*(H)TiCl$_2$(O-2,6-^{i}Pr-C$_6$H$_3$) (**3**)	80	344	84	0.0063 ± 0.00014	55535	1.36
Pn*(H)TiCl$_2$(O-2,6-^{i}Pr-C$_6$H$_3$) (**3**)	100	166	86	0.019 ± 0.00030	53169	1.47
Pn*(H)TiCl$_2$(O-2,6-^{i}Pr-C$_6$H$_3$) (**3**)	120	39	88	0.076 ± 0.0087	29581	1.77
Pn*(H)TiCl$_2$(O-2,4-^{t}Bu-C$_6$H$_3$) (**4**)	80	174	83	0.017 ± 0.00029	49604	1.31
Pn*(H)TiCl$_2$(O-2,4-^{t}Bu-C$_6$H$_3$) (**4**)	100	109	96	0.044 ± 0.0022	49415	1.37
Pn*(H)TiCl$_2$(O-2,4-^{t}Bu-C$_6$H$_3$) (**4**)	120	36	87	0.087 ± 0.0028	42347	1.40

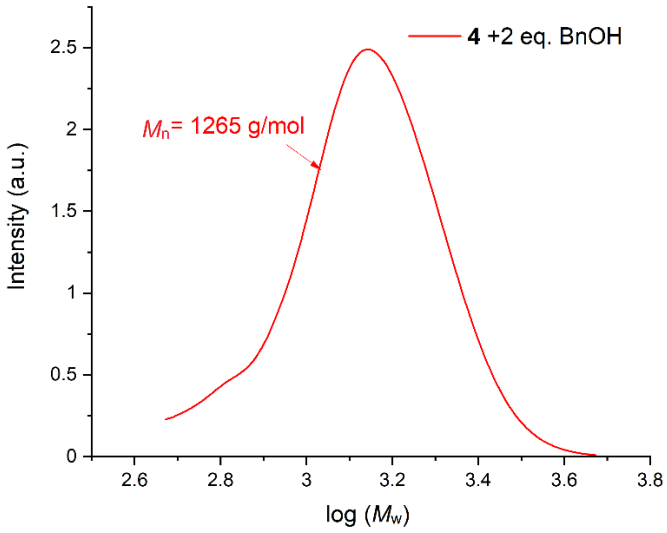

Figure A5.5. GPC trace of PLA produced using Pn*(H)TiCl$_2$(O-2,4-^{t}Bu-C$_6$H$_3$) (**4**) and 2 eq. of BnOH. Polymerisation conditions: toluene-d_8, 120 °C, [LA]$_0$:[Ti]$_0$= 50 and [LA]$_0$= 0.5M.

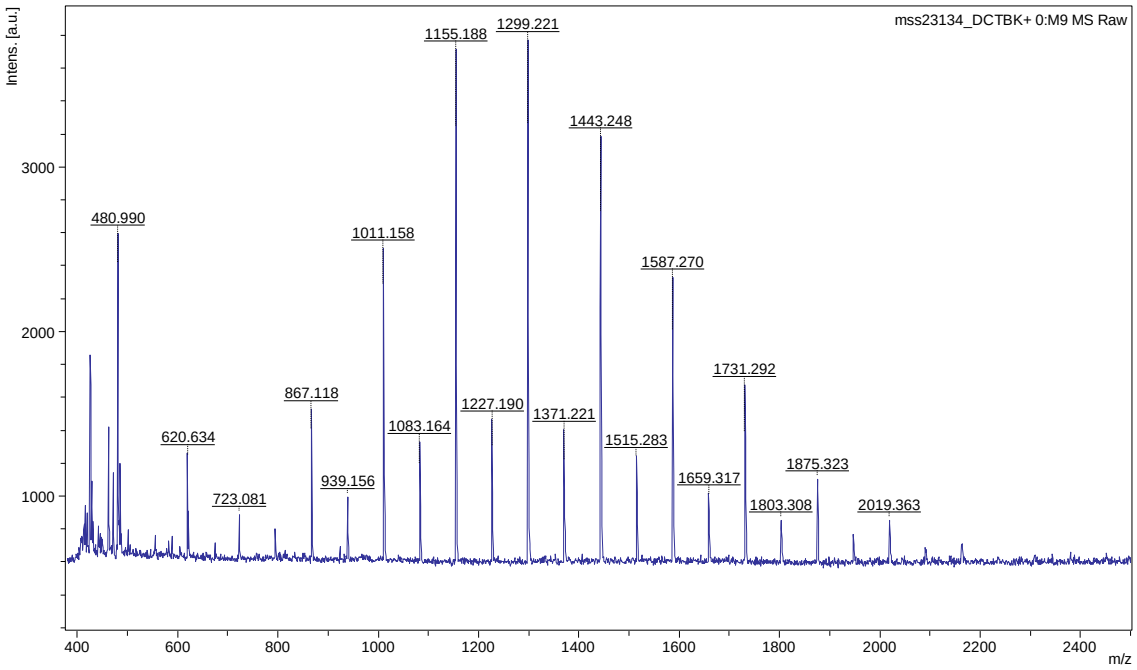

Figure A5.6. MALDI-TOF mass spectrum for the polymer produced by the ROP of *L*-lactide using Pn*(H)TiCl$_2$(O-2,4-^{t}Bu-C$_6$H$_3$) (**4**) and 2 eq. of BnOH. Polymerisation conditions: toluene-d_8, 120 °C, [LA]$_0$:[Ti]$_0$= 50 and [LA]$_0$= 0.5M.

Table A5.2. List of peaks observed in MALDI-TOF mass spectrometry for the polymer produced by the ROP of *L*-lactide using Pn*(H)TiCl$_2$(O-2,4-^{t}Bu-C$_6$H$_3$) (**4**) and 2 eq. of BnOH. Polymerisation conditions: toluene-d_8, 120 °C, [LA]$_0$:[Ti]$_0$= 50 and [LA]$_0$= 0.5M.

m/z	S/N	Intensity	Area
424.976	10	1735	246
426.627	10	1743	278
462.937	7	1313	196
480.99	16	2397	386
620.634	7	1225	142
723.081	4	884	85.9
795.097	3	765	68.8
867.118	8	1387	344
939.156	5	992	130
1011.158	17	2267	745
1083.164	6	1175	401
1155.188	25	3226	1359
1227.19	8	1282	529
1299.221	26	3243	1582
1371.221	7	1200	588
1443.248	21	2710	1493
1515.283	7	1222	232
1587.27	14	1987	1220
1659.317	5	988	176

1731.292	9	1369	927
1803.308	4	853	111
1875.323	6	1105	217
1947.313	3	765	112
2019.363	4	854	133

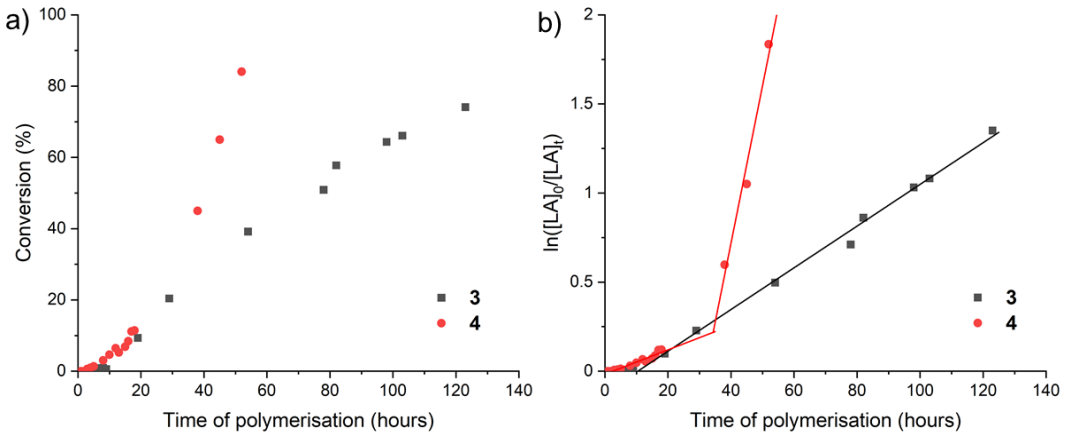

Figure A5.7. a) Percentage conversion and b) $\ln([LA]_0/[LA]_t)$ as a fonction of time for the ROP of *rac*-lactide using Pn*(H)$TiCl_2$(O-2,6-^{i}Pr-C_6H_3) (**3**), Pn*(H)$TiCl_2$(O-2,4-^{t}Bu-C_6H_3) (**4**) and Pn*(H)$TiCl_2$(O-Si$(CH_3)_2{}^t$Bu) (**5**). Polymerisation conditions: toluene-d_8, $[LA]_0$:$[Ti]_0$=50 and $[LA]_0$= 0.5M.

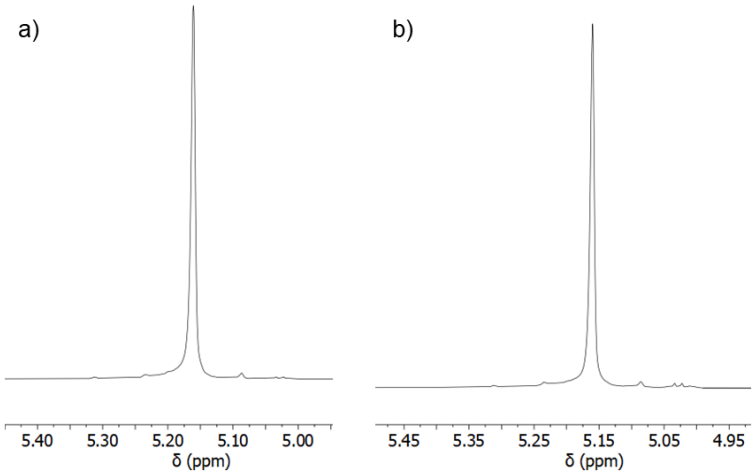

Figure A5.8. $^1H\{^1H\}$ NMR spectrum (chloroform-d_1, 500 MHz, 298K) of the PLLA produced using a) Pn*(H)$TiCl_2$(O-2,6-^{i}Pr-C_6H_3) (**3**) and b) Pn*(H)$TiCl_2$(O-2,4-^{t}Bu-C_6H_3) (**4**). Polymerisation conditions: toluene-d_8, 120 °C, $[LA]_0$:$[Ti]_0$= 50 and $[LA]_0$= 0.5M.

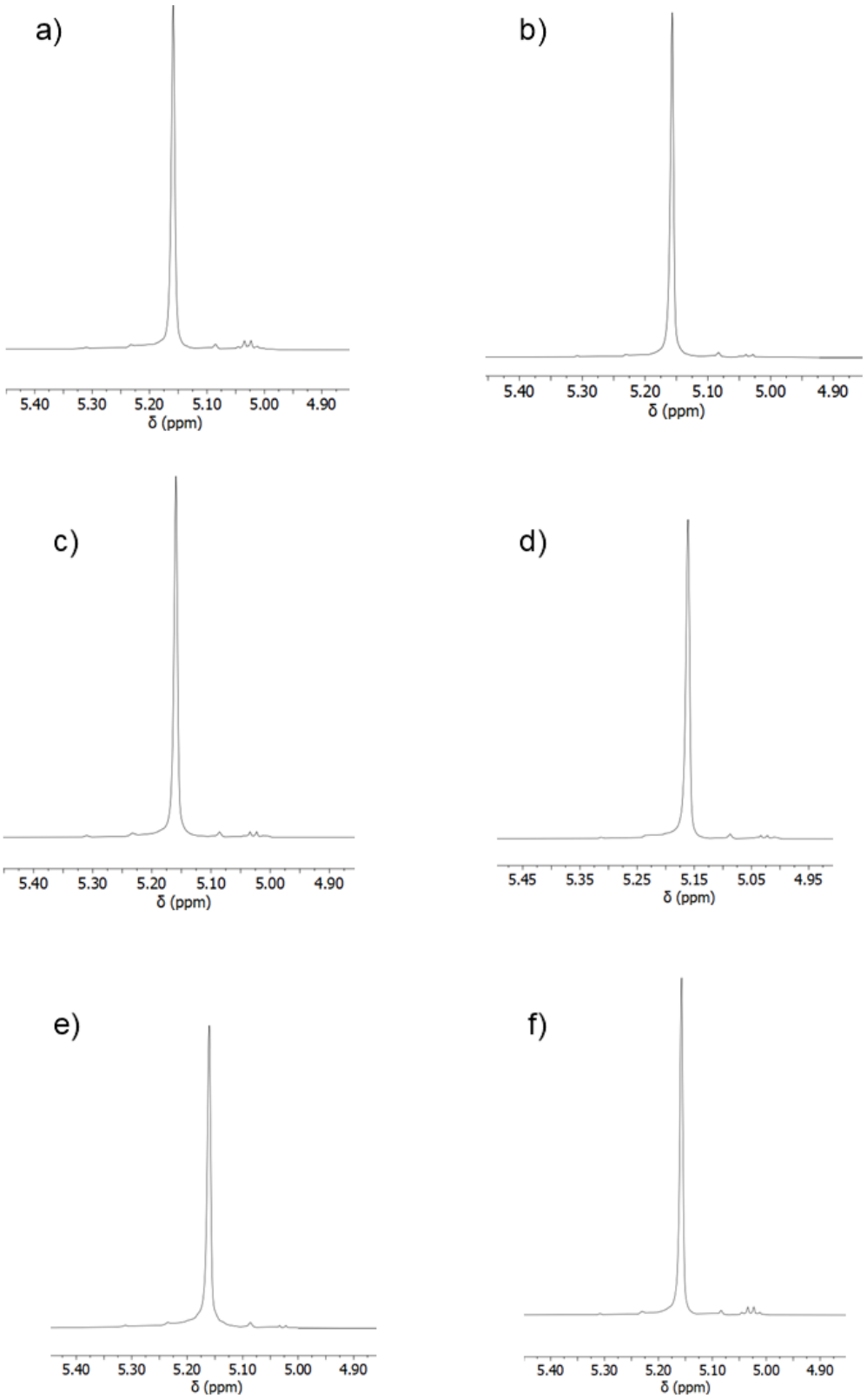

Figure A5.9. $^{1}H\{^{1}H\}$ NMR spectrum (chloroform-d_1, 500 MHz, 298K) of the PLLA produced using Pn*(H)$TiCl_2$(O-2,6-^{i}Pr-C_6H_3) (**3**) ($[LA]_0$:$[Ti]_0$= 20 a), 100 b) and 200 c) and Pn*(H)$TiCl_2$(O-2,4-^{t}Bu-C_6H_3) (**4**) ($[LA]_0$:$[Ti]_0$= 20 d), 100 e) and 200 f). Polymerisation conditions: toluene-d_8, 120 °C and $[LA]_0$= 0.5M.

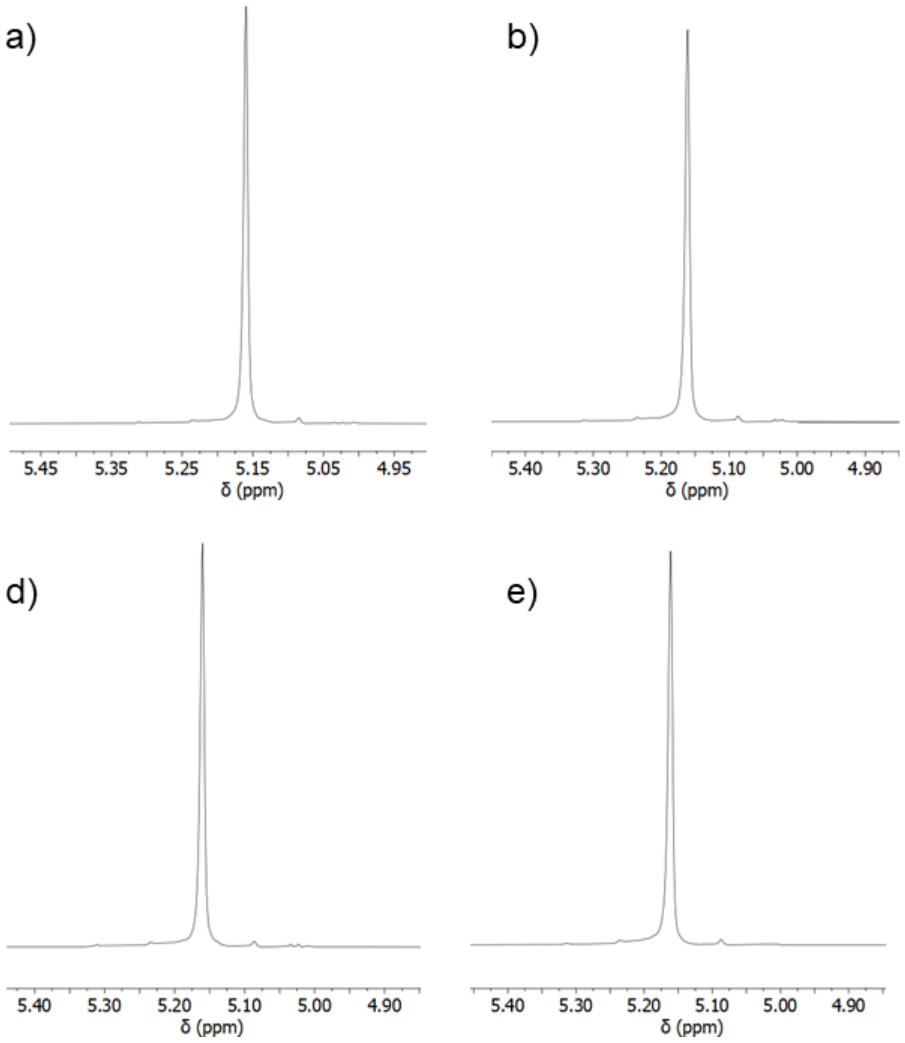

Figure A5.10. $^{1}H\{^{1}H\}$ NMR spectrum (chloroform-d_1, 500 MHz, 298K) of the PLLA produced using Pn*(H)$TiCl_2$(O-2,6-^{i}Pr-C_6H_3) (**3**) (T = 80 °C a) and 100 °C b) and Pn*(H)$TiCl_2$(O-2,4-^{t}Bu-C_6H_3) (**4**) (T = 80 °C d) and 100 °C e). Polymerisation conditions: toluene-d_8, $[LA]_0$:$[Ti]_0$= 50 and $[LA]_0$= 0.5M.

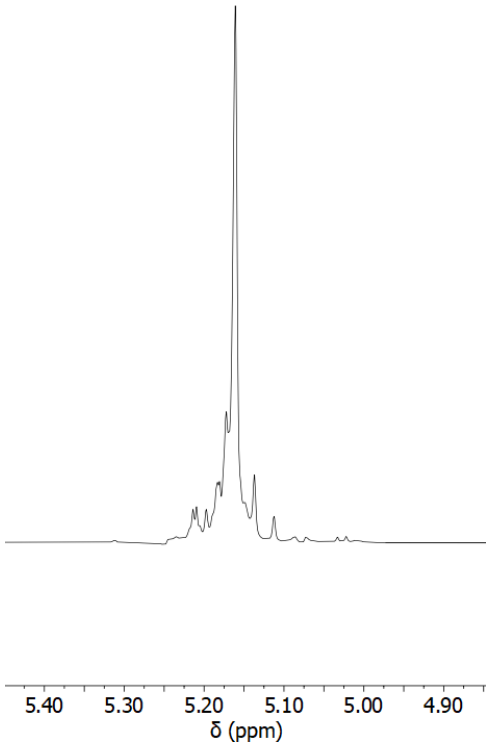

Figure A5.11. $^{1}H\{^{1}H\}$ NMR spectrum (chloroform-d_1, 500 MHz, 298K) of the PLLA produced using Pn*(H)$TiCl_2$(O-2,6-^{i}Pr-C_6H_3) (**3**) with 2 eq. of BnOH. Polymerisation conditions: toluene-d_8, $[LA]_0$:$[Ti]_0$= 50 and $[LA]_0$= 0.5M.

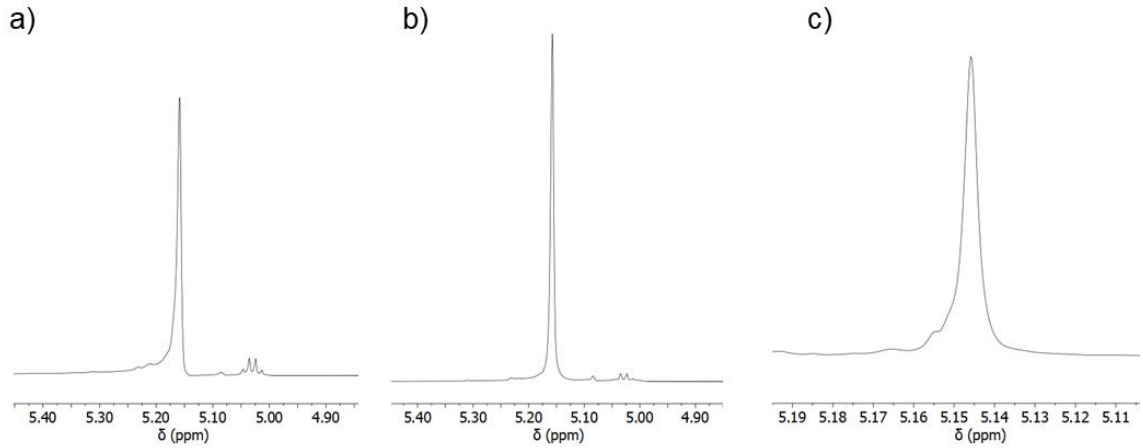

Figure A5.12. $^{1}H\{^{1}H\}$ NMR spectrum (chloroform-d_1, 500 MHz, 298K) of the PDLA produced using a) Pn*(H)$TiCl_2$(O-2,6-^{i}Pr-C_6H_3) (**3**), b) Pn*(H)$TiCl_2$(O-2,4-^{t}Bu-C_6H_3) (**4**) and c) Pn*(H)$TiCl_2$(O-Si(Me)$_2$^{t}Bu) (**5**). Polymerisation conditions: toluene-d_8, 120 °C, $[LA]_0$:$[Ti]_0$= 50 and $[LA]_0$= 0.5M.

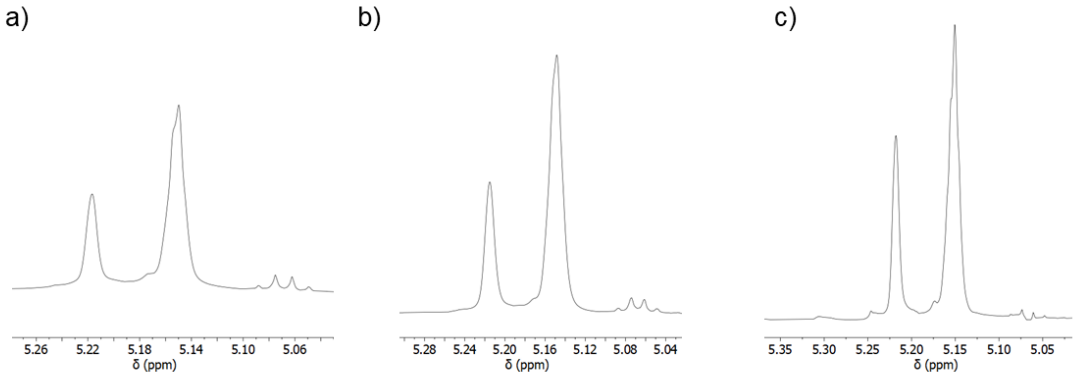

Figure A5.13. $^{1}H\{^{1}H\}$ NMR spectrum (chloroform-d_1, 500 MHz, 298K) of the PLA produced by the ROP of *meso*-lactide using a) Pn*(H)$TiCl_2$(O-2,6-^{i}Pr-C_6H_3) (**3**), b) Pn*(H)$TiCl_2$(O-2,4-^{t}Bu-C_6H_3) (**4**) and c) Pn*(H)$TiCl_2$(O-Si(Me)$_{2t}$Bu) (**5**). Polymerisation conditions: toluene-d_8, 120 °C, $[LA]_0$:$[Ti]_0$= 50 and $[LA]_0$= 0.5M.

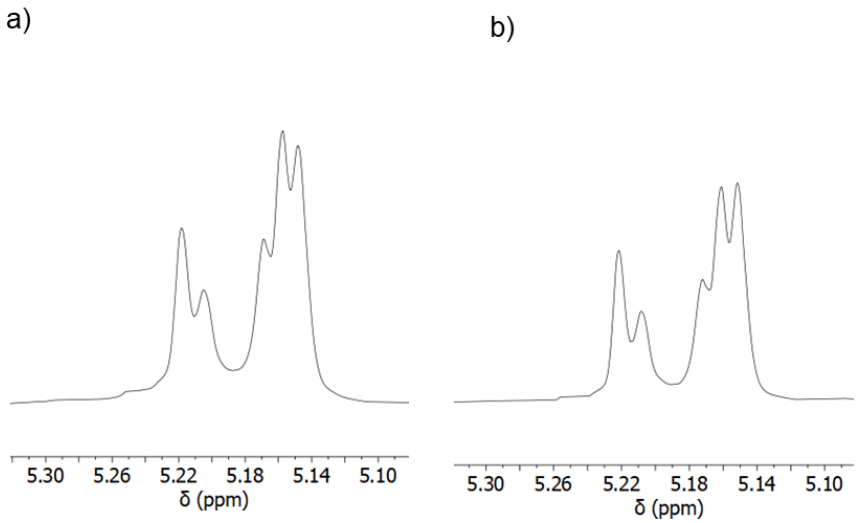

Figure A5.14. $^{1}H\{^{1}H\}$ NMR spectrum (chloroform-d_1, 500 MHz, 298K) of the PLA produced by the ROP of *rac*-lactide using a) Pn*(H)$TiCl_2$(O-2,6-^{i}Pr-C_6H_3) (**3**) and b) Pn*(H)$TiCl_2$(O-2,4-^{t}Bu-C_6H_3) (**4**). Polymerisation conditions: toluene-d_8, 120 °C, $[LA]_0$:$[Ti]_0$= 50 and $[LA]_0$= 0.5M.

Chapter 6

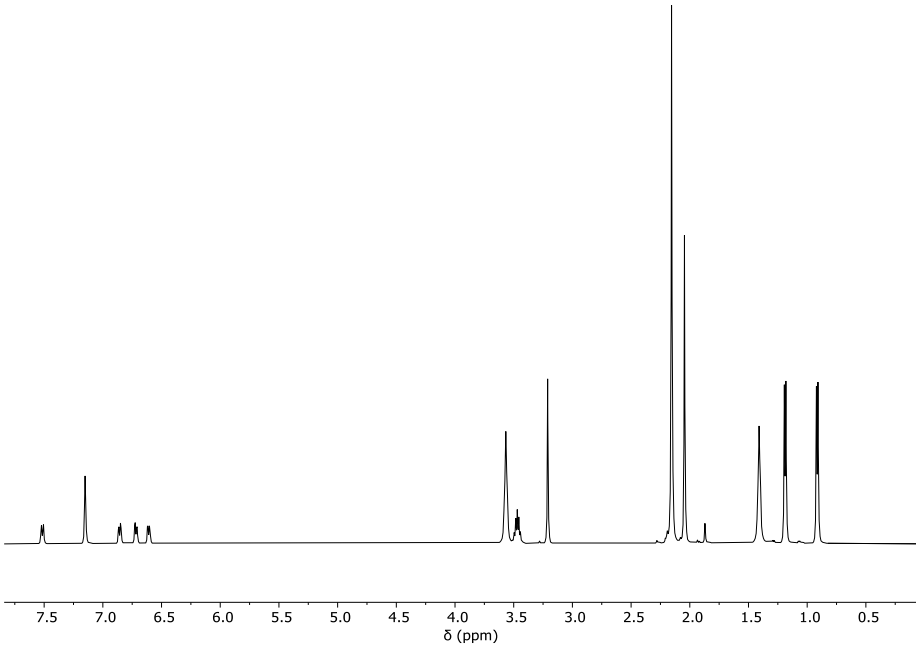

Figure A6.1. ^{1}H NMR spectrum of Pn*ZrCl[(N^{i}Pr)$_2$C(4-OMe-C$_6$H$_4$)] (benzene-d_6, 298 K and 500 MHz).

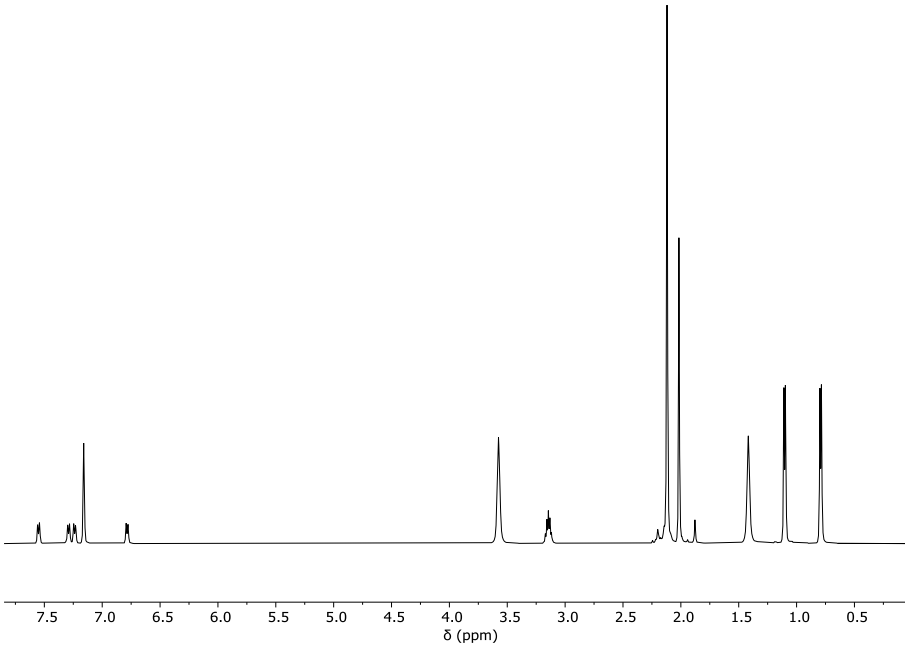

Figure A6.2. ^{1}H NMR spectrum of Pn*ZrCl[(N^{i}Pr)$_2$C(4-CF$_3$-C$_6$H$_4$)] (benzene-d_6, 298 K and 500 MHz).

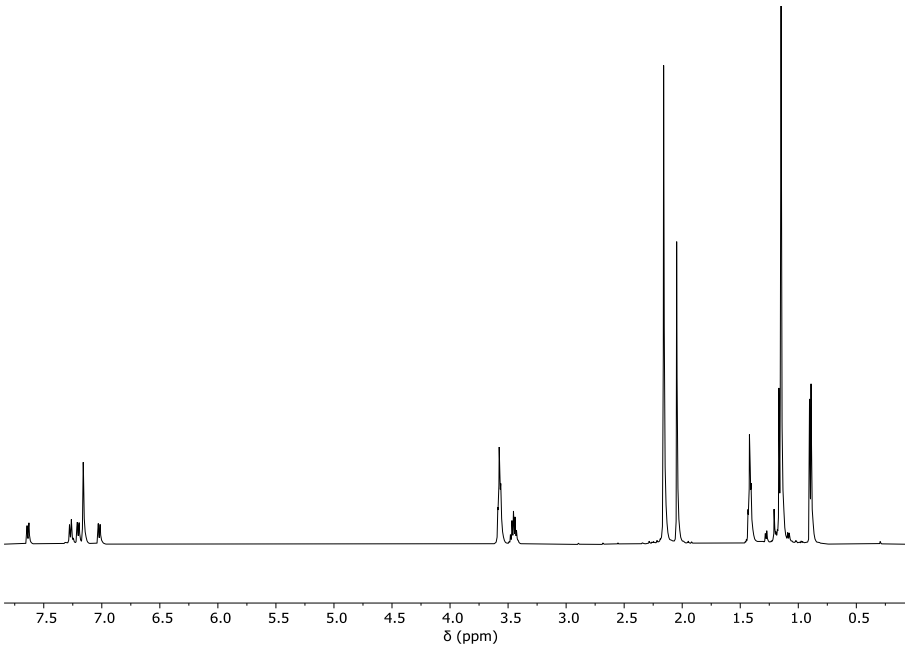

Figure A6.3. ^{1}H NMR spectrum of Pn*ZrCl[(N^{i}Pr)$_2$C(4-^{t}Bu-C$_6$H$_4$)] (benzene-d_6, 298 K and 500 MHz).

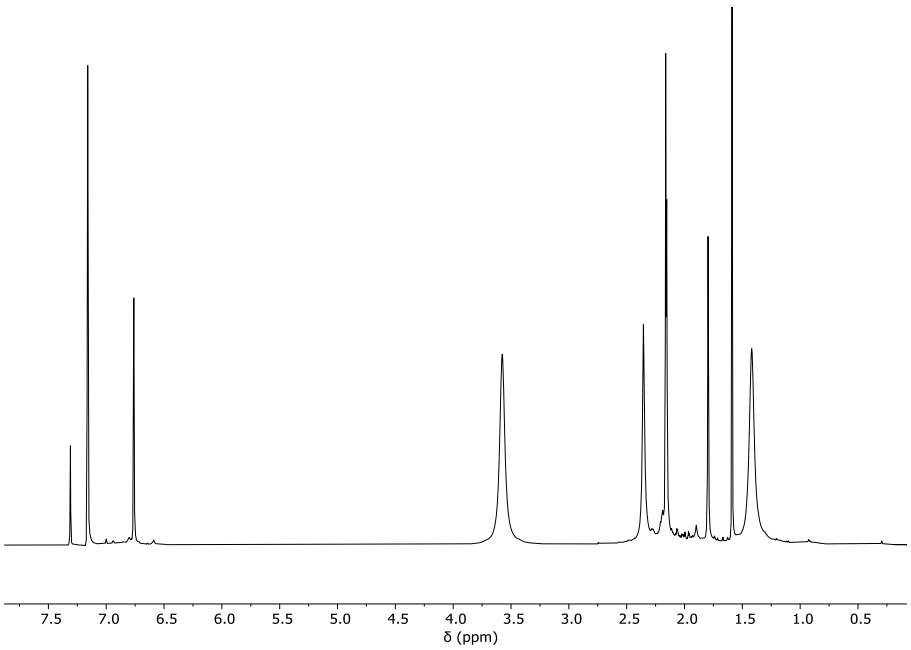

Figure A6.4. ^{1}H NMR spectrum of Pn*ZrCl[(NMes)$_2$CH] (benzene-d_6, 298 K and 500 MHz).

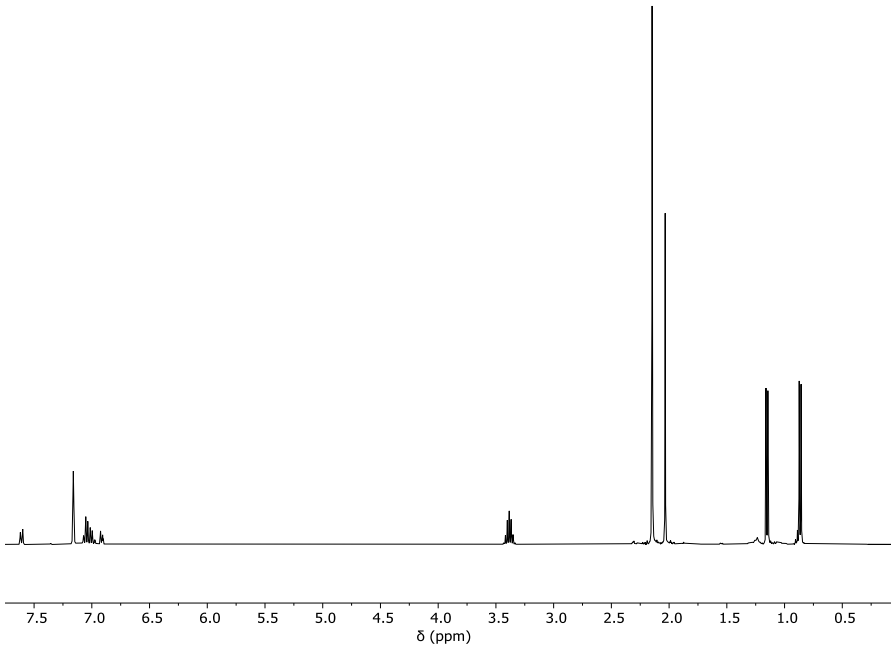

Figure A6.5. ^{1}H NMR spectrum of Pn*ZrCl[($N^{i}Pr)_2C(C_6H_5)$] (benzene-d_6, 298 K and 500 MHz).

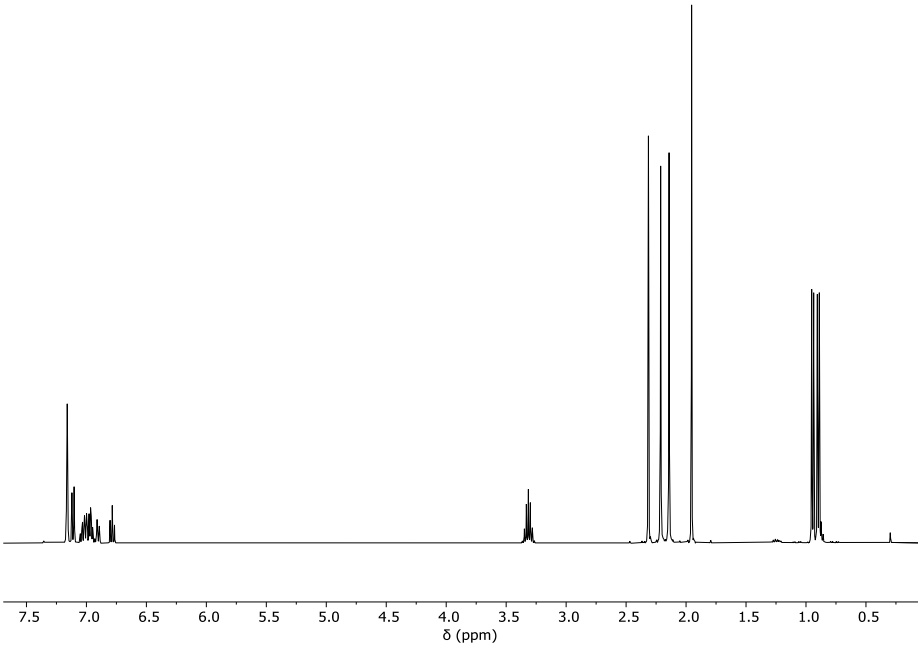

Figure A6.6. ^{1}H NMR spectrum of Pn*Zr(OXyl)[($N^{i}Pr)_2C(C_6H_5)$] (benzene-d_6, 298 K and 500 MHz).

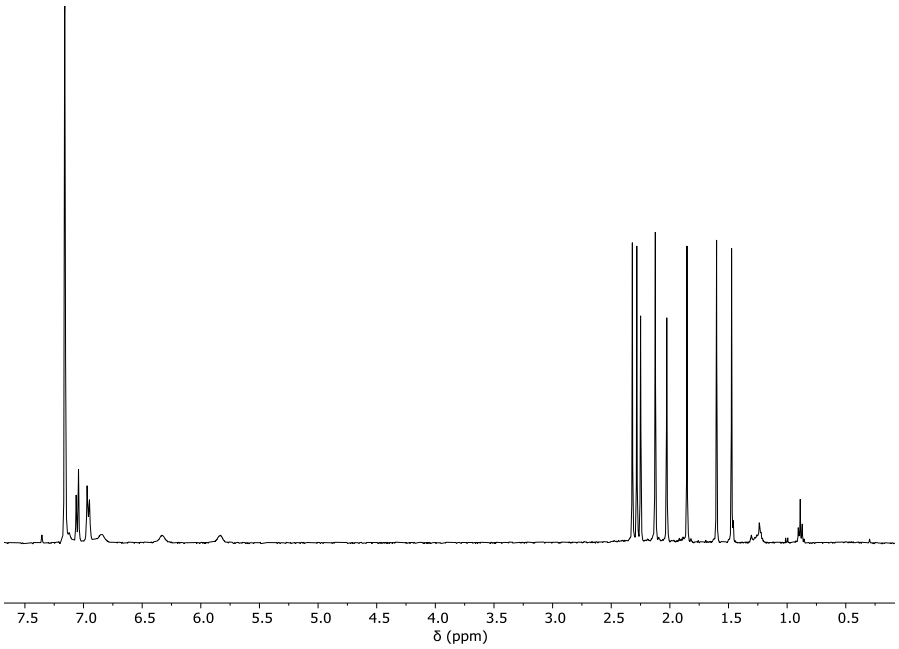

Figure A6.7. ^{1}H NMR spectrum of Pn*ZrCl[(N^{p}Tol)$_2$CH] (benzene-d_6, 298 K and 500 MHz).

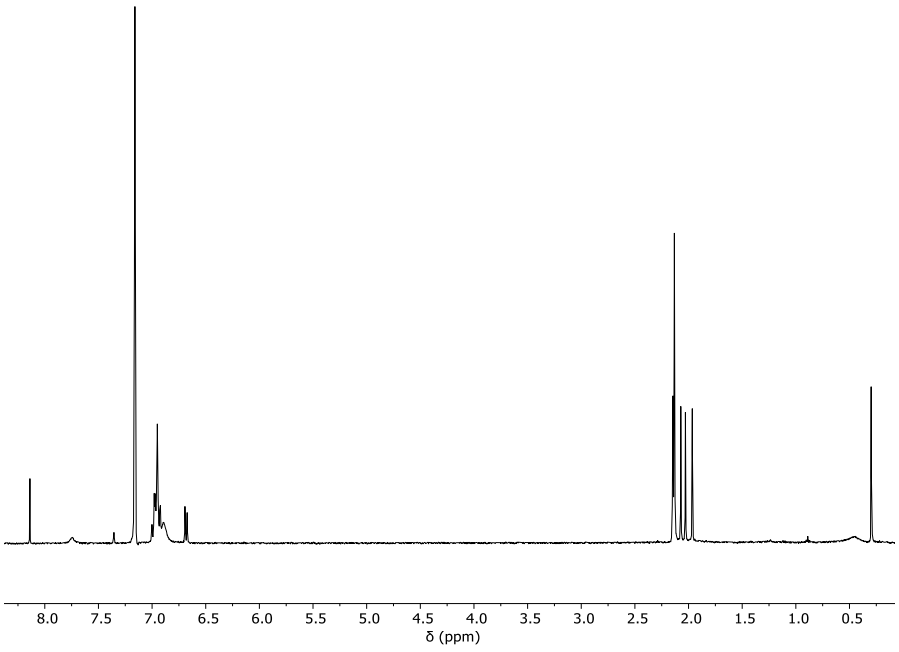

Figure A6.8. ^{1}H NMR spectrum of Pn*Zr[(N^{p}Tol)$_2$CH]$_2$ (benzene-d_6, 298 K and 500 MHz).

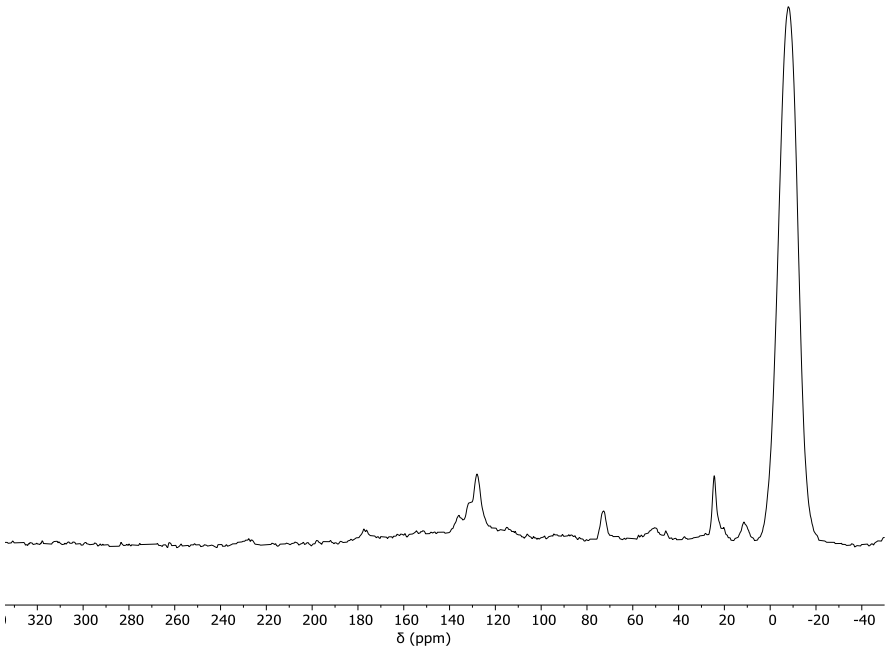

Figure A6.9. ^{13}C CP-MAS (10 kHz) NMR spectrum of sMAO-Pn*ZrCl[$(N^iPr)_2C$(4-OMe-C_6H_4)] **(6_{sMAO})**.

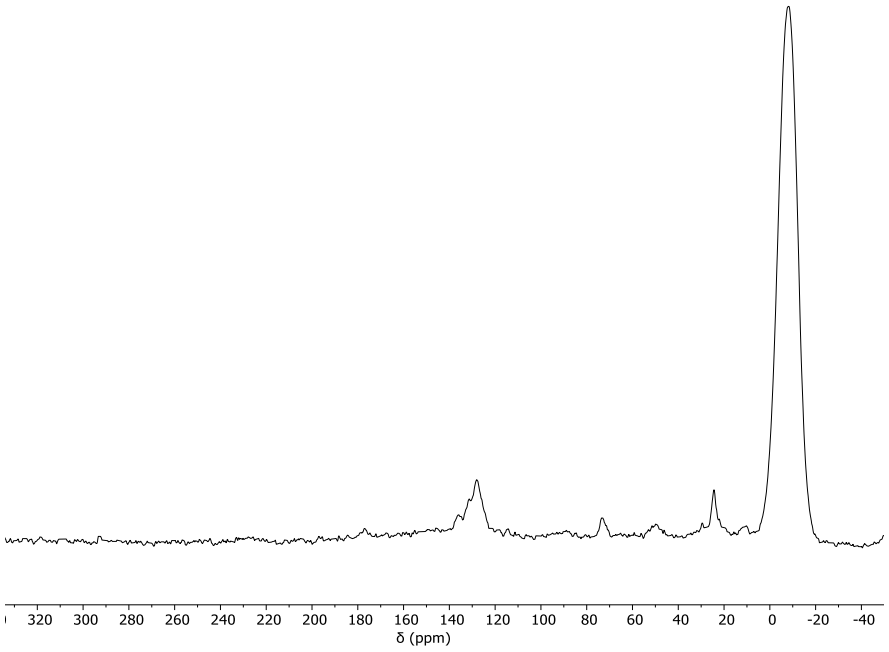

Figure A6.10. ^{13}C CP-MAS (10 kHz) NMR spectrum of sMAO-Pn*ZrCl[$(N^iPr)_2C$(4-CF_3-C_6H_4)] **(7_{sMAO})**.

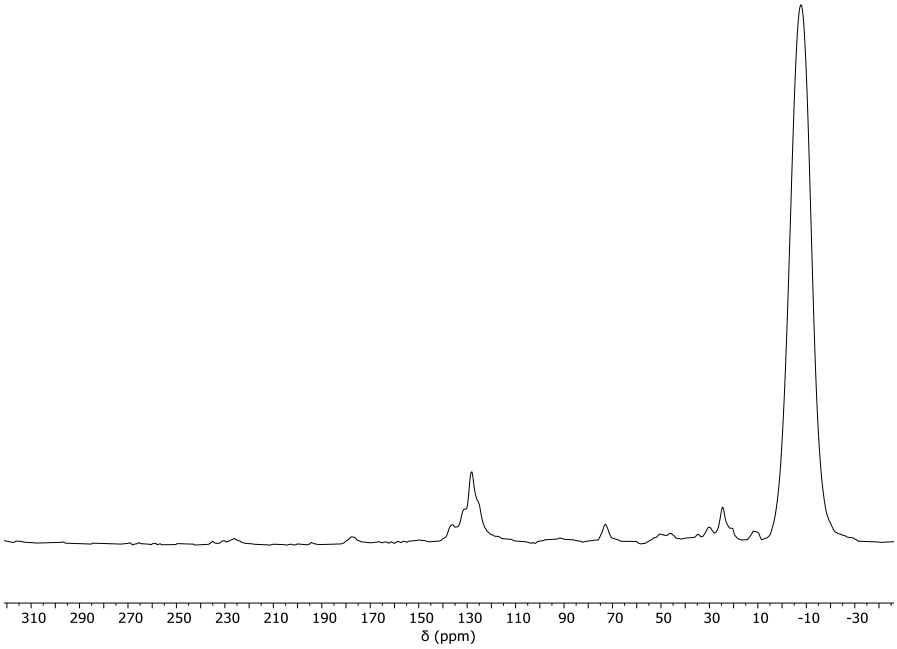

Figure A6.11. ^{13}C CP-MAS (10 kHz) NMR spectrum of sMAO-Pn*ZrCl[(N^{i}Pr)$_2$C(4-^{t}Bu-C$_6$H$_4$)] **(8$_{sMAO}$)**.

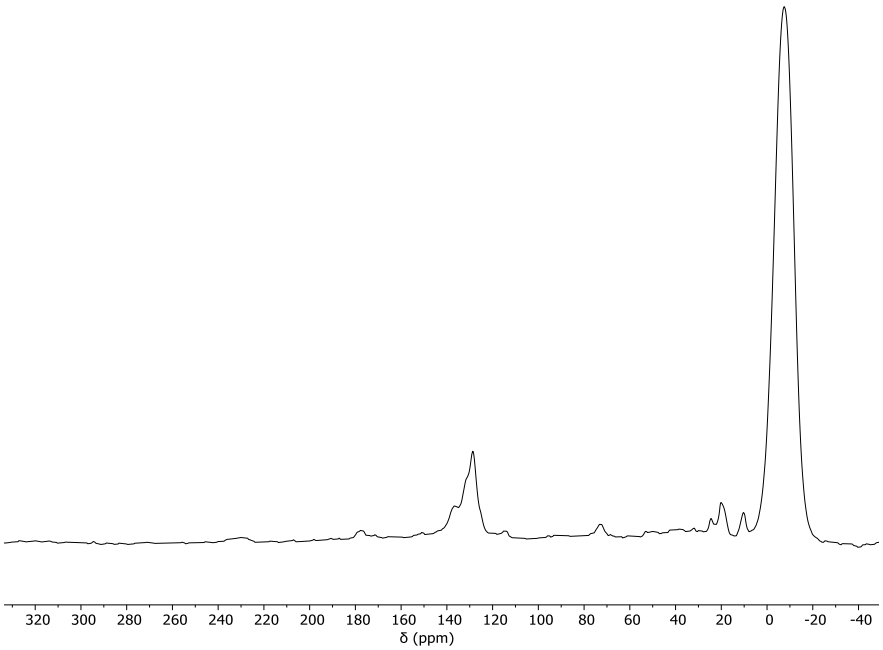

Figure A6.12. ^{13}C CP-MAS (10 kHz) NMR spectrum of sMAO-Pn*ZrCl[(NMes)$_2$CH] **(9$_{sMAO}$)**.

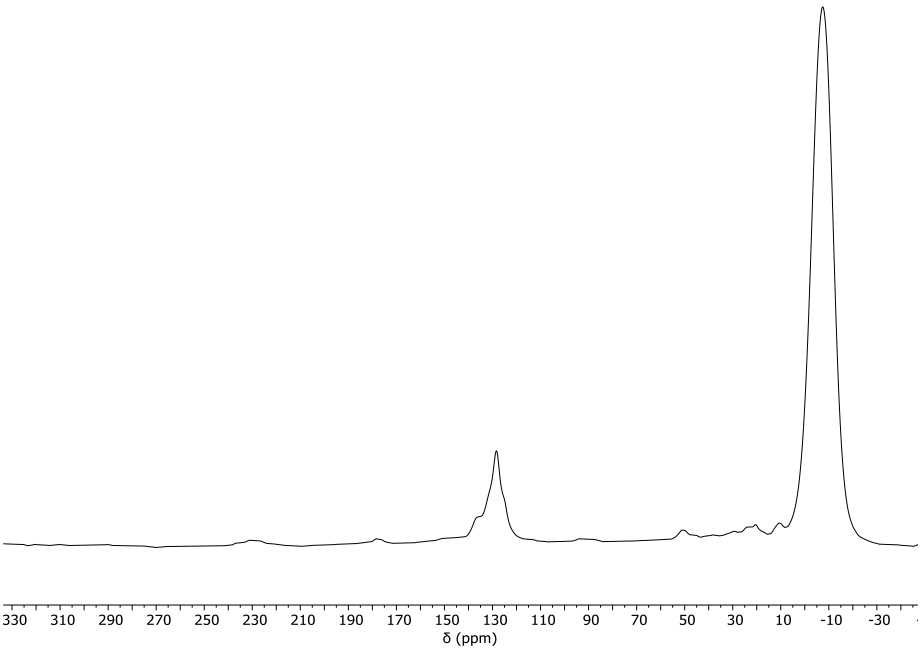

Figure A6.13. ^{13}C CP-MAS (10 kHz) NMR spectrum of sMAO-Pn*Zr(OXyl)[$(N^{i}Pr)_2C(C_6H_5)$] **(11_{sMAO})**.

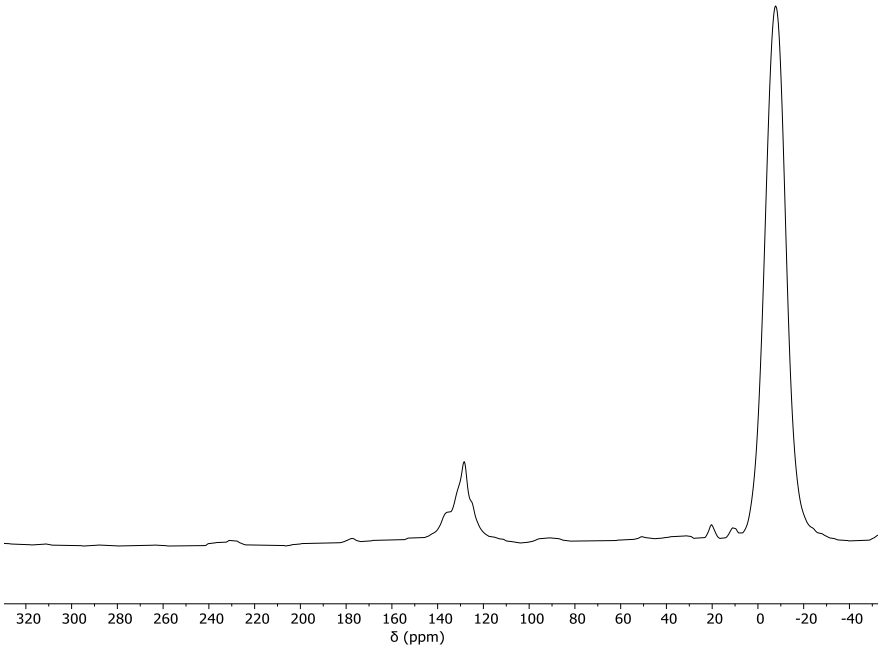

Figure A6.14. ^{13}C CP-MAS (10 kHz) NMR spectrum of sMAO-Pn*ZrCl[$(N^{p}Tol)_2CH$] **(12_{sMAO})**.

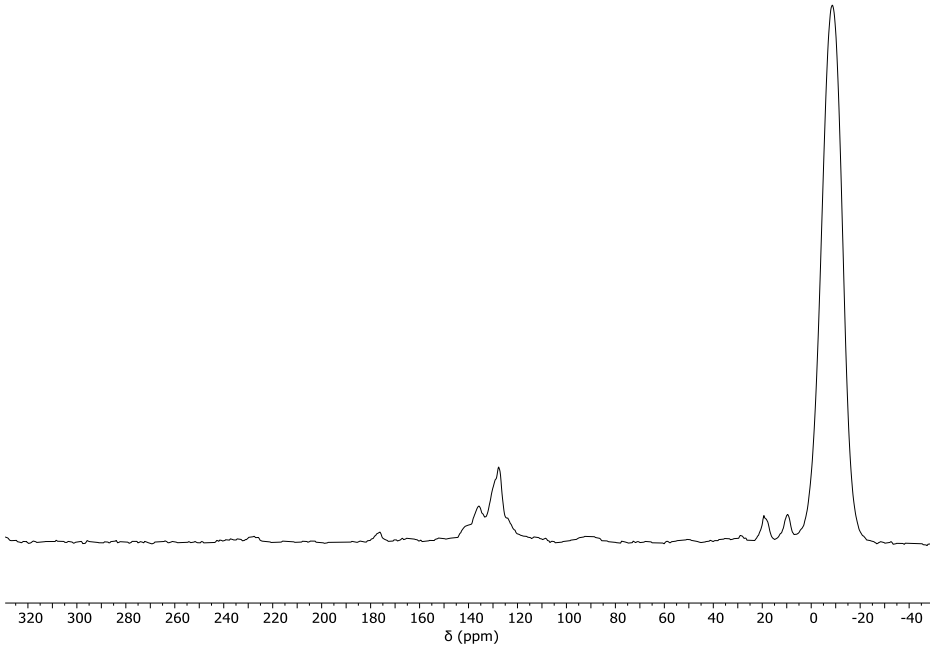

Figure A6.15. ^{13}C CP-MAS (10 kHz) NMR spectrum of sMAO-Pn*Zr[(N^{p}Tol)$_2$CH]$_2$ **(13$_{sMAO}$)**.

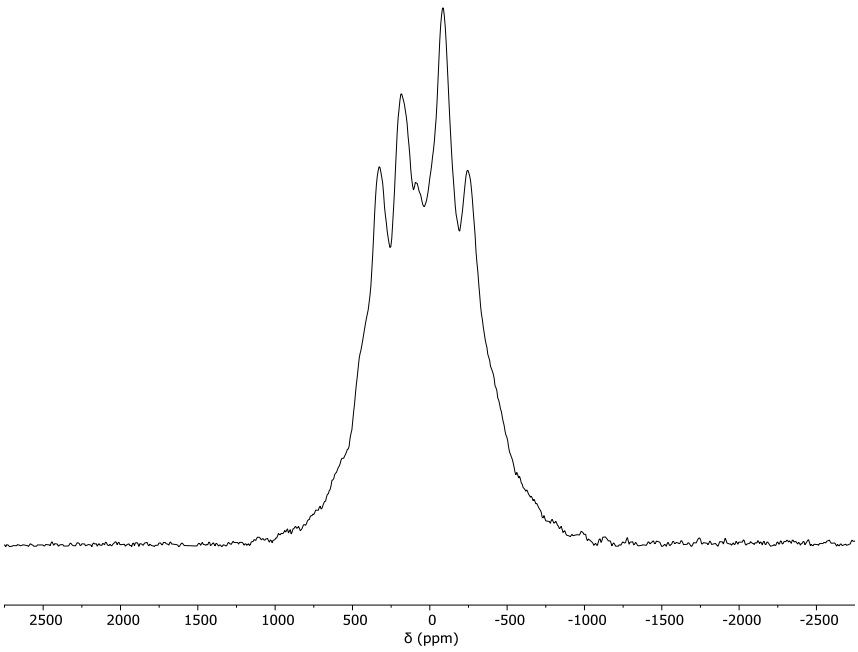

Figure A6.16. ^{27}Al DP-MAS (15 kHz) NMR spectrum of sMAO-Pn*ZrCl[(N^{i}Pr)$_2$C(4-OMe-C$_6$H$_4$)] **(6$_{sMAO}$)**.

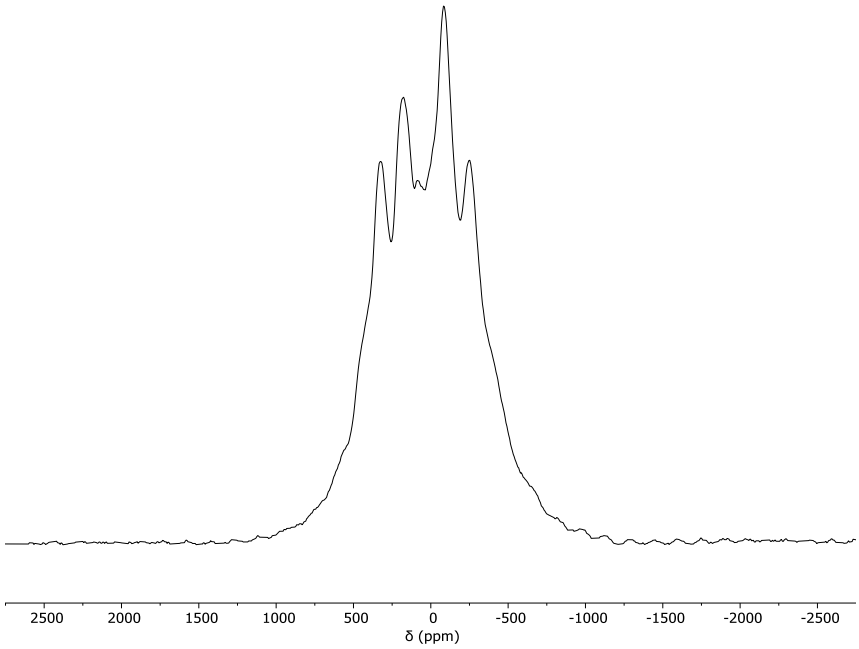

Figure A6.17. ^{27}Al DP-MAS (15 kHz) NMR spectrum of sMAO-Pn*ZrCl[(N^{i}Pr)$_2$C(4-CF$_3$-C$_6$H$_4$)] **(7$_{sMAO}$)**.

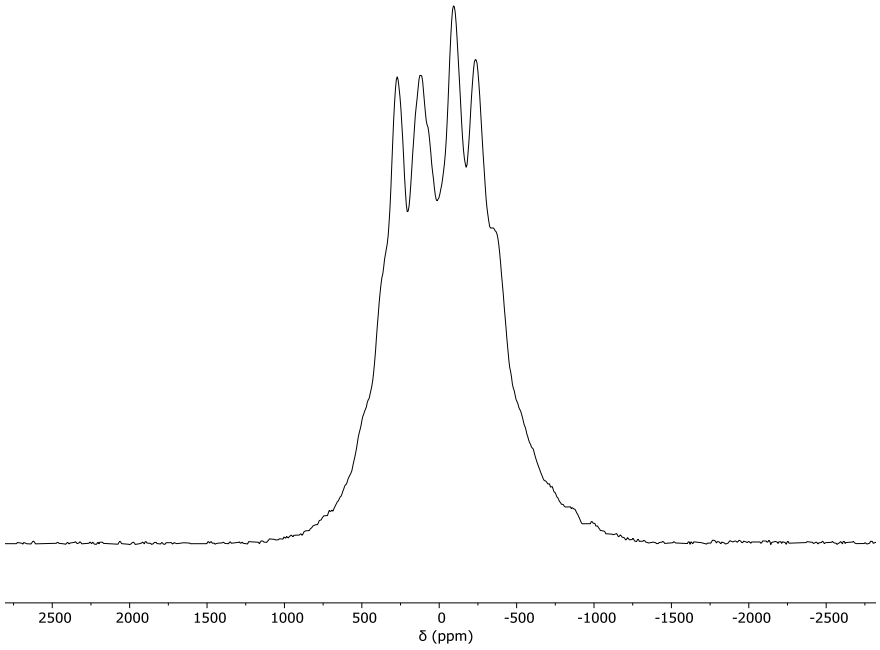

Figure A6.18. ^{27}Al DP-MAS (15 kHz) NMR spectrum of sMAO-Pn*ZrCl[(N^{i}Pr)$_2$C(4-^{t}Bu-C$_6$H$_4$)] **(8$_{sMAO}$)**.

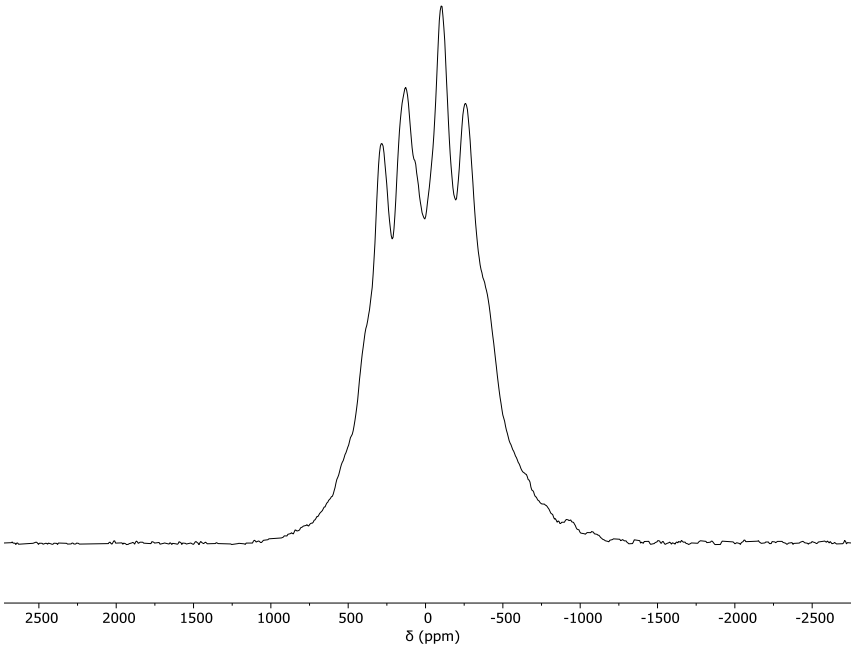

Figure A6.19. ^{27}Al DP-MAS (15 kHz) NMR spectrum of sMAO-Pn*ZrCl[(NMes)$_2$CH] **(9$_{sMAO}$)**.

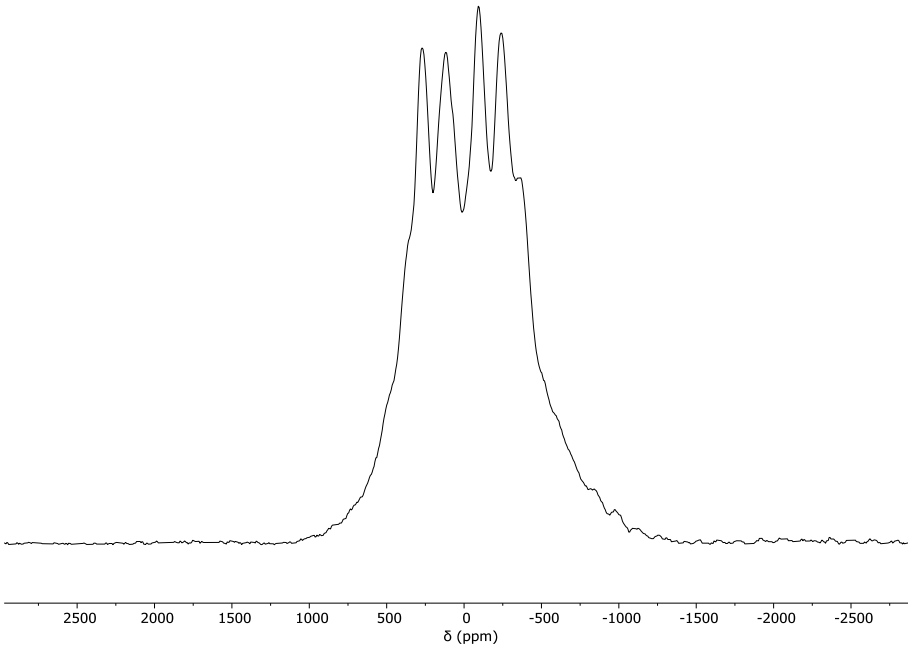

Figure A6.20. ^{27}Al DP-MAS (15 kHz) NMR spectrum of sMAO-Pn*Zr(OXyl)[(N^{i}Pr)$_2$C(C$_6$H$_5$)] **(11$_{sMAO}$)**.

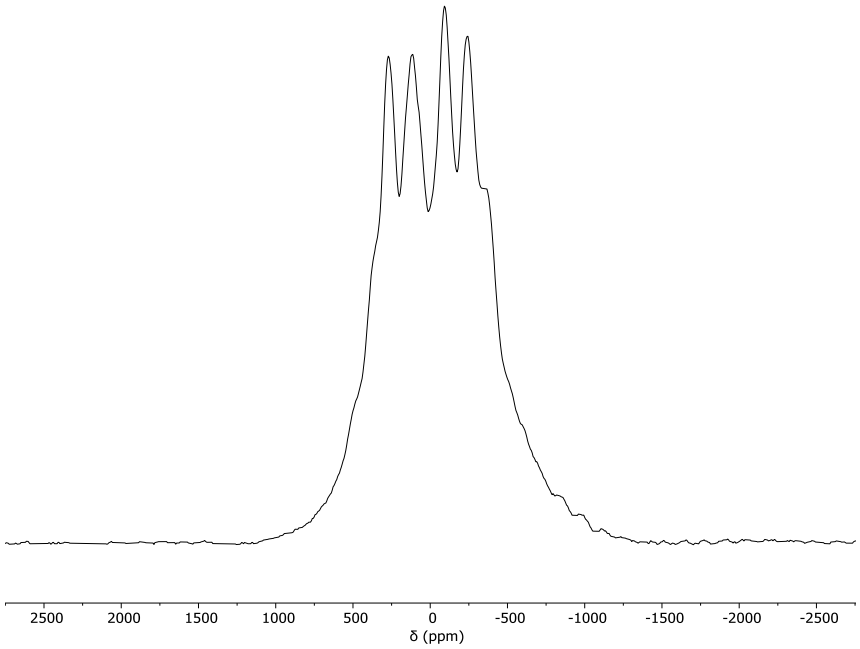

Figure A6.21. ^{27}Al DP-MAS (15 kHz) NMR spectrum of sMAO-Pn*ZrCl[(N^{p}Tol)$_2$CH] **(12$_{sMAO}$)**.

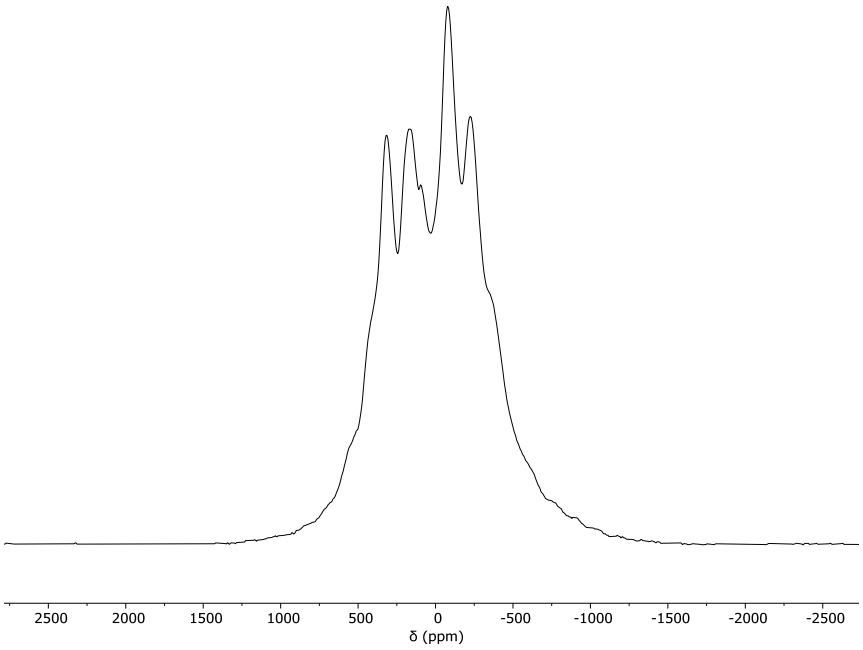

Figure A6.22. ^{27}Al DP-MAS (15 kHz) NMR spectrum of sMAO-Pn*Zr[(N^{p}Tol)$_2$CH]$_2$ **(13$_{sMAO}$)**.

Table A6.1. Slurry-phase styrene homopolymerisation activities, temperature, mass of catalyst and mass of polymer. Polymerisation conditions: 10 minutes, 1000 rpm. 50 mL toluene, 10 mg catalyst, 3.7 mL styrene, $[Al_{sMAO}]_0$:$[Zr]_0$ = 200:1, 150 mg TiBA.

Temperature (°C)	Mass catalyst (mg)		Mass polymer (mg)		Activity ($kg_{PS}/mol_{Ti}/h$)		Average activity ($kg_{PS}/mol_{Ti}/h$)
	1	2	1	2	1	2	
sMAO-Pn*ZrCl[(N^{i}Pr)$_2$C(4-OMe-C$_6$H$_4$)] (6$_{sMAO}$)							
40	11	11.5	412	336	3089	2412	2751
55	9.8	10	281	269	2358	2214	2286
70	9.5	10.2	292	305	2526	2462	2494
sMAO-Pn*ZrCl[(N^{i}Pr)$_2$C(4-CF$_3$-C$_6$H$_4$)] (7$_{sMAO}$)							
40	12.3	11.3	483	476	3220	3449	3335
55	11.5	10.4	343	310	2443	2437	2440
70	11.1	11	411	435	3031	3237	3134
sMAO-Pn*ZrCl[(N^{i}Pr)$_2$C(4-^{t}Bu-C$_6$H$_4$)] (8$_{sMAO}$)							
40	10.3	10.8	121	155	965	1180	1072
55	10.1	9.6	579	400	4705	3416	4061
70	9.5	10.7	407	488	3512	3748	3630
sMAO-Pn*ZrCl[(NMes)$_2$CH] (9$_{sMAO}$)							
40	9.9	9.8	332	336	2745	2806	2776
55	11.9	10.1	403	341	2782	2765	2774
70	9.7	9.5	370	329	3122	2833	2977
sMAO-Pn*ZrCl[(N^{i}Pr)$_2$C(C$_6$H$_5$)] (10$_{sMAO}$)							
55	9.5	9.6	72	75	215	221	218
sMAO-Pn*Zr(OXyl)[(N^{i}Pr)$_2$C(C$_6$H$_5$)] (11$_{sMAO}$)							
40	11.2	12.3	209	222	1539	1492	1516
55	10.8	11	177	204	1351	1529	1440
70	10.6	10.2	185	147	1438	1186	1312
sMAO-Pn*ZrCl[(N^{p}Tol)$_2$CH] (12$_{sMAO}$)							
40	9.5	10.1	215	216	1849	1749	1799
55	9.5	10.7	203	211	1746	1614	1680
70	9.5	9.5	120	158	1032	1359	1195
sMAO-Pn*Zr[(N^{p}Tol)$_2$CH]$_2$ (13$_{sMAO}$)							
40	10.2	10.2	123	170	997	1379	1188
55	10.1	10	200	166	1858	1557	1707
70	10.5	10.4	151	136	1350	1228	1289

Table A6.2. Slurry-phase ethylene homopolymerisation activities, temperature, mass of catalyst and mass of polymer. Polymerisation conditions: 30 minutes, 1000 rpm, 2 bar ethylene, 50 mL hexane, 10 mg catalyst, $[Al_{sMAO}]_0$:$[Zr]_0$ = 200:1, 150 mg TiBA.

Temperature (°C)	Mass catalyst (mg)		Mass polymer (mg)		Activity ($kg_{PE}/mol_{Ti}/h/bar$)		Average activity ($kg_{PE}/mol_{Ti}/h$)
	1	2	1	2	1	2	
sMAO-Pn*ZrCl[(N^{i}Pr)$_2$C(4-OMe-C$_6$H$_4$)] (6$_{sMAO}$)							
40	10	10	65	76	89	104	97
50	10.1	10.3	79	86	107	115	111
60	9.6	9.7	81	88	116	124	120
70	11.6	11.1	102	105	121	130	126
80	10.6	9.5	92	84	119	121	120

sMAO-Pn*ZrCl[(N^{i}Pr)$_2$C(4-CF$_3$-C$_6$H$_4$)] (7$_{sMAO}$)							
40	11.1	11.2	117	138	144	168	156
50	11.1	11.2	132	121	162	147	155
60	13	12.4	178	125	187	138	163
70	10.9	9.7	91	94	114	132	123
80	9.6	9.8	69	71	98	99	98
sMAO-Pn*ZrCl[(N^{i}Pr)$_2$C(4-^{t}Bu-C$_6$H$_4$)] (8$_{sMAO}$)							
40	9.5	9.7	39	61	56	86	71
50	10.7	10.7	71	63	91	81	86
60	11.2	11.2	113	119	138	146	142
70	10.3	10.4	101	103	134	136	135
80	10.6	12	106	135	137	155	146
sMAO-Pn*ZrCl[(NMes)$_2$CH] (9$_{sMAO}$)							
40	10.4	10.6	15	29	20	37	29
50	12.3	10.7	4	27	45	34	40
60	9.4	10.7	28	31	1	40	40
70	11.4	10.1	32	27	38	36	37
80	9.8	11.7	31	34	4	40	42
sMAO-Pn*ZrCl[(N^{i}Pr)$_2$C(C$_6$H$_5$)] (10$_{sMAO}$)							
40	9.9	9.9	100	91	143	130	137
50	9.9	10	102	106	146	151	148
60	9.5	9.5	120	100	179	149	164
70	9.6	9.7	118	119	174	174	174
80	9.6	9.6	112	125	165	185	175
sMAO-Pn*Zr(OXyl)[(N^{i}Pr)$_2$C(C$_6$H$_5$)] (11$_{sMAO}$)							
40	11.9	9.9	45	41	52	57	54
50	9.4	10	38	21	51	26	38
60	10.2	10.3	46	79	57	97	77
70	10.2	10.4	70	69	86	83	85
80	9.7	9.4	59	95	77	127	102
sMAO-Pn*ZrCl[(N^{p}Tol)$_2$CH] (12$_{sMAO}$)							
40	9.8	9.8	71	75	99	104	101
50	9.5	9.6	62	77	89	109	99
60	9.7	10.7	80	89	112	113	113
70	10.4	10.4	78	105	102	138	120
80							
sMAO-Pn*Zr[(N^{p}Tol)$_2$CH]$_2$ (13$_{sMAO}$)							
40	12.7	9	70	44	76	67	72
50	11.5	11.2	60	64	78	86	82
60	10.5	9.5	50	46	72	73	72
70	10.2	10.3	42	60	62	89	75
80	11.5	11.5	49	50	64	66	65

Table A6.3. Slurry-phase activities of copolymerisation of ethylene with styrene, temperature, mass of catalyst, volume of styrene and mass of polymer. Polymerisation conditions: 30 minutes, 1000 rpm, 2 bar ethylene, 50 mL hexane, 10 mg catalyst, $[Al_{sMAO}]_0$: $[Zr]_0$ = 200:1, 150 mg TiBA.

Temperature (°C)	Mass catalyst (mg)		Styrene (µL)	Mass polymer (mg)		Activity ($kg_{Polymer}/mol_{Ti}/h/bar$)		Average activity ($kg_{Polymer}/mol_{Ti}/h$)
	1	2		1	2	1	2	
			sMAO-Pn*ZrCl[(N^{i}Pr)$_2$C(4-OMe-C$_6$H$_4$)] (6$_{sMAO}$)					
40	9.5	10	125	157	235	226	322	274
50	10.1	10.2	125	257	237	349	319	334
60	9.6	9.6	125	259	224	370	320	345
70	10.5	10.2	125	259	235	339	316	327
80	10	10	125	221	240	303	329	316
40	10.2	9.7	62.5	158	251	213	355	284
40	10.1	10.5	250	215	221	292	289	291
40	9.9	10.5	500	184	239	255	313	284
			sMAO-Pn*ZrCl[(N^{i}Pr)$_2$C(4-CF$_3$-C$_6$H$_4$)] (7$_{sMAO}$)					
40	9.5	10.2	125	266	263	381	351	366
50	9.7	9.7	125	209	197	293	276	385
60	10	9.5	125	260	227	354	325	340
70	11.3	10	125	248	216	300	294	297
80	9.6	11.8	125	144	230	204	266	235
40	10.7	9.7	62.5	268	234	342	328	335
40	9.7	10.7	250	356	315	500	401	451
40	9.5	10.8	500252	252	263	361	332	347
			sMAO-Pn*ZrCl[(N^{i}Pr)$_2$C(4-^{t}Bu-C$_6$H$_4$)] (8$_{sMAO}$)					
40	10.3	10.3	125	123	142	164	189	176
50	10.6	11	125	194	201	251	251	251
60	9.6	10.1	125	210	223	299	302	301
70	9.5	9.5	125	280	264	403	380	391
80	9.6	9.8	125	273	352	389	491	440
40	10.1	9.7	62.5	116	104	157	147	152
40	9.9	10	250	185	224	256	306	281
40	10.3	10.8	500	121	133	161	169	165
			sMAO-Pn*ZrCl[(NMes)$_2$CH] (9$_{sMAO}$)					
40	10.6	10.2	125	189	188	244	244	244
50	9.7	9.7	125	93	83	131	117	124
60	9.8	9.9	125	116	159	161	212	187
70	10.1	10.5	125	256	229	335	298	316
80	10.5	11.5	125	211	228	274	271	273
40	10.6	10.5	62.5	219	186	282	242	262
40	9.9	10.3	250	193	185	254	245	251
40	11.6	9.5	500	210	199	248	286	267
			sMAO-Pn*ZrCl[(N^{i}Pr)$_2$C(C$_6$H$_5$)] (10$_{sMAO}$)					
40	8.5	8.5	125	230	256	381	424	403
			sMAO-Pn*Zr(OXyl)[(N^{i}Pr)$_2$C(C$_6$H$_5$)] (11$_{sMAO}$)					
40	11	11	125	224	239	280	299	289
			sMAO-Pn*ZrCl[(N^{p}Tol)$_2$CH] (12$_{sMAO}$)					
40	10.2	10.6	125	319	221	365	284	325
50	10.2	10.9	125	148	109	198	136	167
60	10	9.9	125	188	147	256	202	229
70	11.5	9.6	125	124	116	147	165	156
80	10.2	9.5	125	118	122	158	175	166
40	9.8	9.5	62.5	89	99	124	142	133

40	9.7	10.2	250	85	82	119	110	114
40	9.9	9.7	500	125	103	172	145	158
sMAO-Pn*Zr[(N^{p}Tol)$_2$CH]$_2$ (13$_{sMAO}$)								
40	10.7	9.9	125	138	144	178	200	189

Table A6.4. Slurry-phase activities of copolymerisation of ethylene with 4-NH_2-styrene, temperature, mass of catalyst, volume of styrene and mass of polymer. Polymerisation conditions: 30 minutes, 1000 rpm, 2 bar ethylene, 50 mL toluene, 10 mg catalyst, $[Al_{sMAO}]_0$: $[Zr]_0$ = 200:1, 150 mg TiBA.

Temperature (°C)	Mass catalyst (mg)		Styrene (µL)	Mass polymer (mg)		Activity ($kg_{Polymer}/mol_{Ti}/h/bar$)		Average activity ($kg_{Polymer}/mol_{Ti}/h$)
	1	2		1	2	1	2	
sMAO-Pn*ZrCl[(N^{i}Pr)$_2$C(4-OMe-C$_6$H$_4$)] (6$_{sMAO}$)								
40	11	11.3	125	357	365	1362	1357	1360
sMAO-Pn*ZrCl[(N^{i}Pr)$_2$C(4-CF$_3$-C$_6$H$_4$)] (7$_{sMAO}$)								
40	11.1	10.9	125	310	341	381	427	404
sMAO-Pn*ZrCl[(N^{i}Pr)$_2$C(4-^{t}Bu-C$_6$H$_4$)] (8$_{sMAO}$)								
40	12.6	12.7	125	364	381	397	413	405
sMAO-Pn*ZrCl[(NMes)$_2$CH] (9$_{sMAO}$)								
40	10.8	11.4	125	378	377	478	438	458
sMAO-Pn*Zr(OXyl)[(N^{i}Pr)$_2$C(C$_6$H$_5$)] (11$_{sMAO}$)								
40	10.5	10.2	125	227	239	297	321	309
sMAO-Pn*ZrCl[(N^{p}Tol)$_2$CH] (12$_{sMAO}$)								
40	10.2	10.8	125	365	311	488	393	440
sMAO-Pn*Zr[(N^{p}Tol)$_2$CH]$_2$ (13$_{sMAO}$)								
40	10.5	9.8	125	240	212	315	298	307

Table A6.5. Polystyrene molecular weights and dispersity. Polymerisation conditions: 10 minutes, 1000 rpm. 50 mL toluene, 10 mg catalyst, 3.7 mL styrene, $[Al_{sMAO}]_0$:$[Zr]_0$ = 200:1.

Temperature (°C)	Low M_w ($\times 10^3$ g/mol)	Đ	High M_w ($\times 10^6$ g/mol)	Đ
sMAO-Pn*ZrCl[(N^{i}Pr)$_2$C(4-OMe-C$_6$H$_4$)] (6$_{sMAO}$)				
40	25.3	1.6	1.81	3.1
55	16.7	2.3	1.16	3.6
70	13.0	1.6	1.84	3.4
sMAO-Pn*ZrCl[(N^{i}Pr)$_2$C(4-CF$_3$-C$_6$H$_4$)] (7$_{sMAO}$)				
40	15.1	1.6	2.41	3.3
55	18.2	2.0	1.20	3.8
70	-	-	1.86	3.6
sMAO-Pn*ZrCl[(N^{i}Pr)$_2$C(4-^{t}Bu-C$_6$H$_4$)] (8$_{sMAO}$)				
40	21.3	1.8	2.29	3.7
55	9.5	3.2	2.24	3.9
70	8.9	2.8	2.58	3.5
sMAO-Pn*ZrCl[(N^{i}Pr)$_2$C(C$_6$H$_5$)] (10$_{sMAO}$)				
55	28.9	1.7	1.86	3.3
sMAO-Pn*Zr(OXyl)[(N^{i}Pr)$_2$C(C$_6$H$_5$)] (11$_{sMAO}$)				
40	11.4	1.8	2.34	2.9
55	12.4	1.7	2.21	3.5
70	12.8	1.7	2.32	3.4

sMAO-Pn*ZrCl[(NMes)$_2$CH] (9$_{sMAO}$)				
40	8.4	2.9	2.33	3.4
55	9.3	2.7	2.60	3.5
70	9.3	2.7	2.25	3.4
sMAO-Pn*ZrCl[(N^{p}Tol)$_2$CH] (12$_{sMAO}$)				
40	11.9	1.8	1.92	3.0
55	12.3	1.7	2.36	3.4
70	15.7	1.6	2.24	3.4
sMAO-Pn*Zr[(N^{p}Tol)$_2$CH]$_2$ (13$_{sMAO}$)				
40	12.5	1.7	1.84	3.4
55	15.7	1.5	2.32	3.4
70	14.5	1.6	2.44	3.3

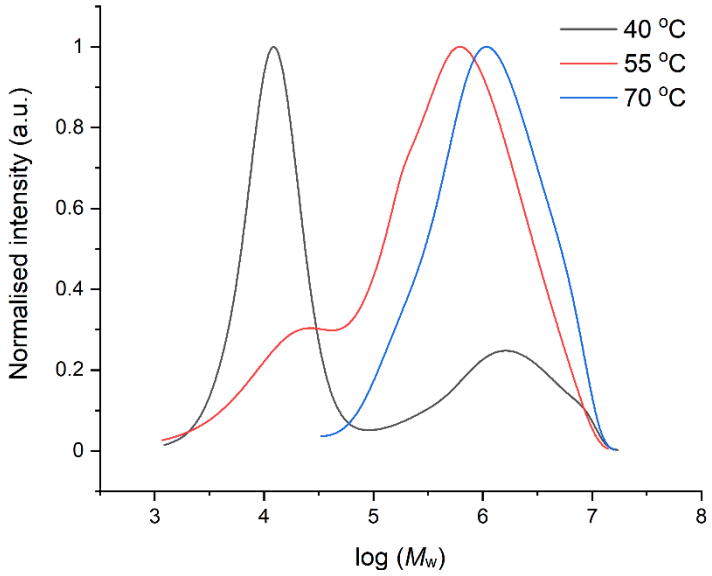

Figure A6.23. Molecular weights distribution of polystyrenes synthesised with Pn*ZrCl[(N^{i}Pr)$_2$C(4-CF$_3$-C$_6$H$_4$)] **(7$_{sMAO}$)** between 40 and 70 °C. Polymerisation conditions: 10 minutes, 1000 rpm. 50 mL toluene, 10 mg catalyst, 3.7 mL styrene, [Al$_{sMAO}$]$_0$:[Zr]$_0$ = 200:1, 150 mg TiBA.

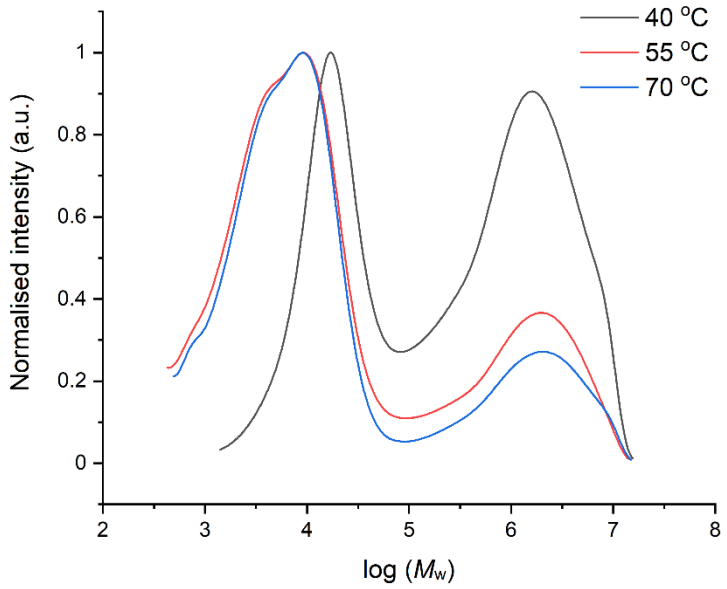

Figure A6.24. Molecular weights distribution of polystyrenes synthesised with Pn*ZrCl[(N^{i}Pr)$_2$C(4-^{t}Bu-C$_6$H$_4$)] **(8$_{sMAO}$)** between 40 and 70 °C. Polymerisation conditions: 10 minutes, 1000 rpm. 50 mL toluene, 10 mg catalyst, 3.7 mL styrene, [Al$_{sMAO}$]$_0$:[Zr]$_0$ = 200:1, 150 mg TiBA.

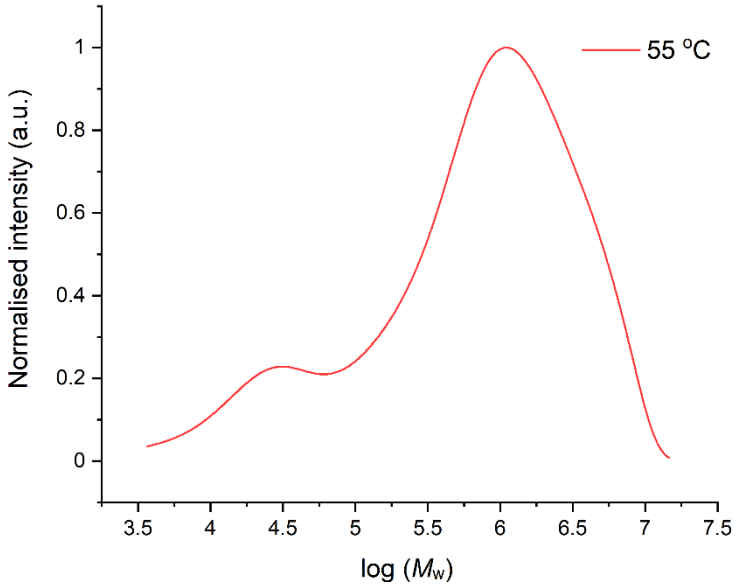

Figure A6.25. Molecular weights distribution of polystyrene synthesised with Pn*ZrCl[(N^{i}Pr)$_2$C(C$_6$H$_5$)] **(10$_{sMAO}$)** at 55 °C. Polymerisation conditions: 10 minutes, 1000 rpm. 50 mL toluene, 10 mg catalyst, 3.7 mL styrene, [Al$_{sMAO}$]$_0$:[Zr]$_0$ = 200:1, 150 mg TiBA.

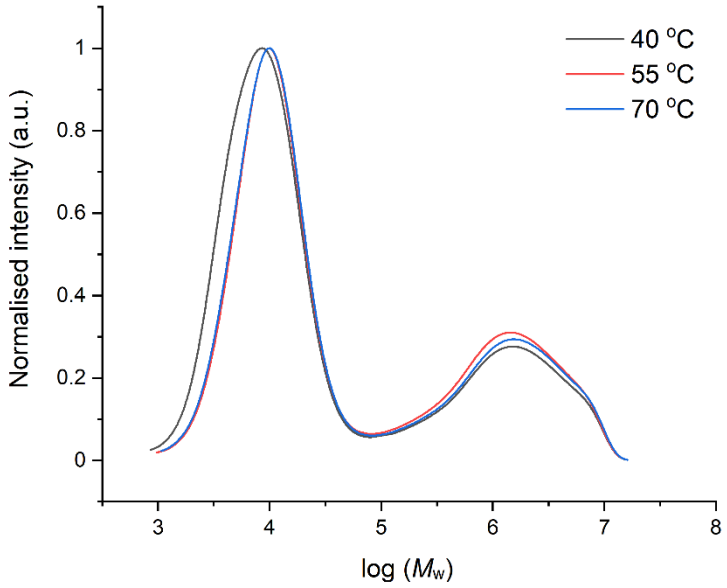

Figure A6.26. Molecular weights distribution of polystyrenes synthesised with Pn*Zr(OXyl)[(N^{i}Pr)$_2$C(C$_6$H$_5$)] **(11$_{sMAO}$)** between 40 and 70 °C. Polymerisation conditions: 10 minutes, 1000 rpm. 50 mL toluene, 10 mg catalyst, 3.7 mL styrene, [Al$_{sMAO}$]$_0$:[Zr]$_0$ = 200:1, 150 mg TiBA.

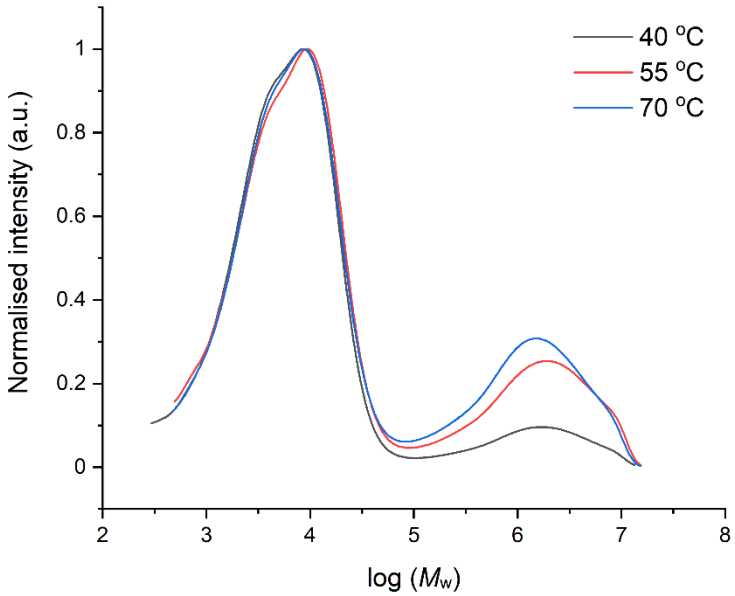

Figure A6.27. Molecular weights distribution of polystyrenes synthesised with Pn*ZrCl[(NMes)$_2$CH] **(9$_{sMAO}$)** between 40 and 70 °C. Polymerisation conditions: 10 minutes, 1000 rpm. 50 mL toluene, 10 mg catalyst, 3.7 mL styrene, [Al$_{sMAO}$]$_0$:[Zr]$_0$ = 200:1, 150 mg TiBA.

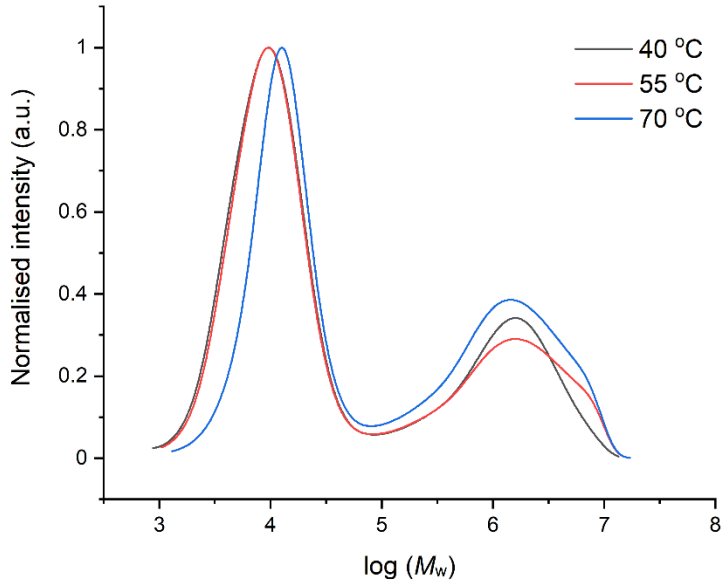

Figure A6.28. Molecular weights distribution of polystyrenes synthesised with Pn*ZrCl[(N^{p}Tol)$_2$CH] **(12$_{sMAO}$)** between 40 and 70 °C. Polymerisation conditions: 10 minutes, 1000 rpm. 50 mL toluene, 10 mg catalyst, 3.7 mL styrene, $[Al_{sMAO}]_0$:$[Zr]_0$ = 200:1, 150 mg TiBA.

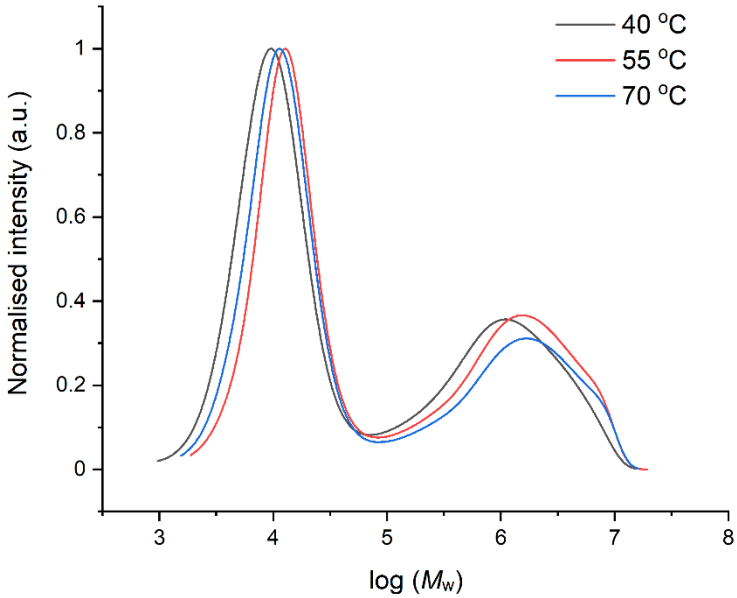

Figure A6.29. Molecular weights distribution of polystyrenes synthesised with Pn*Zr[(N^{p}Tol)$_2$CH]$_2$ **(13$_{sMAO}$)** between 40 and 70 °C. Polymerisation conditions: 30 minutes, 1000 rpm, 2 bar ethylene, 50 mL hexane, 10 mg catalyst, $[Al_{sMAO}]_0$:$[Zr]_0$ = 200:1, 150 mg TiBA.

Table A6.6. Polyethylene molecular weights and dispersity. Polymerisation conditions: 30 minutes, 1000 rpm, 2 bar ethylene, 50 mL hexane, 10 mg catalyst, $[Al_{sMAO}]_0$:$[Zr]_0$ = 200:1, 150 mg TiBA.

Temperature (°C)	M_w ($\times 10^4$ g/mol)	M_n ($\times 10^3$ g/mol)	Đ
sMAO-Pn*ZrCl[(N^{i}Pr)$_2$C(4-OMe-C$_6$H$_4$)] (6$_{sMAO}$)			
40	82.3	17.1	46.5
50	65.4	21.9	29.9
60	54.9	24.9	21.4
70	54.2	26.9	18.8
80	42.4	17.9	21.3
sMAO-Pn*ZrCl[(N^{i}Pr)$_2$C(4-CF$_3$-C$_6$H$_4$)] (7$_{sMAO}$)			
40	118.5	11.7	101.4
50	94.5	9.2	103.1
60	94.8	10.5	90.0
70	77.5	9.9	78.6
80	61.0	11.5	53.0
sMAO-Pn*ZrCl[(N^{i}Pr)$_2$C(C$_6$H$_5$)] (10$_{sMAO}$)			
40	61.0	11.8	51.6
50	56.3	19.6	28.7
60	34.8	2.8	9.9
70	26.5	27.7	9.6
80	31.0	27.6	11.3
sMAO-Pn*Zr(Oxyl)[(N^{i}Pr)$_2$C(C$_6$H$_5$)] (11$_{sMAO}$)			
40	90.6	56.6	16
80	15.9	20.4	7.8
sMAO-Pn*ZrCl[(NMes)$_2$CH] (9$_{sMAO}$)			
40	92.3	32.0	28.8
50	89.5	29.5	30.3
60	65.3	35.8	18.2
80	35.3	36.5	9.8
sMAO-Pn*ZrCl[(N^{p}Tol)$_2$CH] (12$_{sMAO}$)			
40	81.3	12.9	63
50	75.7	12.8	59
60	56.0	14.8	38
70	46.2	16.7	28
80	47.5	17.8	27
sMAO-Pn*Zr[(N^{p}Tol)$_2$CH]$_2$ (13$_{sMAO}$)			
40	50.1	13.0	38.6
50	51.2	13.5	37.9
60	49.4	11.2	44.1
70	37.0	15.7	23.6
80	38.2	13.3	28.8

Figure A6.30. Molecular weights distribution for polyethylene synthesised using Pn*ZrCl[(N^{i}Pr)$_2$C(4-CF$_3$-C$_6$H$_4$)] **(7$_{sMAO}$)** supported on sMAO across the range of temperature 40-80 °C. Polymerisation conditions: 30 minutes, 1000 rpm, 2 bar ethylene, 50 mL hexane, 10 mg catalyst, $[Al_{sMAO}]_0$:$[Zr]_0$ = 200:1, 150 mg TiBA.

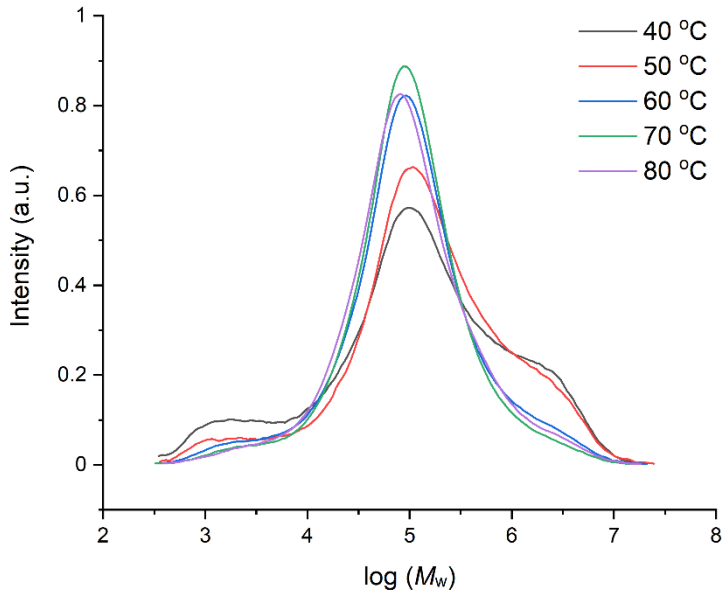

Figure A6.31. Molecular weights distribution for polyethylene synthesised using Pn*ZrCl[(N^{i}Pr)$_2$C(C$_6$H$_5$)] **(10$_{sMAO}$)** supported on sMAO across the range of temperature 40-80 °C. Polymerisation conditions: 30 minutes, 1000 rpm, 2 bar ethylene, 50 mL hexane, 10 mg catalyst, [Al$_{sMAO}$]$_0$:[Zr]$_0$ = 200:1, 150 mg TiBA.

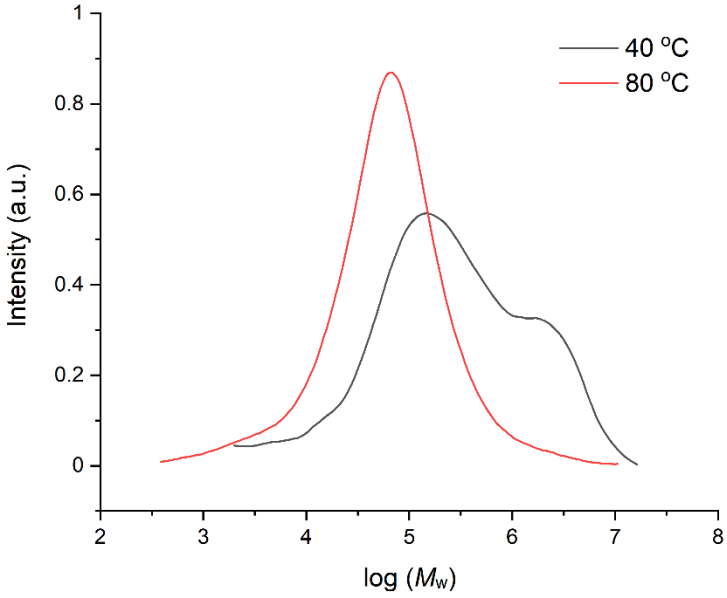

Figure A6.32. Molecular weights distribution for polyethylene synthesised using Pn*Zr(OXyl)[(N^{i}Pr)$_2$C(C$_6$H$_5$)] **(11$_{sMAO}$)** supported on sMAO across the range of temperature 40-80 °C. Polymerisation conditions: 30 minutes, 1000 rpm, 2 bar ethylene, 50 mL hexane, 10 mg catalyst, [Al$_{sMAO}$]$_0$:[Zr]$_0$ = 200:1, 150 mg TiBA.

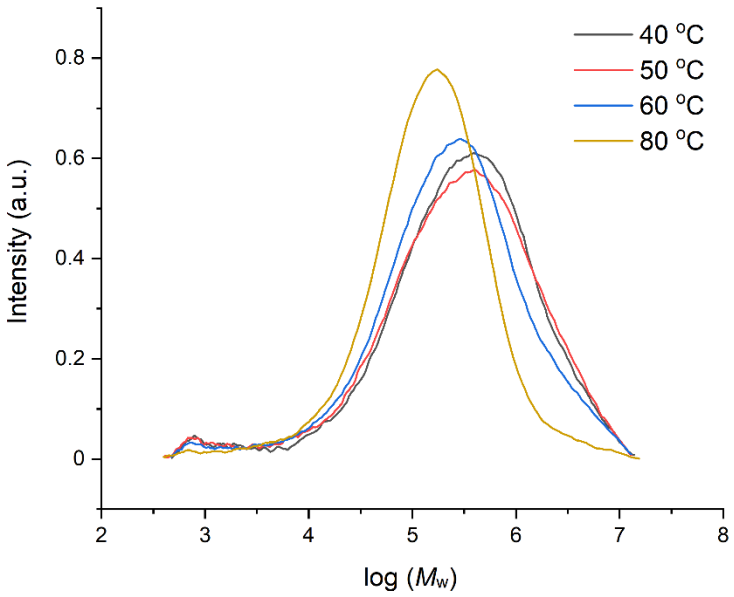

Figure A6.33. Molecular weights distribution for polyethylene synthesised using Pn*ZrCl[(NMes)$_2$CH] **(9$_{sMAO}$)** supported on sMAO across the range of temperature 40-80 °C. Polymerisation conditions: 30 minutes, 1000 rpm, 2 bar ethylene, 50 mL hexane, 10 mg catalyst, $[Al_{sMAO}]_0$:$[Zr]_0$ = 200:1, 150 mg TiBA.

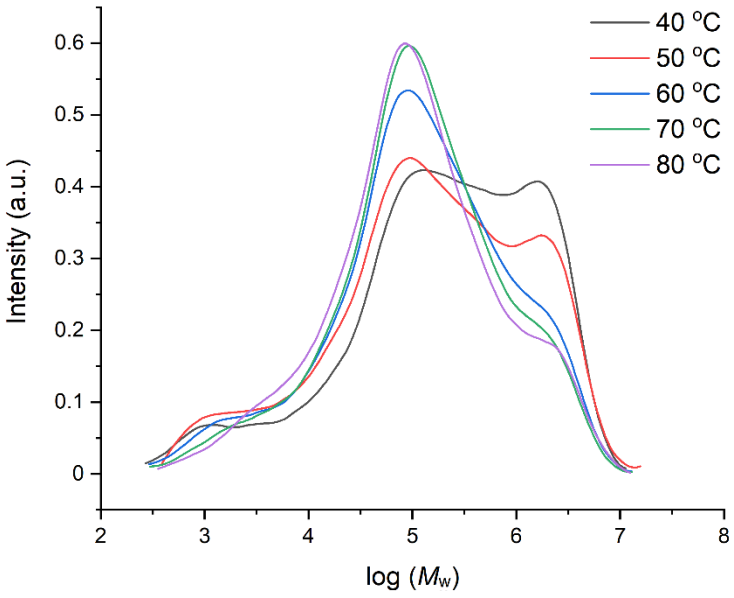

Figure A6.34. Molecular weights distribution for polyethylene synthesised using Pn*ZrCl[(N^{p}Tol)$_2$CH] supported on sMAO **(12$_{sMAO}$)** across the range of temperature 40-80 °C. Polymerisation conditions: 30 minutes, 1000 rpm, 2 bar ethylene, 50 mL hexane, 10 mg catalyst, $[Al_{sMAO}]_0$:$[Zr]_0$ = 200:1, 150 mg TiBA.

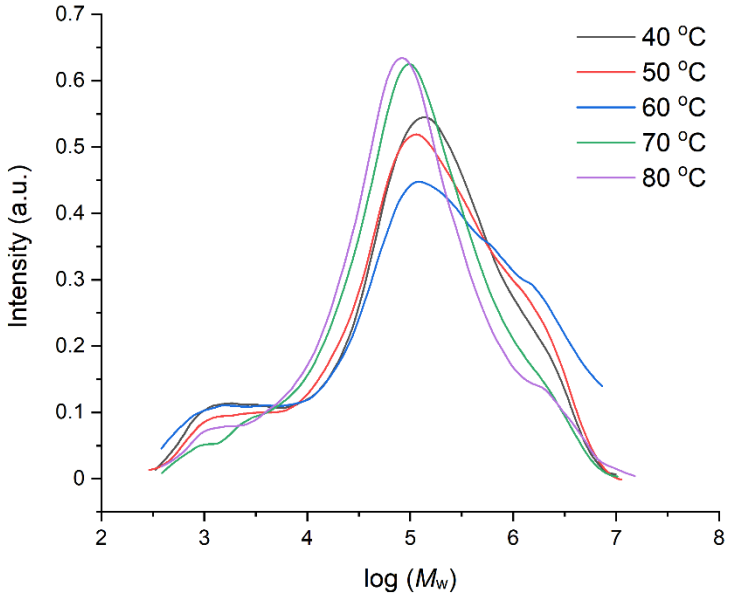

Figure A6.35. Molecular weights distribution for polyethylene synthesised using Pn*Zr[(N^{p}Tol)$_2$CH]$_2$ supported on sMAO **(13$_{sMAO}$)** across the range of temperature 40-80 °C. Polymerisation conditions: 30 minutes, 1000 rpm, 2 bar ethylene, 50 mL hexane, 10 mg catalyst, [Al$_{sMAO}$]$_0$:[Zr]$_0$ = 200:1, 150 mg TiBA.

Table A6.7. Poly(ethylene-co-styrene) molecular weights. Polymerisation conditions: 30 minutes, 1000 rpm, 2 bar ethylene, 50 mL hexane, 10 mg catalyst, [Al$_{sMAO}$]$_0$: [Zr]$_0$ = 200:1, 150 mg TiBA.

Temperature (°C)	Styrene (µL)	M_w (×10^6 g/mol)	M_n (×10^3 g/mol)	Đ
sMAO-Pn*ZrCl[(N^{i}Pr)$_2$C(4-CF$_3$-C$_6$H$_4$)] (7$_{sMAO}$)				
40	125	1.26	7.1	178.2
50	125	Not dissolved		
60	125	Not dissolved		
70	125	Not dissolved		
80	125	Not dissolved		
40	62.5	1.03	9.6	107
40	250	1.17	11.4	102.2
40	500	0.95	7.6	125.4
sMAO-Pn*ZrCl[(NMes)$_2$CH] (9$_{sMAO}$)				
40	125	0.74	11.5	64.1
50	125	0.45	7.4	61.0
60	125	Not dissolved		
70	125	0.30	36.8	8.3
80	125	0.18	24.1	7.5
40	62.5	1.22	19.0	64.0
40	250	0.92	37.0	24.9
40	500	Not dissolved		
sMAO- Pn*ZrCl[(N^{i}Pr)$_2$C(C$_6$H$_5$)] (10$_{sMAO}$)				
40	125	1.22	47.7	26.0

sMAO-Pn*ZrCl[(N^{p}Tol)$_2$CH] (12$_{sMAO}$)				
40	125	0.85	44.3	19.1
50	125	Not dissolved		
60	125	Not dissolved		
70	125	0.50	48.0	10.5
80	125	0.39	38.7	10.1
40	62.5	0.98	32.5	30.3
40	250	0.89	52.5	17.0
40	500	0.70	41.6	16.8

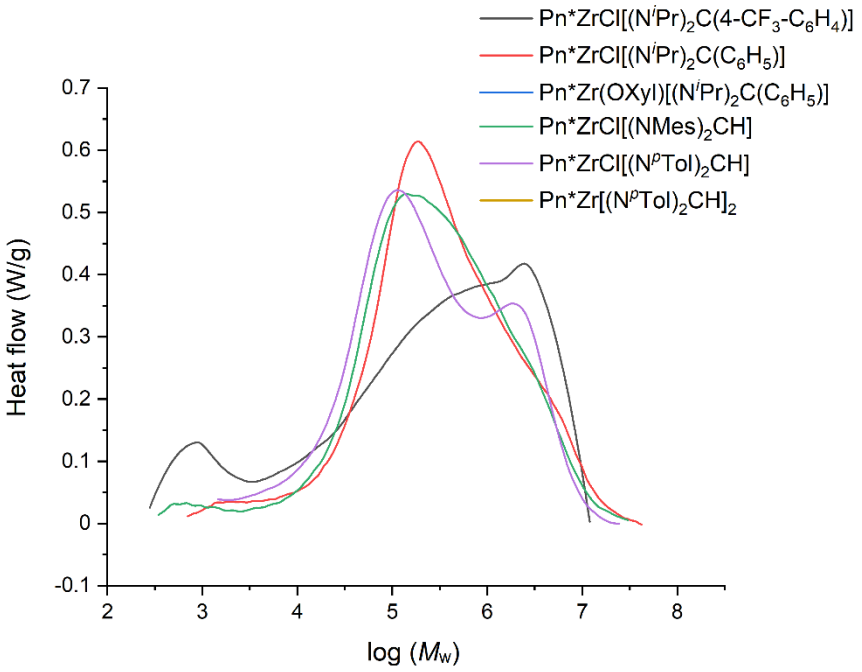

Figure A6.36. Molecular weights distribution for polyethylene synthesised using Pn*ZrCl[RNC(R')NR] supported on sMAO at 40 ° C using 125 µL of styrene. Polymerisation conditions: 30 minutes, 1000 rpm, 2 bar ethylene, 150 mg TiBA, 50 mL hexane, 10 mg catalyst, $[Al_{sMAO}]_0$:$[Zr]_0$ = 200:1, 125 µL styrene.

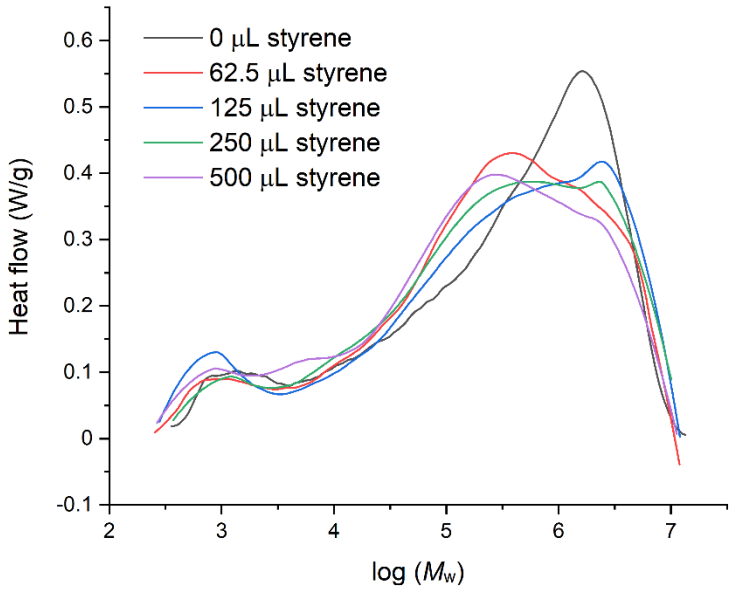

Figure A6.37. Influence of the styrene concentration on the molecular weights distribution for polyethylene synthesised using Pn*ZrCl[(N^{i}Pr)$_2$C(4-CF$_3$-C$_6$H$_4$)] supported on sMAO (**7$_{sMAO}$**) at 40 ° C. Polymerisation conditions: 30 minutes, 1000 rpm, 2 bar ethylene, 150 mg TiBA, 50 mL hexane, 10 mg catalyst, [Al$_{sMAO}$]$_0$:[Zr]$_0$ = 200:1.

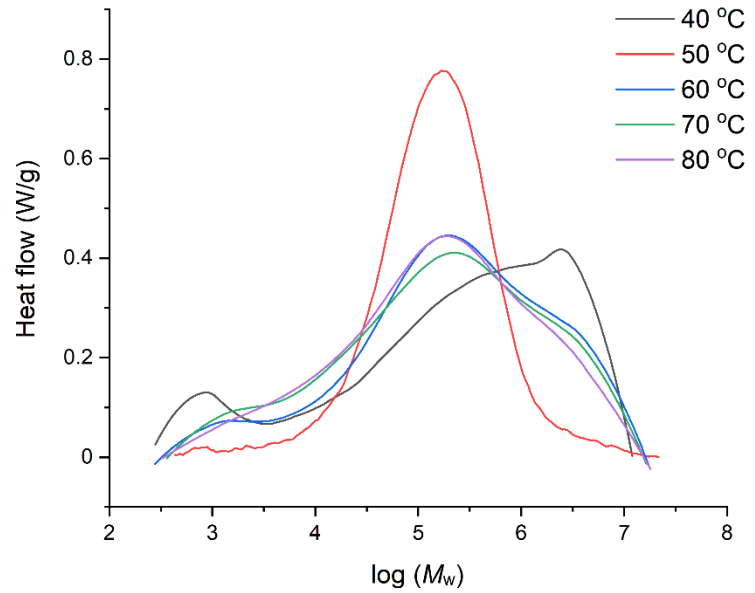

Figure A6.38. Influence of the temperature on the molecular weights distribution for polyethylene synthesised using Pn*ZrCl[(N^{i}Pr)$_2$C(4-CF$_3$-C$_6$H$_4$)] supported on sMAO (**7$_{sMAO}$**) using 125 µL of styrene. Polymerisation conditions: 30 minutes, 1000 rpm, 2 bar ethylene, 50 mL hexane, 150 mg TiBA, 10 mg catalyst, [Al$_{sMAO}$]$_0$:[Zr]$_0$ = 200:1.

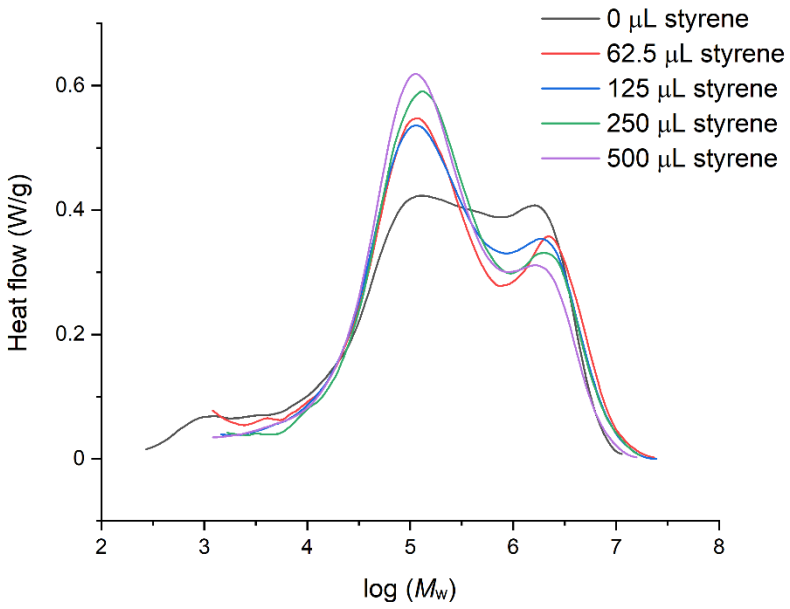

Figure A6.39. Influence of the styrene concentration on the molecular weights distribution for polyethylene synthesised using Pn*ZrCl[(N^{p}Tol)$_2$CH] supported on sMAO (**12$_{sMAO}$**)at 40 ° C. Polymerisation conditions: 30 minutes, 1000 rpm, 2 bar ethylene, 150 mg TiBA, 50 mL hexane, 10 mg catalyst, [Al$_{sMAO}$]$_0$:[Zr]$_0$ = 200:1.

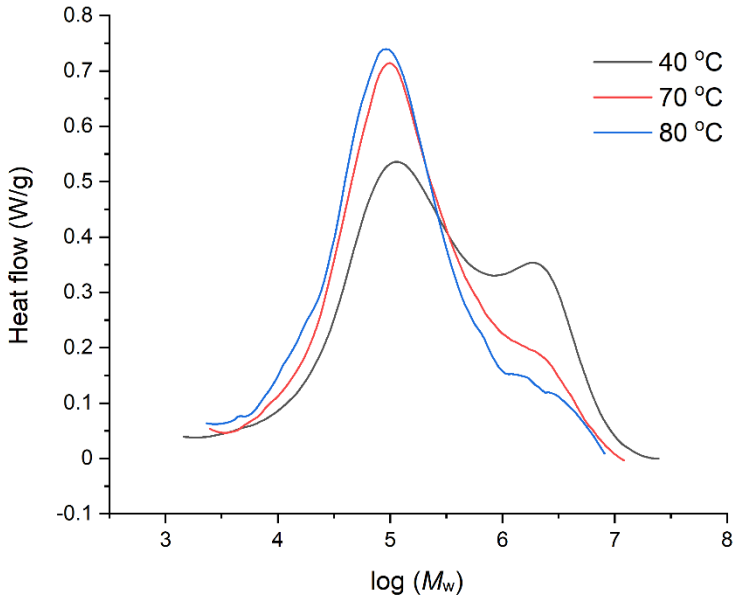

Figure A6.40. Influence of the temperature on the molecular weights distribution for polyethylene synthesised using Pn*ZrCl[(N^{p}Tol)$_2$CH] supported on sMAO (**12$_{sMAO}$**) using 125 µL of styrene. Polymerisation conditions: 30 minutes, 1000 rpm, 2 bar ethylene, 150 mg TiBA, 50 mL hexane, 10 mg catalyst, [Al$_{sMAO}$]$_0$:[Zr]$_0$ = 200:1.

Table A6.8. *Meso* probabilities calculated for the polystyrenes synthesised by Pn*ZrCl[$(NR)_2NR'$] supported on sMAO at 55 °C.

Supported complex	P_m (calculated by $^{13}C\{^1H\}$ NMR)
Pn*ZrCl[$(N^iPr)_2C(4\text{-}OMe\text{-}C_6H_4)$] (**6$_{sMAO}$**)	0.66
Pn*ZrCl[$(N^iPr)_2C(4\text{-}CF_3\text{-}C_6H_4)$] (**7$_{sMAO}$**)	0.40
Pn*ZrCl[$(N^iPr)_2C(4\text{-}^t Bu\text{-}C_6H_4)$] (**8$_{sMAO}$**)	0.54
Pn*ZrCl[$(NMes)_2CH$] (**9$_{sMAO}$**)	0.69
Pn*ZrCl[$(N^iPr)_2C(C_6H_5)$] (**10$_{sMAO}$**)	n/a
Pn*Zr(OXyl)[$(N^iPr)_2C(C_6H_5)$] (**11$_{sMAO}$**)	0.45
Pn*ZrCl[$(N^pTol)_2CH$] (**12$_{sMAO}$**)	0.68
Pn*Zr[$(N^pTol)_2CH]_2$(**13$_{sMAO}$**)	0.55

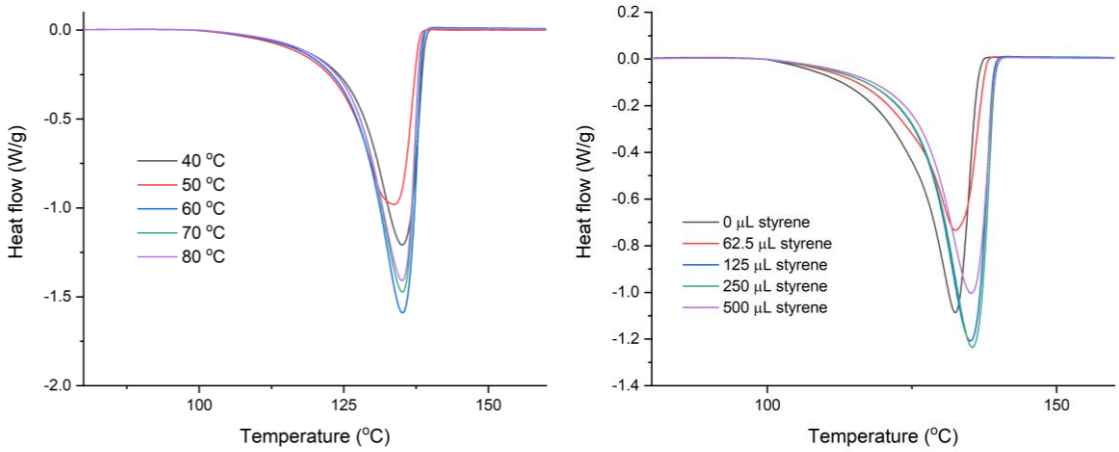

Figure A6.41. DSC curves for copolymers produced by supported Pn*ZrCl[$(N^iPr)_2C(4\text{-}OMe\text{-}C_6H_4)$] (**6$_{sMAO}$**). (Left): 125 µL styrene and T ∈ [40 °C; 80 °C], (right): 40 °C and $V_{styrene}$ ∈ [0 µL; 500 µL]. Conditions: 10 mg catalyst ($[Al]_0$: $[Zr]_0$ = 200:1), 2 bar ethylene, 50 mL hexane, 150 mg TiBA and 30 minutes.

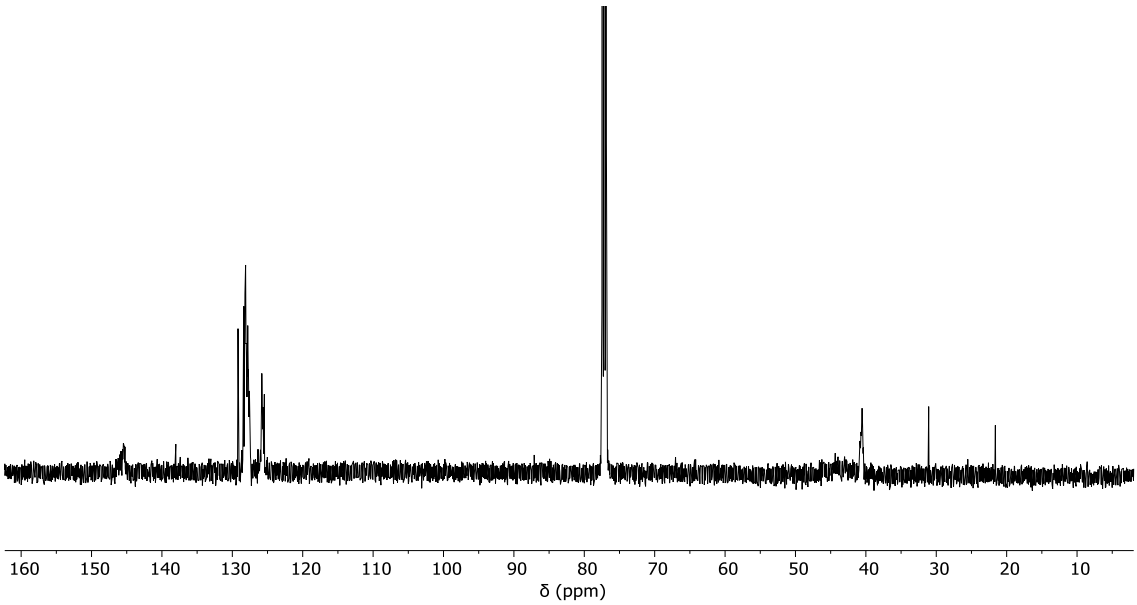

Figure A6.42. $^{13}C\{^{1}H\}$ NMR spectrum of polystyrene produced by sMAO-Pn*ZrCl[$(N^{i}Pr)_2C$(4-$OMe-C_6H_4$)] (**6$_{sMAO}$**) (chloroform-d_1, 298 K, 125 MHz).

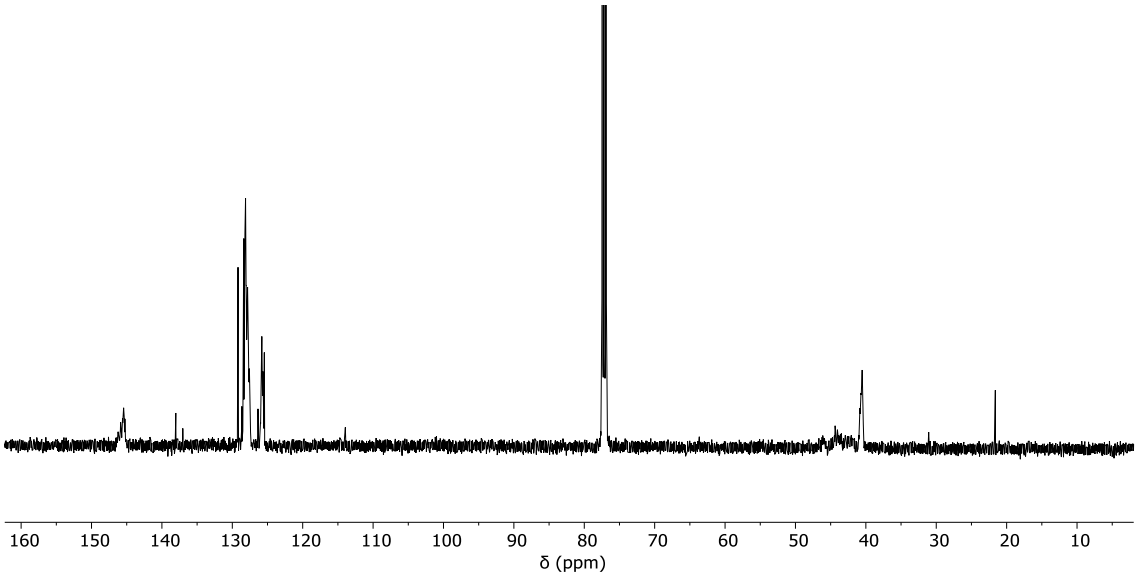

Figure A6.43. $^{13}C\{^{1}H\}$ NMR spectrum of polystyrene produced by sMAO-Pn*ZrCl[$(N^{i}Pr)_2C$(4-CF_3-C_6H_4)] (**7$_{sMAO}$**) (chloroform-d_1, 298 K, 125 MHz).

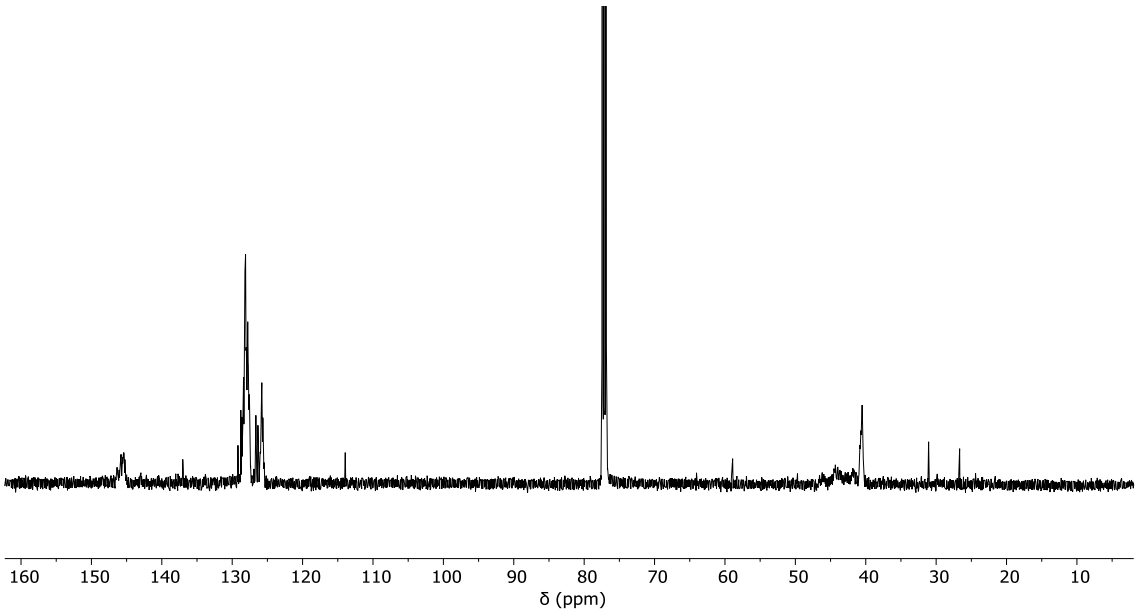

Figure A6.44. $^{13}C\{^{1}H\}$ NMR spectrum of polystyrene produced by sMAO-Pn*ZrCl[$(N^{i}Pr)_2C(4\text{-}^{t}Bu\text{-}C_6H_4)$] (**8$_{sMAO}$**) (chloroform-$d_1$, 298 K, 125 MHz).

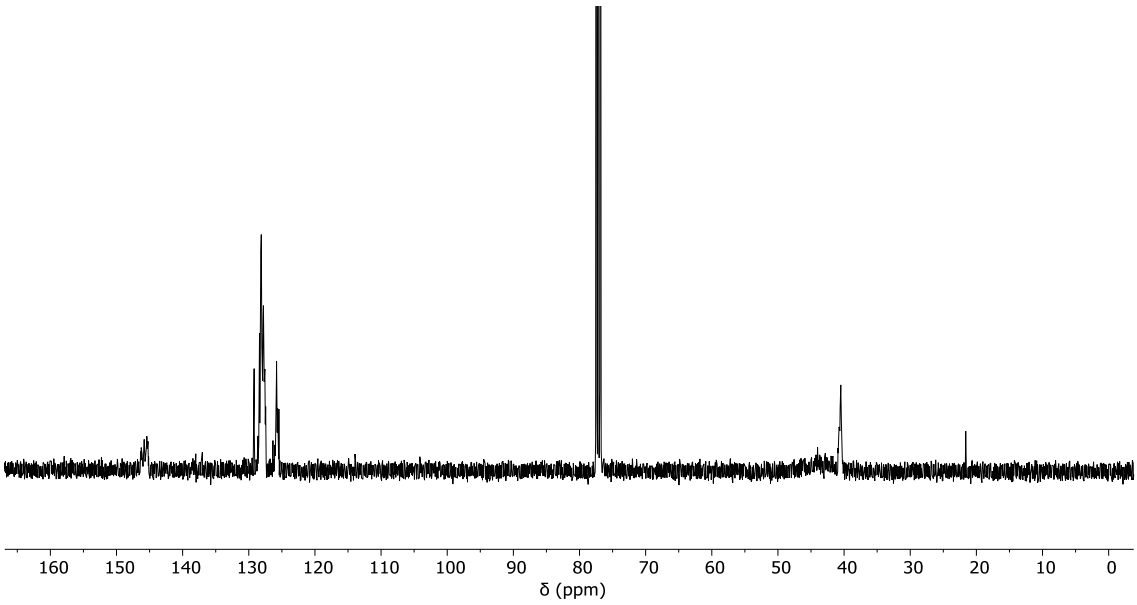

Figure A6.45. $^{13}C\{^{1}H\}$ NMR spectrum of polystyrene produced by sMAO-Pn*ZrC(OXyl)$(N^{i}Pr)_2C(C_6H_5)$] (**11$_{sMAO}$**) (chloroform-d_1, 298 K, 125 MHz).

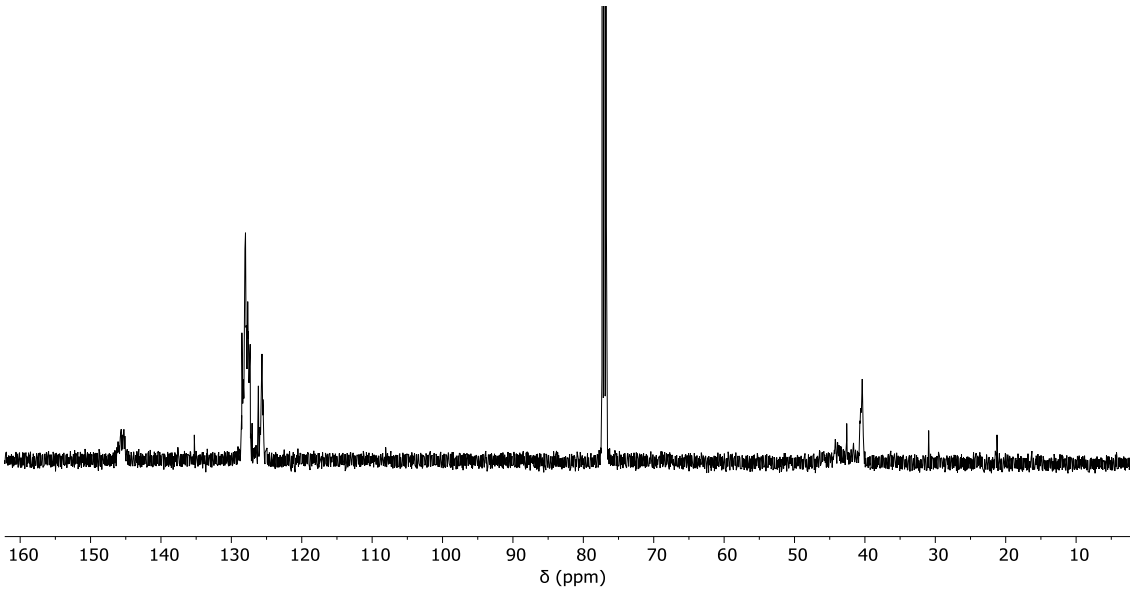

Figure A6.46. $^{13}C\{^{1}H\}$ NMR spectrum of polystyrene produced by sMAO-Pn*ZrCl[$(NMes)_2CH$] (**9$_{sMAO}$**) (chloroform-d_1, 298 K, 125 MHz).

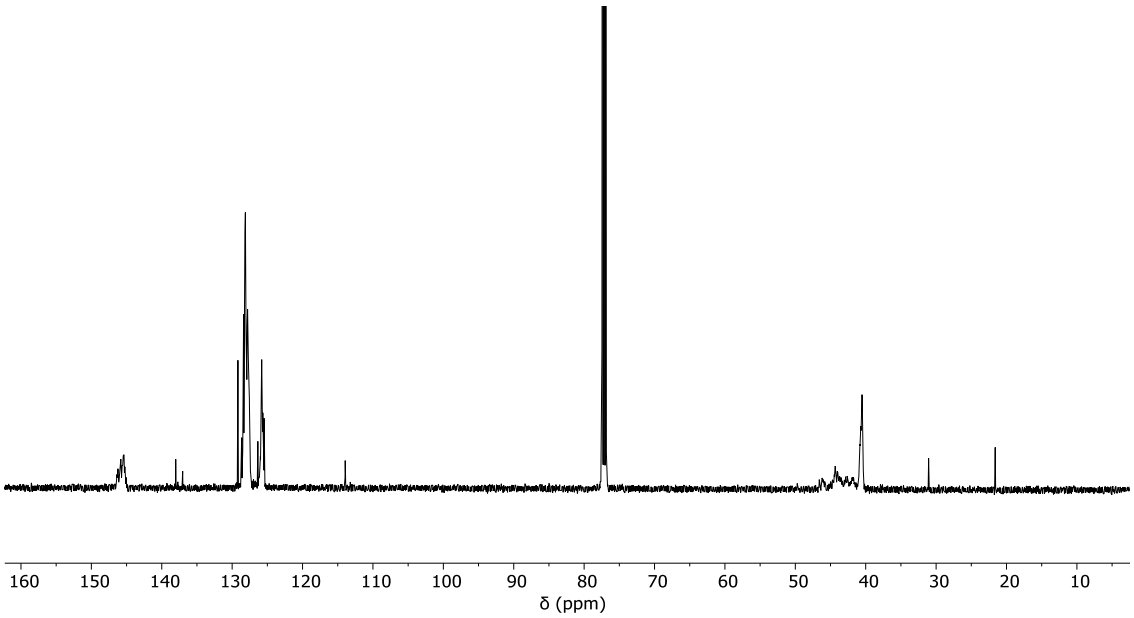

Figure A6.47. $^{13}C\{^{1}H\}$ NMR spectrum of polystyrene produced by sMAO-Pn*ZrCl[$(N^{p}Tol)_2CH$] (**12$_{sMAO}$**) (chloroform-d_1, 298 K, 125 MHz).

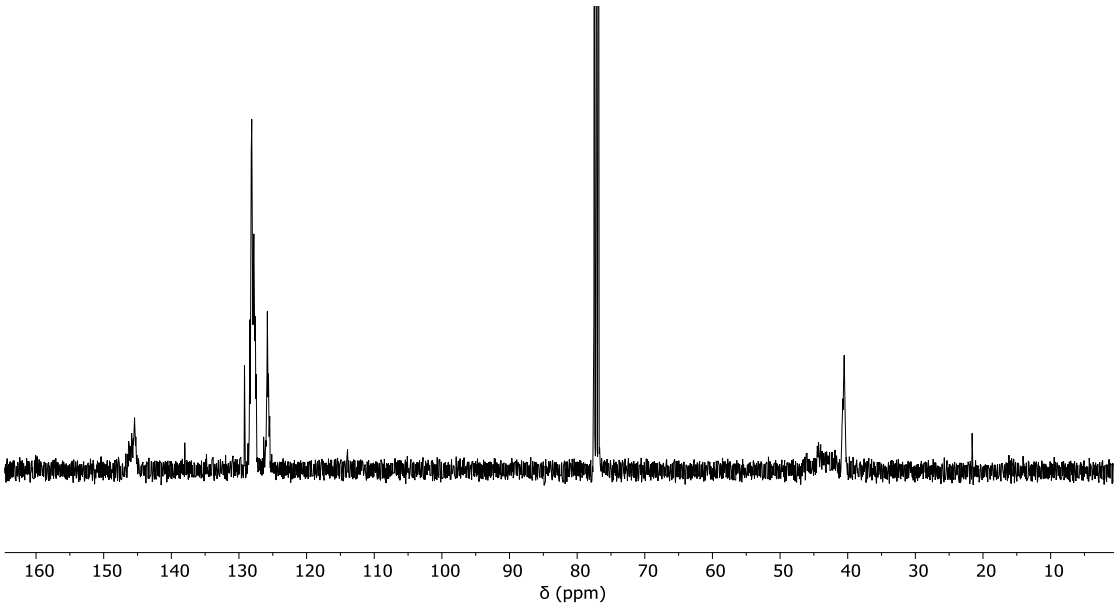

Figure A6.48. $^{13}C\{^{1}H\}$ NMR spectrum of polystyrene produced by sMAO-Pn*Zr[(N^{p}Tol)$_2$CH]$_2$ (**13$_{sMAO}$**) (chloroform-d_1, 298 K, 125 MHz).

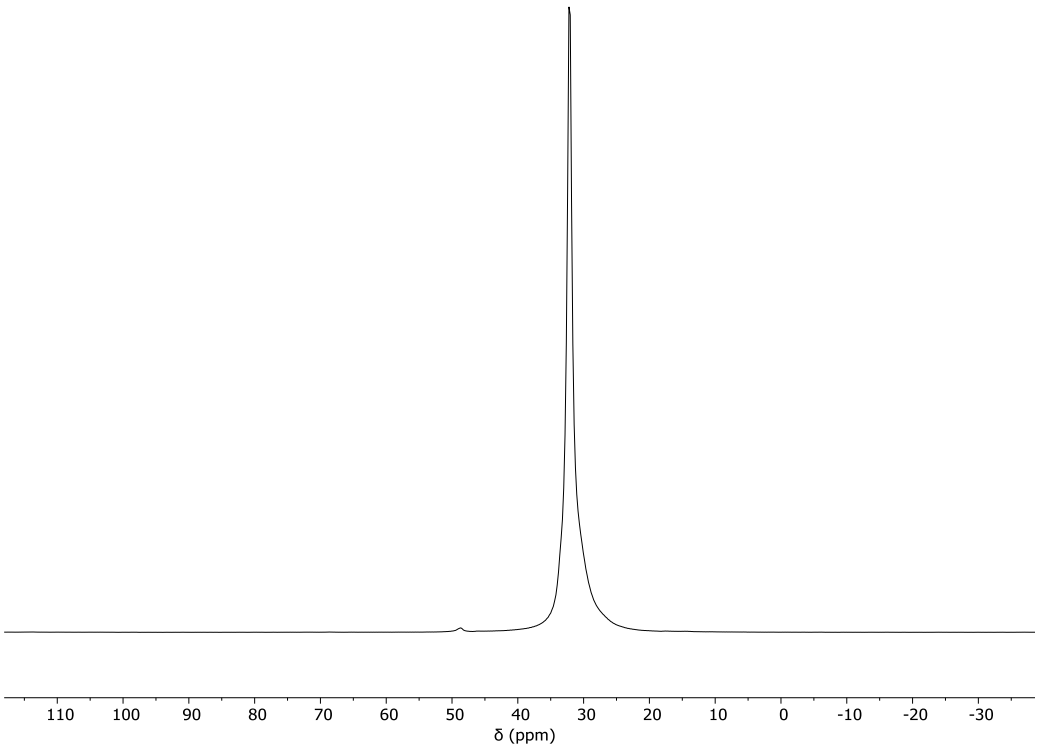

Figure A6.49. ^{13}C CPMAS NMR spectrum of polyethylene produced by sMAO-Pn*ZrCl[(N^{i}Pr)$_2$C(4-^{t}Bu-C$_6$H$_4$)] (**8$_{sMAO}$**) at 40 °C (10 kHz).

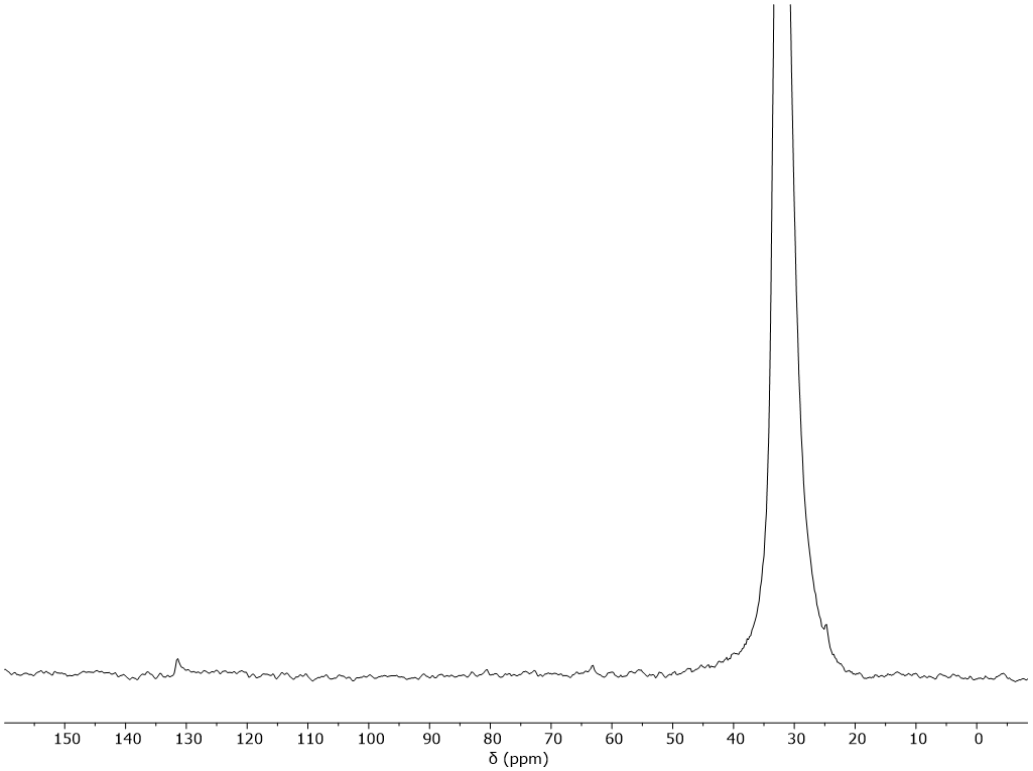

Figure A6.50. ^{13}C CPMAS NMR spectrum of polymer produced by the copolymerisation of ethylene with styrene using sMAO-Pn*ZrCl[(N^{i}Pr)$_2$C(4-^{t}Bu-C$_6$H$_4$)] (**8$_{sMAO}$**) at 40 °C (10 kHz).

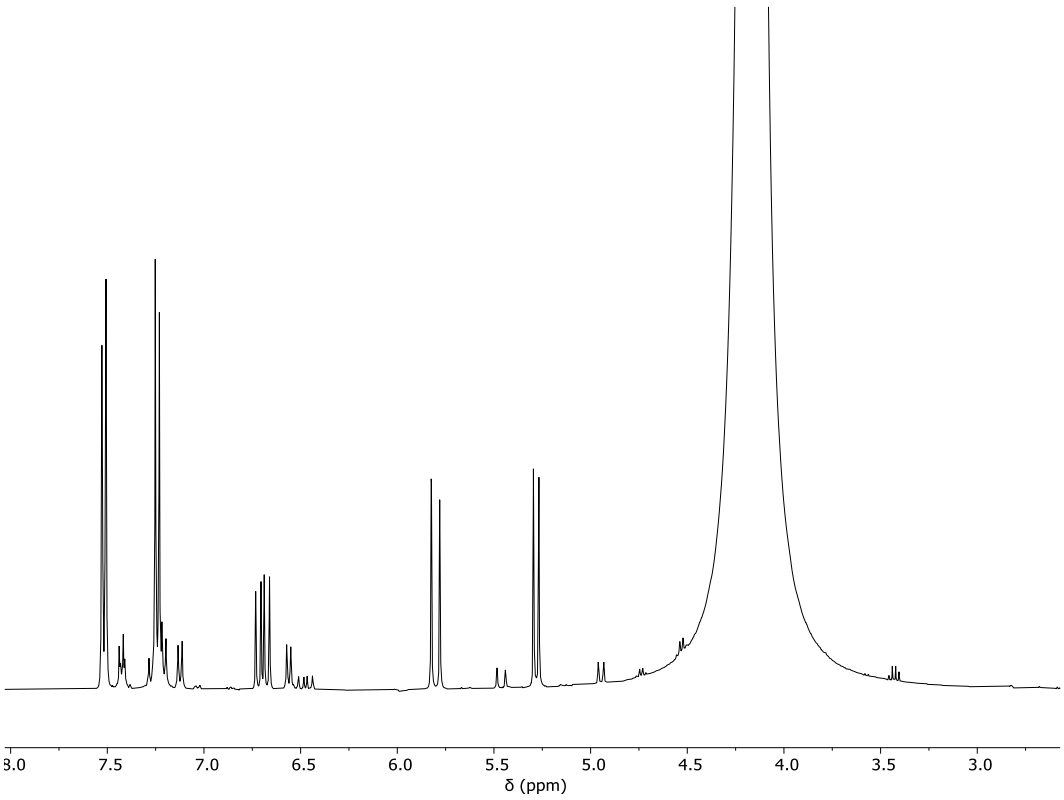

Figure A.51. 13H NMR spectrum of material produced by the attempted copolymerisation of ethylene with 4-NH$_2$-styrene using sMAO-Pn*ZrCl[(N^{i}Pr)$_2$C(4-OMe-C$_6$H$_4$)] (**6$_{sMAO}$**) (dmso-*d*^{6}, 298K, 400MHz).

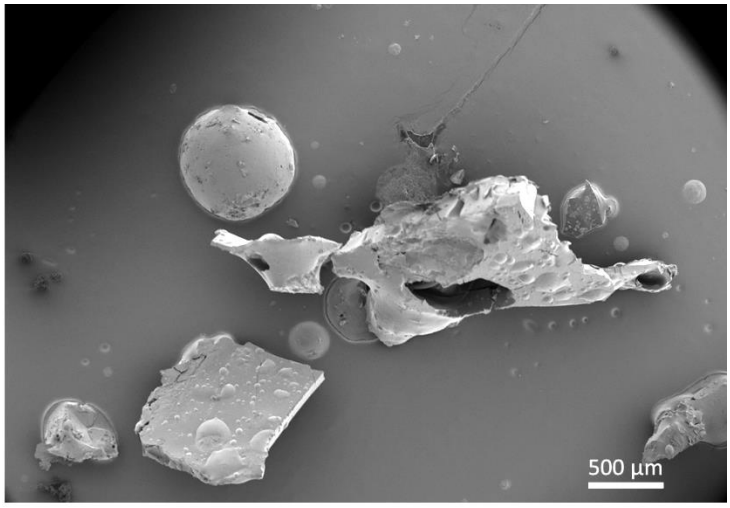

Figure A6.52. SEM image of polystyrene produced by sMAO-Pn*ZrCl[(N^{i}Pr)$_2$C(4-^{t}Bu-C$_6$H$_4$)] (**8$_{sMAO}$**) at 55 °C (x27).

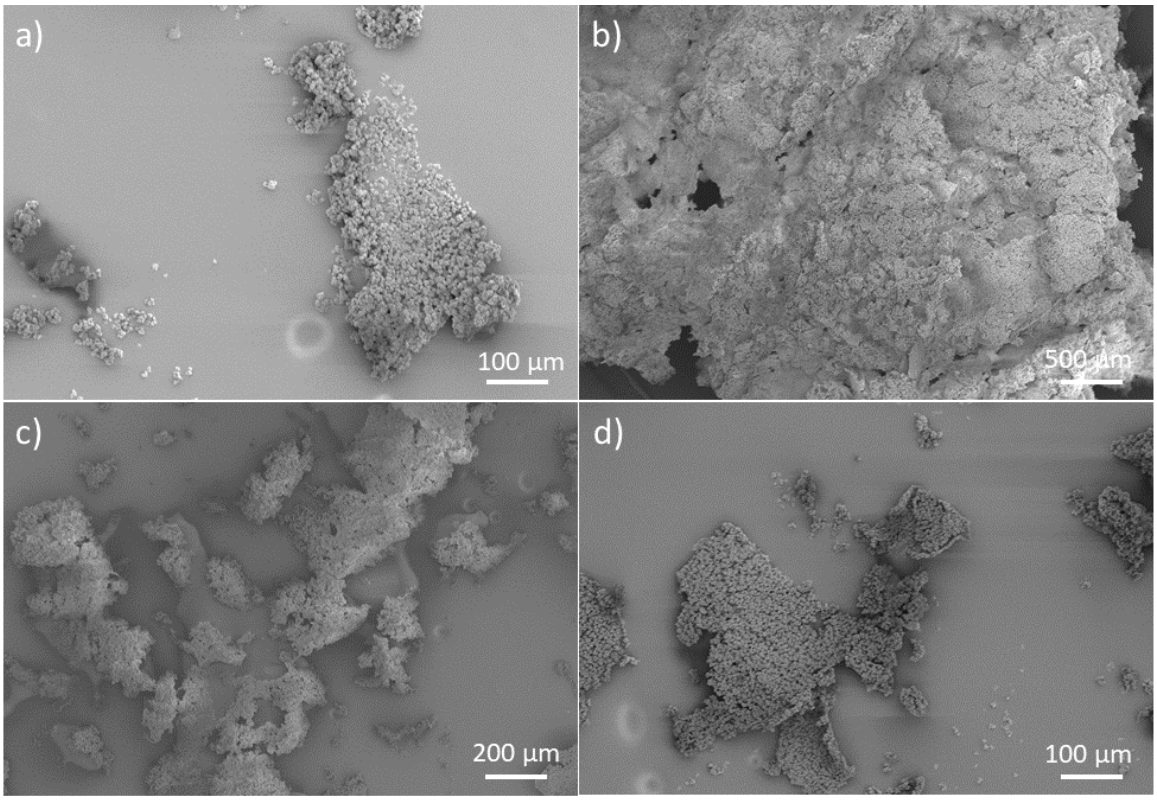

Figure A6.53. SEM images of polyethylenes produced by a) sMAO-Pn*ZrCl[(N^{i}Pr)$_2$C(C$_6$H$_5$)] (**10$_{sMAO}$**) (x120), b) sMAO-Pn*Zr(OXyl)[(N^{i}Pr)$_2$C(C$_6$H$_5$)] (**11$_{sMAO}$**) (x43), c) sMAO-Pn*ZrCl[(N^{p}Tol)$_2$CH] (**12$_{sMAO}$**) (x55) and d) sMAO-Pn*ZrCl[(N^{p}Tol)$_2$CH]$_2$ (**13$_{sMAO}$**) (x110).

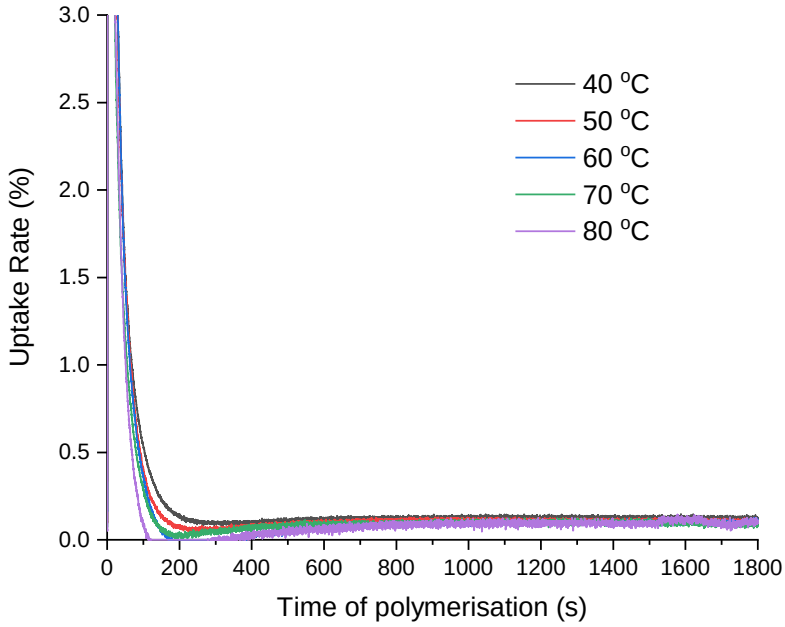

Figure A6.54. Homopolymerisation ethylene uptake rate plots for sMAO-Pn*ZrCl[(N^{i}Pr)$_2$C(4-OMe-C$_6$H$_4$)] (**6$_{sMAO}$**); 10 mg catalyst ([Al$_{sMAO}$]$_0$:[Ti]$_0$ = 200:1), 2 bar ethylene, 50 mL hexane, 150 mg TiBA and 30 minutes.

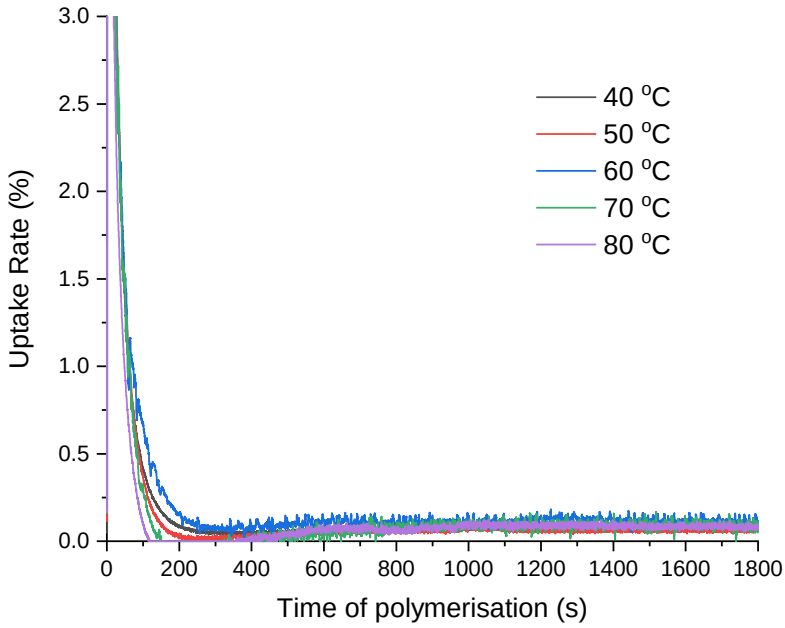

Figure A6.55. Homopolymerisation ethylene uptake rate plots for sMAO-Pn*ZrCl[(N^{i}Pr)$_2$C(4-CF$_3$-C$_6$H$_4$)] (**7$_{sMAO}$**); 10 mg catalyst ([Al$_{sMAO}$]$_0$:[Ti]$_0$ = 200:1), 2 bar ethylene, 50 mL hexane, 150 mg TiBA and 30 minutes.

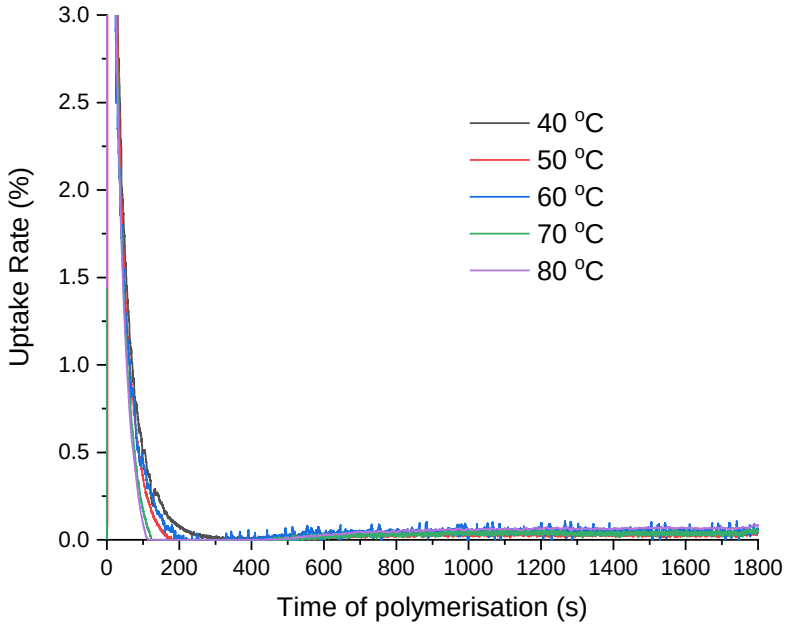

Figure A6.56. Homopolymerisation ethylene uptake rate plots for sMAO-Pn*ZrCl[(N^{i}Pr)$_2$C(4-^{t}Bu-C$_6$H$_4$)] (**8$_{sMAO}$**); 10 mg catalyst ([Al$_{sMAO}$]$_0$:[Ti]$_0$ = 200:1), 2 bar ethylene, 50 mL hexane, 150 mg TiBA and 30 minutes.

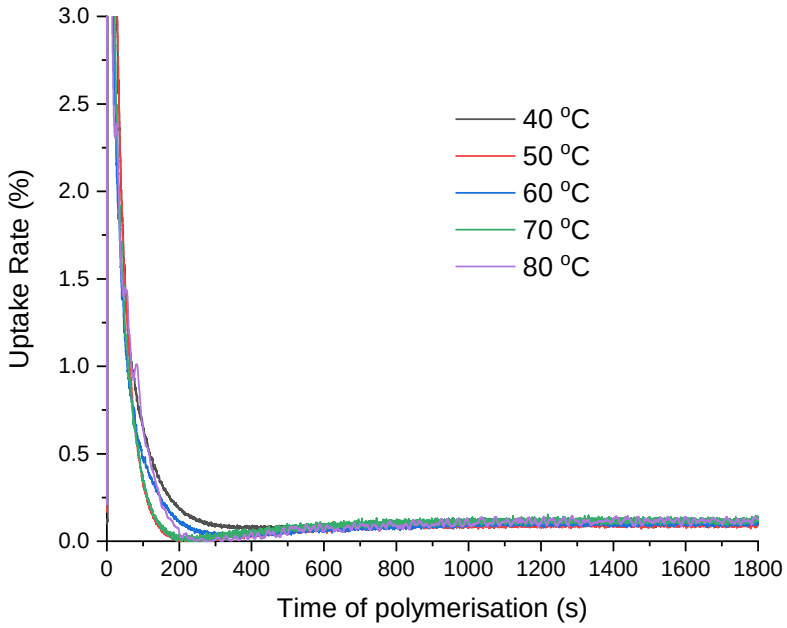

Figure A6.57. Homopolymerisation ethylene uptake rate plots for sMAO-Pn*ZrCl[(NMes)$_2$CH] (**9$_{sMAO}$**); 10 mg catalyst ([Al$_{sMAO}$]$_0$:[Ti]$_0$ = 200:1), 2 bar ethylene, 50 mL hexane, 150 mg TiBA and 30 minutes.

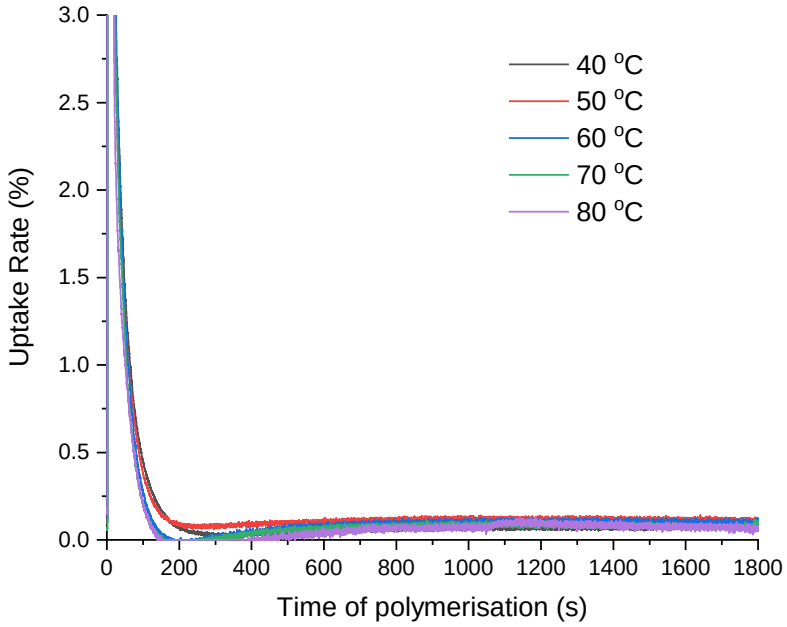

Figure A6.58. Copolymerisation ethylene uptake rate plots for sMAO-Pn*ZrCl[(N^{i}Pr)$_2$C(4-OMe-C$_6$H$_4$)] (**6$_{sMAO}$**); 10 mg catalyst ([Al$_{sMAO}$]$_0$:[Ti]$_0$ = 200:1), 2 bar ethylene, 50 mL hexane, 150 mg TiBA, 125 µL of styrene and 30 minutes.

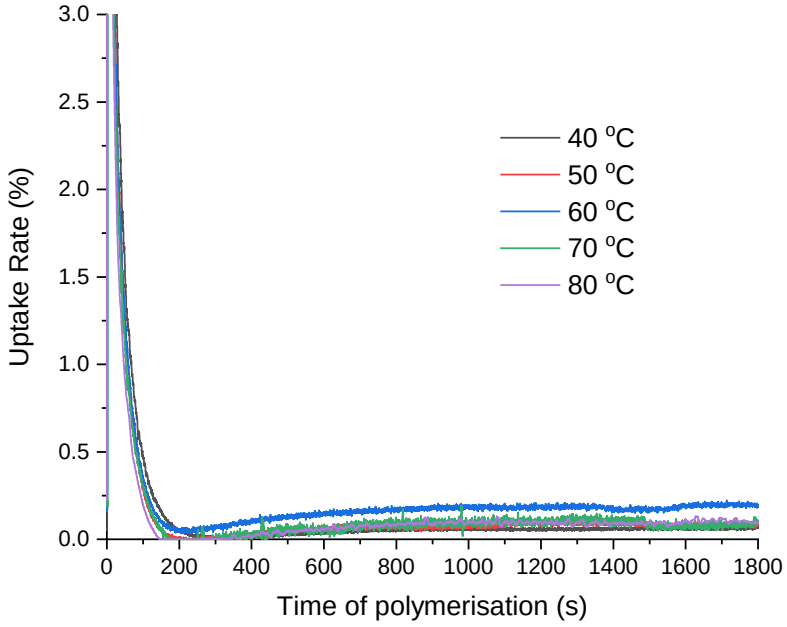

Figure A6.59. Copolymerisation ethylene uptake rate plots for sMAO-Pn*ZrCl[(N^{i}Pr)$_2$C(4-CF$_3$-C$_6$H$_4$)] (**7$_{sMAO}$**); 10 mg catalyst ([Al$_{sMAO}$]$_0$:[Ti]$_0$ = 200:1), 2 bar ethylene, 50 mL hexane, 150 mg TiBA, 125 µL of styrene and 30 minutes.

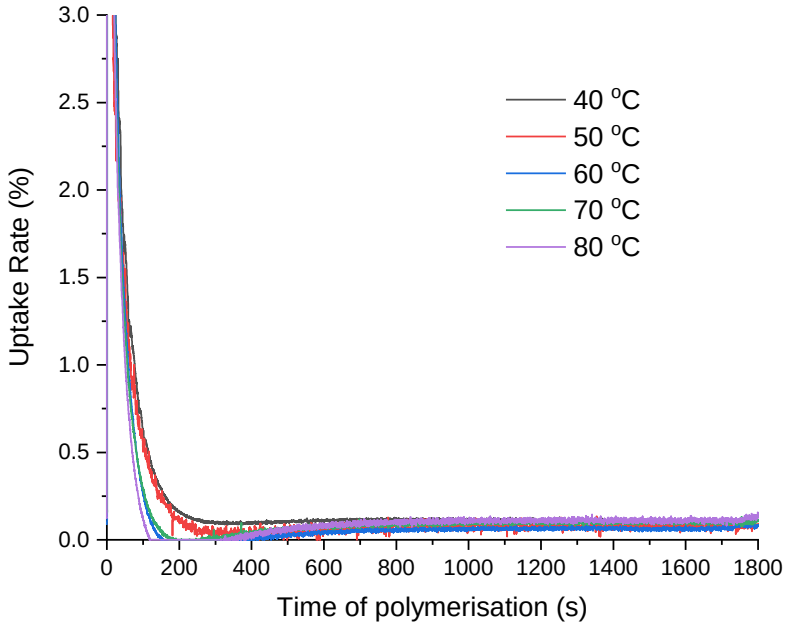

Figure A6.60. Copolymerisation ethylene uptake rate plots for sMAO-Pn*ZrCl[(N^{i}Pr)$_2$C(4-^{t}Bu-C$_6$H$_4$)] (**9$_{sMAO}$**); 10 mg catalyst ([Al$_{sMAO}$]$_0$:[Ti]$_0$ = 200:1), 2 bar ethylene, 50 mL hexane, 150 mg TiBA, 125 µL of styrene and 30 minutes.

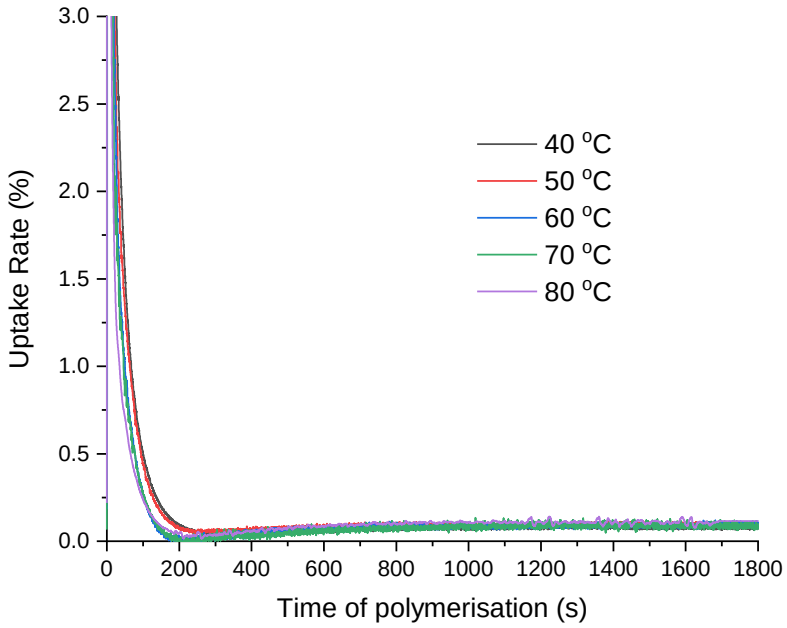

Figure A6.61. Copolymerisation ethylene uptake rate plots for sMAO-Pn*ZrCl[(NMes)$_2$CH] (**9$_{sMAO}$**); 10 mg catalyst ([Al$_{sMAO}$]$_0$:[Ti]$_0$ = 200:1), 2 bar ethylene, 50 mL hexane, 150 mg TiBA, 125 µL of styrene and 30 minutes.

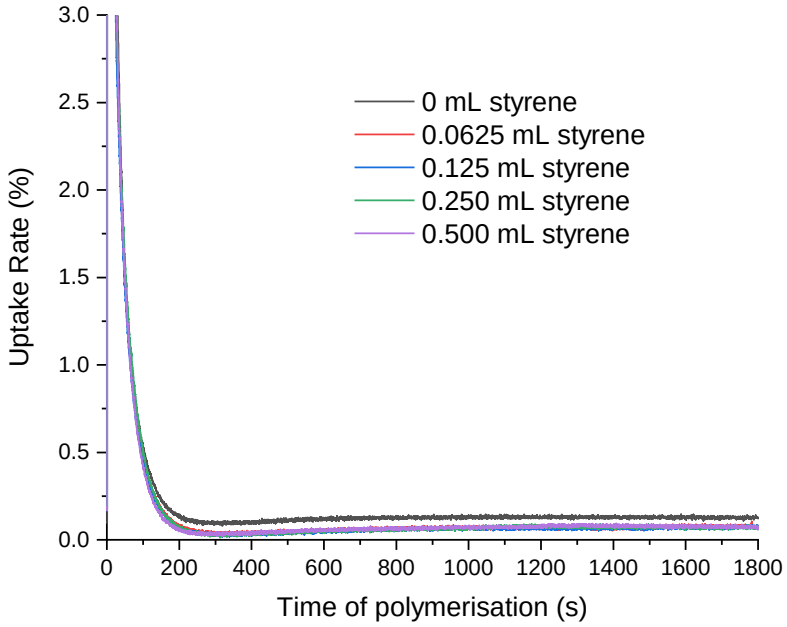

Figure A6.62. Copolymerisation ethylene uptake rate plots for sMAO-Pn*ZrCl[(N^iPr)$_2$C(4-OMe-C_6H_4)] (**6$_{sMAO}$**); 10 mg catalyst ([Al$_{sMAO}$]$_0$:[Ti]$_0$ = 200:1), 2 bar ethylene, 50 mL hexane, 150 mg TiBA, 40 °C and 30 minutes.

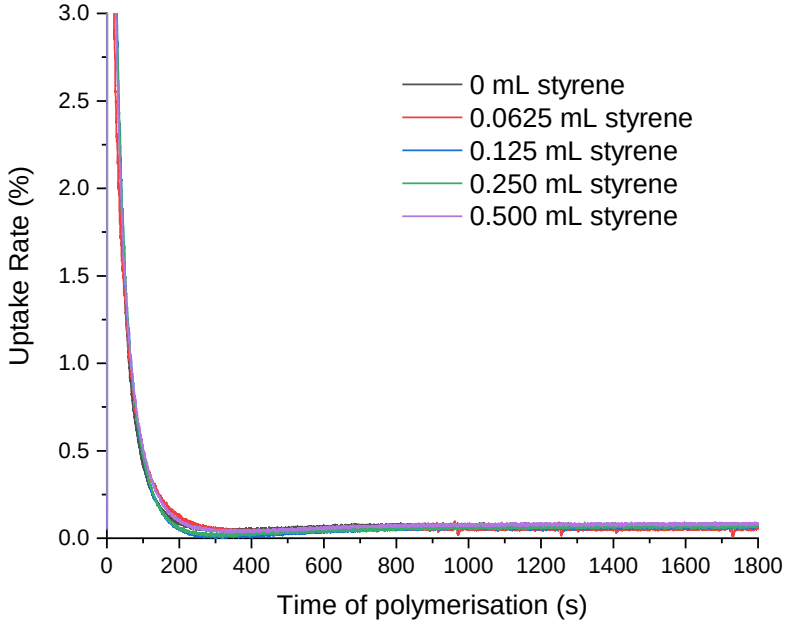

Figure A6.63. Copolymerisation ethylene uptake rate plots for sMAO-Pn*ZrCl[(N^iPr)$_2$C(4-CF_3-C_6H_4)] (**7$_{sMAO}$**); 10 mg catalyst ([Al$_{sMAO}$]$_0$:[Ti]$_0$ = 200:1), 2 bar ethylene, 50 mL hexane, 150 mg TiBA, 40 °C and 30 minutes.

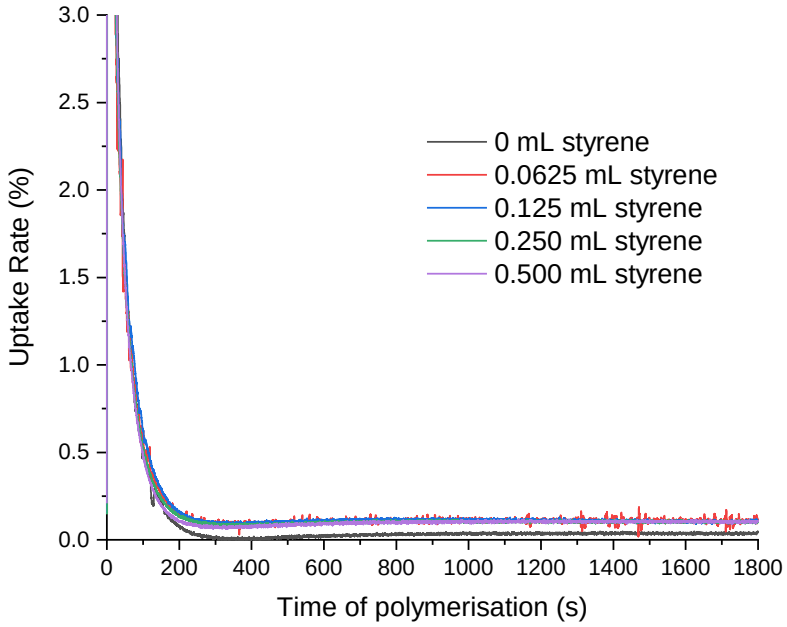

Figure A6.64. Copolymerisation ethylene uptake rate plots for sMAO-Pn*ZrCl[(N^{i}Pr)$_2$C(4-^{t}Bu-C$_6$H$_4$)] (**8$_{sMAO}$**); 10 mg catalyst ([Al$_{sMAO}$]$_0$:[Ti]$_0$ = 200:1), 2 bar ethylene, 50 mL hexane, 150 mg TiBA, 40 °C and 30 minutes.

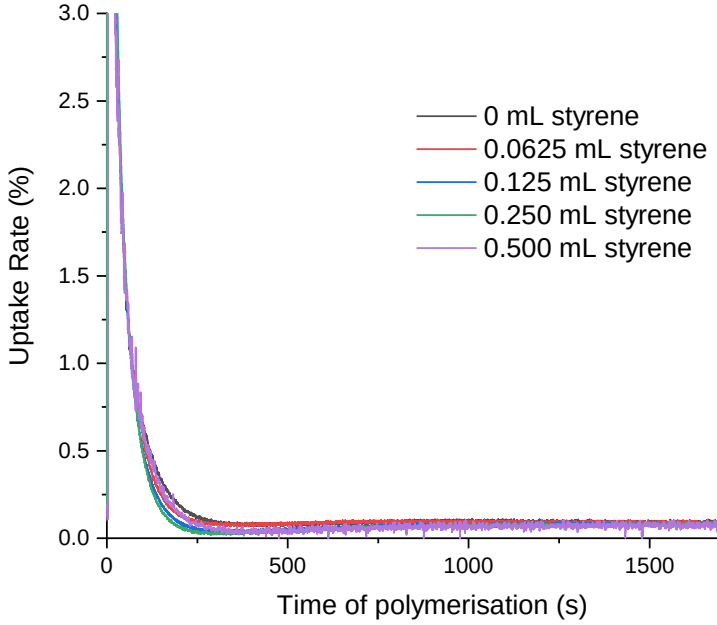

Figure A6.65. Copolymerisation ethylene uptake rate plots for sMAO-Pn*ZrCl[(NMes)$_2$CH] (**9$_{sMAO}$**); 10 mg catalyst ([Al$_{sMAO}$]$_0$:[Ti]$_0$ = 200:1), 2 bar ethylene, 50 mL hexane, 150 mg TiBA, 40 °C and 30 minutes.